Kinetic and mechanistic studies on substitution reactions of multinuclear *cis*-platinum(II) complexes: An experimental and computational investigation

By

Panyako Wangoli Asman

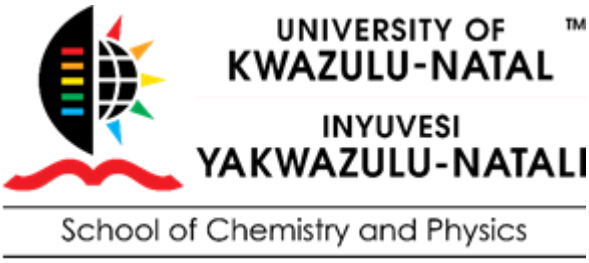

MARCH, 2020

Kinetic and mechanistic studies on substitution reactions of multinuclear *cis*-platinum(II) complexes: An experimental and computational investigation

By

PANYAKO WANGOLI ASMAN **(**Student Number **211560867)**

(B. Sc, M. Sc (Kenyatta University)

Being a thesis submitted to the College of Agriculture, Engineering and Science in fulfilment of the requirements for the award of the degree of

Doctor of Philosophy

of the

University of KwaZulu-Natal

Supervisor: Professor P. A. Ajibade

MARCH 2020

DECLARATION

I, PANYAKO WANGOLI ASMAN**,** declare that;

1. The research in this thesis, except where otherwise indicated, is my original research.
2. This thesis has not been submitted for any degree or examination at other university.
3. This thesis does not contain any other person data unless specifically acknowledged as being sourced from them.
4. This thesis does not contain any other persons' writing, unless specifically acknowledged as being sourced from other researchers. Where other written sources have been quoted, then:
    a. Their words have been re-written but the general information attributed to them has been properly referenced.
    b. In all instances where the exact words of other authors have been used, then their writing has been placed in italics and inside a quotation mark, and referenced.
5. This thesis does not contain text or graphics from the internet copied and pasted, unless specifically acknowledged, and the source being detailed in the dissertation/thesis and in the references section.

Sign 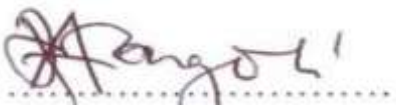 **PANYAKO WANGOLI ASMAN**

Date 12/03/2020 Name

CERTIFICATION

This is to certify that this research is a record of original work carried out by PANYAKO WANGOLI ASMAN under my supervision in the Kinetics Reactions laboratory of the Department of Chemistry, University of KwaZulu Natal in fulfilments of the requirements for the award of Doctor of Philosophy degree in Chemistry.

_12/03/20___ _____

Date Supervisor

P. A. Ajibade
Professor of Inorganic Materials Chemistry
B. Sc (Hons), MSc (Ibadan);
PhD (UniZul); MRSC (London

Dedication

In memory of my beloved mum and dad who over the years of their lives gave me the right advice at the right time and in the right dose, may their souls rest in peace

ACKNOWLEDGEMENTS

Completing this thesis a product of several years' work, I feel deeply indebted to countless people who greatly inspired and supported within the University of KwaZulu Natal and outside University of KwaZulu Natal. First I am deeply gratefully to Prof Peter Ajibade for accepting to co-supervisor the work. Your acceptance to co-supervise this research project brought a renewed inspiration and gave the impetus at a time I needed it most. Thank you for your insightful suggestions and re-organization of the thesis. I am very grateful and may God bless you abundantly.

Secondly I thank all the academic staff in the Chemistry Department at University of KwaZulu Natal, Pietermaritzburg Campus for their open door policy for discussion. Your discussions whenever I visited nourished and enriched my work. In particular I would like to thank Dr. Allen Mambanda for the valuable suggestions and corrections he made to this thesis. I am indebted for his willingness to read and correct my work any time I called upon him. I also extend my appreciation to Dr. D. Reddy. I acknowledge the technical staff for a friendly and enjoyable environment, your assistance during the course of this work is greatly appreciated. I also express my gratitude to Mr Craig Grimmer for NMR analyses, Ms Janse van Resenburg for mass and elemental analysis and Shawn Ball for proper storage and delivery of chemicals. Your support in this study is highly appreciated. I also express my gratitude to International Office and Higher Degrees at UKZN.

I also acknowledge Dr. D. Andala of Multimedia University for proof reading the work; I am much humbled by your character. I also thank Dr. Watanga of Multimedia University for your assistance when things were not right. To Dr. Karanja wa-Thiong'o of Kenyatta University I am much grateful for your initial mentorship during my M. Sc at KU. You inspired me to become an independent researcher and guided me to realize the power of critical reasoning and encouraged me to work towards scientific accomplishment. I also thank University of KwaZulu Natal (UKZN) not only for providing the funding for my research, but also giving a nourishing environment to undertake this study and inspiring me to greatness. The UKZN community receive the greatest gratitude. I acknowledge Multimedia University of Kenya (MMU) for the part-time work that facilitated the finalization of this Doctorate degree. Thank you for the space and the academic environment that enabled the drafting of the published papers and the final thesis draft.

I owe a debt of gratitude for inspiring mentorship, practical guidance, generosity with vast reserves of knowledge accompanied with intellectual honesty and sincerity to Dr. Peter Ongoma and Dr. Grace Kununda. Thank you as well for guiding me. Next I thank my fellow postgraduate students in Chemistry department at Pietermaritzburg campus with whom I shared moments of deep anxiety but sometimes with big excitement. “Most people say that it is the intellect which makes a great scientist,” however, I beg to disagree with this statement and concur with Albert Einstein, “it is the character.” I hereby say “a big thank you so much for your character.” Many thanks to Dr. Wekesa, Olusegun, Dr. Alam, Dr. Rajesh, Dr. Ogweno, Dr. Simba, Dr. Bilaal and Dr. Abimbola. Thank you for your friendship and character. Your presence was very important in the project I felt tremendously solitude. Dr. Wekesa I hope you remember the tea breaks, it was awesome. I also acknowledge Dr. Ollengo of Kimathi University and Dr. Magu at Multimedia University of Kenya (MMU) who has done the final type setting of this document.

I also acknowledge the authors of the articles and reviews I have quoted during the write-up of this thesis. Thank you for your expertise. I am also very grateful to my landlord Terry Petersen for the accommodation during my stay in South Africa. I thank you for your hospitality and generosity you extended to me while staying at your apartment. It was always clean and a comfortable environment.

Finally, this achievement was realized by standing on the shoulders of giants; I therefore greatly thank my parents, brothers and sisters for their greatness. Special thanks to my late dad and mum who passed on during the course of this study. It is for their sacrifice that I am indebted forever. I dedicate this thesis to them. May their souls Rest in Peace. To Maimuna B. M. thank you for your love and support I cherish.

TABLE OF CONTENTS

Chapter One

Chapter Two

Chapter Three

Chapter Four

Chapter Seven

Appendices

LIST OF FIGURES

LIST OF TABLES

ABBREVIATIONS AND SYMBOLS

Å	Angstrom ($1.0 \times 10^{-10} m$)
μL	microliter
kJ	kilojoule
j	joule
^{13}C NMR	Carbon 13 nuclear magnetic resonance
^{1}H NMR	Proton nuclear magnetic resonance
^{195}Pt NMR	Platinum nuclear magnetic resonance
h	Planck's constant ($6.626 \times 10^{-34} Js^{-1}$)
NBO	Natural Bond Orbital
K	Kelvin
MLCT	Metal-to-ligand charge transfer
D	Debyes
dpa	2,2'-dipyridylamine
k_B	Boltzmann's constant ($1.38 \times 10^{-23} JK^{-1}$)
UV-Vis	Ultra violet visible
v/v	volume by volume
k_{obs}	Observed *pseudo* first-order constant
k_2	Second-order rate constant
k_1	Solvolytic path
eV	Electron volt
R	Universal gas constant ($8.3145\ JK^{-1}mol^{-1}$)
DMF-d_7	Deuterated N,N-Dimethylformamide
DMSO-d_6	Deuterated Dimethyl Sulfoxide
D_2O	Deuterium oxide/Deuterated water
M/z	Mass-to-charge ratio
TOF MS	Time-of –flight mass spectrometry
ESI-MS	Electrospray ionization mass spectrometry
ΔE	HOMO-LUMO energy gap
$\Delta H^{\#}$	Activation enthalpy
$\Delta S^{\#}$	Activation entropy
λ	Wavelength (nm)

HOMO	Highest occupied molecular orbital
LUMO	Lowest unoccupied molecular orbital
Nu	Nucleophile
K_a	Acid-dissociation equilibrium constant
mmol	Millimole
Hz	Hertz, s^{-1}
MHz	mega Hertz
d	doublet
dd	doublet of doublets
ddd	doublet of doublets of doublets
t	triplet
Calcd	Calculated
py	pyridine
m	multiplet
s	singlet or second
M	Molarity
I	Ionic strength
Syn-	Synperiplanar
Anti-	Antiperiplanar
A/T	Adenine/Thymine
G/C	Guanine/Cytosine
S-donor	Sulphur-donor
p53	Tumour protein
Cisplatin	*Cis*-diamminedichloroplatinum(II), [*cis*-$Pt(NH_3)_2Cl_2$]
DNA	Deoxyribonucleic Acid
pH	$-\log[H^+]$
TU	Thiourea
DMTU	*N,N'*-dimethylthiourea
TMTU	*N,N,N'N'*-tetramethylthiourea
$	United States Dollar
dpzm	4,4'-dipyrazolylmethane
B3LYP	Becke, 3-parameter, Lee-Yang-Parr
LANL2DZ	Los Alamos National Laboratory 2 Double basis set

mM	Millimolar
DFT	Density Functional Theory
%	per cent
ppm	parts per million
exp	Exponential
g	gram
mL	millilitre
(=CH-)	Methine
K_2PtCl_4	Potassium tetrachloroplatinate
DIPEA	*N,N*-diisopropylethylamine
THF	Tetrahydrofuran
o	*ortho*
m	*meta*
p	*para*
ph	phenyl
tdab	1,3,5-tris(di-2-pyridylamino)benzene
tdat	2,4,6-tris(dipyridin-2-ylamino)–[1,3,5]-triazine
$Pt(dpa)(H_2O)_2$	di-2-pyridylaminodiaquaplatinum(II) (**Pt1**)
$Ph(dpa)Pt(H_2O)_2$	di-2-pyridylaminomethylbenzenediaquaplatinum(II) (**Pt2**)
$o\text{-}Ph(dpa)_2Pt_2(H_2O)_4$	1,2-bis(di-2-pyridylaminomethyl)benzenetetraquaplatinum(II) **(Pt3)**
$m\text{-}Ph(dpa)_2Pt_2(H_2O)_4$	1,3-bis(di-2-pyridylamino-methyl)benzenetetraquaplatinum(II) (**Pt4**)
$p\text{-}Ph(dpa)_2Pt_2(H_2O)_4$	1,4-bis(di-2-pyridylaminomethyl)-benzenetetraquaplatinum(II) (**Pt5**)
$(dpa)_2$-en)	*N,N'*-1,2-Bis(di-2-pyridylamino)ethane (**L2**)
$(dpa)_2$-prop	*N,N'*-1,3-Bis(di-2-pyridylamino)propane (**L3**)
$(dpa)_2$-but	*N,N'*-1,4-*N,N'*-Bis(di-2-pyridylamino)butane (**L4**)
$(dpa)_2$-pent	*N,N'*-1,5-Bis(di-2-pyridylamino)pentane (**L5**)
$(dpa)_2$-hex	*N,N'*-I,6-Bis(di-2-pyridylamino)hexane (**L6**)
$[(dpa)_2\text{-}enPt_2(H_2O)_4]^{4+}$	*N,N'*-1,2-Bis(di-2-pyridylamino)ethanetetraquaplatinum(II) (**PtL2**)
$[(dpa)_2\text{-}propPt_2(H_2O)_4]^{4+}$	*N,N'*-1,3-Bis(di-2-pyridylamino)propanetetraquaplatinum(II) (**PtL3**)
$[(dpa)_2\text{-}butPt_2(H_2O)_4)]^{4+}$	*N,N'*-1,4-Bis(di-2-pyridylamino)butanetetraquaplatinum(II) (**PtL4**)
$[(dpa)_2\text{-}pentPt_2(H_2O)_4)]^{4+}$	*N,N'*-1,5-Bis(di-2-pyridylamino)pentanetetraaquaplatinum(II) (**PtL5**)

$[(dpa)_2\text{-hex}Pt_2(H_2O)_4)]^{4+}$ *N,N'*-1,6-Bis(di-2-pyridylamino)hexanetetraquaplatinum(II) (**PtL6**)

dpab Di-2-pyridylaminobenzene (**C1**)

dpamb Di-2-pyridylaminomethylbenzene (**C2**)

tamb 1,3,5-tris(di-2-pyridylaminomethyl)benzene (**C3**)

tdab 1,3,5-tris(di-2-pyridylamino)benzene (**C4**)

tdat 2,4,6-tris(dipyridin-2-ylamino)–[1,3,5]-triazine (**C5**)

Ptdpab phenyl-dichlorido-2,2'-dipyridinylaminediaquaplatinum(II) $(dpab)Pt(H_2O)_2$, (**PtC1**)

Ptpamb di-2-pyridylaminomethylbenzenediaquaplatinum(II) $(pamb)Pt(H_2O)_2$, (**PtC2**)

Pttab 1,3,5-tris(2,2'dipyridylamino)-benzenehexaquaplatinum(II) $(tab)Pt_3(H_2O)_6$, (**PtC3**)

Pttamb 1,3,5-tris(2,2'dipyridylmethylamino)benzenehexaquaplatinum(II) $(tamb)Pt_3(H_2O)_6$, (**PtC4**)

Pttat 2,4,6-tris(2,2'-dipyridylamino)-1,3,5-triazinehexaquaplatinum(II) $(tat)Pt_3(H_2O)_6$,

2,3-tppda *N,N,N',N'*-tetrakis(2-pyridyl)-2,3-pyridinediamine

2,4-tppda *N,N,N',N'*-tetrakis(2-pyridyl)-2,4-pyridinediamine

2,5-tppda *N,N,N',N'*-tetrakis(2-pyridyl)-2,5-pyridinediamine

2,6-tppda *N,N,N',N'*-tetrakis(2-pyridyl)-2,6-pyridinediamine

2,6-tpmpda *N,N,N',N'*-tetrakis(2-pyridylaminomethyl)-2,6-pyridylamine

$[2,3\text{-tppda}Pt_2(H_2O)_4]^{4+}$ *N,N,N',N'*-tetrakis(2-pyridyl)-2,3-pyridinediaminetetraquaplatinum(II) (**PtL1**)

$[2,4\text{-tppda}Pt_2(H_2O)_4]^{4+}$ *N,N,N',N'*-tetrakis(2-pyridyl)-2,4-pyridinediaminetetraquaplatinum(II) (**PtL2**)

$[2,6\text{-tppda}Pt_2(H_2O)_4]^{4+}$ *N,N,N',N'*-tetrakis(2-pyridyl)-2,6-pyridinediaminetetraquaplatinum(II) (**PtL3**)

$[2,5\text{-tppda}Pt_2(H_2O)_4]^{4+}$ *N,N,N',N'*-tetrakis(2-pyridyl)-2,5-pyridinediaminetetraquaplatinum(II) **(PtL4)**

$[2,6\text{-tpmpda}Pt_2(H_2O)_4]^{4+}$ *N,N,N',N'*-tetrakis(2-pyridylaminomethyl)-2,6-pyridinediaminetetraquaplatinum(II) (**PtL5**)

dpa 2,2'-dipyridylamine

Carboplatin [Pt(NH3)$_2$(O,O-cyclobutane-1,1-dicarboxylate)]

Oxaliplatin [Pt(1,2-*trans*-R,R-diaminoyhexane)(O,O-oxalato)]

BBR3005 $[\{cis\text{-}PtCl(NH_3)_2\}_2(\mu\text{-}NH_2(CH_2)_6NH_2)]^{2+}$ (1,1/c,c)

BBR3005 $[\{trans\text{-}PtCl(NH_3)_2\}_2(\mu\text{-}NH_2(CH_2)_6NH_2)]^{2+}$ (1,1/t,t)

BBR3464 $[\{trans\text{-}PtCl(NH_3)_2\}_2(\mu\text{-}trans\text{-}Pt(NH_3)_2(H_2N(CH_2)_6NH_2)_2\}]^{4+}$

BBR3571	[{*trans*-$PtCl(NH_3)_2$}$_2$(μ-spermidine-N^1,N^8)]$^{3+}$
BBR3610	[{*trans*-$PtCl(NH_3)_2$}$_2$-μ-{*trans*($H_2N(CH_2)_6NH_2(CH_2)_2NH_2(CH_2)_6NH^2$}]$^{4+}$

RESEARCH OUTPUTS

Publications

The following publications are the outputs from this thesis

1. The role of an alkyl-phenyl spacer on the reactivity of novel platinum(II) complexes with thiourea nucleophiles, W. A. **Panyako** and D. Jaganyi, *Int. J. Kinet.*, 2017, **49,** 545-561.

2. The effect of an alkyl chain tether on the kinetics and mechanistic behaviour on bifunctional dinuclear platinum(II) complexes bearing *N,N'*-dipyridylamine ligands. W. A. **Panyako** and G. Kinunda, *New J. Chem.*, 2018, **42**, 214-227.

3. Kinetics and mechanistic studies of polynuclear Pt(II) polypyridyl complexes; a paradigm shift in search of new anticancer agents. W. A. **Panyako**, *Inorg. Chim. Acta*., 2018, **469**, 341-352.

4. The role of annular nitrogen in tuning the reactivity of novel bifunctional Pt(II) complexes appended to pyridyl spacers; a kinetic and mechanistic investigation, W. A. **Panyako**, *Journal of Coordination Chemistry*, DOI: 10.1080/00958972.2017.1371702, Link:http://dx.doi.org/10.1080/00958972.2017.1371702.

Conference Contributions:

1. The Kenya Chemical Society (KCS), 9th International Conference, held at United States International University (USIU) 9th May – 12th May 2017, Oral presentation "The role of alkyl-phenyl spacer on the reactivity of novel platinum(II) complexes with bio-relevant nucleophiles."

2. The South African Chemical Institute (SACI), Inorganic Chemistry Conference 2015, Held at University of Rhodes (28th June – 2nd July 2015), Poster presentation "The role of alkyl-phenyl spacer on the reactivity of novel platinum(II) complexes with bio-relevant nucleophiles."

Abstract

In the search for new metal-based anticancer agents as effective drug candidates, this thesis reports on the kinetics and mechanistic substitution reactions of multinuclear platinum(II) complexes with bio-relevant molecules as a vital step towards novel drug development. The concept of multinuclearity for improving the chemotherapeutic activity has been proven in multinuclear platinum complexes such as BBR3464 and forms the solid basis for this project. The study addresses the problems associated with mononuclear platinum(II) drugs and reports on the design of novel multinuclear bifunctional platinum(II) complexes as potential anticancer therapeutics. The study involves synthesis of mono- and multinuclear platinum(II) complexes with 2,2'-dipyridylamine bridges followed with a detailed study of their reactivity with biological nucleophiles. Their successful substitution reactions support their potential antitumour activity. This leads to the notion that even the most deadly types of cancer may be revolutionised using platinum-based therapy. This further strengthens the search for new Pt(II) metal drugs that operate *via* novel mechanisms in controlling their bio-reactivity. Multinuclear Pt(II) complexes have shown a wider spectrum of activity giving hope of forming clinically relevant candidates. This has been epitomized by favourable reactivity profile of BBR3464, $[\{trans\text{-}PtCl(NH_3)_2\}_2(\mu\text{-}trans\text{-}Pt(NH_3)_2(H_2N(CH_2)_6NH_2)_2\}]^{4+}$, (1,0,1/t,t,t) with fewer side effects compared to cisplatin. This has led to a paradigm shift that validates the development and exploration of new multinuclear Pt(II) drugs with novel mechanism of action. Hence, this investigation illustrates a new approach in designing innovative platinum-based anticancer drugs through tuning the ligand system to regulate the reactivity. A mechanistic understanding of how these multinuclear platinum complexes achieve their novel mechanism is crucial to their clinical success as well as to their improved potency. Details about reaction mechanisms of multinuclear Pt(II) complexes remain to be elucidated in order to gain insight into their cytotoxic effects and factors controlling their bio-reactivity. In summary, this work reports a detailed kinetic and mechanistic study on multiple substitution reactions of multinuclear Pt(II) complexes linked by 2,2'-dipyridylamine ligands. The study mainly concentrated on complexes which offer two or more labile substitution sites chelated to *N,N*-donors in the *cis* position, since similar complexes like cisplatin are used in tumour therapy. The kinetic results presented herein were tuned by a tailored design of the molecular structures of the bridging ligands *via* electronic and steric effects. The investigated complexes shows varying reactivity patterns attributed to electronic and steric effects imparted by the bridging ligands and the bulky pyridyl groups connecting the Pt(II) centres.

Complexes with the structure *cis*–[Pt*NN*$(H_2O)_2]^{2+}$ were investigated since *cis*-$[Pt(NH_3)_2(H_2O)_2]^{2+}$ exhibits anti-tumour activity. The anticancer property of the investigated complexes is believed to stem from the ability of the *cis*-[Pt*NN*$(H_2O)_2]^{2+}$ fragment to bind to DNA bases. The study was tailored through tuning of the chelating ligands. Spectrophotometric acid-base titrations were performed to determine the pK_a values of the coordinated water molecules for the aqua species. Substitution reactions were carried out on aqua platinum(II) complexes under *pseudo* first-order conditions as a function of concentration of nucleophiles and temperature using stopped-flow and UV-visible spectroscopic techniques. The study shows the reaction rates to be greatly influenced by the nature of the chelating ligands; hence, the study was able to correlate kinetic, thermodynamic and structural properties of the designed platinum(II) complexes to their mechanistic interaction with biological molecules. The study suggests an identical reaction mechanism. The small positive values of enthalpy activation and large negative values of entropies of activation support an associative substitution mechanism. The experimental data is also supported by computational calculations by Gaussian 09' using Density Functional theory by the hybrid B3LYP functional. Calculations were carried out with the LANL2DZ atomic orbital basis functions.

CHAPTER 1

1.0 Introduction

1.1 Cancer

Cancer is the abnormal mass of tissue as a result of uncontrolled growth of abnormal cells, impacting on the functioning of bodily tissues and organs. It is a disease that has become very difficult to treat and thus, novel drugs are in high demand[1-3] as it has become a significant cause of death. Latest world cancer statistics shows a global rise of 14.1 million new cancer cases, 8.2 million cancer deaths and 32.6 million people living with cancer within 5 years of diagnosis in 2012 worldwide.[4,5] This figure is on the rise compared to 12.7 million new cases and 7.6 million deaths reported in 2008.[6] The most commonly diagnosed cancers were those of lung (1.8 million, 13.0 %), breast (1.7 million, 11.9 %) and colorectum (1.4 million, 9.7 %). The most common causes of cancer death were cancers of the lung (1.6 million, 19.4 % of the total), liver (0.8 million, 9.1 %) and stomach (0.7 million, 8.8 %).[4,5] Projections based on the GLOBOCAN 2012 estimates predict a substantive increase to in new cancer cases per year due to growth and ageing of the global population. It is reported that more than half of all cancers (56.8 %) and cancer deaths (64.9 %) in 2012 occurred in less developed countries and these proportions are projected to increase further by 2025.[4-6] Schematic maps in Figure 1.1 shows the estimated number of new cancer cases in 21 world areas in 2012.[6] The current statistics shows 18.1 million new cancer cases every year globally and 9.6 million cancer deaths in 2018.[7] From this statistics, it is frightening and challenging to meet the global demand in combating cancer without an essential drug. The pricing of cure drugs has become an issue as the cost of cancer care continues to rise significantly. Due to high cost involved and many impediments of current anticancer therapies there is an urge to discover new agents.

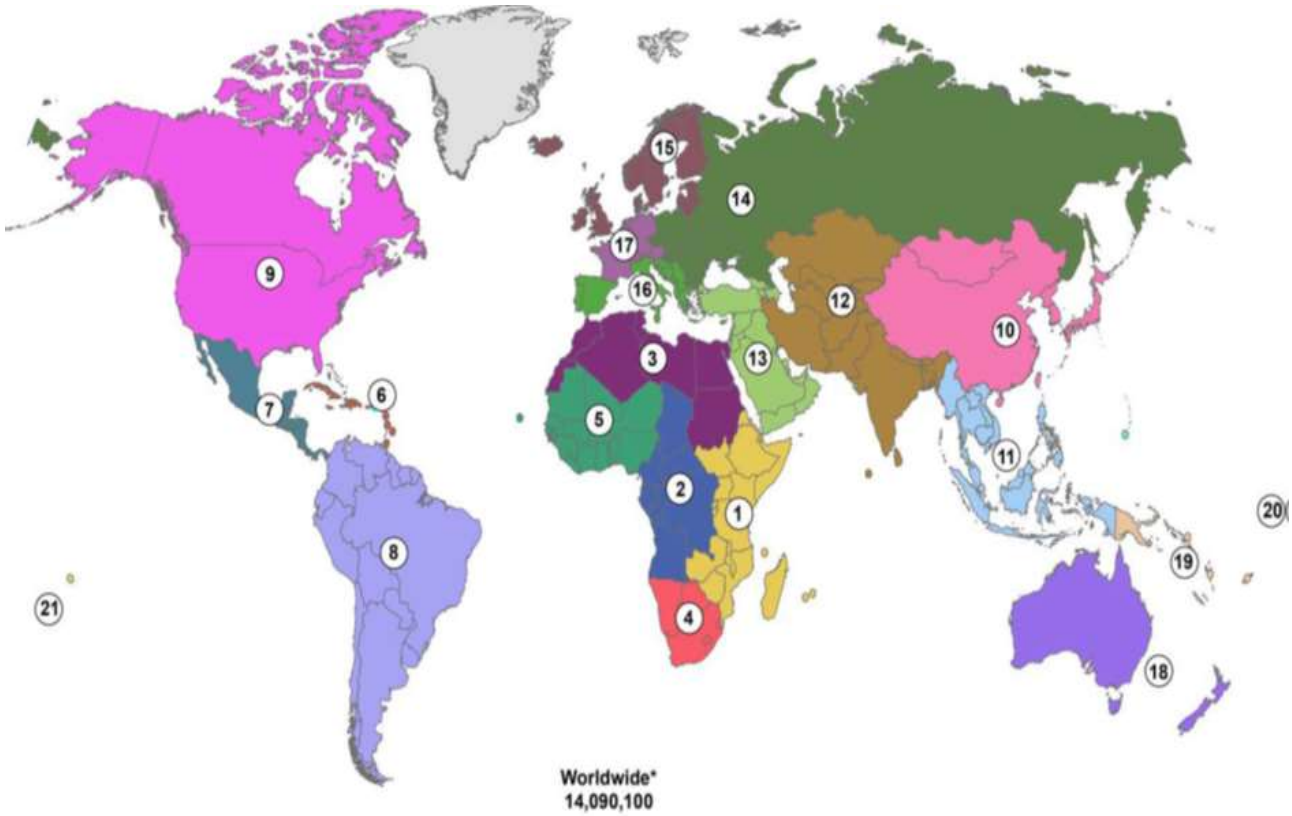

Figure 1.1: Estimated number of new cancer cases in world regions in 2012

*Note: Region estimates do not sum to the worldwide estimate due to calculation method. Source: GLOBOCAN 2012[4].

This rise in cancer cases has an immense burden not only on the large number of lives it touches but also has a significant economic impact. It was estimated that the 12.9 million new cases of cancer diagnosed in 2009 was estimated to cost the world $286 billion that year alone.[8] In 2010, the 13.3 million new cases of cancer diagnosed worldwide were estimated to have cost $290 billion while new cancer cases anticipated to occur by 2030 are projected to cost $458 billion.[9] From these data with the rising economic and personal burden of cancer, there is urgent need for more research to develop new prevention and treatment approaches. From the current statistics, the prevalence of this disease and all associated costs drives towards the search for new anticancer therapeutic drugs and treatments. In the search of these new anticancer drugs with better cytotoxic properties, platinum based polynuclear complexes have become the most promising therapeutics agents.

The present study addresses the latest developments in the design of novel chemotherapeutic agents based on platinum(II), particularly multinuclear chelates with variable bridging ligands. Platinum metal is of interest due to it being "slow metal", that is the ligands exchange on the same time scale as cell division processes.[10,11] This explains their success as anticancer therapeutics. The study aims to develop classical multinuclear platin drugs with new mechanisms of action with maximum efficacy using ligand substitution marking the first step towards clinically improved anti-tumour agents. Evaluating firstly, the kinetic properties of the designed Pt(II) complexes is significantly important in showing their biological activities. Mechanistic knowledge developed from the current study is hoped to be applied for the design of new multinuclear and bifunctional Pt(II) improved anticancer drugs. This is due to multinuclear Pt(II) complexes ability to overcome both intrinsic and acquired resistance to cisplatin. The study highlights their electronic and structural preference to their reactivity. The mechanistic knowledge from this study is essential in the design and development of new bifunctional Pt(II) compounds aimed for use as improved therapeutic agents to treat and control cancer. One aspect of transition metal chemistry that made this investigation more attractive is the geometric and electronic structural diversity that can be achieved through synthetic framework with Pt(II) using different bridging ligands.

1.2 Platinum-Based Anticancer Drugs

Research has shown a significant progress in utilization of transition metal complexes as drugs to treat several human diseases including cancer.[12,13] These metal based compounds have played an enormous impact on medicine as they provide possibilities to design and develop new therapeutic agents that treat different types of diseases. The unique aspects of introducing metals into anti-therapeutic agents are their ability to produce geometries that cannot be generated by organic compounds. Also the positive charge on metal ions produces favourable electrostatic interactions between the ligand and the DNA. This has made metals to have an esteemed place in medicinal chemistry. The development of metal based complexes with platinum as the central atom such as cisplatin or carboplatin has had an enormous impact on current cancer chemotherapy.[14-16] The success and imperfection of cisplatin has triggered intensive work for discovery of thousands of new platinum-based anticancer drugs. Over the past three decades, thousands of platinum compounds have been prepared and screened as potential antitumour drugs.[17] Among the developed platinum based

candidates are five new drugs that is, oxaliplatin, carboplatin, nedaplatin, lobaplatin and heptaplatin[18,19] being used globally or regionally in chemotherapy as shown in Figure 1.2.

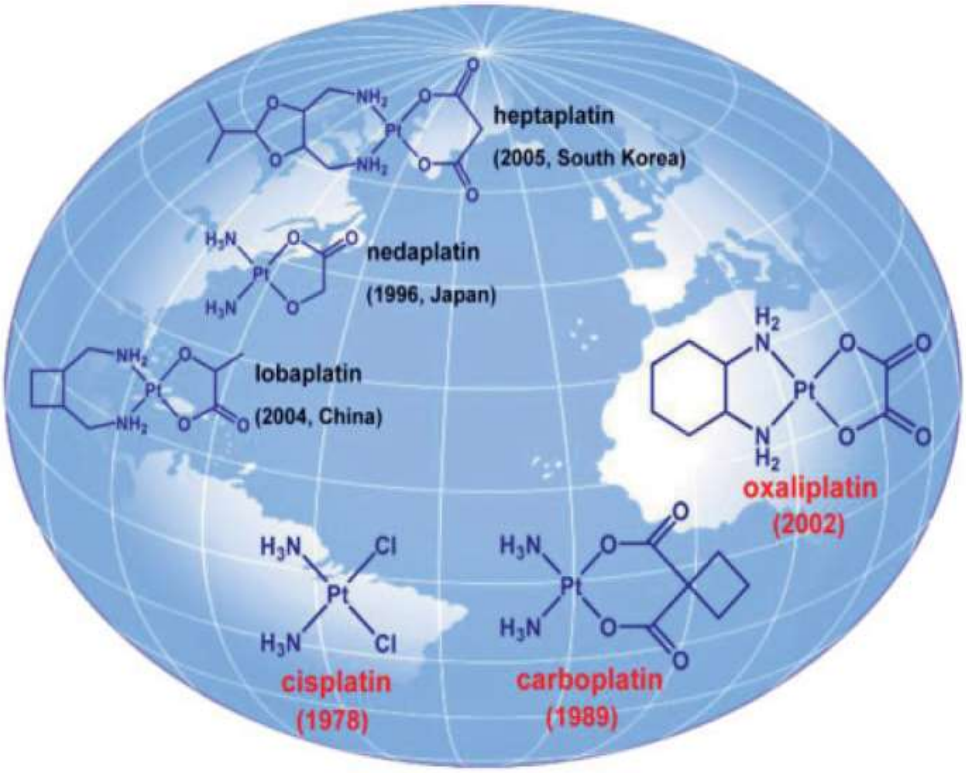

Figure 1.2: Platinum-based antitumour drugs used globally and regionally in chemotherapy.[20,21]

The clinical success of cisplatin has been the main impetus for the evolution and development of the platinum compounds, which currently holds a vital role in metal-based cancer chemotherapy. However, the efficacy and applicability of these platinum based drugs are heavily restricted by their severe systemic toxicities and resistance.[15-17] Although the leading anti-cancer drug cisplatin has been used for over three decades, it is associated with severe side effects ranging from poor specificity[22] to systemic toxicities like nephrotoxicity, neurotoxicity, ototoxicity and emetogenesis which inflict serious disorders or injuries on the patient during treatment.[23-25] In addition, the efficacy of cisplatin is often limited by the intrinsic and acquired resistance possessed by various cancers.[26]

These disadvantages of cisplatin have created a sustained momentum for the improvement of platinum-based anticancer drugs.[27] From the clinical point of view, the current challenge in drug development is to use multinuclear Pt-based chemotherapeutics to treat cisplatin resistant cell lines. This is due to multinuclear metal complexes having a novel mechanism of action. Recent advances in this area have demonstrated a bright prospect in the utilization of di- and multinuclear platinum complexes that have shown great potential for cancer chemotherapy.[28] These complexes contain two or three platinum centres which can each covalently bind to DNA. This enables these complexes to be able to form different range of DNA adducts compared to cisplatin and its analogues.[29] Whereas cisplatin and its analogues predominantly forms 1,2-GG (47-50 %) and 1,2-AG (23-28 %) intrastrand cross-links with DNA,[30] multinuclear platinum complexes are reported to form a variety of intra- and interstrand links between bases two to six nucleotides apart.[31] The binding of $(NH_3)_2Pt^{2+}$ to DNA leads to changes in the DNA structure. NMR studies have shown Pt^{2+} to bind to N7 atoms of a pair of guanine (G) bases on the adjacent strands of DNA. Although the primary target of cisplatin in genomic DNA where it undergoes hydrolysis inside the cell to produce more reactive aquated species. This hydrolysis step is reported to be key step in the activation of the molecule for its binding with cellular targets.[32] Within the cell, the chloride ligands may be substituted by aqua ligands in stepwise to form *cis*-$[PtCl(H_2O)(NH_3)_2]^+$ and *cis*-$[Pt(H_2O)_2(NH_3)_2]^{2+}$ cations. Scheme 1.2 gives a schematic representation of hydrolysis of cisplatin in aqueous solution at physiological pH.[33,34]

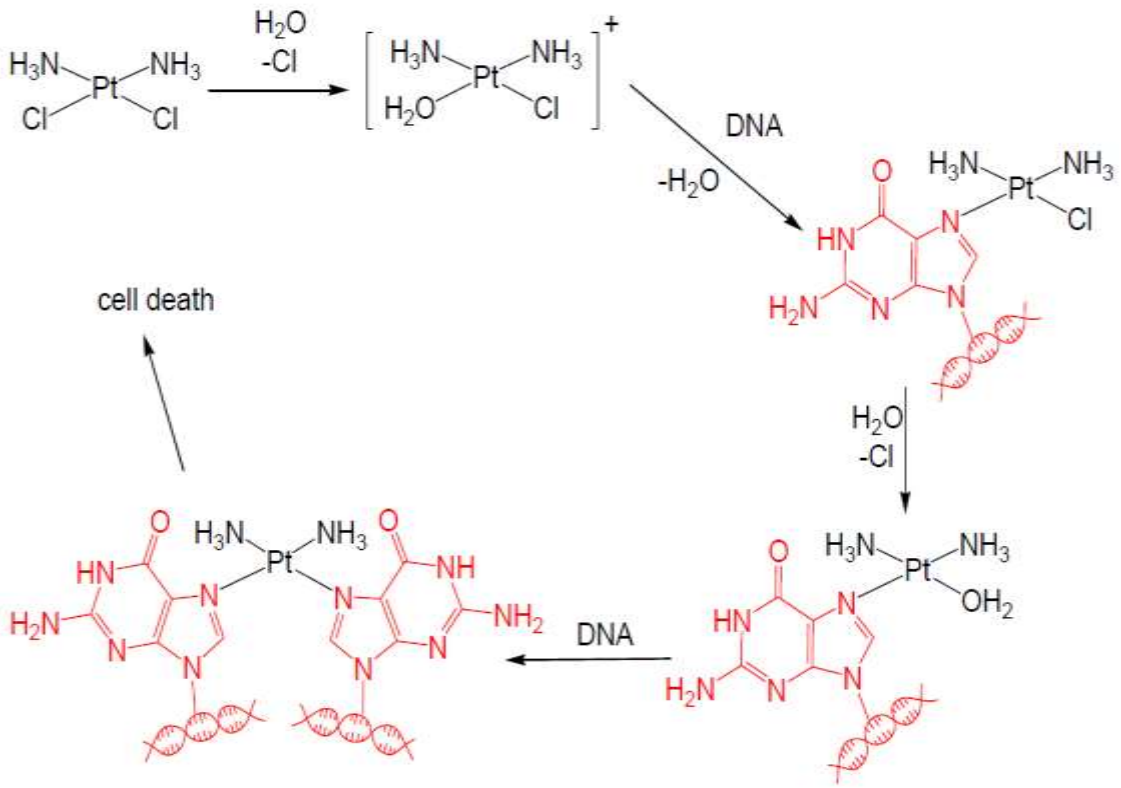

Scheme 1.1 Proposed mechanism of how cisplatin binds to DNA with the body cells.[31]

If aquation occurs in the bloodstream before diffusion, the aqua species is likely to react with non-target cancerous cells leading to toxicity of the drug.[35] This is controlled by high concentration of approximately 104 mM chloride ion forcing the hydrolysis equilibrium to chloride species.[14,15] Once in the bloodstream, there is passive and active diffusion across the cell membrane into the cytoplasm where chloride ion concentration is low, in the range of 4-20 mM favouring aquation process.[36,37] During this process, Pt(II) centre is exposed to a variety of bio-molecules, including sulphur donors like thiols and thioethers which have a high affinity for platinum metal. Although platinum binding to sulphur is kinetically favoured, it binds to more thermodynamically stable nitrogen nucleobases.[38,39] There is a possibility that binding to sulphur donor sites is a temporary reservoir for platinum with subsequent transfer to the N7 sites of purines that initiates cell deaths. The binding of Pt(II) to proximal guanine residues through N7 coordination is proposed to be responsible for the antitumour activity of cisplatin.[31,33,34] The formation of bifunctional adducts for intrastrand cross-linking with DNA is shown in Figure 1.3.

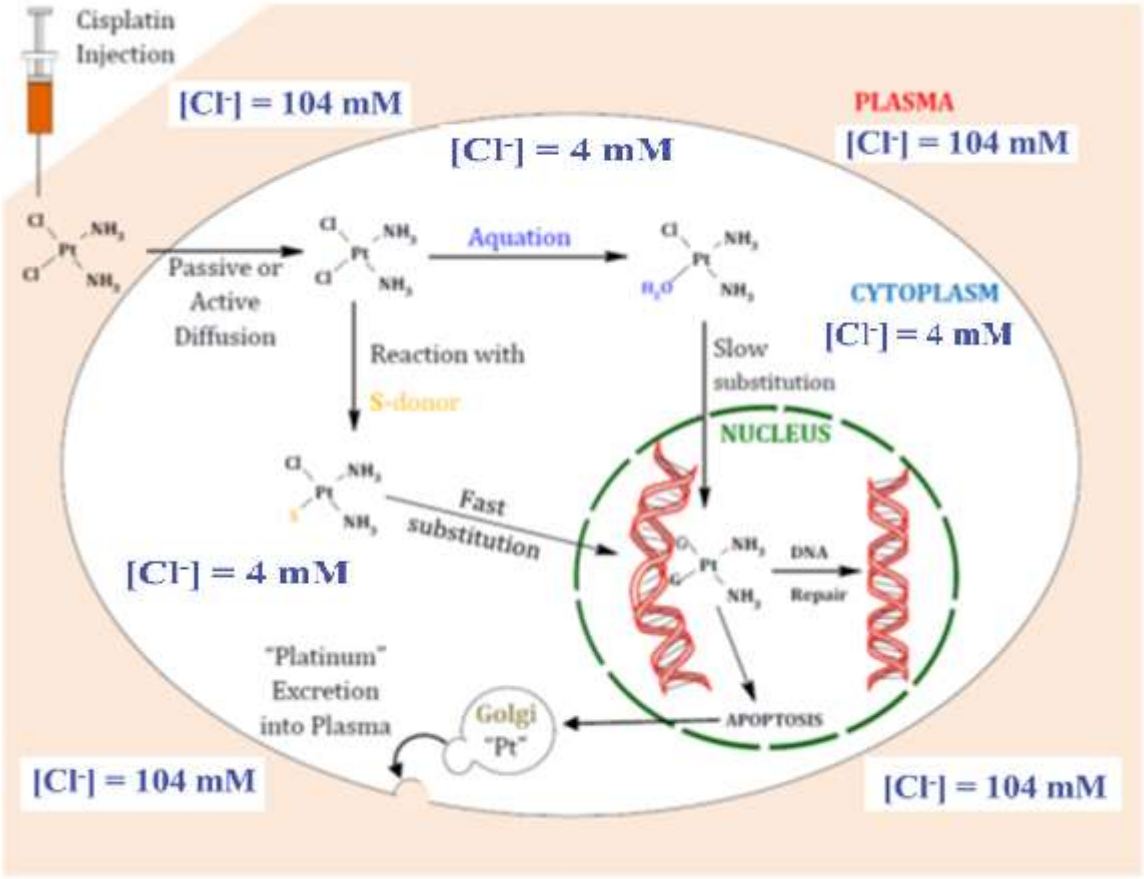

Figure 1.3: DNA interstrands and intrastrands adducts with cisplatin *in vivo*[40,41]

The reason for increasing interest in multinuclear complexes is their ability to form DNA adducts that differ significantly from those of cisplatin and related complexes. Since these complexes are capable of forming a different range of DNA adducts, it is of interest to develop complexes that selectively target non-guanine residues. The focus should be to produce multinuclear platinum complexes that preferentially targets adenine residues in DNA rather than guanine. The specific type of interstrand crosslink formed and the preference for adenine binding may account for the difference in activity between these multinuclear and mononuclear platinum complexes. Another feature is their ability to form long-range adducts with DNA compared to cisplatin and its analogues.[13-16] The clinical development of the di- and multinuclear platinum complexes depend on the understanding of their mechanism of action. Indeed, mechanistic studies of some of the complexes have demonstrated that they produce a high percentage of interstrand adducts.[42]

1.3 Multinuclear platinum complexes

Mononuclear platinum complexes are well established drugs in modern anticancer chemotherapy. However, current approaches to obtain more potent compounds are based on linking two or more platinum centres via bridging ligands to form multinuclear complexes which have shown novel modes of action. Following the advantages of these multinuclear platinum complexes, their investigation remains a new and exciting area in the treatment of human cancers. There is a considerable interest in the antiproliferative properties of multiplatinum species including di- and triplatinum complexes containing dipyridylamine (dpa) binding motif. The properties of the linker such as the length, rigidity, flexibility and charge are the major factors that seem to facilitate their antitumour activities.[43] New complexes undergoing clinical trials like BBR3464, BBR3571, BBR3610 and BBR3611 may be the key to overcoming both the intrinsic and acquired resistance to conventional platinum treatment.[15,16,29, 42,43] As mentioned earlier, their success is based on their ability to form DNA adducts that are structurally different from cisplatin and its analogues. They form two types of DNA interstrand cross-links with bifunctional Pt(II) complexes; the intramolecular and interduplex interstrands. In intramolecular interstrand cross-links, the Pt complex coordinates the bases in one DNA molecule, while in interduplex interstrand it coordinates the bases in two different DNA duplexes.[44] This unique cross-linking capability of multinuclear Pt(II) complexes represents a new and vital aspect in DNA-binding mode and seems to be significant in the working mechanism of these distinct classes of antitumour metallodrugs. With the objective of developing compounds with new modes of action in comparison to the established anticancer agents for treatment of a broader range of tumours with reduced side effects, many metal complexes have been investigated.[45] Despite the successful use of cisplatin for over 40 years, the attempt to design new derivatives with improved biological properties has also lasted as long. Many platinum analogues both mononuclear and multinuclear analogs have been synthesized and screened for anticancer activity in attempt to overcome the limitations of cisplatin.

Thousands of platinum-based drugs have been tested for pre-clinical antitumour activity, but very few have entered clinical trials in the past 30 years. At present several new Pt-based complexes are reported to be in clinical trials or in clinical use giving hope that they may

fulfill the needs for novel antitumour drugs. Some of the multinuclear antitumour Pt(II) complexes that have shown to overcome Pt-drug resistances are shown in Figure 1.4.

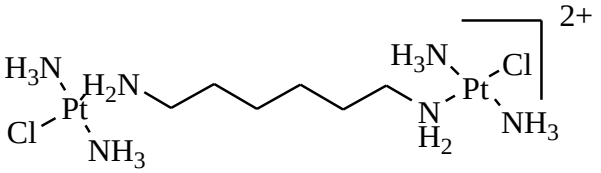

BBR3005

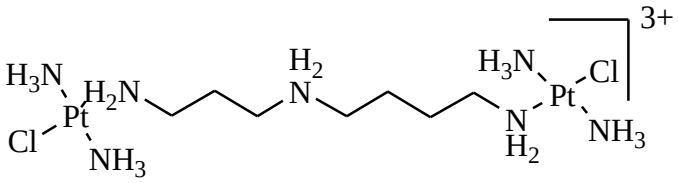

BBR3571

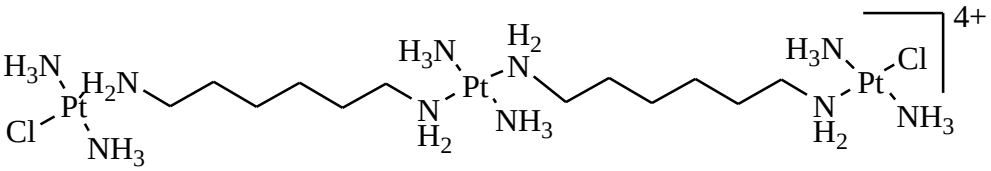

BBR3464

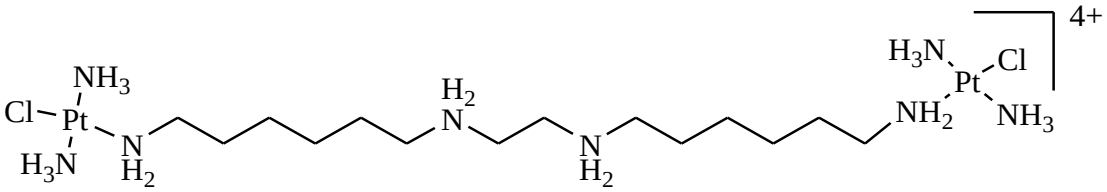

BBR3610

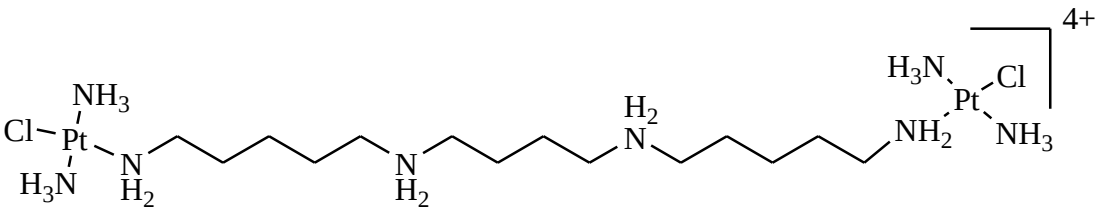

BBR3611

Figure 1.4: The multinuclear agents that have been tested in cisplatin resistant cell-lines

It is reported that these multinuclear platinum complexes with long and flexible α,ω-diamino-alkane linkers can overcome both acquired and intrinsic resistance to anti-tumour activity by forming long-range interstrand and intrastrand, flexible and non-directional adducts with DNA.[46] However, very short and rigid linked multinuclear complexes have also shown promising antitumour activity. However, platinum-platinum distance and flexibility are reported to be the major factors of reduced activity in 4,4'-dipyrazolylmethane (dpzm) ligand. It has been observed that using ligand bridges of the same lengths in Figure 1.5 as those of the BBR complexes show a decrease in activity due to rigidity.[47]

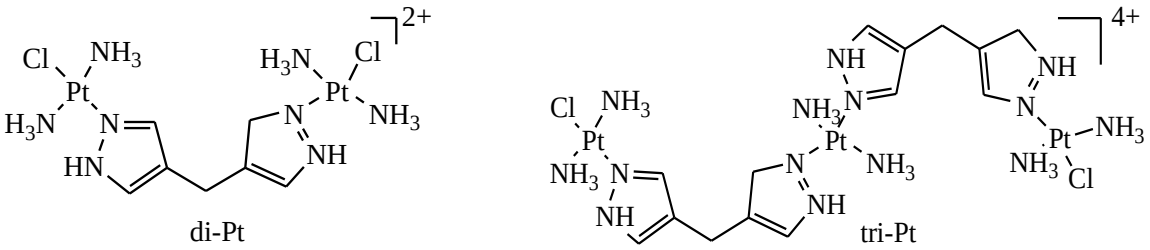

Figure 1.5: *Trans*-$[\{PtCl(NH_3)_2\}_2\mu\text{-dpzm}]^{2+}$ (di-Pt) and the corresponding trinuclear complex *trans*-$[trans\text{-}\{PtCl(NH_3)_2\}_2\text{-}trans\{Pt(dpzm)_2(NH_3)_2\}]^{4+}$ (tri-Pt) linked by the semi rigid 4,4'- dipyrazolylmethane (dpzm) ligand.

These complexes form high levels of DNA interstrand crosslinks (50 %) proposed to be due to the rigid nature of the dpzm ligand that prevents the complexes from forming short-range intrastrand adducts. Despite these complexes showing cytotoxicity, they are not as active as the aliphatic dinuclear and the BBR3464.[46,47] The bifunctional dinuclear complex was reported to bind preferentially at adenine residues;[48] probably because of its pre-association in the minor groove at adenine/thymine (A/T) rich regions.[49] Pre-association in the minor groove at guanine/cytosine (G/C) rich regions has been found to occur at a lower rate.[50] Adenine and guanine are examples of a purine which contains a six and a five atom ring sharing two atoms, while cytosine and thymine are examples of pyrimidine composed of a single six atom ring see Figure 1.6.

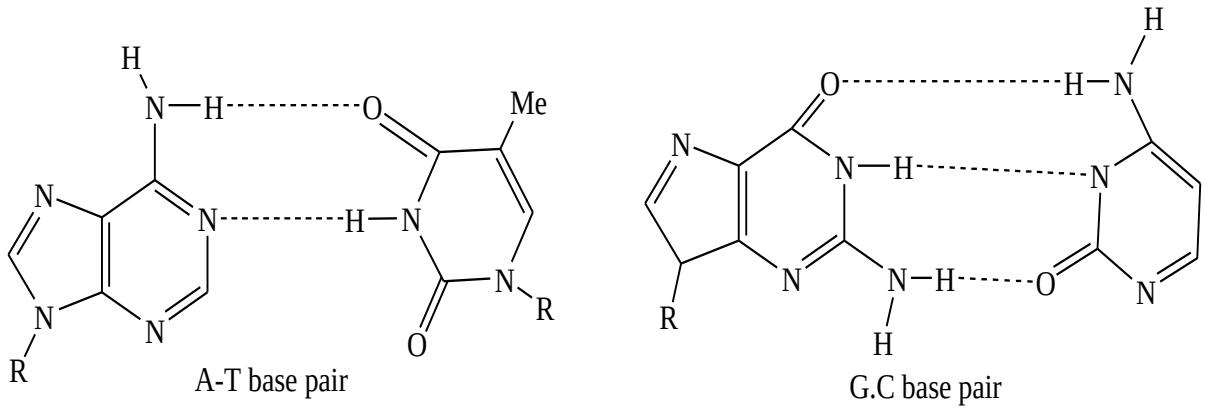

Figure 1.6: The structure of purine and pyrimidine being the two building blocks of nucleic acid. The inter-base hydrogen bonds shown in the dimers strongly stabilize the structure as indicated in the base pairs.[51]

Figure 1.7 shows a DNA strand with minor and major grooves with a base pairs A/T or G/C. Each base pair consists of a purine and a pyrimidine which are complementary and allows them to bond together with hydrogen bonds. The A/T pair forms two hydrogen bonds while G/C forms three. This hydrogen bonding between complementary bases holds the two DNA strands together. This may be the possible reason why charged complexes consisting of di- and trinuclear platinum complexes linked by aliphatic ligands with much hydrogen bonding functionality are able to overcome cisplatin and carboplatin resistance in many important human cancer cell lines.[13,14] These complexes are able to induce conformational changes in DNA, particularly the conversion from B-type to Z- and A-type.[14,15]

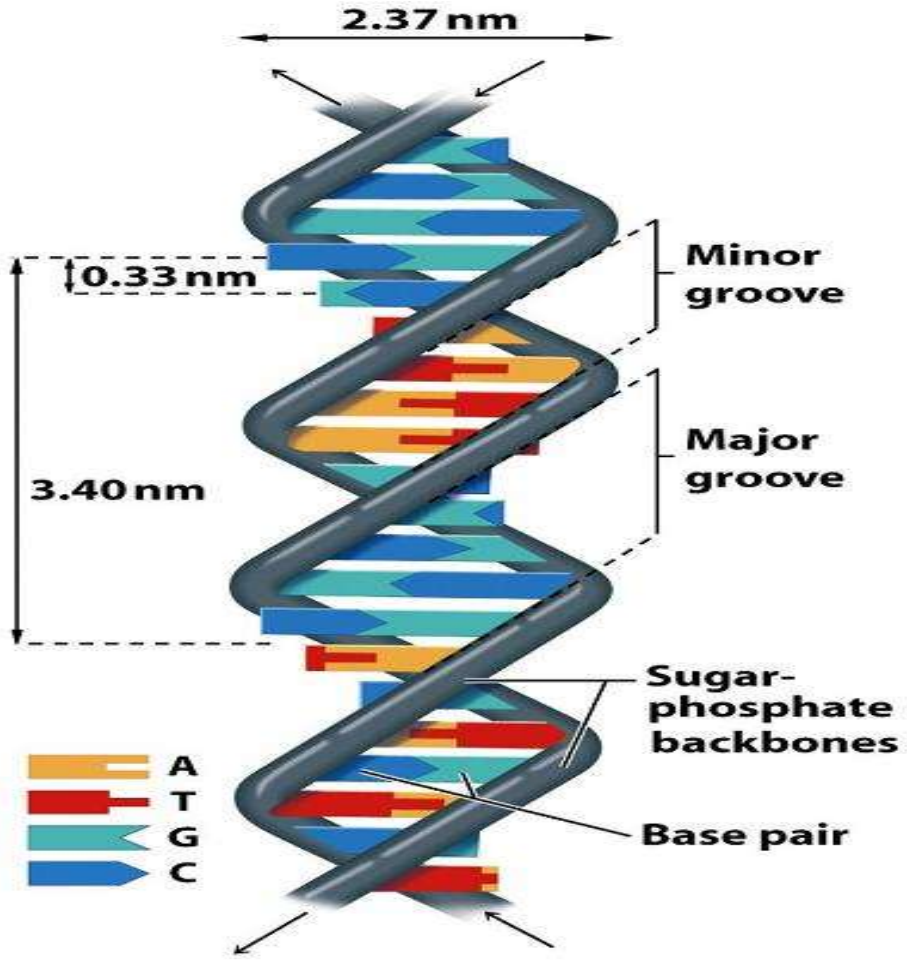

Figure 1.7: Schematic illustration of the double-helix structure of DNA with sugar phosphate backbone. *Inset* is the base pairs A/T and G/C in the major and minor grooves.[52]

The novel dinuclear platinum antitumour drugs just like cisplatin are activated before binding to DNA. As mentioned earlier, this occurs by intracellular activation through aquation to form monoaqua or diaqua species facilitated by lower chloride concentrations below 100 mM inside cells. The platinum anticancer compounds form adducts between neighbouring guanine residues on DNA molecule. The platinum binding is on the N7 position of the imidazole ring of the purine nucleobase of DNA involving guanine and to lesser extend adenine.[53] Monofunctional adducts behave similar to the major adducts of cisplatin while bifunctional cross-links behave distinctly different. As such, dinuclear bifunctional Pt(II) complexes may contribute substantially to the overall drug cytotoxicity due to the synergistic effects of adducts. Figure 1.8 shows intrastrand crosslinks of 1,2-d(G/G) and 1,2-d(G/A) with

the 1,2-d(G/G) motif the dominant feature.[13,54,55] Also minor lesions, 1,2-intrastrand cross-links are formed between adenine and guanine in a d(A/G) adducts as well as a 1,3-intrastrand cross links where two platinated guanines are separated by one base pair-d(GNG).[13,56] This structural information is vital to providing a better understanding of how Pt-based drugs produce their anticancer activity. It is anticipated that using multinuclear bifunctional Pt(II) complexes will efficiently mediate DNA repair pathways in the cell and facilitate design of novel platinum-based drugs with desirable chemotherapeutic properties that surpass the clinical efficacy of cisplatin.

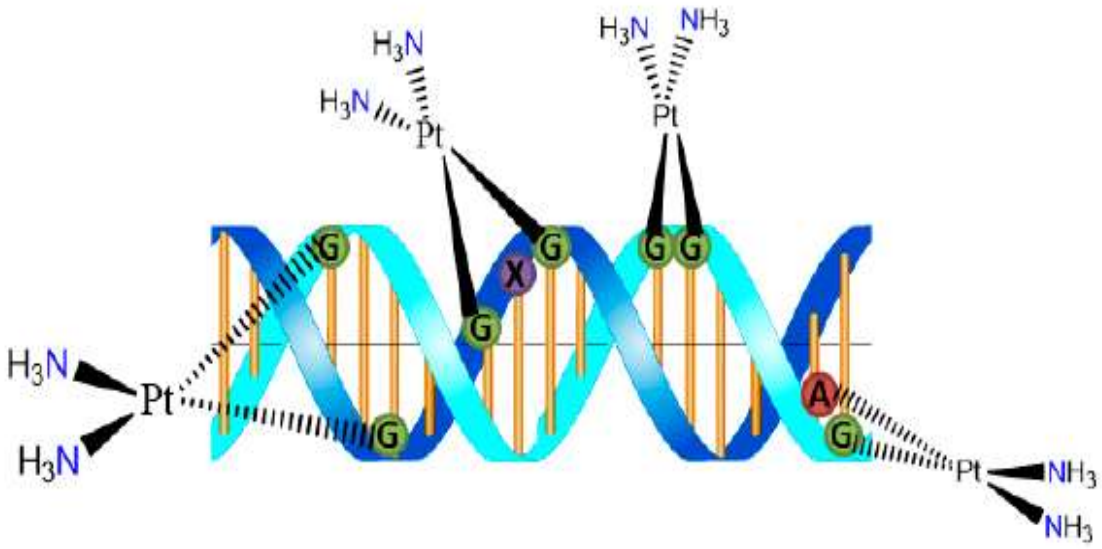

Figure 1.8: Schematic illustrations of DNA adduct formation with cisplatin moiety[57]

Some of the di- and trinuclear Pt(II) complexes investigated in this study have been screened before in literature and showed potential anti-proliferative and cytotoxic activity in different human cancer cell lines. Despite the immense advantages of these multinuclear complexes in overcoming acquired cisplatin resistance, relatively little is known about their mechanism of action and their thermodynamic and kinetic properties. In order to shed some light on the mechanistic implication of these complexes in biological systems, a detailed kinetic study was carried out. The principles of chemical kinetics remain significant in predicting the time span for which these agents maintain their therapeutic effectiveness or efficacy at specified conditions in the body. A deep understanding of the mechanisms of multinuclear Pt(II) anticancer agents will build the basis for the rational design of novel therapeutic and diagnostic agents with improved potency. Such non-classical platinum(II) complexes are

meant to provide a broader clinical spectrum and overcome toxic side effects and acquired drug resistance of cisplatin. Dinuclear Pt(II) complexes are expected to lead to development of new drug derivatives with maximum synergistic effects.

1.4 Aims and Scope of the Study

The present study is a progression of the work on tumour active compounds by Jaganyi with the group[58] and other groups[59] on mechanistic and kinetics of ligand substitution reactions. Their Mechanistic studies on d^8 transition metals especially platinum; ruthenium and palladium compounds have opened new avenues of research that has led to design of completely new anticancer drugs. However, much of the work reported so far has been concerned with reactions in which unidentate ligands are substituted by unidentate nucleophiles. There is less information on the kinetics and mechanistic insight on multinuclear substitution reactions of square-planar complexes. Studies by Jaganyi,[58] van Eldik,[60] and other groups have concentrated on the substitution kinetics of monodentate *trans*-Pt(II) complexes. The kinetics of bidentate ligand exchange reactions of *cis*-configuration have not been fully studied in the same details and magnitude as monodentate ligands. The dinuclear systems with cisplatin configuration merits further studies as potential anti-therapeutic agents due to their resemblance to cisplatin.

The main objective of this study is to synthesize new non-classical derivatives of di- and tri-bifunctional Pt(II) complexes with *cis*-configuration that mimic cisplatin and explore their kinetics and mechanistic investigations. Dinuclear and trinuclear platinum(II) complexes based on the *cis*-[PtX_2(N-N)] geometry, where X_2 are two labile ligands have not been fully explored. These type of complexes are likely to produce similar array of adducts that target DNA like those of cisplatin and may induce similar or even improved selectivity, specificity and potency towards malignant cells. This concept of multinuclearity for improving the chemotherapeutic activity has been proven in multinuclear platinum complexes such as BBR3464 remains the effective approach in the development of anti-cancer therapeutics. This study was also motivated by multinuclear platinum compounds such as BBR3464 having the ability to circumvent the cellular resistance with improved specificity for tumour tissue hence reduced side effects to conventional cisplatin and its analogues.

Since the role of the bridging ligand in controlling the kinetic properties of dinuclear complexes has been a topic of much interest, various designs of organic ligands acting as bridges between the metal ions were utilized. Changes in the ligand system have an influence either on the basicity of the donor or on energies of the unoccupied orbitals and therefore have an impact on the excited state of the complex. The structural and electronic features of the bridges are key factors in the energy or charge-transfer and their influence on the reactivity of these multinuclear Pt(II) complexes are discussed in the respective chapters.

In summary, it is worth mentioning that the subtlety with which the ligands control reactivity of transition metals there are also reciprocal effects from metal ions on the properties of ligands. The intrinsic nature of the metal ion largely determines the reactivity of the metal complex. The lability of the metal complex dictates its reactivity which determines its relevance for use as therapeutic agent. Labile complexes will react fast and indiscriminately thus preventing the drug from reaching the tumour site. Inert complexes will not react significantly to elicit a response. Therefore both the metal and the ligands play vital roles in the recognition of the target molecules. Thus this work focuses on establishing the mechanisms of multinuclear Pt(II) complexes with two binding sites separated by a bridging ligand of variable length and architecture that will react with DNA more rapidly than cisplatin and produce characteristic long-range inter- and intrastrand cross-linked DNA adducts. Figure 1.9 shows the type of Pt(II) complexes investigated consisting of two cisplatin centres linked through tuning the ligand framework of different diamines as linkers. The reactivity of the designed complexes was tuned to depend on the relative position of the binding sites and the variation in the framework structure of the overall ligand. For the first time, the present work gives information on substitution mechanisms of Pt(II) complexes with bidentate ligands as leaving groups in *cis* coordination sphere.

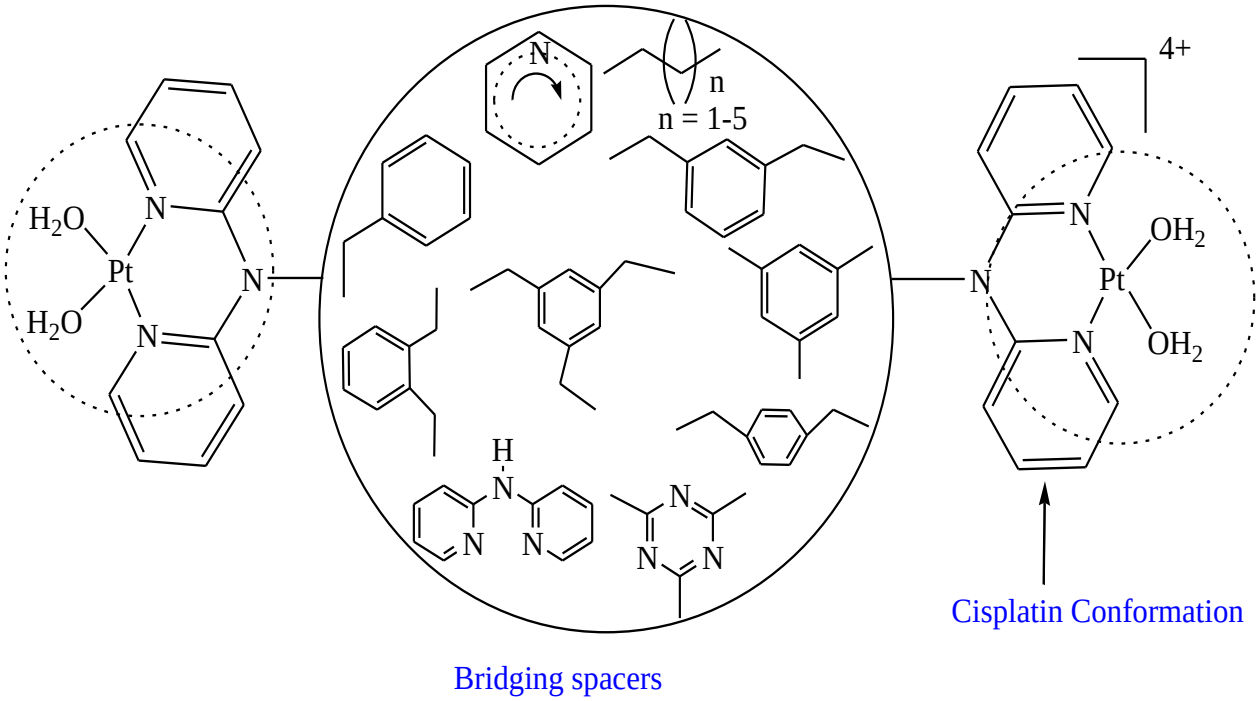

Figure 1.9: Multinuclear cationic platinum(II) complexes in which different bridging motifs were used to tune the kinetics of various complexes in this study.

These novel multinuclear Pt(II) anticancer agents are anticipated to have superior efficacy, increased selectivity for tumour tissue, reduced toxicity, wider spectrum of activity and lack of tumour cell resistance compared to cisplatin. Despite synthetic advances in multinuclear platinum complexes, unified pharmacokinetics of different functional compounds is required. The rationale for designing these new platinum antitumour drugs is to come up with a better understanding of their kinetics and mechanistic substitution reactions. Therefore detailed substitution kinetics along with mechanism of action of these multinuclear platinum complexes represents an excellent starting point in designing new antitumour metallodrugs. In this thesis, kinetics and computational studies of multinuclear Pt(II) complexes were carried out in order to extend our understanding on their mechanistic substitution behaviour with thiourea nucleophiles. To discuss these principles of kinetic stability and structural influence on the reactivity of the investigated metal complexes, density functional theory (DFT) was of great utility. The plethora of successful applications of DFT in coordination chemistry provided a general tool in understanding and predicting the behaviour and chemical reactivity of the complexes. All calculations were performed using the Gaussian 09 suite program.[61] Full geometry optimization was performed in gas phase at *ab-initio*

molecular orbital calculations using the B3LYP/LANL2DZ level of theory to model the structural and electronic properties of the complexes molecular structures. DFT was considered very useful in investigating molecular properties which are difficult to measure experimentally. By comparison of the computational calculations with experimental results, the study demonstrates the value of computational analysis in the understanding of the mechanistic of these reaction processes.

1.4.1 General and specific objectives of this study

As mentioned earlier, numerous publications have documented the synthesis of multinuclear Pt(II) complexes but little has been reported on the kinetics of nucleophile substitution reactions and mechanisms of this anticancer therapeutics. The claims in literature on the behaviour of multinuclear Pt(II) complexes and their novelty mechanisms in their reactivity have provided the impetus to this project. The main aim of this investigation on multinuclear Pt(II) complexes is to obtain drugs of similar anticancer activity but with reduced toxicity and wider spectrum of activity compared to cisplatin. In order to have an explanation on how these multinuclear anticancer drugs behave under biological conditions, a detailed mechanistic insight into their nucleophilic substitution remains vital. This study relies on the core concept of ligand substitution reactions to shed light on the mechanistic insight of bidentate cisplatin drugs from kinetic approach. This study outlines how the bridging ligands connected to platinum(II) centres influence the reactivity of the complexes towards the entering nucleophiles. The bridging spacers are reported to play a significant role in regulating the reactivity of dinuclear Pt(II) complexes by controlling the geometry, the distance between Pt^{2+} ions, steric and electronic features of the metal centre.[58-60] There is need to explore the features that could untangle the differences in antitumour selectivity of multinuclear Pt(II) complexes. The biological activity of multinuclear platinum (II) complexes in this work were modulated by the geometry and number of leaving groups in the coordination sphere of Pt(II) atoms as well as by the nature of the connecting bridging spacers. The main focus is to untangle the question of mechanistic and bioavailability of Pt(II) based drugs in biological systems. This has been underpinned by an in-depth understanding of the factors controlling the bio-reactivity of the Pt(II) based-drugs. As such, the present study addresses plausible reaction mechanisms and rate laws of polynuclear bifunctional Pt(II) complexes that represent a new class of anticancer agents.

This work designed new multinuclear platinum(II) complexes grafted in chapters 3-6 and investigated their rates of substitution with biological nucleophiles. The reactivity of the investigated complexes was tuned by grafting of the bridging spacers shown in Figure 1.9. This thesis reports the substitution reactions of 2,2'-dipyridylamine-chelated mono, di- and trinuclear Pt(II) complexes linked by rigid and flexible bridges. This thesis describes the comparative effect of ligands on thermodynamics and kinetic behaviour of Pt(II) complexes as reported here in.

Thus, the specific objectives of this study are:

(i) To investigate the role of alkyl-phenyl spacer on the reactivity of novel platinum(II) complexes with thiourea nucleophiles.

(ii) To determine the effect of alkyl chain tether on the kinetics and mechanistic behaviour of bifunctional dinuclear platinum(II) complexes bearing *N,N'*-dipyridylamine ligands.

(iii) To understand the role of rigid versus flexible bridging spacers in controlling the reactivity and mechanistic substitution reactions of polynuclear platinum(II) complexes by experimental and computational analysis.

(iv) To understand the influence of chemically tunable annular nitrogen atom in a pyridine ring as a spacer on the reactivity of dinuclear Pt(II) complexes through a kinetic and mechanistic investigation.

In general, it is anticipated that kinetics and mechanistic studies on cancer based drugs will assist in understanding and improving on the current clinical therapeutics. The results could contribute to a better understanding of biochemical mechanism of the investigated Pt(II) complexes. Moreover, substitution reactions of these complexes with biologically relevant nucleophiles could lead to more information on possible interaction modes of cisplatin like Pt(II) complexes with their intended targets. To achieve the outlined objectives, this study investigated the kinetic and mechanistic interactions of *cis*-$[Pt(OH_2)_2]^{2+}$ complexes with biomolecules with the aim of developing a new family of metallo-pharmaceuticals. Detailed knowledge on mechanistic interactions between polynuclear bifunctional Pt(II) complexes with biologically relevant biomolecules is fundamental for design and discovery of new anti-cancer agents. This study correlated kinetic, thermodynamic and structural properties of Pt(II) complexes with their interaction with biological nucleophiles. This study is essential for

mechanistic interpretation of Pt(II) substitution reactions and design a new generation of antitumour therapeutics. The determination of mechanistic substitution was based on the analysis of kinetic and thermodynamic parameters to characterize the reactions. The first mechanistic information was observed from the rate constants measured as a function of concentration of the entering nucleophile. The activation parameters were used to deduce the plausible reaction mechanism.

For a way forward, this study presents a comprehensive mechanistic overview of transformations promoted by Pt(II) with different ligand backbone in nucleophilic medium. The present work provides an account of the reaction mechanism and reactivity rates resulting from coordination to the σ-donor/π-acceptor ligands at the metal centre that triggers the intra- or intermolecular attack of nucleophiles to varying degrees. The computational calculations are consistent with the experimental observations providing fundamental insights into the versatility of the reaction processes. The polynuclear Pt(II) complexes herein represent a completely new paradigm for platinum-based anticancer metallodrugs that may offer great potential as new anticancer agents. It's with the view that understanding the mechanistic action of these complexes may serve as baseline and essential stepping stone for further development of new anticancer therapeutics. Hence the study remains essential as a stepping stone towards the design of new anticancer drug candidates. The kinetic data presented in this study gives useful insights into the factors controlling the reactivity of Pt(II) complexes. It also enhances a deepened understanding of the Pt(II) biomolecular chemistry. Thus, a mechanistic understanding of how metal complexes achieve their biological activities is vital to their clinical success as well as to the rational design of novel compounds with improved potency.

Elucidating the reactivity of platinum complexes and multinuclear level will greatly increase our understanding of the mechanism of action of these metal complexes as drugs. Furthermore, this under investigated area of platinum chemistry could be useful to obtaining a complete picture of multilevel mechanism of action and accurate assessment of multinuclear platinum chemistry as anticancer agents. In a nutshell, cancer is a deadly disease killing millions of people annually as revealed in the introductory part of this chapter; there is need to take bold challenges for the development of novel metal based drugs able to cure

cancer even in late stages. Exploring new structural classes of platinum antitumour drugs structurally different from cisplatin is likely to lead to improved anticancer agents. Structural studies and elucidation of the role of the bridging ligands could explain the Pt-based anticancer drugs DNA binding and repair mechanism and may assist predict the differences of antitumour selectivity for a large number of Pt complexes carried out in this study.

References

1. G. A. Colditz, T. A. Sellers and E. Trapido, *Nat. Rev. Cancer*., 2006, **6**, 75–83.
2. A. Umar, B. K. Dunn and P. Greenwald, *Nat. Rev. Cancer.*, 2012, **12**, 835–848.
3. M. S. Kim, *Biomol. Ther*., 2011, **19**, 371–389.
4. J. Ferlay, I. Soerjomataran, M. Ervik, R. Dikshit, S. Eser, C. Mathers, M. Rebelo, D. M. Parkin, D. Forman and F. Bray, GLOBOCAN 2012, Cancer Incidence and mortality worldwide: IARC Cancer Base No. 11 [Internet]. Lyon, France: International Agency for Research on Cancer. 2013, Available from: http://globocan.iarc.fr, accessed on 10/03/2015.
5. D. Saranath and A. Khanna, *Biomed Res J*., 2014, **1**, 1-5.
6. F. Bray, J. S. Ren, E. Masuyer, J. Ferlay, *Int. J. cancer,* 2013, **132**, 1133-1145.
7. International Agency for Research on Cancer, WHO 2018, Press release.
8. Beaulieu N, Bloom D. E, Bloom L. R, Stein R. M, Breakaway: The global burden of cancer-challenges and opportunities. London, UK: The economic Intelligence Unit; 2009, Available at: https://assets-livestrong-org.s3.amazonaws.com/media/site_proxy/data/c49ced3068f7205319cbledf653dd91e0baee3ba.pdf.
9. D. E. Bloom, E. T. Cafiero, E. Jané-Llopis, S. Abrahams-Gessel, L. R. Bloom, S. Fathima, *et al*. The global economic burden of non-communicable diseases. Geneva, Switzerland: World Economic Forum; 2011.
10. J. Reedijk, *Pure Appl. Chem*., 2011, **83**, 1709-1719.
11. J. Reedijk, *Eur J. Inorg. Chem*., 2009, 1303-1313.
12. S. Rafique, M. Idrees, A. Nasim, H. Akbar and A. Athar, *Biotechnol. Mol. Biol. Rev*., 2010, **5**, 38-45.
13. N. J. Wheate and J. G. Collins, *Curr Med Chem Anticancer Agents*, 2005, **5**, 267-279.
14. B. Lippert, *Cisplatin. Chemistry and Biochemistry of a Leading Anti-cancer Drug*, 1999, Wiley- VCH, Weinheim.
15. N. Farrell, *Transition Metal Complexes as Drug and Chemotherapeutic Agents*, 1989, Kluwer Academic Publishers, Dorderecht.
16. V. Brabec and J. Kasparkova, *Drug Resist. Updat*., 2005, **8**, 131-146.
17. C. X. Zhang and S. J. Lippard, *Curr. Opin. Chem. Biol*., 2003, **7**, 481-489.
18. W. Xiaoyong and G. Zijian, *Chem. Soc. Rev*., 2013, **42**, 202-224.
19. W. Xiaoyong and G. Zijian, *Dalton Trans*., 2008, 1521-1532.

20. M. A. Fuertes, C. Alonso and J. M. Pérez, *Chem. Rev*., 2003, **103**, 645-662; (b) J. J. Wilson and S. J. Lippard, *Chem. Rev*., 2014, **114**, 4470-4495.
21. Á. M. Montańa and C. Batalla, *Curr. Med. Chem*., 2009, **16**, 2235-2260.
22. C. A. Rabik and M. E. Dolan, *Cancer Treat. Rev*., 2007, **33**, 9-23.
23. A. A. Argyriou, P. Polychronopoulos, G. Iconomou, E. Chroni and H. P. Kalofonos, *Cancer Treat. Rev*., 2008, **34**, 368-377.
24. S. R. McWhinney, R. M. Goldenberg and H. L. McLeod, *Mol. Cancer Ther*. 2009, **8**, 10-16.
25. X. Yao, K. Panichpisal, N. Kurtzman and K. Nugent, *Am. J. med. Sci*., 2007, **334**, 115-124.
26. P. Heffeter, U. Jungwirth, M. Jakupec, C. Hartinger, M. Galanski, L. Elbling, M. Micksche, B. Keppler and W. Berger, *Drug Resist. Updates*, 2008, **11**, 1-16.
27. K. S. Lovejoy and S. J. Lippard, *Dalton Trans*., 2009, 10651-10659.
28. N. J. Wheate and J. G. Collins, *Coord. Chem. Rev*., 2003, **241**, 133-145.
29. N. Farrell and L. R. Kelland, (Eds.) Platinum-Based Drugs in Cancer Therapy, Humana Press, Totowa, 2000, 321-338.
30. E. Wong and C. M. Giandomenico, *Chem. Rev*., 1999, **99**, 2451.
31. M. H. Baik, R. A. Friesner and S. J. Lippard, *J. Am. Chem. Soc*., 2003, **125**, 14082.
32. S. E. Miller and D. A. House, *Inorg. Chim Acta*., 1991, **187**, 125-132.
33. R. N. Bose, *Mini Rev Med. Chem*., 2002, **2**, 103-111.
34. P. Pil and S. J. Lippard, Cisplatin and related drugs. Encyclopedia of cancer., 1996, Bertino, J. R., San Diego, CA, USA, Academic Press, 392-410.
35. F. Arnesano and G. Natile, *Coord. Chem. Rev*., 2009, **253**, 2070-2081.
36. E. R. Jamieson and S. J. Lippard, *Chem Rev*., 1999, **99**, 2467-2498.
37. I. Judson and L. R. Kelland, *Drugs*, 2000, **59**, 29-38.
38. M. A. Fuertesa, J. Castillab, C. Alonsoa and J. M. Pérez, *Curr. Med. Chem*., 2003, **10**, 257-266.
39. B. Mu-Hyun, R. A. Friesner and S. J. Lippard, *J. Am. Chem. Soc*., 2003, **125** (46) 14082-14092
40. M. A. Jakupec, M. Galanski and B. K. Keppler, *Rev Phys Biochem Pharm.*, 2003, **146**, 1-53, ISSN: 0303-4240.
41. V. M. Gonzalez, M. A. Fuertes, C. Alonso and J. M. Perez, *Mol Pharmacol*., 2001, **59**, 657.

42. N. Farrell, Y. Qu, L. Feng and B. van Houten, *Biochemistry*, 1990, **29**, 9522.
43. J. Kašpárková, J. Zehnulova, N. Farrell and V. Brabec, *J. Biol. Chem*., 2001, **276**, 22191; (b) M. B. Kloster, J. C. Hannis, D. C. Muddiman and N. Farrell, *Biochemistry*, 1999, **38**, 14731.
44. T. Muchova, S. M. Quintal, N. Farrell, V. Brabec and J. Kašpárková, *J. Biol Inorg. Chem*., 2012, **17**, 239-245.
45. M. Galanski, M. A. Jakupec and B. K. Keppler, *Curr. Med. Chem*., 2005, **12**, 2075-2094.
46. N. Farrell, Y. Qu, U. Bierbach, M. Valsecchi and E. Menta, in *Cisplatin. Chemistry and Biochemistry of a Leading Anticancer Drug* (Ed. Lppert, B), Verlag Helvetica *Chimica Acta*, Zurich, Wiley-VCH, Weinheim, 1999, 479-496.
47. N. J. Wheate, C. Cullinane, L. K. Webster and J. G. Collins, *Anti-Cancer Drug Des*., 2001, **16**, 91.
48. N. J. Wheate, B. J. Evison, A. J. Herlt, D. R. Phillips and J. G. Collins, *Dalton Trans*., 2003, 3486-3492.
49. (a) N. J. Wheate and J. G. Collins, *J. Inorg. Biochem*., 2000, **78**, 313-320; (b) N. J. Wheate, L. K. Webster, C. R. Brodie, J. G. Collins, *Anti-Cancer Drug Des*. 2000, **15**, 313-322.
50. N. J. Wheate, S. M. Cutts, D. R. Phillips, J. R. Aldrich-Wright and J. G. Collins, *J. Inorg. Biochem*., 2001, **84**, 119-127.
51. B. Gary, K'NEX ® DNA Models, http://c3.biomath.mssm.edu/knex/dna.models.knex.html , cited 13/03/2015.
52. A. Klug, *J. Mol. Biol*., 2004, **335**, 3-26.
53. J. Reedijk, *Chem. Rev*., 1999, **99**, 2499-2510.
54. B. A. Donahue, M. Augot, S. F. Bellon, D. K. Treiber, J. H. Toney, S. J. Lippard and J. M. Essigmann, *Biochemistry*., 1990, **29**, 5872-5880.
55. P. M. Pil and S. J. Lippard, *Science*, 1992, **256**, 234-237.
56. V. Brabec, J. Kaspárková, O. Vrána, O. Nováková, J. W. Cox, Y. Qu and N. Farrell, *Biochemistry*, 1999, **38**, 6781-6791.
57. Y. Ellahioui, S. Prasher and S. Gómez-Ruiz, *Inorganics 5,4 review.*, 2017.
58. (a) A. Mambanda and D. Jaganyi, *Dalton Trans.*, 2012, **41**, 908; (b) P. O. Ongoma, and D. Jaganyi, *Dalton Trans*., 2013, **42**, 2724-2734; (c) D. Reddy and D. Jaganyi, *Int. J. Chem. Kinet*., 2011, **43**, 161; (d) D. Jaganyi, F. Tiba, O. Q. Munro, B. Petrović

and Ž. D. Bugarcić, *Dalton Trans*., 2006, **24**, 2943-9; (e) D. Jaganyi, A. Hofmann, and R. van Eldik, *Angew. Chem., Int. Ed*., 2001, **40**, 1680; (f) D. Jaganyi, D. Reddy, A. Gertenbach, A. Hofmann and R. van Eldik, *J. Chem. Soc., Dalton Trans*., 2004, 299-304.

59. (a) J. Bogojeski, Ž. D. Bugarčić, R. Puchta and R. van Eldik, *Eur. J. Inorg. Chem.*, 2010, 5439; (b) N. Hochreuther, S. T. Nandibewoor, R. Puchta, R. van Eldik, *Dalton Trans*., 2012, **41**(2), 512; (c) W. Summa, R. Schiessl, N. Puchta, H. van Eikema, R. van Eldik, *Inorg. Chem*., 2006, **45**, 2948-2959, Ž. D. Bugarčić, J. Bogojeski, B. Petrović, N. Hochreuther, and R. van Eldik, *Dalton Trans*., 2012, **41**, 12329-12345.

60. H. Ertürk, R. Puchta and R. van Eldik, *Eur. J. Inorg. Chem*., 2009, 1331-1338.

61. M. J. Frisch, G. W. Trucks, H. B. Schlegel, G. E. Scuseria, M. A. Robb, J. R. Cheeseman, G. Scalmani, V. Barone, B. Mennucci, G. A. Petersson, H. Nakatsuji, M. Caricato, X. Li, H. P. Hratchian, A. F. Izmaylov, J. Bloino, G. Zheng, J. L. Sonnenberg, M. Hada, M. Ehara, K. Toyota, R. Fukuda, J. Hasegawa, M. Ishida, T. Nakajima, Y. Honda, O. Kitao, H. Nakai, T. Vreven, J. A. Montgomery, Jr., J. E. Peralta, F. Ogliaro, M. Bearpark, J. J. Heyd, E. Brothers, K. N. Kudin, V. N. Staroverov, R. Kobayashi, J. Normand, K. Raghavachari, A. Rendell, J. C. Burant, S. S. Iyengar, J. Tomasi, M. Cossi, N. Rega, J. M. Millam, M. Klene, J. E. Knox, J. B. Cross, V. Bakken, C. Adamo, J. Jaramillo, R. Gomperts, R. E. Stratmann, O. Yazyev, A. J. Austin, R. Cammi, C. Pomelli, J. W. Ochterski, R. L. Martin, K. Morokuma, V. G. Zakrzewski, G. A. Voth, P. Salvador, J. J. Dannenberg, S. Dapprich, A. D. Daniels, O. Farkas, J. B. Foresman, J. V. Ortiz, J. Cioslowski, and D. J. Fox, Gaussian 09, Revision A.1, *Gaussian, Inc*., Wallingford CT, 2009.

CHAPTER 2

2.0 Literature review

2.1 Introduction

The application of metals complexes in the field of medicine has risen tremendously over the past four decades.[1,2] In design of metal-based drugs, transition metals and their reactions have been of importance in the treatment of many diseases like cancer, diabetes, arthritis among others.[3] However, there is little understanding of the mechanism of action of these transition metal-based drugs in biological systems.[4] Carcinostatic properties of platinum complexes particularly cisplatin[5] has given a special impetus to research on interaction of the metal ion and the DNA.[6-8] Due to outstanding properties of cisplatin, anticancer metallodrug developments have been designed to similarity of cisplatin and its analogues.[9-11] Much of this platinum anticancer drug chemistry is based on coordination of the carrier ligand to the metal. This is through being attached to intermediate ligands of varying binding strengths. Platinum-ligand binding makes the kinetics of these complexes to be of importance. However, cisplatin resistance remains a major challenge to successful treatment of cancer.[12,13] The control of Ligand substitution is inherent in platinum coordinated drug mechanisms of action.[14] Multinuclear platinum complexes are able to overcome both intrinsic and acquired resistance to cisplatin. For metal containing compounds to find their way into medicine it is useful to first provide basic information on the bonding of metal complexes and the way they react with biological targets in the cell. The overall goal of this Chapter is to briefly provide core information needed to understand the substitution mechanisms of square planar complexes. This chapter briefly reviews in general terms, the basic principles of the crystal field theory a unifying theory of bonding in metal complexes. This will provide the required theoretical background for the subsequent discussion of the investigated Pt(II) complexes.

2.2 Platinum Chemistry

The discovery of cisplatin and its cancer properties has motivated further exploration into its coordination chemistry and that of related species[15-17] with the ultimate goal of finding new complexes with improved therapeutic properties. The mechanism of substitution of water exchange reactions in square planar complexes is explained by *trans* effect in terms of σ-donation and π back-donation whose relative strengths are quantified by the changes of

electron occupations of 5*d* atomic orbitals in platinum complexes. The *σ*-donation strengths are linearly correlation with the $Pt-H_2O$ (leaving ligand) bond length (*trans* influence). The kinetic *trans* effect is proportionally correlated to the *σ*-donation ability of the *trans* ligand exception are the ligands with strong *π* back-donation ability that stabilizes transition state. The *σ*-donation ability of the ligand is dependent on the σ-donation strength of the coordinated ligand in the *trans* position. A good electronic structural arrangement for square planar is d^8 low spin. The structure utilizes relatively stable metal *d* orbitals. The antibonding molecular orbitals derived from the *d* orbitals consist of four relatively stable d_{yz}, d_{xz}, d_z^2 and d_{xy} and a high-energy lying unstable $d_{x^2-y^2}$ orbitals.

These *d* orbitals play a key role in this transition metal coordination chemistry. The electrons on the metal occupy d orbitals furthest from the direction of ligand approach. In terms of crystal field theory, the d^8 electrons occupy the low-energy d_{yz}, d_{xz}, d_z^2 and d_{xy} orbitals while the high-energy $d_{x^2-y^2}$ orbital remains unoccupied.[18,19] The square planar geometry offers the greatest stabilization since the highest energy orbital $d_{x^2-y^2}$ remains unoccupied. Supposing the ligands lie on the x, y axis, applying classical ligand field theory, the $5d_{x^2-y^2}$ atomic orbitals become LUMO of the Pt(II) due to their largest repulsion with *σ*-donating electron pairs of the ligands. The structure of the complex is a simple square on the x and y axes since there are no ligands along the z-axis. This makes the repulsion of electrons in the d_{xz}, d_{yz} and d_z^2 orbitals to be considerably lower than those of its counterpart octahedral.[20,21] At a higher energy P_z valence orbital in square planar metal complexes is not involved in *σ* bonding, it is available for forming the extra *σ* bond required in associative activation process. The availability of valence orbital attach to additional entering ligand to form a five-coordinate intermediate showing square planar substitutions to proceed by an associative mechanism. Ligands with strong *π* back-donation stabilize the penta-coordinated transition state. Square planar substitution involves σ donation from the filled ligand P_x orbital to vacant metal $5d_{x^2-y^2}$ orbital and *π* back-donation from the filled metal d_{xz} orbital to the antibonding linear combination of the *π* ligand.

2.3 Transition metal *d*-orbitals

From literature review, reactivity of Pt(II) square planar complexes is driven by two effects: σ donation and π back-donation. Their role is quantified by population of $5d_{x^2-y^2}$ and $5d_{xz}$ atomic orbitals respectively. Figure 2.1 shows σ donation and π back-donation ligand interaction between platinum and ligands. The π back-donation increases the total positive charge of the Pt(II) atom and decreases electron density in the *xz* plane. This facilitates a nucleophilic attack in the *xz* plane and stabilizes the corresponding penta-coordinated transition state. The energy of the orbitals actively involved in σ and π interactions is varied by different ligand substitutions on the metal centre. The σ and π acceptance character of various ligand derivatives are understood in terms of electron donating and accepting character and their position on the metal coordination skeleton.

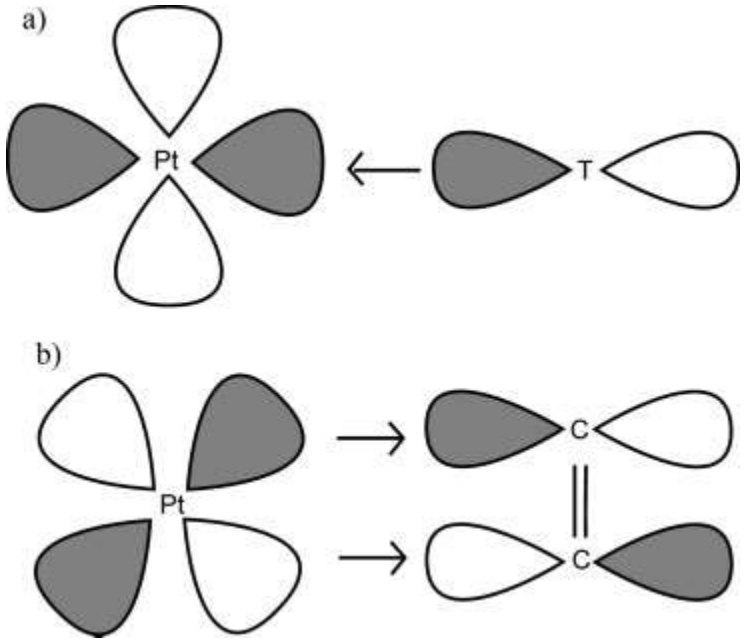

Figure 2.1 (a) σ-donation from the filled ligand P_x orbital to vacant metal 5 $d_{x^2-y^2}$ orbital,[22] (b) *pi* back-donation from the filled metal d_{xz} orbital to the antibonding linear combination of carbon's P_x orbitals of a π back-bonding ligand (C_2H_4).

As the ligands move along the z-axis, *d*-orbitals with a z-component fall in energy. The effect is more in d_z^2 orbitals since its electrons are concentrated in lobes along the z-axis. The $d_{x^2-y^2}$ and d_{xy} orbitals increase in energy. This make the square planar complexes of d^8 to be diamagnetic because of the highest-energy orbital ($d_{x^2-y^2}$) which is greatly destabilized

making pairing in the d_{xy} orbital more favourable than placing an unpaired electron in the $d_{x^2-y^2}$ orbital. This creates a large energy gap between the d_{xy} and $d_{x^2-y^2}$ orbitals. This makes square planar complexes to be exclusively of d^8 metals (Pt^{2+}, Ni^{2+}, Pd^{2+}, Co^{+}, Rh^{+}, Ir^{+}, Cu^{3+}, Ag^{3+} and Au^{3+}) that is all metal orbitals are filled except the $d_{x^2-y^2}$ orbitals which have 16 electrons rather than 18. The 16 electron d^8 square planar complexes are coordinatively and electronically unsaturated.[19] If $d_{x^2-y^2}$ orbital is filled with electrons it weakens the σ bonds with the ligands making it antibonding as shown in Figure 2.2.

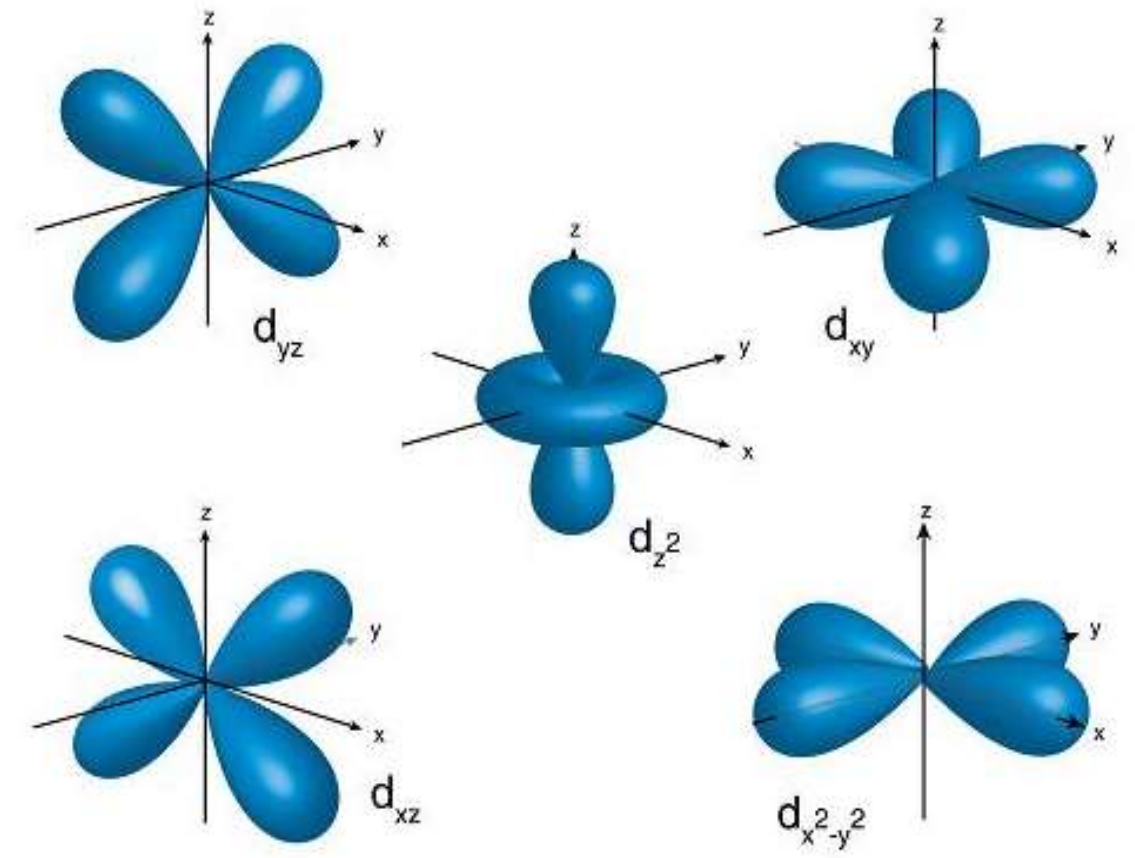

Figure 2.2: The spatial configurations, the shapes and boundary surfaces of the five *d* orbitals.[23]

The d_{xy}, d_{yz} and d_{xz} orbitals bisect the negative charges. They cause a smaller repulsion between the ligand and metal for these orbitals. These orbitals form the degenerate low energy set of energy levels. The energy level splitting of the *d*-orbitals due to their interaction with the ligands in a complex has important structural, kinetic and thermodynamic effects on the chemistry of transition-metal complexes. The splitting of *d* orbitals in the crystal field

model not only depends on the geometry of the complex, but also on the nature of the metal ion, the charge on this ion, and the ligands that surround the metal.

The surfaces enclose the percentage of the total electron probability for the five *d*-orbitals. Four of the five *d*-orbitals consists of four lobes arranged in a plane that is intersected by two perpendicular nodal planes. They have the same shape but different orientations. The fifth *d*-orbital (d_z^2) has a distinct shape but still mathematically equivalent to other orbitals. The orbitals are hinged on understanding the influence of the approaching ligands on the *d*-orbital energies. The *d* orbitals split into two sets; t_{2g} and e_g orbitals, under the influence of crystal field. The nature of the approaching ligands has an influence on the strength of perturbations energy. For instance, more electron donating ligands cause more significant energy perturbations. The extent of perturbations or field splitting caused by the approaching ligands can be predicted from the spectrochemical series.[24,25] These *d* orbitals split into two energy levels; the top consisting of d_{xy}, d_{xz} and d_{yz} and the bottom $d_x^2{}_{-y}{}^2$ and d_z^2.

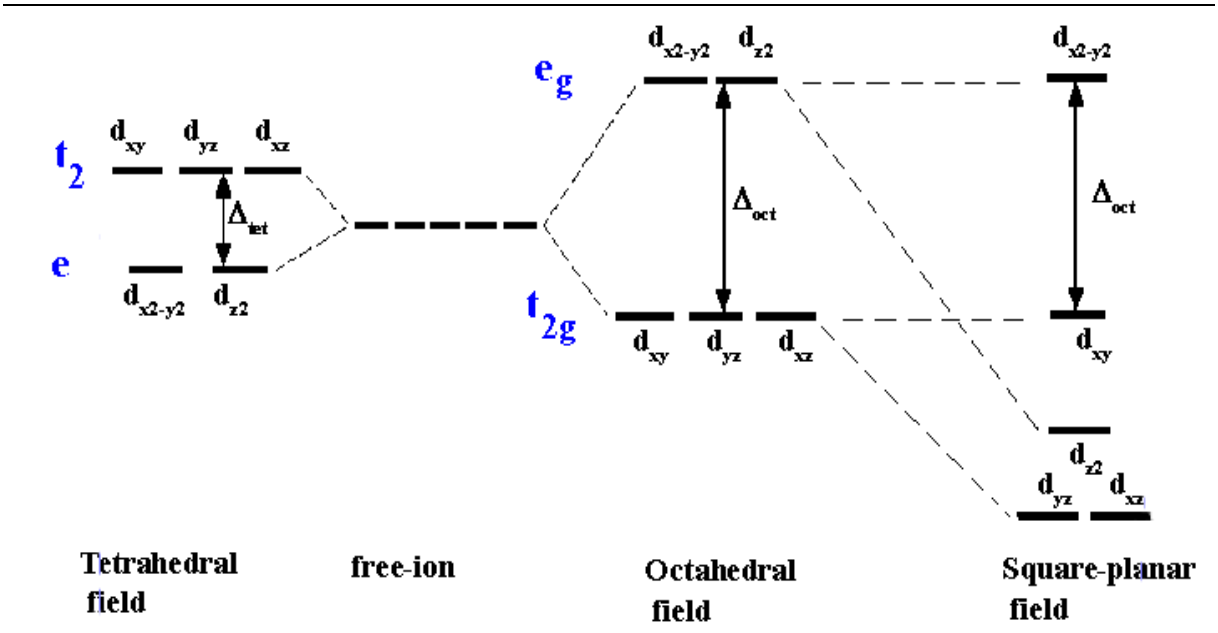

Figure 2.3: Crystal field splitting of *d*-orbitals of a central ion in complexes having different geometries.[26]

In octahedral complexes, the filled ligand orbitals raise the energy of the orbitals with which they overlap directly. Due to the different directions of the *d* orbital lobes, the two e_g orbitals directed towards the axes (d_z^2 and $d_x^2{}_{-y}{}^2$) are more destabilized than other three t_{2g} orbitals with lobes pointing in-between the main axes (d_{xz}, d_{yz}, d_{xy}). In square planar geometry, the d_{xy}

orbital experiences a similar fate, although its overlap is not quite as direct making its increase in energy not to be as severe as in $d_{x^2-y^2}$ orbitals. The d_{z^2} orbitals exhibits some overlap via its "donut" lobe. These *d*-orbitals that point towards the approaching ligands ($d_{x^2-y^2}$ and d_{z^2}) are destabilized by the negative charge of the ligands and move to higher energy levels.[24] The d_{xz} and d_{yz} orbitals are completely perpendicular to the xy-plane and exhibit no overlap with the approaching filled orbitals a factor that strongly stabilizes them by the approaching ligands.

The octahedral complexes can undergo Jahn-Teller distortions which results in the elongation of the z-axis, and shortening of the x and y-axes adopting the square planar symmetry. Due to elongation of z-axis, the degeneracy between the d_{z^2} and $d_{x^2-y^2}$ orbitals is broken resulting in d_{z^2} orbital becoming lower in energy as a result of ligands being further away. Therefore the extreme tetragonal distortion to form square planar complexes removes the z-axis and drops d_{z^2} orbitals to lower energy. Thus Crystal Field Theory (CFT) is important in describing the breaking of degeneracies of electron *d*-orbital states and together with molecular orbital theory to form more realistic and complex ligand field theory (LFT), the study was in a position to chemical bonding process in platinum complexes synthesized. From Figure 2.3 it's clear that the 5*d* orbitals in platinum chemistry complexes are no longer degenerate hence the study used this to explore the implications on the coordination of Pt(II) ion to various ligands.

Thus there is need for an extensive review in developing a detailed understanding of substitution behaviour of bifunctional dinuclear and trinuclear platinum-based anticancer drugs. Understanding the role of σ-donicity and π-acceptor properties of polynuclear Pt(II) complexes and structural complexity and the splitting of *d* orbitals by bridging ligand in controlling reactivity remains a major challenge. The distinctive electronic, chemical and photophysical properties of different transition metals complexes with their various applications are particularly of interest in understanding their interaction with the living cells.

References

1. P. J.Sadler, *Adv. Inorg. Chem.* 1999, **49**, 183–306.
2. M. A. Jakupec, E. Reisner, A. Eichinger,M. Pongratz, V. B. Arion, M.Galanski, C. G. Hartinger and B. K. Keppler, *J. Med. Chem.*, 2005, **48**, 2831.
3. M. R. Berger, M. H. Seelig and A. Galeano, in *Metal Complexes in Cancer Chemotherapy*, ed. B. K. Keppler, VCH, Weinheim, 1993, p. 325.
4. L.Ronconi, Sadler, P. *J. Coord. Chem. Rev.*, 2007, **251**, 1633–1648.
5. B. Rosenberg L. Vancamp and T. Krigas, *Nature*, 1965, **205**, 698.
6. B. P. Esposito and R. Najjar, *Coord. Chem. Rev.*, 2002, **232**, 127.
7. P. Umapathy, *Coord. Chem. Rev*., 1989, **95**, 129.
8. S. Komeda, T. Moulaei, K. K. Woods, M. Chikuma, N. P. Farrell and L. D. Williams, *J. Am. Chem., Soc.* 2006, **128**, 16092
9. J. Kasparkova, O. Vrana, N. Farrell, and V. Brabec, *J. Inorg. Biochem.*, 2004, **98**, 1560–1569.
10. J. J. Wilson, S. J. Lippard, *Inorg. Chem*., 2011, **50**, 3103.
11. J. Malina, J. Kasparkova, N. P. Farrell, and V. Brabec, *Nucleic Acids Research*, 2011, **39,** 720–728.
12. H. P. Varbanov, S. M. Valiahdi,C. R. Kowol, M. A. Jakupec, M. Galanski, B. K. Keppler, *Dalton Trans.*, 2012, **41**, 14404–14415.
13. P. Karmakar, *Transition Met Chem*., 2014, **39**, 727–733.
14. T. Soldatović, S. Jovanović, Ž. D. Bugarčić, R. van Eldik, *Dalton Trans.*, 2012, **41**, 876–884.
15. V. Pichler, S. Göschl, S. M. Meier, A. Roller, M. A. Jakupec, M. Galanski, B. K. Keppler, *Inorg. Chem.*, 2013, **52**, 8151.
16. B. Lippert, *Coord. Chem. Rev*., 1999, 182, 263.
17. S. J. Lippard, *Science*, 1982, **218**, 1075
18. M. E. Howe-Grant and S. J. Lippard, *Metal Ions in Biological Systems*, 1980, Ed. H. Sigel, Marcel Dekker Inc., N.Y.
19. F. A. Cotton and G. Wilkinson, *Advanced Inorganic Chemistry*, 1972, 3rd ed. John Wiley and Sons, Inc.
20. J. R. Sabino and P. Coppens, *Acta Cryst.*, 2003, A**59**, 127–131.
21. C. Corminboeuf, C. S. Wannere, D. Roy, R. B. King and P. V. R. Schleyer, *Inorg. Chem.*, 2006, **45** (1), 214–219.

22. Z. Chval, M. Sip and J. V. Burda, *J. Comput. Chem*., 2008, **29**, 2370.
23. https://socratic.org/chemistry/the-electron-configuration-of-atoms/arrangement-of-electrons-in-orbitals-spd-and-f visited 18 May 2019
24. D. F. Shriver and P. W. Atkins, *Inorganic Chemistry*, 2001, 3rd ed. Oxford University Press, 227-236.
25. J. E. Huheey, E. A. Keiter and R. L. Keiter, *Inorganic Chemistry*: *Principles of Structure and Reactivity*, 1993, 4th ed. Harper Collins College Publishers, 405-408.
26. http://wwwchem.uwimona.edu.jm/courses/CFT.html Visited 18 May 2019

CHAPTER 3

The role of an alkyl-phenyl spacer on the reactivity of novel platinum(II) complexes with thiourea nucleophile

3.1 Introduction

Ligand substitutions on square-planar platinum(II) complexes have attracted continued attention owing to their intrinsic chemical and bio-medical applications in anti-tumour treatment.[1-3] The interaction of these platinum based drugs with DNA is widely accepted as the mechanism responsible for their anticancer activity.[4-6] To understand the chemical and the bio-medical transformations of this platinum metallodrugs with biologically relevant nucleophiles under physiological conditions has been of special concern towards the discovery of potential anti-cancer chemotherapy.[4,5] To achieve this many aspects of substitution reactions on square-planar complexes have been carried out on monofunctional Pt(II) complexes.[7,8] The results reported on substitution reactions of these monofunctional Pt(II) complexes mostly suggest an associative mechanism[9,10], although in some cases dissociative mechanisms have also been reported.[11,12] To date, most attention is focused on this class of platinum complexes despite side effects like toxicity, acquired resistance and narrow spectrum of activity limiting their application as anticancer therapeutics.[13] This has led to considerable interest in the development of multinuclear platinum(II) complexes which are reported to be very promising class of new platinum anticancer drugs.[14-16] Many complexes from this class have shown potential antitumour activity and are reported to circumvent cisplatin resistance cell-lines.[1,2,5,6,15] Recent reports in this area shows bright prospects in the utilization of dinuclear and polynuclear metal complexes in cancer chemotherapy.[4,5,13]

Despite the advantages of these multinuclear platinum complexes, extensive studies have been carried out with regard to cisplatin which is reported to be among the most active metal based anti-tumour agents in clinical use.[17,18] Cisplatin being among the mainstays in cancer chemotherapy has contributed to more detailed studies of monofunctional platinum(II) complexes. However, its narrow spectrum of activity and side effects like nephrotoxicity, ototoxicity, neurotoxicity, nausea, vomiting, myelosuppresion and resistance in tumour cell-

lines[19,20] has led to many different and creative approaches towards the design of innovative new classes of platinum and other metal-based complexes that address the side effects associated with cisplatin. One way of exploring this has been a paradigm shift from the mononuclear to multinuclear platinum complexes that form different intrastrand and interstrand cross-link DNA-adducts with an expanded spectrum of activity.[21-23] This class of complexes have shown to be pharmaceutically significant by the advancement of BBR3464 to clinical trials and exhibiting antitumour activity in both cisplatin-sensitive and resistant cell-lines as well as in p53 mutant tumour models.[24,25]

These complexes consist of two or more platinum centres bridged to either a flexible aliphatic diamine chains or a rigid aromatic ring. Collectively, this class of complexes have been reported to display novel mechanisms of action over classical mononuclear complexes such as cisplatin and its analogues. Results from recent studies by Jaganyi *et al.*,[26] Hofmann *et al.*[27] and Farrell *et al*.[28] shows that reactivity of dinuclear platinum(II) complexes to vary with the bridging linker that connect the two platinum centres. However, the actual thermodynamic or kinetic contribution of the bridge to the mechanism of substitution of the leaving groups still needs to be elucidated, especially in dinuclear and multinuclear Pt(II) complexes. Moreover the molecular geometry, symmetry, steric or electronic connotations adopted by the complexes which play a major role in their reactivity also remains unexplored. Variation in substitution rates by changing the bridging spacer and introduction of more bifunctional platinum centres remains a promising strategy in designing platinum anticancer agents with improved efficacy.[4-6]

In order to gain insight into the substitution reactions of these bifunctional dinuclear Pt(II) complexes, the current study was undertaken to investigate the role of alkyl-phenyl spacer on the multiple substitutions of the complexes with bidentate N^N donors of the form $[Pt(N\text{^}N)X_2]^{2+}$ with biological nucleophiles. The reaction of these complexes with chelating N^N donors with *cis*-$PtCl_2$ configuration mimics the mechanism of cisplatin's anticancer activity. To pursue this perspective another platinum centre was introduced to form dinuclear complexes of the type $[Pt(N\text{^}N)X_2Pt(N\text{^}N)X_2]^{4+}$ by varying the connectivity of the alkyl linker on the phenyl ring in *ortho*, *meta* and *para* positions. This investigation reveals for the first time information on substitution mechanisms of transition metal complexes with

multidentate ligands ($4H_2O$) as leaving groups in *cis* coordination. This study was motivated by the fact that dinuclear platinum(II) complexes have been reported to be promising anticancer-agents owing to their formation of long range intrastrand and interstrand cross-link DNA-adducts.[28-30] The adducts are not common in mononuclear platinum(II) complexes, thus making their mechanism the centre of focus in cancer chemotherapy as they are expected to offer increased anticancer activity over clinically applied mononuclear complexes.

In the current study, the 2,2-dipyridylamine ligand was used due to its unique coordination that forms six membered chelates upon binding to the metal centre and the ability of nitrogen donor ligands to stabilize both low and high oxidation states of complexes.[31,32]These complexes are of special interest because they contain a *cis*-[$PtCl_2$(ammine)$_2$] unit that is structurally related to cisplatin in the sense that they both display two strongly bonded carrier ligands and two labile groups. To assess the utility of these dinuclear Pt(II) series as antitumour probes, their substitution reaction with bio-relevant molecules remains vital to shed light on the mechanism of Pt-based prodrugs. Thiourea nucleophiles were employed due to their differences in nucleophilicity, steric hindrance and their biological relevance. For instance, thiourea (**TU**) is a strong σ-donor with high solubility and can act as a good model compound for thiolate and thioether present in the cells[33] and as a protecting agent to minimize nephrotoxicity in cisplatin treatment.[4] It is also known to act as a chemoprotective agent that alleviates the side effects in the normal tissue[4], while *N,N'*-dimethylthiourea (**DMTU**) highly permeate molecule, decreases injury in a wide variety of biological systems.[34]Additionally its protective effect has been ascribed to its capacity to inactivate reactive oxygen species.[35] It is envisaged that the kinetic tuning of the dinuclear complexes in Figure 3.1 will shed light on their mechanistic interaction with thiourea molecules and also provide a better understanding of platinum metabolism.

This chapter outlines the positional effect of an alkyl-phenyl spacer on the reactivity of Pt(II) complexes: di-2-pyridylaminodiaquaplatinum(II), Pt(dpa)$(H_2O)_2$ (**Pt1**); di-2-pyridylaminomethylbenzenediaquaplatinum(II), Ph(dpa)Pt$(H_2O)_2$ (**Pt2**); 1,2-bis(di-2-pyridylaminomethyl)benzenetetraquaplatinum(II), o-Ph(dpa)$_2$Pt$_2(H_2O)_4$ (**Pt3**); 1,3-bis(di-2-pyridylamino-methyl)benzenetetraquaplatinum(II), m-Ph(dpa)$_2$Pt$_2(H_2O)_4$ (**Pt4**); and 1,4-bis(di-2-pyridylaminomethyl)-benzenetetraquaplatinum(II), p-Ph(dpa)$_2$Pt$_2(H_2O)_4$ (**Pt5**)

shown in Figure 3.1 below. The complexes were synthesized from ligand prepared in Scheme 3.1.

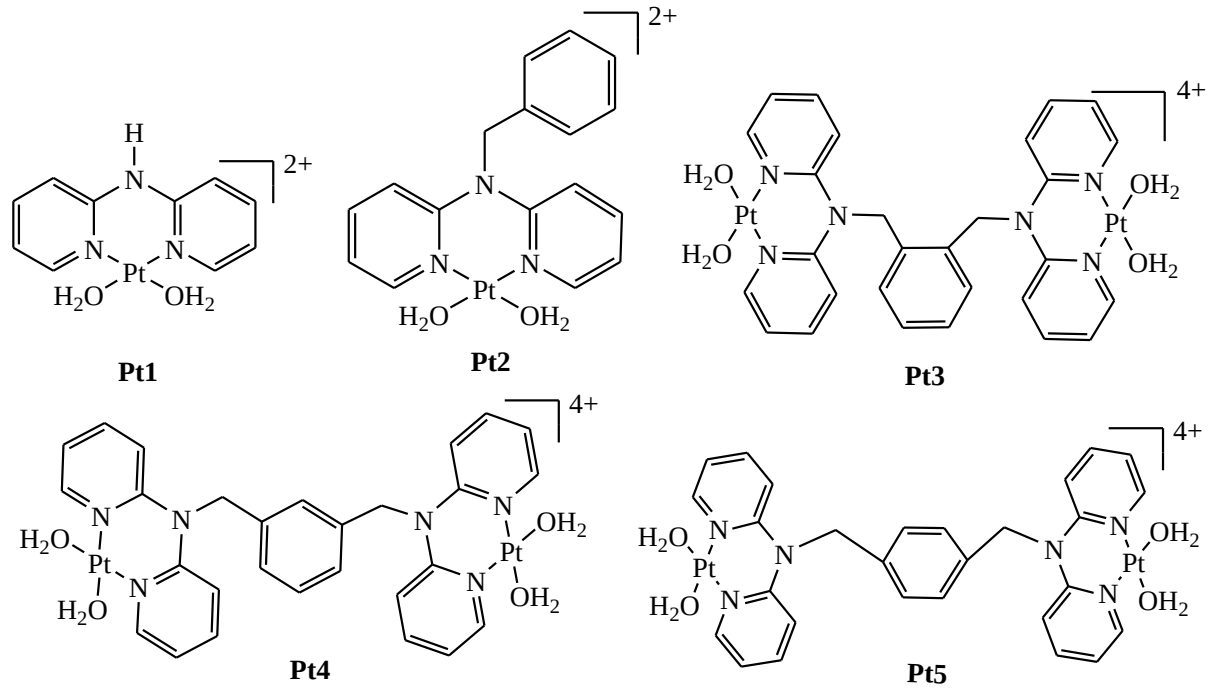

Figure 3.1: The chemical structures and abbreviations for the aquated Pt(II) complexes investigated.

3.2 Experimental Section

3.2.1 Materials and reagents:

The nucleophiles thiourea (**TU**, 99 %), *N,N'*-dimethylthiourea (**DMTU**, 99 %) and *N,N,N'N'*-tetramethylthiourea (**TMTU**, 98 %), 2,2-dipyridylamine 99 %, Benzyl bromide 99 %, 1,2-bis(bromomethyl)benzene 99 %, 1,3-bis(bromomethyl)benzene 99 %, 1,4-bis(bromomethyl)benzene 99 % and $AgClO_4$ 99.99% were all obtained from Sigma Aldrich. K_2PtCl_4 was obtained from Strem chemicals. Ultrapure de-ionized water was used in all experiments. All other reagents were of analytical grade quality and were used without further purification.

3.2.2 Synthesis of ligands

Syntheses of ligands were carried out using standard Schlenk line procedures under dry nitrogen. The ligands namely di-2-pyridylaminomethylbenzene, 1,2-bis(di-2-pyridylaminomethyl)benzene, 1,3-bis(di-2-pyridylaminomethyl)benzene and 1,4-bis(di-2-

pyridylaminomethyl)benzene were prepared according to literature procedure,[36] starting with 2,2'-dipyridylamine and their respective bromo alkyl halide linkers. For each ligand, the respective bromo alkyl halide (0.855 g, 5.00 mmol) was dissolved in 3 mL DMF at room temperature and 2, 2'-dipyridylamine (0.856 g, 5.00 mmol) and KOH (1.137 g, 20.26 mmol) in 5.00 mL DMF added drop wise. The resulting solution was stirred under nitrogen at room temperature for 24 hours and then dried under *vacuo*. The residue was washed with water and extracted with $CHCl_3$ (3 × 50 mL) and the extracts dried over anhydrous sodium sulphate and filtered. The filtrate was taken to dryness under reduced pressure. The residue was chromatographed on silica gel by elution with $CHCl_3$:CH_3OH (5:1). The resulting yellow product was recrystallized from an acetone-water mixture (1:2 v/v). However, synthesis of 1,2-bis(di-2-bromomethyl)benzene was carried out in DMSO and recrystallized in ethyl acetate-petroleum ether. A summary of the synthetic pathway of the ligands is presented in Scheme 3.1.

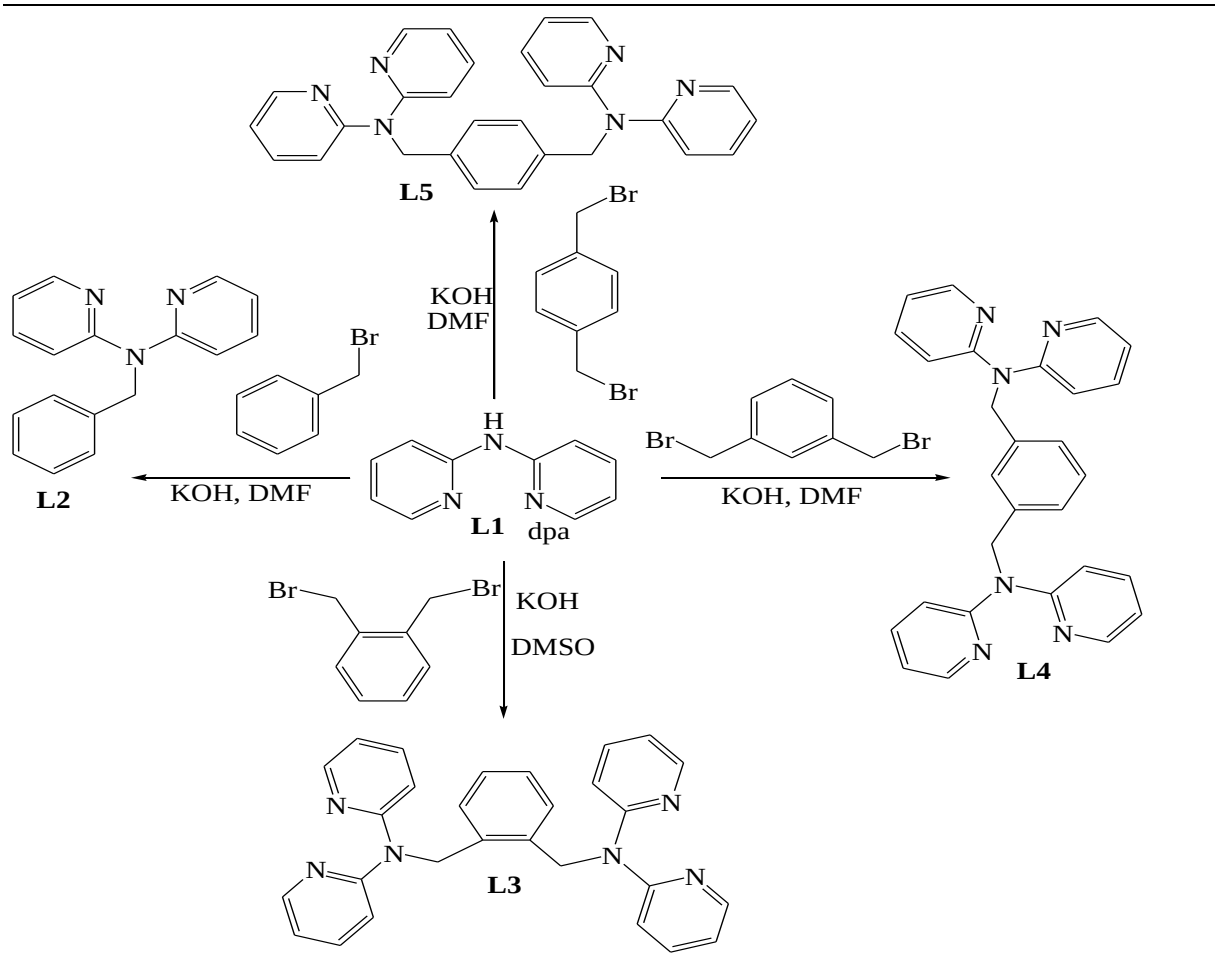

Scheme 3.1: Synthetic pathways in preparation of the bridging ligands

Di-2-pyridylaminomethylbenzene (L2), Yield, 0.277 g, (21 %). Anal. Calcd. for $C_{17}H_{15}N_3$, C, 78.13; H, 5.79; N, 16.08; Found: C, 77.78; H, 5.55; N, 16.48. ^{1}H NMR (400 MHz, $CDCl_3$, 303 K) δ 8.40 (2H, d, py), 7.60 (2H, t, py), 7.37 (2H, d, py), 7.27 (2H, d, ph), 7.20 (1H, t, ph), 7.16 (2H, d, ph), 6.94 (2H, t, py), 5.55 (2H, s, CH_2); ^{13}C NMR (400 MHz, $CDCl_3$, 303K) δ 157.5, 148.6, 139.8, 137.4, 128.0, 117.4, 114.4, 51.3,TOF MS ES$^+$, *m/ z:* 262.134 $[M + H]^+$.

1,2-bis(di-2-pyridylaminomethyl)benzene (L3), Yield, 0.369 g, (37 %). Anal. Calcd. for $C_{28}H_{24}N_6$, C, 75.65; H, 5.44; N, 18.91; Found C, 75.39; H, 5.27; N, 19.28. ^{1}H NMR (400 MHz, $CDCl_3$, 303 K) δ 8.32 (4H, d, py), 7.53 (4H, t, py), 7.27 (2H, d, ph), 7.22 (4H, d, py), 7.04 (2H, t, ph), 6.86 (4H, dd, py), 5.64 (4H, s, CH_2); ^{13}C NMR (400 MHz, $CDCl_3$, 303K) δ157.1, 148.2, 137.3, 136.4, 127.6, 126.4, 117.3, 114.6, 48.3, TOF MS ES$^+$, *m/z:* 445.2141 $[M + H]^+$.

1,3-bis(di-2-pyridylaminomethyl)benzene (L4), Yield, 0.463 g, (46 %). Anal. Calcd. for $C_{28}H_{24}N_6$, C, 75.65; H, 5.44; N, 18.91; Found C, 75.75; H, 5.36; N, 19.19. ^{1}H NMR (400 MHz, $CDCl_3$, 303 K) δ 8.25 (4H, d, py), 7.53 (4H, t, py), 7.27 (2H, d, ph), 7.22 (4H, d, py), 7.04 (2H, t, py), 6.86 (4H, t, py), 5.64 (4H, s, CH_2); ^{13}C NMR (400 MHz, $CDCl_3$, 303K) δ 157.1, 148.1, 139.6, 136.9, 128.4, 125.0, 114.3, 51.1, TOF MS ES$^+$, *m/z:* 445.2136 $[M + H]^+$.

1,4-bis(di-2-pyridylaminomethyl)benzene (L5), Yield, 0.599 g, (59 %). Anal. Calcd. for $C_{28}H_{24}N_6$, C, 75.65; H, 5.44; N, 18.91; Found C, 75.57; H, 5.32; N, 19.27. ^{1}H NMR (400 MHz, $CDCl_3$, 303 K) δ 8.28 (4H, d, py), 7.47 (4H, t, Py), 7.22 (4H, s, ph), 7.13 (4H, d, py), 6.82 (4H, dd, py), 5.43 (4H, s, CH_2); ^{13}C NMR (400 MHz, $CDCl_3$, 303K) δ 157.1, 148.1, 137.6, 137.1, 126.9, 117.1, 114.5, 51.0, TOF MS ES$^+$, *m/z:* 467.1957 $[M + Na]^+$.

3.2.3 Syntheses of Complexes

The complexes were synthesized from their respective ligands according to the literature method by Krebs *et al.*[37] A 50 mL solution of K_2PtCl_4 was stirred and the corresponding molar equivalent of respective ligands dissolved in a small amount of water was added drop-wise. The reaction mixture was refluxed overnight at 50 °C. The resulting platinum(II) complexes were obtained as precipitates, washed with ultrapure water and diethyl ether and finally dried in *vacuo*. The synthesized ligands and complexes were characterized using ^{1}H-^{13}C and ^{195}Pt NMR, mass spectrometry and elemental analysis. It is important to note that

characterization of the complexes was carried out in their chloride form while for kinetic analysis they were aquated to $Pt(L)(H_2O)_n$ (L = bridging ligand L1-L5, n = 2 or 4) (Figure 3.1).

di-2-pyridylaminodichloroplatinum(II) Pt(dpa)(Cl_2), (**Pt1**), Yield, 66 mg, (63 %), Yellow powder, Anal. Calcd. for $C_{10}H_9N_3PtCl_2$, C, 27.54; H, 2.08; N, 9.64; Found C, 27.36; H, 2.29; N, 9.16. ^{1}H NMR (400 MHz, DMSO-d_6, 303K), 8.80 (2H, d, py), 7.98 (2H, t, py), 7.27 (2H, d, py), 7.14 (2H, t, py), 4.04 (1H, s, N-H), ^{13}C NMR (400 MHz, DMSO-d_6, 303K), 170.8., 150.4, 141.0, 119.4, 114.3, 60.1, TOF MS ES$^+$, *m/z:* 437.9808, ^{195}Pt NMR -2103.4 ppm.

di-2-pyridylaminomethylbenzenedichloroplatinum(II) Ph(dpa)$PtCl_2$ (Pt2), Yield, 69 mg, (44 %). Anal. Calcd. for $C_{17}H_{15}N_3PtCl_2$, C, 38.72; H, 2.87; N, 7.97; Found C, 38.46; H, 3.07; N, 8.10. ^{1}H NMR (400 MHz, DMSO-d_6, 303K), 9.05 (2H, d, py), 8.04 (2H, t, py), 7.68(2H, d, py), 7.53 (2H, d, py), 7.36 (2H, t, py), 7.26 (5H, d, ph), 5.43 (2H, s, CH_2); ^{13}C NMR (400 MHz, DMSO-d_6, 303K):153.8, 151.8, 142.1, 136.3, 129.8, 122.1, 117.4, 54.3, TOF MS ES$^+$, *m/z:* 550.0247 [M + Na]$^+$, ^{195}Pt NMR -2189.2 ppm.

1,2-bis(di-2-pyridylaminomethyl)benzenetetrachloroplatinum(II), o-Ph(dpa)$_2$$Pt_2Cl_4$ (**Pt3**), Yield, 75 mg (0.08 mmol) (36 %). Anal. Calcd. for $C_{28}H_{24}N_6Pt_2Cl_4$, C, 34.45, H, 2.48, N, 8.61; Found C, 34.32, H, 2.52, N, 8.56. ^{1}H NMR (400 MHz, DMSO-d_6, 303K), 8.83 (2H, d, py), 8.20 (2H, t, py), 7.96 (2H, d, py), 7.56 (4H, d, py), 7.44 (2H, t, py), 7.26 (4H, d, py), 7.02 (2H, t, ph), 6.92 (2H, d, ph), 5.38 (4H, s, CH_2), ^{13}C NMR (400 MHz, DMSO-d_6, 303K): 157.2, 153.4, 148.6, 138.2, 125.4, 117.6, 113.7, 51.0, TOF MS ES$^+$, *m/z:* 941.05 [M-Cl]$^+$, ^{195}Pt NMR -2187.3 ppm.

1,3-bis(di-2-pyridylamino-methyl)benzenetetrachloroplatinum(II), m-Ph(dpa)$_2$$Pt_2Cl_4$ (Pt4), Yield, 92 mg (0.10 mmol) (44 %). Anal. Calcd. for $C_{28}H_{24}N_6Pt_2Cl_4$, C, 34.45, H, 2.48, N, 8.61; Found C, 34.32, H, 2.52, N, 8.56. ^{1}H NMR (400 MHz, DMSO-d_6, 303K), 8.83 (2H, t, py), 8.22 (2H, d, py), 8.02 (3H, d, py), 7.58 (4H, d, py), 7.44 (3H, d, py), 7.28 (4H, d, ph), 7.02 (2H, d, py), 5.39 (4H, s, CH_2); ^{13}C NMR (400 MHz, DMSO-d_6, 303K): 157.1, 148.8, 138.6, 114.2, 111.3, 54.5, TOF MS ES$^+$, *m/z:* 941.04 [M-Cl].$^+$ ^{195}Pt NMR -2190.6 ppm.

1,4-bis(di-2-pyridylaminomethyl)-benzenetetrachloroplatinum(II), p-Ph(dpa)$_2$Pt$_2$Cl$_4$ Pt5, Yield, 106 mg (0.11 mmol) (51 %). Anal. Calcd. for $C_{28}H_{24}N_6Pt_2Cl_4$, C, 34.45, H, 2.48, N, 8.61; Found C, 34.23, H, 2.34, N, 8.26. ^{1}H NMR (400 MHz, DMSO-d_6, 303K), 8.28 (4H, d, py), 7.63 (4H, t, py), 7.19 (8H, s, py), 6.94 (4H, d, ph), 5.35 (4H, s, CH_2), ^{13}C NMR (400 MHz, DMSO-d_6, 303K): 157.6, 147.9, 137.6, 127.3, 117.6, 115.0, 50.4, TOF MS ES$^+$, *m/z:* 941.05 [M-Cl]$^+$. ^{195}Pt NMR -2194.8 ppm.

3.2.4 Aquation of chloride complexes

Due to the low solubility of the chloride complexes, the complexes were converted to their aqua analogues according to Bugarčić *et al.*[38] procedure. The aqua solutions were prepared from their corresponding chloride complexes by removing the chloride ion using $AgClO_4$. An almost stoichiometric amount of $AgClO_4$ was added to the solution and refluxed for 24 h at 50 ^{o}C in the dark. The white AgCl precipitate that formed was removed by filtration through a 0.45 µm pore membrane filter. This was to ensure complete conversion to aqua and removal of silver ions. The aqua solutions were made to the required concentration using a solution of 0.1 M $HClO_4$ acid. The use of acidic solutions of pH 1.0 ensured that complex solutions are in aqua form and maintained a constant ionic strength of 0.1 M. This ensured that pK_a values were determined at similar ionic strength. The aqua solutions were titrated with NaOH solution to determine the pK_a of the complexes. Whilst for all kinetic studies, a pH of 2.0 and an ionic strength at 0.1 M using $NaClO_4$ was maintained to minimize effects of ionic strength.

3.3 Physical measurements

Characterization of both the ligands and complexes using ^{1}H, ^{13}C and ^{195}Pt NMR spectroscopy were recorded on a Bruker Avance III 500 or Bruker Avance 400 spectrometers at frequencies of 500 or 400 MHz and 125 MHz/100 MHz using either a 5 mm BBOZ probe or a 5 mm TBIZ probe. All proton and carbon shifts were recorded with reference to the relevant solvent signal used. Chemical shift values are given in δ (ppm) of ^{1}H relative to tetramethylsilane ($Si(CH_3)_4$) while ^{195}Pt were externally referenced to $K_2[PtCl_6]$ in D_2O. For mass determination, a Waters Micro-mass LCT Premier spectrometer was employed. Elemental analysis was obtained on a Thermo Scientific Flash 2000. Kinetic studies for fast reactions were monitored using an Applied Photophysics SX20 Stopped-Flow spectrophotometer coupled to an online data acquisition system while a Varian Cary 100 Bio

UV-Visible spectrophotometer thermostated by a Varian Peltier temperature controller to within ±0.05 ^{o}C was used for the slow kinetic measurements. The kinetic traces were analyzed using the Origin 7.5® software package.[39] The pH of the solutions was recorded on a Jenway 4330 conductivity/pH meter. Standard pH calibration buffer solutions (pH = 4.0, 7.0 and 10.0) were used for calibration.

3.4 pK_a Determination of the aqua complexes

To obtain the intrinsic information on the acidity of the complexes and their effect on reactivity, their pK_a values were determined. UV-Vis spectra for the determination of pK_a values were recorded on a Varian Cary 100 Bio spectrophotometer. NaOH was used as the base for spectrophotometric titration in the pH range 1 – 10. To avoid absorbance corrections due to dilution a large volume of the platinum aqua complex (250 mL) was used. Solid NaOH pellets were used initially in the pH range of 1 – 3 after which the Pasteur pipettes were used for drop wise addition of 0.5 M, 0.1 M, 0.05 M and 0.001 M of NaOH solution and similar concentrations for perchloric acid for adjusting the pH.

3.5 Kinetic measurements

Substitution reactions were performed at pH 2.0 where the complexes exist in their aqua form (as predetermined when determining pK_a) and protonation of thiourea nucleophiles ruled out.[40] The rate of substitution of the aqua complexes was determined under *pseudo*-first-order conditions as a function of nucleophile concentration and temperature using stopped flow for fast and UV-Vis spectroscopy for slow reactions by following the change in absorbance at suitable wavelengths (Table S3.1 in the Appendix). All the kinetic runs were fitted by a single exponential to determine the k_{obs}. The activation parameters of $\Delta H^{\#}$ and $\Delta S^{\#}$ were obtained by varying the temperature between 288 *K* and 313 *K* at an interval of 5 *K*. These parameters were calculated from Eyring plots using Equation [3.1] below:

$$In\left(\frac{k_2}{T}\right) = -\frac{\Delta H^{\#}}{RT} + \left[In\left(\frac{k_B}{h}\right)\right] + \frac{\Delta S^{\#}}{R} = \frac{\Delta H^{\#}}{RT} + \left(23.76 + \frac{\Delta S^{\#}}{R}\right) \qquad \text{Eq [3.1]}$$

where k_B and h are Boltzmann's and Planck's constants respectively while *R* is gas constant (8.314 J/mol *K*) and *T* is absolute temperature.

3.6 Computational calculations

Density functional theory (DFT) calculations were performed with the Gaussian 09 programme suite.[41] Geometrical optimizations were carried at B3LYP/LanL2DZ level of theory. B3LYP refers to a three parameter functional hybrid exchange of Becke[42] with functional correlation gradient of Lee, Yang and Parr,[42] whereas LanL2DZ refers to Los Alamos National Laboratory 2 Double ζ basis set.[42] The singlet states were used due to low electronic spin of Pt(II) complexes. The aqua complexes were modelled as cations of overall charge as +2 for mononuclear and +4 for dinuclear Pt(II) complexes. The density functional theory provided the ground state properties of the systems and the electron density. Molecular orbital calculations were performed to give HOMO and LUMO energies using LanL2DZ/B3LYP basis set.

3.7 Results and discussion

3.7.1 pK_a determinations for the aqua Pt(II) complexes

Spectrophotometric acid-base titrations were performed to determine the pK_a values of the coordinated water molecules for the aqua species. This was also used to confirm the number of chloride ligands coordinated to each complex. Figure 3.2 show a typical UV-Vis spectrum recorded during spectrophotometric titration of the aqua complex solution with NaOH. The pK_a values were determined from a characteristic sigmoid curve by locating the inflection point from Boltzmann equation using Origin 7.5® program (Appendix S3.39 – S3.41). Determination of pK_a values for aquated Pt(II) complexes provides supporting evidence for conversion of chloride complexes to aqua complexes.

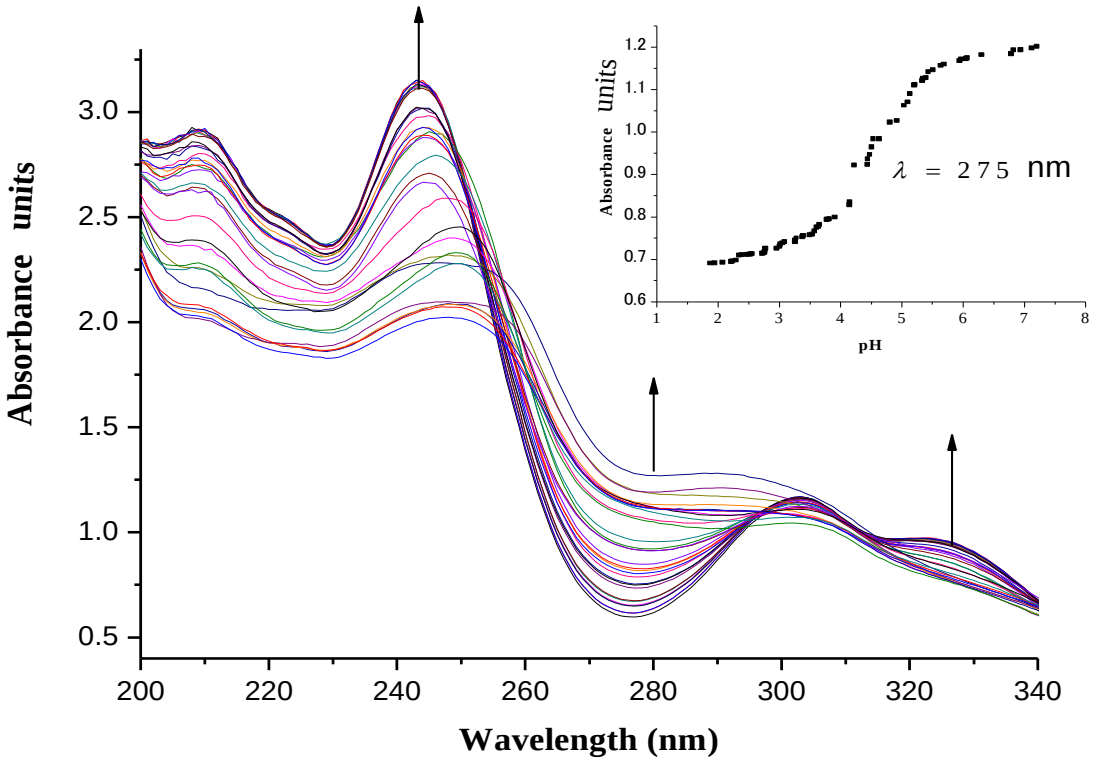

Figure 3.2: UV-Vis spectra of 0.09 mM **Pt1** complex recorded as a function of pH in the range of 2 to 8 at 25 °C, *inset* is a plot of absorbance versus pH at λ = 275 nm.

Table 3.1: A summary of pK_a values obtained for stepwise deprotonation of aqua Pt(II) complexes investigated

Complex	Pt1	Pt2	Pt3	Pt4	Pt5
pK_{a1}	2.72 ± 0.06	2.87 ± 0.02	2.55 ± 0.03	2.39 ± 0.01	2.61 ± 0.01
pK_{a2}	3.80 ± 0.02	6.97 ± 0.11	3.24 ± 0.03	3.65 ± 0.03	3.62 ± 0.01
pK_{a3}	5.68 ± 0.02		5.46 ± 0.02	4.41 ± 0.02	4.16 ± 0.03
pK_{a4}			7.37 ± 0.04	6.90 ± 0.08	7.43 ± 0.01

Boltzmann equation, $y = A_2 + (A_1 - A_2)/(1 + \exp(x - x_0)/\partial x)$, was used in determining the p*K*a values using the Origin 7.5® program (Appendices S3.39 – S3.41).

where A_1 and A_2 are initial and final y values respectively, x_0 = centre, ∂x = width. The y value at x_0 is half way between the two limiting values A_1 and A_2. The y value changes

drastically within a range of x variable. The width of this range is approximately ∂x. The Boltzmann fit gives a sigmoid curve (Appendix Figure S3.39-S3.42).

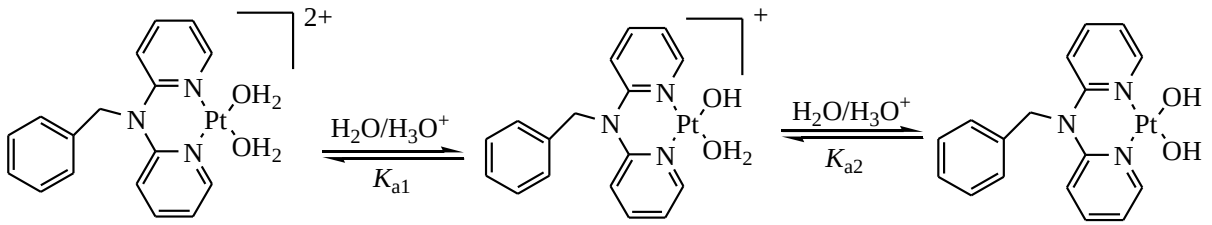

Scheme 3.2: Proposed mechanism for stepwise deprotonation of the diaqua Pt(II) mononuclear complex.

The study shows the nature and conformation of the spacer in the dinuclear complexes to have little influence on the pK_a values as they are of similar magnitude. The *ortho*/*para* orientation effect of the alkyl substituent has a natural consequence of the preferential stabilizing influence as exhibited in this investigation. The effect depends on the position of the alkyl group which exhibits stronger electron donating effect in *para*-position than *ortho* and *meta* positions.[43a-c] The only difference among these three complexes is the position of the alkyl group on the phenyl group. The study notes that the slight change in anchorage position results in a significant difference in their chemical structure, pK_a values and reactivity. This investigation shows that alkyl group's electron donating effect in *ortho*/*para* is stronger than in *meta* position. This is supported by computational calculations (Table 3.3) showing varying bond angles of $C_1N_3C_2$**Pt5** (123.07^o) > **Pt3** (122.72^o) > **Pt4** (118.55^o), representing *para* > *ortho* > *meta*, respectively. Thus, the *meta* complex is more acidic since it only has inductive effects, whereas the *ortho*/*para* complexes experience both inductive and resonance effects. This investigation shows the *ortho*/*para* orientation effect of the alkyl substituent has a natural preferential stabilizing effect. The study shows that substituents' position has an influence on the stability of a complex through both electronic and steric effects. Thus, by having alkyl substituents at *ortho* and *para* positions behave identically but different from that of *meta* position. As such, one would expect *meta* complex to have a significantly different pK_a value as observed in this investigation.

The acidity of complexes shows that the dinuclear complexes are slightly more acidic using first deprotonation for comparison. This difference can be ascribed to the difference in the

overall charge of the complexes which is +2 for the mononuclear and +4 for the dinuclear complexes. Coordination of a second Pt(II) atom results in addition of charges that make the dinuclear platinum complexes more electrophilic thus favouring aqua deprotonation. The results also show that the deprotonation of the subsequent water molecules occurs at higher pH values. This is due to the sequential reduction of the overall charge after each deprotonation, which results in the Pt(II) centre of the aqua/hydroxo species being less electrophilic[8,27] leading to higher pK_a values. Complex **Pt1** showed three pK_a values which are attributed to the two aqua ligands and the pendant acidic proton on N. The proposed deprotonation process can therefore be represented by the equilibrium reaction given in Scheme 3.3 while the pK_a values are summarized in Table 3.1. The results support a stepwise deprotonation. This investigation shows similar behaviour in deprotonation process to previous study by van Eldik[22,27,38] with dinuclear Pt(II) complexes coordinated to 4 aqua ligands that shows four acid dissociation steps. The two aqua ligands coordinated to each platinum centre exhibited different values supporting recent study carried out on similar Pt(II) complexes with the same head group.[43d] This study shows dinuclear complexes to be more acidic than mononuclear analogues due to increased charge as reported in literature.[38]

3.7.2 Computational studies

In order to gain additional insight into the influence of the anchorage position of the alkyl-phenyl spacer on the conformation and possible kinetic properties of the complexes, computational studies was undertaken to determine the structural and electronic properties of the molecules. Computational calculations were used to support experimental data of relative reactivities of the complexes in each series. The computational work was reliably used to predict the stability of complexes and employed structure simulation in aid of understanding the effect of substituent on ligand design with desired properties. The complexes were fully optimized in gas phase and the mapping of their frontier molecular orbitals and selected geometrical parameters summarized in Tables 3.2 and 3.3 respectively. In addition dihedral and basal angles were determined as shown in Figure 3.3 to understand the extent of deviation from the planarity of the ligand around the platinum centre. The optimized structures of dinuclear complexes show that the six-membered chelate rings containing the platinum adopt a twist-boat conformation. The bond angles of the amine nitrogen are close to 120° and are indicative of sp^2 hybridization of the nitrogen atom.[44a] The electron lone pair on nitrogen atom affects cross conjugation of these complexes. The introduction of the alkyl-

phenyl spacer results into a conformation which is dependent on the position of the alkyl group on the phenyl, but all form bowl like cavity. In the case of both *ortho* and *meta* the boat conformation is not part of the cavity created between the two metal centres while in the *para* it is part of the cavity. In *meta* and *para*, the phenyl ring is positioned in the centre of the cavity while in the *ortho* it is away from the cavity. These configurations introduce steric hindrance to the incoming nucleophile to different degrees. DFT calculations shows that there is very little if any electronic effect when the pendant alkyl-phenyl is attached to **Pt2** or used as a spacer in **Pt3** to **Pt5**. Both the NBO charges and the electrophilicity index are similar in magnitude because of Pt(II) centres being in similar environment due to identical atomic and conjugative connectivity to at least five atoms in all directions. A similar resonance pattern in the complexes places little confidence in the accuracy of NBO charges. However, the presence of resonance supports presence of molecular orbitals that extent over to more atoms that lowers energies hence increased stabilization of the complexes to varying levels. The difference between the monomers and the dinuclear complexes is because of the size of the complexes.[44b] These findings are in agreement with the pK_a data which shows a similar trend. One would therefore expect that the reactivity of these complexes will be controlled by steric effect.

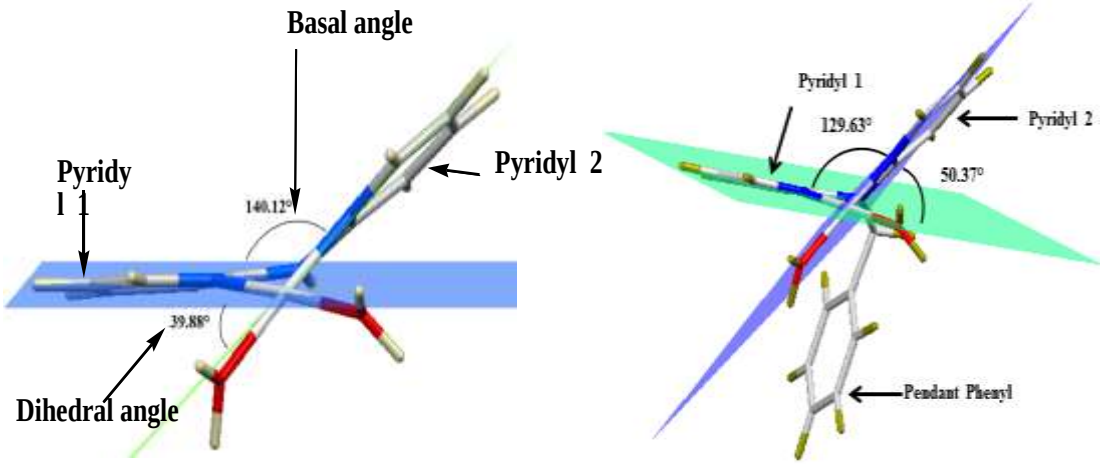

Figure 3.3: DFT-Optimized structures of **Pt1**and **Pt2** showing dihedral and basal angles of the boat conformed pyridine rings.

The mechanism of substitution of aqua exchange in these square planar complexes is explained in terms of σ-donation whose relative strengths are quantified by the changes of electron occupations in 5*d* orbitals. The study shows Pt(II) being a transition metal to be sensitive to the number of *d*-electrons and how they are arrange themselves in the *d*-orbitals.

The geometry is more affected by the surrounding coordination, which is a change in metal ligand bonding strength. This strong σ donation from H^- in **Pt1** shows HOMO orbitals to be localized on the pyridine rings and on the *d*-orbitals of the metal. The negative charge built on the metal by strongly σ-donating –NH-moiety in **Pt1** destabilizes the metal $d\pi$ orbitals thus lowering the $d\pi \rightarrow \pi^*$. This is as a result of increasing electron density on either pyridine ring by conjugation with π-electrons of the pyridine rings. From the molecular point of view, **Pt1** reaction involves $5d_z^2$ orbital which is the highest occupied molecular orbital. As a consequence, this complex strongly repels the incoming nucleophile that leads to its low reactivity compared to **Pt2**. The repulsive effect is greater on d_z^2 orbitals than on the d_{xz}, d_{yz} and d_{xy} orbitals because of its orientation in the direction of the incoming ligands and is preferentially raised in energy. On the contrary the d_{xz}, d_{yz} and d_{xy} orbitals are oriented away from the incoming ligands and are lower in energy. The greater electron transfer from H^- donor to the $5d_z^2$ orbitals of the platinum centre destabilizes these orbitals than the d_{xz} and d_{yz} orbitals. This strong electron transfer to the acceptor pyridyl rings that fills $5d_z^2$ orbitals of metal centre leads to higher stabilization energy of the Pt(II) centre hence slow reactivity. Figure 3.4 shows charge distributions of the dpa ligand *verses* the coordinated metal complex. The better σ-donating H^- increases the electron density on Pt(II) atom hence leads to slow substitution rate.

The study utilized the reactivity index (electrophilicity index, ω) to measure the stabilization in energy when the system acquires an additional electronic charge from the environment.[45-51] This value supports **Pt2** (34.20 eV) to be more reactive than **Pt1** (31.15 eV) which is in line with the experimental data. This difference in the electrophilicity values between the two complexes indicates a measure of energy lowering between the ligand systems due to maximal electron flow between the donor and acceptor. For changes in ligand system the dipole moments decrease in the order **Pt2** (6.44 D) > **Pt1** (2.30 D) which further corroborates with the reactivity of the two moieties. The lower HOMO-LUMO gap, higher dipole moment of **Pt2** illustrates higher reactivity of the complex in comparison to **Pt1**. However, the dinuclear isomers show no clear dipole moment trend in relation to reactivity. The dipole moments followed the order **Pt3** (*ortho)* > **Pt4** (*meta)* > **Pt5** (*para).* This trend reflects the electron density distribution in the complexes. However, dipole forces show insignificant influence on the reactivity of dinuclear complexes. To show the charge transfer in the complexes, frontier molecular orbitals are presented in Figure 3.4.

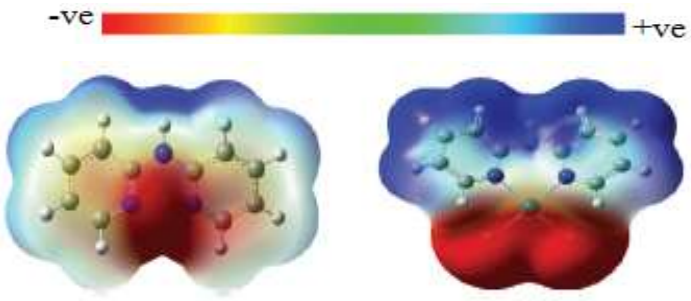

Figure 3.4: The molecular electrostatic potential surface map of the ligand dpa and the metal complex **Pt1** calculated at B3LYP/6-311G^{++} basis sets.

Figure 3.4 was used to obtain a better understanding of the electronic characteristics of the ligand dpa and its Pt(II) complex, (dpa)$PtCl_2$. The nitrogen atoms in both dpa and (dpa)$PtCl_2$ possess a negative charge, in which the pyridyl nitrogen atoms in (dpa)$PtCl_2$ complex are more negative (−0.528) than those in dpa (−0.482) owing to the coordination of the metal to the ligand. The 2,2-dipyridylamine based ligand not only provides a unique coordination platform, but it facilitates a very excellent metal ligand charge transfer mechanism as exhibited by this study.

Table 3. 2: The optimized structures of the molecular frontier orbitals of the studied complexes at B3LYP/LanL2DZ level of theory (iso value =0.02)

Complex	Planarity	HOMO Map	LUMO Map
Pt1	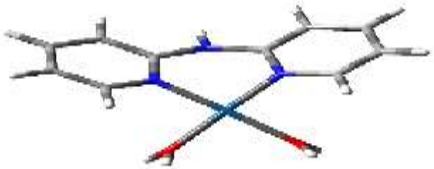		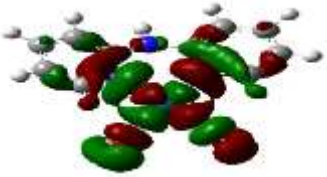
Pt2	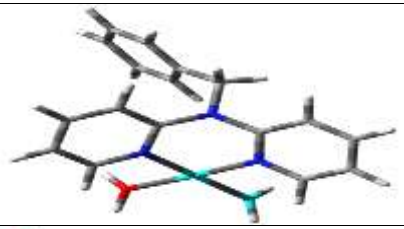		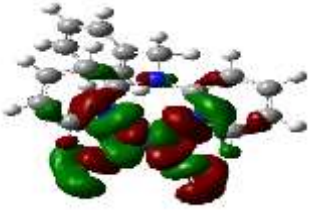
Pt3	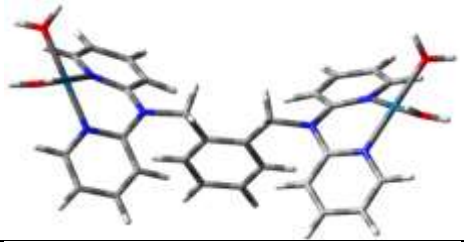	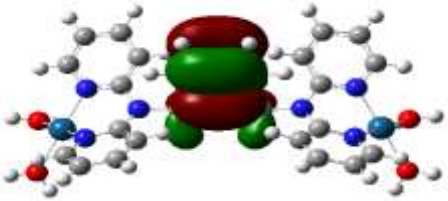	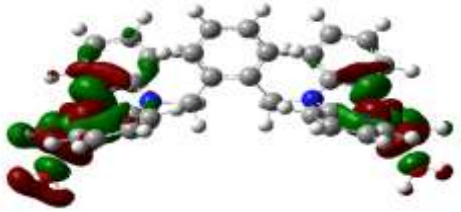
Pt4	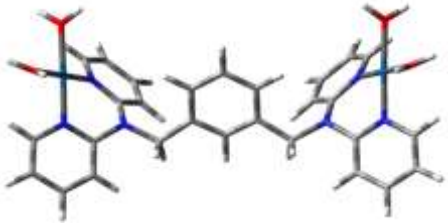	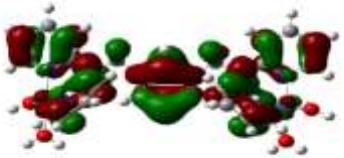	
Pt5	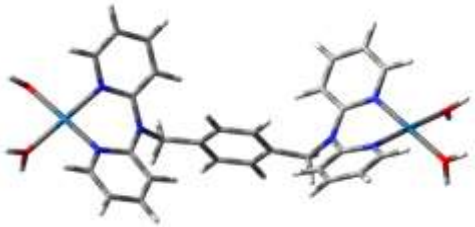	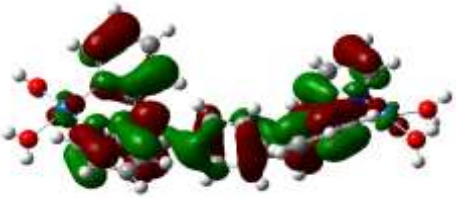	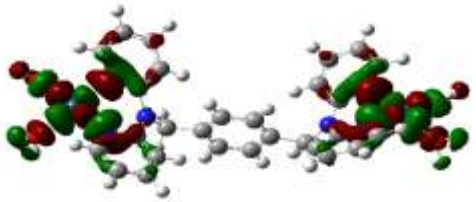

Table 3. 3: A summary of selected DFT data for the investigated complexes

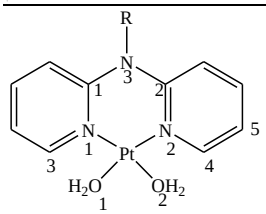

	Pt1	**Pt2**	**Pt3**	**Pt4**	**Pt5**
HOMO-LUMO energy					
LUMO/eV	-9.18	-8.77	-11.64	-11.46	-11.33
HOMO/eV	-13.20	-11.88	-15.82	-15.65	-15.53
ΔE/eV	4.02	3.11	4.18	4.19	4.20
Electrophilicity index (ω)	31.15	34.20	45.10	43.78	43.41
NBO Charges					
Pt_1	0.766	0.760	0.770	0.766	0.771
Pt_2	-	-	0.770	0.766	0.771
N_1	-0.528	-0.518	-0.520	-0.516	-0.520
N_2	-0.528	-0.520	-0.520	-0.517	-0.521
N_3	-0.634	-0.508	-0.501	-0.509	-0.505
Dipole moment (Debye)	2.30	6.44	9.04	5.78	1.78
Bond length (Å)					
C_1-N_3	1.3979	1.4112	1.4189	1.4277	1.4140
C_2-N_3	1.3979	1.4091	1.4189	1.4182	1.4134
C_1-N_1	1.3688	1.3737	1.3751	1.3758	1.3751
C_2-N_2	1.3688	1.3737	1.3751	1.3728	1.3753
Pt-N_1	2.0099	2.0042	2.0039	2.0018	2.0045
Pt-N_2	2.0099	2.0041	2.0039	2.0018	2.0046
$Pt_1 \ldots Pt_2$			11.758	12.088	13.871
Bond angles (^{o})					
$C_1N_3C_2$	127.25	120.30	122.72	118.55	123.07
Dihedral angles	39.88	50.37	43.52	50.13	44.26
Basal angle	140.12	129.63	136.48	129.87	135.74

Where R = H, benzyl

3.7.3 Kinetic measurements

The kinetics of substitution of coordinated aqua ligands were investigated spectrophotometrically using conventional UV-Vis and stopped flow techniques. A typical stopped-flow kinetic trace obtained is shown in Figure 3.5 while Figures 3.6 and 3.7 represents the typical UV-Visible spectrophotometer kinetic traces. For each reaction, the values of k_{obs} were determined at five different concentrations of nucleophile, [Nu]. The k_{obs} values were obtained from nonlinear least squares fit of the experimental data by fitting to Equation [3.2].[11]

$$A_t = A_\infty + (A_0 - A_\infty)\exp^{(-k_{obs}t)} \qquad \text{Eq [3.2]}$$

where A_0, A_t and A_∞ represent the absorbance of the reaction mixture initially, at time *t*, and at the end of the reaction respectively. The second-order rate constant, k_2, for the reaction of each metal complex was obtained from the linear regression of the plots of k_{obs} versus nucleophile concentration using origin 7.5®.[39] Straight-lines with zero or with negligible intercepts were obtained as presented in Figures 3.8 and Figures S3.1– S3.6 in the appendix. A summary of k_2 values determined at 25 °C for the two step reaction are given in Table 3.4. Since it is unlikely for the displacement of four water molecules by thiourea to follow a single kinetic phase, a biphasic reaction is proposed. The proposed mechanism of reaction can be represented by the reaction Scheme 3.3 and the corresponding rate law described by Equation [3.3].

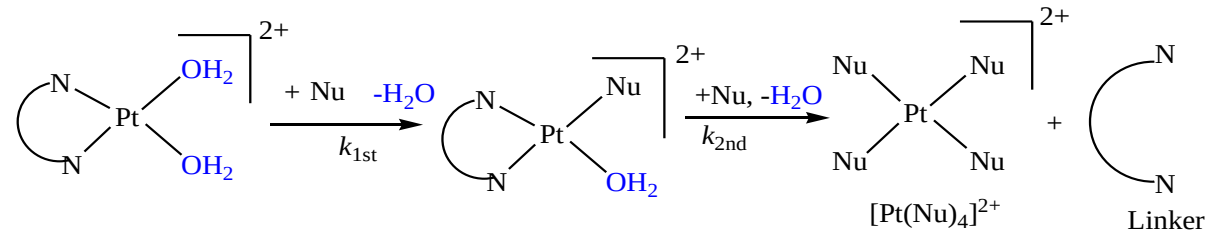

Scheme 3.3: Proposed substitution mechanism showing biphasic substitution at each Pt(II) centre followed by the dechelation process

$$k_{obs(1/2)} = k_1 + k_{2(1st/2nd)}[Nu] \approx k_{2(1st/2nd)}[Nu] \qquad \text{Eq [3.3]}$$

where k_1 = solvent path and is either zero or infinitesimal, k_2 = second-order rate constant for direct path.

The observed *pseudo*-first-order rate constant for substitution reactions occurred through biphasic reaction. This was through a fast substitution of one water molecule from each Pt(II) centre followed by a rapid susbstitution of its *trans* N atom by thiourea since sulphur atom has a strong *trans* effect. The slow phase is attributed to the substitution of the second water molecule from the metal complex followed by a rapid substitution of its *trans* position N atom. The second slow phase of aqua ligand substitution is composed of two simultaneous reactions. This second phase combines displacement of second aqua ligand with simultaneous release of the chelate N^N ligand from the metal complex, forming the final product $[Pt(thiourea)_4]^{2+}$ as supported by the NMR study. The values of $k_{2(2nd)}$ for second aqua substitution and dechelation are slower than the corresponding values of $k_{2(1st)}$ indicating that

steric factor is predominant after the first nucleophile coordination and governs the extent of second step.

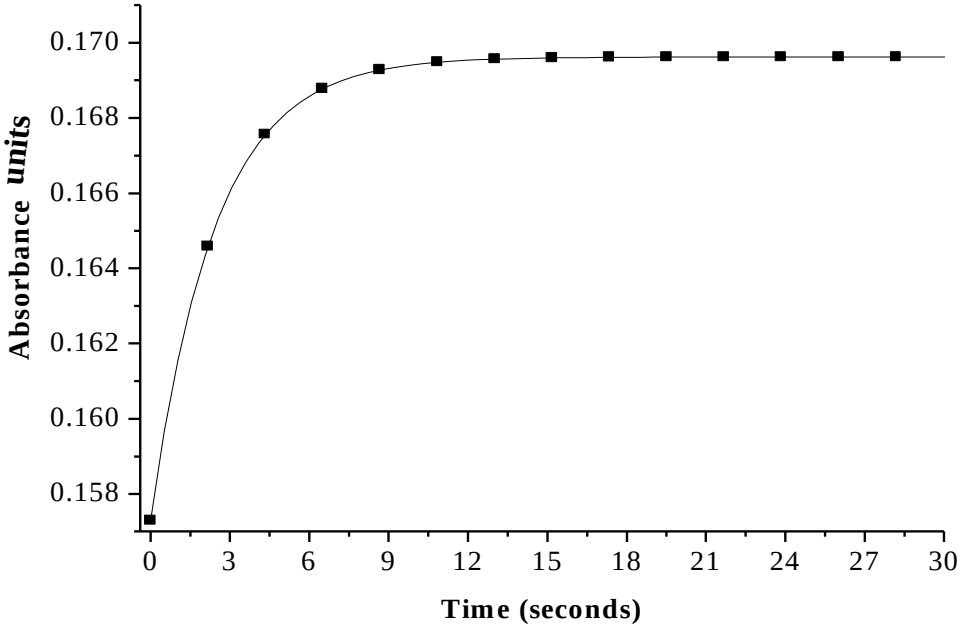

Figure 3.5: A typical kinetic trace showing a substitution step between **Pt2** and **TU** at 290 nm, T = 298 K, pH = 2.0, I = 0.1 M ($NaClO_4$) on the Stopped-flow spectrophotometer

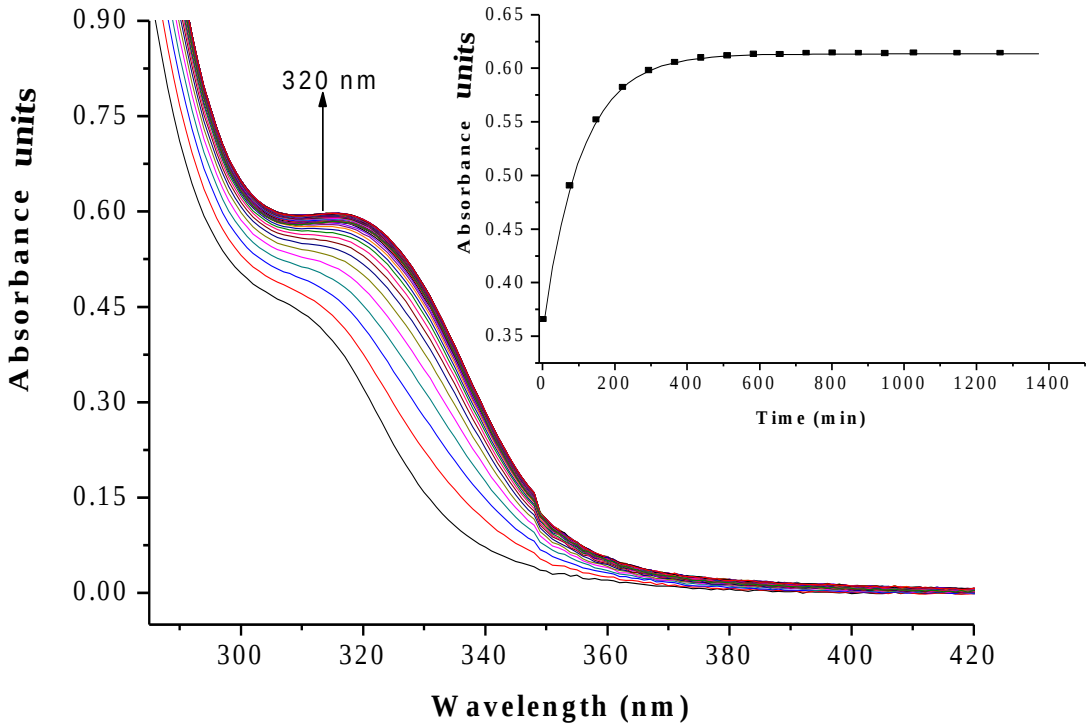

Figure 3.6: Absorbance spectra of 0.16 mM **Pt2** with excess **TU**; *inset* is typical kinetic trace on the UV-Visible spectrophotometer at 320 nm, T =298 K, pH = 2.0 and I = 0.1 M $NaClO_4$

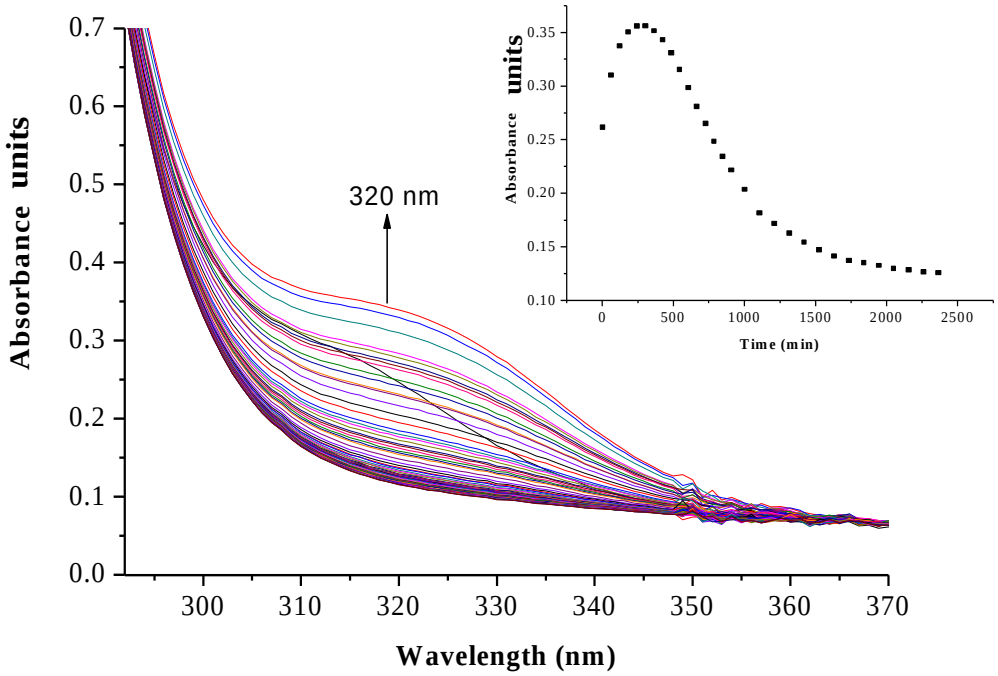

Figure 3.7: The time resolved UV/Vis absorption spectra of 0.33 mM **Pt5** with excess **TU**; *inset* is a kinetic trace for time dependence of absorbance at 320 nm showing a two-step reaction at T = 298 K, pH = 2.0 and I = 0.1 M $NaClO_4$.

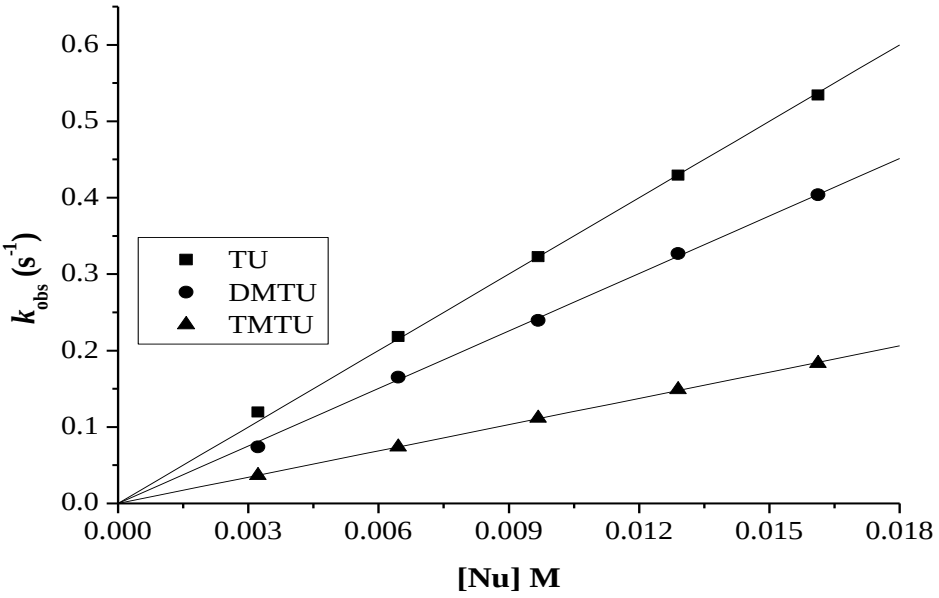

Figure 3.8: Concentration dependence of k_2 for the substitution of the simultaneous aqua ligands in **Pt2** by nucleophiles at pH =2.0, T= 298 K, I = 0.1 M $NaClO_4$.

Table 3.4: A summary of the second order rate constants, k_2, for the simultaneous substitution of aqua ligands ($k_{2(1st)}$ and the dechelation step $k_{2(2nd)}$ at pH = 2.0, T = 298 K, I = 0.1 M $NaClO_4$.

Complex	Nu	second order rate constant/$M^{-1}s^{-1}$	
		$k_{2(1st)}$	$k_{2(2nd)}$ x 10^{-3}
Pt1	**TU**	28.85 ± 0.18	20 ± 3
	DMTU	33.42 ± 0.15	10 ± 1
	TMTU	10.38 ± 0.05	10 ± 1
Pt2	**TU**	33.34 ± 0.27	30 ± 4
	DMTU	25.09 ± 0.19	10 ± 0.1
	TMTU	11.45 ± 0.04	10 ± 0.2
Pt3	**TU**	0.08 ± 0.001	1 ± 0.03
	DMTU	0.02 ± 0.001	1 ± 0.01
	TMTU	0.01 ± 0.001	1 ± 0.01
Pt4	**TU**	0.16 ± 0.004	40 ± 2
	DMTU	0.21 ± 0.003	20 ± 1
	TMTU	0.04 ± 0.002	10 ± 1
Pt5	**TU**	0.04 ± 0.001	3 ± 0.06
	DMTU	0.01 ± 0.001	1 ± 0.01

Note: **TMTU** was too slow on reaction with **Pt5** hence no data was recorded

3.8 Activation parameters

The activation parameters for the reactions were determined from the Eyring plots shown in Figure 3.9 and in the appendix (Figure S3.7 - 3.10). The corresponding values for the activation parameters of $\Delta H^{\#}$ and $\Delta S^{\#}$ are summarized in Table 3.5. These results are temperature depend and are in agreement with an associative substitution mechanism for square planar Pt(II) complexes based on the negative activation entropy values as reported in literature.[11,12,57]

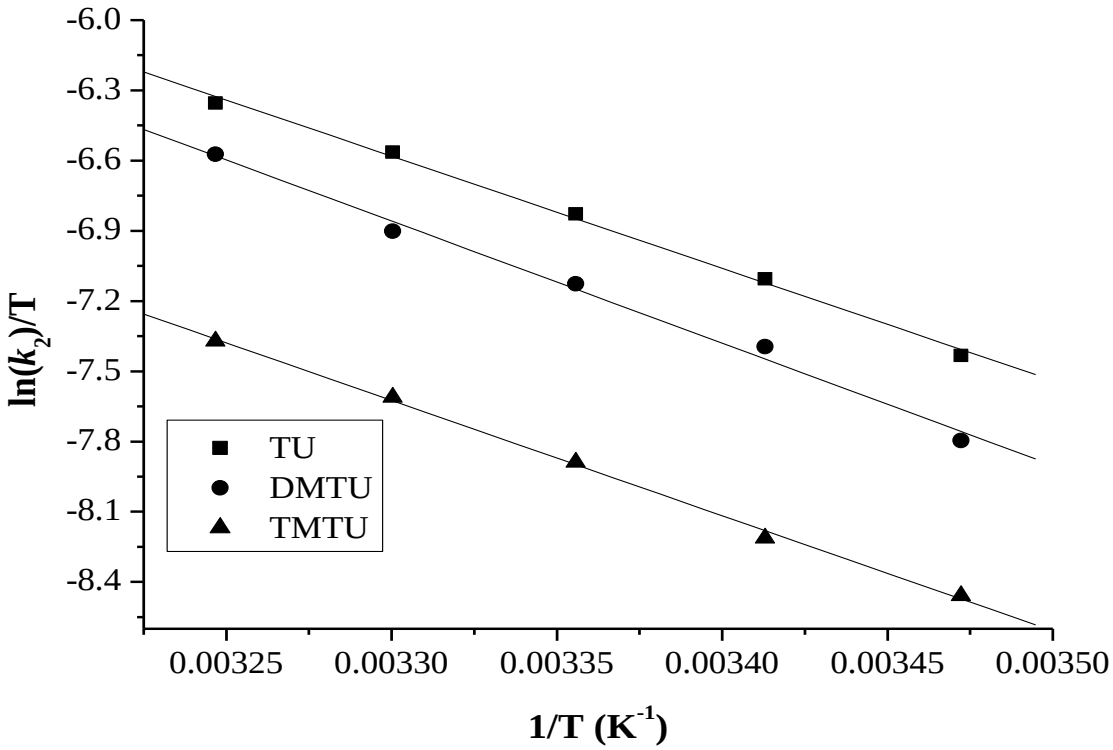

Figure 3.9: Eyring plots for the determination of the activation parameters for the aqua substitution of **Pt2** with respective nucleophiles I = 0.1 M $NaClO_4$, pH = 2.0.

Table 3.5: A summary of the activation parameters for the simultaneous substitution of aqua ligands and the dechelation step of the studied Pt(II) complexes

Complex	**Nu**	Activation Enthalpy/ $kJmol^{-1}$		Activation entropy/ $JK^{-1}mol^{-1}$	
		$\Delta H_1^{\#}$	$\Delta S_1^{\#}$	$\Delta H_2^{\#}$	$\Delta S_2^{\#}$
	TU	33.78 ± 0.6	-143 ± 2	22.27 ± 0.6	-246 ± 2
Pt1	**DMTU**	33.19 ± 1.8	-144 ± 6	22.60 ± 0.9	-254 ± 3
	TMTU	44.39 ± 1.0	-115 ± 3	60.76 ± 3.5	-112 ± 12
	TU	39.81 ± 0.3	-121 ± 1	20.54 ± 0.8	-249 ± 2
Pt2	**DMTU**	43.47 ± 1.7	-111 ± 5	26.74 ± 0.9	-241 ± 3
	TMTU	40.86 ± 0.8	-126 ± 3	41.02 ± 1.5	-179 ± 5
	TU	29.17 ± 0.5	-192 ± 2	16.78 ± 0.1	-266 ± 1
Pt3	**DMTU**	26.37 ± 0.5	-229 ± 2	12.48 ± 0.3	-291 ± 1
	TMTU	39.03 ± 0.3	-183 ± 1	20.14 ± 0.1	-255 ± 1
	TU	19.07 ± 0.3	-226 ± 1	35.31 ± 0.9	-181 ± 3
Pt4	**DMTU**	26.83 ± 0.6	-201 ± 2	27.49 ± 0.6	-221 ± 2
	TMTU	33.52 ± 0.2	-191 ± 1	31.05 ± 1.1	-209 ± 4
	TU	32.25 ± 1.4	-193 ± 4	20.63 ± 0.6	-260 ± 2
Pt5	**DMTU**	37.00 ± 0.7	-196 ± 2	32.52 ± 0.6	-225 ± 2

3.9 Substitution reaction

From the kinetic studies, the substitution proceeds via a two-step associative mechanism. The first step was attributed to simultaneous substitution of the labile aqua ligands at each platinum centre. To confirm the second step as the displacement of the ligand, substitution reaction of complex **Pt2** as a chloride with **TU** (6 equivalents) was monitored by ^{1}H NMR and ^{195}Pt NMR spectroscopy. Respectively, Figures 3.10 and 3.11 shows arrays of ^{1}H and ^{195}Pt NMR spectra for the reaction. The pyridyl protons (H_a) were monitored due to their proximity to N-donor atoms coordinated to the metal centre. The proton resonances of this unreacted chloride complex (**Pt2)** labelled H_a appear at δ = 9.05 ppm and δ = -2189.2 ppm on ^{1}H and ^{195}Pt NMR spectra respectively. During the course of reaction, these resonances shifted upfield to δ = 8.40 ppm and δ = -3889.2 ppm on ^{1}H and ^{195}Pt NMR respectively. This shift is attributed to the complexation between the metal and the ligand. This is because on coordination, the metal centre pulls electron density from the pyridyl rings causing deshielding of protons to lower field as indicated by H_a in Figure 3.10. The study shows that on coordination of the metal to the ligand, changes electron distribution within the ligand.

The peak at -2189.2 ppm on ^{195}Pt NMR spectrum is indicative that the platinum is coordinated to two nitrogen atoms[52] while the peak at -3889.2 ppm in Figure 3.11 shows the formation of $[Pt(\mathbf{TU})_4]^{2+}$ complex[22] due to the excess thiourea displacing the ligand. The formation of the $[Pt(\mathbf{TU})_4]^{2+}$ complex supports the reaction mechanism proposed in Scheme 3.3. From these observations, it can be concluded that the second step is due to the displacement of the dipyridylamine ligand due to strong *trans*-effect of sulphur on coordination of **TU** to Pt(II) centre. These results are in accordance to the previous work reported on Pt(II) complexes of the type $[L_2PtX_2]$ where X = anionic leaving group; L = ammonia, amine, pyridine.[53-55] Also studies on mononuclear dipyridylamine bidentate Pt(II) complexes appended to alkyl flexible backbone recently reported[54b] show similar behaviour of this ligand head group to undergo dechelation process.

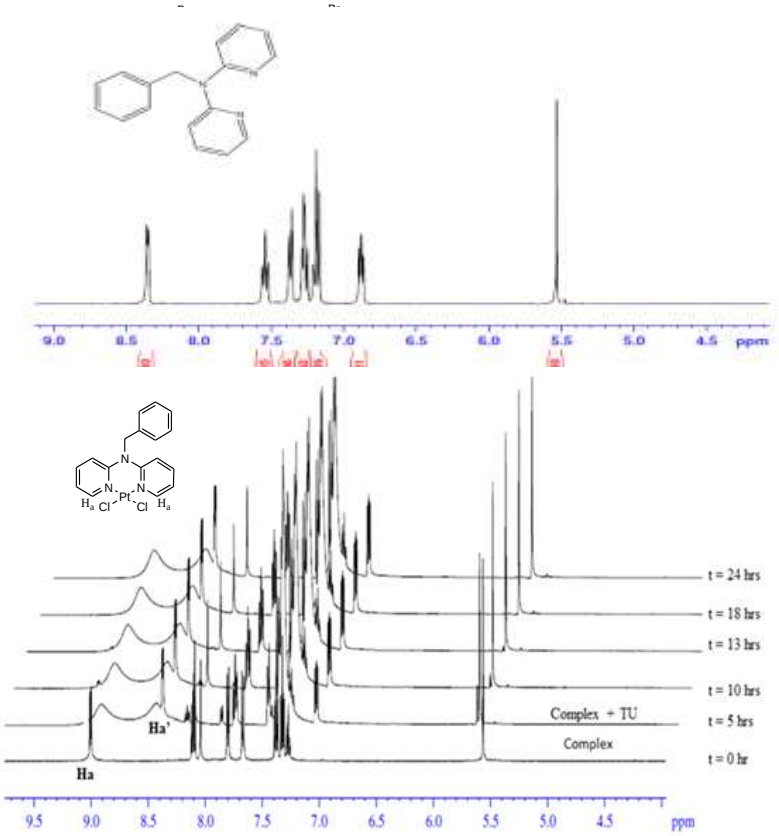

Figure 3.10: Time-dependent changes in the ^{1}H NMR spectra array of **Pt2** upon addition of 6 equivalents of **TU** in DMF-d_7. The complex undergoes dechelation to form free ligand (starting material) also shown in Figure S3.13 (Appendix).

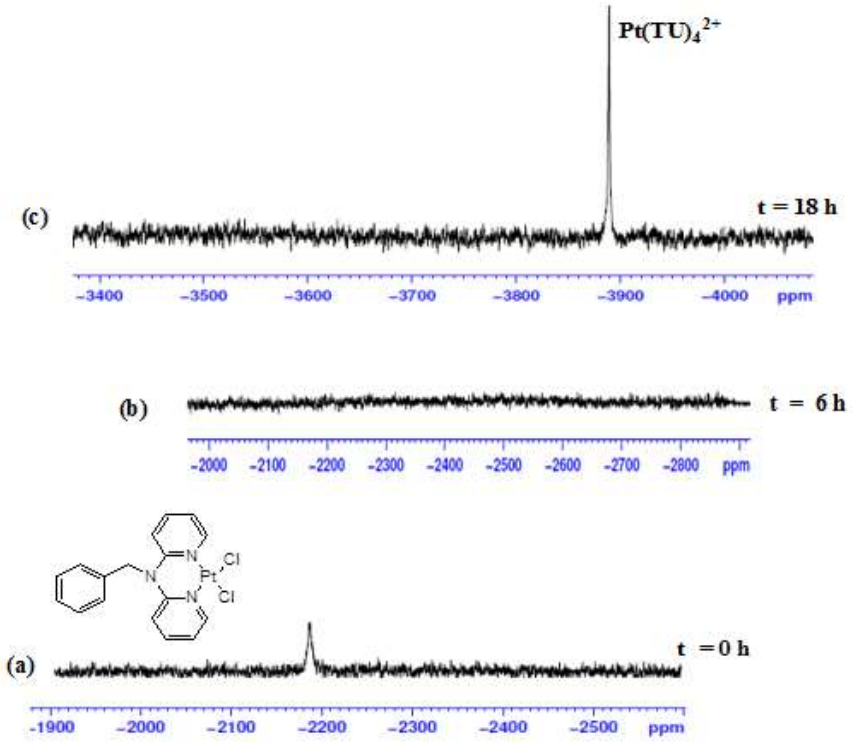

Figure 3.11: (a) Time dependent ^{195}Pt NMR chemical shift of **Pt2** in DMF-d_7 showing a peak at -2189.2 ppm. (b) Addition of 6 equivalents of **TU** leads to the disappearance of the peak at -2189.2 ppm. (c) The peak at -3889.2 ppm is attributed to the formation of $[Pt(\mathbf{TU})_4]^{2+}$ complex.

3.10 Discussion

In this chapter, the role of alkyl-phenyl moiety as a pendant and a spacer group on the reactivity Pt(II) complexes with multi-substitution of four aqua ligands with thiourea nucleophiles of different electronic and steric demands was investigated. The general reactivity in terms of $k_2$values increased in the order **Pt2** (33.34 $M^{-1}s^{-1}$) > **Pt1** (28.85 $M^{-1}s^{-1}$) > **Pt4** (0.16 $M^{-1}s^{-1}$) > **Pt3** (0.08 $M^{-1}s^{-1}$) > **Pt5** (0.04 $M\text{-}^{1}s^{-1}$) as shown in Table 3.4, with **TU** as the entering nucleophile. The observed reactivity trend is in line with the overall electrophilicity as well as steric demands of the complexes which is the controlling factor in case of dinuclear complexes. The trend in reactivity of dinuclear complexes is suggested to be interplay of inductive and resonance effects and geometrical make-up of the compounds. Coordination geometry is significantly influenced by ligand field stabilization energy as well as steric demand.

The study shows mononuclear Pt(II) complexes to react faster than their dinuclear analogues. This is in agreement with earlier report by Adnan *et al.*[56] who attributed the cause to increased amount of steric demand in dinuclear Pt(II) complexes compared to mononuclear complexes. The study suggests the "cage in-effect" due to the linker and coordination position to cause steric hindrance that reduces the rates of ligand exchange reactions in dinuclear complexes. The difference in reactivity between the two mononuclear complexes is attributed mostly attributed to the electronic effects. The slow reactivity of **Pt1** is due to the stronger σ-donor property of H^- which increases electron density around the ligand system in comparison to the $-CH_2-$ group. The study shows a strong influence of the bridging moiety on the molecular and electronic properties of the complexes.[57] This is supported by DFT data in Table 3 which shows a higher negative charge density (-0.634) on the amine nitrogen (N_3) in **Pt1** compared to **Pt2** with (-0.508). This is further supported by the electrophilicity index values and the short C_1-N_3 and C_2-N_3 bond lengths in **Pt1**compared to **Pt2**. The stronger electron donation of H^- compared to $-CH_2-$ is also evident in the HOMO-LUMO energy gap (ΔE) difference between the two complexes. It is important to note that energy gap is an important stability index. The large gap of **Pt1** (4.02 eV) compared to **Pt2** (3.11 eV) implies high stability for this complex. The net result is a system that is more electronegative in **Pt1** than in **Pt2**. In addition to the electronic effect is the entrapment of the nucleophile in the cavity created the two pyridine rings. The basal angle for **Pt1** (140.12°) is bigger than that of **Pt2** (129.63°) which means more effective collisions between the metal and the nucleophile.

Since dinuclear Pt(II) complexes as anticancer agents are expected to offer an advantage over mononuclear analogues, this study introduced a second Pt(II) centre to show comparison in reactivity with related mononuclear complex. Introduction of a second platinum centre in **Pt2** to form dinuclear Pt(II) complex leads to structural and conformational differences that influences their chemical reactivity. This difference in the three dinuclear complexes is aided by the incorporation of an aminomethyl spacer that provides greater flexibility to the complexes. This results in the twisting of complexes to form cavities of different shapes and sizes. The inorganic hybrid architectures show novel chemical and physical properties of the investigated dinuclear Pt(II) complexes.

The reactivity of the dinuclear complexes is approximately 100 times slower than the mononuclear complexes. The reactivity trend can be summed up as **Pt4** (*meta)* > **Pt3** (*ortho)* > **Pt5** (*para)* even though the reactivities are small. In these complexes, there are two types of cavities which influence the reactivity. These are the cavity due to the twisting of the two pyridine rings attached to the Pt-atoms and the cavity created due to the formation of the dinuclear complex. The first cavity is measured by determining the basal angle as shown in Figure 3.2 and values tabulated in Table 3.3. The basal angle shows **Pt4** to have the smallest angle compared to **Pt3** and **Pt5** which are comparable. One would therefore expect the cavity in **Pt4** to entrap the incoming nucleophile much better than **Pt3** and **Pt5** resulting in higher reactivity which is in agreement with the observed results. Looking at the bowl-like cavity between the two platinum centres it is noted that the $–CH_2$- and the phenyl that form the pendant attachment introduce steric hindrance at a different degree to each complex on both side of the platinum atom. For instance, the twisting of pyridyl rings in **Pt5** causes the coordinated metal ions to be maximally shielded and thus prevented from nucleophilic attack. This is very different to the mononuclear complexes that do not experience this type of steric hindrance and therefore accounting for the difference in reactivity between the two types of systems.

The shape and size of these cavities also influence the effectiveness of the entrapment of the incoming nucleophile exhibiting the difference in reactivity.[58,59] The DFT data shows that the electronic effect of all the three dinuclear complexes are very similar, suggesting that the difference in reactivity is mostly due to the structural conformation.[60] This is in agreement with previous studies[60] showing the bridging linker to confer special structural properties on the metal complexes that controls their reactivity and stability. Investigation of structural differences in dinuclear Pt(II) complexes shows steric effect of the spacer through cavities realized through changing the anchorage position which supports previous study by Mambanda and Jaganyi.[60] This study shows the dinuclear complexes to have a cage effect through adopting bowl-shaped molecular structures that controls reactivity. The decrease in the rate of substitution of dinuclear complexes is attributed to steric contributions imposed by the cavities of the complexes to varying degrees as shown by the different size and shape of cavities as shown by Figures 3.34 and 3.34 (appendix). The data obtained in this study supports the previous studies by Mambanda and Jaganyi,[60] that subtle differences in the

structural makeup of the linker can have a greater influence on the reactivity of dinuclear Pt(II) complexes.

In contrast to previous studies where metal-metal distance has an influence on the reactivity of dinuclear complexes, this chapter reports reactivity to be mainly dependent on conformational makeup and to smaller extent electronic contribution in the *ortho*, *meta* and *para* complexes to varying levels. The electronic structure calculations suggest that the geometries observed for dinuclear complexes are highly dependent on steric factors. Any small electronic preference for a particular dinuclear complex is overshadowed by steric preferences. From these results, the steric properties of the dinuclear complexes are observed to be dependent on the positions of alkyl/phenyl substituents. However, the stability of the complexes is proposed to be maximized when steric and electronic parameters reinforce each other.

The substitution of the aqua ligands by nucleophiles **TU**, **DMTU** and **TMTU** showed a clear dependence on the steric hindrance of the nucleophile. However, in **Pt1** and **Pt4, DMTU** was found to be slightly faster than **TU**; this enhanced reactivity is attributed to the inductive effect introduced by the two methyl groups on **DMTU** which over compensates the steric effect.[61] The small but positive enthalpy and large negative entropy confirm the associative mode of mechanism for all the investigated complexes. This is an indication that the mechanistic reactions of these complexes are characterized by bond formation in the transition state.[62,63] The activation parameters also imply a good degree of ligand participation in the transition state and a more compact transition state than that of the starting reactants.[64]

3.11 Conclusion

The substitution kinetics of mono and dinuclear Pt(II) complexes with 2,2'-dipyridylamine units connected by alkyl-phenyl spacer was investigated. The results shows that upon coordination of the metal atoms to the pyridyl rings of 2,2'-dipyridylamine the complex adopts inclined planes with varying dihedral and basal angles. When the two metals are joined together through a bridging ligand, the dinuclear complexes form bowl-like cavities

whose shape and size are very dependent on the position to which the phenyl moiety is joined to the complex. The study has shown that the reactivities of these complexes are controlled by steric effect which is due to the architectural framework of the complexes. The mononuclear complexes being less sterically hindered compared to the dinuclear complexes, as such are 100 times more reactive. The cavities formed due to the presence of the pyridine rings and the $–CH_2-$ and phenyl group as the linker, plays a key role in influencing the entrapment of the incoming nucleophile which in turn controls the reactivity of these complexes. These results indicate that small differences in the anchor positions can result in significant changes in reactivity through steric and electronic interactions with the substrates when they enter the substrate-binding pocket. The findings show that substitution positions affect the complex stability and thus their kinetic properties through the electronic inductive effect and the steric effect. Our findings on the anchor positions in dinuclear Pt(II) complexes can influence both steric and electronic control can form a strong base for future design of polynuclear Pt(II) anticancer agents.

The substitution behaviour of all the complexes followed a two-step substitution reaction where the first step is the displacement of one aqua ligand while the second step involves dechelation process when the second water molecule is displaced. The activation parameters confirmed the mode of mechanism to be associative in nature. The displacement of the linker following coordination of excess nucleophile to the congested platinum(II) centre suggest a possibility of instability of the system which could limit its application as an anticancer agent. The study for the first time has provided an insight into how multiple substitutions; in this case four aqua ligands are substituted by biological nucleophiles.These results suggest that tuning the geometric structure may be an effective molecular design strategy towards potent anticancer agents. The knowledge generated herein has provided a better understanding of the interactions of these Pt(II) complexes with nitrogen and sulphur containing biomolecules and is likely to assist in the development of new platinum-based anticancer agents with improved efficacy.

References

1. B. Lippert, *Cisplatin. Chemistry and Biochemistry of a Leading Anti-cancer Drug*, Wiley- VCH, Weinheim, 1999, 3-27.
2. N. Farrell, *Transition Metal Complexes as Drug and Chemotherapeutic Agents*, Kluwer Academic Publishers, Dorderecht,1989, 8-30, 46-54.
3. U. Fekl and K. I. Goldberg, *Adv. Inorg. Chem*., 2003, **54**, 260-270.
4. J. Reedijk, *Chem. Rev*., 1999, **99**, 2499-2510.
5. V. Brabec and J. Kasparkova, *Drug Resist. Updat*., 2005, **8**, 131-146.
6. E. Wong and C. M. Giandomenico, *Chem. Rev*., 1999, **99**, 2451-2466.
7. (a) D. Jaganyi, D. Reddy, J. A. Gertenbach, A. Hofmann and R. van Eldik, *J. Chem. Soc. Dalton Trans.*, 2004, **2**, 299-304. (b) D. Jaganyi, A. Hofmann and R. van Eldik, *Angew. Chem. Int. Ed.*, 2001,**40**, 1680-1683.
8. A. Hofmann, D. Jaganyi,O. Q. Munro,G. Liehr and R. van Eldik, *Inorg. Chem*., 2003, **42**, 1688-1700.
9. R. A. Henderson, *The Mechanisms of Reactions at Transition Metal Sites*, Oxford University Press, Oxford, 1993, 1-22.
10. R. G. Wilkins, *Kinetics and Mechanism of Reactions Transition Metal Complexes*, VCH, Weinheim, 2nd edn,1991, 199-201, 221-242.
11. J. D. Atwood, *Inorganic and Organometallic Reaction Mechanisms*, 1997, Wiley-VCH Inc., NY, 2nd edn. 43-61; J. D. Atwood, *Inorganic Organometallic Reaction Mechanisms*; Brook/Cole: Monterey, CA,1985, 82-83.
12. K. A. Connors, *Chemical Kinetics*: *The Study of Reaction Rates in Solution*, Wiley-VCH, New York, 1990, 1-22, 57-68, 177-180.
13. A. K. Gorle, A. J. Ammit, L. Wallace, F. R. Keene and J. G. Collins, *New J. Chem*., 2014, **38**, 4049-4059.
14. T. Boulikas, A. Pantos, E. Bellis, and P. Christofis, *Cancer Ther*. , 2007, **5**, 537-583.
15. N. J. Wheate and J. G. Collins, *Coord. Chem. Rev*., 2003, **241**, 133-145.
16. U. Olszewski and G. Hamilton, *Med. Chem*., 2010, **10**, 293-301.
17. A. A. El-Sherif, and M. M. Shoukry, *Inorg. Chim. Acta*, 2007, **360**, 473-487.
18. M. A. Barry, A. C. Behnkeand A. Eastman, *Biochem. Pharm-macol*., 1990, 4**0**, 2353-2362.
19. J. Lokich, *Cancer Invest*., 2001, **19**, 756-760.
20. S. Shibata, A. Ochi and K. Mori, *Neurol. Med. Chir*., 1990, **30**, 242-245.

21. T. Soldatović, Ž. D. Bugarčić and R. van Eldik, *Dalton Trans*., 2009, 4526-4532.
22. H. Ertürk, J. Magut, R. Puchta and R. van Eldik, *Dalton Trans*., 2008, 2759-2766.
23. M. D. Hall and T. W. Hambley, *Coord.Chem. Rev*., 2002, **232**, 49-56.
24. N. Farrell, Y. Qu, and M. P. Hacker, *J. Med. Chem.*,1990, **33**, **8**, 2179-2184.
25. N. Farrell, T. G. Appleton, Y. Qu,J. D. Roberts, A. P. Soares-Fontes, K. A. Skov, P. Wu and Y. Zou, *Biochemistry*, 1995, **34**, 15480-15486.
26. D. Jaganyi, V. M. Munisamy and D. Reddy, *Int. J. Chem. Kinet*., **38**, 202-210.
27. A. Hofmann and R. van Eldik, *J. Chem. Soc. Dalton Trans*., 2003, 2979-2985.
28. J. W. Cox, S. J. Berners-Price, M. S. Davies, W. Barlage, Y. Qu and N. Farrell, *Inorg. Chem*., 2000, **39**, 1710-1709.
29. T. Banerjee, P. Dubey, R. Mukhopadhyay, *Biochimie*, 2012, **94**, 494-502.
30. J. Malina, J. Kasparkova, N. Farrell and V. Brabec, *Nucleic Acids Research*, 2010, 1-9.
31. R. Guilard and K. M. Kadish, *Chem. Rev*., 1988, **88**, 1121-1146; D. G. Brown, P. K. Byers and A. J. Canty, *Organometallics*, 1990, **9**, 1231-35; A. J. Canty, *Acc. Chem. Res*., 1992, **25**, 83-90.
32. E. Sauvageot, R. Marion, F. Sguerra, A. Grimault, R. Daniellou, M. Hamel, S. Gaillard and J. Renaud, *Org. Chem. Front*., 2014, **1**, 639-644.
33. M. T. Ashby, *Comm. Inorg. Chem*., 1990, **10**, 297–313.
34. (a) W. E. Curtis, M. E. Muldrow, N. B. Parker, R. Barkley, S. L. Linas and J. E. Repine, *Proc. Natl. Acad. Sci.* USA, 1988, **85**, 3422-3425; (b) R. C. Sprong, C. J. M. Aarsman, J. F. L. M. van Oirschot and B. S. van Asbeck, *J. Lab. Med*., 1997, **129**, 470-481.
35. (a) M. De Agazio and M. Zacchini, *Plant Cell Environ*., 2001, **24**, 237-244; (b) K. Matsumoto, H. Aizawa, H. Inoue, H. Koto, S. Fukuyama and N. Hara, *Eur. J. Pharmacol*., 2000, **403**, 157-161.
36. A. Bianca, D. J. Bray, J. K. Clegg, K. Gloe, G. Karsten, O. Kataeva, F. L. Lindoy, J. C. McMurtrie, P. J. Steel, C. J. Sumbyand M. Wenzel, *Dalton Trans.*, 2006, 4783-4794.
37. S. Fakih, W. C. Tung, D. Eierhoff, C. Mock, and B. Krebs, *Z. Anorg. Allg. Chem.*, 2005, **631**, 1397-1402; M. J. Rauterkus, S. Fakih, C. Mock and I. P. Krebs, *Inorg. Chim Acta*, 2003, 350, 355-365.

38. (a) J. Bogojeski, Ž. D. Bugarčić, R. Puchta, and R. van Eldik, *Eur. J. Inorg. Chem.*, 2010, 5439-5445; (b) S. Jovanović, B. Petrović, D. Čanović and Ž. D. Bugarčić, *Int. J. Chem. Kinet*., 2011, **43**,99-106; (c) N. Hochreuther, S. T. Nandibewoor, R. Puchta, R. van Eldik, *Dalton Trans*., 2012, **41**, 512-522; (d) W. Summa, R. Schiessl, N. Puchta, H. van Eikema and R. van Eldik R, *Inorg. Chem*., 2006, **45**, 2948-2959.

39. V.B. Origin7.5^{TM} SRO in Origin Lab Corporation, Northampton, One, Northampton, MA, 01060, USA, 2003.

40. W. C. Schiessl, N. K. Summa, C. F. Weber, S. Gubo, C. Duecker-Benfer, R. Puchta, H. van Eikema and R. van Eldik, *Z. Anorg. Allg. Chem*., 2005, **631**, 2812-2819.

41. M. J. Frisch, G. W. Trucks, H. B. Schlegel, G. E. Scuseria, M. A. Robb, J. R. Cheeseman, G. Scalmani, V. Barone, B. Mennucci, G. A. Petersson, H. Nakatsuji, M. Caricato, X. Li, H. P. Hratchian, A. F. Izmaylov, J. Bloino, G. Zheng, J. L. Sonnenberg, M. Hada, M. Ehara, K. Toyota, R. Fukuda, J. Hasegawa, M. Ishida, T. Nakajima, Y. Honda, O. Kitao, H. Nakai, T. Vreven, J. A. Montgomery, Jr., J. E. Peralta, F. Ogliaro, M. Bearpark, J. J. Heyd, E. Brothers, K. N. Kudin, V. N. Staroverov, R. Kobayashi, J. Normand, K. Raghavachari, A. Rendell, J. C. Burant, S. S. Iyengar, J. Tomasi, M. Cossi, N. Rega, J. M. Millam, M. Klene, J. E. Knox, J. B. Cross, V. Bakken, C. Adamo, J. Jaramillo, R. Gomperts, R. E. Stratmann, O. Yazyev, A. J. Austin, R. Cammi, C. Pomelli, J. W. Ochterski, R. L. Martin, K. Morokuma, V. G. Zakrzewski, G. A. Voth, P. Salvador, J. J. Dannenberg, S. Dapprich, A. D. Daniels, O. Farkas, J. B. Foresman, J. V. Ortiz, J. Cioslowski, and D. J. Fox, Gaussian 09, Revision A.1, Gaussian, Inc., Wallingford CT, 2009.

42. (a) A. D. Becke, *J. Chem. Phys.* 1993, **98**, 1372-1384, 5648-5642. (b) C. Lee, W. Yang and R. G. Parr, *Phys. Rev. B.*,1988, **37**, 785-795; (c) P. J. Stephens, F. J. Devlin, C. F. Chabalowski and M. J. Frisch, *J. Phys. Chem*., 1994, **98**, 1623-1627; (d) B. Miehlich, A. Savin, H. Stoll and H. Preuss, *Chem. Phys. Lett.*, 1989, **157**, 200-206.

43. (a) Y. Huang, M. Zhang, L. Ye, X. Guo, C. C. Han, Y. Li and J. Hou, *J. Mater. Chem*., 2012, **22**, 5700-5705; (b) M. T Rogers, *J. Phys Chem*., Sect. A 105, 2001, 2374-2383. (c) Ž. J. Bratislav, D. M. Aleksandar, V. Željko and O. J. Ivan, *J. Serb. Chem. Soc.*, 2007, **72,** 1191-1200.

44. (a) H. Gornitzka and D. Stalke, Organometallics, 1994, **13**, 4398-4405; (b) I. M. Wekesa and D. Jaganyi, *Dalton Trans*., 2014, **43**, 2549-2558.

45. (a) R. G. Parr and W. Yang, 1989, *Density functional theory of atoms and molecules* (New York: Oxford University Press) 3-350; (b) P. K. Chattaraj and S. Giri, *Annu. Rep. Prog. Chem. Sect. C: Phys. Chem*.2009, **105**, 13-39; (c) P. K. Chattaraj, *Chemical Reactivity Theory: A Density Functional View* 2009, (Florida: Taylor & Francis/CRC Press) 109-112.

46. R. G. Pearson, *Chemical Hardness - Applications from Molecules to Solids*,1997, VCH Wiley: Weinheim. 27-63.

47. P. K. Chattaraj, *Special Issue* of *J. Chem. Sci.* on *Chemical Reactivity*, 2005, **117**, 561-571.

48. P. Geerlings, F. De Proft and W. Langenaeker, *Chem. Rev*., 2003,**103**, 1793-1873.

49. (a) R. G. Parr, L. V. Szentpaly and S. Liu, *J. Am. Chem. Soc*., 1999, **121**, 1922-1924; (b) P. K. Chattaraj, U. Sarkar and D. R. Roy, *Chem. Rev*., 2006, **106**, 2065-2091.

50. K. R. Ram and S. Soumen, *Annu. Rep. Prog. Chem., Sect. C*, 2010, **106**, 118-162.

51. (a) K. D. Sen and D. M. P. Mingos, *Structure and bonding: chemical hardness*, 1993, **80**, 103-108; (b) R. G. Parr and R. G. Pearson, *J. Am. Chem. Soc*., 1983, **105** 7512-7516; (c) R. G. Pearson, *Chemical hardness: Applications from molecules to solids*, 1997, (Weinheim: Wiley-VCH). 12-33.

52. B. M. Still, P. G. A. Kumar, J. R. Aldrich-Wright and W. S. Price, *Chem. Soc. Rev*., 2007, **36**, 665-686.

53. P. O. Ongoma and D. Jaganyi, *Dalton Trans*., 2013, **42**, 2724-2734.

54. (a) P. O. Ongoma and D. Jaganyi, *Transition Met Chem*., 2014, **39**, 407-420; (b) G. Kinunda and D. Jaganyi, *Transition Met. Chem*., 2016, **41**, 235-248. (b)

55. (a) A. A. Shoukry, *J. Chem. Sci*., 2013, 125, 643-651.

56. S. A. Adnan and K. Mika, *Curr. Med. Chem.*, 2006, **13**, 1337-1357.

57. (a) M. L. Tobe, In *Comprehensive Coordination Chemistry*; Wilkinson, G, Ed.; Pergamon Press: Oxford,U.K., 1987, **1**, 311-329. (b) F. Basolo and R. G. Pearson, *Mechanisms of Inorganic Reactions*; Wiley: New York, 1968, 299-354; (c) C. H. Langford and H. B. Gray, *Ligand Substitution Processes*; W. A. Benjamin: New York, 1965, 20-28, 43-65. (d) F. Basolo, *Coord. Chem. Re*v., 1996, **154**, 151-161.

58. D. I. Jodrell, T. R. J. Evans, W. Steward, D. Cameron, J. Prendiville, C. Aschele, C. Noberasco, M. Lind, J. Carmichael, N. Dobbs, G. Camboni, B. Gatti and F. Braud De, *Eur. J. Cancer*, **40**, 2004, 1872-1877.

59. (a) S. Sakaki, B. Biswas and M. Sugimoto, *J. Chem. Soc. Dalton Trans.,* 1997, 803-809*;* M. D. Su and S. Chu, *Inorg. Chem*., 1988, **37**, 3400-3406; (b) S. Kozuch, C. Amatore, A. Jutand and S. Shaik, O*rganometallics*, 2005, **24**, 2319-2330.

60. A. Mambanda, and D. Jaganyi, *Dalton Trans*., 2012, **41**, 908-920.

61. D. Jaganyi, F. Tiba, O. Q. Munro, B. Petrović and Ž. D. Bugarcić, *Dalton Trans*., 2006, **24**, 2943-2949.

62. H. Ertürk, A. Hofmann, R. Puchta and R. van Eldik, *Dalton Trans.*, 2007, 2295-2301.

63. A. Mandal, P. Karmakar, S. Mallick, B. K. Bera, S. Mondal, S. Ray and A. K. Ghosh, *J. Chem. Sci.*, 2012, **124**, 801-807.

64. B. K. Bera, S. Ray, S. Mondal, P. Karmakar, A. Mandal, S. Mallick and A. K. Ghosh, *J. Chem.*, 2013, **42**, 441-458.

CHAPTER 4

The effect of an alkyl chain tether on the kinetics and mechanistic behaviour of bifunctional dinuclear platinum(II) complexes bearing *N,N'* dipyridylamine ligands

4.1 Introduction

Although platinum based-drugs, such as cisplatin, oxaliplatin and carboplatin have become the mainstays of cancer chemotherapy, problems of resistance and side effects that includes severe ototoxicity neurotoxicity,[1-5] nausea, vomiting and nephrotoxicity[6,7] have limited their clinical use. This has motivated the development of other platinum anticancer drugs that are less toxic, with less cross resistance and with broader spectrum of activity.[8-10] Novel platinum(II) drugs, distinctive from cisplatin and its analogues in terms of structure and the nature of Pt-DNA adducts, are viewed to improve the biological profile of platinum anticancer agents by circumventing or complementing cisplatin specific biological processes in DNA repair. This study is in search for new multinuclear platinum(II) complexes which represent a completely new paradigm shift in the development of novel anticancer agents.[11-13]

Multinuclear complexes contain two or more platinum centres that can bind to DNA forming long range flexible and non-directional DNA adducts that induces DNA conformational changes.[14-17] This has been shown by complexes bridged by aliphatic diamines showing higher cytotoxic activity in cisplatin-resistant cell-lines.[10,12,14,18-20] This class of complexes have overcome both acquired and intrinsic resistance due to their ability to form long range DNA adducts.[9-12] The amphiphilic nature of the amine linkers, coupled with charge dispersion along their carbon backbone, results in an enhanced cellular uptake of the anticancer drug. This cytotoxic potency of these anticancer agents is strictly regulated by their electronic and structural conformations.[21,22] These characteristic variations are attributed to the coordinating ligands that connect platinum nuclei.[23-27] The best activity for such class of complexes have been reported for BBR3464, $[\{trans\text{-}PtCl(NH_3)_2\}_2(\mu\text{-}trans\text{-}Pt(NH_3)_2(H_2N(CH_2)_6NH_2)_2\}]^{4+}$, (1,0,1/t,t,t) the first trinuclear bifunctional DNA binding agent to undergo phase II clinical trials. Furthermore, it is also the first and only non-cisplatin analogue introduced into human body.[28-32] Although

multinuclear complexes have been reported to prevent tumour growth, their exact underlying molecular and kinetic mechanisms remains unexplored.

To provide information on substitution mechanisms of multinuclear Pt(II) complexes and estimate their reactivity inside the cell, determination of substitution kinetics remains vital. Furthermore, kinetic studies are of interest to shed light on complex metabolism and predict treatment response in cancer patients.[33] The current study, for the first time, is investigating the substitution reactions of tetraqua dinuclear Pt(II) complexes having [*cis*-Pt(*N,N'*)$(H_2O)_2$] molecular structure with alkyl backbone that mimic cisplatin. Similarity of such new drug candidates to cisplatin will provide insight understanding of anticancer property of Pt(II) drugs. This is also with the view that Pt(II) complexes with *cis* geometry have a higher efficacy in antitumour cell lines than those with *trans*-geometry. To obtain these complexes, a series of 2,2'-dipyridylamine chelate-appended to alkyl chain tether of variable length (n = 2 - 6) was used. The only variable was–(CH_2)n- moiety in the spacer which allowed the effect of alkyl chain on the behaviour of Pt(II) complexes with *cis*-geometry to be probed.

Five novel dinuclear Pt(II) complexes from 2,2'-dipyridylamine chelate-appended to alkyl chain *viz.*, *N,N'*-1,2-Bis(di-2-pyridylamino)ethanetetraquaplatinum(II) $[(dpa)_2\text{-en}Pt_2(H_2O)_4]^{4+}$ (**PtL2**), *N,N'*-1,3-Bis(di-2-pyridylamino)propanetetraquaplatinum(II) $[(dpa)_2\text{-prop}Pt_2(H_2O)_4]^{4+}$ (**PtL3**), *N,N'*-1,4-Bis(di-2-pyridylamino)butanetetraquaplatinum(II) $[(dpa)_2\text{-but}Pt_2(H_2O)_4)]^{4+}$ (**PtL4**), *N,N'*-1,5-Bis(di-2-pyridylamino)pentanetetraaquaplatinum(II) $[(dpa)_2\text{-pent}Pt_2(H_2O)_4)]^{4+}$ (**PtL5**), *N,N'*-1,6-Bis(di-2-pyridylamino)hexanetetraquaplatinum(II) $[(dpa)_2\text{-hex}Pt_2(H_2O)_4)]^{4+}$ (**PtL6**), were synthesized and their substitution reactions with biologically relevant nucleophiles of thiourea investigated. The mononuclear dipyridylamine complex **PtL1***, cited from literature[41b] was included for comparison purposes. Figure 4.1 shows the molecular presentation of these complexes in their aquated form. The thiourea biomolecules were of interest due to their role as chemoprotective agents.[34-37] The nucleophiles *viz* thiourea (**TU**), *N,N'*-dimethylthiourea (**DMTU**) and *N,N,N'N'*-tetramethylthiourea (**TMTU**) were chosen as representatives of the targets and competitors[38] of platinum drugs in the cellular environment. They have strong affinity towards platinum centre and good solubility. Also due to their relatively fast reactions

with Pt(II) complexes, it makes this set of nucleophiles convenient for preliminary experiments.[39-41a]

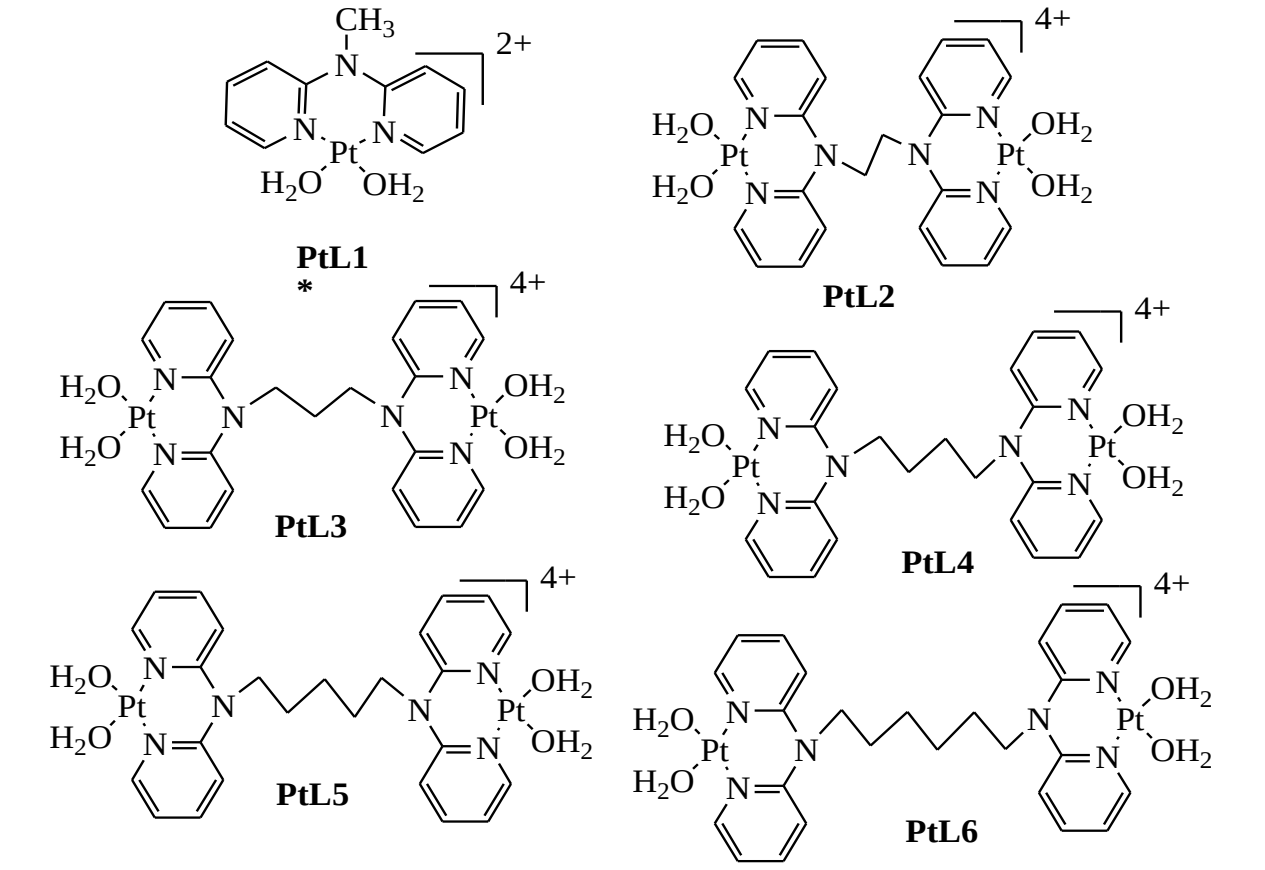

Figure 4.1: Chemical structures and abbreviations for the tetraqua Pt(II) complexes investigated

4.2 Experimental Section

4.2.1 Materials and methods

All starting materials were of analytical grade and were obtained from commercial sources and used without further purification. The nucleophiles thiourea (**TU**, 99 %), *N,N'*-dimethylthiourea (**DMTU**, 99 %) and *N,N,N'N'*-tetramethylthiourea (**TMTU**, 98 %) and the starting materials 1,2-diiodoethane, 99 %, 1,3-diiodopropane, 99 %, 1,4-diiodobutane, 99 %, 1,5-diiodopentane, 97 % and 1,6-diiodohexane, 97 %, $AgClO_4$ 99.99 % were obtained from Sigma Aldrich. K_2PtCl_4 and 2,2'-dipyridylamine (dpa) were obtained from Strem chemicals. De-ionized water from was used in all experiments.

4.2.2 Synthesis of the Ligands

N,N'-1,2-Bis(di-2-pyridylamino)ethane (**dpa**)$_2$**-en**) (**L2**), *N,N'*-1,3-Bis(di-2-pyridylamino)propane **(dpa)$_2$-prop (L3)**, *N,N'*-1,4-*N,N'*-Bis(di-2-pyridylamino)butane **(dpa)$_2$-but (L4)**, *N,N'*-1,5-Bis(di-2-pyridylamino)pentane **(dpa)$_2$-pent** (**L5**), and *N,N'*-I,6-Bis(di-2-pyridylamino)hexane **(dpa)$_2$-hex** (**L6**), were synthesized following a reported procedure by Krebs *et al*.[42] To a suspension of KOH (0.023 mol, 1.30 g) in 30 mL of DMSO was added 2,2'-dipyridylamine (dpa) (5.00 mmol, 0.856 g). The suspension was stirred at room temperature for 24 h and the respective linker of *α,ω*-iodoalkane (2.5 mmol) added drop-wise. The mixture was stirred for another 5 hours and quenched with 50 mL of water thereafter. The desired products were extracted with chloroform (4×30 mL) and the organic layer was dried over anhydrous magnesium sulphate. The solvent was removed under reduced pressure and the product recrystallized from dichloromethane/hexane mixture to obtain pure solids or oil. These ligands were characterized using ^{1}H, ^{13}C, NMR, mass spectroscopy and elemental analysis. General syntheses of the ligands is indicated in Scheme 4.1

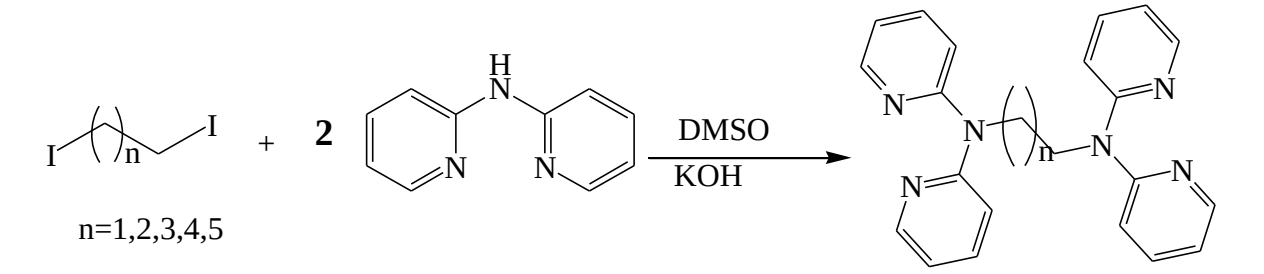

Scheme 4.1: General synthetic route for alkyl-dipyridylamine ligands

The structures of the of the synthesized alkyl-2,2'-dipyridylamine ligands prepared by the method in Scheme 4.1 are given in Scheme 4.2. Although the ligands display similar coordination chemistry, their reactivity on coordination to metal centres was controlled by the alkyl diamine spacers linking the 2,2'-dipyridylamine chelating ligand. Unlike in the previous Chapter where 2,2'-dipyridylamine was linked to an alkyl-phenyl spacer, this Chapter employed a more flexible linker alkyl chain to form ditopic ligands with aliphatic core. The ligands possess two di-2-pyridylamine subunits separated by aliphatic spacers. The synthesized ligands were reacted with two equivalents of $K_2[PtCl_4]$ precursor to yield the Pt(II) chloride complexes.

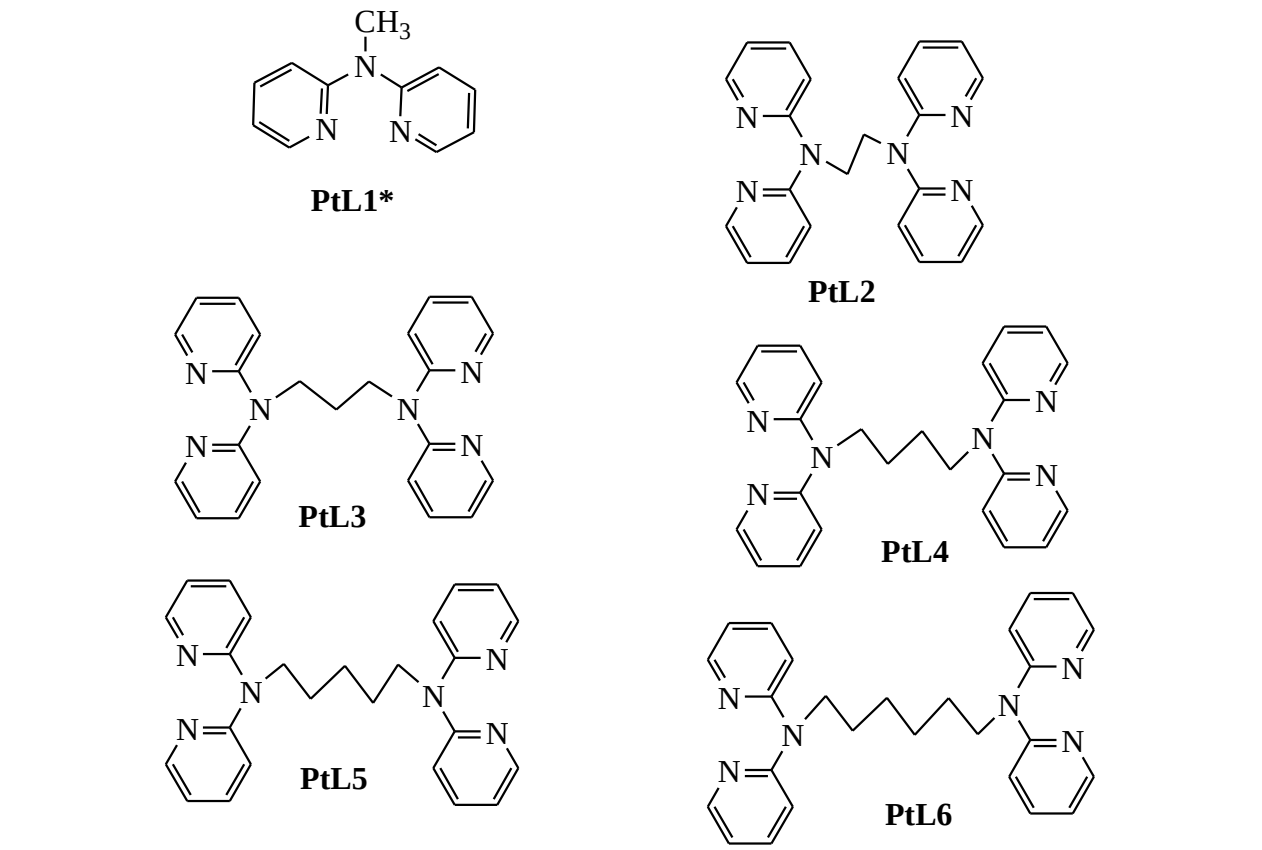

Scheme 4.2: Aliphatic chain bridging ligands coordinated to platinum atoms to form bifunctional dinuclear Pt(II) complexes

***N,N'*-1,2-Bis(di-2-pyridylamino)ethane $(dpa)_2$-en (L2),** Yield: 548.3 mg, 60 %, (white needle crystalline powder). ^{1}H NMR (400 MHz, $CDCl_3$): δ 8.26 (dd, 4H), 7.60 (dd, 4H), 7.55 (td, 4H), 6.85 (dd, 4H), 1.78 (brs, 4H). ^{13}C NMR (400 MHz, $CDCl_3$): 154.0, 147.8, 137.8, 116.4, 111.7 and 41.0. Anal. Calcd. for $C_{22}H_{20}N_6$: C 71.74, H 5.43, N 22.83; Found: C 72.12, H 5.28, N 23.18, TOF MS ES$^+$: *m/z* = $[M+H]^+$ = 369.452

***N,N'*-1,3-Bis(di-2-pyridylamino)propane $(dpa)_2$-prop (L3)**, Yield: 577.8 mg, 60 %, (yellow needle crystalline powder).^{1}H NMR (400 MHz, $CDCl_3$): δ 8.24 (dd, 4H), 7.58 (dd, 4H), 7.54 (t, 4H), 6.83(dd, 4H), 4.19(brs, 2H), 2.04 (brs, 4H). ^{13}C NMR (400 MHz, $CDCl_3$): 154.4, 148.3, 138.3, 116.9, 112.2, 41.5 and 25.8. Anal. Calcd. for $C_{23}H_{22}N_6$: C 72.25, H 5.76, N 21.99; Found: C 72.52, H 5.56, N 21.72, TOF MS ES$^+$: *m/z* = 383.1987 $[M+H]^+$.

***N,N'*-1,4-*N,N'*-Bis(di-2-pyridylamino)butane $(dpa)_2$-but (L4)**, Yield: 601.9 mg, 61 %, (yellow cubic like crystals).^{1}H NMR (400 MHz, $CDCl_3$): δ 8.30 (dd, 4H), 7.48 (dd, 4H), 7.03 (t, 4H), 6.82 (dd, 4H), 4.19 (m, 4H), 1.76 (brs, 4H). ^{13}C NMR (400 MHz, $CDCl_3$): 157.5, 148.4, 137.1, 116.9, 114.9, 48.1 and 25.8. Anal. Calcd. for $C_{24}H_{24}N_6$: C 72.73, H 6.06, N 21.21; Found: C 73.11, H 6.40, N 21.17, TOF MS ES$^+$: *m*/*z* = 419.1791 $[M+Na]^+$.

***N,N'*-1,5-Bis(di-2-pyridylamino)pentane $(dpa)_2$-pent (L5),** Yield: 628.3 mg, 61 %, (yellow oil).^{1}H NMR (400 MHz, $CDCl_3$): δ 8.18 (dd, 4H), 7.37 (dd, 4H), 6.94 (d, 4H), 6.70 (dd, 4H), 4.03 (m, 4H), 1.62 (m, 2H), 1.27 (m, 4H). ^{13}C NMR (400 MHz, $CDCl_3$): 157.4, 148.3, 137.1, 116.8, 114.6, 48.4, 28.1 and 24.6. Anal. Calcd. for $C_{25}H_{26}N_6$: C 73.17, H 6.34, N 20.49; Found: C 73.13, H 5.93, N 20.87, TOF MS ES$^+$: *m*/*z* = 411.2292 $[M+H]^+$.

***N,N'*-I,6-Bis(di-2-pyridylamino)hexane $(dpa)_2$-hex (L6)**, Yield: 653.0 mg, 63 %, (yellow oil).^{1}H NMR (400 MHz, $CDCl_3$): δ: 8.13 (dd, 4H), 7.33 (dd, 4H), 6.88 (d, 4H), 6.66 (dd, 4H), 4.25 (m, 4H), 1.49 (m, 4H), 1.40 (m, 4H). ^{13}CNMR (400 MHz, $CDCl_3$): 157.4, 148.2, 137.0, 116.8, 114.6, 48.2, 28.1 and 26.8. Anal. Calcd. for $C_{26}H_{28}N_6$: C 73.58, H 6.60, N 19.81; Found: C 73.24, H 6.34, N 20.44, TOF MS ES$^+$: *m*/*z* = 425.2441 $[M+H]^+$.

4.2.3 Preparation of the platinum(II) Complexes

The chloride forms of the Pt(II) complexes were synthesized using a general procedure reported by Krebs *et al*.[42] To a stirred solution of K_2PtCl_4 (0.5 mmol, 0.2075 g) in 50 mL of water, a solution of alkyldiamine (0.25 mmol) of the bridging spacer dissolved in 10 mL ethanol was added drop wise. The reaction mixture was then refluxed at 50 °C for 24 h. The resulting yellow precipitates was filtered off, washed with ultrapure water, ethanol and diethyl ether and dried in vacuum.

***N,N'*-1,2-Bis(di-2-pyridylamino)ethanetetrachloroplatinum(II) $[(dpa)_2$-$enPt_2(Cl_4)]$ (PtL2),** Yield: 165.5 mg, 74 %. ^{1}H NMR (400 MHz, DMSO-d_6): δ 8.77 (dd, 4H), 7.97(dd, 4H), 7.29 (dd, 4H), 7.11(ddd, 4H), 2.53 (brs, 4H). ^{13}C NMR (400 MHz, DMSO-d_6): 151.6, 151.0, 141.9, 119.6,

120.4 and 19.7. Anal. Calcd. for $C_{22}H_{20}Cl_4N_6Pt_2$: C 29.33, H 2.22, N 9.33; Found: C 29.64, H 2.81, N 9.15.

***N,N'*-1,3-Bis(di-2-pyridylamino)propanetetrachloroplatinum(II) [(dpa)$_2$-propPt$_2$(Cl$_4$)] PtL3,** Yield: 159.2 mg, 70 %. ^{1}H NMR (400 MHz, DMSO-d_6): δ 8.24 (dd, 4H), 7.58 (dd, 4H), 7.54 (t, 4H), 6.83 (dd, 4H), 4.19 (brs, 2H), 2.04 (brs, 4H). ^{13}C NMR (400 MHz, DMSO-d_6): 154.4, 148.3, 138.3, 116.9, 112.2, 41.5 and 25.8. Anal. Calcd. for $C_{23}H_{22}Cl_4N_6Pt_2$: C 30.20, H 2.41, N 9.19; Found: C 29.94, H 2.25, N 8.99.

***N,N'*-1,4-Bis(di-2-pyridylamino)butanetetrachloroplatinum(II) [(dpa)$_2$-butPt$_2$(Cl$_4$)] PtL4,** Yield: 152 mg, 66 %. ^{1}H NMR (400 MHz, DMSO-d_6): δ 8.78 (dd, 4H), 8.05 (dd, 4H), 7.51 (d, 4H), 7.24 (dd, 4H), 4.23 (brs, 4H), 1.96 (brs, 4H). ^{13}C NMR (400 MHz, DMSO-d_6): 153.9, 152.6, 142.4, 122.7, 117.9, 50.5 and 25.1. Anal. Calcd. for $C_{24}H_{24}Cl_4N_6Pt_2$: C 31.03, H 2.59, N 9.05; Found: C 30.90, H 2.76, N 8.18.

***N,N'*-1,5-Bis(di-2-pyridylamino)pentanetetrachloroplatinum(II) [(dpa)$_2$-pentPt$_2$(Cl$_4$)] PtL5,** Yield: 156.5 mg, 66 %. ^{1}H NMR (400 MHz, DMSO-d_6): δ 8.81 (dd, 4H), 8.03 (dd, 4H), 7.49 (d, 4H), 7.27 (dd, 4H), 4.16 (t, 4H), 1.91 (m, 2H), 1.72 (m, 4H). ^{13}C NMR (400 MHz, DMSO-d_6): 153.4, 151.8, 141.6, 121.9, 117.1, 50.2, 31.3 and 26.5. (Anal. Calcd. for $C_{25}H_{26}Cl_4N_6Pt_2$: C 31.85, H 2.76, N 8.92; Found: C 32.27, H 2.80, N 8.17.

***N,N'*-1,6-Bis(di-2-pyridylamino)hexanetetrachloroplatinum(II) [(dpa)$_2$-hexPt$_2$(Cl$_4$)] PtL6,** Yield: 145.7 mg, 61 %.^{1}H NMR (400 MHz, DMSO-d_6): δ 8.79 (dd, 4H), 8.06 (dd, 4H), 7.54(d, 4H), 7.26 (dd, 4H), 4.15 (br, 4H), 1.65 (m, 8H). ^{13}C NMR (400 MHz, DMSO-d_6): 154.2, 152.6, 142.4, 122.4, 118.1, 50.8, 32.1 and 28.3. Anal. Calcd. for $C_{26}H_{28}Cl_4N_6Pt_2$: C 32.63, H 2.93, N 8.79; Found: C 32.95, H 2.89, N 8.34.

4.3 Instrumentation and physical measurements

Characterization of the ligands and complexes were recorded using similar instruments and similar procedure as in Chapter three. Kinetic studies and pH of solutions were also repeated as reported by Panyako and Kinunda.[43] Various methods outlined in the previous were used to confirm the prepared ligands and complexes.

4.3.1 Preparation of solutions for kinetic analysis

Due to the low solubility of the chloride complexes (**PtL1-PtL6**) for kinetic solutions, they were converted to their aqua analogues according to literature procedure.[44-47] The solutions of the aqua complexes were prepared by reaction of a known amount of chloride Pt(II) complex with $AgClO_4$ in molar ratio of 1:3.98 respectively in 0.1 M $HClO_4$. The mixture was stirred at 40 - 50 ^oC for 48 hrs in the dark to protect it from light. After cooling the AgCl precipitate was removed by filtration through a 0.45 µm pore membrane filter. The filtrate was diluted with 0.1 M $HClO_4$ solution to final concentrations of the respective complex solutions.

4.3.2 p*K*a determination of the aqua complexes

The acidity of the aqua ligands coordinated to the metal centre was determined through pK_a titrations. NaOH was used as the base for spectrophotometric titration in the pH range 1 – 10 at 25 °C. Large volumes of the platinum aqua complex (300 mL) were used during titration to avoid absorbance corrections due to dilution. Crushed NaOH pellets were used in the pH range of 1 – 3 after which the Pasteur pipettes were used for drop wise addition of 0.5 M, 0.1 M, 0.05 M and 0.001 M of NaOH solution. After addition of the base, samples of about 500 µL were taken in ampoules and their pH recorded. After determining the pH the samples in the ampoules were discarded to avoid possible chloride ion contamination from the pH electrode. 2.0 mL solution of platinum aqua complex was placed in a cuvette in UV-Vis spectroscopy to determine absorbance as a function of pH.

4.4 Kinetic measurements

All kinetic measurements were performed under *pseudo*-first-order conditions. The nucleophile concentration was at least 40-fold excess over that of the Pt(II) complexes in all reactions. This ensured at least 10-fold of nucleophile concentration at each platinum centre hence forced the reaction to completion. Spectral changes resulting from mixing the dinuclear Pt(II) complex and nucleophile solutions were recorded over the wavelength range 200 to 800 nm to establish a suitable wavelength at which kinetic measurements could be performed. A summary of the wavelengths used for each nucleophile is found in Table S4.1 in the appendices. The temperature was controlled throughout all kinetic experiments within an accuracy of ± 0.05 ^{o}C. For the determination of the activation parameters (enthalpies and entropies) the rate of reaction was measured as a function of temperature, over a temperature range of 15 and 40 ^{o}C at intervals of 5 ^{o}C. The rate constants reported represent an average value of at least six to eight independent kinetic runs for reactions performed on the stopped flow and in triplicates for those carried out on the UV-Visible spectrophotometer. Six to eight kinetic runs ensured reproducibility that ensured a benchmark upon which the reliability of the experiment was tested. This reproducibility ensured transparency, credibility and confidence in the analysis. The k_{obs} values were obtained from nonlinear least-squares by fitting the exponential function in Equation [4.1] to the time dependent absorbance.[48a]

$$A_t = A_\infty + (A_0 - A_\infty)\exp^{(-k_{obs}t)} \qquad \text{Eq [4.1]}$$

where $A_{0,}$ A_t and A_∞ represent the absorbance of the reaction mixture initially, at time t, and at the end of the reaction, respectively. Activation parameters were determined from a linear least-square analysis of ln(k_2/T) versus 1/T using the Eyring plots.

4.5 Computational calculations

Computational calculations for parameters such as chemical potential, chemical hardness and electrophilicity indices, density functional theory (DFT) were performed as in Chapter three. The optimized structures of frontier molecular orbitals and other key geometrical data are presented in Tables 4.1 and 4.2 respectively. The dihedral and basal angles of the complexes were obtained from optimized structures of respective complexes as indicated in Figure 4.2 and values

summarized in Table 4.2. Computational calculations were used to correlate structural properties to the chemical and kinetic behaviour of the compounds.

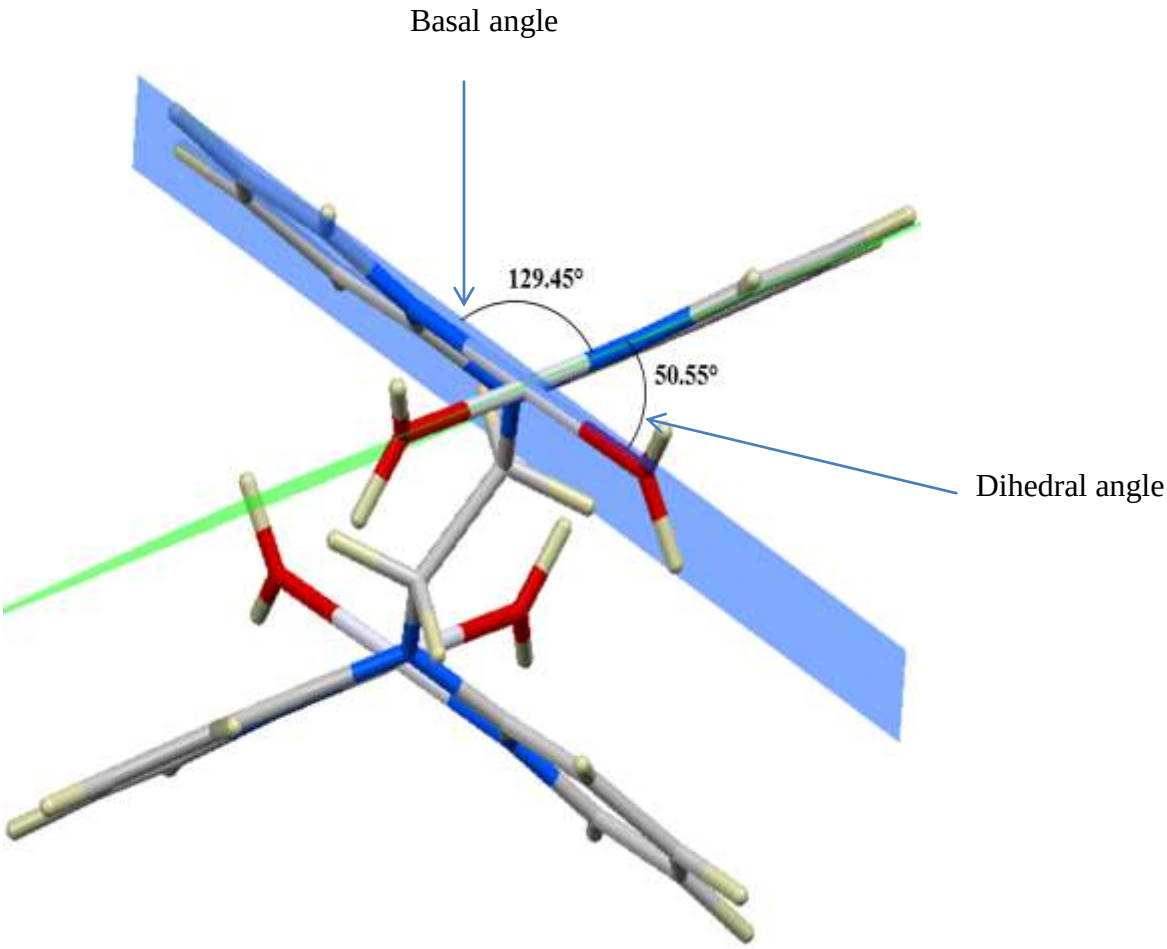

Figure 4.2: DFT-optimized structure of **PtL2** showing the dihedral and basal angles between boat conformed pyridyl groups.

The two pyridyl rings of each dpa have similar dihedral angles because of similar spatial repulsion. The values of these angles for the complexes are summarized in Table 4.1. Thus, preorganization is shown by the alkyl chain to endow conformational stability. The preorganization is achieved by the alkyl chain to impose electronic and steric effects that restrict the dipyridylamine dihedral angles. As expected a longer chain linking the two Pt centres increases distance between them and decrease hindrance. This is shown by almost similar dihedral and basal angles suggesting that increase in alkyl chain or size of these complexes

provide little steric effect in the immediate vicinity of the platinum atoms. Although there may be the possibility of "pi-stacking" forces or π-π interactions between the neighboring aromatic rings, have no significant role on the behaviour of the complexes. Almost similar dihedral angles in the complexes suggest complementary direct electrostatic interactions between polarized atoms of substituents are not a dominant factor in the repulsion of aromatic rings. Since the metal centres are in similar electronic environment of 2,2-dipyridylamine back-bone and the only variant is the alkyl bridge. Thus the study can state confidently the alkyl spacer to control both reactivity and conformations of the complexes rather than π-π interactions. Also according to electrostatic model, it is the electron withdrawing groups that enhance "π-stacking" interaction since they withdraw electrons from π bonds thus reducing electrostatic repulsion. The electron donating groups used attenuate π-π interactions[48b] thus reducing possibility of this factor in playing a major role in reactivity of the investigated complexes. The large values of ΔE in Table 4.2 are attributed to delocalization rather than to electrostatic interactions due to Pt(II) centres being in similar electronic environment. There is possibility of π-π interactions controlled by electrostatic interactions but there major energetic contribution comes from other factors. As such, the alkyl linker is proposed to be the main factor controlling the reactivity due to its electron releasing ability.

Table 4.1: DFT optimized geometrical structures of HOMO and LUMO frontier molecular orbitals of the investigated platinum(II) complexes at B3LYP/LANL2DZ level theory (Isovalue = 0.02).

Complex	Planarity	HOMO map	LUMO map
PtL2	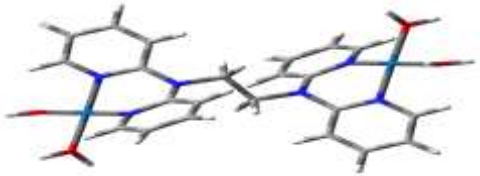	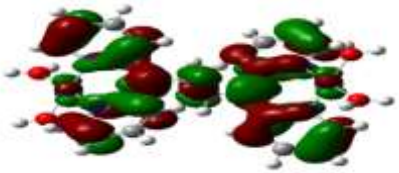	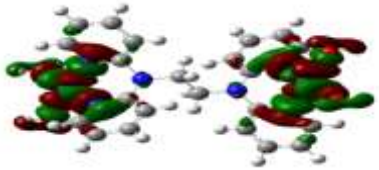
PtL3	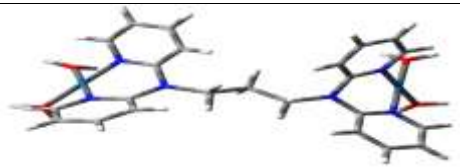	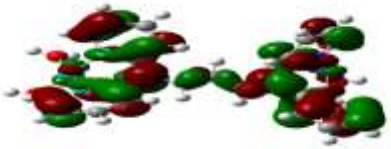	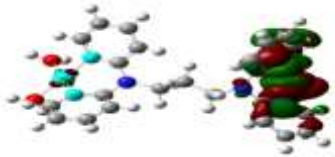
PtL4	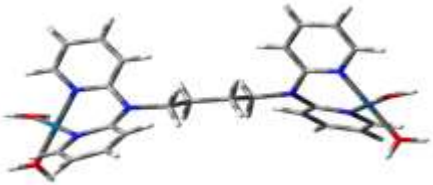	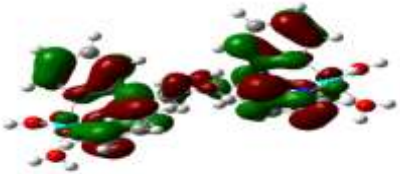	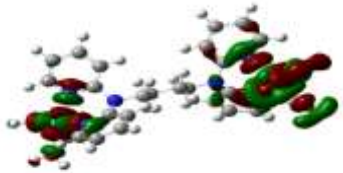
PtL5	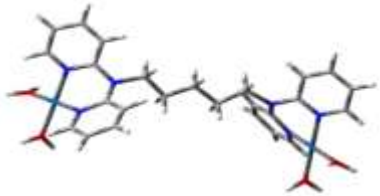		
PtL6	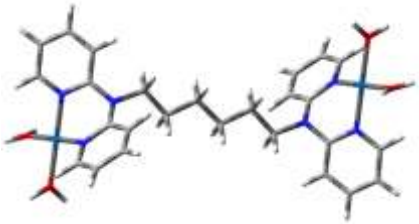		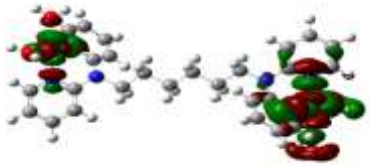

Table 4.2: Computed bond lengths and angles, natural atomic bond orbital (NBO) charges, HOMO-LUMO energy gap for the dinuclear Pt(II) complexes.

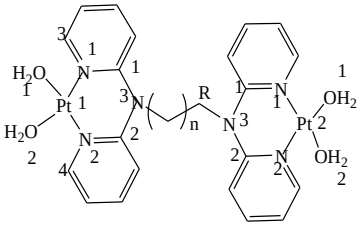

	PtL2	PtL3	PtL4	PtL5	PtL6
HOMO-LUMO energy					
LUMO/eV	-12.33	-11.99	-11.63	-11.37	-11.13
HOMO/eV	-16.66	-16.23	-15.85	-15.52	-15.26
ΔE/eV	4.34	4.24	4.22	4.15	4.13
Electrophilicity index (ω) (eV)	48.44	46.96	44.74	43.49	42.09
NBO Charges					
Pt_1	0.776	0.771	0.770	0.767	0.767
Pt_2	0.776	0.771	0.770	0.767	0.767
N_1	-0.517	-0.516	-0.518	-0.518	-0.518
N_2	-0.515	-0.516	-0.517	-0.517	-0.518
N_3	-0.536	-0.513	-0.513	-0.509	-0.509
Dipole moment (Debye)	0.5785	5.5062	3.3977	4.6459	1.3105
Bond length (Å)					
N_3-R	1.4972	1.5004	1.5043	1.5050	1.5067
Pt_1-Pt_2	9.44	9.70	11.58	12.47	14.03
Bond angles (^{o})					
Dihedral	50.55	50.47	50.28	50.06	50.30
Basal	129.45	129.53	129.72	129.94	129.70

4.6 Acidity and pK_a titrations of the aqua Pt(II) complexes

The acidity of the complexes in this study is discussed based on the first deprotonation. A typical spectrum obtained during the pH titrations is shown in Figure 4.3. Looking at the first deprotonation, the trend for the pK_{a1} values shows that acidity of the coordinated aqua ligands depends on length of the alkyl bridge between the metal centres decreasing in acidity as the alkyl chain (the distance) increases.[49-51] The pK_a values were determined from Boltzmann Equation 4.2 by fitting a characteristic sigmoid curve and locating the inflection point using the Origin 7.5® program.The pK_a values of the deprotonated complexes are summarized in Table 4.3 while the proposed deprotonation mechanism is represented in equilibrium reaction in Scheme 4.3.

$$y = A_2 + (A_1 - A_2)/(1 + \exp(x - x_0)/\partial x) \qquad \text{Eq [4.2]}$$

where A_1 and A_2 are initial and final y values respectively, x_0 = centre, ∂x = width. The y value at x_0 is half way between the two limiting values A_1 and A_2. The y value changes drastically within a range of x variable. The width of this range is approximately ∂x.

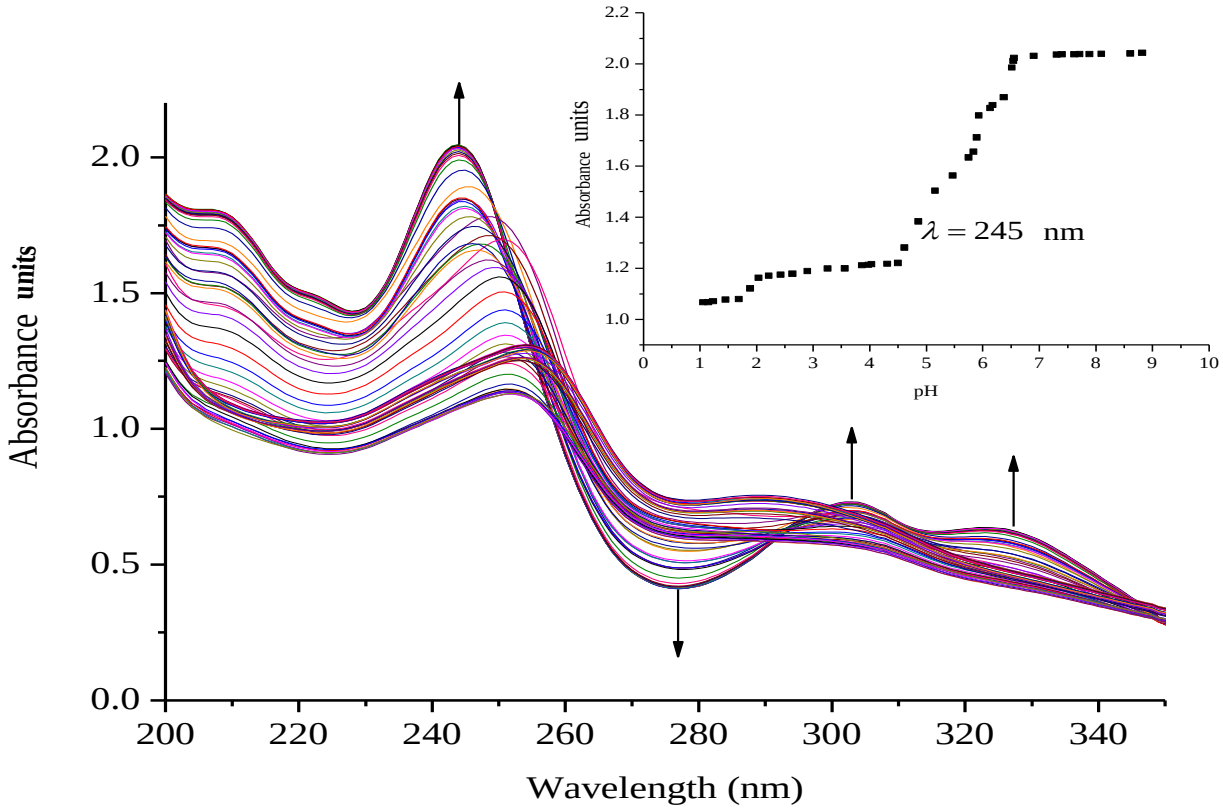

Figure 4.3: UV-Vis spectral changes for the titration of 0.05 mM **PtL2** within the pH range of 1 to 10*; Inset* shows the titration curve at λ = 245nm.

Table 4.3: pK_a values for the four stepwise deprotonation equilibrium of the tetraqua Pt(II) complexes.

Complex	PtL1*	PtL2	PtL3	PtL4	PtL5	PtL6
pK_{a1}	5.24 ± 0.07*	2.11 ± 0.01	2.27 ± 0.01	2.34 ± 0.01	2.47 ± 0.03	2.71 ± 0.06
pK_{a2}	6.19 ± 0.04*	3.74 ± 0.03	3.60 ± 0.01	3.39 ± 0.04	3.44 ± 0.03	3.49 ± 0.01
pK_{a3}	-	4.89 ± 0.04	4.58 ± 0.02	4.88 ± 0.01	4.68 ± 0.05	4.74 ± 0.04
pK_{a4}	-	6.45 ± 0.01	6.38 ± 0.01	6.53 ± 0.02	6.33 ± 0.06	7.04 ± 0.06

pK_a values for **PtL1*** were obtained from reference[41b.]

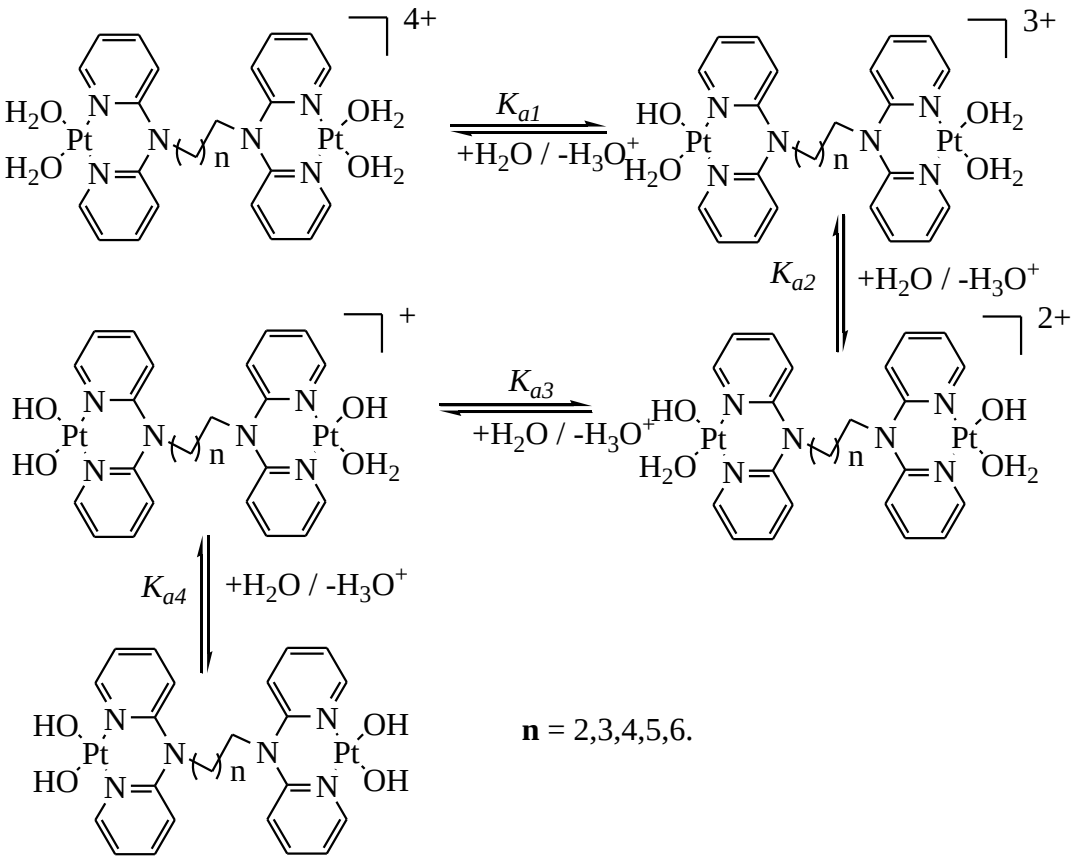

Scheme 4.3: Proposed stepwise deprotonation of the four aqua ligands on dinuclear Pt(II) complexes.

The difference in the acidity of dinuclear complexes is attributed to the metal-metal distance through charge addition and also to the inductive effects of the alkyl chain. Complexes with shorter distances between the platinum(II) centres undergo addition of single charges that enhances electrophilic and acidity due to close proximity of Pt^{2+} ions.[52,53] The mutual charge addition of each Pt(II) centre becomes weaker as the distance between the metal centres becomes longer as shown by the current study. This is evident from the pK_{a1} trend in the acidity of the complexes **PtL2** > **PtL3** > **PtL4** > **PtL5** > **PtL6**. The electronic effect of alkyl group on the pyridine rings is suggested to increase electron density on pyridine nitrogen atoms making them stronger donors. The strength of inductive effect is dependent on length of alkyl chain. The trend shows the longer alkyl chain to stabilize the platinum centres due to their increased inductive effect which is also supported by the slight increase in bond lengths N_3-R across the homologous series as shown in Table 2. As a result, the aqua ligands become more basic hence high pK_a

values. An increase in electron density around the platinum atom leads to a stronger σ bond and increased intrinsic basicity of the complexes. This increased inductive effect of alkyl moieties enhances negative charge around platinum centres that results in their stability. This study shows that the strength of the σ bond is related to the pK_{a1} values of the deprotonated aqua ligands. In addition the study shows dinuclear complexes to be more acidic than the mononuclear. This difference is attributed to the difference in the overall charge of the complexes which is +2 for the mononuclear and +4 for the dinuclear complexes. Coordination of a second Pt(II) atom results in addition of charges that make the dinuclear platinum complexes more electrophilic thus favouring aqua deprotonation. Because of the overall charge of +4 on the dinuclear Pt(II) complexes the aqua ligands are more acidic compared to the reference mononuclear complex **PtL1***.

The stability of these complexes is due to each metal centre possessing a delocalized electronic structure with boat conformation.[42] This makes the Pt centres to be in a conjugated six membered ring that causes the electron density to be delocalized into the ring hence shielding of alkyl protons. The inductive effect of the alkyl group is reported to be transmitted to the Pt(II) centres *via* the lone pair on nitrogen being delocalized over the amide group. The lone pair of electrons on nitrogen atom affects cross conjugation of the complexes. As such the NBO charges on Pt centres do not change significantly since the surrounding environment has identical atomic and conjugative connectivity.[54a] From such complexes, the NBO charge on the metal is not readily quantified due to being in a delocalized system.[54b] Due to chelation, the metal ions with positive charge in the complexes are stabilized through resonance. This behaviour is supported by the raising of frontier orbitals in Table 4.1. The positively charged Pt^{2+} ion becomes stabilized as the alkyl chain increases indicating increased inductive effect as the alkyl chain length increases.[55,56] This observation is in agreement with the negative charge being stabilized as one moves from $sp^3 \rightarrow sp^2$ closer to positively charged nucleus. This is also supported by the general decrease in electrophilicity index across the complexes as the alkyl chain increases. The results also show the subsequent pK_a values to increase with subsequent deprotonation; this observation is attributed to the lowering of the overall charge from +4 to +1. This decrease in the overall charge decreases the electrophilicity and the acidity of the metal centres making it more difficult to

deprotonate the consequent coordinated aqua ligand due to formation of hydroxo species. The pK_a studies show that the complexes undergo four stepwise deprotonation an observation reported in our first study and also previous investigation by van Eldik *et al*.[57]

4.7 Kinetic results

The substitution kinetics of the coordinated aqua ligands in the complexes was followed spectrophotometrically by the change in the absorbance at suitable wavelengths as a function of nucleophile concentration and time. Figures 4.4 and 4.5 show typical spectral changes for the slow reaction steps of complexes with odd and even number of carbons in the alkyl chain (**PtL3**) and (**PtL6**) respectively. The *inset* in the spectra is a kinetic trace of time dependence of the absorbance at a particular wavelength from which the *pseudo*-first-order rate constants k_{obs} were obtained by fitting single exponential function.

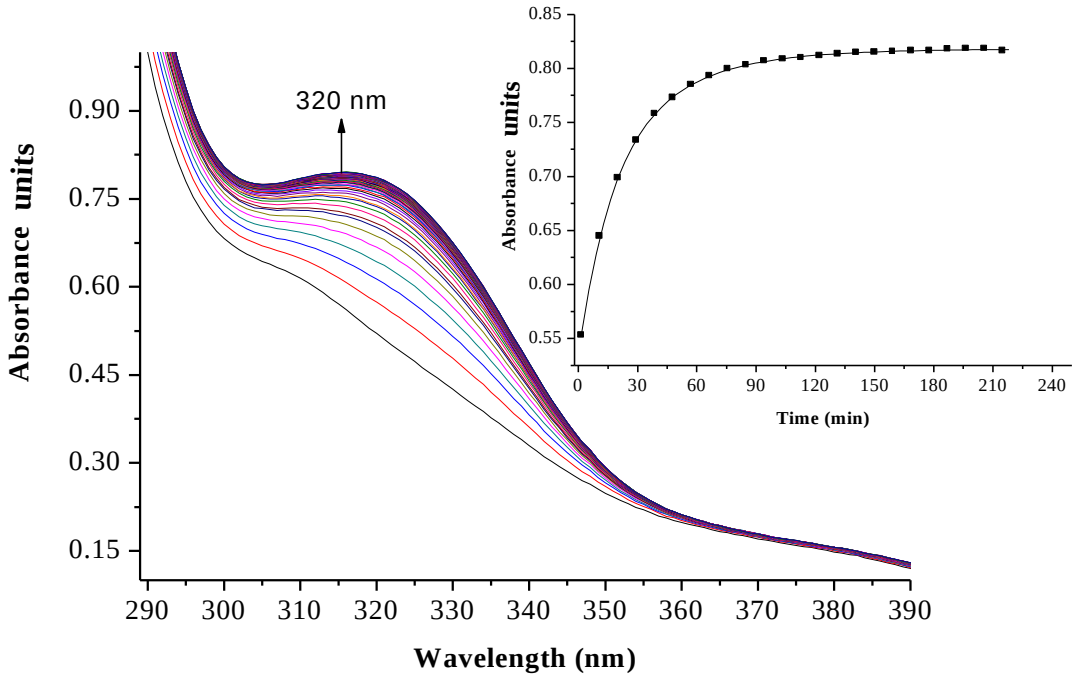

Figure 4. 4: UV-Vis spectral changes observed during the reaction between 0.34 mM **PtL3** with 0.068 M **TU**; *inset* is a typical kinetic trace at 320 nm, T = 298 K, pH = 2.0 and I = 0.1 M $NaClO_4$.

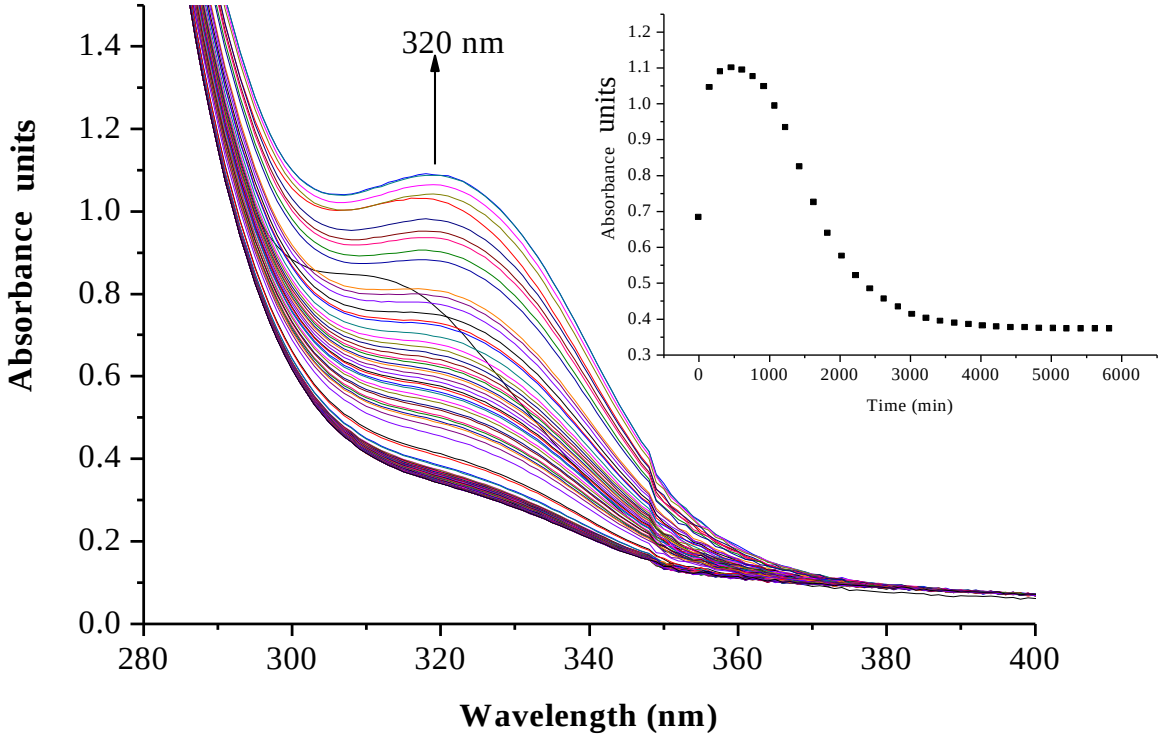

Figure 4.5: UV-Vis spectral changes observed during the reaction between 0.34 mM **PtL6** with 0.068 M **TU**; *inset* is a typical kinetic trace for time dependence of absorbance at 320 nm, T = 298 K, pH = 2.0 and I = 0.1 M $NaClO_4$.

Plots of k_{obs} against nucleophile concentrations resulted in a linear dependence second-order rate constants, k_2 with no significant intercepts as shown in Figures 4.6, 4.7 and S4.1-S4.3 in the Appendix. The summary of the second order rate constants are shown in Table 4.4. Based on this observation, Equation [4.3] presents the corresponding rate laws for the consecutive reaction steps.

$$k_{obs(1,2,3)} = k_1 + k_2[Nu] \approx k_2[Nu] \qquad \text{Eq [4.3]}$$

where k_1 = rate constant for solvent path and k_2 = rate constant for direct path, [Nu] = nucleophile concentration. The contribution of the solvent through the solvolytic path (k_1) is negligible or absent. The values of k_2 obtain from the linear regression analysis from Equations 4.2 and 4.3 are summarized in Table 4.4.

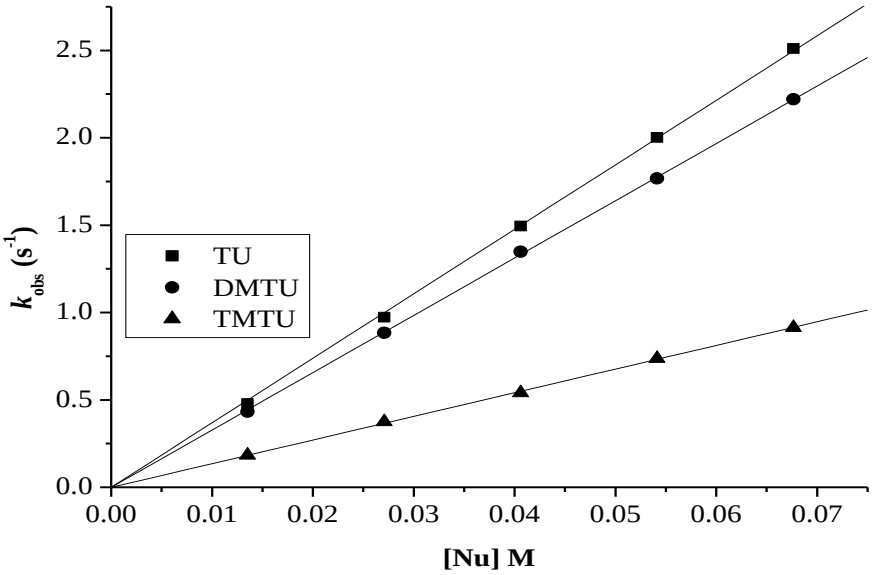

Figure 4.6: Plots of $k_{obs(1)}$ versus nucleophile concentration for the reaction of **PtL2** at pH = 2.0, T = 298K, I = 0.1 M $NaClO_4$.

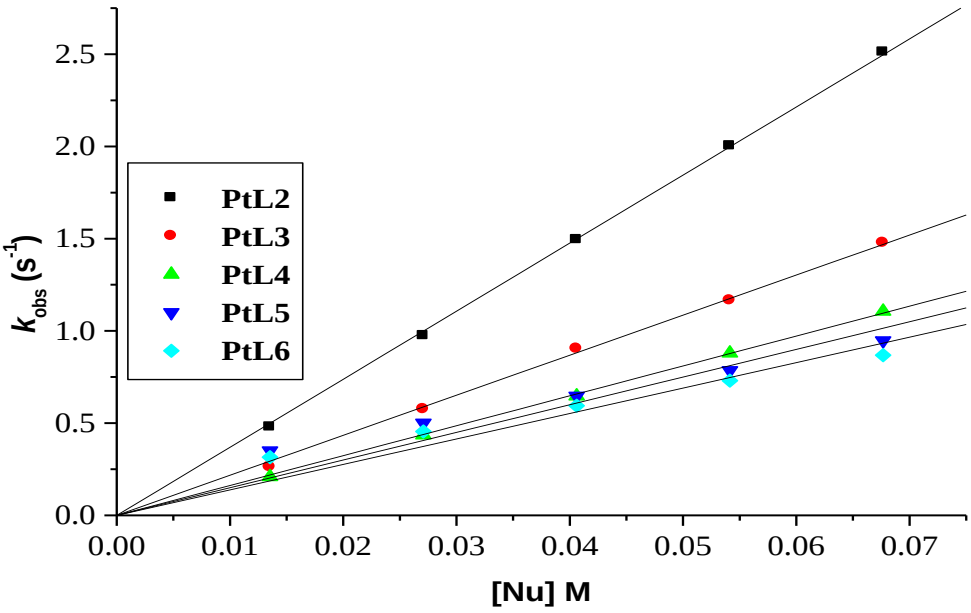

Figure 4.7: Plots of $k_{obs(1)}$ versus thiourea concentration for the reaction of the dinuclear platinum(II) complexes at pH = 2.0, T = 298K, I = 0.1 M $NaClO_4$.

Table 4.4: A summary of the second order rate constants, $k_{obs(1,2,3)}$, for displacement of coordinated aqua ligands and the chelation step at pH = 2.0, T = 298K, I = 0.1 M $NaClO_4$

Complex	Nu	Second-order rate constant/$M^{-1}s^{-1}$		
		$k_{2(1st)}$	$k_{2(2nd)}$ x10^{-2}	$k_{2(3rd)}$ x10^{-3}
PtL1*	**TU**	38.70 ± 0.60	106 ± 3	-
	DMTU	48.80 ± 0.50	2 ± 0.1	
	TMTU	22.80 ± 0.40	-	
PtL2	**TU**	36.90 ± 0.18	4 ± 0.2	-
	DMTU	32.79 ± 0.11	7 ± 0.1	-
	TMTU	13.53 ± 0.06	1 ± 0.1	-
PtL3	**TU**	21.71 ± 0.22	7 ± 0.1	-
	DMTU	17.43 ± 0.18	3 ± 0.1	-
	TMTU	9.71 ± 0.16	3 ± 0.1	-
PtL4	**TU**	16.20 ± 0.10	11 ± 0.6	5 ± 0.09
	DMTU	13.57 ± 0.02	6 ± 0.1	3 ± 0.03
	TMTU	7.04 ± 0.08	4 ± 0.06	too slow
PtL5	**TU**	10.92 ± 0.14	5 ± 0.02	-
	DMTU	13.45 ± 0.24	3 ± 0.05	-
	TMTU	6.28 ± 0.04	0.8 ± 0.01	-
PtL6	**TU**	10.21 ± 0.03	8 ± 0.09	0.5 ± 0.02
	DMTU	12.60 ± 0.23	3 ± 0.04	0.7 ± 0.02
	TMTU	5.10 ± 0.04	2 ± 0.04	too slow

Data for **PtL1*** extracted from the work by Jaganyi and Kinunda.[41b]

4.8 Activation parameters

The values of activation parameters $\Delta H^{\#}$ and $\Delta S^{\#}$ were calculated from Eyring plots Figures 4.8, 4.9 and Figures S4.4-S4.7 in the appendix using Eq [3.1] in the previous Chapter. They were determined from the temperature dependence of rate constant. The data obtained for activation parameters is given in Table 4.5.

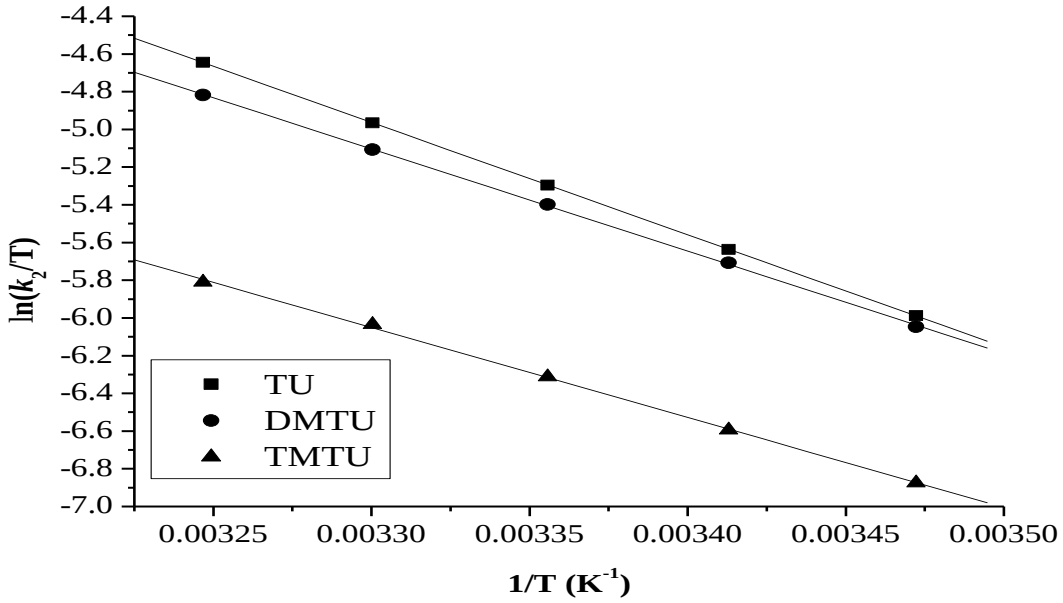

Figure 4.8: Eyring plots for first substitution step of **PtL2** with different nucleophiles at pH = 2.0, I = 0.1 M $NaClO_4$.

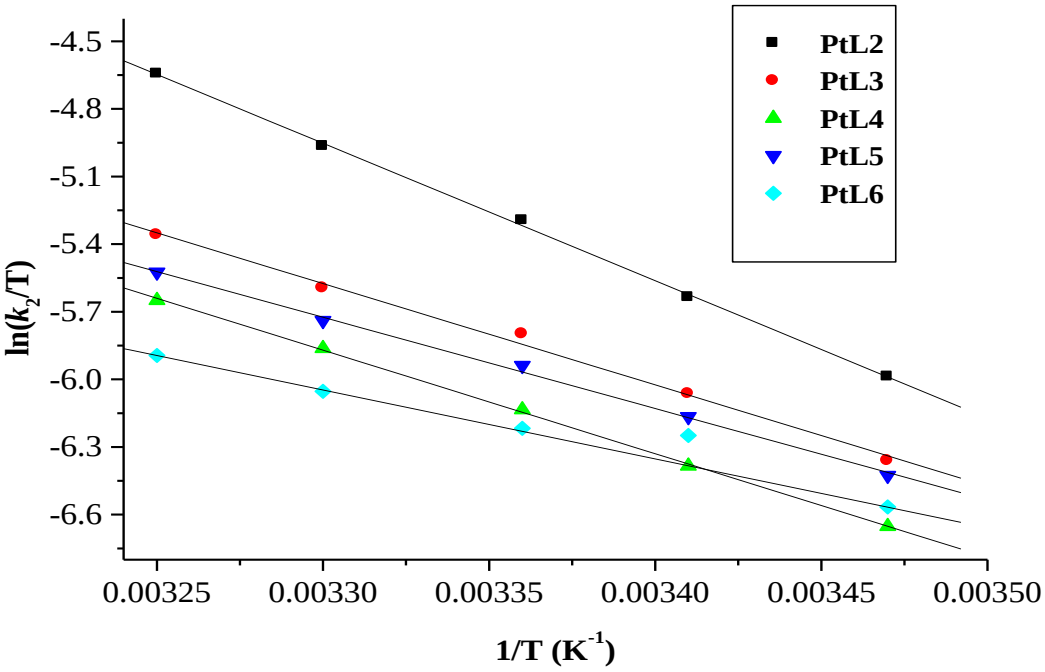

Figure 4.9: Eyring plots for first substitution step of dinuclear platinum(II) complexes with thiourea at pH = 2.0, I = 0.1 M $NaClO_4$

Table 4.5: Activation parameters for the substitution of aqua ligands by nucleophiles and dissociation of the bridging linker

Complex	Nu	Activation Enthalpy/ kJmol^{-1}			Activation entropy/ J mol^{-1}K^{-1}		
		$\Delta H_1^{\#}$	$\Delta H_2^{\#}$	$\Delta H_3^{\#}$	$\Delta S_1^{\#}$	$\Delta S_2^{\#}$	$\Delta S_3^{\#}$
PtL2	**TU**	49.53 ± 0.1	24.41 ± 0.3	-	-76 ± 1	-226 ± 1	-
	DMTU	45.09 ± 0.4	32.52 ± 0.3	-	-92 ± 1	-206 ± 1	-
	TMTU	39.69 ± 0.6	46.12 ± 1.6	-	-117 ± 2	-155 ± 5	-
PtL3	**TU**	36.53 ± 1.1	23.05 ± 0.1	-	-123 ± 4	-219 ± 1	-
	DMTU	21.01 ± 0.5	40.08 ± 0.5	-	-177 ± 2	-170 ± 2	-
	TMTU	47.39 ± 0.7	37.21 ± 0.6	-	-94 ± 2	-180 ± 2	-
PtL4	**TU**	37.30 ± 0.6	23.37 ± 0.3	24.16 ± 0.9	-124 ± 2	-218 ± 1	-232 ± 3
	DMTU	39.60 ± 0.4	29.70 ± 0.3	29.57 ± 1.2	-117 ± 1	-205 ± 1	-220 ± 4
	TMTU	39.58 ± 0.5	29.40 ± 1.1	-	-125 ± 2	-201 ± 4	-
PtL5	**TU**	32.90 ± 0.6	44.62 ± 0.5	-	-137 ± 2	-149 ± 2	-
	DMTU	49.54 ± 1.1	46.61 ± 0.8	-	-82 ± 4	-146 ± 3	-
	TMTU	48.93 ± 0.3	30.65 ± 0.4	-	-92 ± 1	-208 ± 1	-
PtL6	**TU**	24.74 ± 0.2	30.26 ± 0.4	11.55 ± 0.1	-167± 1	-194 ± 1	-293 ± 0.1
	DMTU	18.44 ± 0.1	27.02 ± 0.2	22.51 ± 0.3	-189 ± 0.4	-211 ± 1	-255 ± 1
	TMTU	71.15 ± 1.4	43.57 ± 0.5	-	-19 ± 5	-153 ± 2	-

The small but positive $\Delta H^{\#}$ and large negative values of $\Delta S^{\#}$ supports an associative mechanism. The low enthalpy values are attributed to bond formation and participation of the entering ligand in the transition state. The large negative values of entropies signify a more compact transition state than that of the reactants.[58]

4.9 Substitution reaction

The displacement reactions involving these complexes lead to two types of behaviour that is dependent on the "odd or even" effect of methylene groups in the aliphatic chain.[59-61] Except for **PtL2**, complexes with even number of methylene groups [n = 4, 6], (**PtL4** and **PtL6**), have *anti*-conformation (Figure S4.32) and show three kinetic steps in their reactions while those with odd groups [n = 3, 5], (**PtL3** and **PtL5**) show *syn* conformation with two reaction steps. These conformations are in agreement with observation by Albrecht and other groups who also observed the odd-even effect.[62] As such different substitution behaviour is expected due to different architectural framework. The *syn* conformation restricts Pt(II) centres in the same plane making them kinetically equivalent. This equivalency at Pt(II) centres results in simultaneous substitution at the two metal centres as shown by this study. The second slow step is governed by steric hindrance of the first nucleophile coordination and is joined by a dechelation process. The study shows the displacement of the labilized amine spacer from two Pt(II) ions to occur concurrently. Similar behaviour of a single kinetic step release of two metal ions from the spacer in dinuclear complexes has also been reported by Basollote *et al*.[63]

However, in the *anti*-conformational configuration, the study proposes first step to fast substitution of water molecule at each Pt(II) centre followed by a slow displacement of second water molecule that involves the stepwise displacement of labilized alkyl spacer as a result of the strong *trans* effect of thiourea ligands.However, **PtL2** showed two reaction steps instead of the expected three steps due to its ability to exhibit either *syn*- or *anti*-conformations (Scheme 4.4). This is partly attributed to its ability to interconvert by rotations around the single bond by approximately $6\times10^{9}s^{-1}$ at 25 °C[64] and also due to the shorter spacer between the two Pt(II) centres. Due to the proximity of the metal centres, the study suggests a single kinetic step to release the two metal centres from the spacer.

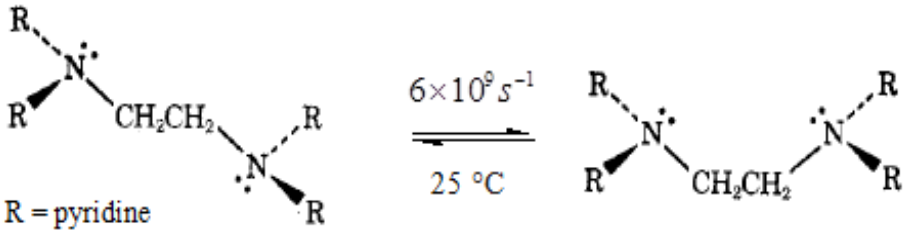

Trans (*anti*-)-conformer *Gauche (syn-)*-conformer

Scheme 4.4: Possible conformational shifts of **PtL1**as either *trans* or *gauche* conformation[64].

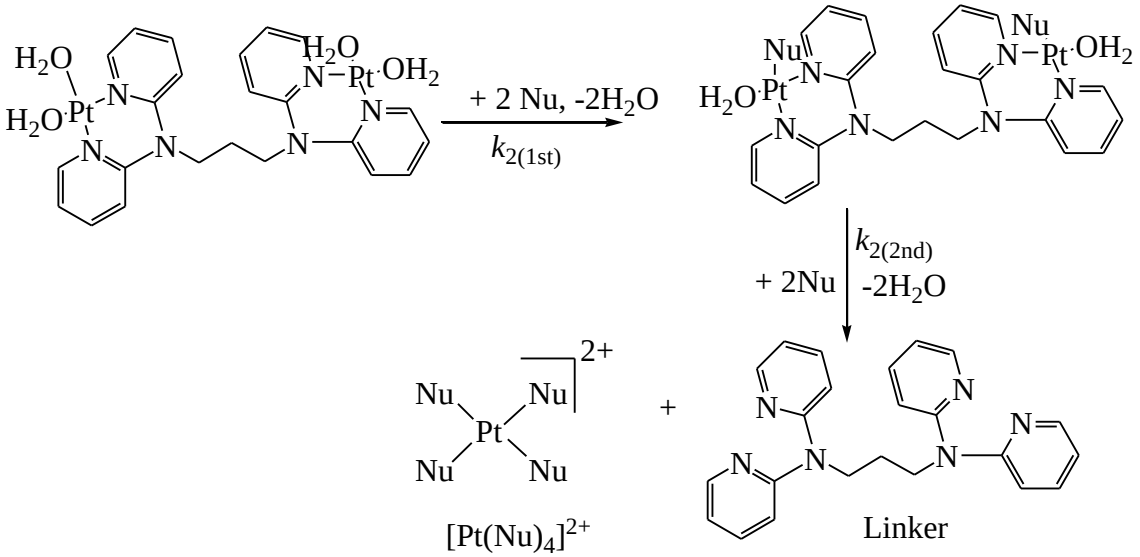

Scheme 4.5: Proposed substitution mechanism for odd numbered alkyl chain (n = 3, 5). Note: even numbered alkyl chain (n = 4, 6) shows three steps due to stepwise displacement of the alkyl diamine linker.

To show that the complexes undergo a dechelation process, substitution reaction of the chloride complexes with 6 equivalents of **TU** was carried out. The reaction products were analyzed using ^{1}H and ^{195}Pt NMR spectroscopic. The ^{195}Pt NMR of **PtL6** in DMSO-d_6 at -2175 ppm was indicative that the platinum centres were coordinated to two nitrogen atoms (PtN_2Cl_2).[65] Upon addition of 6 equivalents of **TU** to the chloride complex solution leads to the shifting of PtN_2Cl_2

peak from -2175 ppm to -3909.1 ppm. This confirmed the formation of $[Pt(\mathbf{TU})_4]^{2+}$ complex[66-68]as expected from *cis* isomers of ($PtNNCl_2$) when reacted with thiourea. The complex reacts completely with thiourea to give $[Pt(\mathbf{TU})_4]^{2+}$ because of the large *trans* effect as proposed in Scheme 4.5. The^{1}H NMR study shows σ effect that reduces electron density from the ligand that leads to downfield shift. The ^{1}H NMR spectrum of complex **PtL6** of the alkyl protons (Ha) shifts to 1.65 ppm compared to Hb at 1.40 ppm of the ligand (Figure 4.10). This downfield shift indicates deshielding of alkyl protons attributed to reduced electron density on coordination to the metal centre. This decrease in electron density causes alkyl protons to resonate downfield. This shifts support the presence of σ inductive effects causing the shifts of protons of free ligands and their coordinated forms. Due to the *cis* configuration of this class of complexes, the strong *trans* effect on coordination to thiourea labilizes the linker that leads to the dechelation as supported in Figures 4.10 and 4.11.

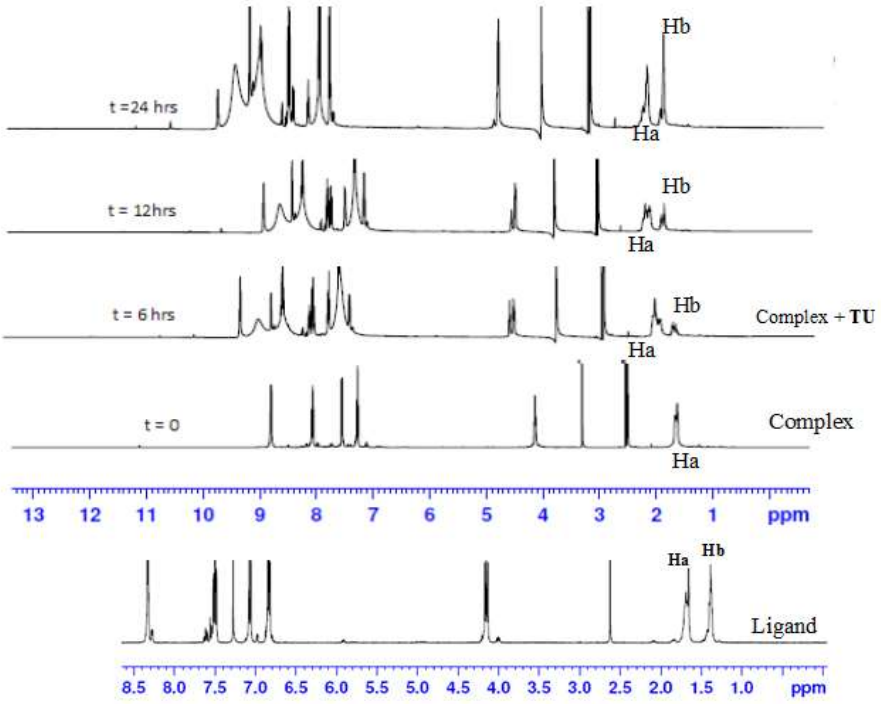

Figure 4.10: Time-dependent changes in the ^{1}H NMR spectrum of **PtL5** upon addition of 6 equivalents of **TU** in DMSO-d_6. The complex undergoes dechelation to form the free ligand (starting material) after 24 hrs.

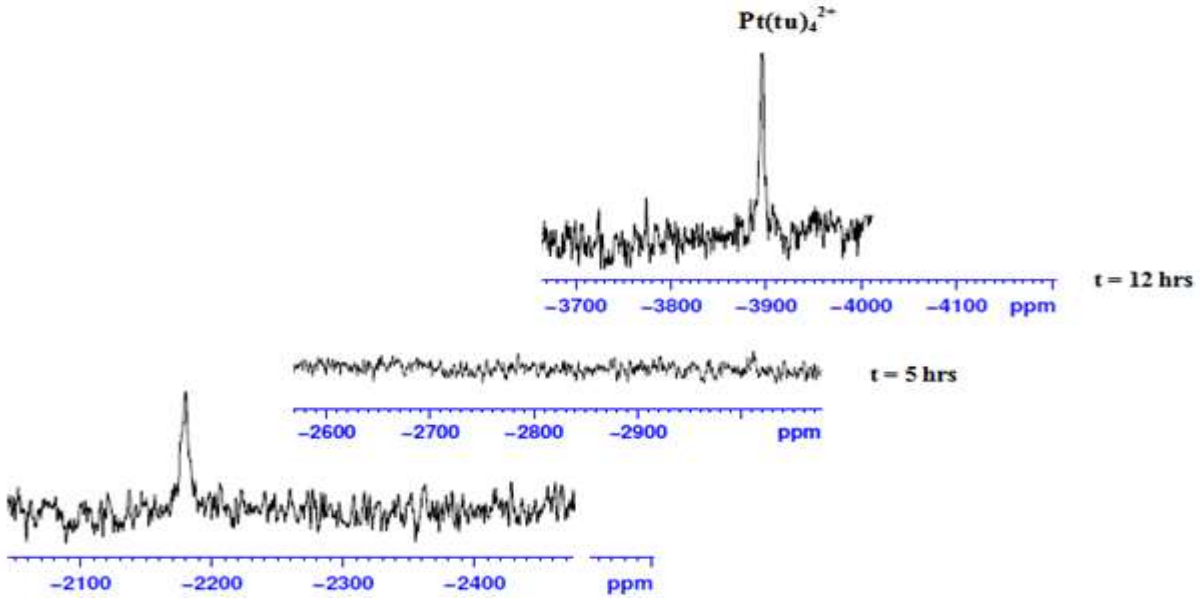

Figure 4. 11: Time-dependent changes in the ^{195}Pt NMR spectrum of **PtL5**, upon addition of 6 equivalents of TU in DMSO-d_6 the peak at -2175 ppm disappears and reappears at -3909.1 ppm indicating the formation of $[Pt(TU)_4]^{2+}$ complex.[69]

4.10 Discussion

The substitution behaviour of dinuclear dipyridylamine Pt(II) complexes with varying alkyl chain was investigated. The first substitution step follows the trend **PtL1** > **PtL2** > **PtL3** > **PtL4** > **PtL5** > **PtL6** supporting the view that alkyl chain length has an influence on the reactivity. This trend is attributed to the stronger σ-donation as the alkyl chain increases that lead to stabilization of the metal centres through increased σ-donicity.[70] The longer alkyl groups increases the electron density around the Pt(II) centres through inductive process. This is enhanced by the lone pair of electrons on the amine nitrogen making them more σ electron donating leading to a decrease in electrophilicity at the metal centres. The electrophilicity of the complexes; **PtL2** (48.44) > **PtL3** (46.96) > **tL4** (44.74) > **PtL5** (43.49) > **PtL6** (42.09) eV is in agreement with the reactivity trend. The electronic effect in these complexes is also supported by DFT calculations that shows raised frontier orbitals as the alkyl chain increases (Table 4.2). The position of HOMO and LUMO levels suggest the amount of charge in the alkyl chain. The low lying LUMO orbitals in short alkyl spacers indicate less σ effect to the dipyridyl rings. The nitrogen's lone pair and inductive effect of longer alkyl chain increases electron density to the HOMO making the complexes better nucleophiles.[71]

However, HOMO-LUMO energy gap, Δ*E*, reflects a contradicting trend from that of the kinetic data. The Pt(II) complex with the least reactivity, **PtL6,** has the smallest HOMO-LUMO energy gap (Δ*E* = 4.13 eV) while the most reactive complex, **PtL2**, has the highest energy gap (ΔE = 4.34 eV). Increased inductive electron donation raises both the HOMO and LUMO due to increasing chain length as shown in Figure 4.12. This increase in energy is in line with the expectation of electron donating groups to raise the energy of molecular orbitals.

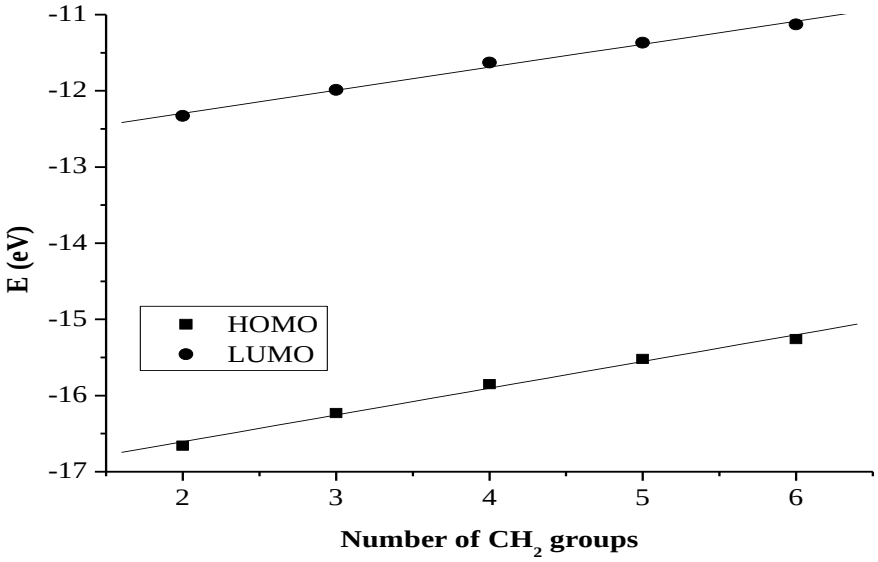

Figure 4.12: Linear correlation between chain length and HOMO/LUMO orbital energy levels.

The results from the current study were compared to previous work[72,73] where bis(2-pyridylmethyl)amine (bpma) head group was appended to the alkyl bridge of variable length. The findings in this chapter show an opposite trend to that previously reported by Jaganyi and Mambanda.[72] Although both studies used flexible alkyl linkers, the difference is attributed to different head functionalities at the termini *viz* bis(2-pyridylmethyl)amine and 2,2'-dipyridylamine. The decrease in reactivity of 2,2-dipyridylamine Pt(II) complexes was observed as the –(CH_2)n- moiety increased due to the linker being in *cis*-position relative to the leaving group. The trend in reactivity of this class of bidentate Pt(II) complexes is attributed to the strong *σ*-ability of the –(CH_2)n- moiety in *cis*-position to the leaving group that causes accumulation of electron density around the metal centre. However, this trend is opposite to kinetic studies

reported of the ligand substitution of dinuclear Pt(II) complexes with flexible linker with bis(2-pyridylmethyl)amine functionality. This head group forms monodentate dinuclear Pt(II) complexes of which reactivity increases with increase in chain length due to *trans*-effect. The high *trans*-effect[74-76] of bis(2-pyridylmethyl)amine linked platinum(II) complexes enhances the rate of substitution through ground state destabilization. It shows the stronger effect of *trans* ligand to accommodate the excess electronic charge added to the central metal by the entering ligand. Comparing these two studies, they suggest that *cis* ligands are not as effective as *trans* ligands in lowering the activation energy of ligand → metal σ bonding. This observation is in agreement with classical explanation; *trans* effect causes electrostatic destabilization of the ligand in the *trans* position. Thus, the study supports the electronic properties of the alkyl spacer to dictate the strength of its *trans* effect in bis(2-pyridylmethyl)amine functionality as the chain length increases.From the two reactivity trends it shows that *cis* and *trans* effects have an opposite net effect. While the *trans* effect accelerates the rate of substitution through ground state destabilization, the *cis* effect decelerates substitution rates through accumulation of electron density around the metal centre.

This study has shown that reactivities of dinuclear Pt(II) complexes may be manipulated by the geometry of the complexes ranging from relationship of diamine bridge to leaving group to the nature of the diamine bridge. It further shows the complexes investigated to be stabilized as the alkyl chain increases, a trend also previously reported by van Eldik[47,52] and Jaganyi.[77] The stability of the complexes was attributed to stronger σ inductive effects in *cis* configuration due to accumulation of electron density around the Pt(II) centre as alkyl chain increases. From these findings the structural features and reactivity pattern of the investigated dinuclear Pt(II) complexes are governed by both steric and electronic effects arising from the methylene bridge.

Steric factors are expected to be influenced by the size of the complex and the preferential conformations of the complexes. The study shows that increasing chain length increases the distance between the metal complexes reducing steric hindrance, hence reactivity is expected to increase. Since this is not the case, the slow reactivity of complexes with longer alkyl chain is

attributed to the electronic factors to play a key role. The study also investigated the reactivity of the entering nucleophiles based on their steric and electronic demands. This investigation shows reactivity to be dependent on the steric influence of the entering nucleophile. The reactivity order of the nucleophiles followed the trend **TU** > **DMTU** > **TMTU**. However, in some cases where **DMTU** is faster than **TU**, the enhanced reactivity is attributed to the inductive effect by the two methyl groups.[78] The second and third steps are much slower since they governed by the steric hindrance caused by coordination of the first nucleophile. In cases where kinetic data is not reported, this was attributed to the slow reactivity of the nucleophile involved.

4.11 Conclusion

This chapter has provided a comprehensive investigation on the effect of alkyl chain on the mechanistic substitution reactions of *cis*-dinuclear Pt(II) complexes with tetraqua ligands. The study shows the length and parity of the flexible linker to be influential parameters on the transitional properties of the metal complexes. The study supports literature findings that the length of alkyl chain has a significant influence on structural and electronic properties of the complexes. The kinetic behaviour of the complexes is controlled by conformations and electronic effect of the alkyl spacers. An increase in alkyl chain into the Pt(II) coordination sphere results in a decrease in acidity of the coordinated tetraqua ligands and hence higher stability of the complexes. The results also show the number of substitution steps to be controlled by the odd-even effect of the alkyl spacer. The absence of separate kinetic steps for the release of both Pt(II) ions in the odd numbered alkyl chain suggests an apparent single process of dechelation. The mechanism of substitution is associative in nature as shown by small but positive values of enthalpy and large negative values of entropy. The ability of these complexes to undergo ligand exchange makes them potential candidates to build chemotherapeutic agents for drug delivery. However, the displacement of the labilized chain linker due to strong *trans* effect by S-donor nucleophiles may limit the application of this family of complexes as anticancer agents. This work has provided a useful approach in tuning the reactivity of new but promising dinuclear platinum anticancer candidates. These results are beneficial in understanding the antitumour activity and toxicity of dinuclear bifunctional Pt(II) complexes.

References

1. P. Gamez,P. de Hoog, O. Roubeau, M. Lutz,W. L. Driessen, A. L. Spek and J. Reedijk, *Chem. Commun.*, 2002, 1488-1498; (b) P. Gamez, P. de Hoog, M. Lutz,A. L. Spek and J. Reedijk, *Inorg. Chim. Acta.*, 2003, **351**, 319-326.
2. P. de Hoog, P. Gamez, M. Leuken, O. Roubeau, B. Krebs and J. Reedijk, *Inorg. Chim. Acta.*, 2004, **357**, 213-218.
3. S. Demeshko, G. Leibeling, S. Dechert and F. Meyer, *Dalton Trans.*, 2004, 3782-3787.
4. C. Seward W. I. Jia, R. Y. Wang and S. Wang, *Inorg. Chem.*, 2004, **43**, 978-985.
5. W. I. Jia, D. R. Bai, T. McCormick, Q. D. Liu, M. R. Motala, R. Y. Wang, C. Seward, Y. Tao and S. Wang, *Chem. Eur. J.*, 2004, **10**, 994-1006.
6. E. Wong and C. M. Giandomenico, *Chem. Rev*., 1999, **99**, 2451-2466.
7. E. R. Jamieson and S. J. Lippard, *Chem. Rev*., 1999, **99**, 2467-2498.
8. J. R**e**edijk, *Proc. Natl. Acad. Sci.*, USA 2003, **100**, 3611-3616.
9. N. J. Wheate and J. G. Collins, *Coord. Chem. Rev.*, 2003, **241**, 133-145.
10. N. Farrell, Y. Qu, U. Bierbach, M. Valsecchi and E. Menta, *Chemistry and Biochemistry of Leading Anticancer Drug* (Ed. Lippert, B), Verlag Helvetica *Chimica Acta*, Zurich, Wiley-VCH, Weinheim, 1999, 479-496.
11. (a) N. Farrell, *Comments Inorg. Chem*., 1995, **16**, 373-389; (b) N. Farrell, in S. B Howell (Ed.) Platinum and Other Metal Coordination Compounds in cancer Chemotherapy, Plenum Press, New York, 1991, 81-82.
12. E. Raymond, S. Faivre, S. Chaney, J. Woynarowski and E. Cvitkovic, *Mol. Cancer Therapeut*., 2002, **1**, 227-235.
13. D. Wong and S. J. Lippard, *Nature Rev. Drug Disc*., 2005, **4**, 307-320.
14. J. Kasparkova, J. Novakova, O. Vrana, N. Farrell and V. Brabec, *J. Biol. Inorg. Chem*., 1999, **38**, 10997-11005.
15. J. Kasparkova, J. Zehnulova, N. Farrell and V. Brabec, *J. Biol. Inorg. Chem*., 2002**, 277**, 48076-48086.
16. J. W. Cox, S. J. Berners Price, M. S. Davies, W. Barlage, Y. Qu and N. Farrell, *Inorg. Chem*., 2000, **39**, 1710-1715.

17. M. S. Ali,K. H. Whitmire,T. Toyomasi, Z. H. Siddikand A. R. Khokhar, *J. Inorg. Biochem*., 1999, **77**, 231-238.
18. S. Komeda, M. Lutz, L. A. Spek, M. Chikuma and J. Reedijk, *Inorg. Chem*., 2000, **39**, 4230-4236.
19. A. J. Kraker, J. D. Hoeschele,W. L. Elliot, H. D. Showalter, A. D. Sercel and N. Farrell, *J. Med. Chem*., 1992, **35**, 4526-4532.
20. Y. Qu and N. Farrell, *J. Am. Chem. Soc*., 1991, **113**, 4851-4857.
21. Y. Qu and N. Farrell, *Inorg. Chem*., 1992, **31**, 930-932.
22. U. Bierbach, Y. Qu, T. W. Hambley, J. Peroutka,H. L. Nguyen,M. Doedee and N. Farrell, *Inorg. Chem*., 1999, **38**, 3535-3542.
23. N. Farrell, Y. Qu and M. P. Hacker, *J. Med. Chem*., 1990, **33**, 2179-2184.
24. A. Gund and B. K. Keppler, *Angew. Chem*., 1994, **106**, 198-2005.
25. R. Mital, T. S. Srivastata, H. K. Parekh and M. P. Chitnis, *J. Inorg. Biochem*., 1991, **41**, 93-103.
26. H. M. Mansuri-Torshizi, T. S. Srivastata, H. K. Parekh, and M. P. Chitnis, *J. Inorg. Biochem.*, 1992, **45**, 135-148.
27. Y. Qu, H. Rauter, A. P. Soares Fontes, R. Bandarage, L. R. Kelland and N. Farrell, *Med. Chem*., 2000, **43**, 3189-3192.
28. R. A. Ruhayel, S. Janina, J. S. Langner, M. J. Oke,S. J. Berners-Price, Z. I. Ibrahim and N. Farrell, *J. Am. Chem. Soc*., 2012, **134**, 7135-7146.
29. N. Farrell, *Metal Ions Biol. Syst*., 2004, **41**, 252−296.
30. S. Komeda, "Unique platinum-DNA interactions may lead to more effective platinum-based antitumour drugs," *Metallomics*, 2011, **3,** 650-655.
31. J. B. Mangrum and N.Farrell, *Chem. Commun.*, 2010, **46**, 6640-6650.
32. P. Perego, C. Caserini, L. Gatti, N. Carenini, S. Romanelli, R. Supino, D. Colangelo, I. Viano, R. Leone, S. Spinelli, G. Pezzoni, C. Manzotti, N. Farrell and F. Zunino, *Mol. Pharmacol*., 1999, **55**, 528-534.
33. R. Jarzynka, A. Topolski, M. Uzarska and R. Czajkowski, *Inorg. Chim. Acta*., 2014, **413**, 60-67.
34. J. Reedijk, *Chem. Rev.*, 1999, **99**, 2499-2510.

35. W. E. Curtis, M. E. Muldrow, N. B. Parker, R. Barkley, S. L. Linas and J. E. Repine, *Proc. Natl. Acad. Sci.* USA, 1988, **85**, 3422-3428.
36. A. A. Shoukry, *J. Chem. Sci.*, 2013, 1**25**, 643-651.
37. K. Matsumoto, H. Aizawa, H. Inoue, H. Koto, S. Fukuyama and N. Hara, *Eur. J. Pharmacol*., 2000, **403**, 267-275.
38. P. Pil and S. J. Lippard, *Specific Binding of Chromosomal Protein HMGI to DNA Damaged by the Anticancer Drug Cisplatin*. *Science*, 1992, **256**, 234-236.
39. B. Petrović, Ž. D. Bugarčić, A. Dees, I. Ivanović-Burmazović, F. W. Heinemann, R. Puchta, S. N. Steinmann, C. Corminboeuf and R. van Eldik, *Inorg. Chem*., 2012, 1516-1529.
40. M. T. Ashby, *Comments Inorg. Chem.*, 1990, **10**, 297-313.
41. (a) S. G. Murray and F. R. Hartley, *Chem. Rev.*, 1981, **81**, 365-441; (b) G. Kinunda and D. Jaganyi, *Transition Met. Chem*., 2016, **41**, 235-248.
42. (a) S. Fakih, W. C. Tung, W. D. Eierhoff,C. Mock and B. Krebs, *Z. Anorg. Allg. Chem*., 2005, **631**, 1397-1402. (b) M. J. Rauterkus, S. Fakih, C. Mock, I. Puscasu and B. Krebs, *Inorg. Chim. Acta*, 2003, **350**, 355-365.
43. W. A. Panyako and G. Kinunda, *New J. Chem.*, 2018, **42**, 214-227.
44. J. Bogojeski, Ž. D.Bugarčić, R. Puchta and R. van Eldik, *Eur. J. Inorg. Chem.*, 2010, 5439-5445.
45. S. Jovanović, B. Petrović, D. Čanović and Ž. D. Bugarčić, *Int. J. Chem. Kinet*., 2011, **43**, 99-106.
46. N. Summa, W. Schiessl, R. Puchta, R. van Eikema and R. van Eldik, *Inorg. Chem*., 2006, **45**, 2948-2959.
47. N. Hochreuther, S. T. Nandibewoor, R. Puchta and R. van Eldik, *Dalton Trans*., 2012, **41**, 512-522.
48. (a) J. D. Atwood, *Inorganic and Organometallic Reaction Mechanisms*, John Wiley & Sons, Canada, 1985, 82-83. (b) F. Cozzi, F. Ponzini, R. Annunziat, M. Cinquini and J. S. Siegel, *Angew. Chem., Int. Ed. Engl*., 1995, **34**, 1019-1020.
49. T. Soldatovic´, S. Jovanovic´, Z. D. Bugarc˘ic´ and R. van Eldik, *Dalton Trans*., 2012, **41**, 876-884.

50. Y. Chen, H. Wang and J. Wang, *J. Phy. Chem*. B., 2014, **17**, 4630-4635.
51. I. Francolini, V. Taresco, F. Crisante, A. Martinelli, L. D'Ilario, and A. Piozzi, *Int J. Mol Sci.*, 2013, **14**(4), 7356–7369.
52. W. A. Panyako and D. Jaganyi, *Int. J. Kinet.*, 2017, **49,** 545-561.
53. H. Ertürk, A. Hofmann, R. Puchta and R. van Eldik, *Dalton Trans.*, 2007, 2295- 2301.
54. (a) V. Rai and I. N. N. Namboothiri, *Eur. J. Org. Chem*., 2006, 4693-4703; (b) F. Weinhold and R. L. Clark, *Discovering Chemistry with Natural Bond Orbitals*, 2012, 132–133, New Jersey: John Wiley & Sons.
55. R. Tandon, T. A. Nigst and H. Zipse, *Eur. J. Org. Chem*., 2013, 5423-5430.
56. O. Exner, *J. Phys. Org. Chem*., 1999, **12**, 265-274; (b) M. Charton, *J. Phys. Org. Chem*., 1999, **12**, 275-282; (c) V. Galkin, *J. Phys. Org. Chem*., 1999, **12**, 283-288; (d) O. Exner, M. Charton and V. Galkin, *J. Phys. Org. Chem*., 1999, **12**, 289-290.
57. H. Stephanie, R. Puchta and R. van Eldik, *Inorg. Chem*., 2011, **50**, 8984-8996.
58. A. Mandal, P. Karmakar,S. Mallick, B. K. Bera, S. Mondal, S. Ray and A. K. Ghosh, *J. Chem. Sci.*, 2012, **124**, 801-807.
59. G. Pistolis, A. K. Andreopoulou, A. Malliaris, J. K. Kallitsis, *J. Phys.Chem. B*., 2005, **109**, 11538-11543.
60. Y. Qu, N. J. Scarsdale, M. C. Tran and N. Farrell, *J. Biol. Inorg. Chem.*, 2003, **8,** 19−28; Y. Qu, N. J. Scarsdale, M. C. Tran and N. Farrell, *J. Inorg. Biochem.*, 2004, **98**, 1585−1590; Y. Qu, M. C. Tran and N. Farrell, *J. Biol. Inorg. Chem.*, 2009, **14**, 969−977.
61. M. J. Birenne, J. Gabard, M. Leclercq, J. M. Lehn, M. Cesario,C. Pascard, M. Cheve and G. Dutruc-Rosset, *Tetrahdron Lett*., 1994, **35**, 8157-8167.
62. (a) M. Albrecht and S. Kotila, *Angew. Chem. Int. Ed. Engl.* 1995, **34**, 2134-2137; (b) M. Albrecht, *Chem. Soc. Rev*., 1998, **27**, 281-288; (c) M. Albrecht, I. Janser, H. Houjou and R. Frohlich, *Chem. Eur. J*., 2004,**10**, 2839-2850; (d) M. Albrecht and R. Frohlich *Bull. Chem. Soc. Jpn*., 2007, **80,** 797-808. (e) C. T. Imrie and P.A. Henderson,*Chem, Soc. Rev*., 2007, **36**, 2096-2124.
63. M. G. Basallote, J. Durán, M. J. Fernández-Trujillo and M. A. Máñez, *J. Chem. Soc. Dalton Trans.*,1999, 3817–3823.

64. E. Eliel and H. Wilen, *Stereochemistry of Organic Compounds*, Wiley, New York, 1994, 596-599.
65. B. M. Still,P. G. A. Kumar,J. R. Aldrich-Wright and W. S. Price, *Chem. Soc. Rev*., 2007, **36**, 665-686.
66. H. Ertürk, R. Puchta and R. van Eldik, *Eur. J. Inorg. Chem*., 2009, **10**, 1331-1338.
67. K. Zamani, A. Mobini Khaledi, N. Foroughifar, K. Faghihi and V. Mahdavi, *Turk J. Chem*., 2003, **27**, 71-75.
68. H. Ertürk, J. Magut, R. Puchta and R. van Eldik, *Dalton Trans*., 2008, 2759-2766.
69. P. O. Ongoma and D. Jaganyi D, *Dalton Trans*., 2013, **42**, 2724-273.
70. (a) D. Reddy and D. Jaganyi, *Int. J. Chem. Kinet*., 2011, **43**, 161-174; (b) A. Hofmann, L. Dahlengburg and R. van Eldik, *Inorg. Chem*., 2003, **42**, 6528-6538.
71. O. Exner and S. Böhm, *Eur. J. Org. Chem*., 2007, 2870-2876.
72. A. Mambanda and D. Jaganyi, *Dalton Trans*., 2011, **40**, 79-91.
73. A. Mambanda, D. Jaganyi, S. Hochreuther and R. van Eldik, *Dalton Trans*., 2010, **39**, 3595-3608.
74. B. Pinter, V. van Speybroeck, M. Waroquier, P. Geerlings and F. de Proft, *Phys. Chem. Phys*., 2013, **15**, 17354-17365.
75. (a) C. H. Langford and H. B. Gray, *Ligand Substitution Processes*, W. A. Benjamin, Inc., New York, 1966, 27-33, 79-81; (b) F. Basolo, *Mechanisms of Inorganic Reactions*, American Chemical Society, 1965, 23-32.
76. (a) B. Coe and S. Glenwright, *Coord. Chem. Rev*., 2000, **203**, 5-80; (b) E. M. Shustorovich, M. Porai-Koshits, Y. Buslaev, *Coord. Chem. Rev*., 1975, **17**, 1-98.
77. P.O. Ongoma and D. Jaganyi, *Transition. Met. Chem*., 2014, **39**, 407-420; D. Jaganyi, V. M. Munisamy and D. Reddy, *Int. J. Chem. Kinet*., 2006, **38**, 202-210.
78. D. Jaganyi, F. Tiba, O. Q. Munro, B. Petrović and Ž. D. Bugarcić, *Dalton Trans*., 2006, **24**, 2943-2949.

CHAPTER 5

Kinetics and mechanistic study of polynuclear platinum(II) polypyridyl complexes: A paradigm shift in search of new anticancer agents

5.1 Introduction

The search for more efficacious Pt-based drugs other than cisplatin has been amplified due to the steady rise in cancer deaths globally.[1,2] The clinical use of cisplatin and its analogous is restricted by dose-limiting deleterious side effects such as nausea, ototoxicity, nephrotoxicity, neurotoxicity, myelosuppression, and acquired resistance.[3-5] This search has been extended to multinuclear platinum(II) complexes such as BBR3464 and *N,N,N',N'',N*''-hexakis(2-pyridylmethyl)-1,3,5-tris(aminomethyl)-benzene which have shown cytotoxicity in some cell lines.[6-8] This class of complexes multinuclear Pt((II)] has distinctive mechanisms of action compared to mononuclear analogues.[9,10] They have shown the potential to expand the spectrum of treatable tumours and to overcome clinical resistance in cisplatin cell lines.[11-13] Their increased cytotoxicity is due to different types of intra- and interstrand DNA cross-linking adducts which they form.[14,15] This is due to their ability to form flexible, non-directional and mainly interstrand DNA-adducts that enhances conformational changes that leads to improved antitumour activity.[16,17] This improved antitumour activity has made them a class of clinically relevant drug candidates.[18,19] The distinct molecular characters of pharmacological action of multinuclear complexes is contributed by the rigidity/flexibility of the bridging ligands in conjunction with the intra-metal distances that offer the possibility of forming both intra- and inter-strand DNA cross-linking adducts.The presence of more than one platinum centre causes formation of multiple adducts that disrupt DNA's helical structure with improved replication and transcription.[20,21] This is promoted by multinuclear Pt(II) complexes having appropriate metal-metal separation which is significant in polymetallic biosites. This improved mutagenicity is integrated to reach maximum level due to synergy of linking metal moieties.

In the development of the proposed antitumour agents, the present study utilized 2,2'-dipyridylamine as the core chelating agent to synthesize multi and mononuclear Pt(II) analogues. The influence of this ligand on the reactivity of Pt(II) complexes and the ligand's

ability to modulate the potential toxicity[22]of the metal complexes is of interest. Both mononuclear and multinuclear Pt(II) and Pd(II) complexes based on this core have showed high cytotoxicity as potential anticancer agents[23-25] which shows an area full of prospects that can be explored to give potential anticancer drug candidates. They form complexes with *cis* configuration similar to cisplatin which are likely to produce similar array of adducts with DNA but with improved biological consequences than cisplatin.[26] This study focuses on *cis*-conformers since *cis*/*trans* structure-activity relationship of platinum antitumor complexes, exemplified by cisplatin shows that only the *cis* geometry is therapeutically active. The complexes are designed by tuning the steric and electronic effects on reactivity. It is projected that such tuning of the lability of antitumour Pt(II) complexes may improve the efficacy and overcome the side effects of the present anticancer agents. The complexes designed herein are good models for mechanistic and kinetic studies and suggest potential prospects as anticancer drugs with *N*-donor ligands.[27] The study further tunes the complexes by incorporating methylene groups and heteroanalogues of benzene by replacing =CH- units with isovalent atoms of nitrogen. Such tuning of the linker remains vital to determine the influence of nitrogen on cytotoxicity of antitumour agents and as a π-acceptor atom on the reactivity of metal complexes.[28] In corporation of such chelating ligands that can interact with free or protein bound metal ions is important in understanding mechanistic activities of newly designed chemotherapeutics. The scope of this study focuses on ligand substitution reaction mechanisms and to determine the rate laws consistent with Pt(II) complexes which offer two labile reaction sites in nucleophilic medium. The mechanistic overview is based on experimental and computational calculations into the following synthesized complexes: phenyl-dichlorido-2,2'-dipyridinylaminediaquaplatinum(II) (dpab)Pt$(H_2O)_2$ (**Ptdpab**); di-2-pyridylaminomethylbenzenediaquaplatinum(II) (pamb)Pt$(H_2O)_2$ (**Ptpamb**); 1,3,5-tris(2,2'dipyridylamino)-benzenehexaquaplatinum(II) (tab)$Pt_3(H_2O)_6$ (**Pttab**); 1,3,5-tris(2,2'dipyridylmethylamino)benzenehexaquaplatinum(II) (tamb)$Pt_3(H_2O)_6$ **(Pttamb)**; and 2,4,6-tris(2,2'-dipyridylamino)-1,3,5-triazinehexaquaplatinum(II) (tat)$Pt_3(H_2O)_6$, (**Pttat**).

To gain insight into the mechanistic substitution reactions of these polynuclear Pt(II) complexes with biological nucleophiles, *viz* thiourea (**TU**), *N*,*N*'-dimethylthiourea (**DMTU**)

and *N*,*N*,*N*',*N*'-tetramethylthiourea (**TMTU)**, a full kinetic and mechanistic investigation was undertaken. The study determined the kinetics and bioactivity of trinuclear Pt(II) complexes with 6-aqua ligands with sulphur donor molecules for the first time. The nucleophiles studied are of special interest as they represent targets and competitors of anticancer platinum-based therapeutics in the cellular cell lines and also play a role as chemoprotective agents.[29,30]The specific roles of these nucleophiles has been outlined in the chapter three and published.[31] To achieve this objective, the study determined the influence of structural flexibility and rigidity on reactivity of complexes shown in Figure 5.1. All the complexes are ligated by 2'2-dipyridylamine backbone that ensures a similar structure to cisplatin. However, the ancillary ligands are varied to investigate their influence on their substitution reactions. Such tailoring of the backbone linker is anticipated to improve bio-stability and bioavailability of these trinuclear Pt(II) complexes as anti-tumour agents. Hence the goal of this investigation is to contribute towards a mechanistic understanding of the interaction of multinuclear Pt(II) complexes with biologically relevant molecules. This is due to multinuclear Pt(II) complexes showing wider spectrum of activity that has given hope of forming clinically relevant candidates. This makes this class of complexes the most promising alternatives to cisplatin since they can provide significant cytostatic activity in several cisplatin resistant tumour cell lines. This chapter shows how tailoring the backbone of the metal complex leads to dramatic changes in their acidity and reactivity. This tailoring of the bridging ligands is envisaged to provide special delivery carriers to selectively transport metal-based agents tumour cell-lines.

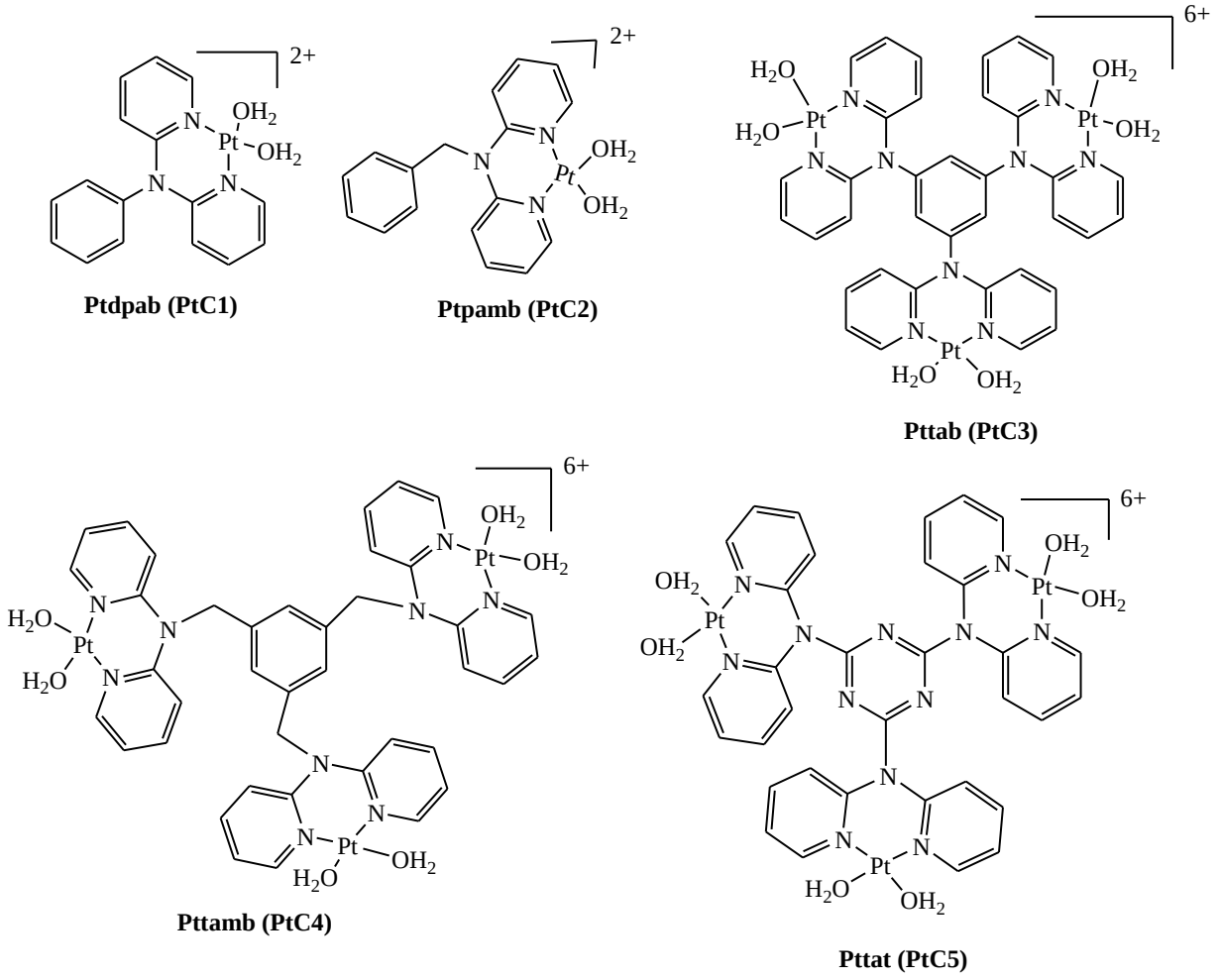

Figure 5.1: Schematic structures and abbreviations for the aqua Pt(II) complexes investigated

5.2 Experimental Section

5.2.1 Materials and methods

All starting materials were obtained from commercial sources and used as received without further purification. The nucleophiles **TU**, 99 %, **DMTU**, 99 % and **TMTU**, 98 %, benzyl bromide, 98 %, bromobenzene, 99 %, cyanuric chloride (2,4,6-trichloro-1,3,5-triazine), 99 %, 1,3,5-tribromobenzene, 98 % and 1,3,5-tris(bromomethyl)benzene, 97 %, $AgClO_4$ 99.99 %, were obtained from Sigma Aldrich while K_2PtCl_4 and 2,2'-dipyridylamine (dpa) were obtained from Strem chemicals. De-ionized water was used in all experiments.

5.2.2 Synthesis of ligands

Three ligands namely **di-2-pyridylaminobenzene, di-2-pyridylaminomethylbenzene**, and **1,3,5-tris(bromomethyl)benzene** were synthesized according to literature procedures.[32,33a] A weighed amount of bromo-alkyl halide (0.855 g, 5.00 mmol) was dissolved in 3 mL DMF at room temperature and 2,2'-dipyridylamine (0.856 g, 5.00 mmol) and KOH (1.137 g, 20.26 mmol) in 5.00 mL DMF added drop wise. The resulting solution was stirred under nitrogen at room temperature for 24 hours and dried under vacuum. The residue was washed with water and extracted into $CHCl_3$ (3×50 mL). The extracts were dried over anhydrous sodium sulphate and filtered. The filtrate was dried under vacuum and chromatographed on silica gel with $CHCl_3$:CH_3OH (5:1) v/v. The resulting yellow product was recrystallized from an acetone-water mixture.

1,3,5-Tris(di-2-pyridylaminomethyl)benzene was prepared by reacting di-2-pyridylamine (0.856 g, 5 mmol) with potassium hydroxide (1.121 g, 20 mmol) in 5 mL of DMSO. The mixture was stirred for 1 hour and 1,3,5-tris(bromomethyl)benzene (0.595 g, 1.667 mmol) added and stirred for an additional 48 hours. Water was added drop-wise to induce crystallization. On standing, a yellow powder formed and was filtered off, washed with plenty of water and recrystallized from an ethyl acetate-petroleum ether mixture. The synthesized ligands were characterized using ^1H, ^{13}C NMR, mass spectrometry and elemental analysis.

Di-2-pyridylaminobenzene (dpab), Yield, 0.604 g, (49 %). ^1H NMR (400 MHz, $CDCl_3$, 303 K) δ 8.28 (2H, d, py), 7.68 (2H, t, py), 7.60 (2H, d, py), 7.57 (2H, d, ph), 7.20 (1H, t, ph), 7.16 (2H, d, ph), 6.94 (2H, t, py) ppm. ^{13}C NMR (100 MHz, $CDCl_3$, 303 K) δ 157.5, 148.6, 139.5, 117.4, 112 ppm. Anal. Calcd. for $C_{16}H_{13}N_3$, C, 78.13, H, 5.79, N, 16.08, Found C, 78.34, H, 5.45, N, 16.34; TOF MS ES^+ *m/z:* $[M+H]^+$= 248.309.

Di-2-pyridylaminomethylbenzene (dpamb), Yield, 0.277 g, (21 %). ^1H NMR (400 MHz, $CDCl_3$, 303 K)δ 8.40 (2H, d, py), 7.60 (2H, t, py), 7.37 (2H, d, py), 7.27 (2H, d, ph), 7.20 (1H, t, ph), 7.16 (2H, d, ph), 6.94 (2H, t, py), 5.55 (2H, s, CH_2) ppm, ^{13}C NMR (100 MHz, $CDCl_3$, 303 K) δ157.5, 148.6, 139.8, 137.4, 128.0, 117.4, 114.4, 51.3 ppm.Anal. Calcd for $C_{17}H_{15}N_3$,

C, 78.13, H, 5.79, N, 16.08, Found C, 77.78, H, 5.55, N, 16.48, TOF MS ES^+ (*m/z)*: $[M+H]^+$= 262.134.

1,3,5-tris(di-2-pyridylaminomethyl)benzene (tamb), Yield, 0.578 g (55 %). For $C_{39}H_{33}N_9$, ^{1}H NMR (400 MHz, $CDCl_3$, 303 K) δ8.22 (6H, d, py), 7.40 (6H, t, py), 7.09 (3H, s, ph), 6.92 (6H, d, py), 6.81 (6H, t, py), 5.34 (6H, s, CH_2) ppm. ^{13}C NMR (100 MHz, $CDCl_3$, 303 K) δ 157.4, 148.6, 139.5, 136.6, 124.0, 117.0, 114.5, 51.6 ppm. Anal. Calcd. for $C_{39}H_{33}N_9$, C, 74.67, H, 5.30, N, 20.10, Found C, 74.27, H, 5.12, N, 19.86, TOF MS ES^+ (m/z): $C_{39}H_{34}N_9^+$= 628.2937.

1,3,5-tris(di-2-pyridylamino)benzene (tdab) was prepared according to literature procedure using 1,3,5-tribromobenzene and di-2-pyridylamine *via* copper-mediated Ullmann condensation.[34] A mixture of 1,3,5-tribromobenzene (0.525 g, 1.67 mmol) in dichloromethane (30 mL), di-2-pyridylamine (0.856 g, 5 mmol) in dichloromethane (20 mL), potassium carbonate (0.8976 g, 6.448 mmol) in water (10 mL) and copper (II) sulphate pentahydrate (0.1355 g, 0.5428 mmol) in water (10 mL) was stirred overnight at room temperature and evaporated to dryness under vacuum. The dried mixture was ground in a mortar and 5 drops of chloromethane added and heated at 210 ^{o}C for 8 hours under nitrogen. The mixture was cooled to room temperature and dissolved in a mixture of dichloromethane (50 mL) and water (50 mL). The organic layer was washed with water (3×50 mL), dried over Na_2SO_4, and concentrated to give a yellow residue that was purified by chromatographic column using tetrahydrofuran (THF) and hexane (3:1) v/v to obtain a brown solid. The brown solid was recrystallized from a mixture of CH_2Cl_2 – hexane to give a white crystalline compound.

1,3,5-tris(di-2-pyridylamino)benzene (tdab), Yield, 0.302 g, (57 %).^{1}H NMR (400 MHz, $CDCl_3$, 303 K) δ 8.28 (6H, d, py), 7.56 (6H, dd, py), 7.14 (6H, d, py), 6.91 (6H, dd, py), 3.16 (3H, s, ph) ppm,^{13}C NMR (100 MHz, $CDCl_3$, 303 K) δ 158.0, 148.7, 146.8, 137.9, 120.6, 118.9, 117.9 ppm. Anal. Calcd for $C_{36}H_{27}N_9$: C, 73.83, H, 4.65, N, 21.52, Found C, 73.41, H, 4.81, N, 21.88.

2,4,6-tris(dipyridin-2-ylamino)–[1,3,5]-triazine (tdat) was prepared according to Gamez *et al.* method.[35] The synthesis was *via* sequential substitution of the three chlorides of cyanuric chloride by 2,2'-dipyridylamine. 2,4,6-trichloro-[1,3,5]-triazine (cyanuric chloride) (0.307 g, 1.67 mmol) was dissolved in 25 mL tetrahydrofuran (THF) and 3 equivalent moles of *N,N*-diisopropylethylamine (DIPEA, 'Hünig's base' 0.646 g, 5.00 mmol) added while stirring. The resulting yellow solution was cooled down to 0 ^{o}C. Subsequently, a solution of 2, 2'-dipyridylamine(0.856 g, 5.00 mmol) in THF (20 mL) was added drop-wise and the reaction mixture stirred at 0 ^{o}C for 1 hour. The reaction mixture was warmed to room temperature and refluxed for 48 hours at 67 ^{o}C. The resultant white precipitate was isolated on a glass filter washed with THF (3×20 mL) and with ethanol (3×20 mL) to remove DIPEA.

2,4,6-tris(dipyridin-2-ylamino)–[1,3,5]-triazine (tdat), Yield 0.296 g (30 %). ^{1}H NMR (400 MHz, $CDCl_3$, 303 K) δ 8.35 (6H, d, py), 7.51 (6H, dd, py), 7.42 (6H, d, py), 7.03 (6H, dd, py) ppm, ^{13}C NMR (100 MHz, $CDCl_3$, 303 K) δ165.8, 154.9, 148.2, 137.3, 122.9, 120.8 ppm.Anal. Calc. for $C_{33}H_{24}N_{12}$, C, 67.34, H, 4.11, N, 28.55, Found C, 66.98, H, 4.08, N, 28.80; TOF MS ES^{+} (m/z): $[M+Na]^{+}$ = 611.2141.

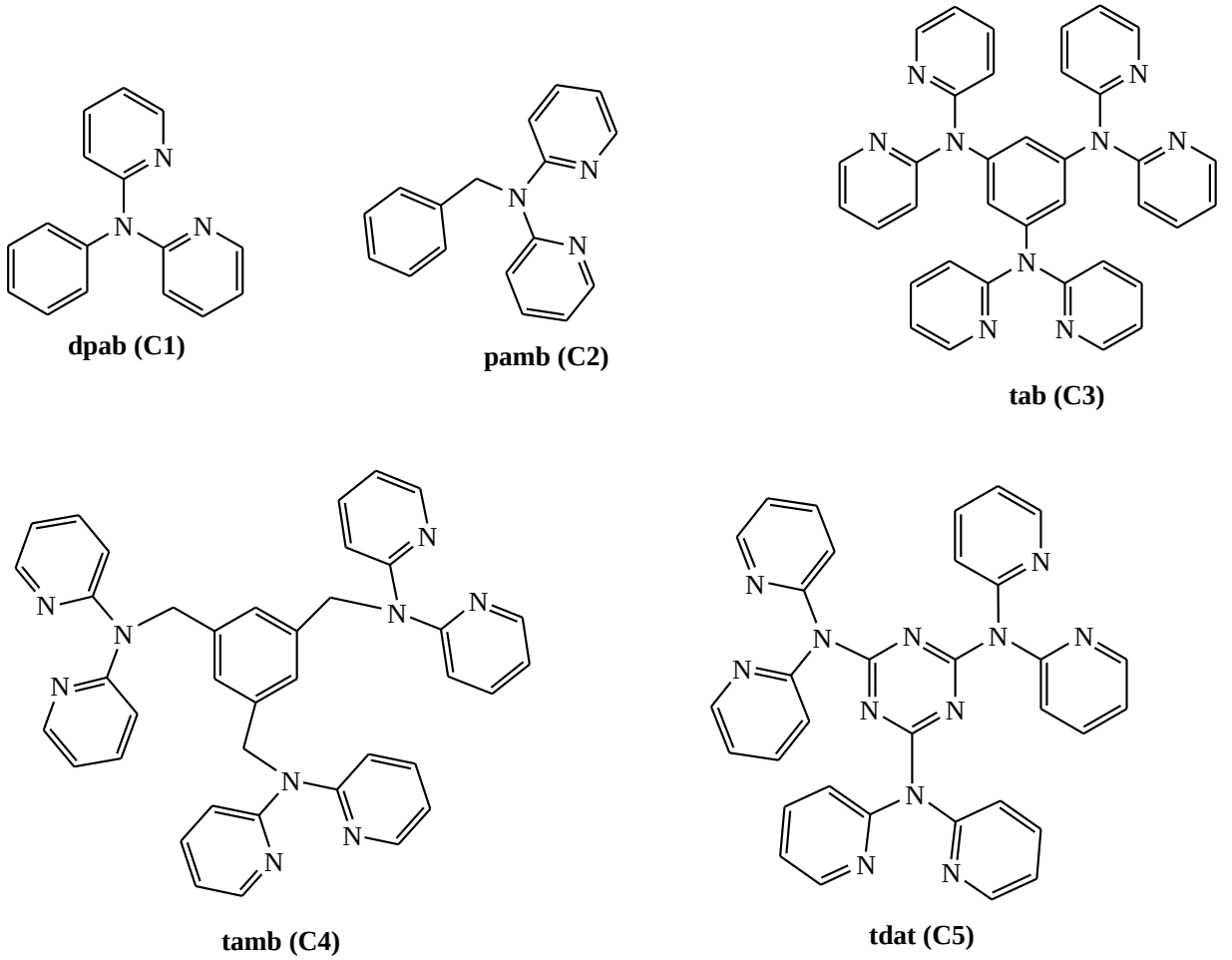

Scheme 5.1: molecular structures of the 2,2'-dipyridylamine ligands coordinated to platinum metal ions in this study

In this study to improve on the efficacy or spectrum of activity the carrier ligands were modified by introducing C_3-symmetric ligands as shown in Scheme 5.1. Investigating C_3-symmetric ligands remains of great importance due to their unique coordination chemistry and reaction mechanisms. The scope of this investigation was the potential of applying C_3-symmetric ligands in designing of the desired therapeutic drugs. Using this selected C_3-symmetric carrier ligands, this study took into consideration different factors that influence the property of antitumour complexes such as geometry, steric hindrance, flexibility, electrostatic effects, lipophilicity and electronic factors. From the ligand backbone, the complexes in Figure 5.1 are similar to cisplatin but the alteration of the ligand system and increased number of platinum centres may cause changes in therapeutic profiles and the development of drug resistance. A better understanding of the carrier process of the Pt(II) complexes is greatly needed for further exploration for these platinum-based complexes as antitumour agents. For clarity, the ligands

were abbreviated as C1 to C5 on coordination to the platinum centres. On coordination the Pt(II) complexes were denoted as **PtC1** to **PtC5** respectively. The rigidity verses flexibility of the ligands exerted an important impact on the structural diversities of the resulting coordination Pt(II) complexes.

5.2.3 Preparation of PtC1, PtC2 and PtC4

The complexes were synthesized from their respective ligands according to a reported procedure.[36] A 50 mL solution of K_2PtCl_4 was stirred and the corresponding molar equivalent of respective ligands dissolved in a small amount of ethanol was added drop-wise. The reaction mixture was refluxed overnight at 50 °C. The resulting platinum(II) complexes were obtained as precipitates, washed with ultrapure water and diethyl ether and dried in vacuum overnight. They were characterized with similar techniques as ligands.

PtC1, Yield, 55 mg, (35 %). ^{1}H NMR (400 MHz, DMSO-d_6) δ 11.12 (s, 1H), 8.80(d, 3H), 7.96 (t, 3H), 7.28 (d, 3H), 7.12 (d, 3H) ppm, ^{13}C NMR (100 MHz, DMSO-d_6) δ, 153.7, 148,6, 137.6, 117, 112.4 ppm, ^{195}Pt NMR -2105 ppm. Anal. Calcd. for $C_{16}H_{13}N_3PtCl_2$, C, 37.35, H, 2.55, N, 8.17, Found C, 37.52, H, 3.02, N, 7.84,TOF MS ES$^+$, *m/z:* $[M\text{-}Cl]^+$ = 479.0607.

PtC2, Yield, 69 mg, (44 %).^{1}H NMR (400 MHz, DMSO-d_6) δ8.83(d, 2H), 8.04 (t, 2H), 7.68 (d, 2H), 7.53 (d, 2H), 7.36 (t, 1H), 7.26 (ddd, 4H), 5.43 (s, 2H) ppm, ^{13}C NMR (100 MHz, DMSO-d_6, 303 K) δ, 153.4, 151.7, 148.4, 141.3, 136.2, 129.2, 127.3, 117.8, 114.8, 53.7 ppm, ^{195}Pt NMR -2189.2 ppm. Anal. Calcd. for $C_{17}H_{15}N_3PtCl_2$, C, 38.72, H, 2.87, N, 7.97, Found C, 38.46, H, 3.07, N, 8.10; TOF MS ES$^+$, *m/z:* $[M+Na]^+$ = 550.0247.

PtC4, Yield, 120 mg, (53 %). ^{1}H NMR (400 MHz, DMSO-d_6) δ 8.83 (d, 6H), 8.04 (s, 3H), 7.74 (d, 4H), 7.30 (d, 14H), 5.34 (s, 6H) ppm, ^{13}C NMR (100 MHz, DMSO-d_6 303 K) δ, 153.5, 152.0, 141.5, 137.4, 127.3, 121.6, 116.8 and 53.9, ^{195}Pt NMR -2190.3 ppm. Anal. Calcd. for $C_{39}H_{33}N_9Pt_3Cl_6$, C, 32.84, H, 2.33, N, 8.84, Found C, 32.36, H, 2.51, N, 8.60; TOF MS ES$^+$, *m/z:* $[M\text{-}Cl]^+$ = 1390.0830.

5.2.4 Synthesis of complexes PtC3 and PtC5

These complexes were synthesized according to the procedure reported by Corey *et al.*[37,38] Synthesis of [$(PtCl_2)_3$(tdab), **PtC3**] and [$(PtCl_2)_3$ (tdat), **PtC5**]: 93.9 mg (0.160 mmol) of tdat was dissolved in 6 mL $CH_2Cl_2$and placed in a reaction tank. Benzene (4 mL) and a solution of K_2PtCl_4 (200 mg, 0.481 mmol) in a mixture of 3 mL of H_2O and 5 mL of DMSO were layered upon the solution of tdat in the reaction tank. The yellow K_2PtCl_4/H_2O/DMSO solution sank through the layer of benzene and settled upon the tdat/CH_2Cl_2 layer. The solvents were allowed to diffuse for two weeks at ambient temperature under nitrogen to dryness. Yellow crystalline solids were obtained weighed and characterized.

PtC3, Yield, 108 mg, (49 %). ^{1}H NMR (400 MHz, DMSO-d_6) δ 8.88 (d, 6H), 7.96 (t, 6H), 7.30 (d, 6H), 7.12 (t, 6H), 3.48 (s, 3H) ppm, ^{13}C NMR (100 MHz, DMSO-d_6 303 K) δ, 154.5, 152.2, 142.5, 137.4, 127.3, 121.6, 116.8 ppm, ^{195}Pt NMR -2103.5 ppm. Anal. Calcd. for $C_{33}H_{27}N_9Pt_3Cl_6$, C, 29.41, H, 2.02, N, 9.35, Found C, 29.63, H, 1.98, N, 9.10.

PtC5, Yield, 118 mg, (53 %). ^{1}H NMR (400 MHz, DMSO-d_6) δ 8.80 (d, 6H), 7.96 (t, 6H), 7.30 (d, 6H), 7.10 (t, 6H) ppm, ^{13}C NMR (100 MHz, DMSO-d_6) δ, 157.4, 154.8, 146.2, 137.2, 122.9, 120.8, 117.2 ppm, ^{195}Pt NMR -2104.2 and -2155.6 ppm. Anal. Calcd. for $C_{33}H_{24}N_{12}Pt_3Cl_6$, C, 28.59, H, 1.74, N, 12.12, Found C, 28.93, H, 1.54, N, 11.80; TOF MS ES$^+$, *m/z:* $[M\text{-}Cl]^+$ = 1351.0259.

5.3 Preparation of complex solutions for kinetic analysis

Owing to poor solubility of the chloride complexes they were converted to aqua analogues according to reported method.[39-43] Aqua solutions were prepared by refluxing chloride complexes with equivalent amount of silver perchlorate. Perchlorate salts are preferred due to their high solubility in water and are kinetically stable. The solutions were refluxed at 40-50 ^{o}C for 48 hours in 0.1 M $HClO_4$ (50 mL). Perchlorate salts and $HClO_4$ acid were used as inert electrolytes and ClO_4^- anion is non-complexing ion. It provides strong acidity with minimal

interference since it is weakly nucleophilic. Increased acidity results from the conjugate base of $HClO_4$ acid, ClO_4^- anion that has its negative charge distributed equally over the four oxygen atoms. This delocalization of the conjugate base, ClO_4^- anion, contributes to the increased acidity of $HClO_4$ acid than HCl acid. Also $HClO_4$ acid is not susceptible to hydrolysis. As such $HClO_4$ acid and perchlorate salts were used to adjust ionic strength in kinetic studies where other electrolytes might complex the metal ion. The AgCl precipitate was removed by filtration through 0.45 µmilli-pore membrane filter. The removal of the Cl^- ions by Ag^+ to form $AgCl_{(s)}$ ensured presence of platinum aqua species, $[Pt(OH_2)_2]^{2+}$ in the solution and ClO_4^- as the counter ion.. This is supported by the pK_a values that indicate at pH 2.0 the major species involved in kinetics processes are aqua species.The resulting aqua solutions were titrated with NaOH solution to determine the pK_a values of the complexes for kinetic investigations.

5.4 Preparation of aqua complexes for pK_a determination

Spectrophotometric pH titrations were carried out on UV-Vis spectra on a Varian Cary 100 Bio spectrophotometer. NaOH was used as the base for spectrophotometric titration in the pH range 1 – 10. To avoid absorbance corrections due to dilution a large volume of the platinum aqua complex (250 mL) was used. To avoid leaching of chloride ions, 500 µL of the sample taken in ampoules were placed on the electrode and pH recorded then discarded. The pH was adjusted by adding 0.01, 0.05, 0.10 and 0.50 M solutions of either NaOH or $HClO_4$ acid. The pH of the solution was maintained at pH 2.0 based on the pK_a study and the ionic strength was maintained at 0.1 M using $NaClO_4$.

5.5 Kinetic measurements

Spectral changes resulting from mixing the trinuclear Pt(II) complex and nucleophile solutions were recorded over the wavelength range 200 to 800 nm to establish a suitable wavelength at which kinetic measurements were performed. A summary of the used wavelength for each nucleophile is summarized in Table S5.1 (Appendix). All kinetic measurements were performed under *pseudo*-first-order conditions at least 20 fold and 60-fold excess of the nucleophile over that of the metal concentration for mononuclear and trinuclear complexes respectively. This ensured at least 10-fold of nucleophiles concentration at each platinum

centre hence forced the reaction to completion. The temperature was controlled throughout all kinetic experiments within an accuracy of ±0.05^{o}C. Activation parameters ($\Delta H^{\#}$ and $\Delta S^{\#}$) were measured as a function of temperature over a temperature range of 15 to 40 ^{o}C at an interval of 5 ^{o}C. The reported rate constants represent an average value of at least six to eight independent kinetic runs for each set of experimental conditions on the stopped flow and a triplicate for UV-Visible spectrophotometer. All data obtained from both the UV-Visible and stopped flow spectrophotometric techniques were fitted to first-order exponential function to generate the pseudo-first-order rate constants (k_{obs}). The reactions were followed by the changes in absorbance at suitable wavelengths for both fast reactions on the stopped flow and slow ones on the UV-Vis spectrophotometer.

5.6 Computational Calculations

Similar computational calculations were carried out as in the previous two chapters. The optimized molecular structures are presented in Figure 5.2 while the labeling of the atoms is shown in Figure 5.3. The DFT-optimized structure of **PtC1** shows the dihedral and basal angles between two pyridyl groups chelated to Pt(II) centre. Selected bond lengths, bond angles and other parameters are given in Table 5.1.

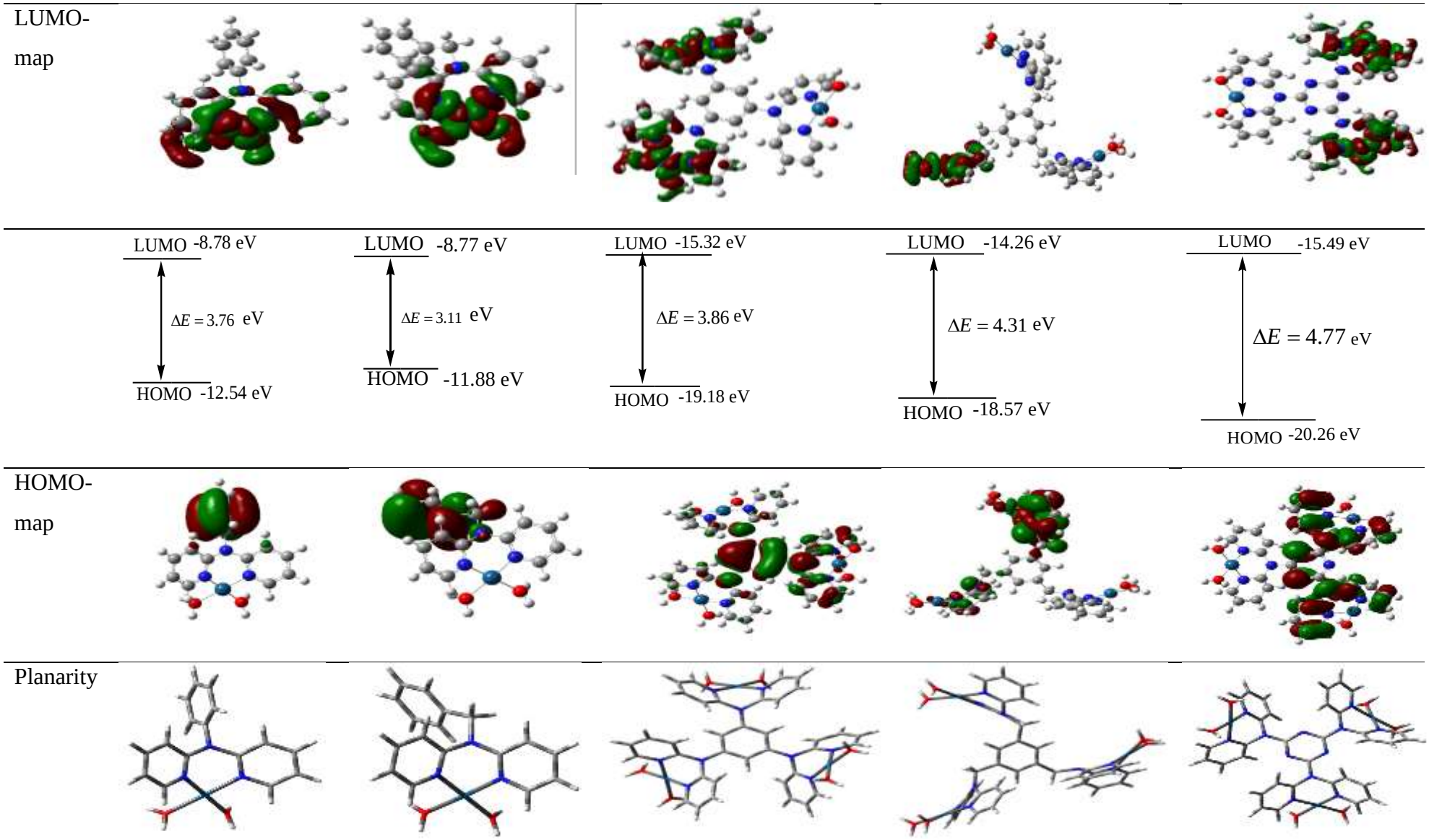

Figure 5.2: DFT optimized structures of HOMO and LUMO frontier molecular orbitals of the platinum(II) complexes at B3LYP/LANL2DZ level theory (Isovalue = 0.02).

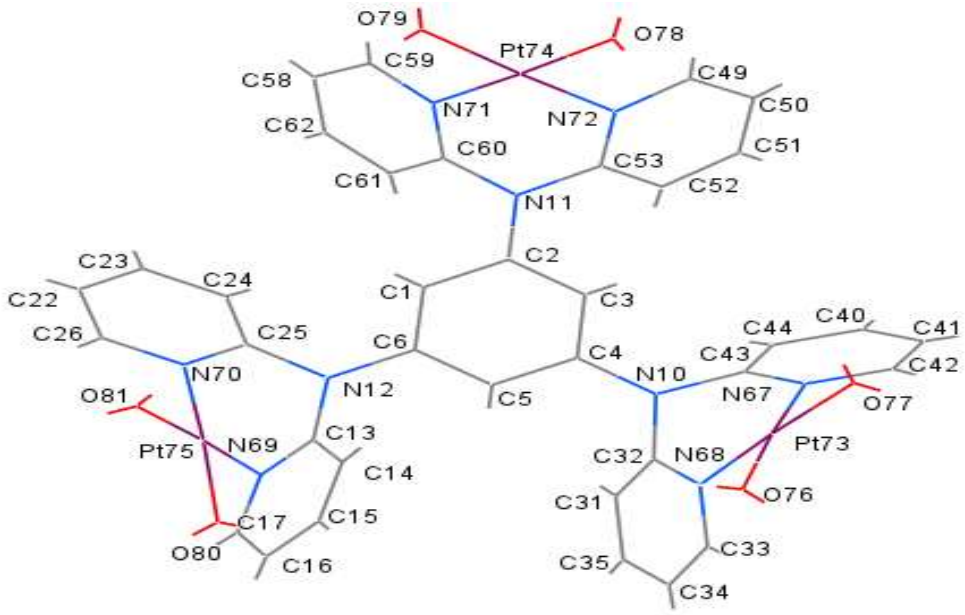

Figure 5.3: Optimized molecular structure of **PtC3** showing the coordination spheres of the complex. Hydrogen atoms were not labelled for clarity. Extracted data is summarized in Table 5.1.

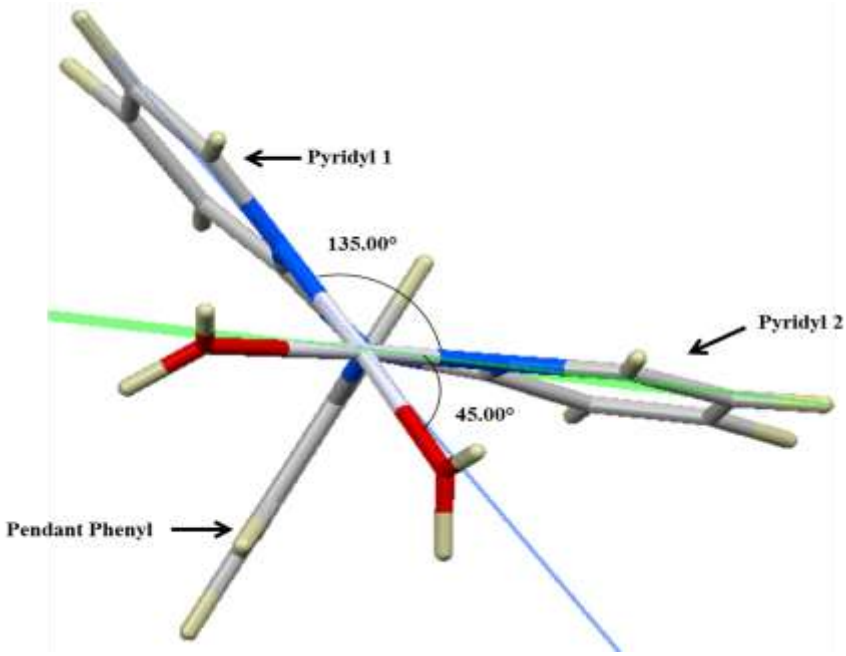

Figure 5.4: DFT-optimized structure of **PtC1** showing the dihedral and basal angle between two pyridyl groups. The dihedral and basal angles have minimal effect on the reactivity of the complexes.

Table 5.1: Selected bond lengths (Å), bond angles (degrees) and NBO charges for the various atoms of the complexes

Complex		**PtC1**	**PtC2**	**PtC3**	**PtC4**	**PtC5**
HOMO-LUMO ΔE						
LUMO/eV		-8.78	-8.77	-15.32	-14.26	-15.49
HOMO/eV		-12.54	-11.88	-19.18	-18.57	-20.26
ΔE/eV		3.76	3.11	3.86	4.31	4.77
Electrophilicity index (ω) (eV)		30.22	34.20	77.09	62.41	66.88
NBO Charges on: Pt		0.755	0.760	0.786	0.781	0.786
				0.786	0.772	0.786
				0.786	0.772	0.786
Dipole moment (Debye)		5.9126	6.4378	2.6377	4.6285	2.7545
Inter-atomic distance (Å)	C4-N10	1.4736	1.5128	1.4530	1.5026	1.4122
	C32-N10	1.4135	1.4112	1.4391	1.4195	1.4477
	C43-N10	1.4135	1.4091	1.4391	1.4199	1.4467
Intermetallic distance (Å)	Pt73-Pt74			9.0082	11.1296	8.7157
	Pt73-Pt75			9.8967	11.5317	9.7200
	Pt74-Pt75			9.8964	12.6557	9.7201
Dihedral angle between pyridyl rings (°)		45	50.37	55.84	40.23	54.49

Inter-atomic distance were obtained from Figure 5.2

5.7 Determination of pK_a values for the aqua complexes

The pK_a titration studies were carried out to ascertain the acidity of the complexes. The aim of pK_a determination was to ascertain the active species containing the more labile Pt-$(H_2O)_2$ prevails in solution. This ensured that kinetic studies were carried out with complexes in their aqua rather than in the less reactive deprotonated aqua/hydroxo form. The pK_a titrations showed all the complexes to exist in aqua species at pH 2.0. Basing on this pK_a titration data, reaction of aqua complexes were performed at pH 2.0 to ensure that the complexes exist as aqua species. A typical UV-Vis spectrum recorded during spectrophotometric titration of the six-aqua complex with NaOH is shown in Figure 5.5. The pK_a values were determined from Boltzmann Equation 5.1 by fitting a characteristic sigmoid curve and locating the inflection point using the Origin 7.5® program. The pK_a values of the deprotonated complexes are summarized in Table 5.2 while the proposed deprotonation mechanism is represented in equilibrium reaction in Scheme 5.2 for mononuclear analogue.

$$y = A_2 + (A_1 - A_2)/(1 + \exp(x - x_0)/\partial x) \qquad \text{Eq [5.1]}$$

where A_1 and A_2 are initial and final y values respectively, x_0 = centre, ∂x = width. The y value at x_0 is half way between the two limiting values A_1 and A_2. The y value changes drastically within a range of x variable. The width of this range is approximately ∂x.

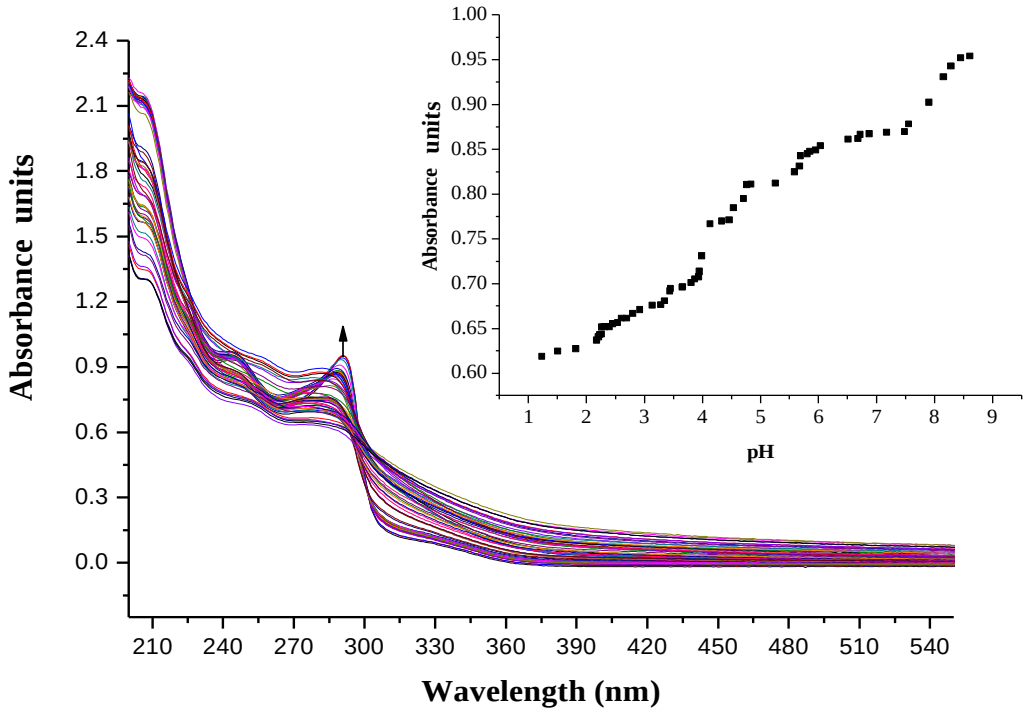

Figure 5.5: UV/Vis spectra for the titration of 1.3 mM **PtC5** complex recorded as a function of pH in the range of 2 to 10 at 25 ^{o}C, *Inset* plot of absorbance versus pH at λ = 295 nm.

Table 5.2: A summary of pK_a values obtained for stepwise deprotonation of aqua Pt(II) complexes investigated

Complex	PtC1	PtC2	PtC3	PtC4	PtC5
pKa$_1$	2.32 ± 0.01	2.87 ± 0.02	2.37 ± 0.08	2.53 ± 0.02	2.23 ± 0.02
pKa$_2$	4.53 ± 0.02	6.97 ± 0.11	3.30 ± 0.01	3.17 ± 0.01	3.34 ± 0.10
pKa$_3$			4.02 ± 0.01	3.60 ± 0.01	4.03 ± 0.02
pKa$_4$			4.78 ± 0.08	4.30 ± 0.01	4.66 ± 0.08
pK_{a5}			6.73 ± 0.07	5.42 ± 0.03	5.70 ± 0.04
pK_{a6}			8.45 ± 0.01	7.46 ±0.07	7.99 ± 0.03

The pK_a values are in the order **PtC5 > PtC1** > **PtC3** > **PtC4** > **PtC2** which corroborates the electronic properties of the bridging ligands. The trend shows complexes with rigid linkers to have lower pK_a values compared to those with methylene groups. The reduced acidity of the complexes with flexible linkers is attributed to the inductive effect of methylene linker that increases electron density on the dipyridyl rings.[39,41] This makes deprotonation of the coordinated aqua ligands difficult due to increased electron density around the Pt(II) centre. The higher electron density in these compounds is supported by DFT calculations that show raised HOMO orbitals in complexes possessing methylene linkers. Raised HOMO orbitals signify addition of electrons to the respective orbitals. On the other hand, the low-lying LUMO orbitals in rigid complexes **PtC1**, **PtC3** and **PtC5** augment a better π-back-donation of electrons from the metal centre to the pendant phenyl ring. This effect lowers electron occupation in the 5d_{xz} orbital by a π back-donation. This decreases electron density on the Pt(II) atom in the xz plane leading to stabilization of the pentacoordinated transition state. The π back-donation to the heterocyclic ligand in complex **PtC5** stipulates the transfer of negative charge into its delocalized π-system, the LUMO. The study shows the negative charge to be shared by more atoms in **PtC5** in Scheme 5.2 which is favourable for its reactivity. The low lying LUMO orbitals account for extensive delocalization in the complex. Electronic factors in rigid complexes are also exhibited by bond lengths of the atoms. For instance, the short C4-N10 in rigid complexes (1.4122–1.4736 Å) are indicative of partial double bond character (sp^2 hybridization) compared to methylene linked complexes with longer bond length (1.5026–1.5128 Å) indicating single bond character (sp^3 hybridization). This findings show more extended and effective delocalization in rigid complexes than flexible analogues. As such, higher acidity in rigid complexes is expected due to more effective π-back donation. This results are also in agreement with literature report[44a,45-47] showing methylene group to have inductive effect. The introduction of methylene spacers destroys the conjugacy of the complexes hence reduced acidity and reactivity.[48-50a]

The subsequent deprotonation values are higher due to lowering of overall charge of the complex. The decrease in charge in trinuclear complexes from 6^+ to 5^+ decreases the electrophilicity of the metal centres decreasing the acidity the complexes upon formation of

hydroxo species. Thus, increase in pK_a trend reported is due to the decrease in the overall charge of the complexes. The higher pH values recorded for subsequent deprotonation was due to formation of the hydroxo species. Higher pH values are recorded due to hydroxo-aqua species in the solutions which are less reactive towards the entering ligands.

The introduction of nitrogen atoms in the backbone of benzene (**PtC5**) lead to an increase in acidity of the coordinated aqua molecules. This is due to the π-accepting properties of triazine that reduce electron density from the metal centres. This increases electrophilicity of the metal centres hence lower pK_a values. This is also supported by low lying HOMO orbitals that suggest removal of electrons from HOMO orbitals. Increased π-back bonding in **PtC5** is further supported by shorter C4-C10, C2-C11 and C6-N12 bond lengths (1.4122 Å) compared to N10-C32, N10-C43, N11-C53, N11-C60, N12-C13, N12-C25 (1.4477 Å). The variation in bond lengths in this complex indicates flow of electrons from 5*d* orbitals of the metal to the antibonding orbitals of triazine ring. Similar observation was also reported by Wang *et al.,*[38] and El-Ghayoury *et al*.[50b] Thus, the presence of hetero-atoms in the benzene ring enhances the transfer of negative charge into its π delocalized system that supports resonance as proposed in Scheme 5.2. The resonance property of the compound has a significant effect on both bond lengths and the acidity of the coordinated aqua ligands in this complex.[51] The conjugate base of this complex is proposed to enjoy resonance stabilization making it more acidic. This is reflected in the out-of ring nitrogen atoms showing sp^2 hybridization while the inner benzene nitrogen atoms possess high electron density due to increased π-back bonding in triazine backbone. Thus, the resonance effect on pK_a values in **PtC5** moiety agrees with predictable behaviour of the complex.

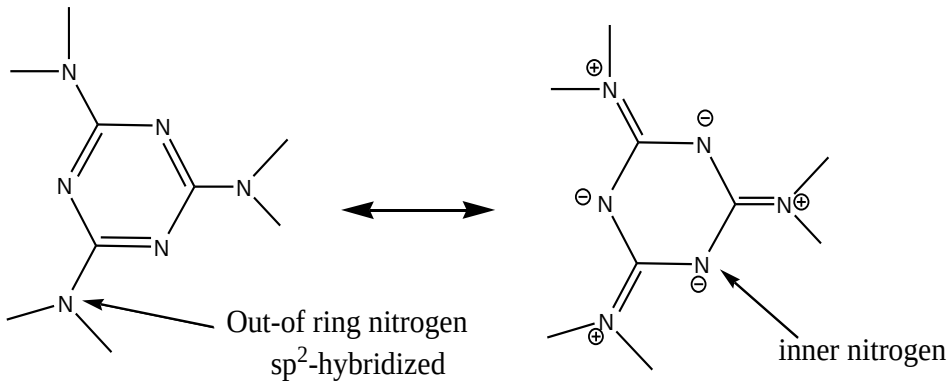

Scheme 5.2: The resonance hybrid structures of **PtC5** complex with 1,3,5-triazine backbone

5.8 Kinetic studies

The substitution reactions of coordinated aqua ligands with bio-relevant nucleophiles *viz.* **TU**, **DMTU** and **TMTU** was carried out under *pseudo*-first-order conditions using conventional UV-Visible spectrophotometry and stopped flow techniques. The suitable wavelengths for kinetics were determined by premixing equal volume of the complex with that of nucleophile in a tandem cuvette then mixing the solutions. A typical spectral change in a kinetic trace is shown Figure 5.6. The subsequent decrease in absorbance indicates the presence of two subsequent reaction steps of **PtC5** with **TU**. The recorded kinetic traces were fitted to a single exponential function. Figure 5.7 shows typical plots of absorbance verses time for **PtC5** with **TU** and **DMTU** on the stopped flow while part (c) shows the kinetic trace with **TMTU** on the UV-Vis spectrophotometer.

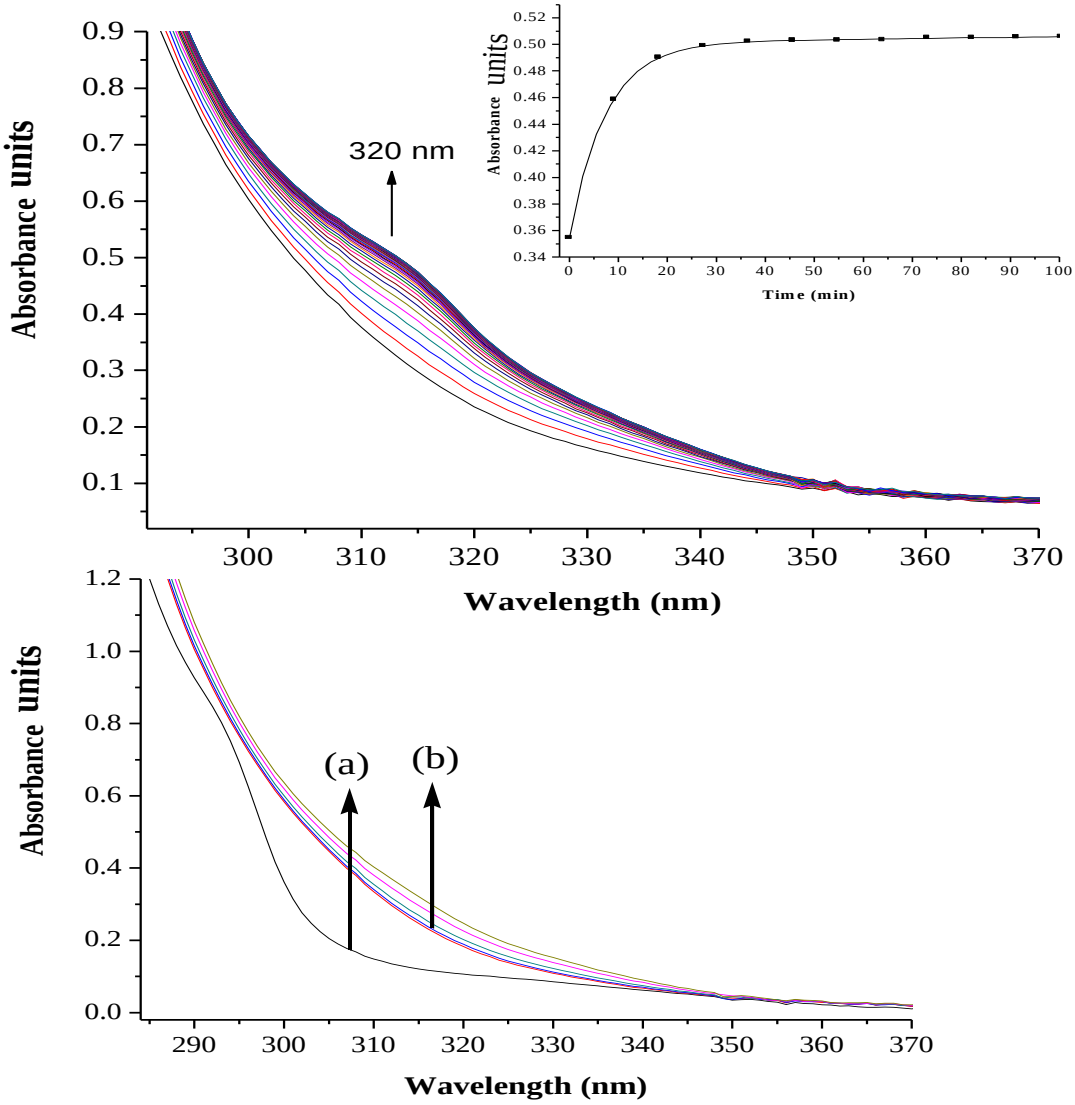

Figure 5.6: UV-Vis spectral changes during the reaction of 0.04 mM **PtC5** with 0.041M **TU** at T = 298 K, pH = 2.0 and I = 0.1 M $NaClO_4$. (a) Initial spectrum before adding **TU** and (b) spectrum at t = 30 s; Successive spectra were recorded at an intervals of 5 min.

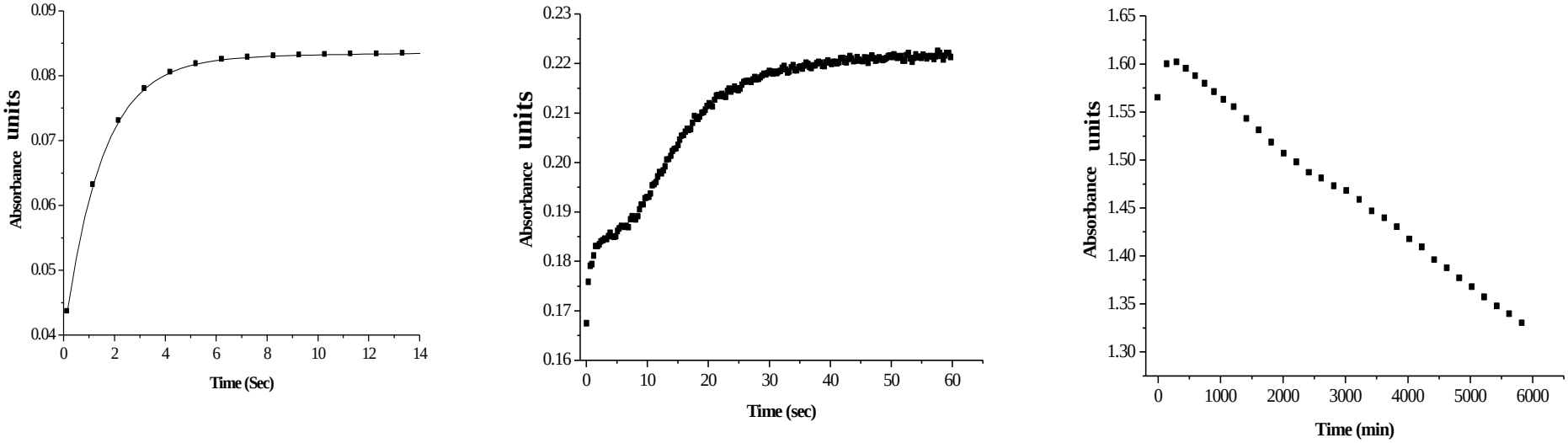

(a) **(b)** **(c)**

Figure 5.7: Typical kinetic traces showing a fast substitution reaction step of **PtC5** with (a) **TU** (b) **DMTU** on the stopped-flow while (c) is the last two steps of **TMTU** on UV-Vis spectrophotometer at T = 298 *K*, pH = 2.0, *I* = 0.1 M $NaClO_4$. The first step of **TMTU** was observed on the stopped-flow while the third step of **DMTU** was recorded on UV-Vis spectrophotometer.

The observed *pseudo*-first order constants, k_{obs} were obtained as average values of six to eight independent kinetic runs for each experimental condition on the stopped-flow and in triplicates on UV-visible spectrophotometry. As mentioned in the previous chapter, these many runs showed reproducibility that illustrated the precision between run replicates. The values of k_{obs}, were plotted against the entering nucleophile concentration. The plots are linear with zero or negligible intercept as shown in Figures 5.8, 5.9 and S5.3–S5.5 in the Appendices. The rate constants (k_2) are linearly dependent on the concentration of entering of nucleophile. The $k_{obs(1,2,3)}$ is expressed by Equation [5.2].

$$k_{obs(1,2,3)} = k_{2(1st,\ 2nd,3rd)}[Nu] \qquad \text{Eq [5.2]}$$

The second-order rate constants for reaction steps of the corresponding complexes at 25 ^{o}C are summarized in Table 5.3.

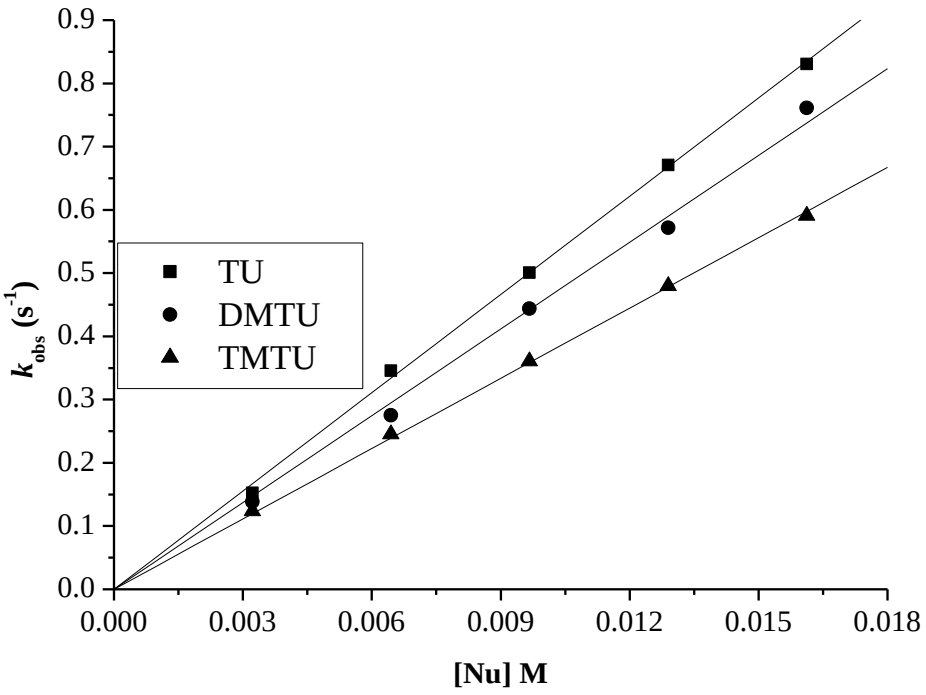

Figure 5.8: Plots of $k_{obs(1)}$ versus nucleophile concentration for the reaction of **PtC1** at pH = 2.0, T = 298 K, I = 0.1 M $NaClO_4$.

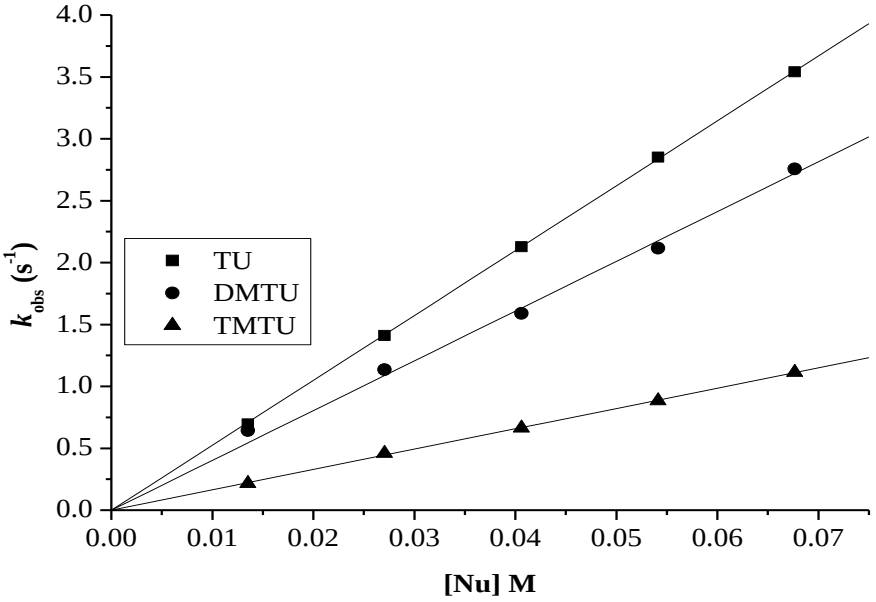

Figure 5.9: Plots of $k_{obs(1)}$ versus nucleophile concentration for the reaction of **PtC5** at pH = 2.0, T = 298 K, I = 0.1 M $NaClO_4$.

Table 5.3: A summary of the second order rate constants, k_2, for the reaction of the investigated complexes at pH = 2.0, T = 298 K and at I = 0.1 M $NaClO_4$

Complex	**Nu**	2^{nd} order rate constant/$M^{-1}s^{-1}$		
		$k_{2(1st)}$	$k_{2(2nd)}$ x10^{-2}	$k_{2(3rd)}$ x10^{-3}
PtC1	**TU**	51.78 ± 0.40	4 ± 0.30	-
	DMTU	45.74 ± 0.77	1 ± 0.02	-
	TMTU	37.06 ± 0.22	-	-
PtC2	**TU**	33.34 ± 0.27	3 ± 0.40	-
	DMTU	25.09 ± 0.19	1 ± 0.01	-
	TMTU	11.45 ± 0.04	1 ± 0.02	-
PtC3	**TU**	40.71 ± 0.22	5 ± 0.30	
	DMTU	37.23 ± 0.55	1 ± 0.01	
	TMTU	15.64 ± 0.26	-	-
PtC4	**TU**	27.87 ± 0.25	6 ± 0.40	-
	DMTU	20.84 ± 0.14	2 ± 0.04	-
	TMTU	6.73 ± 0.05	0.5 ± 0.01	-
PtC5	**TU**	52.41 ± 0.11	4 ± 0.10	-
	DMTU	40.21 ± 0.68	64 ± 0.30	4 ± 0.1
	TMTU	16.43 ± 0.09	7 ± 0.10	Too slow

5.9 Activation parameters

To investigate thermodynamic and chemical stability of the complexes, reactivity was performed at various temperatures (15 to 40 °C. This enabled examine the changes in thermodynamic stability *viz* the enthalpy, $\left(\Delta H^{\#}\right)$ and the entropy, $\left(\Delta S^{\#}\right)$ of activation. These activation parameters were determined from the Eyring plots illustrated in Figures 5.10 and 5.11 and (Figures 5.6-5.8) in the appendix using Eyring Equation 3.1. The complexes showed kinetic stability at all temperatures that conferred thermostability of the investigated class of Pt(II) complexes.

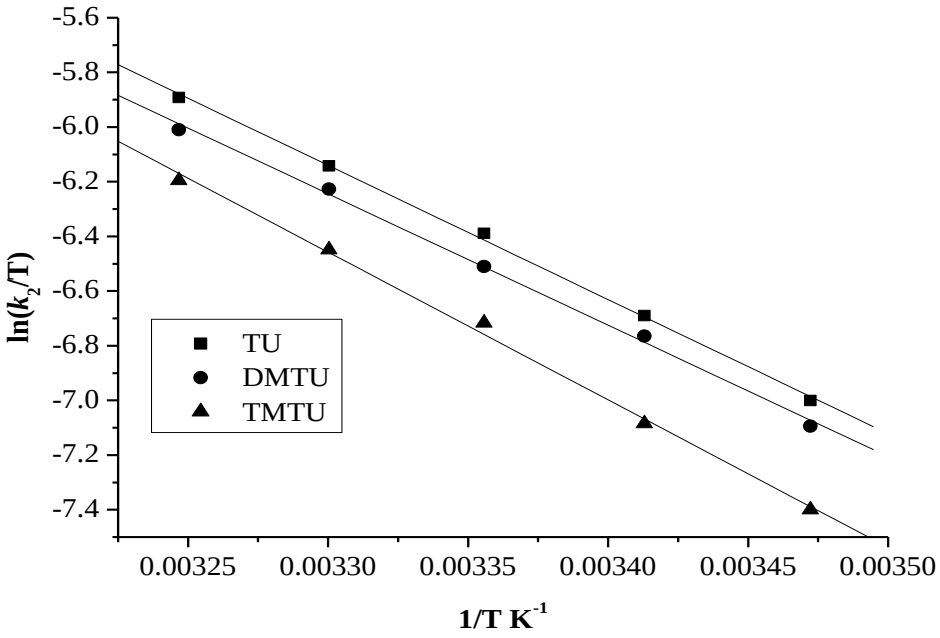

Figure 5.10: Eyring plots for first substitution step of **PtC1** monitored on stopped-flow spectrophotometer at I = 0.1 M $NaClO_4$, pH = 2.

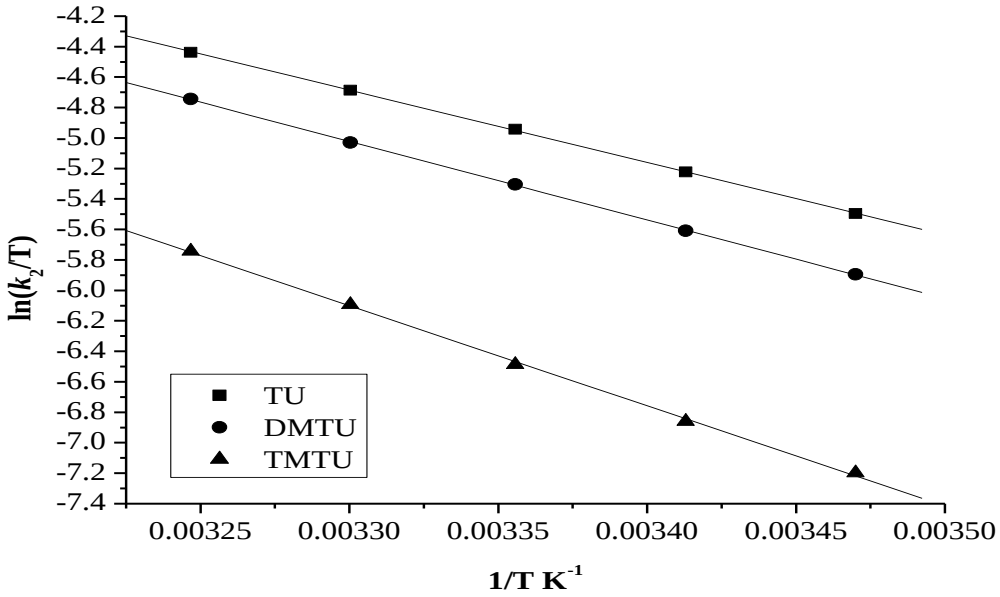

Figure 5.11: Eyring plots for the first substitution step of **PtC5** monitored on stopped-flow spectrophotometer at I = 0.1 M $NaClO_4$, pH = 2.0.

Table 5.4: A summary of the activation parameters for the substitution of aqua ligands pH = 2.0 and at I = 0.1 M $NaClO_4$

Complex	Nu	Activation Enthalpy/ kjmol^{-1}		Activation entropy/ J mol^{-1}K^{-1}	
		$\Delta H_1^{\#}$	$\Delta S_1^{\#}$	$\Delta H_2^{\#}$	$\Delta S_2^{\#}$
PtC1	**TU**	40.83 ± 0.9	-114± 3	21.91 ± 0.4	-229 ± 1
	DMTU	39.97± 1.2	-118±4	29.89±0.4	-213 ± 1
	TMTU	44.93 ± 1.5	-103 ± 5	-	-
PtC2	**TU**	39.81 ± 0.3	-121±1	20.54± 0.8	-249±2
	DMTU	43.47 ± 1.7	-111±6	26.74± 0.9	-241±3
	TMTU	40.86 ± 0.8	-126±3	41.02± 1.5	-179±5
PtC3	**TU**	39.58 ± 0.8	-108± 3	28.20± 1.0	-209 ± 3
	DMTU	40.48 ± 0.7	-106± 2	33.33±0.8	-200 ± 3
	TMTU	53.30± 1.2	-66± 4	-	-
PtC4	**TU**	38.60 ± 0.9	-116±3	23.31±0.3	-221 ± 1
	DMTU	30.00 ± 0.5	146± 2	30.41±0.6	-204 ±2
	TMTU	45.22± 1.1	-104 ± 4	44.48 ± 0.1	-164 ± 1
PtC5	**TU**	39.49 ± 0.3	-107 ± 1	32.80 ± 0.4	-194 ± 1
	DMTU	44.04± 1.4	-94 ± 5	30.80 ± 0.5	-165 ±2
	TMTU	52.10 ±0.8	-74± 3	51.09 ± 1.3	-121 ± 4

The small positive enthalpies and significantly large negative entropy values support an associative mode of substitution mechanism commonly reported for the Pt(II) square-planar complexes.[52-55] In this mode of mechanism, the ML_3X complex binds to the incoming ligand Y to form a five-coordinate intermediates $(ML_3XY)^{\#}$ as shown in Scheme 5.2. Substitution of X results in a 16 electron complex ML_3Y in which the negative activation entropy indicates an increase in the order of the transition state relative to the reactants.[52,53] The small positive enthalpy values reported in Table 4 is attributed to bond formation before bond breaking in the transition state.[54,55]

5.10 Substitution reaction

Since it is unlikely for the entering nucleophile to displacement six water molecules by a single kinetic phase, a biphasic reaction is proposed at each metal centre. The first step is attributed to fast substitution of one water molecule at each metal centre. The second phase is composed of two simultaneous reactions; where the second water molecule is displaced followed by a dechelation process. The extent of the second step was governed by the steric hindrance caused

by coordination of the first nucleophile. The much slower second step was joined by the displacement of the labilized linker due to the strong *trans* effect of thiourea coordination. The proposed reaction mechanism with thiourea as the entering nucleophile is shown in Scheme 5.3. This shows S-donor ligands as strong and efficient nucleophile that can compete with DNA for binding to Pt(II) complexes.

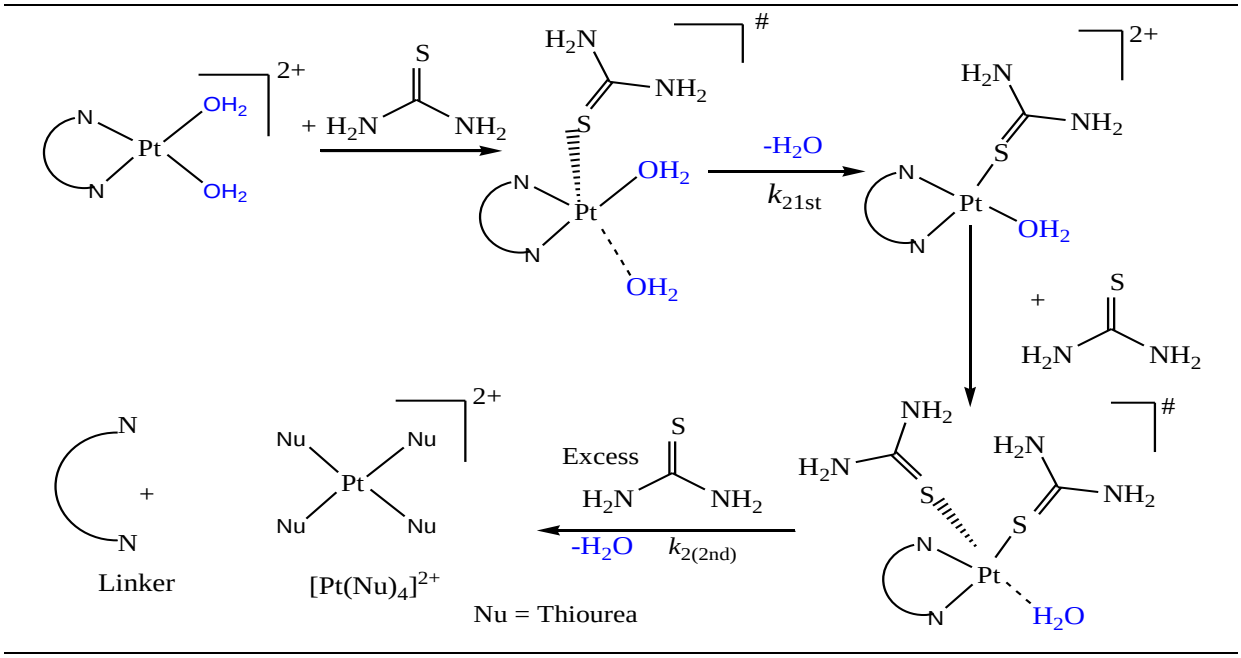

Scheme 5.3: Proposed substitution mechanism showing biphasic substitution at each Pt(II) centre followed by the dechelation process

The dechelation step was confirmed using ^{1}H and ^{195}Pt NMR kinetics by monitoring coordination details of the reactants and products (Figures 5.12 and 5.13). Coordination of the ligand to the metal ion causes ^{1}H chemical shifts. Figure 5.12 shows an array of ^{1}H NMR spectra for the reaction between **PtC3** with 6 equivalents of thiourea. The spectra show net chemical shifts of the coordinated pyridyl protons indicating changes in their coordination environment. The dipyridyl protons denoted $\mathbf{H_a}$ were monitored due their proximity to *N*-donor atoms when coordinated to the metal centre. Their resonance on the chloride complex appear downfield at δ = 8.88 ppm that indicates coordination of platinum atom. This downfield shift is due to the change in electron density on coordination to the metal atom. On reaction with excess **TU** the $\mathbf{H_a}$ protons shift to $\mathbf{H_a}$', which appear upfield at δ = 8.28 ppm similar to those of

uncoordinated ligand. A decrease in electron density on the pyridyl by the σ effect yields to this downfield shift at all ring positions on complexation.

A signal peak shown at δ = -2103.5 ppm by ^{195}Pt NMR is consistent with platinum(II) complexes with *cis*-PtN_2Cl_2 configuration.[56,57] On reaction with 6 equivalents of **TU** shows a peak at -3905.6 ppm with no reaction intermediates (Figure 5.12). This shifting of the peak indicates the preference of Pt(II) to coordinate to sulphur-donor ligands. The study show Pt-N adducts to be converted to Pt-S adducts.[58] The peak at -3906.6 ppm on ^{195}Pt NMR denotes formation of $[Pt(\mathbf{TU})_4]^{2+}$ complex when reacted with excess thiourea.[59,60] From experimental data both the ^{1}H and ^{195}Pt NMR support the complexes to undergo displacement of the linker induced by strong *trans* effect of the sulphur donor atoms.[61]

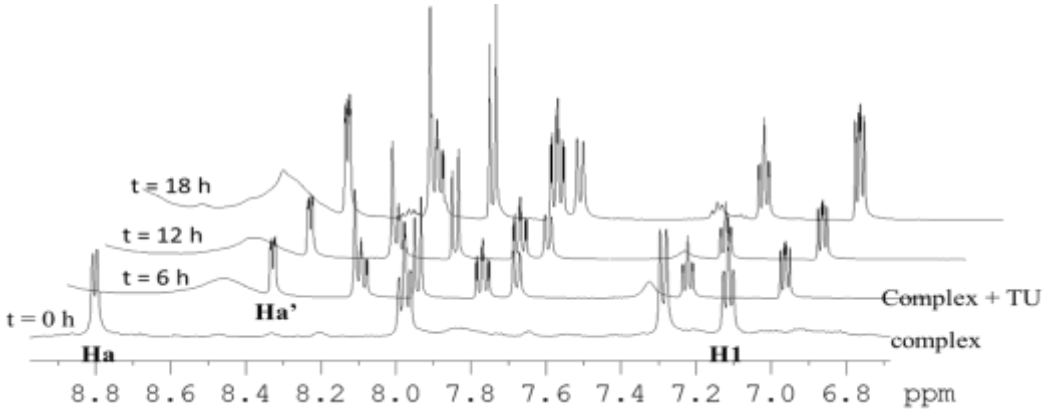

Figure 5.12: Time dependent stacked plot of ^{1}H NMRspectra of **PtC3**with 6 equivalents of **TU** undergoing dechelation to liberate the bridging linker.

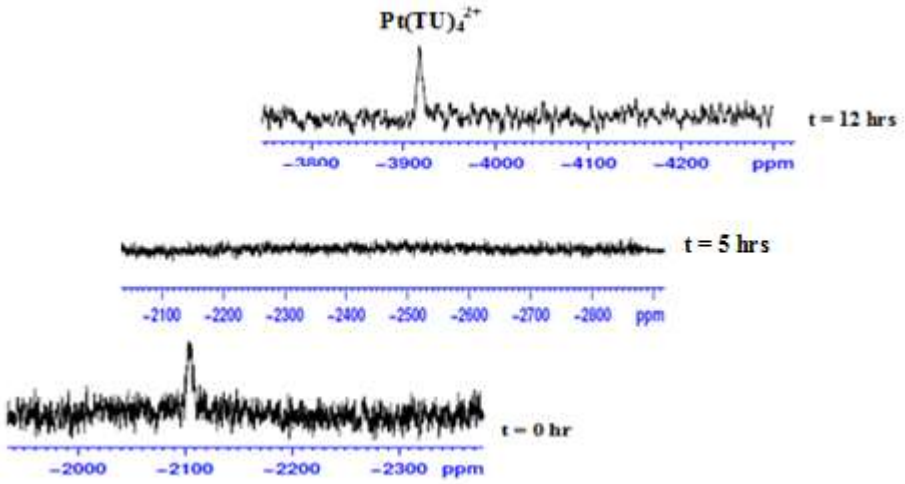

Figure 5.13: Time dependent ^{195}Pt NMR shifts of **PtC3** in DMF forms $[Pt(\mathbf{TU})_4]^{2+}$ on reaction with excess **TU**.

5.11 Discussion

This chapter reports on the reactivity of mono and trinuclear dipyridylamine Pt(II) complexes with biologically relevant molecules. With a view of shedding light on the role of rigidity verses flexibility of bridging moieties, the study shows that introducing methylene groups in the backbone of a complex significantly reduces its reactivity. However, the effect is opposite when a hetero atom or rigidity is introduced as the two enhances reactivity. The experimental results verifies this by showing a reactivity trend of **PtC5** > **PtC1** > **PtC3** > **PtC2** > **PtC4** with **TU** as the entering nucleophile. The trend is governed by both steric and electronic effects arising from the methylene spacers and heteroatoms in the backbone of the ligands. The high reactivity of **PtC5** is due to the decrease of electron density at the Pt(II) centre caused by enhanced π-back-donation *to* π^* orbitals of triazine ligand. The stronger π-acceptor of triazine stabilizes transition state by accepting electron density that is donated by the entering nucleophile to the metal centre. This increases electrophilicity at the Pt(II) centres that leads to high reactivity which is reflected in its lower pK_a values of the coordinated water ligands. This is caused by the presence of electronegative nitrogen atoms which leads to greater π-back-donation from metal centre to the triazine ring. On the other hand, complexes with flexible ligands (**PtC2** and **PtC4)** show slower reactivity than with rigid spacers (**PtC1** and **PtC3**). The study suggests methylene groups to increase electron density on the pyridyl rings and prevent

effective π-back bonding.[62] Also the presence of lone pair electrons on the amine nitrogen makes them stronger σ donors than rigid counterparts. Thus, a combination of rigidity and delocalization accounts for the enhanced reactivity of rigid appended complexes. Rigidity verses flexibility of the ligands along with the number of aqua ligands make an impact on the structural diversities of entangled Pt(II) complexes making a significant influence on their reactivity. Complexes with rigid linkers showed high reactivity.

The high reactivity of **PtC5** is also attributed to the increase in the number of ring electrons when =CH- are replaced by nitrogen atoms. Each nitrogen atom introduces two additional electrons making triazine ring to have six non-bonding electrons in addition to its π-electrons. This unshared pair of electrons to some extent is delocalized and become part of the aromatic π-electron system in both ground and excited states.[63] This complex shows high π accepting property but decreased σ-donor strength as electronegativity is within the ring is increased. This leads to delocalization of the $d\pi$ electrons from the metal to the empty π^* orbitals of the triazine ring. The electron withdrawing effect of 1,3,5-triazine cycle is supported by the lowered HOMO orbitals and wider HOMO-LUMO gap (ΔE = 4.77 eV) Table 5.1. The withdrawal of electron density lowers and stabilizes the HOMO orbitals. This is also reinforced by the presence of low-lying LUMO orbitals which increases π-back-bonding. It should also be noted that in **PtC3**, the amino nitrogen lone pair does not favour conjugation with the central benzene ring due to steric interactions with *ortho* hydrogen atoms. Hence there is reduced π-back donation compared to **PtC5**. In **PtC5** the amino nitrogen lone pair conjugates with triazine ring due to absence of *ortho* hydrogen atoms.

Two consecutive steps were observed for trinuclear complexes **PtC3** and **PtC4** which supports the notion that the three platinum centres are in the same chemical environment. In contrast, **PtC5** shows more reaction steps with sterically hindered nucleophiles supporting the likelihood of fluxionality of the complex in solution.[64,65] The complex is reported to undergo dynamic interchange of chemically inequivalent groups.[65,65] The rotations and unsymmetrical nature of **PtC5** in solution presents the possibility of chemically distinct metal centres as shown in Figure 5.14. However, this behaviour was not observed in **PtC3**. The ^{195}Pt NMR shows a

single peak (Figure 5.14) that corresponds to one set of dipyridyl unit coordinated to Pt centre from the central benzene. This supports the previous study on **PtC3** which had a symmetric structure in solution with all the three dipyridyl units in the same chemical environment.[38] Similarly, **PtC4** showed a single ^{195}Pt NMR spectrum at -2190.3 ppm. This value is consistent with N_2-$PtCl_2$ environment. Single peaks in **PtC3** and **PtC4** supports the number of substitution steps suggesting all the three metal atoms to be chemically equivalent.

In **PtC5** an increase in π electrons makes the complex to have a fluxional behaviour. This fluxionality favours the "up and down" structure that keeps the platinum centres in chemically different environment contrary to the expected symmetry of C_3 conformation. The "up and down" structure, is as a result of the axial and equatorial pyridyl groups undergoing inter-conversion through dynamic process in which the ring undergoes chair conformational change. This makes the electronic structure of **PtC5** to be different from **PtC3** that accounts for the difference in the kinetic and chemical shifts in **PtC5**.[66] The two peaks at -2104.2 ppm and -2156.6 ppm in the ratio of 2:1 by ^{195}Pt NMR spectra indicates platinum centres to be a chemically different environment. Based on this observation different number of substitution steps is expected from fluxional behaviour of **PtC5**.

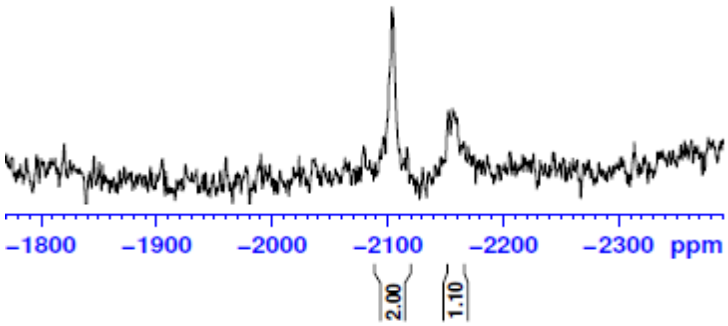

Figure 5.14: ^{195}Pt NMR spectra of complex **PtC5** in DMSO-d_6, showing two inequivalent Pt(II) peaks

On reaction of **PtC5** with 6 equivalents of **TU**, the two peaks disappears signifying two independent platinum peaks. The study suggests the difference in the kinetic behaviour of

trinuclear complexes to be influenced by the degree of conjugation of the amino nitrogen lone pair of electrons of the dipyridylamine unit with the central aromatic ring. The rates of reactions were dependent on the nature of entering nucleophile governed by steric effects in the order: **TMTU** < **DMTU** < **TU**.[59,67]

5.12 Conclusion

This chapter has illustrated that the nature of bridging ligand between the metal centre and the pendant linker has a significant influence on the reactivity of the complexes. It shows that conformational rigidity enhances reactivity while incorporation of methylene groups retards reactivity. The acceleration in the reactivity in rigid complexes is attributed to the effective π-bonding between the metal centre and the pendant rings. On the contrary, introduction of methylene groups prevents such effective π-back bonding and increases electron density that results in a slower nucleophilic substitutions. The study further shows that replacement of –CH groups with N in the phenyl ring accelerates reactivity. Thus, the study shows that the π-accepting property of triazine ring increases the electrophilicity on the Pt(II) metal centre which increases nucleophilic substitution. The Low positive values of enthalpy of activation and significantly large negative values of entropy of activation parameters indicate an associative mechanism of substitution. The successful application of ligand substitution in multinuclear Pt(II) complexes marks the first step to development of new polynuclear antitumour agents. The route to novel anticancer drugs is based on mechanistic knowledge.

Mechanistic insight on reactions of polynuclear Pt(II) complexes under biological and physiological conditions remains the basis for development of novel antitumour drugs. Such inventions and explorations will most likely provide an alternative to modern cancer treatment. After successful substitution reactions of these complexes, further research needs to explore how these compounds bind to DNA molecule at physiological pH and physiological concentrations. Significant progress is proposed in platinum based anticancer agents based on mechanistic understanding of the DNA binding. Therefore, a mechanistic understanding of how metal based drugs achieve their activities is vital to their clinical significance as well as the rational design of new anticancer compounds with improved potency. Further investigation

needs to test the complexes in a range of cancer cell lines and in both *in vitro* and *in vivo* for their anticancer action. Apart from anticancer testing, the complexes need to be tested against antibacterial to explore a multifaceted approach. This will provide an insight on the essential of the complexes that can lead to important contributions to drug discovery.

References

1. W. Yanqing, W. Xiaoyong, W. Jing, Z. Yongmei, H. Weijiang and G. Zijian, *Inorg. Chem*., 2011, **50**, 12661-12668.
2. I. Ali, W. A. Wani, K. Saleem and A. Haque, *Anti-Cancer Agents in Medicinal Chemistry*, 2013, **13**, 296-306.
3. L. Ronconi, A. M. Pizarro, R. J. McQuitty and P. J. Sadler, *Chem. Eur. J*., 2011, **17**, 12051-12058.
4. A. M. Florea and D. Büsselberg, *Cancers*., 2011, **3**, 1351-1371.
5. N. J. Wheate and J. G. Collins, *Curr. Med. Chem.-Anti-Cancer Agents*, 2005, **5**, 267-279.
6. Y. M. Zhao, J. W. He, P. F. Shi, J. H. Zhu, L. Qiu, L. P. Lin and Z. J. Guo, *Dalton Trans.* 2006, 2617−2619.
7. N. J. Wheate and J. G. Collins, *Coord. Chem. Rev*., 2003, **241**, 133-145
8. M. Frezza, S. Hindo, D. Chen, A. Davenport, S. Schmitt, D. Tomco and Q. P. Dou, *Curr. Pharm. Des*., 2010, **16**, 1813-1825.
9. X. Y. Wang and J. Z. Guo, *Dalton Trans.*, 2008, 1521−1532.
10. N. J. Wheate, S. Walker, G. E. Craig and R. Oun, *Dalton Trans*., 2010, **39,** 8113- 8127.
11. S. A. Adnan and Mika K, *Curr. Med. Chem.*, 2006, **13**, 1337-1357.
12. Wang X. Y, *Anti-Cancer Agents Med. Chem.*, 2010, **10**, 396−411.
13. J. B. Mangrum and N. Farrell, *J. Chem. Soc. Chem. Comm*., 2010, **46**, 6640-6650.
14. D. M. Fan, X. L. Yang, X. Y. Wang, S. C. Zhang, J. F. Mao, J. Ding, L. P. Lin, Z. J. Guo, *J. Biol. Inorg. Chem.* 2007, **12**, 655−665.
15. M. X. Lin, X. Y. Wang, J. H. Zhu, D. M. Fan, Y. M. Zhang, J. F. Zhang and Z. J. Guo, *Apoptosis*, 2011, **16**, 288−300.
16. J. D. Roberts, J. Petroutka and N. Farrell, *J. Inorg. Biochem*., 1999, **77**, 51-57
17. X. Wang and Z. Guo, *Chem. Soc. Rev*., 2013, **42**, 202-224.
18. R. A. Ruhayel, J. S. Langner, M. J. Oke, J. Susan, S. J. Berners-Price, I. Zgani and N. Farrell, *J. Am. Chem. Soc*., 2012, **134**, 7135-7146.
19. Z. Yongmei, H. Weijiang, S. Pengfei, Z. Jianhui, Q. Lin, L. Lipng and G. Zijian, *Dalton Trans.*, 2006, 2617-2619.

20. J. H. Zhu, Y. M. Zhao, Y. Y. Zhu, Z. Y. Wu, M. X. Lin, W. J. He, Y. Wang, G. J. Chen, L. Dong, J. F. Zhang, Y. Lu and Z. J. Guo, *Chem.-Eur. J.*, 2009, **15**, 5245−5253.
21. G. J. Kumar, H. V. S. S. Bomma, E. Srihari, S. Shrivastava, V. G. M. Naidu, K. Srinivas and V. J. Rao, *Med. Chem. Res*., 2013, **22**, 5973-5981.
22. L. Ronconi and P. J. Sadler, *Coord. Chem. Rev*., 2007, **251**, 1633-1648.
23. M. J. Rauterkus, S. Fakih, C. Mock, I. Pascasu and B. Krebs, *Inorg. Chim. Acta*., 2003, **350**, 355-365.
24. I. Puscasu, C. Mock, M. J. Rauterkus, A. Röndigs, G. Tallen, S. B. Gangopadhyay, J. E. A. Wolff and B. Krebs, *Z. Anorg. Allg. Chem*., 2001, **627**, 1292-1298.
25. M. J. Bloemink, H. Engelking, S. Karentzopoulos, B. Krebs and J. Reedijk, *Inorg. Chem*., 1996, **35**, 619-627
26. R. B. Weiss and M. C. Christian, *Drugs*, 1993, **46**, 360-377
27. J. Bogojeski and Ž. D. Bugarčić, *Transion Met. Chem*., 2011, **36**, 73-78.
28. M. V. Beusichem and N. Farrell, *Inorg. Chem*., 1992, **31**, 634-639.
29. J. Reedijk, *Chem. Rev.*, 1999, **99**, 2499-2510.
30. W. E. Curtis, M. E. Muldrow, N. B. Parker, R. Barkley, S. L. Linas and J. E. Repine, *Proc. Natl. Acad. Sci.* USA, 1988, **85**, 3422-3425.
31. A. W. Panyako and D. Jaganyi, *Int. J. Chem. Kinet* 1–17, 2017.
32. A. Bianca, D. J. Bray, J. K. Clegg, K. Gloe, G. Karsten, O. Kataeva, F. L. Lindoy, J. C. McMurtrie, P. J. Steel, C. J. Sumbyand M. Wenzel, *Dalton Trans.*, 2006, 4783-4794.
33. C. Tu, J. Lin, Y. Shao and Z. Guo, *Inorg. Chem.*, 2003, **42**, 5795-5797.
34. J. Pang, Y. Tao, S. Freiberg, Y. Xiao-Ping, M. D'Iorio and S. Wang, *J. Mater. Chem*., 2002, **12**, 206-212.
35. N. Wannarit, O. Roubeau, S. Youngme and P. Gamez, *Eur. J. Inorg. Chem*., 2013, 730-737.
36. S. Fakih, W. C. Tung, D. Eierhoff, C. Mock, and B. Krebs, *Z. Anorg. Allg. Chem.*, 2005, **631**, 1397-1402.
37. S. Corey, J. Pang and S. Wang, *Eur. J. Inorg. Chem*., 2002, 1390-1399.
38. Q. De Liu, W. Jia, G. Wu and S. Wang, *Organometallics*, 2003, **22**, 3781–3791.

39. J. Bogojeski, Ž. D. Bugarčić, R. Puchta and R. van Eldik, *Eur. J. Inorg. Chem.*, 2010, 5439-5445.
40. S. Jovanović, B. Petrović, D. Čanović and Ž. D. Bugarčić, *Int. J. Chem. Kinet*., 2011, **43**, 99-106.
41. N. Hochreuther, S. T. Nandibewoor, R. Puchta, R. van Eldik, *Dalton Trans*., 2012, **41**, 512-522.
42. T. Soldatović, Ž. D. Bugarčić and R. van Eldik, *Dalton Trans*., 2009, 4526-4532.
43. N. Summa, R. Schiessl, N. Puchta, H. van Eikema and R. van Eldik R, *Inorg. Chem*., 2006, **45**, 2948-2958.
44. (a) D. Jaganyi, A. Hofmann and van R. Eldik, *Angew. Chem. Int. Ed.*, 2001, **40**, 1680-1683; (b) N. Hochreuther, R. Puchta, R. van Eldik, *Inorg*. *Chem*., 2011, **50**, 8984-8996.
45. J. Tournon and M. A. El-Bayoumi, *J. Am. Chem. Soc*., 1971, **93**, 6396-6398.
46. R. Tandon, T. A Nigst and H. Zipse, *Eur. J. Org. Chem*., 2013, 5423-5430.
47. H. Ertürk, A. Hofmann, R. Puchta and R. van Eldik, *Dalton Trans.*, 2007, 2295-2301
48. F. G. Bordwell and G. J. McCollumn, *J. Org. Chem*., 1976**, 41**, 2391-2395.
49. K. B. Wiberg, J. Ochterski and A. Streitwieser, *J. Am. Chem. Soc*., 1996, **118**, 8291-8299.
50. (a) P. C. Hiberty and C. P. Byrman, *J. Am. Chem. Soc*., 1995, **117**, 9875-9880. (b) D. G. Branzea, A. Fihey, T. Cauchy, A. El-Ghayoury,and N. Avarvari, *Inorg. Chem.*, 2012, **51**, 8545−8556.
51. F. G. Bordwell J. E. Bares, J. E. Bartmess, G. J. McCollumn, M. V. D. Puy, N. R. Vanier and W. S. Matthews, *J. Org. Chem*., 1977, **42**, 315-321.
52. J. D. Atwood, *Inorganic and Organometallic Reaction Mechanisms*, 2nd Ed., Wiley-VCH, New York, 1997,749-771.
53. (a) M. L. Tobe and J. Burgess, *Inorganic Reaction Mechanisms*; Addison-Wesley Longman: Essex, England, 1999, 209-215 (b) R. G. Wilkins, *Kinetics and Mechanisms of Reactions of Transition Metal Complexes*; VCH: Weinheim, Germany, 1991, 136-151; (c) F. Basolo, *Coord. Chem. Re*v., 1996, **154**, 151-161.
54. A. Mandal, P. Karmakar, S. Mallick, B. K. Bera, S. Mondal, S. Ray and A. K. Ghosh, *J. Chem. Sci.*, 2012, **124**, 801-807.

55. A. Mandal, B. K. Bera, S. Mallick, S. Mondal, P. Karmakar and A. K. Ghosh, *Inorg. Chem. Indian J*., 2010, **5**, 176-180.

56. (a) B. M. Still, P. G. A. Kumar, J. R. Aldrich-Wright and W. S. Price, *Chem. Soc. Rev*., 2007, **36**, 665-686.

57. (a) E. Gabano, E. Marengo, M. Bobba, E. Robotti, C. Cassino, M. Botta and D. Osella, *Coord. Chem. Rev*., 2006, **250**, 2158-2174; (b) P. S. Pregosin, *Coord. Chem. Rev*., 1982, **44**, 247-291.

58. T. Soldatović, M. Shoukry, R. Puchta, Ž. D. Bugarčić and R. van Eldik, *Eur. J. Inorg. Chem*., 2009, 2261-2270.

59. P. O. Ongoma and D. Jaganyi, *Dalton Trans*., 2013, **42**, 2724-2734.

60. (a) H. Ertürk, R. Puchta and R. van Eldik, *Eur. J. Inorg. Chem*., 2009, **10**, 1331-1338; (b) H. Ertürk, J. Magut, R. Puchta and R. van Eldik, *Dalton Trans*., 2008, 2759-2766

61. P. O. Ongoma and D. Jaganyi, *Transition Met. Chem*., 2014, **39**, 407-420.

62. B. Petrovic, Ž. D. Bugarčić, A. Dees, I. Ivanovic-Burmazovic, F. W. Heinemann, R. Puchta, S. N. Steinmann, C. Corminboeuf and R. van Eldik, *J. Inorg. Chem*., 2012, **51**, 1516-1529; (b) E. C. Constable, C. Thompson, N. Armaroli, V. Belzani and M. Maestri *Polyhedron*, 1992, **11**, 2707-2709.

63. *C.* Maxim, A. Matni, M. Geoffroy, M. Andruh, N. G. R. Hearns, R. Clérac and N. Avarvari, *New J. Chem*., 2010, **34**, 2319-2327.

64. M. C. Carrión, A. Guerrro, F. A. Jalón, B. R. Manzano and A. de la Hoz, *Inorg. Chem*., 2003, **42**, 885-895.

65. A. Gelling, M. D. Olsen, K. G. Orrell, A. G. Osborne and V. Šik, *J. Chem.Soc., Dalton Trans*., 1998, 3479-3488

66. G. A. Webb, *Nucl. Magn. Reson*., 2009, **38**, 68-93.

67. A. Shaira and D. Jaganyi, *J. Coord. Chem*., 2014, **67**, 2843-2857.

CHAPTER 6

The role of annular nitrogen in tuning the reactivity of novel bifunctional Pt(II) complexes appended to pyridyl spacers: A kinetic and mechanistic investigation

6.1 Introduction

The discovery of cisplatin as an effective antineoplastic drug has played a key role in the fight against cancer. However, its induced side effects limits its therapeutic efficacy prompting the search for novel Pt(II) complexes as potential anticancer drugs.[1,2] This has led to a paradigm shift to more non-classical platinum-based drugs with new mechanism of action.[2] As such, significant efforts have been made in the design of dinuclear Pt(II) complexes that may provide wide spectrum of chemotherapeutic activity with improved clinical profile. Among these novel complexes, metal *N*-heterocyclic complexes have recently gained considerable attention because they perfectly fit prerequisites for efficient drug design and fast optimization.[1,2b] Moreover, most N-heterocyclic dinuclear Pt(II) complexes have shown higher cytotoxicity than cisplatin.[2] Above all, their substitution reactions has attracted continuous attention due to their intrinsic[3,4] and bio-medical applications as potential anticancer drugs.[5,6] They have shown slow substitution reaction rates compared to other d^8 square planar complexes which is important in cancer chemotherapy.[7] This review focuses on developing new family of anti-therapeutics through modification of the coordination spheres.[8,9]

The antitumour activity of dinuclear and multinuclear Pt(II) complexes have demonstrated novel mechanism of action. This has created an interest in understanding their mechanistic interaction with biomolecules. The anticancer properties of these dinuclear Pt(II) complexes stems from the ability of cisplatin [*cis*-$Pt(NH_3)_2Cl_2$] fragment to bind to DNA bases. To improve the efficacy and cytotoxicity of mononuclear Pt(II) complexes, innovative dinuclear Pt(II) complexes can be designed by connecting two or more Pt(II) metals by a different spacer.[10,11] This has been epitomized by a trinuclear Pt(II) complex BBR3464 that has shown a significant clinical use in cisplatin resistant cell lines.[12] This has aroused interest in designing new dinuclear and multinuclear platinum(II) complexes with improved activity and lower toxicity. This paper is based on the view that dinuclear and polynuclear Pt(II)

complexes represent a novel class of promising antitumour agents with potential clinical significance.[13]

Thus, dinuclear Pt(II) complexes with *N*,*N*-donors that mimic cisplatin constitutes a model system that may assist in exploring the mechanistic activity of dinuclear Pt(II) complexes. To explore this area, this review investigated a mechanistic study of heterocyclic compounds as potential anticancer therapeutics. The study employed pyridine whose derivatives with Pt(II) complexes have shown good antitumour activity. Pyridine was chosen as a bridging ligand due to its important role in regulating the reactivity of dinuclear complexes by controlling geometric symmetry, steric and electronic features of the complexes. The anticancer activity of pyridine derived complexes arises from the presence of nitrogen atom and through tuning substituents to different positions on the pyridyl ring. These derivatives are reported to act as σ-donors and also as fairly effective π-acceptors.[14] These nitrogen aromatic heterocyclic ligands have relatively low lying π^* orbitals hence form stable complexes with transition metals. In addition they are involved in π-π stacking with purine and pyrimidine bases which leads to complex formation with DNA-adducts.[15] The stability of the metal complexes is due to metal-ligand back bonding from the metal *d* orbitals to the π system of pyridine.[16-18] The weakly π-accepting ability of pyridine is expected to trigger new physical and chemical properties to reactivity of platinum based drugs. The ultimate aim of the modifications of the parent drug is to make related analogues that produce a different spectrum of DNA lesions and circumvent the problem of resistance to cisplatin.

Thus, anticancer complexes of the type *cis*-[PtX_2-L-PtX_2] (L = pyridine, X = H_2O) were synthesized and their mechanistic study evaluated by nucleophilic displacement of the aqua ligands. The ligand (L) was tuned by attaching substituents to different positions. These dinuclear platinum(II) complexes offer two labile substitution sites with two non-leaving N-donors in *cis*-position that gives a bifunctional DNA binding at each platinum centre.[19] These complexes have the ability to circumvent cellular resistance and also form DNA adducts that differ significantly from those formed by cisplatin and related complexes.[20] It is envisaged that this class of novel Pt(II) complexes may be of potential clinical significance with enhanced efficacy and apoptosis.[21]

The pyridine functionalized dinuclear Pt(II) complexes targeted in this study are: *N,N,N',N'*-tetrakis(2-pyridyl)-2,3 pyridinediaminetetraquaplatinum(II) [**2,3-tppdaPt$_2$(H$_2$O)$_4$]$^{4+}$** (**PtL1**); *N,N,N',N'*-tetrakis(2-pyridyl)-2,4-pyridinediaminetetraquaplatinum(II) [**2,4-tppdaPt$_2$(H$_2$O)$_4$]$^{4+}$** (**PtL2**); *N,N,N',N'*-tetrakis(2-pyridyl)-2,6-pyridinediaminetetraquaplatinum(II) [**2,6-tppdaPt$_2$(H$_2$O)$_4$]$^{4+}$** (**PtL3**); *N,N,N',N'*-tetrakis(2-pyridyl)-2,5-pyridinediaminetetraquaplatinum(II) [**2,5-tppdaPt$_2$(H$_2$O)$_4$]$^{4+}$** (**PtL4**) and *N,N,N',N'*-tetrakis(2-pyridylaminomethyl)-2,6-pyridinediaminetetraquaplatinum(II) [**2,6-tpmpdaPt$_2$(H$_2$O)$_4$]$^{4+}$** (**PtL5**).

The bio-relevant nucleophiles *viz.*, thiourea (**TU)**, *N,N'*-dimethylthiourea **(DMTU)** and *N,N,N'N'*-tetramethylthiourea **(TMTU)** were selected as representatives of the targets and competitors of Pt(II) complexes at cellular level.[22] They were preferred because they contain sulphur which has important role inside blood and cells. These biomolecules play significant roles as component of the cell and performs a wide array of functions[23,24] from side effects caused by interaction with sulphur thiols in the body. For instance, **TU** is clinically used as a protecting agent to minimize nephrotoxicity of cisplatin drugs.[25] Investigation of the mechanistic features of dinuclear Pt(II) complexes with bio-relevant molecules highlighted their substitution kinetics. The study shows the nature of backbone ligands as well as the donor characteristic of entering ligands to play an important role on the substitution kinetics on dinuclear Pt(II) complexes containing dipyridyl linkers. The experimental work is supported by computational calculations. The structures of the investigated complexes are given in Figure 6.1 below.

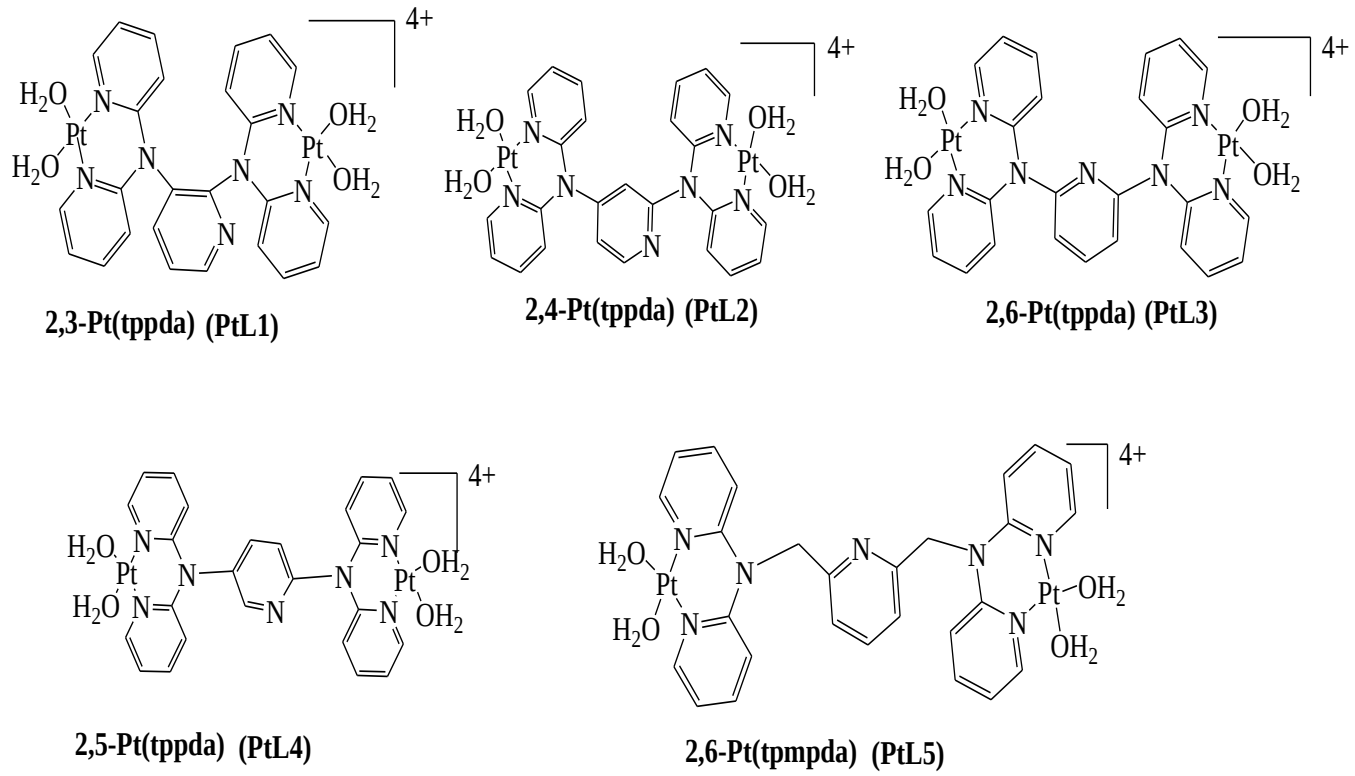

Figure 6.1: Chemical structures and abbreviations for the investigated aqua Pt(II) complexes.

Note: For clarity and simplicity, the abbreviations in the brackets are used in the text to represent the complexes. For characterization, chloro complexes were used.

6.2 Experimental Section

6.2.1 Reagents and methods

All starting chemicals and solvents were of the highest purity grade from commercial sources and were used without further purification. The nucleophiles thiourea **TU**, 99 %), **DMTU**, 99 %, **TMTU**, 98 %, 2,3-dibromopyridine 97 %, 2,4-dibromopyridine 97 %, 2,5-dibromopyridine 98 %, 2,6-dibromopyridine 98 % and 2,6-bis(chloromethyl)pyridine 99 %, were obtained from Sigma-Aldrich. $AgClO_4$ (99.99 %) was stored under nitrogen and used as supplied. K_2PtCl_4 and 2,2'-dipyridylamine (dpa) were obtained from Strem chemicals. De-ionized water was used in all experiments.

6.2.2 Synthesis of ligands

The ligands were synthesized by methods described in the literature.[26] Syntheses of both the ligands and the complexes were carried out under dry N_2 atmosphere using standard Schlenk-line techniques. 0.856 g (5 mmol) of 2,2'-dipyridylamine, 0.3709 g (1.57 mmol) of either 2,3; 2,4; 2,5; and 2,6; of dibromopyridine, 0.7480 g (5.37 mmol) of anhydrous potassium carbonate, and 0.1129 g (0.45 mmol) of cupric pentahydrate were mixed in a 50 mL round bottomed flask. The resultant mixture was heated under N_2 at 220 ^oC for 12h. The reaction mixture was cooled and a mixture of dichloromethane (DCM) and water added to dissolve the solid particles. The DCM extracts were dried over anhydrous Na_2SO_4, filtered and dried under vacuum. The crude product was recrystallized from acetone and water mixture to give brown solids of *N,N,N',N'*-tetrakis(2-pyridyl)-2,3-pyridinediamine (**2,3-tppda**); (*N,N,N',N'*-tetrakis(2-pyridyl)-2,4-pyridinediamine (**2,4-tppda**); *N,N,N',N'*-tetrakis(2-pyridyl)-2,5-pyridinediamine (**2,5-tppda**); and *N,N,N',N'*-tetrakis(2-pyridyl)-2,6-pyridinediamine (**2,6-tppda**). Since the ligands are isomers and have similar formulation the position of the substituents were included to denote the position of the substituents.

N,N,N',N'-tetrakis(2-pyridyl)-2,6-pyridinediamine **(2,6-tppda)** was synthesized using established methods.[27] A weighed amount of 2,2'-dipyridylamine 0.856 g (5 mmol) and potassium hydroxide 0.838 g (14.74 mmol) were stirred in dimethylformamide (7 mL) for 1h then 2,6-bis(chloromethyl)pyridine 0.257 g (1.46 mmol) was added. The solution was then stirred at room temperature for 60h and adjusted to 60 ^oC and stirred further for 12h. The solution mixture was dried and reduced under pressure and a large amount of water added. The mixture was extracted with 3 x 50 mL chloroform, dried over anhydrous sodium sulphate, filtered, dried under vacuum and recrystallized from acetone and water to give yellow powder.

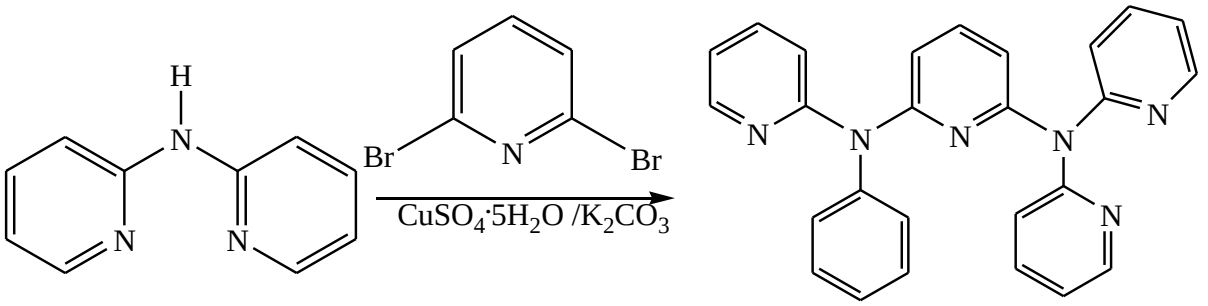

Scheme 6.1: General synthesis of the ligands appended to pyridine spacer **(2,6-tppda)**

The ligands were designed in order to obtain knowledge on the effect of nitrogen atom situated in various positions in pyridine ring on isomeric disubstituted pyridine-platinum(II) derivatives. Changing the position of substituents on the pyridine spacer is projected to provide a powerful tool for complex design with favourable therapeutic properties with selected transition metals. The modifiability was exploited in designing platinum pyridine complexes which have been reported by Farrell and co-workers[28] to greatly enhance cytotoxicity equivalent to cisplatin by varying planarity. A general synthetic sequence in order to access the carrier pyridine shown in Scheme 6.2 is depicted in Scheme 6.1.

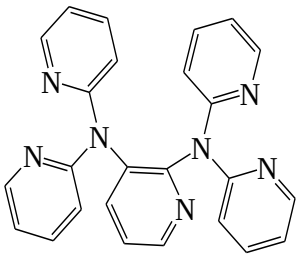

2,3-tppda (L1)

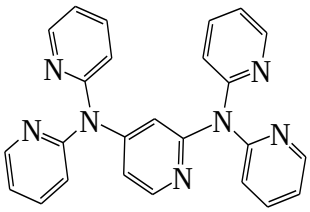

2,4-tppda (L2)

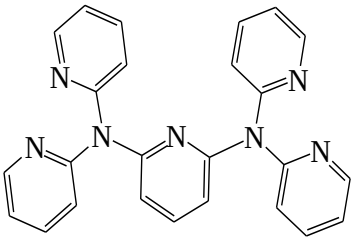

2,6-tppda (L3)

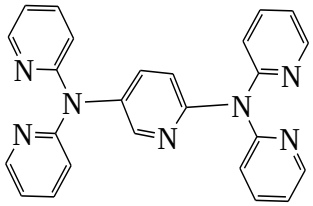

2,5-tppda (L4)

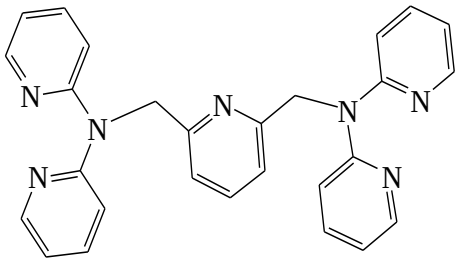

2,6-tpmpda (L5)

Scheme 6.2: Chemical structures of bis –functional rigid pyridine linkers tuned through modifying the positions of the substituents.

The variation of the ligand sphere as in Scheme 6.2 above was used to induce changes in the electron distribution when coordinated to the metal centres and in turn modified thermodynamic parameters and chemical reactivity of the complexes. The structural property of the pyridine ligand and the position of the substituents on the heterocyclic pyridine ring system have an influence on the acidity and overall reactivity of the coordinated metal centre. The pyridine ligands are preferable due to their relatively low MLCT energy when coordinated to Pt(II) system which mainly involves electron transfer from metal *d*-orbitals to π^* orbitals of the ligand.[29] The pyridyl rings feature different geometries and separation lengths which major tunes the reactivity of the Pt-pyridine complexes. The loss of planarity of these bridging ligands may be ascribed to the conformational arrangement of the pyridine rings.[30] Thus the aim of this chapter was to establish how the insertion of the tuned pyridyl spacer unit affects the thermodynamic and kinetic properties of Pt(II) complexes.

6.2.2.1 Characterization of the bridging ligands

***N,N,N',N'*-tetrakis(2-pyridyl)-2,3-pyridinediamine** (**2,3-tppda**); Yield, 0.420 g (64 %).^{1}H NMR ($CDCl_3$, 400 MHz): δ 8.28 (d, 4H), 7.60 (t, 5H), 7.54 (d, 4H), 7.08 (d, 2H), 6.84 (t, 4H). ^{13}C NMR (400 MHz, $CDCl_3$, 303K) δ 157.5, 154.2, 148.8, 147.8, 138.0, 119.4, 118.7, 116.4, 111.8. For $C_{25}H_{19}N_7$ Found: C, 71.78; H, 4.35; N, 23.24; Calcd. C, 71.92; H, 4.59; N, 23.49 %. TOF MS ES^+, *m/z:* 440.1929 $[M + Na]^+$.

***N,N,N',N'*-tetrakis(2-pyridyl)-2,4-pyridinediamine (2,4-tppda)**; Yield, 0.488 g (74 %). ^{1}H NMR ($CDCl_3$, 400 MHz): δ 8.28 (d, 4H), 7.60 (t, 5H), 7.57 (d, 4H), 7.08 (d, 2H), 6.86 (t, 4H). ^{13}C NMR (400 MHz, $CDCl_3$, 303K) δ 157.2, 154.2, 148.8, 137.8, 120.2, 118.8, 116.4, 111.8. For $C_{25}H_{19}N_7$ Found: C, 71.62; H, 4.65; N, 23.74; Calcd. C, 71.92; H, 4.59; N, 23.49 %. TOF MS ES^+, *m/z:* 418.2096 $[M + H]^+$.

***N,N,N',N'*-tetrakis(2-pyridyl)-2,5-pyridinediamine** (**2,5-tppda**); Yield, 0.435 g, (66 %). ^{1}H NMR ($CDCl_3$, 400 MHz): δ 8.28 (d, 4H), 7.64 (m, 5H), 7.60 (d, 5H), 6.86 (t, 5H). ^{13}C NMR (400 MHz, $CDCl_3$, 303K) δ 155.2, 154.0, 148.4, 147.5, 138.4, 116.4, 111.8. For $C_{25}H_{19}N_7$ Found: C, 71.78; H, 4.35; N, 23.24; Calcd. C, 71.92; H, 4.59; N, 23.49 %. TOF MS ES^+, *m/z:* 440.1597 $[M + Na]^+$.

***N,N,N',N'*-tetrakis(2-pyridyl)-2,6-pyridinediamine (2,6-tppda)**; Yield, 0.529 g, (81 %). ^{1}H NMR ($CDCl_3$, 400 MHz): δ 8.36 (d, 4H), 7.52 (d, 6H), 7.10 (m, 9H). ^{13}C NMR (400 MHz, $CDCl_3$, 303K) *δ* 157.4, 156.2, 154.2, 147.8, 138.2, 119.6, 112.3. For $C_{25}H_{19}N_7$ Found: C, 71.78; H, 4.35; N, 23.24; Calcd. C, 71.92; H, 4.59; N, 23.49 %. TOF MS ES$^+$, *m/z:* 440.1430 [M + Na] $^+$.

***N,N,N',N'*-tetrakis(2-pyridylaminomethyl)-2,6-pyridylamine** (**2,6-tpmpda**); Yield 0.327 g (50 %). ^{1}H NMR ($CDCl_3$, 400 MHz): δ 8.30 (d, 4H), 7.53 (t, 4H), 7.40 (t, 1H), 7.23 (d, 4H), 7.12 (d, 2H), 6.86 (t, 4H), 5.58 (s, 4H). ^{13}C NMR (400 MHz, $CDCl_3$, 303K) *δ* 153.8, 148.1, 138.0, 117.2, 114.6, 112.0, 34.60. For $C_{27}H_{23}N_7$ Found: C, 72.89; H, 4.98; N, 22.27; Calcd. C, 72.79; H, 5.20; N, 22.01 %. TOF MS ES$^+$, *m/z:* 446.2095 [M + H] $^+$.

6.2.3 Synthesis of complexes

The complexes were prepared according to literature methods.[31] The chloro-platinum(II) complexes were obtained by reaction of the corresponding ligands with K_2PtCl_4. A solution of 0.100 g (0.24 mmol) of the ligands dissolved in small amount of absolute ethanol was added to a stirred solution of 0.1984 g (0.48 mmol) of K_2PtCl_4 in 50 mL ultrapure water. The reaction was refluxed at 50 ^{o}C for 24 h. The resultant yellow precipitates were filtered, washed with ultrapure water and diethyl ether and dried in *vacuo.* .

[2,3-bis(di-2-pyridylamino)pyridine]tetrachloroplatinum(II) ^{1}H NMR (DMSO-d_6, 400 MHz): δ 8.82 (d, 4H), 7.98 (t, 5H) 7.30 (d, 5H) 7.08 (d, 5H),). ^{13}C NMR (400 MHz, DMSO-d_6, 303K) *δ* 150.7, 141.4, 119.9, 114.3, Anal. Calcd. for $C_{25}H_{19}N_7Pt_2Cl_4$ C, 31.63, H, 2.02, N, 10.33, Found C, 31.21, H, 2.34, N, 10.20, Pt NMR -2103.2 ppm

[2,4-bis(di-2-pyridylamino)pyridine]tetrachloroplatinum(II) ^{1}H NMR (DMSO-d_6, 400 MHz): δ 8.81 (d, 4H), 7.98 (t, 5H) 7.30 (d,5H), 7.12 (t, 5H), ^{13}C NMR (400 MHz, DMSO-d_6, 303K) *δ* 152.9, 141.8, 119.9, 114.3, Anal. Calcd. for $C_{25}H_{19}N_7Pt_2Cl_4$ C, 31.63, H, 2.02, N, 10.33, Found C, 31.94, 1.98, N, 10.57, Pt NMR -2156.7 ppm.

[2,5-bis(di-2-pyridylamino)pyridine]tetrachloroplatinum(II) ^{1}H NMR (DMSO-d_6, 400 MHz): δ 8.80 (d, 4H), 7.97 (t, 6H), 7.26 (d, 4H), 7.12 (t, 5H). ^{13}C NMR (400 MHz, DMSO-d_6, 303K) δ 150.3, 140.7, 119.5, 114.7, Anal. Calcd. for $C_{25}H_{19}N_7Pt_2Cl_4$ C, 31.63, H, 2.02, N, 10.33, Found C, 31.14, H, 1.84, N, 9.97, TOF MS ES$^+$, *m/z:* 913.9711 [M - Cl]$^+$, Pt NMR -2101.2 ppm.

[2,6-bis(di-2-pyridylamino)pyridine]tetrachloroplatinum(II) ^{1}H NMR (DMSO-d_6, 400 MHz): δ 8.81 (d, 4H), 7.98 (t, 5H), 7.32 (d, 5H) 7.12 (t, 5H),). ^{13}C NMR (400 MHz, DMSO-d_6, 303K) δ 150.7, 141.0, 119.5, 114.3, Anal. Calcd. for $C_{25}H_{19}N_7Pt_2Cl_4$ C, 31.63, H, 2.02, N, 10.33, Found C, 31.32, H, 2.38, N, 9.87, TOF MS ES$^+$, *m/z:* 913.9739 [M - Cl]$^+$, Pt NMR -2103.5 ppm.

[2,6-bis(di-2-pyridylaminomethyl)pyridine]tetrachloroplatinum(II) ^{1}H NMR (DMSO-d_6, 400 MHz): δ 8.80 (d, 4H), 8.00 (t, 5H), 7.30 (d, 5H) 7.15 (t, 5H), 3.32 (s, 4H). ^{13}C NMR (400 MHz, DMSO-d_6, 303K) δ 157.4, 148.7, 138.1, 125.4, 118.4, 114.7, 50.8, Anal. Calcd. for $C_{25}H_{23}N_7Pt_2Cl_4$, C, 33.18, H, 2.37, N, 10.03, Found C, 32.84, 1.98, N, 9.67, ^{195}Pt NMR -2103.5 ppm.

6.3 Physical measurements

^{1}H, ^{13}C and ^{195}Pt NMR spectra of the ligands and Pt(II) complexes were recorded on a Bruker Avance III 500 or Bruker Avance 400 spectrometers at frequencies of 400 MHz and 125 MHz/100 MHz using either a 5 mm BBOZ probe or a 5 mm TBIZ probe. All proton and carbon shifts were recorded with reference to the relevant solvent signal used. Chemical shift values are given in δ (ppm) of ^{1}H relative to tetramethylsilane ($Si(CH_3)_4$) while ^{195}Pt NMR were external referenced to K_2PtCl_6 in D_2O. Mass of ligands and complexes was determined using a Waters Micro-mass LCT Premier spectrometer while elemental analysis was obtained on a Thermo Scientific Flash 2000. Kinetic studies for fast reactions were monitored using an Applied Photophysics SX20 stopped-flow spectrophotometer coupled to an online data acquisition system. A Varian Cary 100 Bio UV-Visible spectrophotometer thermostated by a Varian Peltier temperature controller to within ±0.05 ^{o}C was used for the slow kinetic measurements. The kinetic traces were analysed using the Origin 7.5® software package.[32]

The pH of the solutions was recorded on a Jenway 4330 pH meter calibrated using standard buffer solutions of pH 4.0, 7.0 and 10.0.

6.4 Preparation of the dinuclear Pt(II) aqua complexes

Due to the low solubility of chloride complexes for substitution kinetics, they were converted to aqua analogues according to literature procedures.[33-37] They were prepared by stirring the chloride complexes with four mole equivalents of $AgClO_4$ in 0.01M $HClO_4$ acid. The solution was refluxed for 24 h at 50 ^oC in the dark to protect it from light. The AgCl precipitate was removed by filtration through a 0.45 µm pore membrane filter. These aqua solutions were titrated with NaOH solution to determine the pK_a of the complexes whilst for kinetic investigations; the pH of the solution was maintained at 2.0 based on the pK_a study and the ionic strength at 0.1 M using $NaClO_4$.

6.5 pK_a determination of the aqua complexes

To obtain the intrinsic information on the acidity of the complexes and as a measure of the electrophilicity of the metal centre, their pK_a values were determined by spectral titrations. To avoid absorbance corrections due to dilution of a large volume of the platinum(II) aqua complex (300 mL) was used. Crushed NaOH pellets were used between the pH range of 1–3 after which the Pasteur pipettes were used for drop wise addition of small aliquots 0.5 M, 0.1 M, 0.05 M and 0.001 M of NaOH solution. Similar concentrations of perchloric acid were used for adjusting the pH. After addition of the base, samples of about 500 µL were taken in ampoules and their pH recorded. The samples in the ampoules were discarded to avoid possible chloride ion contamination through leaching from the pH electrode. The pK_a of 2.0 mL aqua solution of platinum complex was analysed using UV/Vis spectroscopy.

6.6 Kinetic measurements

Spectral changes resulting from mixing of equal volumes of dinuclear Pt(II) complex and nucleophile solutions were recorded over the wavelength range 200 to 800 nm to establish a suitable wavelength at which kinetic measurements could be performed. A summary of the used wavelength for each nucleophile can be found in Table S6.1 (Appendix). All kinetic measurements were performed under *pseudo*-first-order conditions at least 40 fold excess of the nucleophile over that of the metal complexes concentrations. This ensured at least 10-fold

of nucleophiles concentration at each platinum centre hence forced the reaction to completion under first order kinetics. The rates of reaction were followed spectrophotometrically by measuring changes in optical density over a period of time at some selected wavelength in the ultraviolet region. All data obtained from both the UV-Visible and the stopped flow spectrophotometric techniques were fitted to first-order double exponential function to generate the *pseudo*-first-order rate constants (k_{obs}) for fast reactions (Figure 6.4). Single exponent function was used for slow reactions on the UV-Vis spectroscopy (Figure 6.5). The observed *pseudo*-first-order rate constants (k_{obs}) were calculated as the average value of from 6-8 independent kinetic runs and are summarized in Tables S6.2–S6.6 (Appendices). To obtain the concentration dependence of the rate constants the reactions were studied at a minimum of five concentrations of excess nucleophile at 25 ^{o}C. The second-order rate constants (k_2) were obtained from straight-line plots of k_{obs} versus nucleophile (Figure 6.5). The intercepts of these plots pass through zero indicating that the reverse reaction does not contribute to the values of k_{obs}. Activation parameters were obtained from a linear least-square analysis using $\ln(k/T)$ verses $1/T$.

6.7 Computational calculations

In order to gain additional insight into the influence of changing substituents positions on the structural and electronic properties of the complexes, density functional theory (DFT) study using Gaussian 09 software package[38] was employed. The molecular structure calculations of fully optimized platinum(II) complexes were performed by using Becke-3-Lee Yang Parr (B3LYP) density functional theory (DFT) with LANL2DZ basis set in ground state.[39,40] The geometries were fully optimized at B3LYP/LANL2DZ level for all the atoms in the gas phase to model the structural and electronic properties of molecular structures. The singlet states were used due to low electronic spin of platinum(II) complexes. The ground-states electronic structures were calculated in order to determine the energies of the molecular orbitals used for the determination of the HOMO and LUMO positions and related electron distributions. The energy difference between the HOMO and LUMO orbitals was adjustable by the electronic character and the position of the substituents on the pyridine spacer. Apart from the density functional theory providing the ground state properties, the molecular structure and electron density of the systems which played a key role in this study also provided important information on conformations and planarity of the complexes. The computed energies of

some of the frontier molecular orbitals using DFT method at the B3LYP/LANL2DZ level are presented in Table 6.1.

Table 6. 1: Electron density plots of the HOMO and LUMO orbitals computed at B3LYP/LANL2DZ level of theory (Isovalue = 0.02).

Name	Planarity	HOMO Map	LUMO Map
PtL1	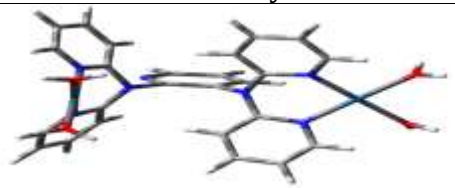	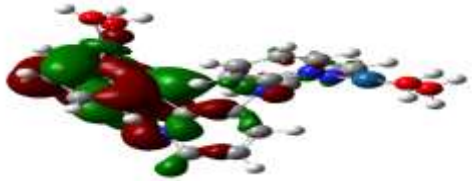	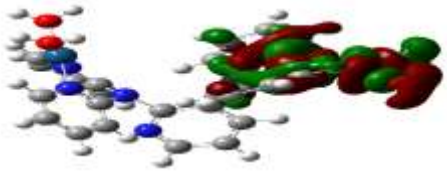
PtL2	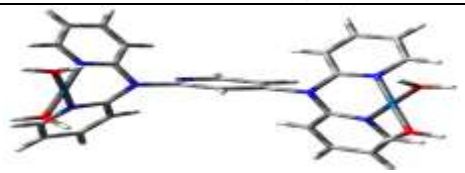	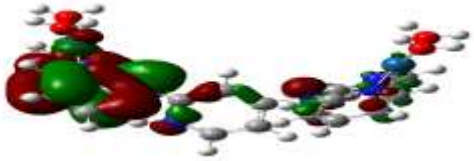	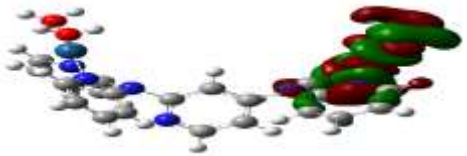
PtL3	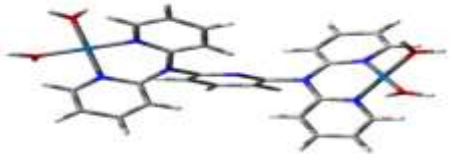	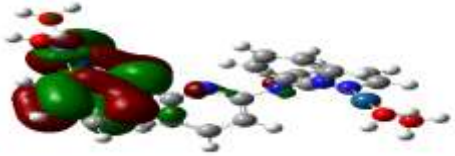	
PtL4	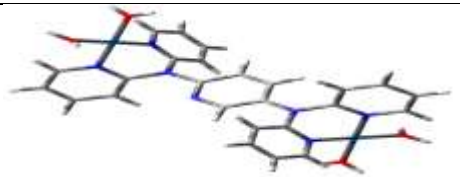	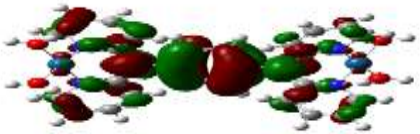	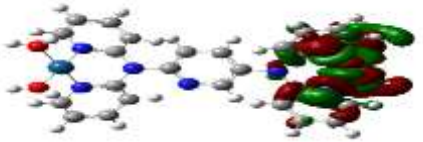
PtL5	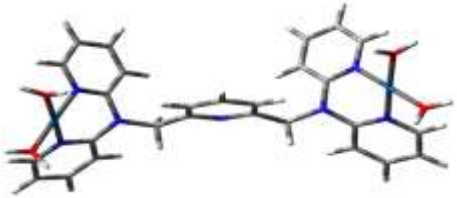		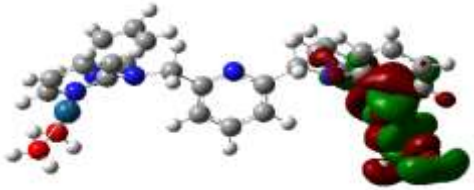

Table 6.2: Selected bond lengths and angles, natural atomic bond orbital (NBO) charges, HOMO-LUMO energy gap and other computation parameters.

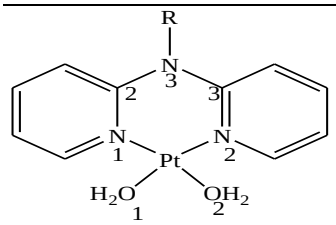

	PtL1	PtL2	PtL3	PtL4	PtL5
HOMO-LUMO energy					
LUMO/eV	-12.62	-12.12	-12.06	-12.05	-11.49
HOMO/eV	-16.77	-16.25	-16.19	-15.49	-15.69
ΔE/eV	4.15	4.13	4.13	3.44	4.20
Electrophilicity index (ϖ)	51.94	48.64	48.23	55.12	43.97
NBO Charges					
Pt_1	0.773	0.769	0.774	0.779	0.776
Pt_2	0.766	0.766	0.770	0.773	0.776
Dipole moment (Debye)	6.60	9.01	2.93	3.07	6.94
Bond lengths (Å)					
R-N3	1.4721	1.4719	1.4531	1.4443	1.4965
N3-C2	1.4225	1.4318	1.4288	1.4335	1.4191
N3-C3	1.4225	1.4318	1.4270	1.4324	1.4288
Pt_1-Pt_2	8.11	9.49	10.40	10.94	12.32
Bond angles (^{o})					
$C_2N_3C_3$	117.40	118.33	123.82	115.89	118.49
Dihedral angle between the planes of pyridine spacer and Pt centres	90.0	89.98	70.0	69.43	62.58

Where R = pyridine, methylpyridine

6.8 Results and discussions

6.8.1 Acidity of the aqua Pt(II) complexes

The pK_a titrations were carried out to ascertain the best pH for the kinetics studies. This was necessary for conceptual understanding of the complexes reactivity and critical in formulation of viable reaction mechanism of metallodrugs. The pK_a values were determined by spectrophotometric pH titrations in aqueous solution at 25 ^{o}C. Figure 6.2 below shows an example of the spectral changes observed during the pH titration of **PtL2** with NaOH base. The pK_a values were determined from Boltzmann Equation by fitting a characteristic sigmoid curve and locating the inflection point using the Origin 7.5® program using Equation 6.1.The respective pK_a values are summarized in Table 3.

$$y = A_2 + (A_1 - A_2)/(1 + \exp((x - x_0)/dx) \qquad \text{Eq [6.1]}$$

where, *y* represents the absorbance value, A_1= the initial absorbance value (baseline response), A_2 = final absorbance value (maximum response), x_0 = centre, concentration that provokes a response halfway between A_1 and A_2) and dx = width of the rapidly varying part of the curve as determined by Origin™.

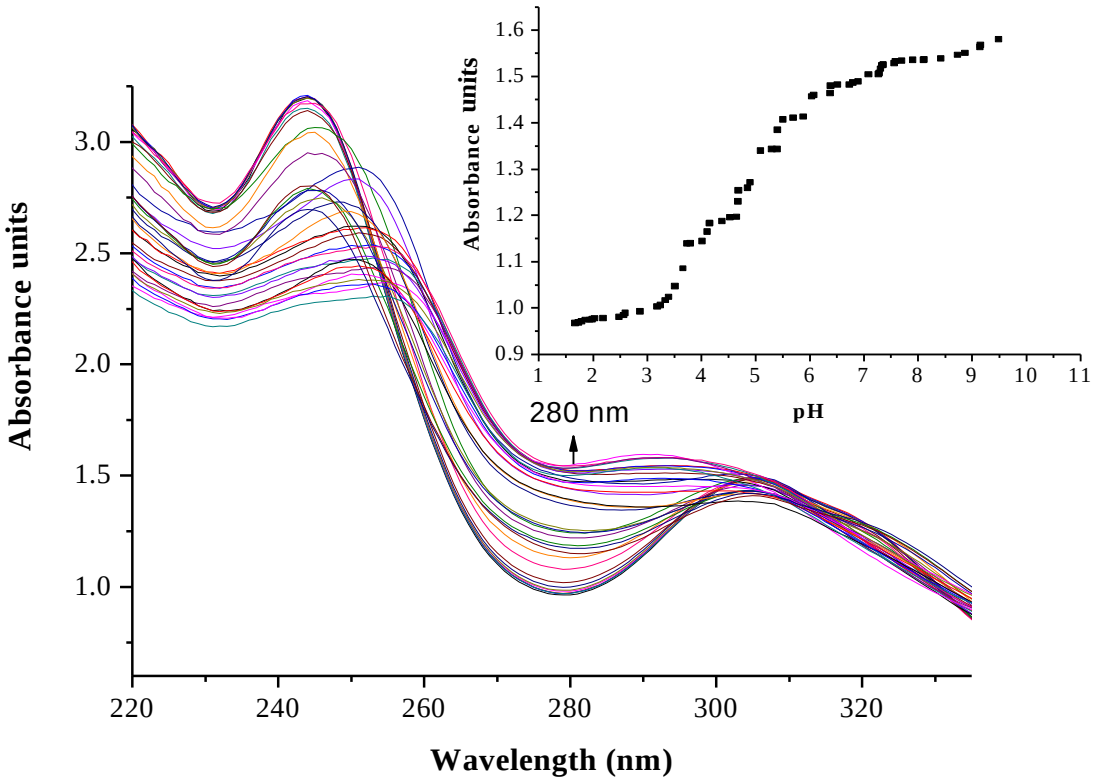

Figure 6.2: UV/Vis spectrum of 0.07 mM **PtL2** complex recorded as a function of pH in the range of 2 to 10 at 25 ^{o}C, *Inset* Plot of absorbance versus pH at λ = 280 nm.

Table 6. 3: A summary of pK_a values obtained for stepwise deprotonation of aqua Pt(II) complexes investigated

Complex	PtL1	PtL2	PtL3	PtL4	PtL5
pKa_1	2.62 ± 0.03	2.57 ± 0.02	2.45 ± 0.02	2.60 ± 0.03	2.75 ± 0.01
pKa_2	3.36 ± 0.02	3.60 ± 0.03	3.08 ± 0.02	3.78 ± 0.02	3.80 ± 0.01
pKa_3	3.92 ± 0.07	4.12 ± 0.01	3.53 ± 0.02	4.78 ± 0.09	4.98 ± 0.03
pKa_4	5.09 ± 0.07	5.11 ± 0.09	5.08 ± 0.01	5.95 ± 0.06	6.49 ± 0.01

The trend in the pK_a values slightly increases in the order **PtL3 > PtL2** > **PtL4** > **PtL1** > **PtL5**. Although the values are similar in magnitude, the slight difference could be ascribed to the consequence of stabilization by the electronegative nitrogen and delocalization in the ring depending on its position. This is because the pyridine spacer can function as σ-donor using the lone pair of electrons on nitrogen or as π-acceptor by using delocalized orbitals in the ring. This induces variation in electron distribution around metal centres making the position of substituents relative to nitrogen in the ring to influence the chemical properties of the complexes.The electron donating effect of methylene groups in **PtL5** enhances basicity due to inductive donor effect supporting our previous study presented in Chapter 5 and also supported in literature by van Eldik.[41] Scheme 6.3 shows the proposed four stepwise deprotonation of the aqua ligands of the complexes.

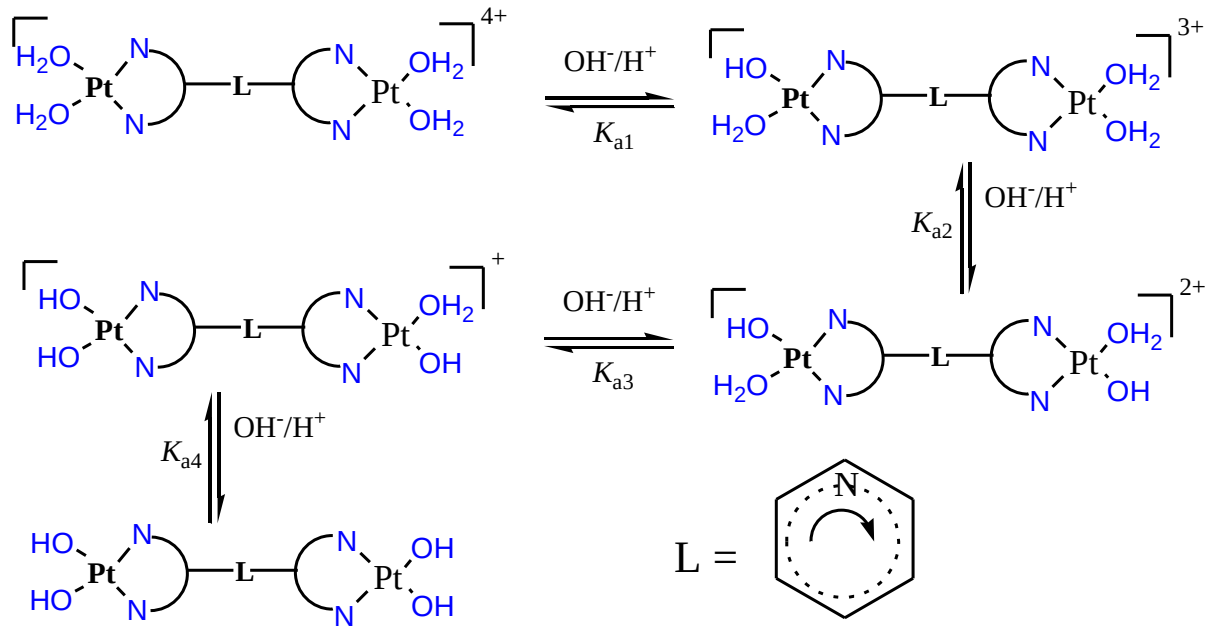

Scheme 6.3: Stepwise deprotonation of the aqua complexes with NaOH during pK_a titrations

6.8.2 Kinetic studies

The substitution reactions of coordinated aqua ligands of these dinuclear Pt(II) complexes with thiourea based nucleophiles showed two consecutive reaction steps. Based on the observed data, a plausible mechanism for substitution of the complexes is proposed in Scheme 6.3. The study proposes a biphasic reaction involving a rapid substitution of one aqua ligand followed by a slow phase of second aqua ligand occurring concurrently by the

displacement of the linker. This is supported by the kinetic traces that gave excellent fit to a double exponential function as shown in Figures 6.3 and 6.4.

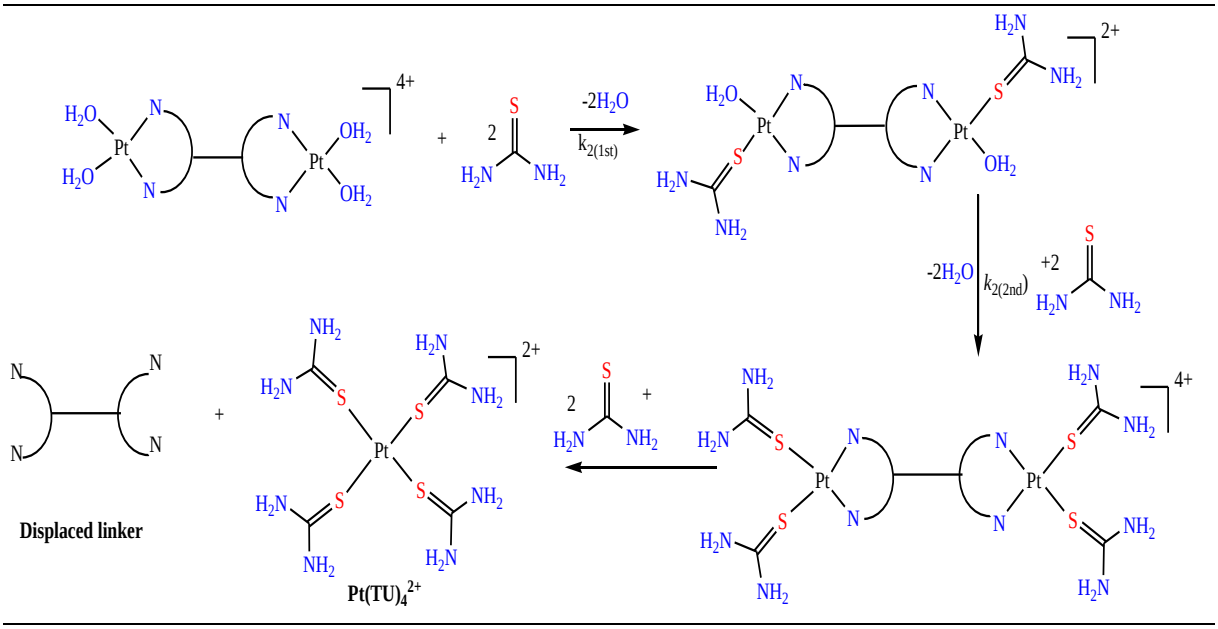

Scheme 6.3: Proposed biphasic substitution reaction at each metal centre, the reaction occurs simultaneously at the two Pt(II) centres.

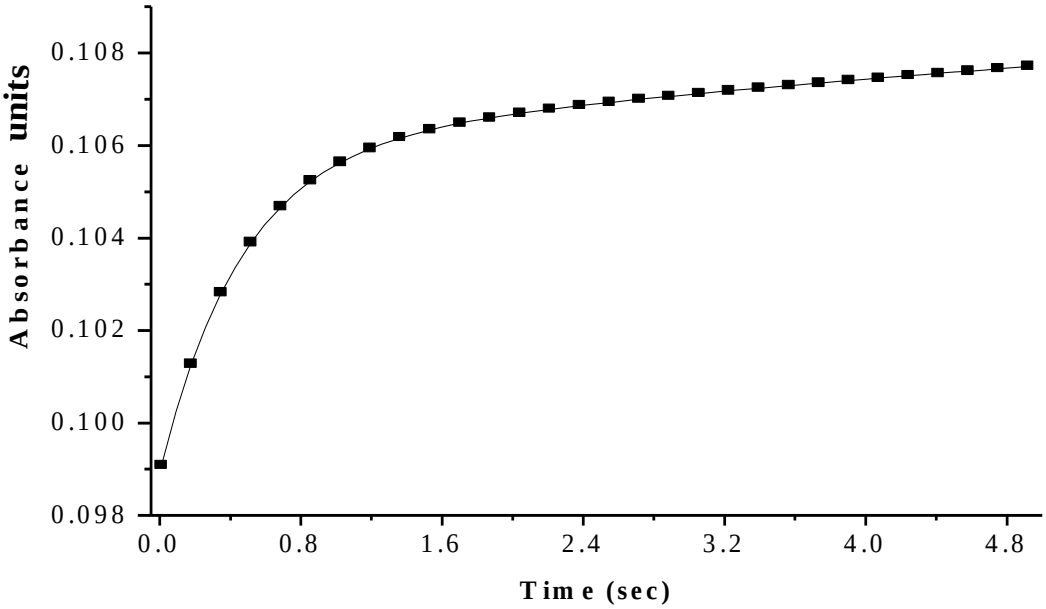

Figure 6. 3: A typical kinetic trace for a two-step reaction between **PtL4** and **TU** at T = 298 K, pH = 2.0, I = 0.1 M ($NaClO_4$) on the stopped-flow. The trace was

fitted to a double exponential function by following the growth in absorbance at 300 nm.

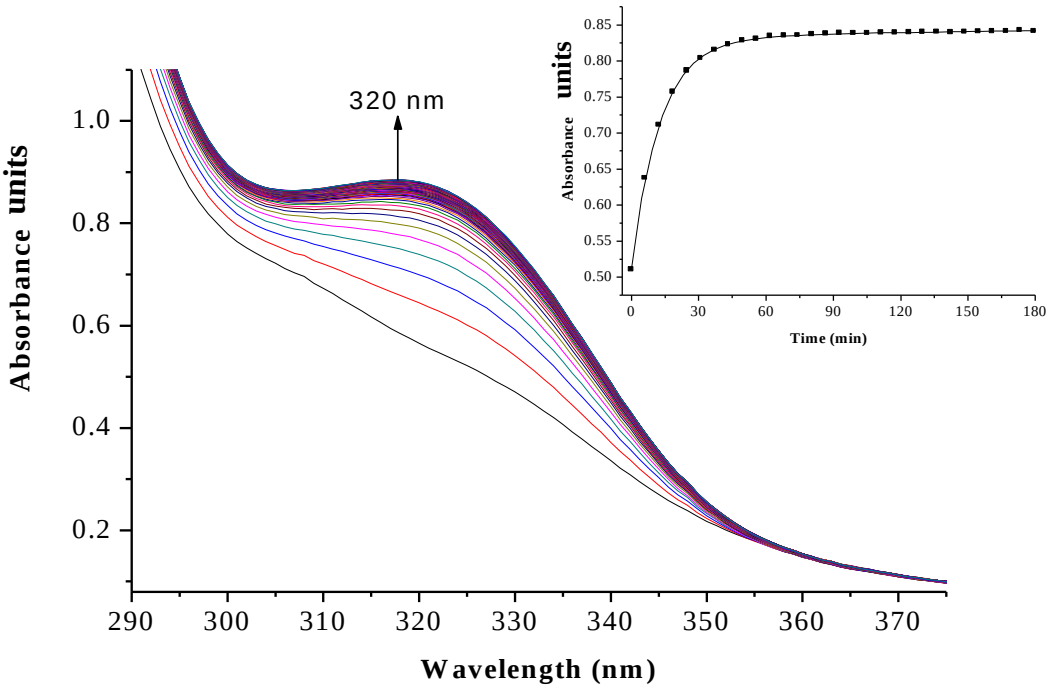

Figure 6.4: Time-resolved UV-Vis spectra of 0.17 mM **PtL4** with 0.068 M **TU**; *inset* is typical kinetic trace on the UV-Visible spectrophotometer at 320 nm of absorbance verses time, at T =298 K, pH = 2.0 and I = 0.1 M $NaClO_4$.

The *pseudo*-first-order rate constants were obtained from the kinetic traces plotted against the entering nucleophile concentration. The plots showed linear dependence of k_{obs} versus nucleophile concentration for all the studied reactions (Figures 6.4 and S6.1-S6.4 in the appendices). The first substitution step $k_{2(1st)}$ is attributed to the simultaneous displacement of one water molecule on each platinum centre while the second step is displacement of second water molecule that occurs concurrently with the dechelation process. The subsequent reaction of $[(\mathbf{TU})_2\text{-Pt–L–Pt–}(\mathbf{TU})_2]^{4+}$ with excess nucleophile leads to the displacement of the linker, L and formation of $[Pt(\mathbf{TU})_4]^{2+}$ complex as supported by ^{1}H and ^{195}Pt NMR kinetics (Scheme 6.3). The dependence of the observed *pseudo*-first-order rate constants $k_{obs(1)}$ and $k_{obs(2)}$ on the concentration of entering nucleophile followed the rate law given in Equation [6.2] below.

$$k_{obs(1,2)} = k_2[Nu] \quad [6.2]$$

where, k_2 represent second-order rate constants first and second substitution reactions.

The substitution of the aqua ligands by nucleophiles **TU**, **DMTU** and **TMTU** showed a clear dependence on the steric demands of the nucleophiles.[42-44] The study suggests a two-step reaction mechanism: The first step, attributed to a rapid substitution of one water molecule at platinum(II) centre by thiourea nucleophiles. The second step is the slow phase substitution of the second aqua ligand occurring concurrently with a dechelation process. As expected, increasing steric hindrance of the entering nucleophile, that is **TU**, **DMTU** and **TMTU** slows down the ligand substitution reactions, since the bulkier nucleophiles find it increasingly difficult to closely approach the metal centre.[45]

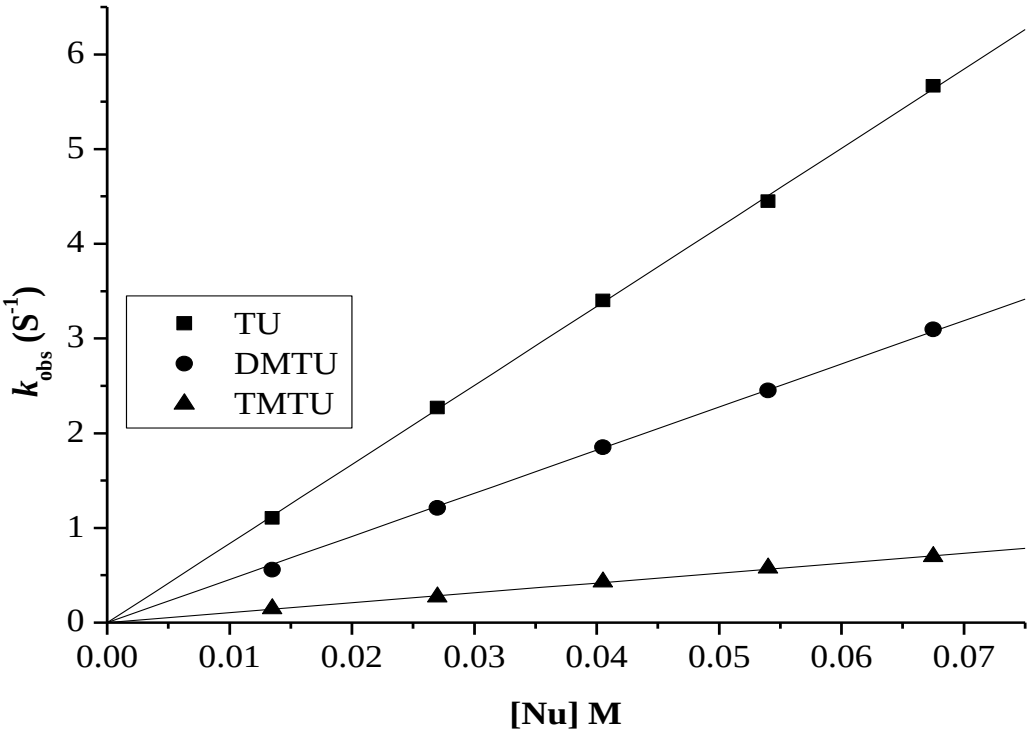

Figure 6.5: Concentration dependence of $k_{2(1st)}$ for the substitution of the aqua ligands in **PtL5** by nucleophiles at: pH =2.0, T = 25 ^{o}C, I = 0.1 $NaClO_4$.

6.9 Activation parameters

Determination of ligand substitution mechanism relied on the activation parameters *viz.*,enthalpy and entropy. They were determined from temperature dependence of a rate

constant from the Eyring plots Figures 6.6 and (S6.5-S6.8 in the appendices) using Equation [3.1] in Chapter three. The typical experimental results obtained are summarized in Table 6.4.

The low but positive values of $\Delta H_1^{\#}$ and $\Delta H_2^{\#}$ represents the energy required for bond making process. The highly negative entropy values of ($\Delta S_1^{\#}$ and $\Delta S_2^{\#}$) suggests a more compact transition state than the reactants which supports ligand participation in transition state to form a five-coordinate transition state. The small positive values of enthalpies and large negative values of entropies of activation strongly suggest ligand participation in the transition state which supports an associative mechanism of ligand substitution.

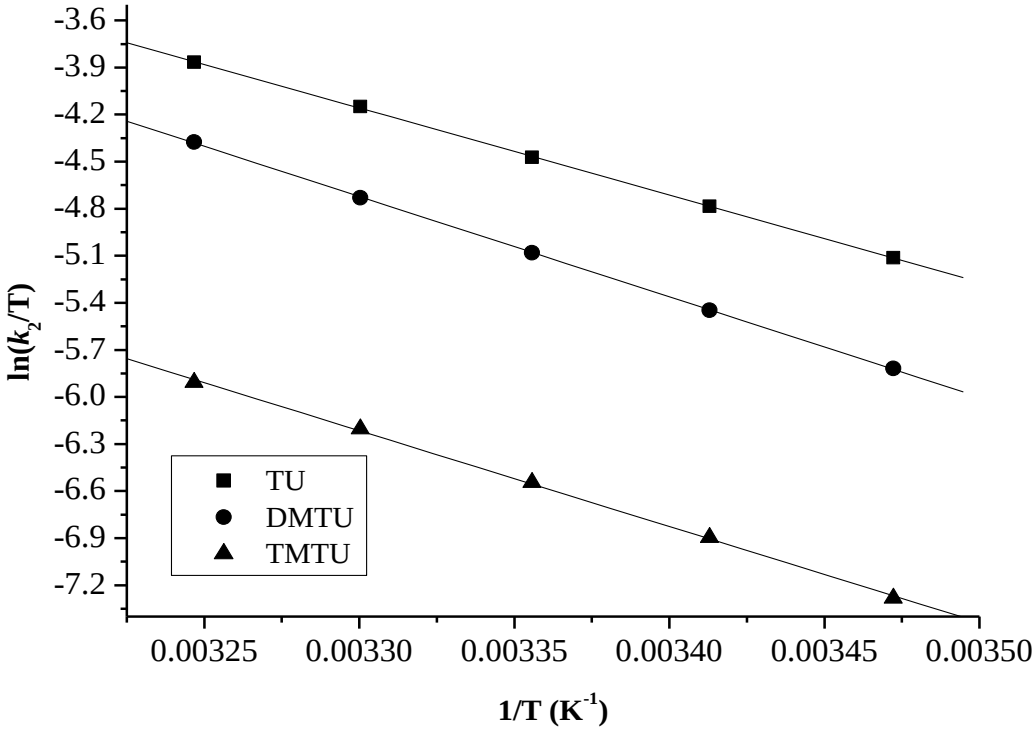

Figure 6.6: Eyring plots of ln(k_2/T) verses 1/T for the reaction between **PtL5** with thiourea nucleophiles at I = 0.1 M $NaClO_4$, pH = 2 for temperature range of 15 to 40 ^{o}C.

Table 6.4: A summary of the kinetic data for the reaction of the systems investigated with respective nucleophiles

Complex	Nu	**2nd order rate constants/$M^{-1}s^{-1}$**		**Activation enthalpy/kJ/mol**		**Activation entropy/J/mol/K**	
		$k_{2(1st)}$	$k_{2(2nd)} \times 10^{-2}$	$\Delta H_1^{\#}$	$\Delta H_2^{\#}$	$\Delta S_1^{\#}$	$\Delta S_2^{\#}$
PtL1	**TU**	39.67 ± 0.25	6 ± 0.03	42.78 ± 0.7	18.97 ± 0.2	-98 ± 2	-237 ± 1
	DMTU	36.70 ± 0.13	2 ± 0.01	55.45 ± 0.3	28.04 ± 0.5	-56 ± 1	-217 ± 1
	TMTU	7.21 ± 0.03	1 ± 0.05	35.10 ± 0.6	37.89 ± 0.9	-137 ± 2	-183 ± 3
PtL2	**TU**	39.16 ± 0.13	9 ± 0.06	39.95 ± 0.7	38.22 ± 0.5	-107 ± 2	-165 ± 2
	DMTU	20.87 ± 0.10	4 ± 0.04	57.76 ± 0.5	31.88 ± 0.3	-53 ± 2	-193 ± 1
	TMTU	6.77 ± 0.01	1 ± 0.05	45.80 ± 0.9	40.56 ± 0.4	-102 ± 3	-154 ± 1
PtL3	**TU**	45.81 ± 0.32	7 ± 0.04	36.10 ± 0.4	20.45 ± 0.5	-119 ± 1	-235 ± 2
	DMTU	37.43 ± 0.03	2 ± 0.04	61.17 ± 0.5	27.44 ± 0.3	-37 ± 2	-218 ± 2
	TMTU	7.01 ± 0.06	1 ± 0.01	45.08 ± 0.9	22.73 ± 0.4	-105 ± 3	-232 ± 1
PtL4	**TU**	49.08 ± 1.05	6 ± 0.02	47.17 ± 0.4	18.33 ± 0.2	-81 ± 1	-237 ± 1
	DMTU	35.90 ± 0.19	4 ± 0.02	54.74 ± 0.2	35.50 ± 0.5	-59 ± 1	-188 ± 2
	TMTU	7.38 ± 0.02	2 ± 0.02	46.51 ± 0.7	35.56 ± 0.5	-101 ± 2	-189 ± 1
PtL5	**TU**	83.48 ± 0.37	4 ± 0.06	46.14 ± 0.3	18.57 ± 0.1	-80 ± 1	-239 ± 1
	DMTU	45.54 ± 0.31	2 ± 0.03	53.17 ± 0.3	32.02 ± 0.8	-62 ± 1	-204 ± 3
	TMTU	10.46 ± 0.09	1 ± 0.02	50.80 ± 0.8	14.25 ± 1.1	-82 ± 3	-257 ± 4

6.10 Discussion

In this chapter the effect of position of annular nitrogen on the reactivity of isomeric dinuclear Pt(II) complexes attached to a pyridine spacer was investigated. The complexes under investigation had substituents in α (2-), β (3-) or γ (4-) positions. The substitution reaction of the complexes followed the order **PtL5** (83.48 $M^{-1}s^{-1}$) > **PtL4** (49.08 $M^{-1}s^{-1}$) > **PtL3** (45.81 $M^{-1}s^{-1}$) > **PtL1** (39.67 $M^{-1}s^{-1}$) ≈ **PtL2** (39.16 $M^{-1}s^{-1}$) with **TU** as the entering nucleophile. The second step was attributed to a dechelation of the bridging spacer caused by the strong *trans* effect of sulphur-donor nucleophiles as confirmed by ^{1}H and ^{195}Pt NMR kinetics in Figures 6 and 7 respectively. The ^{1}H NMR spectra of the complexes show proton signals downfield compared to those of the uncoordinated ligands. This downfield shift of the dipyridyl protons denoted "H_a" in the complexes is attributed to the change in the electron density as a result of their proximity to Pt(II) centre. This is caused by σ inductive effect that decreases the electron density from the ligand which makes a downfield shift. The σ *i*nductive effect has a significant deshielding effect on protons closer to Pt(II) centre. At positions far from metal centre, the σ effect is small and shielding is expected for metals that have significant π-back bonding to the ligand.[45b]

On reaction with 6 equivalents of **TU**, the protons (H_a) at δ = 8.81 ppm undergoes upfield shift to $H_{a'}$ δ = 8.20 ppm similar to those of uncoordinated ligand. This shifting indicates the displacement of the ligand from the metal when reacted with excess nucleophile. This observation is in line with the data obtained from ^{195}Pt NMR. The spectrum at -2103.5 ppm on ^{195}Pt NMR indicates platinum coordinated in a bidentate mode to two nitrogen atoms.[46-48] On reaction with 6 equivalents of **TU** the peak at -2103.5 ppm to -3911.7 ppm indicates formation of $[Pt(\mathbf{TU})_4]^{2+}$ complex an earlier observation by van Eldik and group.[49] Both ^{1}H and ^{195}Pt NMR confirms the complexes to undergo displacement of the bridging ligand.

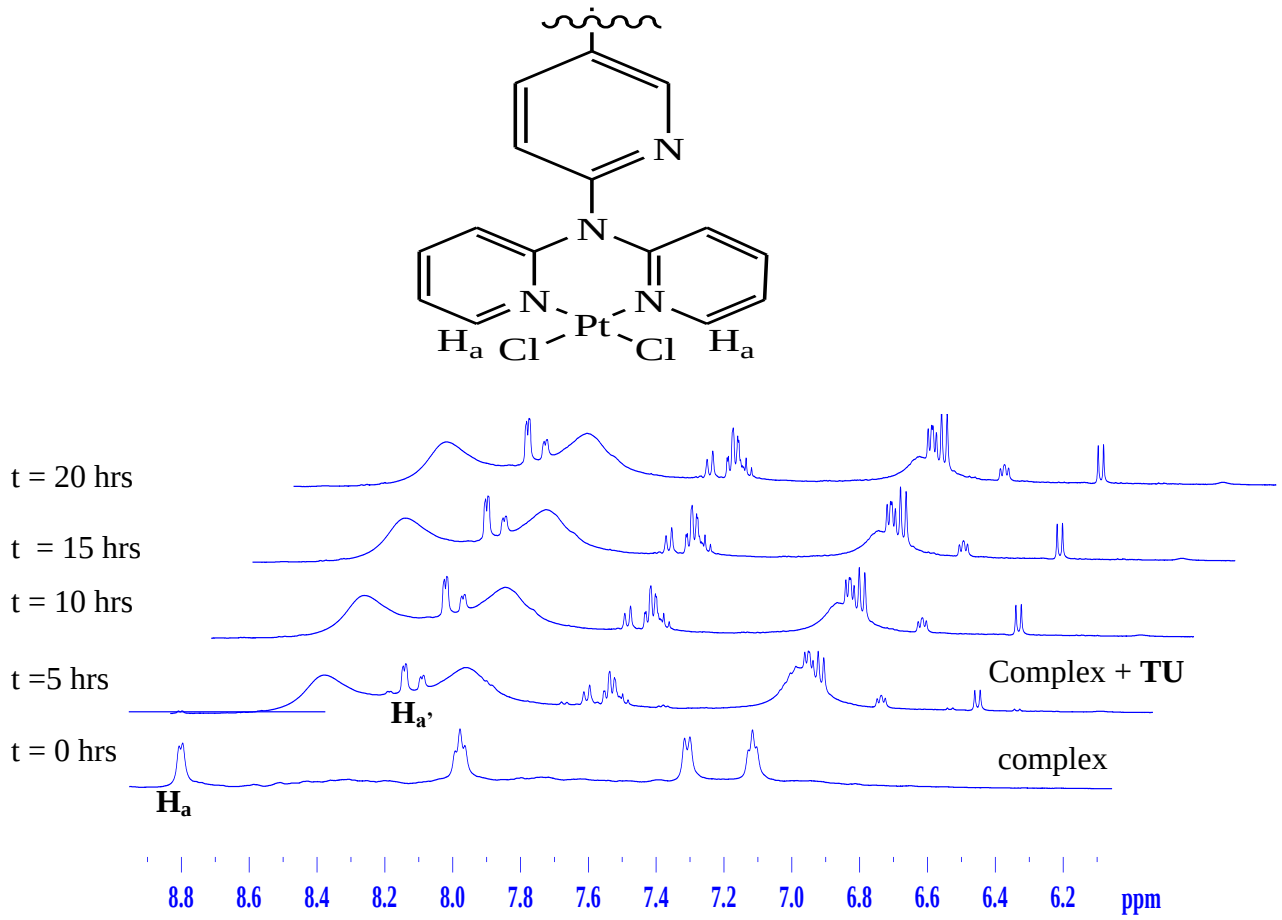

Figure 6.7: Time dependent stacked plot of ^{1}H NMR spectra of **PtL3** with 6 equivalents of TU undergoing dechelation to form the bridging ligand.

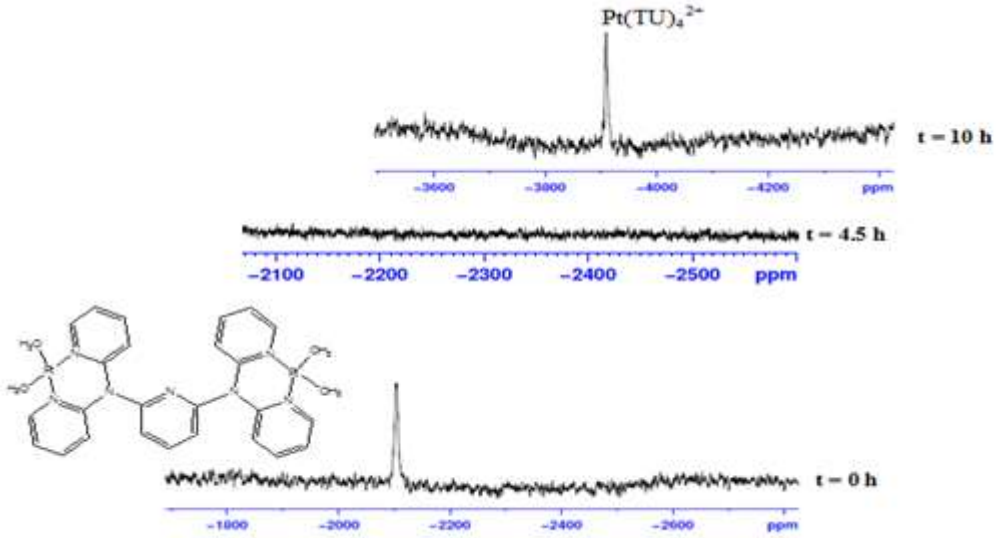

Figure 6.8: Time dependent ^{195}Pt NMR shifts of **PtL3** in DMF leading to formation of $[Pt(\mathbf{TU})_4]^{2+}$ on reaction with excess **TU**.

The planarity and reactivity demonstrates that the pendant pyridine is drastically affected by metal binding. The reactivity trend corroborates with both electronic and geometric structures of the complexes. The study also suggests steric factor to come into play depending on the dihedral angle between the spacer and the dipyridyl plane with the metal centre. The orientation of the pyridine axial ligand causes major differences in complexes stabilities and influences their electronic distribution. The reactivity varied depending on the position of the substituents *viz.*, α (2-), *β* (3-) or *γ* (4-). The positions are polarized due to electronegativity of the nitrogen atom which acts as an electron sink hence creating a positive charge at 2-, 4- and -6 positions. This is due to the *π* density being more delocalized on the nitrogen atom on*α* and γ carbons than β carbon. This makes substituents in positions 2-, 4-, and -6 to be stabilized by positively charged carbon atoms.[50]

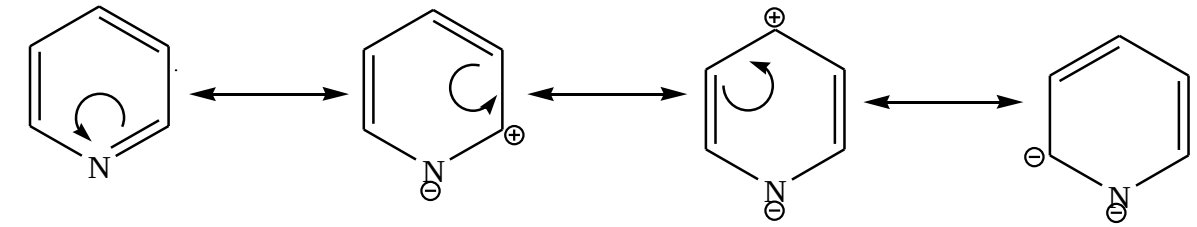

Scheme 6.5: The mesomeric structures of pyridine showing resonance stabilization in 2-, 4- and 6- positions

The high reactivity of **PtL4** compared to **PtL1**, **PtL2** and **PtL3** is due to its increased planarity and enhanced *π*-back donation between nitrogen atom in the central pyridyl ring and the Pt(II) centres. This is supported by its smaller HOMO-LUMO gap.[51-54] This is attributed to the competitive resonance interaction between nitrogen atom and dipyridyls coordinated to Pt(II) centres. The coordination in the 2,5 (*para*) strongly affect the substitution kinetics and electrochemical properties of this complex. This investigation clearly shows the position of substituents to strongly affect the properties of dinuclear platinum(II) complexes. It shows increased planarity between the central pyridine ring and the platinum centres which enhances electron flow and a better orbital overlap that leads to reduced HOMO–LUMO (ΔE) gap hence its high reactivity.[55-58] The planarity in this complex shows a significant *π*-back-bonding from the filled *dπ*-orbitals of the metal to low lying *π** of the pyridine spacer. Due to the extended delocalization of the *π* system there is enhanced planarity of **PtL4**, hence maximum *π*-back-bonding from the metal to the pyridine ring orbitals. Its high reactivity is supported by computational analysis data presented in Table 6.2. The shorter R-N3 bond

length (1.4443 Å) supports electron flow from the *d*-orbitals of the metal to the anti-bonding molecular orbitals of the ligand (the pyridine spacer). The high reactivity of **PtL4** can be explained by effective π-back-bonding effect of the in-plane pyridine that enhances $d_{yz} \rightarrow \pi^*$ electron transfer. This is due to the plane of the pyridine ring and the metal coordination plane being more planar which is important as it allows mixing of the filled Pt-d_{xz} with the empty π^* orbitals of pyridine. The in-plane pyridine in this complex enhances that planarity and extends conjugation between the central pyridine ring and the metal centre. Due to planarity of this complex, there is substantial π-conjugation that leads to larger overlap of π and π^* orbitals of the metal and ligand than in non-planar analogues. The smaller HOMO-LUMO energy supports effective conjugation of the extended π-system. This increases the π-back bonding which makes it more electrophilic for the entering nucleophile to attack.

The DFT optimized structures of **PtL1**, **PtL2** and **PtL3** shows more tilted metal centres from pyridine plane. This tilting places the metal centres out of plane with pyridine ring forcing the complexes to adopt non-planar configuration. The non-planarity destroys delocalization and resonance hence limiting the intermolecular π-orbital overlap of these complexes. The results indicates substituents in the 2,3- and 2,4-positions, have higher out of plane angles as shown in Figure 8. The dihedral angle denoted **b** is perpendicular between the coordination plane of platinum atom and the plane of pyridine ring in **PtL1** and **PtL2**. The study suggests the presence of Pt-pyridine π-bonding to have an overlap of the filled d_{yz} orbitals with the vacant π^* of pyridine. The reason for almost similar k_2 values for **PtL1** (39.67 Ms^{-1}) and **PtL2** (39.16 Ms^{-1}) is due to similar dihedral angles having same electronic effects as well as steric effects. If the π^* orbitals of pyridine have a nodal plane through the six-membered ring, π-back donation takes place *via* $d_{xy} \rightarrow \pi^*$ if it is perpendicular to pyridine otherwise it is *via* $d_{yz} \rightarrow \pi^*$ if it is coplanar.[59,60] However, using an out of plane angle $\approx 90°$ the interaction involves $d_{xy} \rightarrow \pi^*$ reported to be insignificant.[58] The study suggests complexes with smaller dihedral angles ($< 90°$) to experience $d_{yz} \rightarrow \pi^*$ interactions. Angle **b** in Figure 8 has two effects on the metal-ligand interaction. The angle involves $d_{yz} \rightarrow \pi^*$ interaction when the metal /pyridine ligand are not perpendicular and $d_{xy} \rightarrow \pi^*$ when the two planes of the metal to ligand are perpendicular to each other.[59,60]

Steric repulsions in *ortho* position makes the two planes to be perpendicular and to have $d_{xy} \rightarrow \pi^*$ interaction involving metal/pyridine π-bond.[61] The planarity leads to electron withdrawing lowering electron occupation in the $5d_{xz}$ orbital by π-back donation hence higher reactivity. The metal/pyridine ligand contribution to the frontier orbitals is dependent on mutual positions of *d* orbitals and the π^* orbitals on the ligand. Effects of such variation have been demonstrated by varying the positions of the substituents on the pyridine spacer. However, in some complexes the degree of σ and π bonding effect is cancelled out to a great extent by the influence of steric interactions.

The variation in dipole moments in these complexes indicates differing electronegativities. Different dipole moments on the complexes are indicative of varying electronic interactions depending on the substituents position. This variation is due to the pyridine spacer being able to act as either σ/π moiety. As such, the dipole moment reflects the electron density distribution in the complexes in different states.

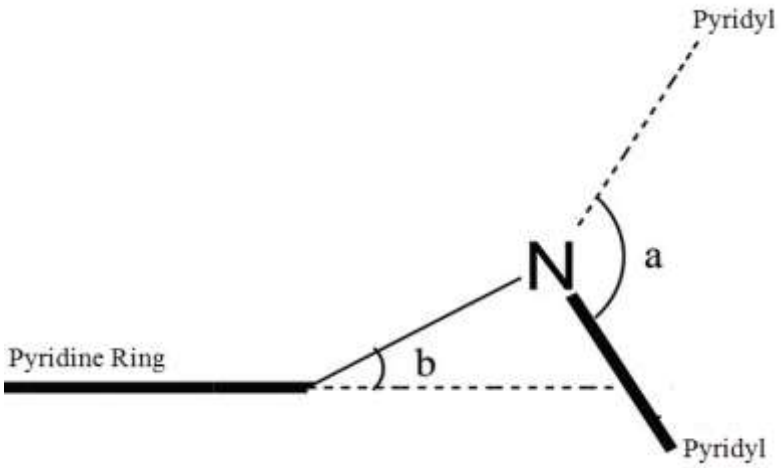

Figure 6.9: Structure of out of plane angle between Pt(II) plane and the pyridine spacer plane;(a ≈ 120°) indicating amine nitrogen to be sp^2 hybridized

The proximity of peripheral groups leads to formation of cavities that entrap the incoming nucleophile. The wider cavity of **PtL5** in Figure S36 in the appendices offers a larger volume for nucleophile entrapment. This is due to incorporation of methylene spacer within the framework of **PtL5** that forms a bowl cavity with a deeper cavity. The difference in the size of the cavities is supported by the wider platinum-platinum distance in the order **PtL5** (12.32 Å) > to **PtL3** (10.40 Å) > **PtL2** (9.49 Å) > **PtL1** (8.11 Å). The reactivity trend indicates the

effect of the size of the cavity. Sterically constrictive cavities minimize the accessibility and amount of nucleophile entrapped *via* encapsulation. The nucleophile is limited inside sterically constrictive cavities of **PtL1**, **PtL2** and **PtL3** while in **PtL5** is quickly trapped hence fast reactivity. The insertion of methylene groups in **PtL5** increases planarity a factor that supports its high reactivity.[62] The study shows planar complexes to have high reactivity than perpendicular conformers. It can therefore be concluded that planar conformers are less stable than the corresponding perpendicular ones.

Comparison of the kinetic data in the current study to those reported in literature[63-65] support reactivity to depend on the nature of the ligand. Dinuclear Pt(II) complexes with semi/rigid linkers shows reactivity to significantly depend on the ability of the ligand to decrease electron density at the metal centre through π-back bonding. This study supports reactivity of dinuclear Pt(II) complexes with rigid ligands to be controlled by geometry and π-back donation. However, in dinuclear Pt(II) complexes, with flexible (-CH_2)n- moiety the trend in reactivity is attributed to strong σ-donor ability of the alkyl chain.

6.11 Conclusion

This work has shown that the electronic and geometric symmetry of dinuclear Pt(II) complexes appended to pyridine spacer can be modulated by substituents positions. This has been illustrated by tuning the reactivity of the complexes by the position of nitrogen atom. The study shows annular nitrogen to enhance the electronic communication and thus provides an opportunity for tailoring the electronic properties of the complexes. The different dihedral angles between pyridine spacer and the platinum metal affect both structural and electronic properties of the complexes. The study shows enhanced reactivity in complexes with smaller dihedral angles between the pyridine spacer and the metal than those that are perpendicular. It was shown that electronic properties are significantly dependent on the position of substituents relative to annular nitrogen in the ring. However, steric factors also come into play in complexes with perpendicular dihedral angles with minimal electronic factors controlling reactivity.

The substitution of the aqua ligands proceeds *via* a two-step reaction pathway which is associatively activated. The results have shown that while planar structures ensure π-conjugation, the linking positions on the pyridine spacer also plays a significant role in determining the extent of this π-conjugation. Thus, steric effects derived from the molecular conformations and electronic effects shows a great influence on the reactivity of these pyridine derivative complexes. The study shows the synergistic σ/π properties of pyridine bridging ligand to control the reactivity of the complexes. This experimental data is well supported by computational calculations which are reliable in predicting the stability of the complexes. Through computational analysis, the study used structure simulations to provide a full understanding of the role played by annular nitrogen and the effect of substituent positions on pyridine as the bridging ligand. It is my hope that the knowledge generated herein will assist in designing novel dinuclear Pt(II) complexes in which interface between extended π conjugation strands and the metal centres could lead to active anticancer complexes with varying reactivity that can be used for treatment of different tumours. The successful study of ligand substitution reported in this thesis marks the first step towards pharmaceutical development of this class of complexes as antitumour agents.

References

1. K. Misra, I. Mitra, G. K. Ghosh, S. Mukherjee, B. Misini, L. Wolfgang and S. C. Moi, *Transition. met. chem.,* 2014, **39**, 789-796; (b) K. Misra, G. K. Ghosh, I. Mitra, S. Mukherjee, V. P. Reddy, L. Wolfgang B. Misini, C. Jagadeesh C. S. Mukhopadhyay and S. C. Moi, *RSC Adv.*, 2015, **5**, 12454-12462.
2. N. J. Wheate, S. Walker, G. E. Craig and R. Oun, *Dalton Trans.,* 2010, **39**, 8113; (b) J. Malina, J. Kasparkova, N. P. Farrell and V. Brabec, *Nucleic Acids Research.*, 2010, 1–9.
3. P. A. Chaloner, *Coord. Chem. Rev*., 1986, **72**, 1-195; (b) P. A. Chaloner, *Coord. Chem. Rev*., 1988, **89**, 1-5.
4. F. Basolo, *Coord. Chem. Rev*., 1996, **154**, 151-161; Basolo F, and Pearson R. G, *Mechanism of inorganic reactions, A study of metal complexes in solutions*, 1967, 345-351.
5. B. K. Keppler, Metal complexes in cancer chemotherapy, (ed) VCH, Weinheim and New York,1993, 429-463.
6. N. P. Johnson, J. P. Hoeschele and R. O.Rahn, *Chem. Biol. Interactions*., 1980, **30**, 151-169.
7. M. A. Fuertes, C. Alonso and J. M. Perez, *Chem. Rev*., 2003, **103**, 645-662.
8. D. Chatterjee, A. Mitra, A. Sengupta and S. Basak, *Inorg. Chim. Acta*., 2005, **358**, 2900-2908.
9. A. Alireza and A. Samie, *J. mater. Chem. Eng*., 2013, **4**, 111-115.
10. G. Schroder, B. Lippert, M. Sabat, C. J. L. Lock, K. Faggiani, B. Song and H. Sigel,*J. Chem. Soc., Dalton Trans*., 1995, 3767-3776.
11. E. Wong and C. M. Giandomenico, *Chem. Rev*., 1999, **99**, 2451-2466.
12. P. K. Ghosh, S. Saha and A. Mahapatra, *Chem. Cent. J*, 2007, 71-80.
13. J. Zhang, L. Wang, Z. Xing, D. Liu, J. Sun, X. Li, and Y. Zhang, *Med. Chem.,* 2010, **10**, 272−282.
14. M. Subhasis, N. Debabrata, A. Mandal, M. Subala, B. B. Kumar, K. Parnajyoti and K. A. Ghosh, *Int. J. Res. Chem. Environ*., 2012, **2**, 275-282.
15. M. R. Shehata, *Transition Met. Chem*., 2001, **26**, 198-204.
16. G. Zhao and H. Lin, *Curr. Med. Chem.*, 2005, **5**, 137-147.
17. J. Kasparkova, N. Farrell, V. Brabec, *J. Biol. Chem*., 2000, **275**, 15789-15798.
18. S. L. Hollis, A. R. Amundsen, E. W. Stern, *J. Med. Chem*., 1989, **32**, 128-136.

19. V. Brabecand J. Kasparkova, *Drug Resist.Updat*., 2005, **8**, 131-146
20. V. Brabec, J. Kasparkova, O. Vrana, O. Novakova, J. W. Cox, Y. Qu and N. Farrell, *Biochemistry*, 1999, **38,** 6781-6790.
21. W. Yanqing, W. Xiaoyong, W. Jing, Z. Yongmei, H. Weijiang and G. Zijian, *Inorg. Chem*., 2011, **50**, 12661-12668.
22. P. Pil and S. J. Lippard, *Science*, 1992, **256**, 234-237.
23. D. Jaganyi, F. Tiba, O. Q. Munro, B. Petrović and Ž. D. Bugarčić, *Dalton Trans*., 2006, **24**, 2943-2949.
24. J. Breet, R. van Eldik, *Inorg. Chem*., 1984, **23**, 1865-1869.
25. M. A. Jakupec, M. Galanski, B. K. Keppler, *Rev. Physiol. Biochem. Pharmacol.*, 2003, **146**, 1-54.
26. A. Bianca, D. J. Bray, J. K. Clegg, K. Gloe, G. Karsten, O. Kataeva, F. L. Lindoy, J. C. McMurtrie, P. J. Steel, C. J. Sumby and M. Wenzel, *Dalton Trans.*, 2006, 4783-4794.
27. J. J. M. Amoore, C. J. Kepert, J. D. Cashion, B. Moubaraki, S. M. Neville, K. S. Murray, Chem.--Eur. J. 2006, **12**, 8220-8227.
28. N. P. Farrell, T. T. B. Ha, J. P. Souchard, F. L. Wimmer, S. Cros, N. P. Johnson, *J. Med. Chem.*, 1989, **32**, 2241.
29. T.-J.J. Kinnunen, M. Haukka, T.A. Pakkanen. J. Organomet. Chem., 2002, 8, 654.
30. M. C. Aragoni, M. Arca, S. J. Coles, M. C. Alonso, S. L. Coles, R. P. Davies, M. B. Hursthouse, *Cryst Eng Comm*., 2016, 18, 5620–5629.
31. (a) J. Bogojeski, Ž. D. Bugarčić, R. Puchta, and R. van Eldik, *Eur. J. Inorg. Chem.*, 2010, 5439-5445; (b) S. Jovanović, B. Petrović, D. Čanović and Ž. D. Bugarčić, *Int. J. Chem. Kinet*., 2011, **43**, 99-106; (c) W. Summa, R. Schiessl, N. Puchta, H. van Eikema and R. van Eldik R, *Inorg. Chem*., 2006, **45**, 2948-2959.
32. V.B. Origin7.5^{TM} SRO in Origin Lab Corporation, Northampton, One, Northampton, MA, 01060, USA, 2003.
33. (a) J. Bogojeski, Ž. D. Bugarčić, R. Puchta and R. van Eldik, *Eur. J. Inorg. Chem.*, 2010, 5439-5445; (b) R. W. Hay and A. K. Basak, 1982, *J. Chem. Soc., Dalton Trans,*1819-1829.
34. Jovanović S, Petrović B, Čanović D. and Ž. D, Bugarčić, *Int. J. Chem. Kinet*., 2011, **43**, 99-106.

35. N. Hochreuther, S. T. Nandibewoor, R. Puchta, R. van Eldik, *Dalton Trans*., 2012, **41**, 512-522.

36. T. Soldatović, Ž. D. Bugarčićand R. van Eldik, *Dalton Trans*., 2009, 4526-4531.

37. N. Summa, R. Schiessl, N. Puchta, H. van Eikema and R. van Eldik, *Inorg. Chem*., 2006, **45**, 2948-2959.

38. M. J. Frisch, G. W. Trucks, H. B. Schlegel, G. E. Scuseria, M. A. Robb, J. R. Cheeseman, G. Scalmani, V. Barone, B. Mennucci, G. A. Petersson, H. Nakatsuji, M. Caricato, X. Li, H. P. Hratchian, A. F. Izmaylov, J. Bloino, G. Zheng, J. L. Sonnenberg, M. Hada, M. Ehara, K. Toyota, R. Fukuda, J. Hasegawa, M. Ishida, T. Nakajima, Y. Honda, O. Kitao, H. Nakai, T. Vreven, J. A. Montgomery, Jr., J. E. Peralta, F. Ogliaro, M. Bearpark, J. J. Heyd, E. Brothers, K. N. Kudin, V. N. Staroverov, R. Kobayashi, J. Normand, K. Raghavachari, A. Rendell, J. C. Burant, S. S. Iyengar, J. Tomasi, M. Cossi, N. Rega, J. M. Millam, M. Klene, J. E. Knox, J. B. Cross, V. Bakken, C. Adamo, J. Jaramillo, R. Gomperts, R. E. Stratmann, O. Yazyev, A. J. Austin, R. Cammi, C. Pomelli, J. W. Ochterski, R. L. Martin, K. Morokuma, V. G. Zakrzewski, G. A. Voth, P. Salvador, J. J. Dannenberg, S. Dapprich, A. D. Daniels, O. Farkas, J. B. Foresman, J. V. Ortiz, J. Cioslowski and D. J. Fox, Gaussian 09, Revision A.1, Gaussian, Inc., Wallingford CT, 2009.

39. (a) A. D. Becke, *J. Chem. Phys.* 1993, **98**, 1372, 5648-5652; (b) C. Lee, W. Yang, R. G. Parr, *Phys. Rev. B.*,1988, **37**, 785-789; (c) P. J. Stephens, F. J. Devlin, C. F. Chabalowski and M. J. Frisch, *J. Phys. Chem*., 1994, **98** 1623-1627.

40. (a) B. Miehlich, A. Savin, H. Stoll and H. Preuss, *Chem. Phys. Lett.*, 1989, **157**, 1089-1098. (b) P. J. Hay and W. R. Wadt, *J. Chem. Phys.,* 1985, **82**, 299-310; (c) M. G. B. Drew, S. Nag and D. Datta, *Inorg. Chim. Acta*., 2008, **361**, 417-421.

41. N. Hochreuther, R. Puchta, R. van Eldik, *Inorg. Chem*., 2011, **50**, 8984-8996.

42. P. O. Ongoma and D. Jaganyi, *Transition Met Chem.,* 2014, **39**, 407-420.

43. A. Mambanda, D. Jaganyi, S. Hochreuther, S. Nandibewoorand R.van Eldik, *Dalton Trans*., 2010, **39**, 3595-3608.

44. D. Reddy and D. Jaganyi, *Dalton Trans*., 2008, 6724-6731.

45. A. Hofmann, L. Dahlenburg and R. van Eldik, *Inorg. Chem*., 2003, **42**, 6528-6538. (b) C. R. Johnson, W. W. Henderson and R. E. Shepherd, *Inorg. Chem*., 1984, **23**, 2754.

46. B. M. Still, P. G. A. Kumar, J. R. Aldrich-Wright and W. S. Price, *Chem. Soc. Rev*., 2007, **36**, 665-686.

47. P. S. Pregosin, *Coord. Chem. Rev*., 1982, **44**, 247-291.
48. E. Gabano, E. Marengo, M. Bobba, E. Robotti, C. Cassino, M. Botta and D. Osella, *Coord. Chem. Rev*., 2006, **250**, 2158-2174.
49. (a) H. Ertürk, R. Puchta and R. van Eldik, *Eur. J. Inorg. Chem*., 2009, **10**, 1331-1338; (b) H. Ertürk, J. Magut, R. Puchta and R. van Eldik, *Dalton Trans*., 2008, 2759-2766.
50. A. Waldemar, A. Grimison and R. Hoffmann, *J. Am. Chem. Soc*., 1969, **91**, 2590-2599.
51. (a) R. G. Pearson, *J. Am. Chem. Soc*., 1988, **110**, 2092-2097; (b) R. G. Pearson, *J. Org. Chem*., 1989, **54**, 1423-1430.
52. Z. Zhou and R. G. Parr, *J. Am. Chem. Soc*., 1990, **112**, 7371-7379.
53. M. D. Diener and J. M. Alford, *Nature*, (London), 1998, **393**, 668-671.
54. D. E. Manolopoulos, J. C. May and S. E. Down, *Chem. Phys. Lett*., 1991, **181**, 105-111.
55. K. Parimala and V. Balachandran, *Spectrochim. Acta Part A*., 2011, **81**, 711-723.
56. M. M. Islam, M. D. Bhiuyan, T. Bredow and A. C. Try, *Comput. Theor. Chem*., 2011, **967**, 165-170.
57. Y. O. Lee, T. Pradhan, K. No and J. S. Kim, Tetrahedron, 2012, **68**, 1704-1711.
58. M. Arivazhagan, V. P. Subhasini and A. Austine, *Spectrochim. Acta Part A*., 2012, **86**, 205-213.
59. F. D. Rochon, A. L. Beauchamp and C. Bensimon, *Can. J. Chem*, 1996, **74**, 2121-2130.
60. Y. Maeda, H. Hashimoto, I. Kinoshita and T. Nishioka, *Inorg. Chem*., 2014, **53**, 661-663.
61. T. A. Albright, R. Hoffmann, J. C. Thibeault and D. L. Thorn, *J. Am. Chem. Soc*., 1979, **99**, 718-726.
62. K. K. Scott, L. T. Ngoc, G. Scott and W. Weiming, *J. Am. Chem. Soc*., 2010, **132**, 390-395.
63. A. W. Panyako and D. Jaganyi, *Int. J. Kinet.*, 2017, **49,** 545-561.
64. G. Kinunda and D. Jaganyi, *Transition met. Chem*., 2014, **39**, 939-949.
65. T. Soldatovic´, S. Jovanovic´, Ž. D. Bugarc˘ic´ and R. van Eldik, *Dalton Trans*., 2012, **41**, 876.

CHAPTER 7

7.1 Summary and future recommendations

A brief review on multinuclear platinum(II) compounds, including their synthetic methods, chemical reactions and important structural features are presented. The work highlights the role linker and experimentally assesses the linker properties in the design of new anticancer drug candidates. The Pt(II) complexes investigated in this work were representatives of diverse groups of functional bridging ligands. The study was designed towards an improved understanding of mechanism of action of platinum(II) anticancer drugs. The aim was geared towards the design of rational drugs that can overcome the limitations of platinum drugs in clinical practice like intrinsic or acquired resistance and severe side effects. To achieve our goal the study focused on development of non-classical *cis* platinum compounds with more than one platinum centre. The dinuclear and polynuclear Pt(II) complexes exhibit anticancer activity, have broad cytotoxic profiles and overcome cisplatin resistance.[1-4] This class of Pt(II) complexes form different Pt-DNA adducts and display different spectrum of anticancer activity compared to mononuclear analogues.[5,6] The commercially available 2,2'-dipyridylamine was used as supporting ligand. The ligand has the ability to form mononuclear, dinuclear and trinulear complexes.[7-9] Employing different bridging backbones yielded new platinum complexes with discrete and polymeric architectures. The kinetics and mechanistic behaviours of these Pt(II) complexes are reviewed with reference to experimental and computational concepts surrounding their structural and electronic properties. More emphasis is put on multinuclear complexes since their mechanistic reactions have not been studied in the same details as the mononuclear analogues.[10,11]

The coordination chemistry of Pt(II) with dpa and its derivatives was the centre of focus. Pt(II) complexes of dpa and its derivatives was investigated as anticancer agents due to their structural similarity to cisplatin.[12],[13] By combing platinum centres it may be possible to produce synergistic benefits to anticancer drugs. In solution form, structure relationships underlying the interaction of Pt(II) complexes with dpa attached to various spacers has been probed. Proposed substitution mechanisms, rate laws and thermodynamic and kinetic data are presented in chapters 3 to 6. The findings show the complexes to undergo successful ligand exchange making the employed bridging ligands potential candidates for drug delivery. The

successful multi-substitution mechanism of these complexes signifies them to be promising anticancer agents with potential clinical significance. With such a huge number of biologically active complexes, this study outlined a systematic examination the effect of the spacer on the conformation and reactivity of the compounds. Since toxicity of these metal-based drugs also depends on the ligands bound to the metal, a wider study on the effect of the spacer ligand was investigated.

The study involved engineering of organic-inorganic hybrid architectures which have a potential application in material science and in drug application. Tuning and modification of coordination spheres of Pt(II) complexes using varying spectator ligands will enable develop antitumour complexes of varying reactivity that can treat different types of tumours. For comparison, this study designed varying bridging ligands with N-donor atoms. The bridging ligands provided the linkage between the metal centres of binuclear and trinuclear assemblies and controlled distances, relative orientations of the complexes as well as inter-complex electron and energy transfer processes. The platinum coordination complexes displayed interesting variations in their architectures that led to variation in their reactivity. By varying the bridging ligands, we extracted reactivity patterns across the series which can be used to predict the trends among and across the investigated series. The study reveals the spacers to be key components that control electronic communication between the metal centres, steric effects and thereby the properties of the complexes.

We based our study on developing Pt(II) complexes that offer two labile substitution sites with two non-leaving N-donors in *cis*-position that gives a bifunctional DNA binding at each platinum centre.[14-16] From structural view point the bridging ligands were arranged in four sets. The first one comprised of semi–rigid linkers composed of aromatic and a methylene flexible linker. The second set in chapter four was based on aliphatic linker as the spacer. In this set of complexes aliphatic chain influences physicochemical and conformational properties. Chapter five of this study focuses on starburst complexes that contain 2,2-dipyridylamino groups with a C_3 symmetry. Complexes in starburst molecules involved appending to a central benzene or to a 1,3,5-triazine core. The starburst dpa derivatives 1,3,5-tris(di-2-pyridylamino)benzene, tdab and 2,4,6-tris(di-2-pyridylamino)1,3,5-triazine, tdat, were employed. Each of the ligands tdab and tdat have three dpa subunits arranged around

the central as chelating donors to three metal centres. This series formed polynuclear Pt(II) complexes with three cisplatin-like metal centres appended to varying ligand backbone.

Comparing the reactivity trend in these four schemes, this investigation reveals that using the alkyl-phenyl linker in chapter three, reactivity depends on the position on the methylene group. The methylene group exhibits a stronger electron donating effect in *para* position.In this study isomeric 1,2-bis(di-2-pyridylaminomethyl)benzene 1,3-bis(di-2-pyridylaminomethyl)benzene and 1,4-bis(di-2-pyridylaminomethyl)benzene ligands showed marked different coordination behaviours. The dinuclear Pt(II) connected to isomeric ligands showed alkyl group to donate electrons to varying degrees. The electron donating effect of alkyl groups is evidenced by elevated HOMO and LUMO levels. Variation in the reactivity of this set of complexes showed electronic and steric properties of the ligands to play a crucial role depending on the position of alkyl on the pendant phenyl spacer. Structural rigidity of the central pendant phenyl ring also plays a significant role in the reactivity of this series. The study shows that coordination of metals to alkyl-phenyl spacers facilitates formation of unique architectures and environment for kinetic reactions. This investigation shows alkyl-phenyl spacers to form bowl-shaped metallocavitands to varying degrees. The presence of cavitands in alkyl-phenyl spacers introduced steric hindrance leading to slow reactivity of this series. These results provide valuable information for isomeric dinuclear Pt(II) molecular design and shows where to attach the alkyl spacer on the pendant phenyl group to achieve a slow or faster reaction.

The second investigation employed aliphatic chain as bridging ligands. Coordinating two Pt(II) metals to an alkyl chain linker gives rise to translocation of the coordinated metal outside the cavity unlike the alkyl-phenyl spacers which form cavities. Using the flexible aliphatic chain linkers demonstrated the “odd – even” effect. This effect was attributed to packing differences in the molecular structure between chains having odd and even number of methylene groups. The number of substitution steps in flexible aliphatic chain linkers was dictated by odd and even conformation. The spacer size (aliphatic chain length) has an influence on the structural makeup and controls the reactivity of the complex. Aliphatic linkers show electrostatic interactions between platinum centres which become weaker on lengthening the bridging linker. On comparison the aliphatic linker shows electronic factors

to be dominant on complexes reactivity while in alkyl-phenyl spacers reactivity is dominated by conformations and steric factors. The study shows that insertion of alkyl-phenyl unit within the framework of the dinuclear complexes dampens reactivity by approximately 100 times slower than those appended to flexible aliphatic linkers. The interaction strength and exchange kinetics was optimized in specific assemblies by changing the ligand structure coordinating to metal centres. Since our objective was to study the influence of the nature of the bridging ligand on the thermodynamic and kinetic properties of Pt(II) complexes, the results indicate that the bridging ligand has an influence on the reactivity and stability of complexes towards biomolecules as well as possible electronic and steric interactions between metal centres.

The third study of this investigation involved assembling three platinum starburst ligands of dpa. Three starburst trinuclear platinum complexes of 2,2'-dipyridylamino derivatives were synthesized. Reactivity of trinuclear complexes was tuned through rigidity and flexibility by perturbing the spacers attached to the central benzene or 1,3,5-triazine. This study envisaged shedding light on rigid verses flexible linkers and the increased charge in the complexes. The complexes investigated this class of complexes displayed versatile structures where a combination of factors played important role in their reactivity. For instance conjugation of the amino nitrogen lone pair of the dpa unit with the central aromatic unit of the ligand and steric interactions play a key role in the reactivity of these complexes. This series shows slightly higher reactivity compared to the complexes appended to aliphatic chain and much more reactive to complexes attached to alkyl-phenyl spacers. Higher reactivity of this series was expected due to their rigidity, high positive charge, electrostatic and to some extent hydrogen-bonding interactions.

This class of complexes shows a higher extent of electronic delocalization by modulating the geometric constraints of the system making it more rigid. The study used a mesitylene moiety to bridge three 2,2'-bis(pyridylmethyl)amine units. This ligand is more rigid than the aliphatic ones in the second study, and similar to dinuclear complexes connected to the alkyl-phenyl spacers but more flexible than pure aromatic linkers. This study was based on the view that design of a more rigid ligand than aliphatic ligands, but more flexible than pure aromatic linkers may be favourable for DNA cross linking. The complex from mesitylene linker shows a higher reactivity compared to dinuclear alkyl-phenyl linked complexes

probably due to increased nuclear charge of positive six and its structural make-up. The study shows that rigidity, flexibility of the linker as well as distances between metal centres greatly controls reactivity of trinuclear complexes investigated. The remarkable differences within this series and to other complexes are due to a combination of many factors, including geometry, steric hindrance, flexibility electrostatic effects and lipophilicity. The choice of ligands in this series offers a possibility of a wide variation in donor-acceptor interaction and molecular flexibility. Introduction of methylene groups destroys conjugacy and lowers both the acidity and reactivity of the complexes. The study further shows that replacement of the methyne (=CH-) groups with nitrogen atoms enhances reactivity. The results show a significant difference in the thermodynamic and kinetic behaviour when the bridge is varied. The intermetallic distances and the conjugated π-electron nature of the bridge in particular triazine backbone controlled reactivity. The presence of methylene linkers reduced reactivity of the complexes through σ-donicity. Complexes with π-acceptor ability showed higher electrophilicity as supported by lower pK_a values and higher reaction rate constants as compared to σ-donor ligands like aliphatic linkers which increase electron density on the metal centre decreasing electrophilicity and acidity.

The fourth investigation of our study restricted rotational freedom and limited interaction within the linker by imparting rigidity using rigid pyridine spacer. The four Pt(II) complexes in this series attached to pyridine spectator ligand are isomers and similar reactivity behaviour are expected. The study shows the complexes to have similar coordination behaviour and almost similar reactivity rates. These findings support our previous study of the alkyl-phenyl spacer, the position of substituent on the spectator ligand to strongly affect the chemical reactivity of the complex. The complexes indicate the position of the substituent and ligand modification to greatly influence the behaviour and thermodynamic and kinetic data of the complexes. These findings justifies our core focus that the spectator ligand can be tuned for vital properties such as reactivity, solubility and acidity of Pt(II) complexes for their application as antitumour agents.[17,18] Varying the spectator ligand and positioning of substituents may offer possibilities to design novel complexes of desired structural and chemical properties.

The introduction of heteroatom (nitrogen atom) in different positions increases π-accepting properties of this type of complexes. The π-back donation is greatly influenced by the position of the annular nitrogen in the pyridine spacer. This is supported by quite remarkable planarity in some complexes that lead to extended conjugation and an increase in delocalized π-system. The enhanced reactivity is attributed to combined effects of planarization, rigidification and inductive effects of the bridging spacers. Among the studied complexes, 2,3- and 2,4-pyridinediamine tetraqua Pt(II) complexes show a lower reactivity compared to 2,5 and 2,6-pyridinediamine tetraqua Pt(II) due to steric interaction of the vicinal and adjacent platinum groups. Steric repulsions in *ortho* position is proposed to bring the two planes to be perpendicular to each other. This involves $d_{xy} \rightarrow \pi^*$ contribution in the bonding of the two *cis* Pt-$(H_2O)_2$ reducing the Pt-pyridine π-bond. The study suggests complexes with smaller dihedral angles have higher reactivity due to $d_{yz} \rightarrow \pi^*$ interaction with a significant π-back bonding as a result of enlarged conjugated system and increased planarity. This series showed increased reactivity than those with alkyl-phenyl spacer and aliphatic linkers due to presence of a heteroatom nitrogen due to increased π-back bonding effect of the pyridine spacer. From this work, Pt(II) complexes with chelating heterocyclic pyridine ligands represents a particularly new class of coordination complexes from the view point of their structural and kinetic properties.

Despite the close similarity between the coordination chemistry of the investigated Pt(II) complexes in this study, they show different thermodynamics and kinetic properties as documented. The study shows that the primary motif of these complexes mainly depends on the features of the spacers such as length, rigidity and orientation of the donor atoms. This has been confirmed by the four studies carried out in this thesis. The variation of the bridging linker enabled a systematic study on the influence of different bridging ligands on the thermodynamic (pK_a values of coordinated aqua ligands) and kinetic properties of the Pt(II) complexes. The study indicates that control of thermodynamics and kinetics of ligand substitution is a key element in design of metal-based drugs. The study shows that in designing new anticancer agents, several structural features can be strategically modified. Modification of ligands directly affects the nature of the complex and the resulting Pt-DNA adducts and cellular repair pathways.[19-22]

In summary, the study gives an up to date overview of the anticancer chemistry of the platinum(II) complexes with an emphasis on new strategies that can be used to develop new antitumour agents. Methodologies' involving bulky aromatic ligands, aliphatic nitrogen ligands, spacers containing nitrogen atom (pyridine) and dinuclear and trinuclear Pt(II) complexes in the design of agents analogous to cisplatin are presented. This study shows that the kinetic and mechanistic behaviour of polynuclear platinum complexes may be modulated by the geometry and number of leaving groups in the coordination sphere of platinum atoms as well as the nature of the bridging ligands to the platinum centres. Bridging ligands play important roles in regulating the reactivity by controlling the geometric symmetry, steric and electronic features and intermetallic distances in dinuclear and trinuclear Pt(II) complexes. This investigation shows that structural modification may be used in tuning the reactivity of anticancer prodrugs. The increased charge in polynuclear Pt(II) complexes of 4+ or 6+, the presence of at least two Pt coordination units capable of DNA binding are remarkable departures from cisplatin structural paradigm. A higher overall charge on the platinum atom is also a way of tuning the reactivity of Pt(II) complexes towards prodrug design. Since DNA binding is the mechanistic paradigm by which cytotoxic platinum complexes are believed to exert their antitumour activity, the development of polynuclear platinum(II) complexes represents an approach to systematically alter this cellular response induced by cisplatin by changing the nature and structure of the DNA lesion induced.[23,24] Elucidating the mechanism of action of this new class of anticancer agents may lead to design better and more specific drugs for treatment of cancer. Proof of utility of this approach is given by the entry of trinuclear Pt(II) complex BBR3464 to human Phase II trials.[25-27]

Inclusion, the study shows associative mechanism of substitution reactions as supported by activation parameters (the low positive values of enthalpy and large negative values of entropy). Substitution reactions of these Pt(II) complexes with S-donor ligands which have strong *trans* effects lead to the facile release of the coordinated linkers. This was collectively supported by ^{1}H and ^{195}Pt NMR results. The ability of the designed complexes to undergo ligand exchange makes them potential chemotherapeutic drug candidates. The findings also offer the possibility of assembling polynuclear Pt(II) whose reactivity and cytotoxicity can be fine-tuned by selection of bridging ligands. Thus, the study provides a potential strategy in designing novel anticancer platinum drug candidates. It is with the hope that kinetic and mechanistic data obtained from this work could contribute to the future design of potential

Pt(II) complexes as anticancer therapeutic agents. Further investigations of polynuclear platinum complexes will allow us to better understand their interaction with DNA and to fully elucidate their mechanism of DNA cleavage. The results show that using coordination chemistry it is possible to design novel therapeutic agents by modifying the ligand around the metal centre. On the basis of our findings, it can be concluded that structural modifications controls the reactivity of dinuclear and trinuclear Pt(II) complexes and is expected to substantially modulate the DNA binding mode and DNA damage process and lead to an improved antitumor efficacy of this class of platinum complexes.

7.2 Future recommendations

The substitution reactions in this work need to be expanded to a broader study involving *invivo* and *in vitro* cytotoxicity assays to evaluate the sensitivity of the complexes togive more information regarding their mechanistic reactions. On this aspect, the study recommends for cancer screening of these complexes to reveal their activity as anticancer therapeutics.

The study also recommends bio-computational/bioinformatics studies using docking software to shed light how the investigated complexes interact with biological systems.Software applications like DOCK and Autodock match potential ligands will assist in calculating steric constraints and bond energies essential in drug design. Thus, bioinformatics will beessential to reveal biological insights in DNA-ligand interactions and also provide a basis for identification of novel mechanisms for synthetic metallodrugs. Bioinformatics will significantly reduce the time and cost for developing new anticancer drugs and exploit many different paradigms.

The future development in this area should compare the bifunctional verses trifunctional complexes and include other parameters such as intercalation, photosensitivity redox properties and photo-caged platinum into play. From industrial point of view these complexes possess both steric and electronic properties which are essential in tuning the reactivity of metal-based drugs. The study also recommends that the catalytic activities of these Pt(II) complexes to be tested in organic synthesis.

Despite significant efforts to design new antitumour agents based on Pt(II) in effort to overcome cisplatin resistance or enhance its antitumour activity, other transition metal complexes need to be brought on board for investigation in similar magnitude. In order to find compounds with greater antitumour activity and less toxicity and resistance compared to cisplatin, the study recommends other noble metals such as ruthenium, Pt(IV), gold, rhenium among others with slow ligand exchange to be investigated in a similar mechanistic perspective. The study also recommends investigation of mixed metal bifunctional and trifunctional like Ru-Pt, Pt-Pd, Ru-Pd compounds attached to intercalator as antitumour agents. There is need for this new approach as it may lead to synergised metal-based anticancer drugs.

The study also proposes future investigation to vary the two ancillary ligands on the square planar Pt(II) complex, to try and tune the HOMO-LUMO gap to suit the anticancer therapeutic properties. By carefully controlling the HOMO-LUMO gap by employing smart ancillary ligand groups minding the toxicity as well may be key to finding suitable compounds with desired anticancer therapeutic properties.

Finally, for this work to gain more clinical significance, further investigation needs to be carried out at physiological concentrations and physiological pH. The complexes need to be tested on a panel of cancer cell lines for their antiproliferative effects as well as *in vitro* and *in vivo*.

References

1. V. Brabec, J. Kasparkova, O. Vrana, O. Novakova, J.W. Cox, Y.Qu and N. Farrell. *Biochemistry*, 1999, **38**, 6781-6790.
2. S. Komeda, M. Lutz, A. L. Spek, M. Chikuma, J. Reedijk, *J. Inorg. Chem.*, 2000, **39**, 4230.
3. J.W. Cox, S.J. Berners-Price, M.S. Davies, Y. Qu, N. Farrell. *J. Am. Chem. Soc*., 2001, **123**, 1316.
4. Ž.D. Bugarčić, J. Bogojeski, B. Petrović, S. Hochreuther and R. van Eldik. *Dalton Trans.*, 2012, **41**, 12329.
5. N. J. Wheate and J. G. Collins, *Coord. Chem. Rev.*, 2003, **241**, 133.
6. J. Reedijk, *Proc. Natl. Acad. Sci. USA*, 2003, **100**, 3611.
7. S. Gloria, P. Wang and K. M. Rao, *Z. Anorg. Allg. Chem.* 2012, **638**, 634–640.
8. H. G. Zhu, M. Strobele, Z. Yu, Z. Wang, H. J. Meyer and X. Z. You, *Inorg. Chem. Commun.*, 2001, **4**, 577.
9. (a) K. Y. Ho, W. Y. Yu, K. K. Cheung and C. M. Che, Chem. Commun., 1998, 2101; (b) K. Y. Ho, W. Y. Yu, K. K. Cheung and C. M. Che, *Dalton Trans*., 1999, 1581.
10. W. A. Panyako *and* D. Jaganyi, *Int. J. Kinet.*, 2017, **49,** 545-561.
11. W. A. Panyako, *Inorg. Chim. Acta*., 2017, **469** 341-352.
12. C. Tu, J. Lin, Y. Shao and Z. Guo, *Inorg. Chem.*, 2003, **42**, 5795.
13. S. Fakih, W. C. Tung, D. Eierhoff, C. Mock and B. Krebs, *Z. Anorg. Allg. Chem.*, 2005, **631**, 1397
14. W. A. Panyako, *Inorg. Chim. Acta*., 2018, **469**, 341-352.
15. W. A. Panyako and G. Kinunda, *New J. Chem.*, 2018, **42**, 214-227.
16. W. A. Panyako, *Journal of Coordination Chemistry,* DOI: 10.1080/00958972.2017.1371702, Link:http://dx.doi.org/10.1080/00958972.2017.1371702.
17. J. Reedijk, Chem Rev., 1999, **99**, 2467.
18. G.K. Ghosh, K. Misra, M. Bashkim, W. Linert, S. C. Moi, J Solut Chem., 2013, **42**, 526
19. V. Brabec and J. Kasparova. *Drug Resist. Updates*, 2005, **8**, 131.
20. (a) N. Farrell, Y. Qu. *Inorg. Chem.*, 1989, **28**, 341, (b) N. Farrell, S.G. de Almeida and K.A. Skov. *J. Am. Chem. Soc.*, 1988, **110**, 5018, (c) J.D. Roberts, B. van Houten, Y. Qu, and N.P. Farrell. *Nucleic Acids Res.*, 1989, **17**, 9719, (d) A. Kraker, W. Elliott,

B. van Houten, N. Farrell, J. Hoeschele and J. Roberts. *J. Inorg. Biochem.*, 1989, **36**, 160.

21. N. J. Wheate, S. Walker, G. E. Craig and R. Oun, *Dalton Trans., 2010*, **39**, 8113
22. B. Spingler, D. A. Whittington, S. J, Lippard, *J. Inorg. Chem*., 2001, **40**, 5596.
23 . J. B. Mangrum and N. P. Farrell, *J. Chem. Soc. Chem. Comm.*, 2010, **46**, 6640–6650.
24 . J. Malina, N. P. Farrell and V. Brabec, *Chem. Asian. J.*, 2011, **6**, 1566–1574.
25. N. P. Farrell, *Comments Inorg. Chem*., 1995, **16**, 373–389.
26. Y. Qu and N. P. Farrell, *J. Am. Chem. Soc*., 1991, **113**, 4851–4857.
27 . N. Farrel, Y. Qu, and M.P. Hacker, *J. Med. Chem*., 1990, **33**, 2179–2184.

APPENDICES

APPENDIX 1 (Chapter 3)

A summary of wavelengths used for kinetic measurements for the investigated complexes, some of their kinetic traces, k_{obs} for reactions at different concentrations and temperatures and characterization of complexes using ^{1}H NMR, TOF ES^{+} mass spectra, ^{13}C NMR and ^{195}Pt NMR are given in the following tables.

Table S3.1: Wavelengths for kinetic measurements used in the study

Complex	Nucleophile	Wavelength (λ) (nm)	
		Stopped-flow	UV-Vis
Pt1	**TU**	302	320
	DMTU	304	320
	TMTU	372	335
Pt2	**TU**	290	320
	DMTU	297	320
	TMTU	362	335
Pt3	**TU**	-	320
	DMTU	-	320
	TMTU	-	335
Pt4	**TU**	295	320
	DMTU	302	320
	TMTU	-	335
Pt5	**TU**	-	320
	DMTU	-	320

Table S3.2: Average observed rate constants, k_{obs}, s^{-1}, for the displacement of the aqua ligands in Pt1 with the nucleophiles, at pH = 2.0, *T* = 298 *K*, *I* = 0.1 M $NaClO_4$.

TU		**DMTU**		**TMTU**	
Conc., M	k_{obs} (s^{-1})	Conc., M	k_{obs} (s^{-1})	Conc., M	k_{obs} (s^{-1})
0.016125	0.46507	0.016125	0.53823	0.016125	0.16678
0.012900	0.37804	0.012900	0.42854	0.012900	0.13549
0.009675	0.27471	0.009675	0.32435	0.009675	0.100026
0.006450	0.18156	0.006450	0.21642	0.006450	0.06559
0.003225	0.09115	0.003225	0.11429	0.003225	0.03334

Table S3.3: Average observed rate constants, k_{obs}, s^{-1}, for the displacement of the aqua ligands in Pt2 with the nucleophiles, at pH = 2.0, *T* = 298 *K*, *I* = 0.1 M $NaClO_4$.

TU		DMTU		TMTU	
Conc., M	k_{obs} (s^{-1})	Conc., M	k_{obs} (s^{-1})	Conc., M	k_{obs} (s^{-1})
0.016125	0.53421	0.016125	0.40385	0.016125	0.18325
0.012900	0.42926	0.012900	0.32699	0.012900	0.14884
0.009675	0.32268	0.009675	0.23933	0.009675	0.11175
0.006450	0.21844	0.006450	0.16504	0.006450	0.07404
0.003225	0.11941	0.003225	0.07383	0.003225	0.03665

Table S3.4: Average observed rate constants, k_{obs}, s^{-1}, for the displacement of the aqua ligands in Pt3 with the nucleophiles, at pH = 2.0, *T* = 298 *K*, *I* = 0.1 M $NaClO_4$.

TU		DMTU		TMTU	
Conc., M	k_{obs} (s^{-1})	Conc., M	k_{obs} (s^{-1})	Conc., M	k_{obs} (s^{-1})
0.06554	0.00547	0.03277	0.00037249	0.03277	0.00043881
0.05243	0.00438	0.02622	0.00027446	0.02622	0.00034446
0.03932	0.00329	0.01966	0.00017524	0.01966	0.00026116
0.02622	0.00221	0.01311	0.000074805	0.01311	0.00017935
0.01311	0.00172	0.00655	-	0.00655	-

Table S3.5: Average observed rate constants, k_{obs}, s^{-1}, for the displacement of the aqua ligands in Pt4 with the nucleophiles, at pH = 2.0, *T* = 298 *K*, *I* = 0.1 M $NaClO_4$.

TU		DMTU		TMTU	
Conc., M	k_{obs} (s^{-1})	Conc., M	k_{obs} (s^{-1})	Conc., M	k_{obs} (s^{-1})
0.06554	0.00686	0.03277	0.00692	0.03277	0.00119
0.05899	0.00604	0.02622	0.00571	0.02622	0.00101
0.05243	0.00487	0.01966	0.00422	0.01966	0.0008433
0.04588	0.00389	0.01311	0.00276	0.01311	0.0006780
0.03932	0.00283	0.00655	0.0017	0.00655	-

Table S3.6: Average observed rate constants, $k_{obs,}$ s^{-1}, for the displacement of the aqua ligands in Pt5 with the nucleophiles, at pH = 2.0, *T* = 298 *K*, *I* = 0.1 M $NaClO_4$.

TU		DMTU	
Conc., M	k_{obs} (s^{-1})	Conc., M	k_{obs} (s^{-1})
0.06554	0.00208	0.03277	0.000312098
0.05899	0.00169	0.02622	0.00021890
0.05243	0.00116	0.01966	0.000125087
0.04588	0.000770	0.01311	0.0000524387
0.03932	0.000388	0.00655	-

Table S3.7: Temperature dependence of $k_2/M^{-1}s^{-1}$, for the displacement of the aqua ligands in Pt1 by the nucleophiles at 60-fold at pH = 2.0, *I* = 0.1 M $NaClO_4$

TU		DMTU		TMTU	
1/T (K^{-1})	**ln(k_2/T)**	**1/T (K^{-1})**	**ln(k_2/T)**	**1/T (K^{-1})**	**ln(k_2/T)**
0.00325	-6.52595	0.00325	-6.46389	0.00325	-7.37407
0.00330	-6.76178	0.00330	-6.60769	0.00330	-7.65613
0.00336	-6.98913	0.00336	-6.82303	0.00336	-7.99708
0.00341	-7.21908	0.00341	-7.10967	0.00341	-8.25904
0.00347	-7.44286	0.00347	-7.33615	0.00347	-8.57767

Table S3.8: Temperature dependence of $k_2/M^{-1}s^{-1}$, for the displacement of the aqua ligands in Pt2 by the nucleophiles at 60-fold at pH = 2.0, *I* = 0.1 M $NaClO_4$

TU		DMTU		TMTU	
1/T (K^{-1})	**ln(k_2/T)**	**1/T (K^{-1})**	**ln(k_2/T)**	**1/T (K^{-1})**	**ln(k_2/T)**
0.00325	-6.35449	0.00325	-6.67358	0.00325	-7.37117
0.00330	-6.5635	0.00330	-6.9020	0.00330	-7.61058
0.00336	-6.82819	0.00336	-7.12701	0.00336	-7.88858
0.00341	-7.10562	0.00341	-7.39446	0.00341	-8.21252
0.00347	-7.43243	0.00347	-7.79678	0.00347	-8.45753

Table S3.9: Temperature dependence of k_2/$M^{-1}s^{-1}$, for the displacement of the aqua ligands in Pt3 by the nucleophiles at 120-fold at pH = 2.0, *I* = 0.1 M $NaClO_4$

TU		DMTU		TMTU	
1/T (K^{-1})	ln(k_2/T)	1/T (K^{-1})	ln(k_2/T)	1/T (K^{-1})	ln(k_2/T)
0.00319	-10.48580	0.00319	-13.82076	0.00319	-13.19318
0.00325	-10.66789	0.00325	-14.00274	0.00325	-13.42711
0.0033	-10.84185	0.00330	-14.15325	0.00330	-13.67822
0.00336	-11.03832	0.00336	-14.34648	0.00336	-13.94746
0.00341	-11.25652	0.00341	-14.51345	0.00341	-14.21231

Table S3.10: Temperature dependence of k_2/$M^{-1}s^{-1}$, for the displacement of the aqua ligands in Pt4 by the nucleophiles at 120-fold at pH = 2.0, *I* = 0.1 M $NaClO_4$

TU		DMTU		TMTU	
1/T (K^{-1})	ln(k_2/T)	1/T (K^{-1})	ln(k_2/T)	1/T (K^{-1})	ln(k_2/T)
0.00319	-10.67890	0.00319	-10.65415	0.00319	-12.12458
0.00325	-10.81009	0.00325	-10.79645	0.00325	-12.34087
0.00330	-10.93324	0.00330	-10.99439	0.00330	-12.54795
0.00336	-11.05304	0.00336	-11.16501	0.00336	-12.77525
0.00341	-11.18281	0.00341	-11.34947	0.00341	-13.00655

Table S3.11: Temperature dependence of k_2/$M^{-1}s^{-1}$, for the displacement of the aqua ligands in Pt5 by the nucleophiles at 120-fold at pH = 2.0, *I* = 0.1 M $NaClO_4$

TU		DMTU	
1/T (K^{-1})	ln(k_2/T)	1/T (K^{-1})	ln(k_2/T)
0.00319	-11.87870	0.00319	-13.91809
0.00325	-12.06123	0.00325	-14.17822
0.00330	-12.25211	0.00330	-14.40920
0.00336	-12.45643	0.00336	-14.68359
0.00341	-11.73708	0.00341	-14.93611

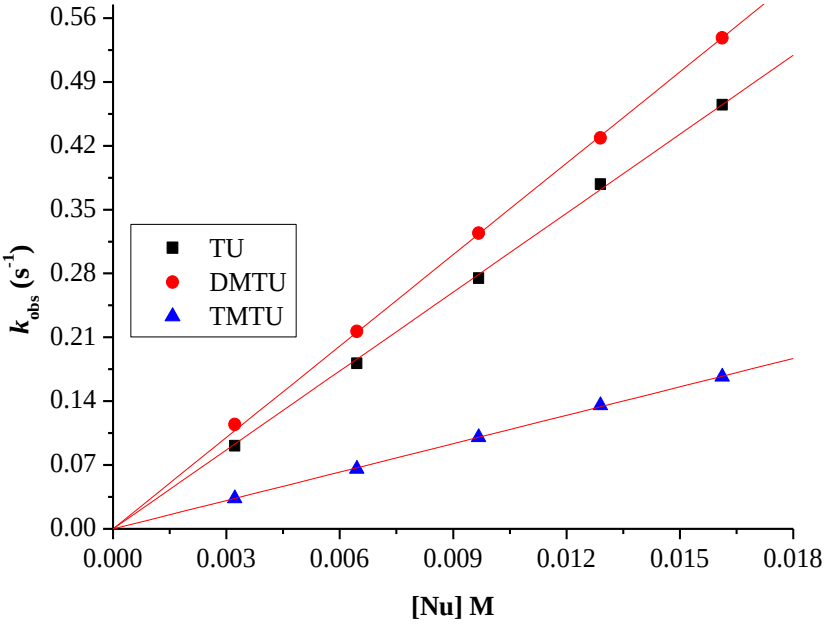

Figure S3.1: Dependence of the *pseudo* first-order rate constants (k_{obs}) on the concentrations of the nucleophiles for the aqua substitution for Pt1 in $NaClO_4$ (I = 0.1 M) at 298 K.

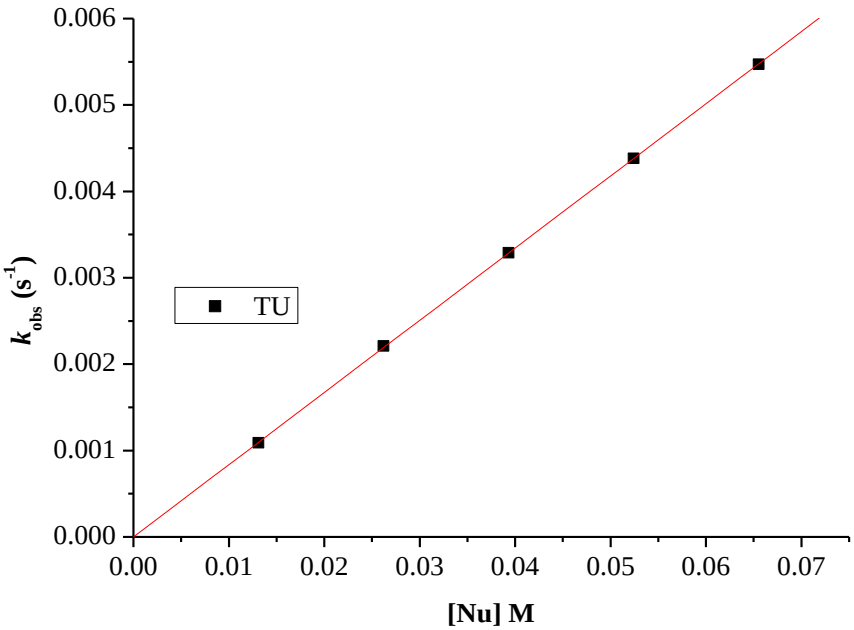

Figure S3.2: Dependence of the *pseudo* first-order rate constants (k_{obs}) on the concentrations of the nucleophiles for the aqua substitution of Pt3 in $NaClO_4$ (I = 0.1 M) at 298 K.

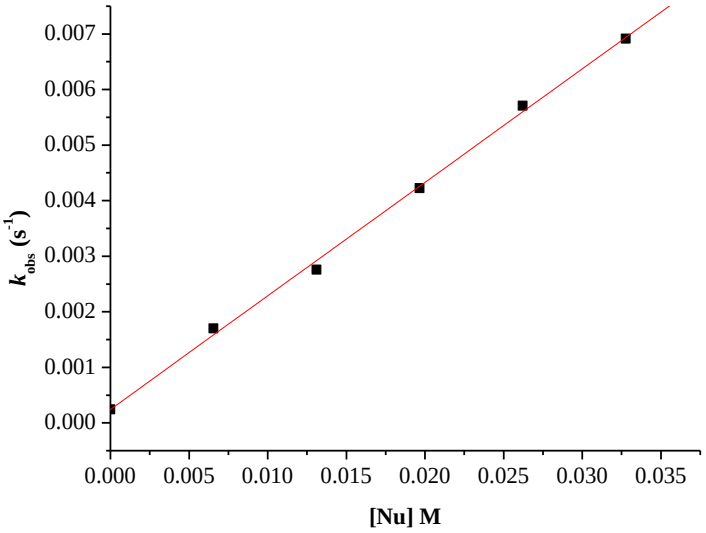

Figure S3.3: Dependence of the *pseudo* first-order rate constants (k_{obs}) on the concentrations of the DMTU for the aqua substitution for Pt3 in $NaClO_4$ (I = 0.1 M) at 298 K.

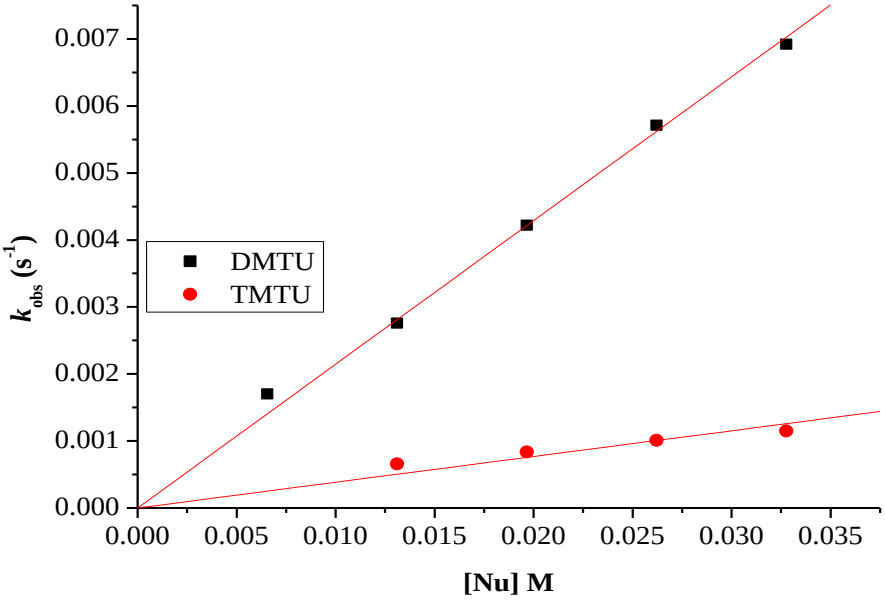

Figure S3.4: Dependence of the *pseudo* first-order rate constants (k_{obs}) on the concentrations of DMTU and TMTU for the aqua substitution of Pt4 in $NaClO_4$ (I = 0.1 M) at 298 K.

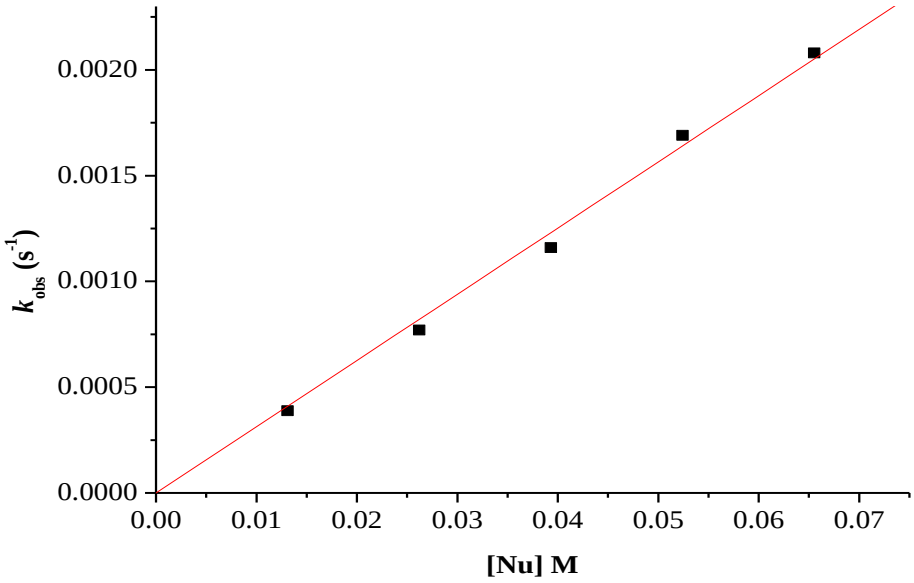

Figure S3.5: Dependence of the *pseudo* first-order rate constants (k_{obs}) on the concentrations of TU for the aqua substitution for Pt5 in $NaClO_4$ (I = 0.1 M) at 298 K.

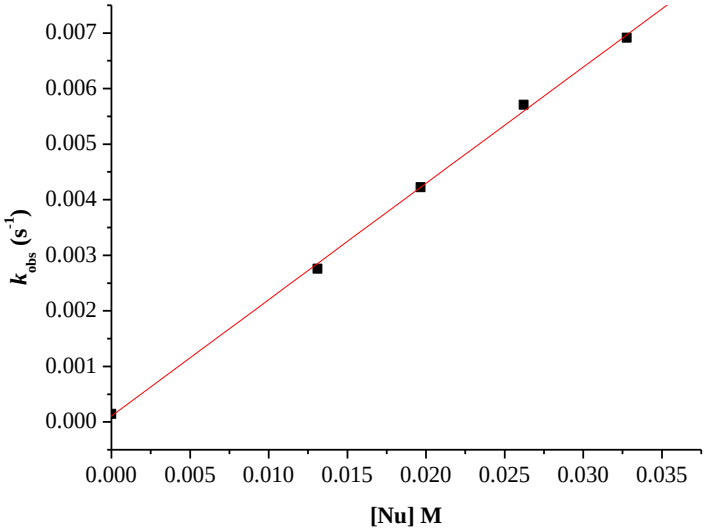

Figure S3.6: Dependence of the *pseudo* first-order rate constant (k_{obs}) on the concentrations of DMTU for the aqua substitution of Pt5 in $NaClO_4$ (I = 0.1 M) at 298 K.

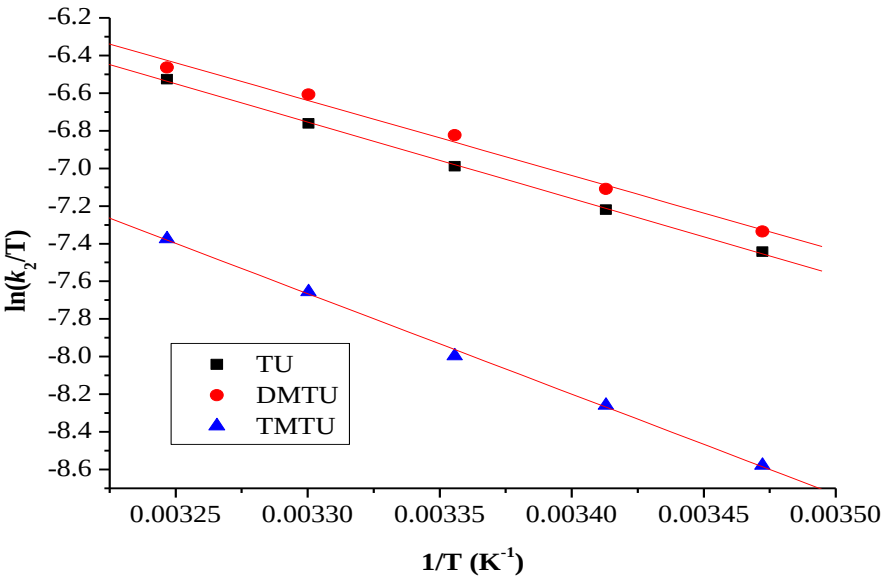

Figure S3.7: Eyring plots obtained for Pt1 with the nucleophiles for the substitution reactions over the temperature range 288 – 308 K in $NaClO_4$ (*I* = 0.1 M).

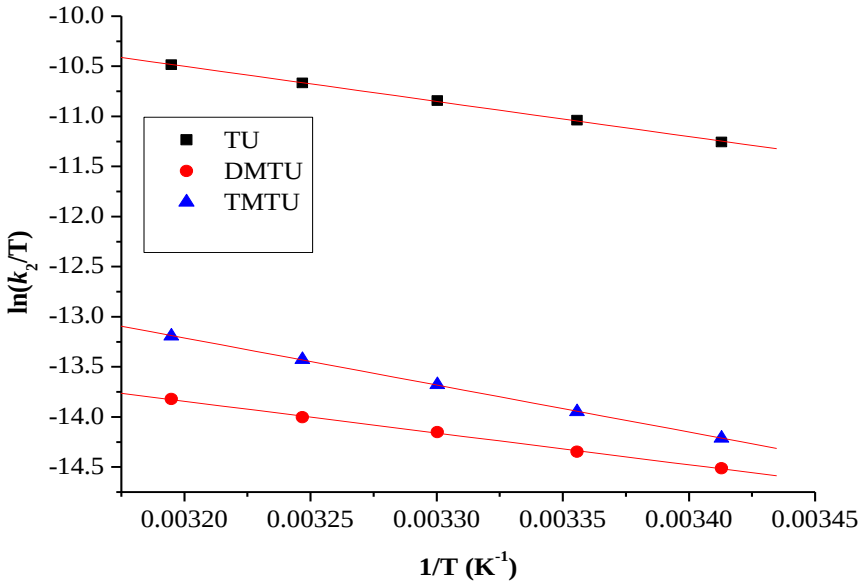

Figure S3.8: Eyring plots obtained for Pt3 with the nucleophiles for the substitution reactions over the temperature range 288 – 308 *K* in $NaClO_4$ (*I* = 0.1 M).

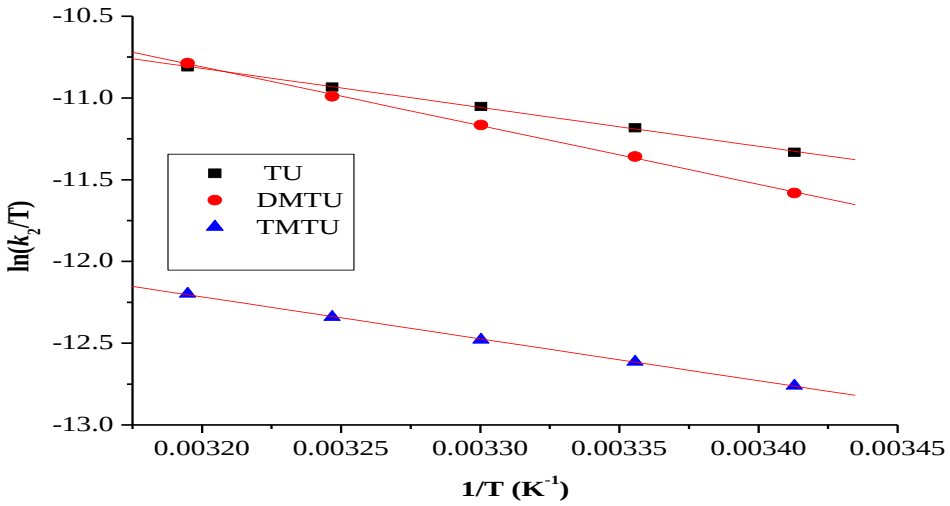

Figure S3.9: Eyring plots obtained for Pt4 with the nucleophiles for the substitution reactions over the temperature range 288 – 308 *K* in $NaClO_4$ (*I* = 0.1 M).

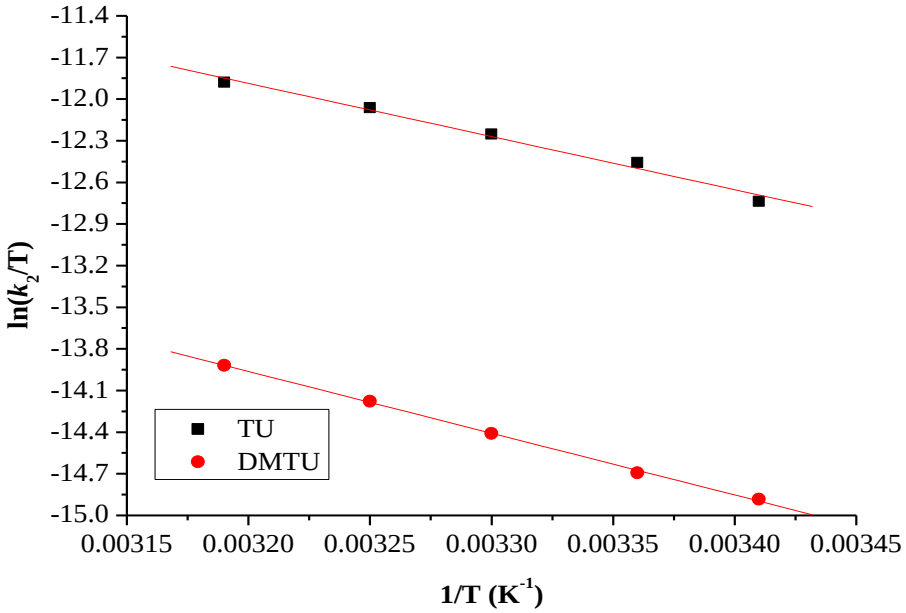

Figure S3.10: Eyring plots obtained for Pt5 with the nucleophiles for the substitution reactions over the temperature range 288 – 308 *K* in $NaClO_4$ (*I* = 0.1 M).

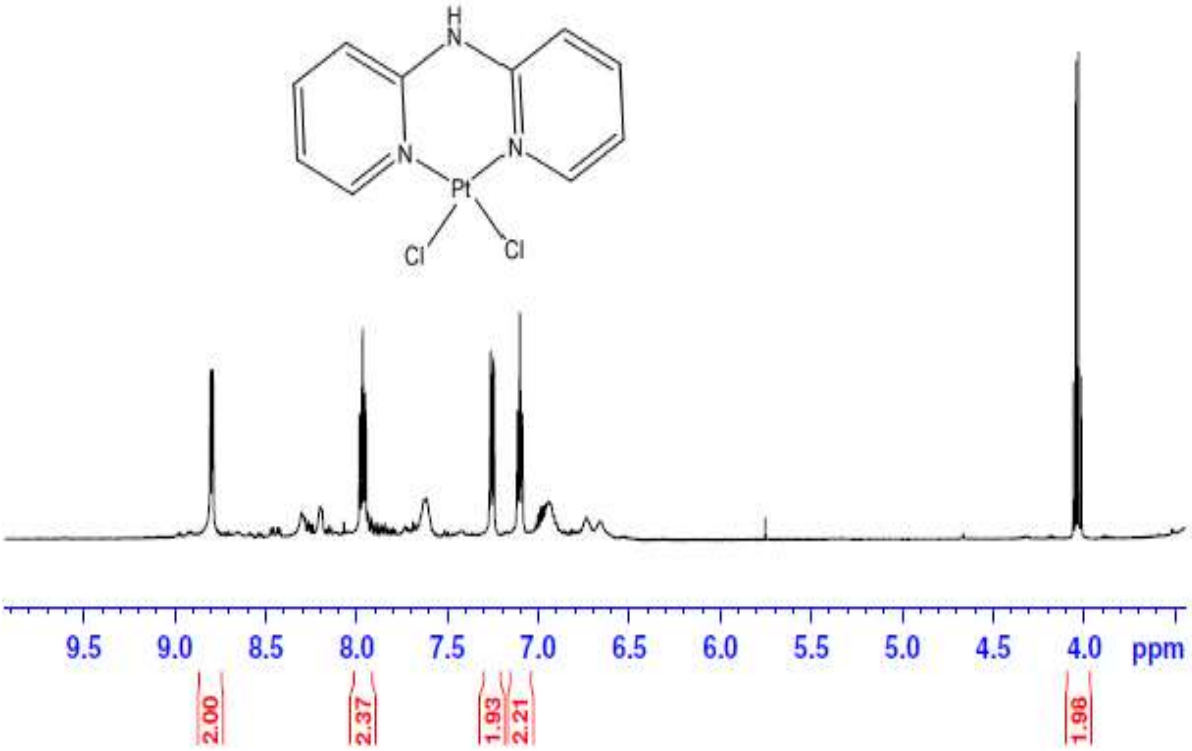

Figure S3.11: **^{1}H NMR spectrum of di-2-pyridylaminodichloroplatinum(II) (Pt1) in DMSO-d_6.**

Elemental Composition Report Page 1

Single Mass Analysis
Tolerance = 5.0 PPM / DBE: min = -1.5, max = 50.0
Element prediction: Off
Number of isotope peaks used for i-FIT = 3

Monoisotopic Mass, Odd and Even Electron Ions
31 formula(e) evaluated with 1 results within limits (all results (up to 1000) for each mass)
Elements Used:
C: 10-15 H: 5-15 N: 0-5 Cl: 0-2 Pt: 0-1

Asman Panyako
CL10 2 (0.017) Cm (1:31)

TOF MS ES-
5.22e+003

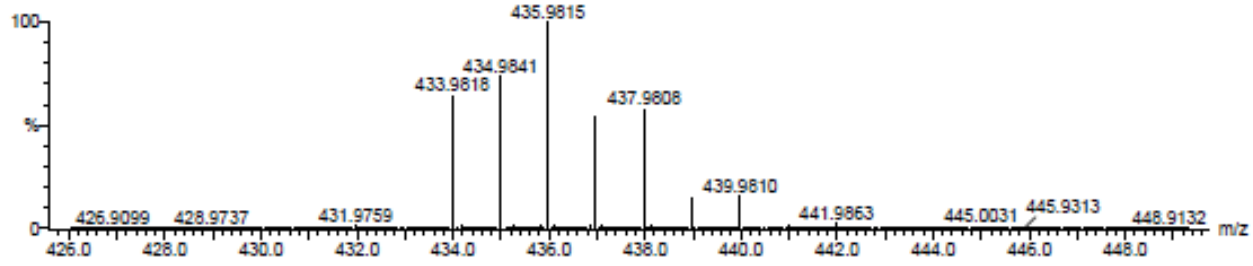

Minimum:				-1.5			
Maximum:		5.0	5.0	50.0			
Mass	Calc. Mass	mDa	PPM	DBE	i-FIT	i-FIT (Norm)	Formula
435.9815	435.9821	-0.6	-1.4	8.0	379.0	0.0	C10 H9 N3 Cl2 Pt

Figure S3.12: **TOF ESI mass spectrum for Pt1**

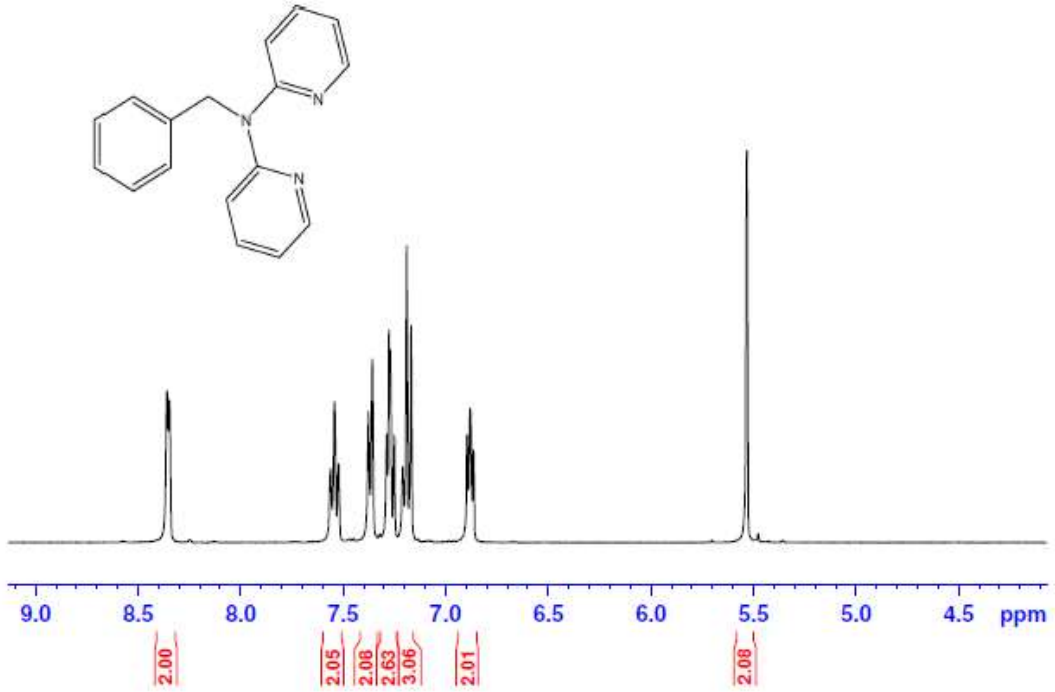

Figure S3.13: **^{1}H NMR spectrum of di-2-pyridylaminomethylbenzene in$CDCl_3$**

Elemental Composition Report Page 1

Single Mass Analysis
Tolerance = 50.0 PPM / DBE: min = -1.5, max = 50.0
Element prediction: Off
Number of isotope peaks used for i-FIT = 3

Monoisotopic Mass, Even Electron Ions
3 formula(e) evaluated with 1 results within limits (all results (up to 1000) for each mass)
Elements Used:
C: 15-20 H: 15-20 N: 0-5
Asman Panyako
L1 14 (0.222) Cm (1:30)

TOF MS ES+
1.68e+004

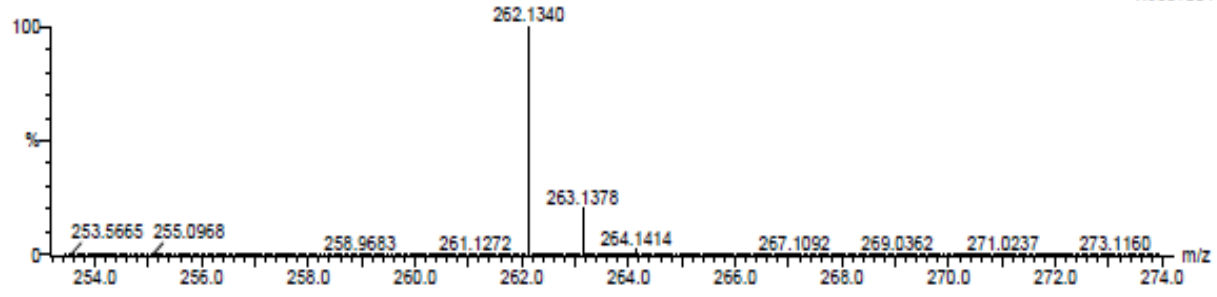

Minimum:				-1.5			
Maximum:		5.0	50.0	50.0			
Mass	Calc. Mass	mDa	PPM	DBE	i-FIT	i-FIT (Norm)	Formula
262.1340	262.1344	-0.4	-1.5	11.5	380.7	0.0	C17 H16 N3

Figure S3.14: **TOF ESI mass spectrum of di-2-pyridylaminomethylbenzene**

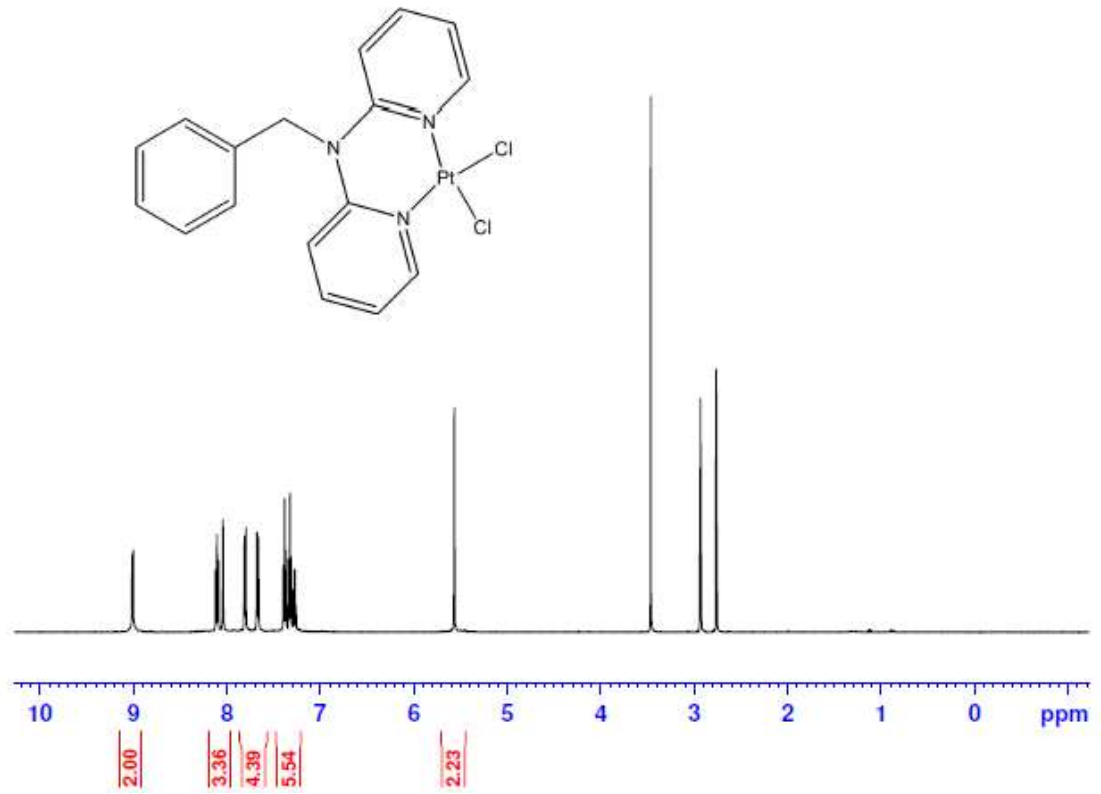

Figure S3.15: **^{1}H NMR spectrum of Pt2 in DMF-d_7.**

Elemental Composition Report **Page 1**

Single Mass Analysis
Tolerance = 5.0 PPM / DBE: min = -1.5, max = 50.0
Element prediction: Off
Number of isotope peaks used for i-FIT = 3

Monoisotopic Mass, Odd and Even Electron Ions
25 formula(e) evaluated with 1 results within limits (all results (up to 1000) for each mass)
Elements Used:
C: 15-20 H: 15-20 N: 0-5 Na: 1-1 Cl: 0-2 Pt: 0-1

Asman Panyako
CL1 26 (0.444) Cm (1:29)

TOF MS ES+
4.56e+003

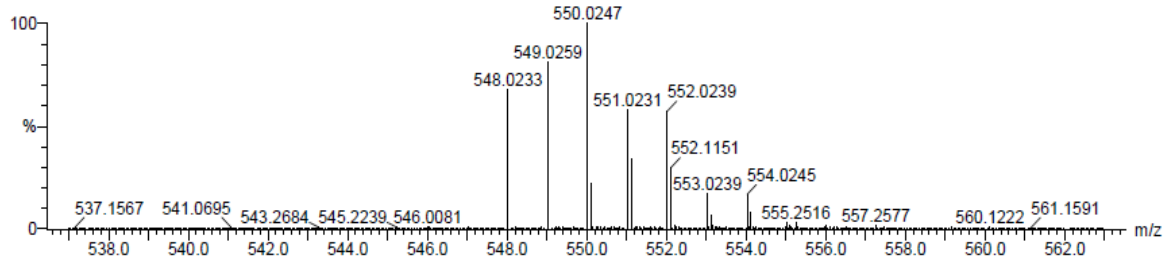

Minimum:				-1.5			
Maximum:		5.0	5.0	50.0			
Mass	Calc. Mass	mDa	PPM	DBE	i-FIT	i-FIT (Norm)	Formula
550.0247	550.0267	-2.0	-3.6	11.0	376.5	0.0	C17 H16 N3 Na Cl2 Pt

Figure S3.16: **TOF ESI mass spectrum of Pt2**

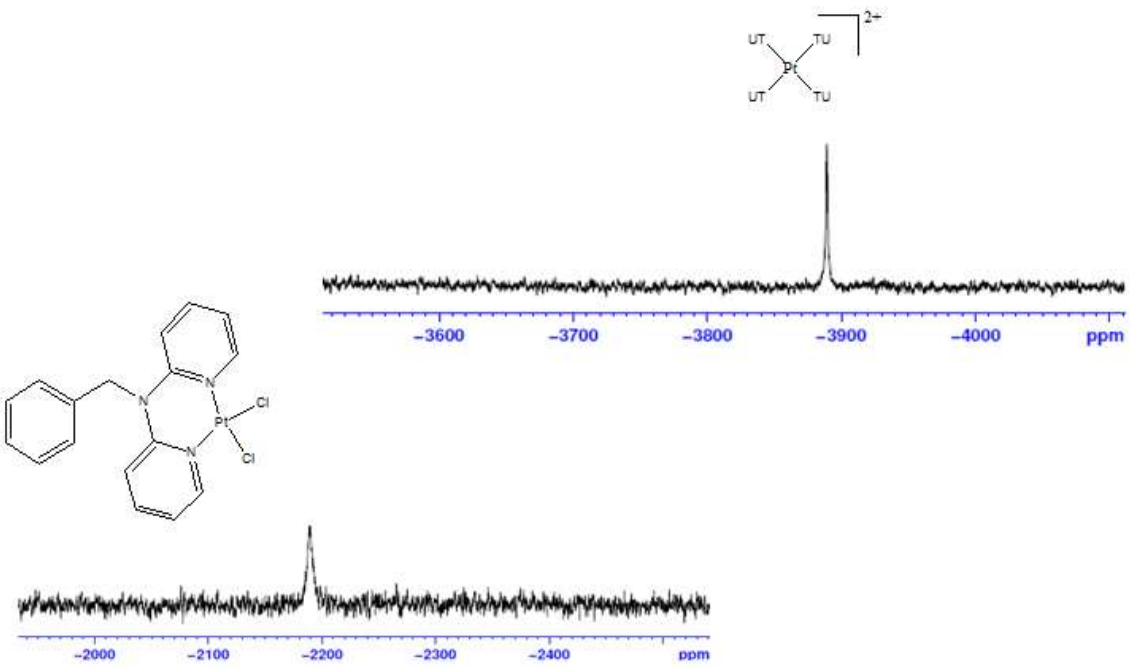

Figure S3.17: **^{195}Pt' NMR spectrum of Pt2 in DMSO-d_6 showing the shifting of the peak from -2189.2 ppm to -3889.2 ppm indicating dechelation process**

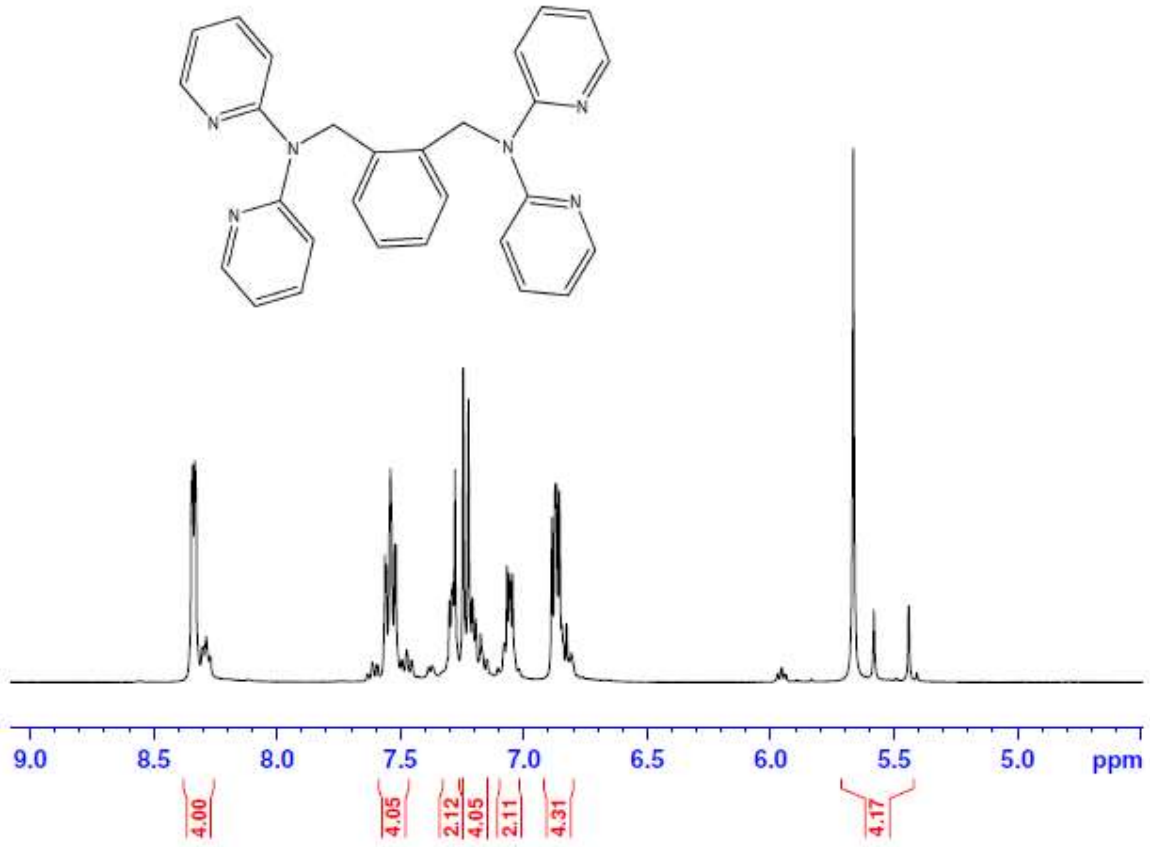

Figure S3.18: **^{1}H NMR spectrum of 1,2-bis(di-2-pyridylaminomethyl)benzene**

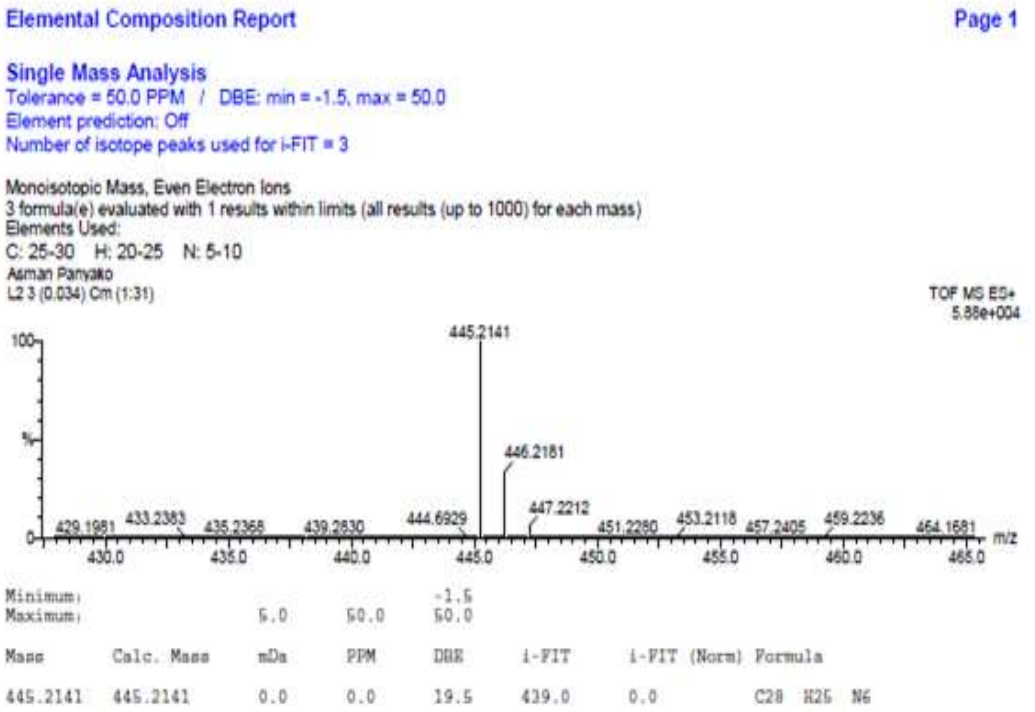

Figure S3.19: **TOF ESI mass spectrum of 1,2-bis(di-2-pyridylaminomethyl)benzene**

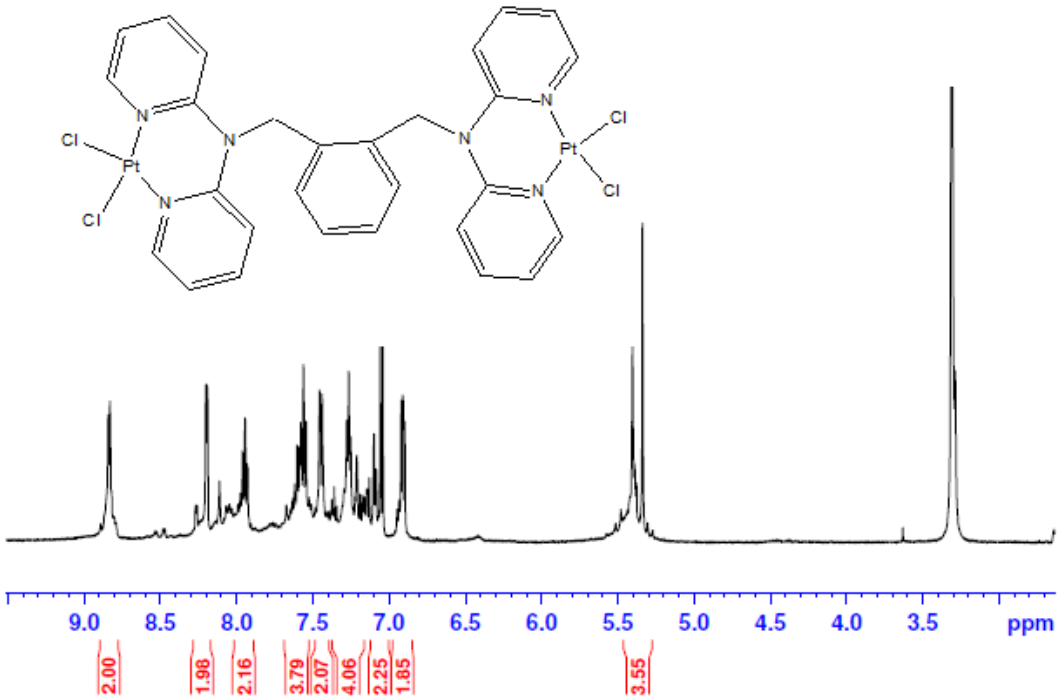

Figure S3.20: **^{1}H NMR spectrum of Pt3**

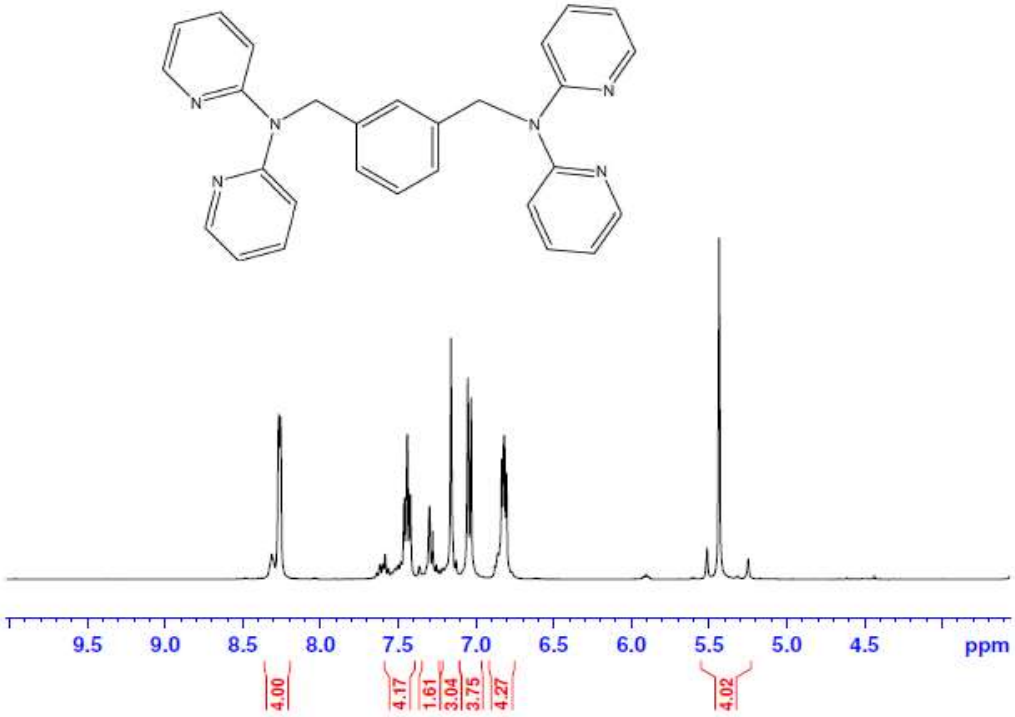

Figure S3.21: **^{1}H NMR spectrum of 1,3-bis(di-2-pyridylaminomethyl)benzene**

Elemental Composition Report Page 1

Single Mass Analysis
Tolerance = 50.0 PPM / DBE: min = -1.5, max = 50.0
Element prediction: Off
Number of isotope peaks used for i-FIT = 3

Monoisotopic Mass, Even Electron Ions
2 formula(e) evaluated with 1 results within limits (all results (up to 1000) for each mass)
Elements Used:
C: 25-30 H: 25-30 N: 5-10
Asman Panyako
L3 30 (0.495) Cm (1:30)

TOF MS ES+
5.53e+004

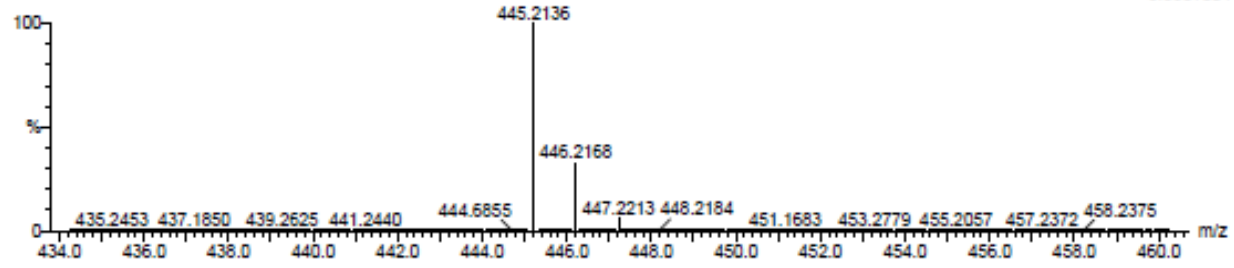

Minimum:				-1.5			
Maximum:		5.0	50.0	50.0			
Mass	Calc. Mass	mDa	PPM	DBE	i-FIT	i-FIT (Norm)	Formula
445.2136	445.2141	-0.5	-1.1	19.5	432.4	0.0	C28 H25 N6

Figure S3.22: **TOF ESI mass spectrum of 1,3-bis(di-2-pyridylaminomethyl)benzene**

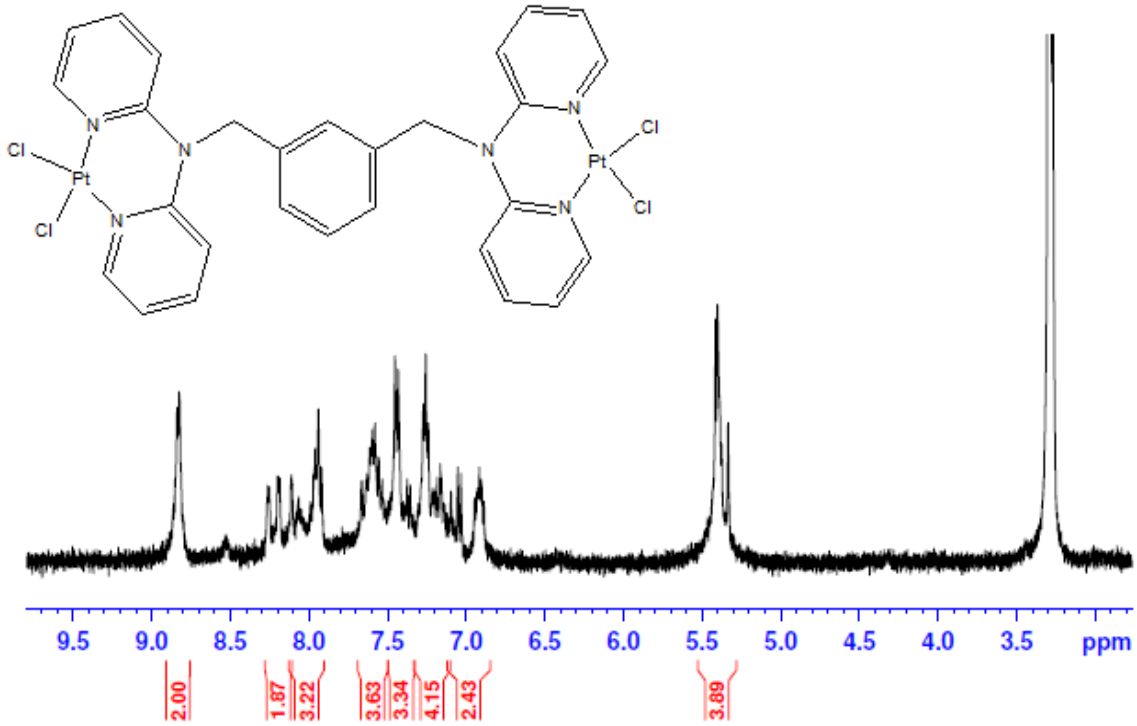

Figure S3.23: **^{1}H NMR spectrum of Pt4 in DMSO-d_6.**

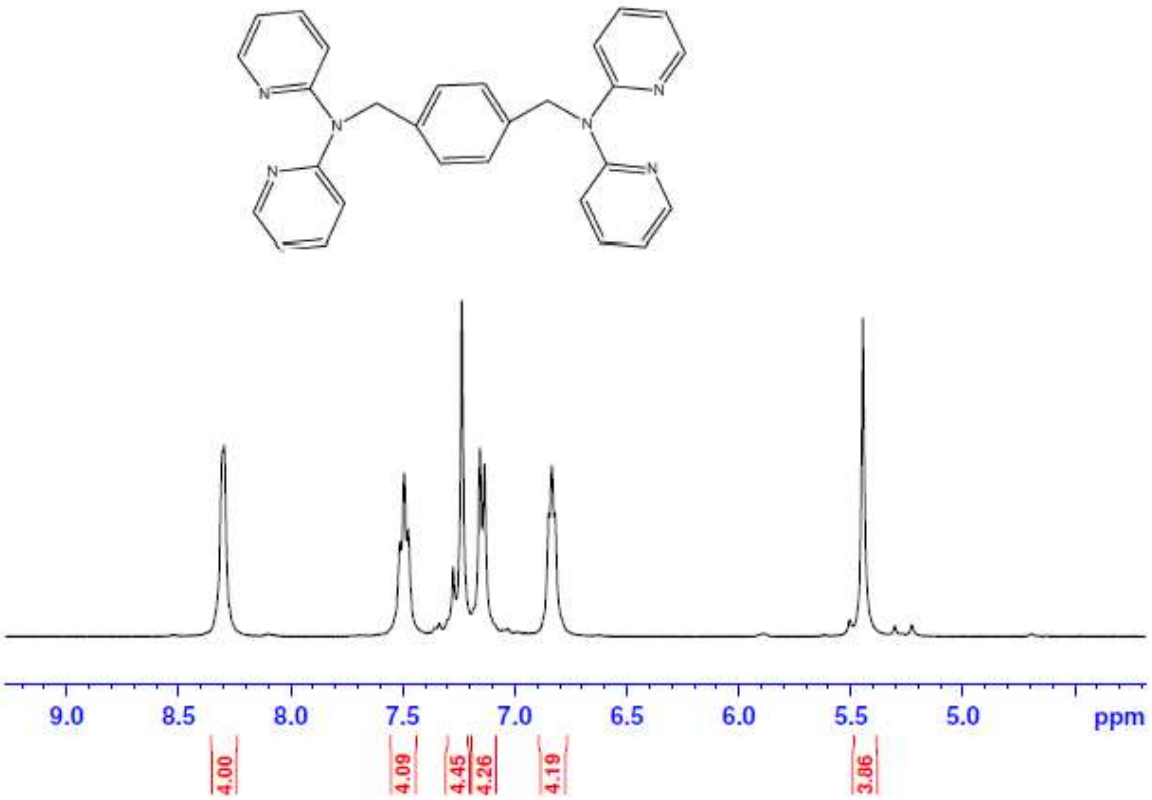

Figure S3.24: **^{1}H NMR spectrum of 1,4-bis(di-2-pyridylaminomethyl)benzene**

Elemental Composition Report Page 1

Single Mass Analysis
Tolerance = 5.0 PPM / DBE: min = -1.5, max = 50.0
Element prediction: Off
Number of isotope peaks used for i-FIT = 3

Monoisotopic Mass, Even Electron Ions
5 formula(e) evaluated with 1 results within limits (all results (up to 1000) for each mass)
Elements Used:
C: 25-30 H: 20-25 N: 5-10 Na: 0-1
Asman Panyako
L13 3 (0.034) Cm (1:31)

TOF MS ES+
2.93e+004

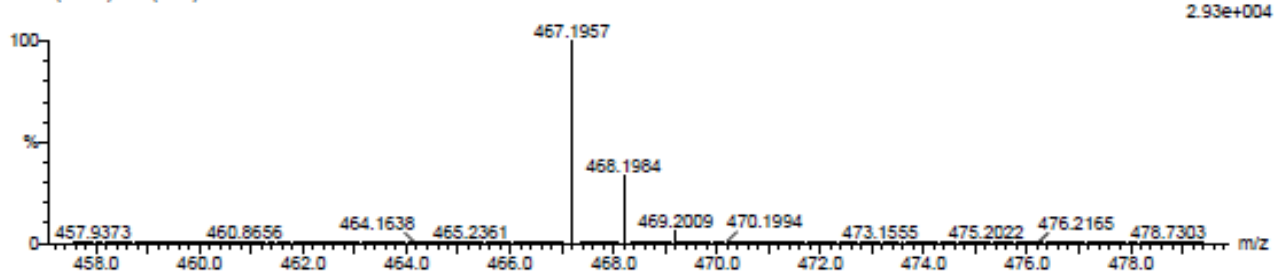

Minimum:				-1.5			
Maximum:		5.0	5.0	50.0			
Mass	Calc. Mass	mDa	PPM	DBE	i-FIT	i-FIT (Norm)	Formula
467.1957	467.1960	-0.3	-0.6	19.5	385.8	0.0	C28 H24 N6 Na

Figure S3.25: TOF ESI mass spectrum of 1,4-bis(di-2-pyridylaminomethyl)benzene

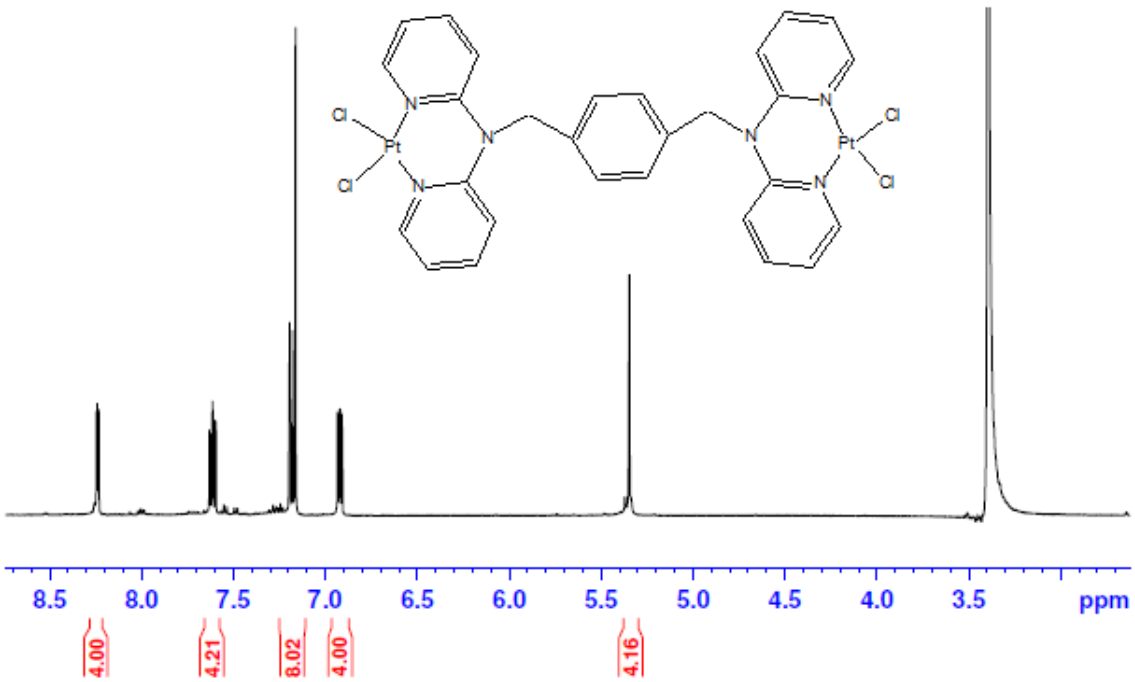

Figure S3.26: ^{1}H NMR spectrum of Pt5 in DMSO-d_6.

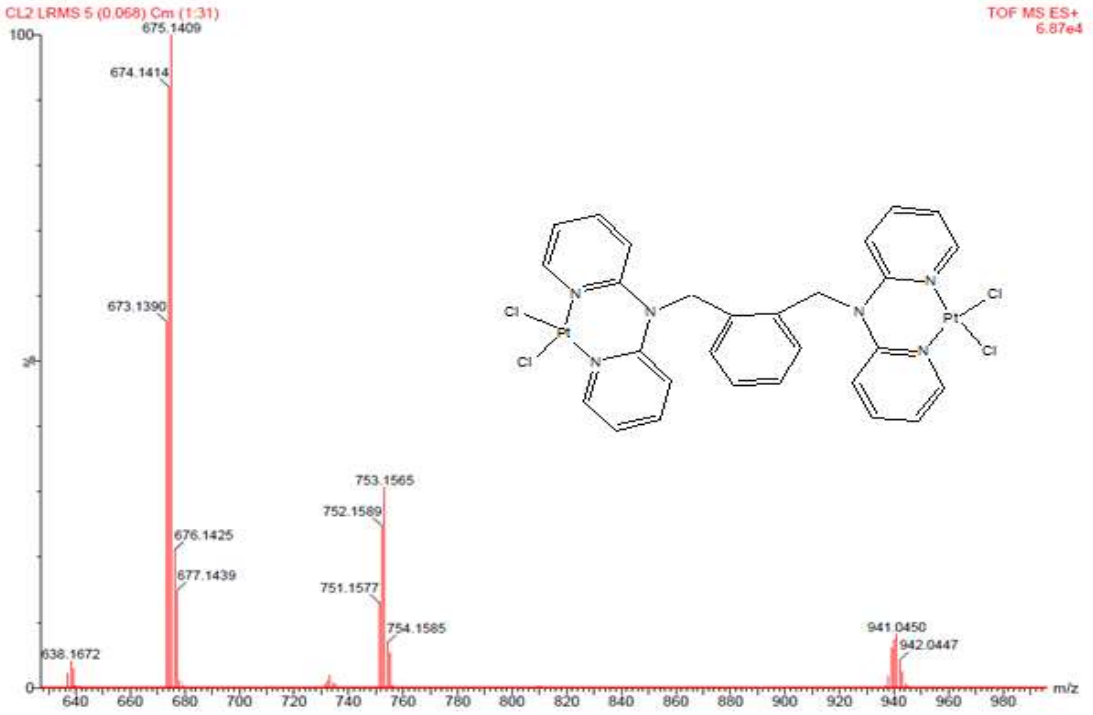

Figure S3.27: TOF ESI mass spectrum of Pt3

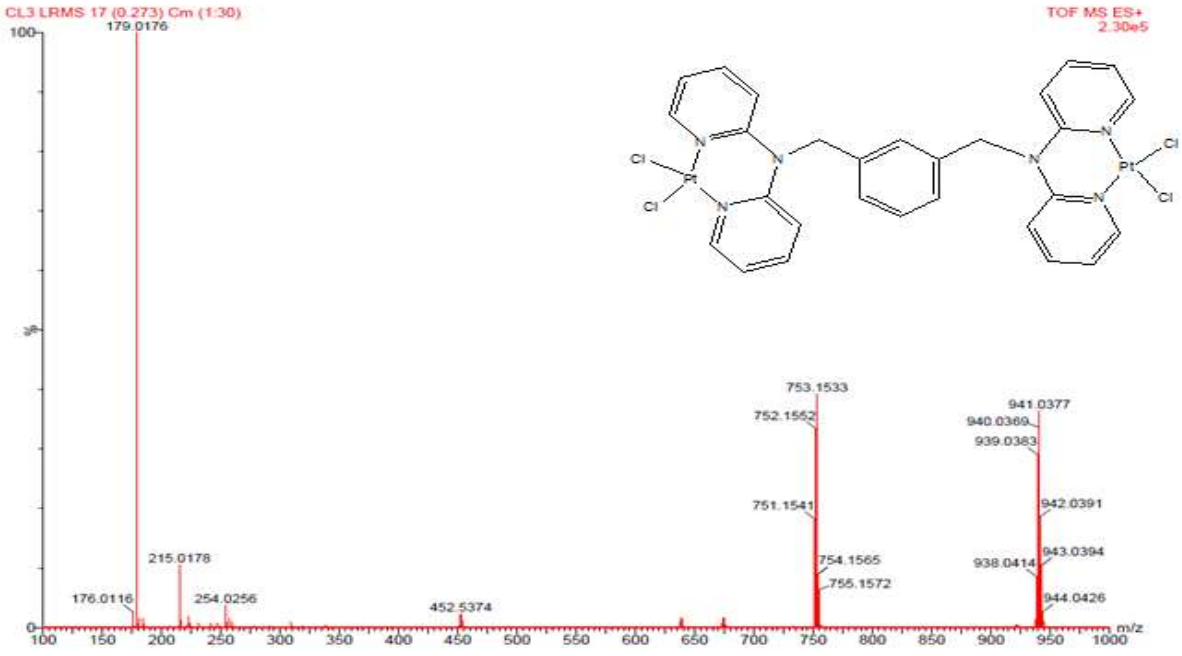

Figure S3.28: TOF ESI mass spectrum of Pt4

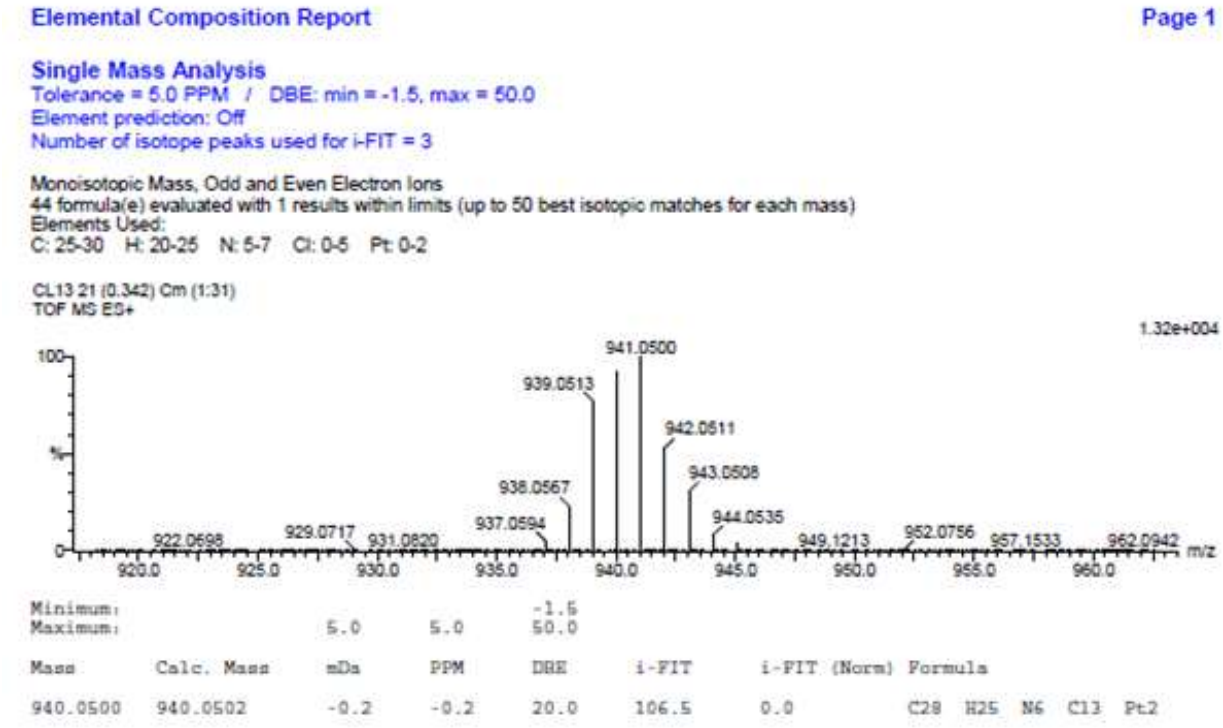

Elemental Composition Report Page 1

Single Mass Analysis
Tolerance = 5.0 PPM / DBE: min = -1.5, max = 50.0
Element prediction: Off
Number of isotope peaks used for i-FIT = 3

Monoisotopic Mass, Odd and Even Electron Ions
44 formula(e) evaluated with 1 results within limits (up to 50 best isotopic matches for each mass)
Elements Used:
C: 25-30 H: 20-25 N: 5-7 Cl: 0-5 Pt: 0-2

CL13 21 (0.342) Cm (1:31)
TOF MS ES+

1.32e+004

Minimum:				-1.5			
Maximum:		5.0	5.0	50.0			
Mass	Calc. Mass	mDa	PPM	DBE	i-FIT	i-FIT (Norm)	Formula
940.0500	940.0502	-0.2	-0.2	20.0	106.5	0.0	C28 H25 N6 Cl3 Pt2

Figure S3.29: TOF ESI mass spectrum of Pt5

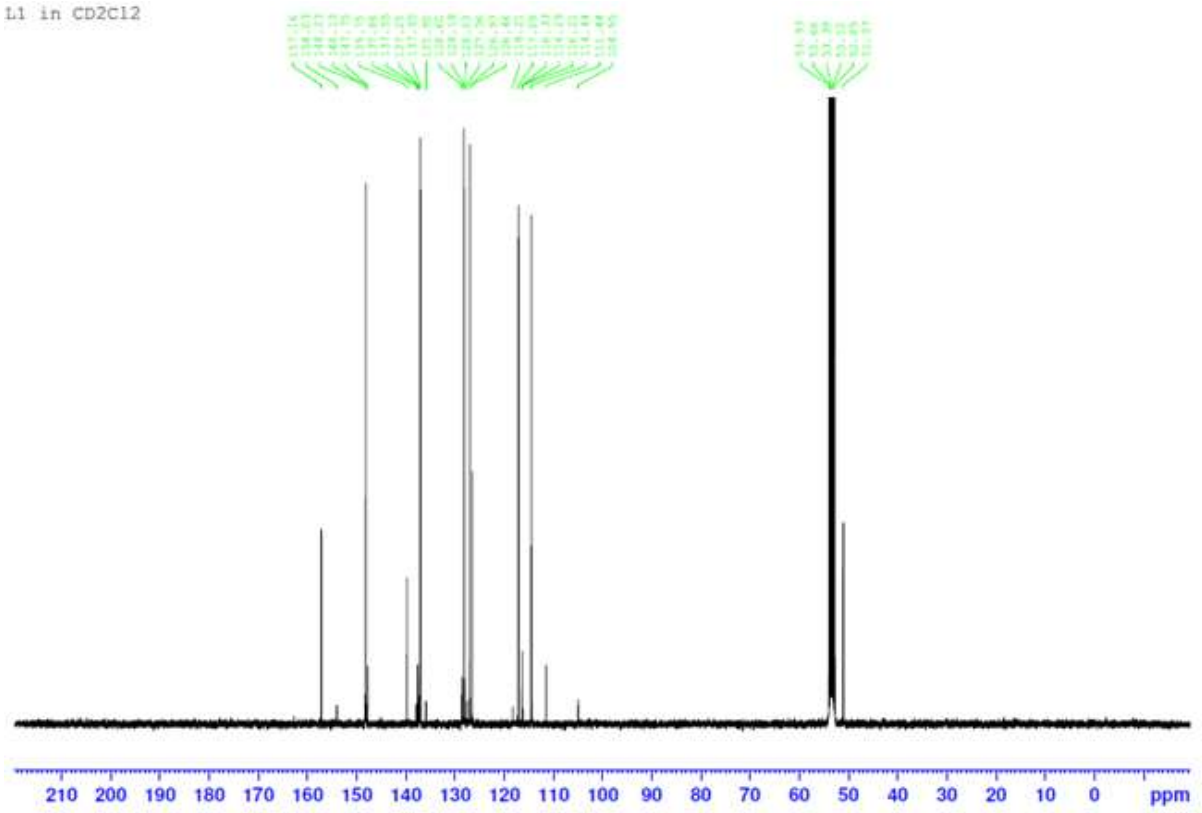

Figure S3.30: ^{13}C NMR spectrum of di-2-pyridylaminomethylbenzene in $CDCl_3$.

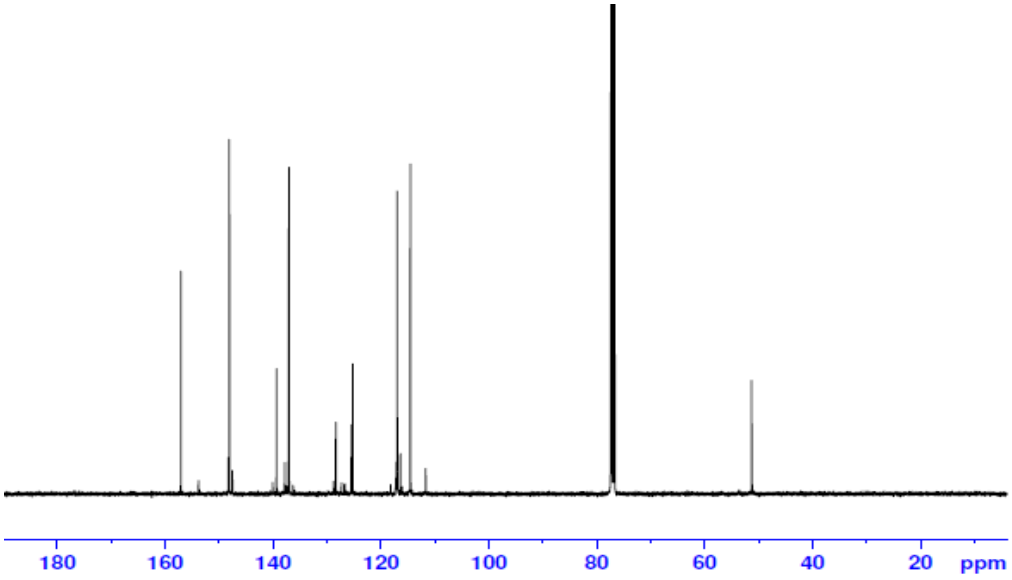

Figure S3.31: **^{13}C NMR spectrum of di-2-pyridylaminomethylbenzene in $CDCl_3$.**

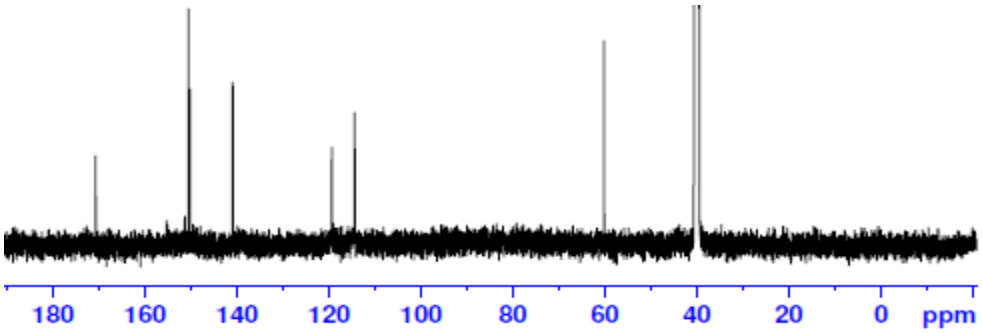

Figure S3.32: **^{13}C NMR spectrum of Pt1 in DMSO-d_6.**

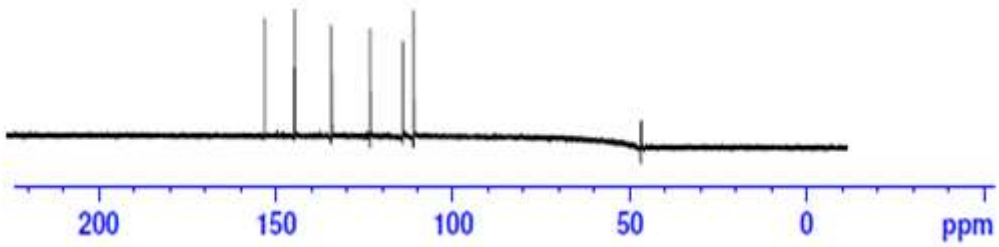

Figure S3.33: **^{13}C NMR spectrum of Pt5 in DMSO-d_6.**

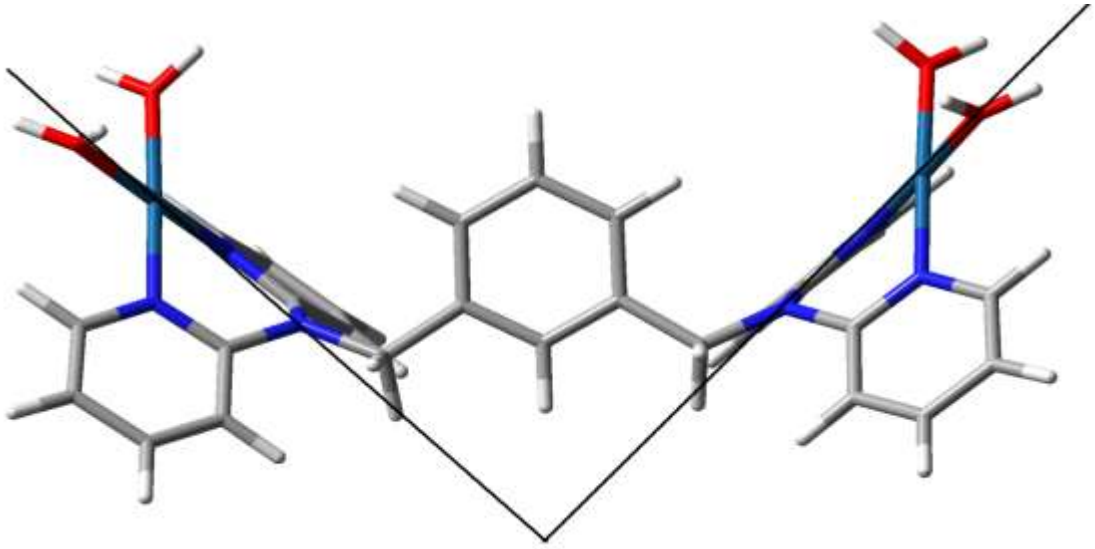

Figure S3.34: **Bowl shaped structure of complex Pt4; proposed for encapsulation of the nucleophiles causing acceleration in substitution kinetics of the complex**

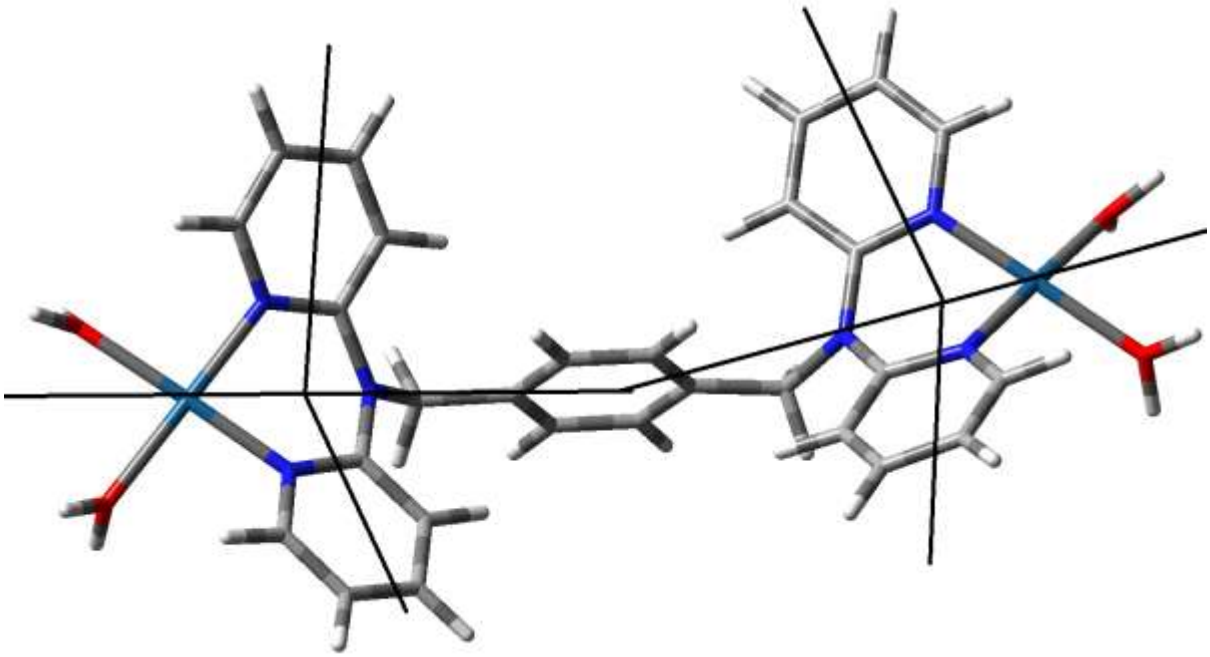

Figure S3.35: **Slip-up structure of complex Pt5; reducing the cavity for encapsulation of the entering nucleophiles retarding substitution kinetics of the complex**

Incorporating methylene spacers in *meta* positions forms cavitand bowl with enforced cavity than in *ortho* and *para* positions. These differences are also reflected in their reactivity.

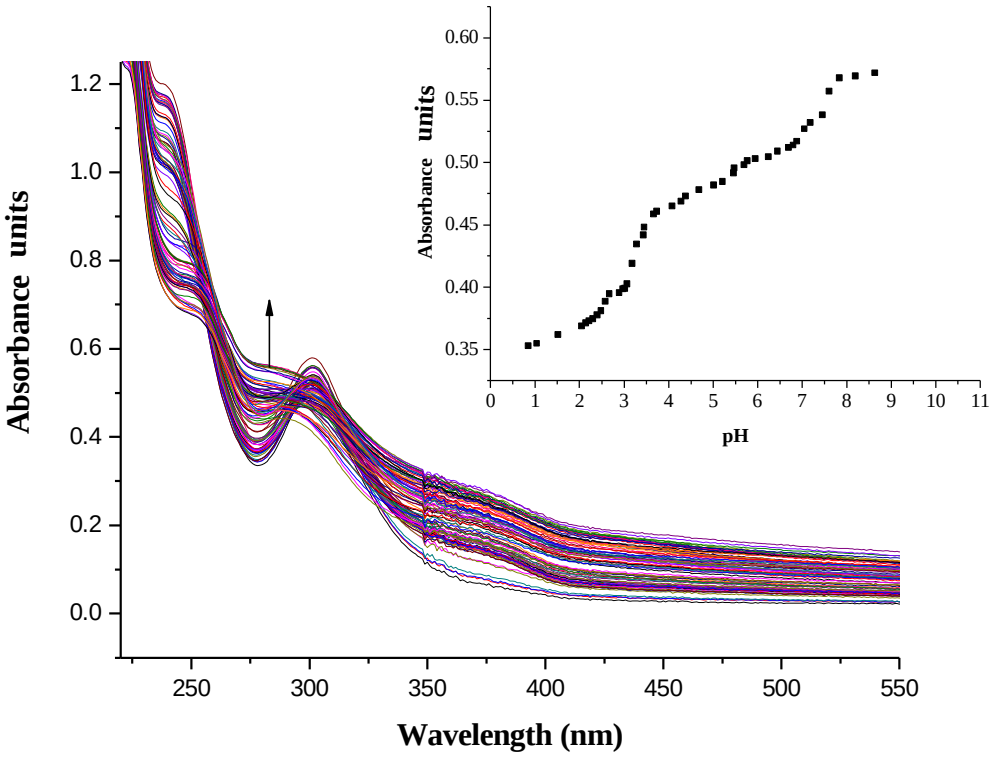

Figure S3.36*:* **UV-Vis spectra of 0.05 mM Pt3 complex recorded as a function of pH in the range of 2.0 - 8.0 at 25 °C, inset is a plot of absorbance versus pH at λ = 275 nm.**

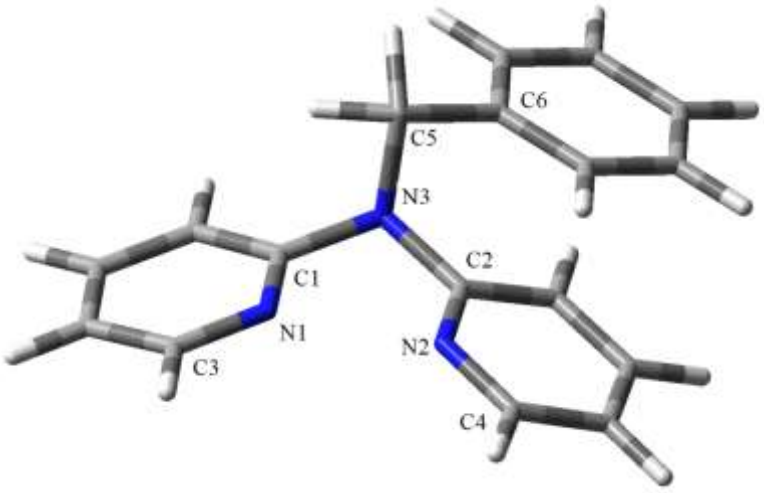

Figure S3.37: Structure of Di-2-pyridylaminomethylbenzene showing angle C1N3C2 to be 109° (*sp*^{3} hybridized)

Table S3.12: Selected bond lengths and angles of the ligand versus the complex (**Pt2**)

	Bond lengths and angle of the ligand (°/Å)	Bond lengths and angle of the complex (°/Å)
C1 – N3	1.4700	1.4112
C2 – N3	1.4700	1.4091
C1 – N1	1.3436	1.3737
C2 – N2	1.3436	1.3759
C4 – N2	1.3436	1.3749
C3 – N1	1.3436	1.3744
C5 – N3	1.4700	1.5128
C5 – C6	1.5400	1.5208
C1N3C2	109.47	120.30
C6C5N3	84.56	112.82

The variations in bond lengths and bond angles show that ligands perturb the electronic structures and electron transport properties of the metal frameworks.

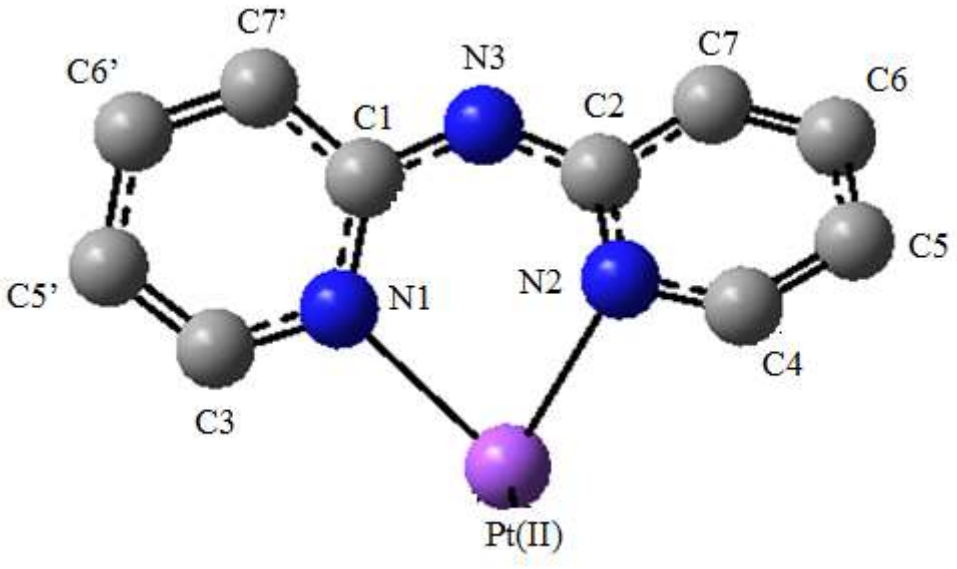

Figure S3.38: **Structure of dipyridylamine indicating angle C1N3C3 to be ≈ 120° (*sp*^{2}) hybridized) on coordination to the metal centre. As such the metal centre becomes stabilized through resonance.**

The atoms of N1, C1, N3, C2, N2 and Pt(II) are located in a conjugated six-membered ring. Due to conjugation, the electron density of Pt(II) is delocalized into the rings causing deshielding in case of alkyl spacers as bridging ligands.

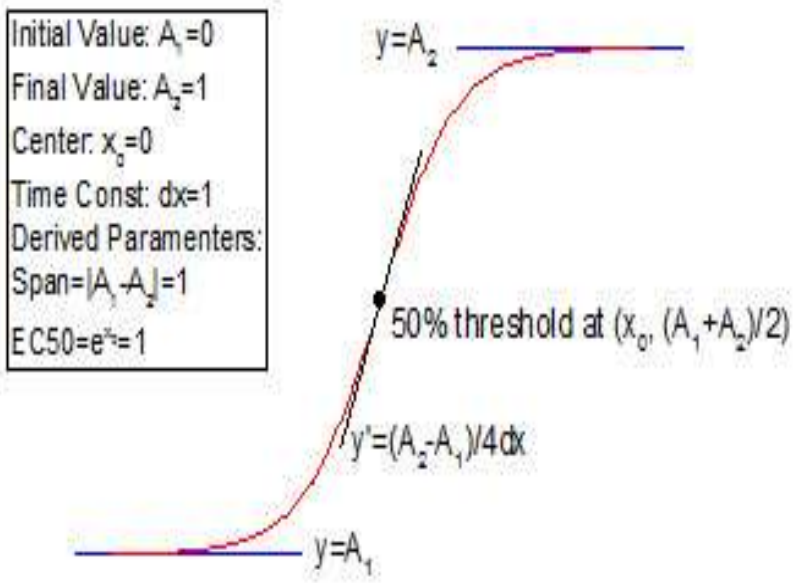

Figure S3.39: **Fitting Boltzmann Equation to a titration curve in determination of pK_a constants**

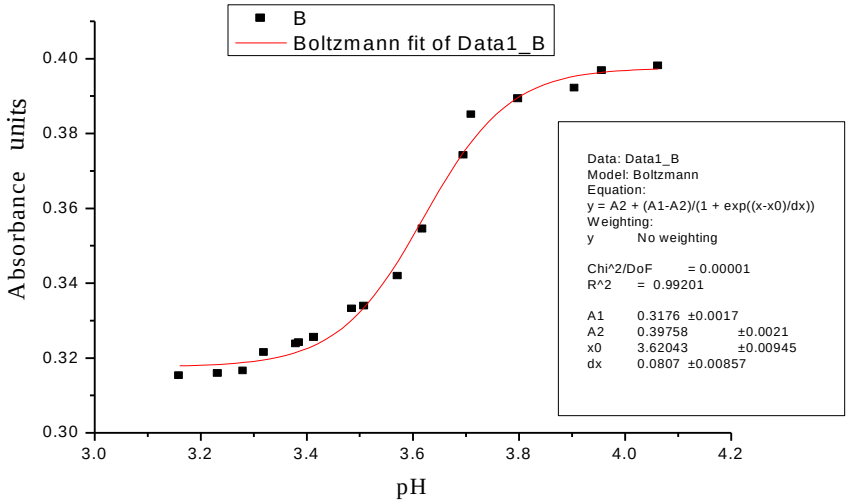

Figure S3.40: **Determination of Second dissociation constant (pK_{a2}) for Pt5 using Boltzmann equation from the sigmoid curve at the inflection point**

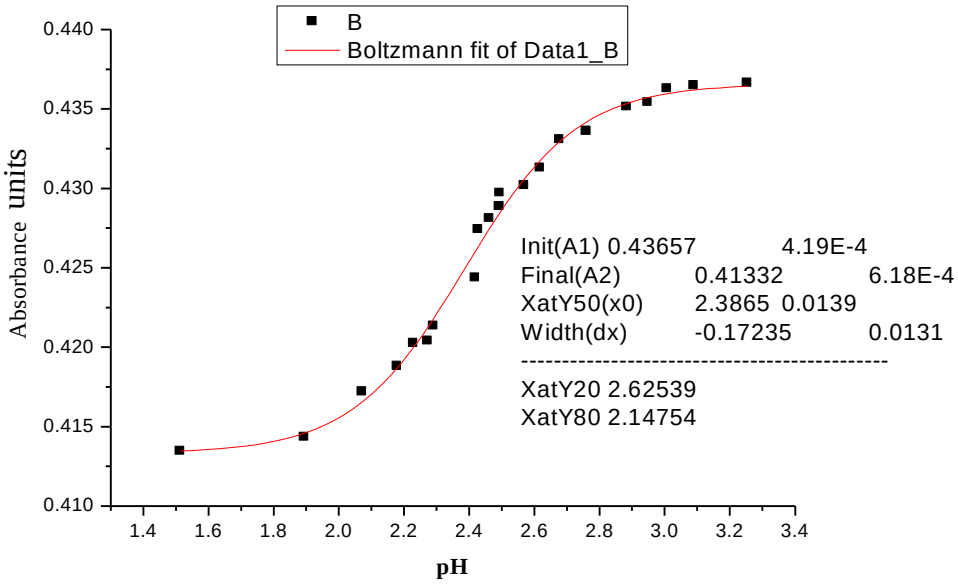

Figure S3.41: **Determination of first dissociation constant (pK_{a1}) for Pt4 using Boltzmann equation from the sigmoid curve at the inflection point**

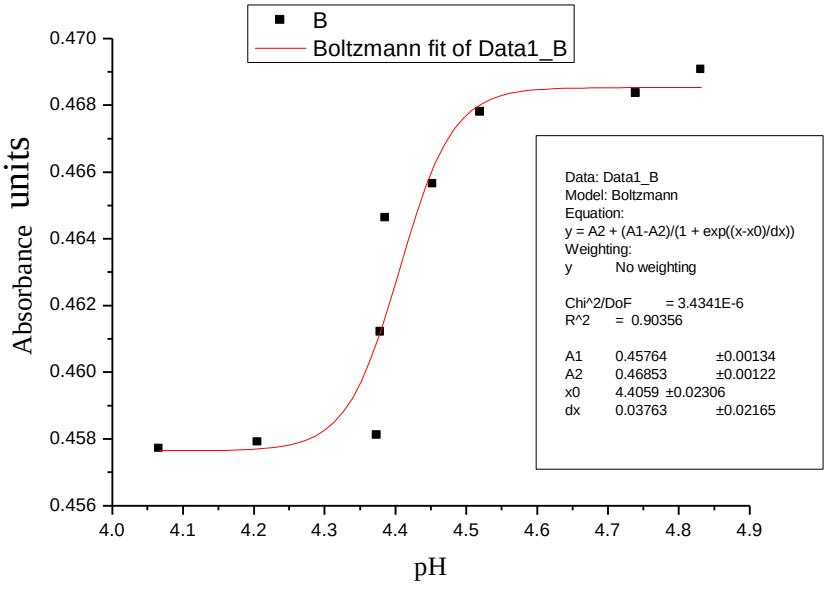

Figure S3.42: **Determination of Second dissociation constant (pK_{a2}) for Pt4 using Boltzmann equation from the sigmoid curve at the inflection point**

APPENDIX 2 (CHAPTER 4)

A summary of wavelengths used for kinetic measurements for the investigated complexes, some of their kinetic traces, k_{obs} for reactions at different concentrations and temperatures and characterization of complexes using ^{1}H NMR, TOF ES^{+} mass spectra, ^{13}C NMR and ^{195}Pt' NMR are given in the following tables.

Table S4.1: Summary of the wavelengths used for monitoring kinetic reactions

Complex	Nucleophile	Wavelength (λ) (nm) Stopped-flow	UV-Visible
PtL2	**TU**	300	320
	DMTU	303	320
	TMTU	363	335
PtL3	**TU**	298	320
	DMTU	300	320
	TMTU	362	335
PtL4	**TU**	290	320
	DMTU	292	320
	TMTU	355	335
PtL5	**TU**	305	320
	DMTU	305	320
	TMTU	363	335
PtL6	**TU**	302	320
	DMTU	305	320
	TMTU	363	335

Table S4.2: Average observed rate constants, $k_{obs(1)}$, s^{-1}, for the displacement of the aqua ligands in PtL2 with the nucleophiles, at pH = 2.0, *T* = 298 *K*, *I* = 0.1 M $NaClO_4$.

TU		**DMTU**		**TMTU**	
Conc., M	$k_{obs(1)}$ (s^{-1})	Conc., M	$k_{obs(1)}$ (s^{-1})	Conc., M	$k_{obs(1)}$ (s^{-1})
0.06767	2.51096	0.06767	2.22029	0.06767	0.91433
0.05414	2.00193	0.05414	1.76683	0.05414	0.73637
0.04060	1.49424	0.04060	1.34718	0.04060	0.54065
0.02707	0.97325	0.02707	0.88399	0.02707	0.37482
0.01353	0.47818	0.01353	0.43177	0.01353	0.18377

Table S4.3: Average observed rate constants, $k_{obs(1)}$, s^{-1}, for the displacement of the aqua ligands in PtL3 with the nucleophiles, at pH = 2.0, *T* = 298 *K*, *I* = 0.1 M $NaClO_4$.

TU		DMTU		TMTU	
Conc., M	$k_{obs(1)}$ (s^{-1})	Conc., M	$k_{obs(1)}$ (s^{-1})	Conc., M	$k_{obs(1)}$ (s^{-1})
0.06767	1.47659	0.06767	1.19614	0.06767	0.64526
0.05414	1.16443	0.05414	0.94017	0.05414	0.53802
0.04060	0.90321	0.04060	0.70801	0.04060	0.40478
0.02707	0.57557	0.02707	0.44803	0.02707	0.26212
0.01353	0.26107	0.01353	0.21551	0.01353	0.10746

Table S4.4: Average observed rate constants, $k_{obs(1)}$, s^{-1}, for the displacement of the aqua ligands in PtL4 with the nucleophiles, at pH = 2.0, *T* = 298 *K*, *I* = 0.1 M $NaClO_4$.

TU		DMTU		TMTU	
Conc., M	$k_{obs(1)}$ (s^{-1})	Conc., M	$k_{obs(1)}$ (s^{-1})	Conc., M	$k_{obs(1)}$ (s^{-1})
0.06767	1.10612	0.06767	0.91759	0.06767	0.42164
0.05414	0.87857	0.05414	0.73711	0.05414	0.32454
0.04060	0.64594	0.04060	0.55036	0.04060	0.22417
0.02707	0.43478	0.02707	0.36521	0.02707	0.13206
0.01353	0.20861	0.01353	0.18141	0.01353	0.04116

Table S4.5: Average observed rate constants, $k_{obs(1)}$, s^{-1}, for the displacement of the aqua ligands in PtL5 with the nucleophiles, at pH = 2.0, *T* = 298 *K*, *I* = 0.1 M $NaClO_4$.

TU		DMTU		TMTU	
Conc., M	$k_{obs(1)}$ (s^{-1})	Conc., M	$k_{obs(1)}$ (s^{-1})	Conc., M	$k_{obs(1)}$ (s^{-1})
0.06767	0.94658	0.06767	1.03145	0.06767	0.42850
0.05414	0.78492	0.05414	0.84216	0.05414	0.33427
0.04060	0.64649	0.04060	0.64524	0.04060	0.25431
0.02707	0.49981	0.02707	0.47911	0.02707	0.17346
0.01353	0.34995	0.01353	0.30294	0.01353	0.08759

Table S4.6: Average observed rate constants, $k_{obs(1)}$, s^{-1}, for the displacement of the aqua ligands in PtL6 with the nucleophiles, at pH = 2.0, T = 298 K, I = 0.1 M $NaClO_4$.

TU		DMTU		TMTU	
Conc., M	$k_{obs(1)}$ (s^{-1})	Conc., M	$k_{obs(1)}$ (s^{-1})	Conc., M	$k_{obs(1)}$ (s^{-1})
0.06767	0.86819	0.06767	0.83580	0.06767	0.34655
0.05414	0.73014	0.05414	0.67843	0.05414	0.27283
0.04060	0.59426	0.04060	0.51663	0.04060	0.21317
0.02707	0.45489	0.02707	0.36303	0.02707	0.13459
0.01353	0.31510	0.01353	0.20789	0.01353	0.06650

Table S4.7: Average observed rate constants, $k_{obs(2)}$, s^{-1}, for the dechelation of the linker in PtL2 with the nucleophiles, at pH = 2.0, T = 298 K, I = 0.1 M $NaClO_4$.

TU		DMTU		TMTU	
Conc., M	$k_{obs(2)}$ (s^{-1})	Conc., M	$k_{obs(2)}$ (s^{-1})	Conc., M	$k_{obs(2)}$ (s^{-1})
0.06767	0.00224	0.06767	0.00404	0.06767	0.00070
0.05414	0.00165	0.05414	0.00315	0.05414	0.00056
0.04060	0.0010	0.04060	0.00214	0.04060	0.00042
0.02707	0.00045	0.02707	0.00135	0.02707	0.00029
0.01353	0.00011	0.01353	0.00038	0.01353	0.00014

Table S4.8: Average observed rate constants, $k_{obs(2)}$, s^{-1}, for the dechelation of the linker in PtL3 with the nucleophiles, at pH = 2.0, T = 298 K, I = 0.1 M $NaClO_4$.

TU		DMTU		TMTU	
Conc., M	$k_{obs(2)}$ (s^{-1})	Conc., M	$k_{obs(2)}$ (s^{-1})	Conc., M	$k_{obs(2)}$ (s^{-1})
0.06767	0.00413	0.06767	0.00156	0.06767	0.00150
0.05414	0.00310	0.05414	0.00122	0.05414	0.00115
0.04060	0.00221	0.04060	0.00083	0.04060	0.00080
0.02707	0.00110	0.02707	0.00046	0.02707	0.00044
0.01353	0.00019	0.01353	0.00011	0.01353	0.00010

Table S4.9: Average observed rate constants, $k_{obs(2)}$, s^{-1}, for the substitution of the aqua ligands in PtL4 with the nucleophiles, at pH = 2.0, *T* = 298 *K*, *I* = 0.1 M $NaClO_4$.

TU		DMTU		TMTU	
Conc., M	$k_{obs(2)}$ (s^{-1})	Conc., M	$k_{obs(2)}$ (s^{-1})	Conc., M	$k_{obs(2)}$ (s^{-1})
0.06767	0.00654	0.06767	0.00446	0.06767	0.00250
0.05414	0.00498	0.05414	0.00348	0.05414	0.00201
0.04060	0.00410	0.04060	0.00252	0.04060	0.00147
0.02707	0.00217	0.02707	0.00155	0.02707	0.00091
0.01353	0.00070	0.01353	0.00092	0.01353	0.00042

Table S4.10: Average observed rate constants, $k_{obs(2)}$, s^{-1}, for the dechelation of the linker in PtL5 with the nucleophiles, at pH = 2.0, *T* = 298 *K*, *I* = 0.1 M $NaClO_4$.

TU		DMTU		TMTU	
Conc., M	$k_{obs(2)}$ (s^{-1})	Conc., M	$k_{obs(2)}$ (s^{-1})	Conc., M	$k_{obs(2)}$ (s^{-1})
0.06767	0.00309	0.06767	0.00184	0.06767	0.00060
0.05414	0.00241	0.05414	0.00145	0.05414	0.00049
0.04060	0.00172	0.04060	0.00103	0.04060	0.00038
0.02707	0.00103	0.02707	0.00058	0.02707	0.00027
0.01353	0.00036	0.01353	0.00021	0.01353	0.00016

Table S4.11: Average observed rate constants, $k_{obs(2)}$, s^{-1}, for the substitution of the aqua ligands in PtL6 with the nucleophiles, at pH = 2.0, *T* = 298 *K*, *I* = 0.1 M $NaClO_4$.

TU		DMTU		TMTU	
Conc., M	$k_{obs(2)}$ (s^{-1})	Conc., M	$k_{obs(2)}$ (s^{-1})	Conc., M	$k_{obs(2)}$ (s^{-1})
0.06767	0.00469	0.06767	0.00194	0.06767	0.00185
0.05414	0.00359	0.05414	0.00150	0.05414	0.00163
0.04060	0.00251	0.04060	0.00111	0.04060	0.00143
0.02707	0.00143	0.02707	0.00067	0.02707	0.00118
0.01353	0.00044	0.01353	0.00028	0.01353	0.00095

Table S4.12: Average observed rate constants, $k_{obs(3)}$, s^{-1}, for the substitution of the aqua ligands in PtL4 with the nucleophiles, at pH = 2.0, *T* = 298 *K*, *I* = 0.1 M $NaClO_4$.

TU		DMTU	
Conc., M	$k_{obs(2)}$ (s^{-1})	Conc., M	$k_{obs(2)}$ (s^{-1})
0.06767	0.00043892	0.06767	0.00022370
0.05414	0.00036983	0.05414	0.00018269
0.04060	0.00030034	0.04060	0.00014294
0.02707	0.00023688	0.02707	0.00010620
0.01353	0.00015745	0.01353	0.00006588

Table S4.13: Average observed rate constants, $k_{obs(2)}$, s^{-1}, for the substitution of the aqua ligands in PtL6 with the nucleophiles, at pH = 2.0, *T* = 298 *K*, *I* = 0.1 M $NaClO_4$.

TU		DMTU	
Conc., M	$k_{obs(2)}$ (s^{-1})	Conc., M	$k_{obs(2)}$ (s^{-1})
0.06767	0.000044457	0.06767	0.000055227
0.05414	0.000036853	0.05414	0.000046590
0.04060	0.000030241	0.04060	0.000036916
0.02707	0.000022912	0.02707	0.000027835
0.01353	0.000015720	0.01353	0.000020254

Table S4.14: Temperature dependence of $k_2/M^{-1}s^{-1}$, for the displacement of the aqua ligands in PtL2 by the nucleophiles at 120-fold at pH = 2.0, *I* = 0.1 M $NaClO_4$

TU		DMTU		TMTU	
1/T (K^{-1})	ln(k_2/T)	1/T (K^{-1})	ln(k_2/T)	1/T (K^{-1})	ln(k_2/T)
0.00325	-4.64485	0.00325	-4.81834	0.00325	-5.80987
0.00330	-4.96562	0.00330	-5.10753	0.00330	-6.03467
0.00336	-5.29547	0.00336	-5.39908	0.00336	-6.31208
0.00341	-5.63597	0.00341	-5.70705	0.00341	-6.59488
0.00347	-5.98855	0.00347	-6.04632	0.00347	-6.87473

Table S4.15: Temperature dependence of k_2/$M^{-1}s^{-1}$, for the displacement of the aqua ligands in PtL3 by the nucleophiles at 120-fold at pH = 2.0, *I* = 0.1 M $NaClO_4$

TU		DMTU		TMTU	
1/T (K^{-1})	ln(k_2/T)	1/T (K^{-1})	ln(k_2/T)	1/T (K^{-1})	ln(k_2/T)
0.00325	-5.35899	0.00325	-5.76252	0.00325	-6.01404
0.00330	-5.59484	0.00330	-5.88652	0.00330	-6.29297
0.00336	-5.79889	0.00336	-6.04239	0.00336	-6.60151
0.00341	-6.06392	0.00341	-6.19096	0.00341	-6.94986
0.00347	-6.36160	0.00347	-6.32252	0.00347	-7.29111

Table S4.16: Temperature dependence of k_2/$M^{-1}s^{-1}$, for the displacement of the aqua ligands in PtL4 by the nucleophiles at 120-fold at pH = 2.0, *I* = 0.1 M $NaClO_4$

TU		DMTU		TMTU	
1/T (K^{-1})	ln(k_2/T)	1/T (K^{-1})	ln(k_2/T)	1/T (K^{-1})	ln(k_2/T)
0.00325	-5.64941	0.00325	-5.77924	0.00325	-6.66437
0.00330	-5.86293	0.00330	-6.02583	0.00330	-6.90796
0.00336	-6.13415	0.00336	-6.29428	0.00336	-7.19244
0.00341	-6.38471	0.00341	-6.55584	0.00341	-7.46058
0.00347	-6.65256	0.00347	-6.85609	0.00347	-7.72969

Table S4.17: Temperature dependence of k_2/$M^{-1}s^{-1}$, for the displacement of the aqua ligands in PtL5 by the nucleophiles at 120-fold at pH = 2.0, *I* = 0.1 M $NaClO_4$

TU		DMTU		TMTU	
1/T (K^{-1})	ln(k_2/T)	1/T (K^{-1})	ln(k_2/T)	1/T (K^{-1})	ln(k_2/T)
0.00325	-5.52510	0.00325	-5.48022	0.00325	-6.43019
0.00330	-5.73966	0.00330	-5.75781	0.00330	-6.73446
0.00336	-5.93927	0.00336	-6.13522	0.00336	-7.06629
0.00341	-6.16591	0.00341	-6.44271	0.00341	-7.41237
0.00347	-6.42657	0.00347	-6.81639	0.00347	-7.74960

Table S4.18: Temperature dependence of $k_2/M^{-1}s^{-1}$, for the displacement of the aqua ligands in PtL6 by the nucleophiles at 120-fold at pH = 2.0, I = 0.1 M $NaClO_4$

TU		DMTU		TMTU	
1/T (K^{-1})	ln(k_2/T)	1/T (K^{-1})	ln(k_2/T)	1/T (K^{-1})	ln(k_2/T)
0.00325	-5.89373	0.00325	-6.11154	0.00325	-6.35065
0.00330	-6.05289	0.00330	-6.23335	0.00330	-6.74529
0.00336	-6.21753	0.00336	-6.35752	0.00336	-7.24276
0.00341	-6.39268	0.00341	-6.47978	0.00341	-7.72905
0.00347	-6.56600	0.00347	-6.61352	0.00347	-8.26895

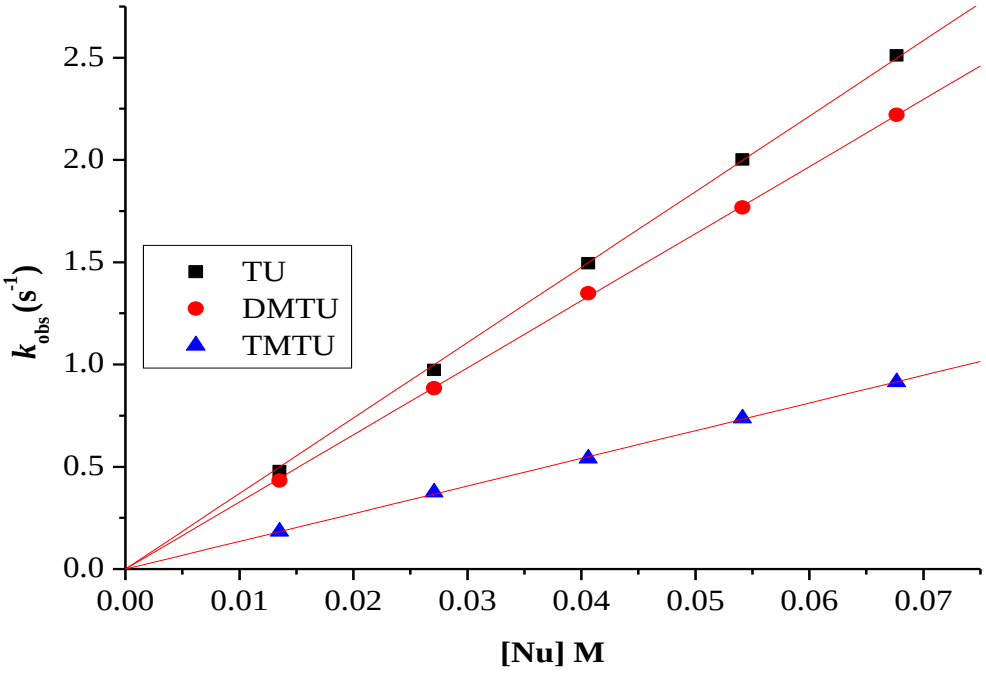

Figure S4.1: Dependence of the *pseudo* first-order rate constants (k_{obs}) on the concentrations of the nucleophiles for the aqua substitution for PtL2 in $NaClO_4$ (I = 0.1 M) at 298 *K.*

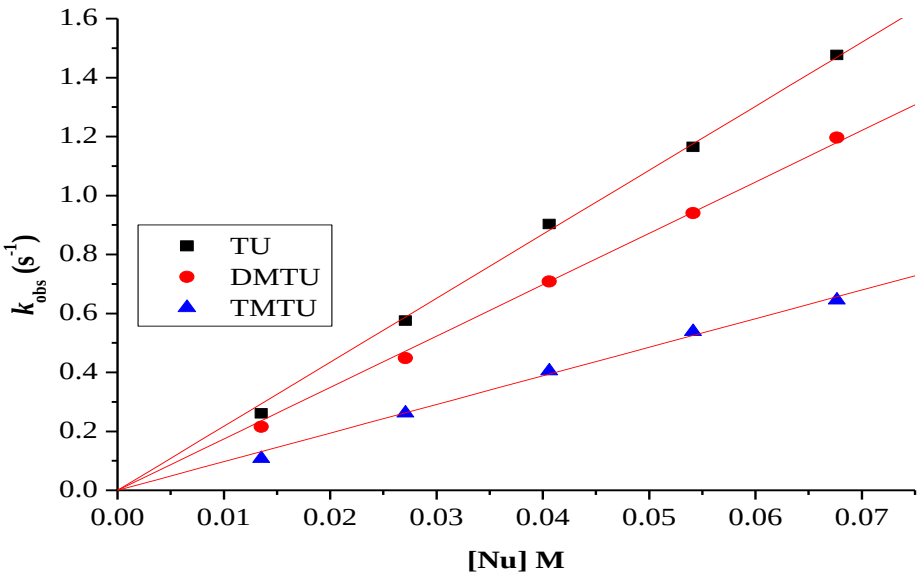

Figure S4.2: Dependence of the *pseudo* first-order rate constants (k_{obs}) on the concentrations of the nucleophiles for the aqua substitution for PtL3 in $NaClO_4$ (I = 0.1 M) at 298 K.

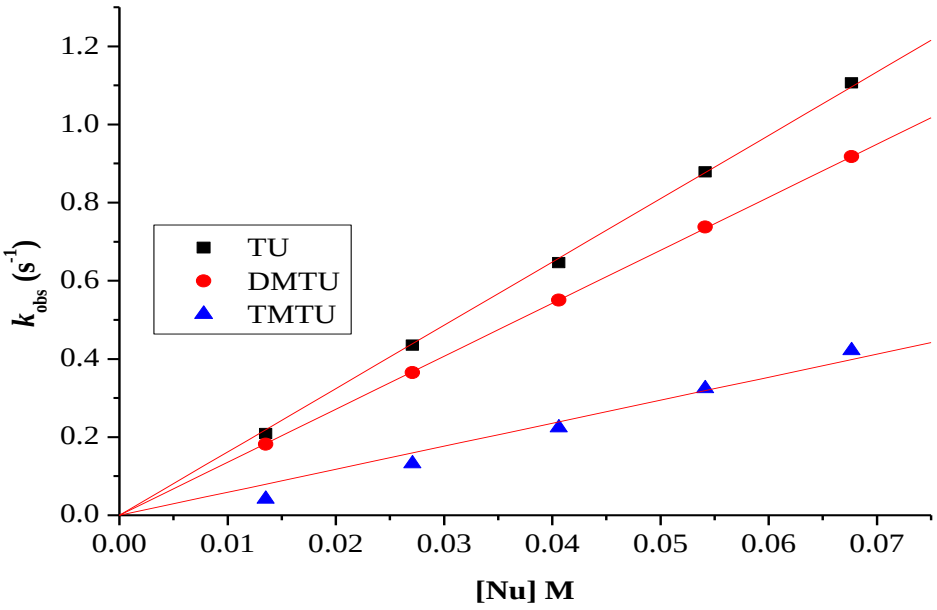

Figure S4.3: Dependence of the *pseudo* first-order rate constants (k_{obs}) on the concentrations of the nucleophiles for the aqua substitution for PtL4 in $NaClO_4$ (I = 0.1 M) at 298 K.

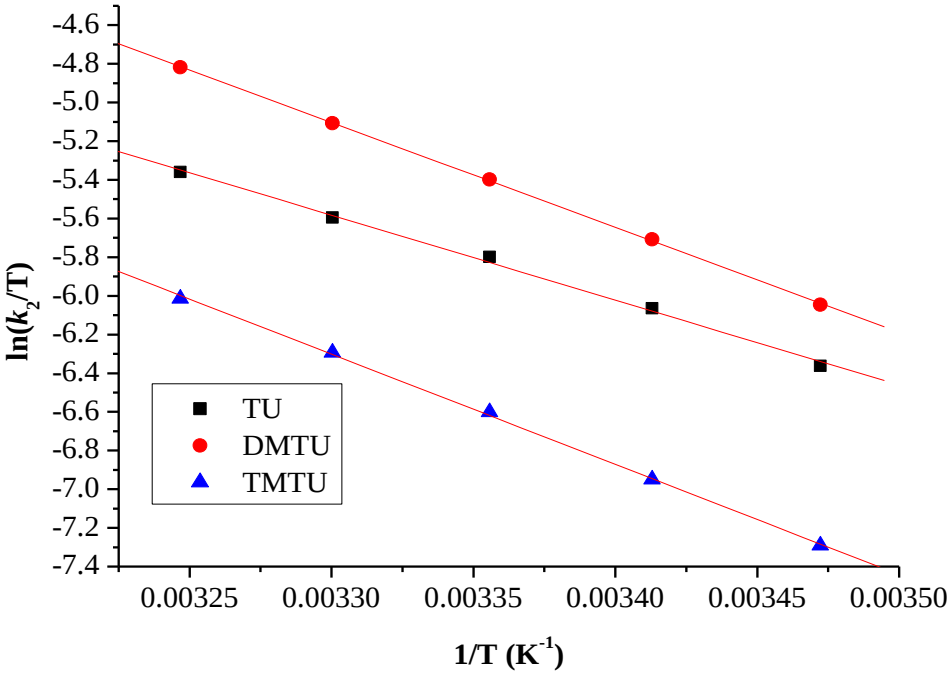

Figure S4.4: Eyring plots obtained for PtL3 with the nucleophiles for the substitution reactions over the temperature range 288 – 308 *K* in $NaClO_4$ (*I* = 0.1 M).

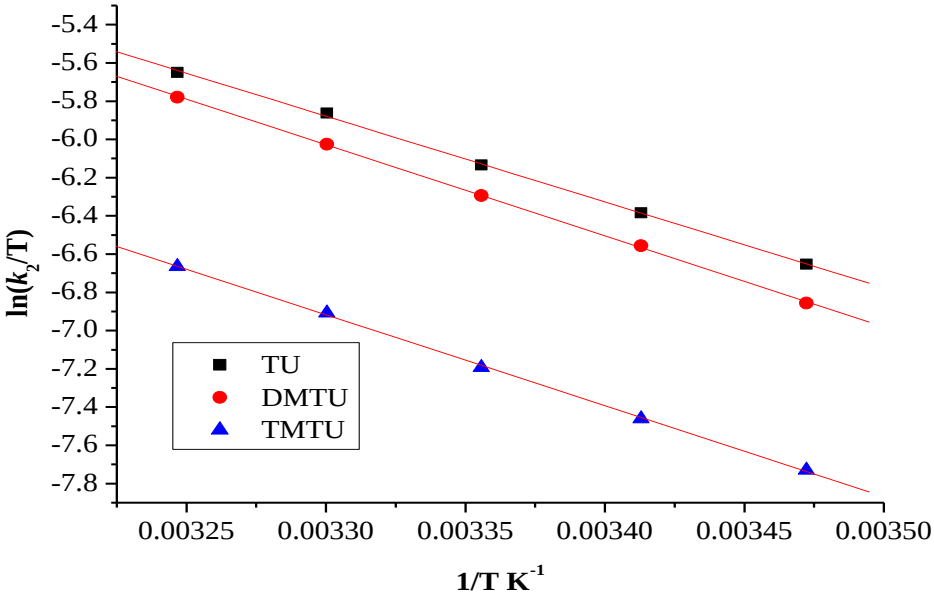

Figure S4.5: Eyring plots obtained for PtL4 with the nucleophiles for the substitution reactions over the temperature range 288 – 308 *K* in $NaClO_4$ (*I* = 0.1 M).

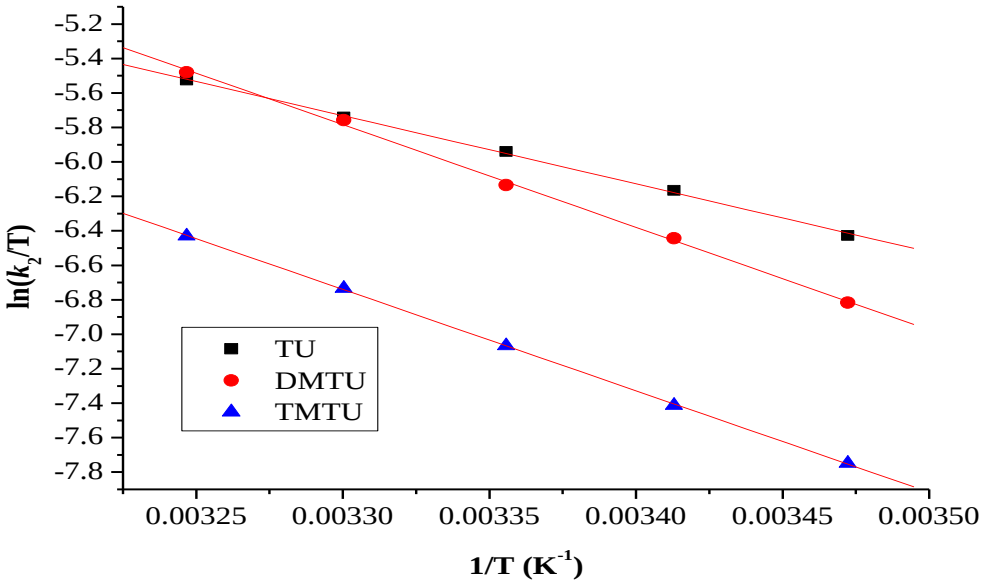

Figure S4.6: Eyring plots obtained for PtL5 with the nucleophiles for the substitution reactions over the temperature range 288 – 308 *K* in $NaClO_4$ (*I* = 0.1 M).

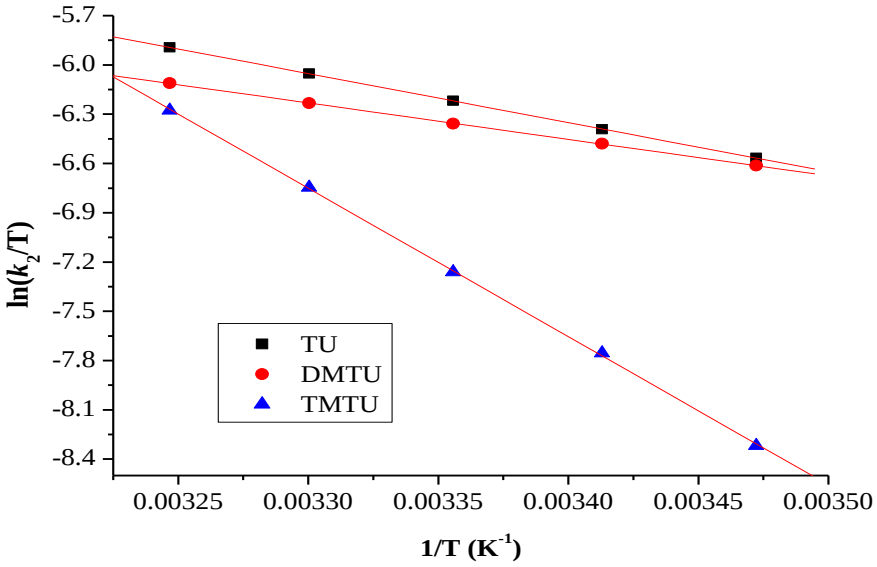

Figure S4.7: Eyring plots obtained for PtL6 with the nucleophiles for the substitution reactions over the temperature range 288 – 308 *K* in $NaClO_4$ (*I* = 0.1 M).

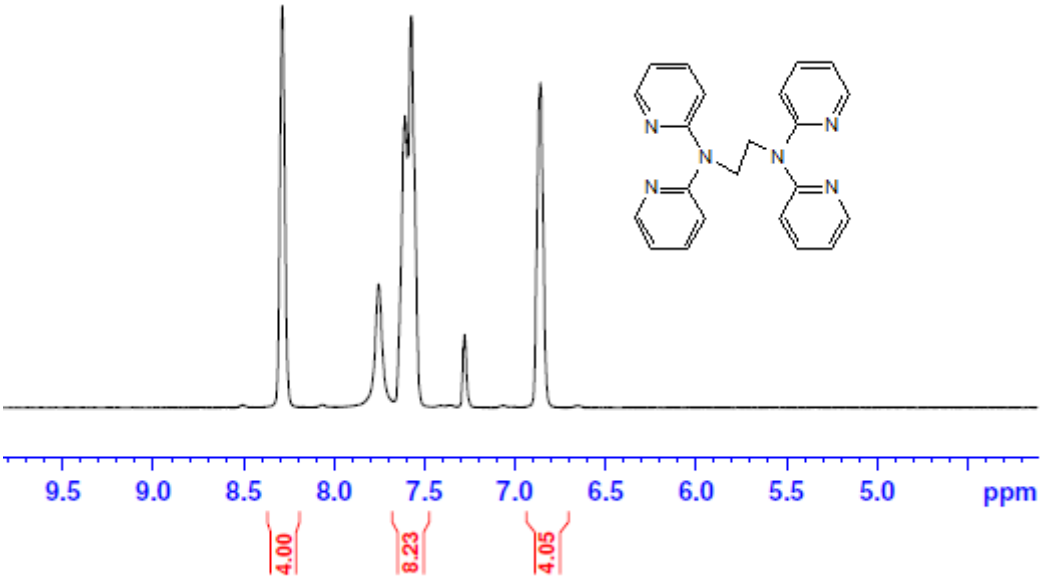

Figure S4.8: **^{1}H NMR spectrum of *N,N'*-1,2-bis(di-2-pyridylamino)ethane (dpa_2en) (L2) in $CDCl_3$.**

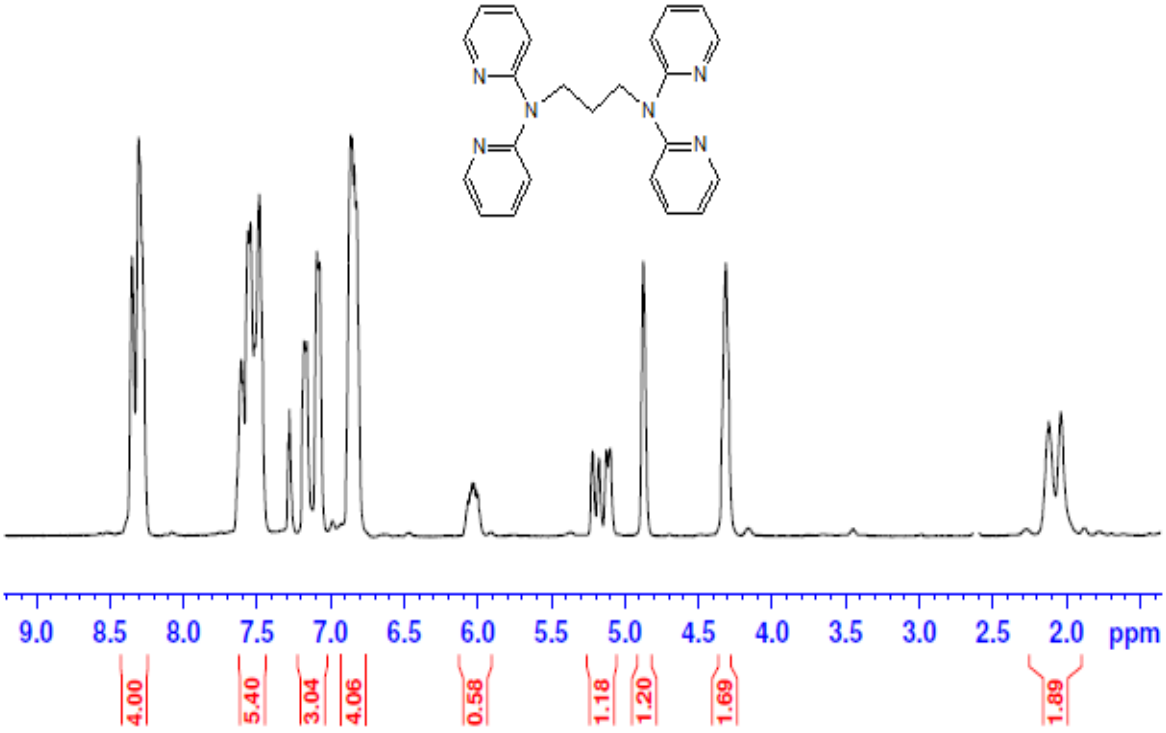

Figure S4.9: **^{1}H NMR spectrum of *N, N'*-1,3-bis(di-2-pyridylamino)propane (dpa_2Prop) (L3), in $CDCl_3$.**

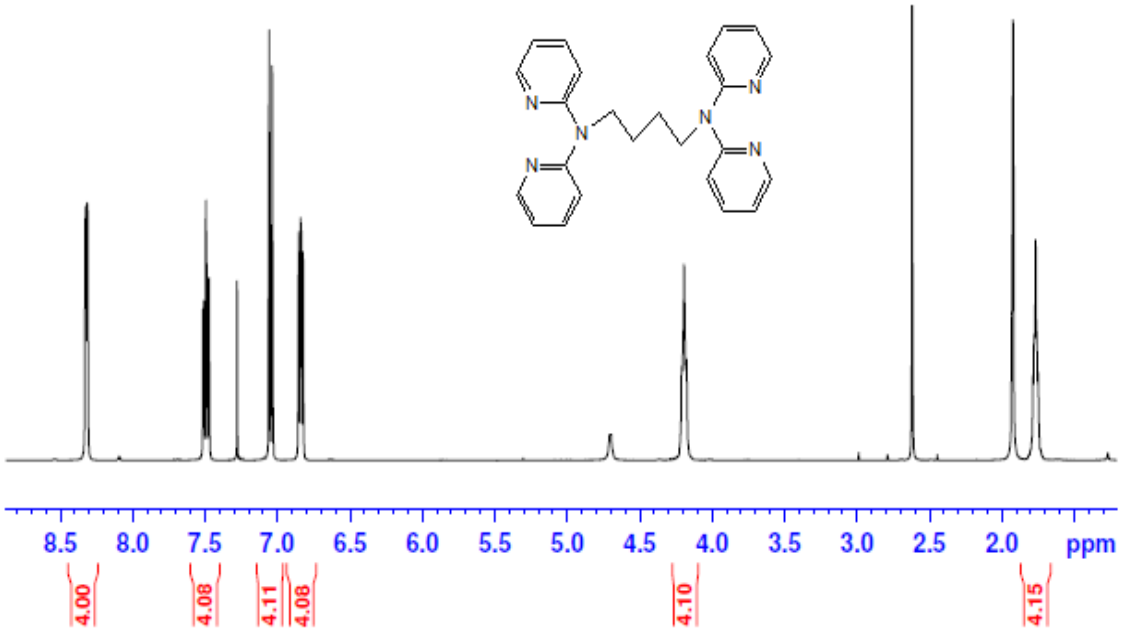

Figure S4.10: ^{1}H NMR spectrum of *N, N'*-1,4-bis(di-2-pyridylamino)butane (dpa_2But) (L4), in $CDCl_3$.

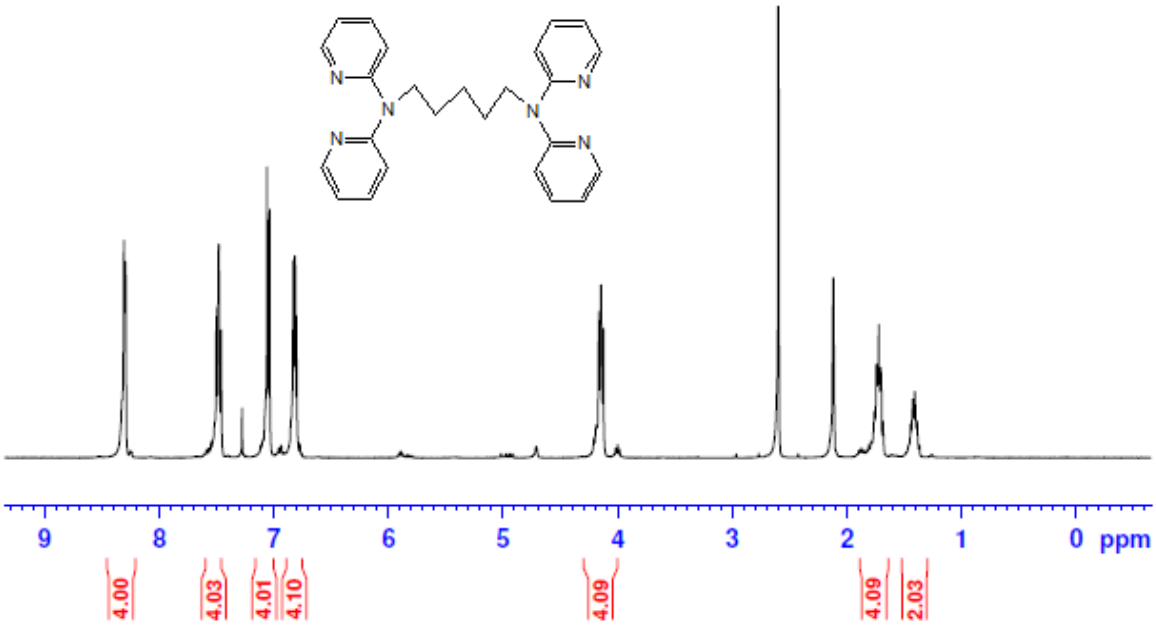

Figure S4.11: ^{1}H NMR spectrum of *N, N'*-1,5-bis(di-2-pyridylamino)pentane dpa_2Pent) (L5) in $CDCl_3$.

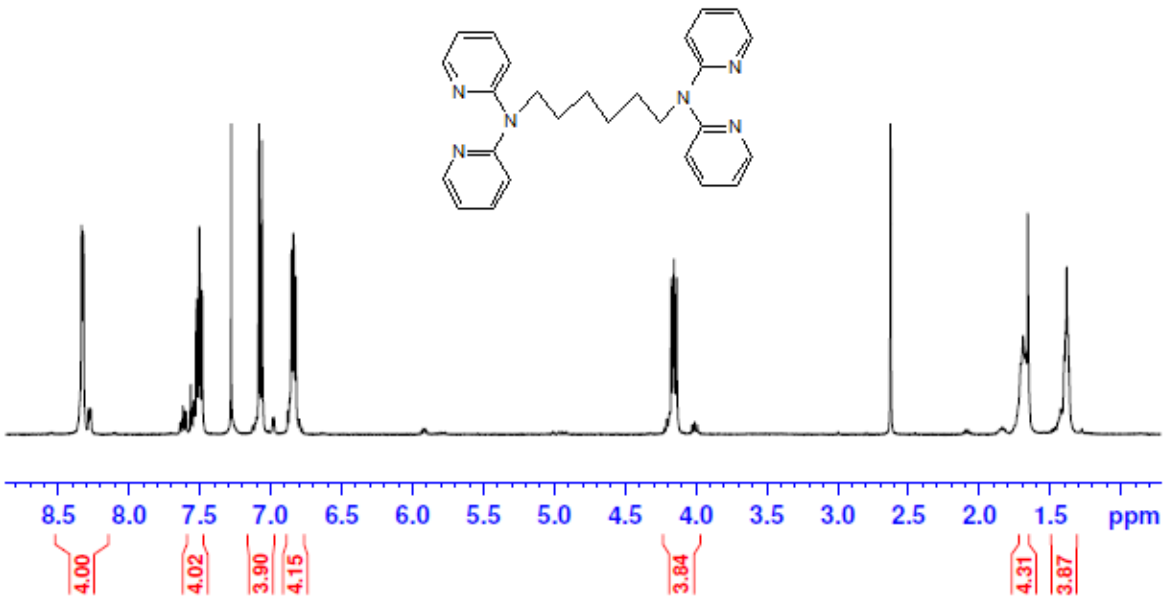

Figure S4.12: **^{1}H NMR spectrum of *N, N'*-1,6-bis(di-2-pyridylamino)hexane (dpa_2Hex) (L6) in $CDCl_3$.**

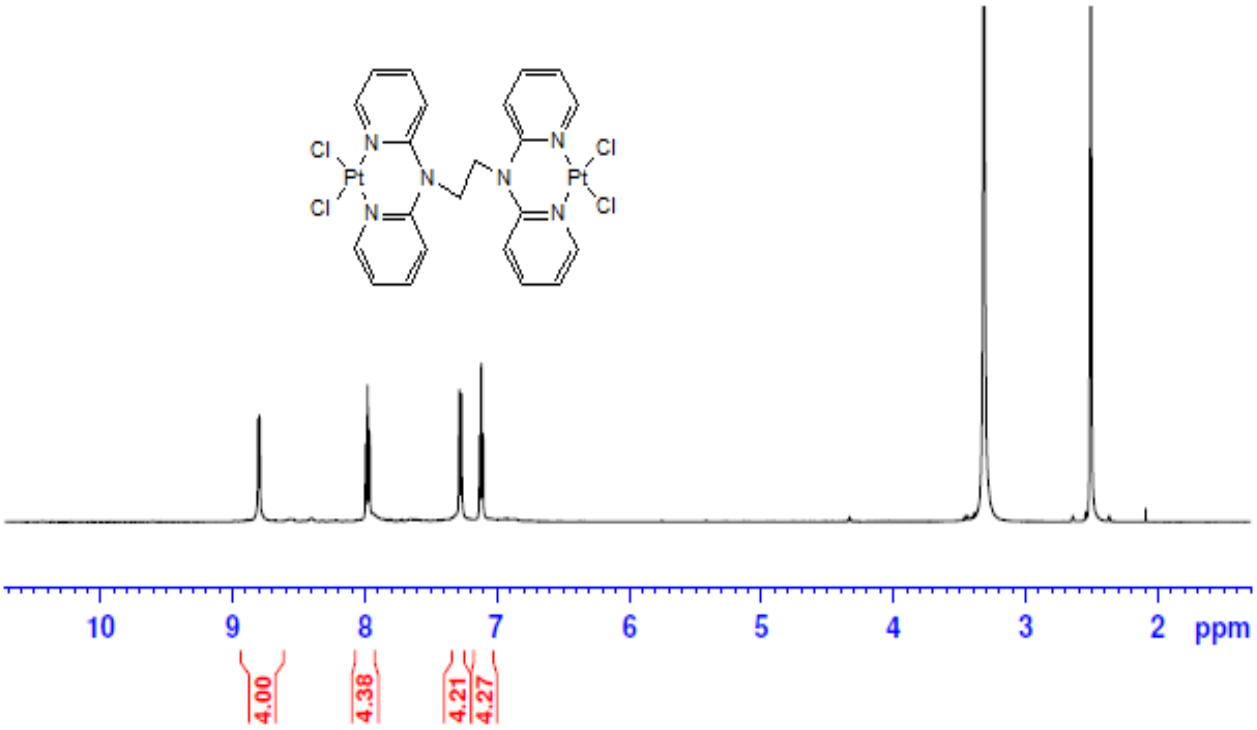

Figure S4.13: **^{1}H NMR spectrum of PtL2 in DMSO-d_6.**

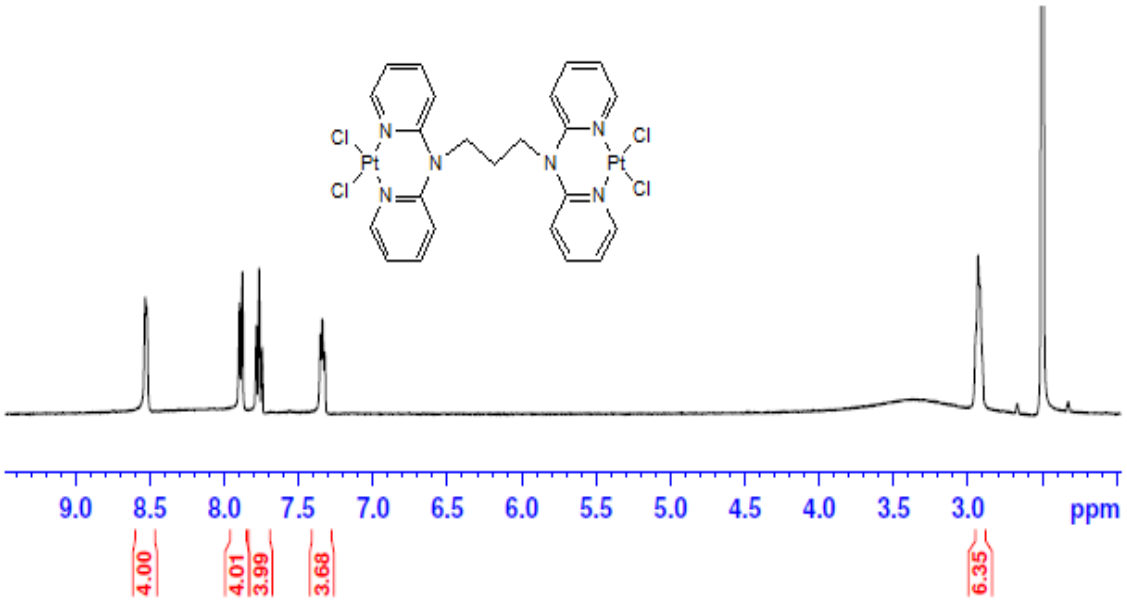

Figure S4.14: **^{1}H NMR spectrum of PtL3 in DMSO-d_6.**

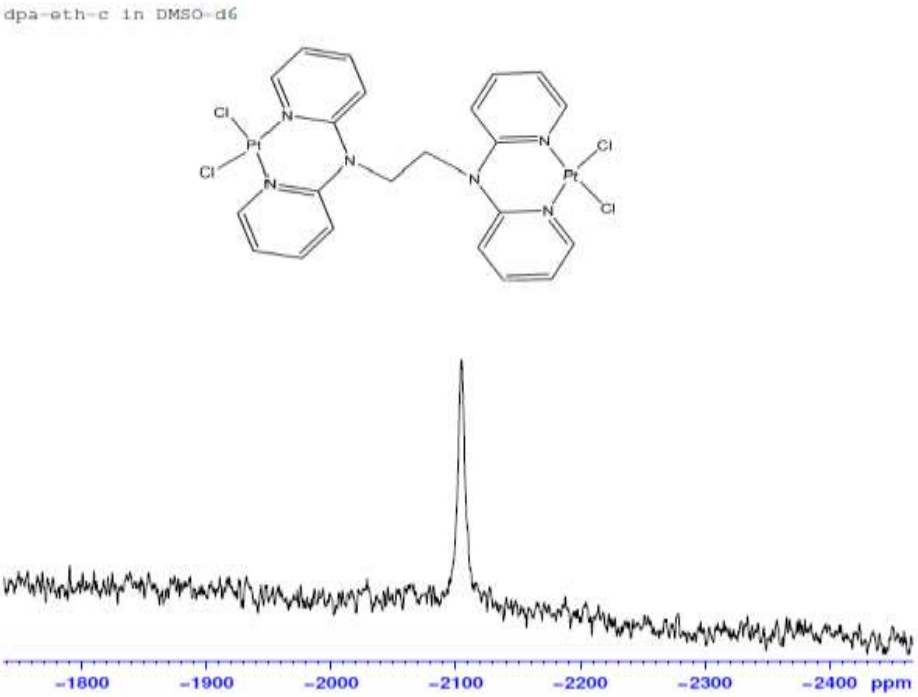

Figure S4.15: **^{195}Pt NMR spectrum of PtL2 in DMSO-d_6.**

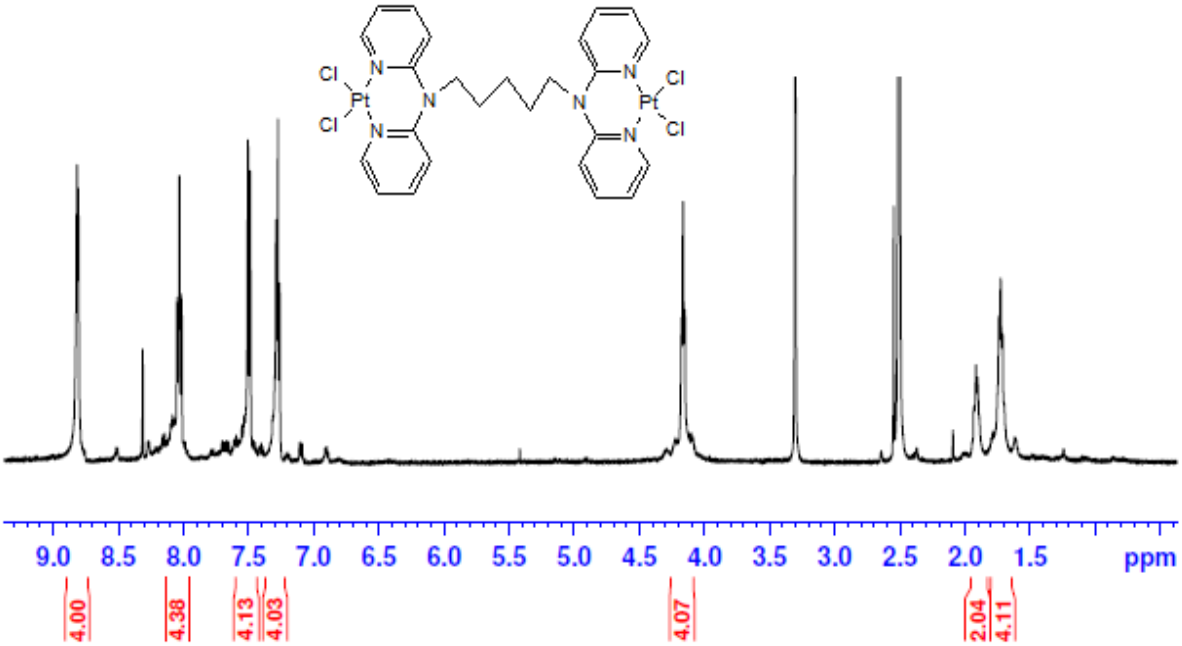

Figure S4.16: **^{1}H NMR spectrum of PtL5 in DMSO-d_6.**

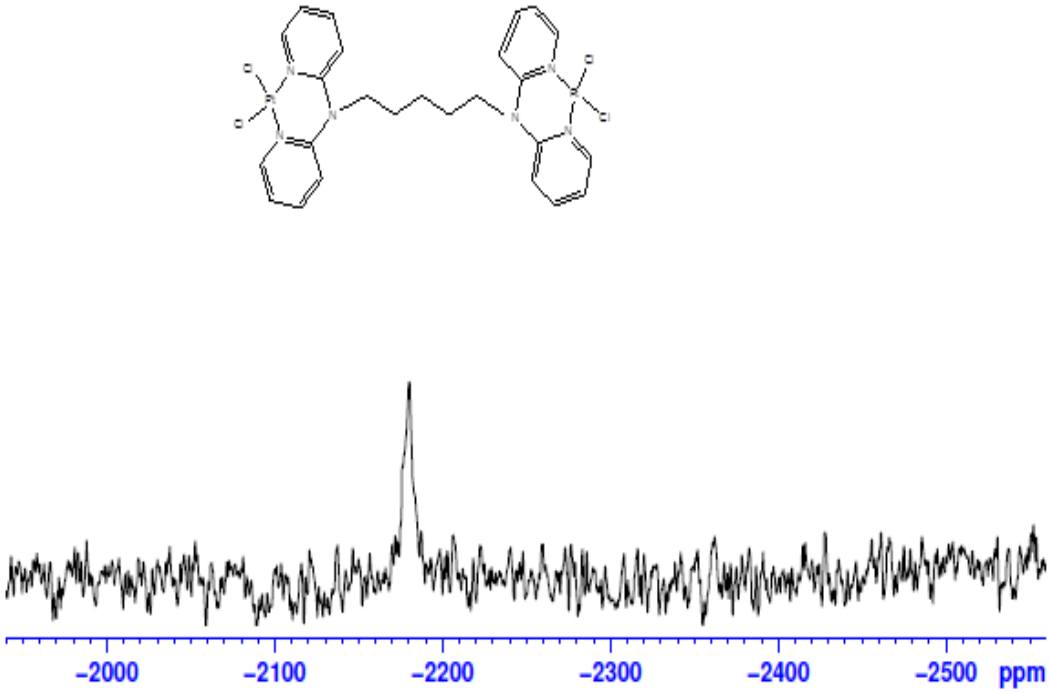

Figure S4.17: **^{195}Pt NMR spectrum of PtL5 in DMSO-d_6.**

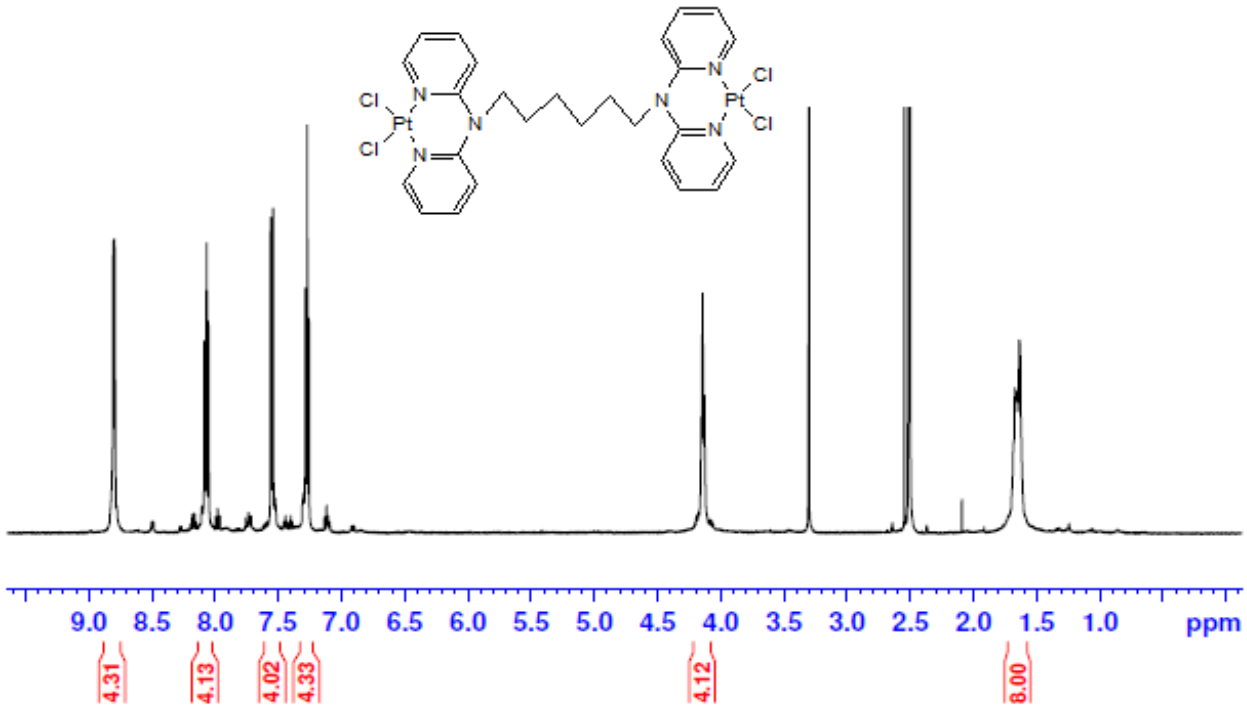

Figure S4.18: **^{1}H NMR spectrum of PtL6 in DMSO-d_6.**

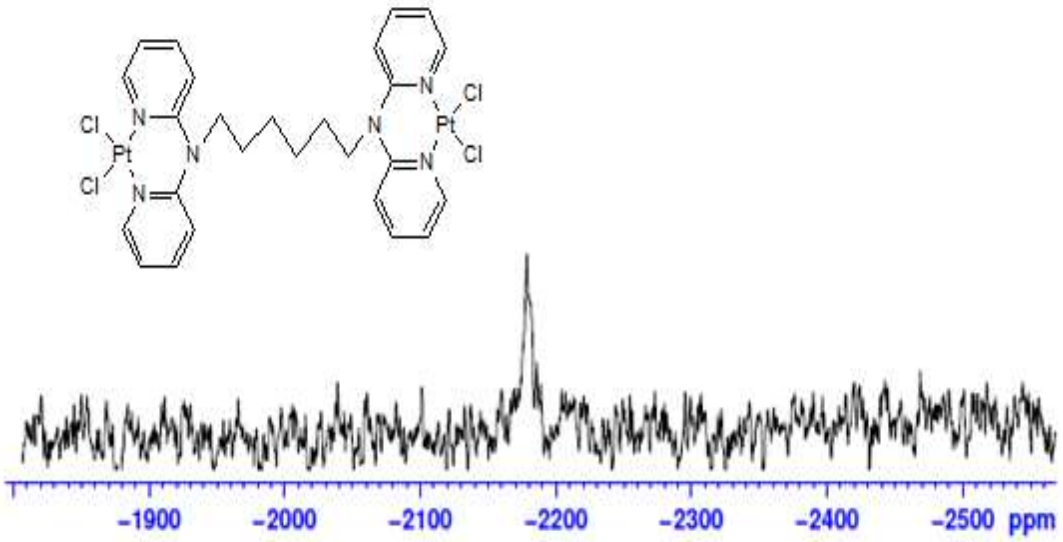

Figure S4.19: **^{195}Pt NMR spectrum of PtL6 in DMSO-d_6.**

Elemental Composition Report **Page 1**

Single Mass Analysis
Tolerance = 5.0 PPM / DBE: min = -1.5, max = 50.0
Element prediction: Off
Number of isotope peaks used for i-FIT = 3

Monoisotopic Mass, Even Electron Ions
3 formula(e) evaluated with 1 results within limits (all results (up to 1000) for each mass)
Elements Used:
C: 20-25 H: 20-25 N: 5-10

Grace Kinunda
dpa2 pnp 2 (0.017) Cm (1:31)

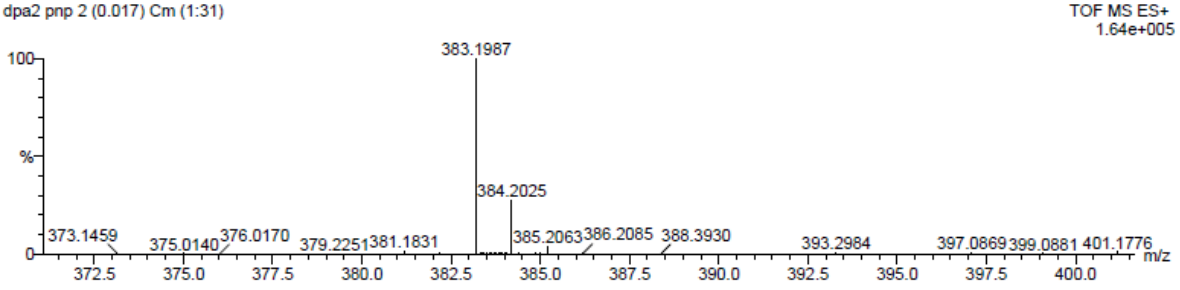

Minimum:				-1.5			
Maximum:		5.0	5.0	50.0			
Mass	Calc. Mass	mDa	PPM	DBE	i-FIT	i-FIT (Norm)	Formula
383.1987	383.1984	0.3	0.8	15.5	553.0	0.0	C23 H23 N6

Figure S4.20: **TOF ESI mass spectrum of *N,N'*-1,3-bis(dipyridylamino)propane (dpa_2Prop)**

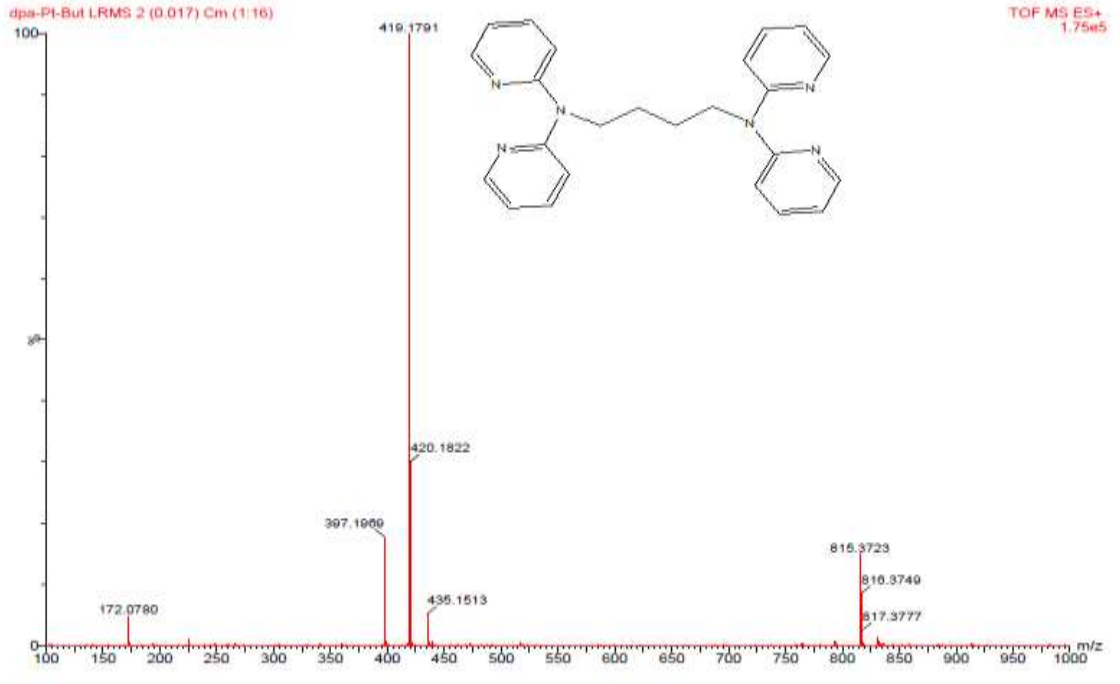

Figure S4.21: **TOF ESI mass spectrum of *N,N'*-1,4-bis(dipyridylamino)butane (dpa_2But)**

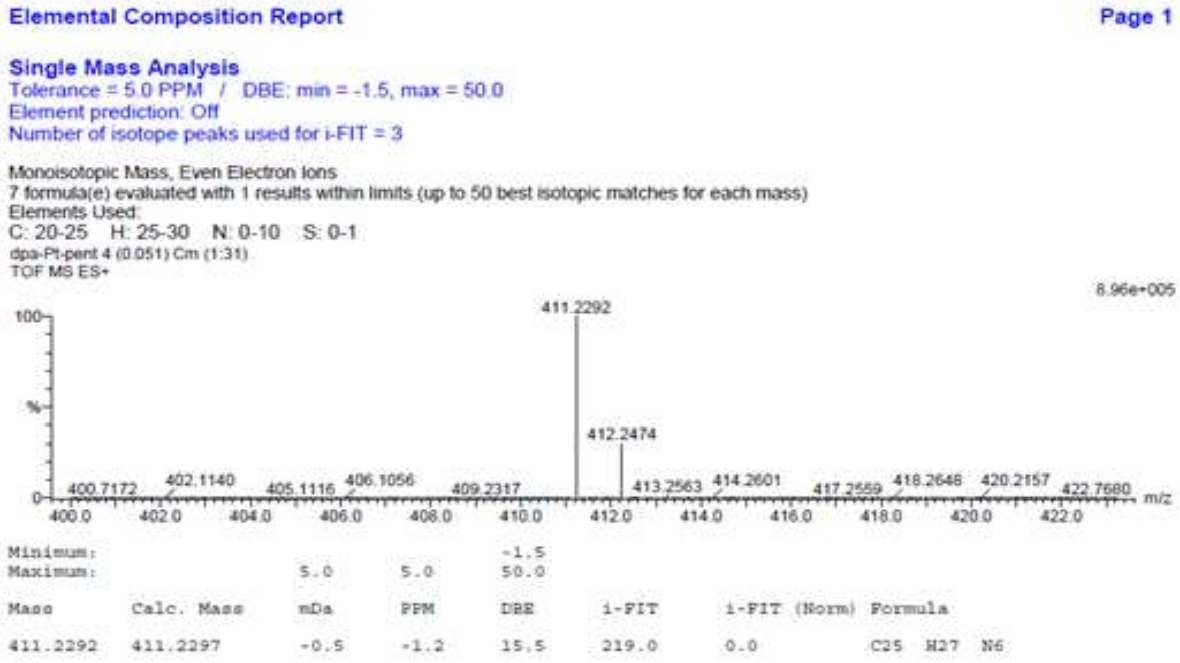

Figure S4.22: **TOF ESI mass spectrum of *N,N'*-1,5-bis(dipyridylamino)pentane (dpa_2Pent)**

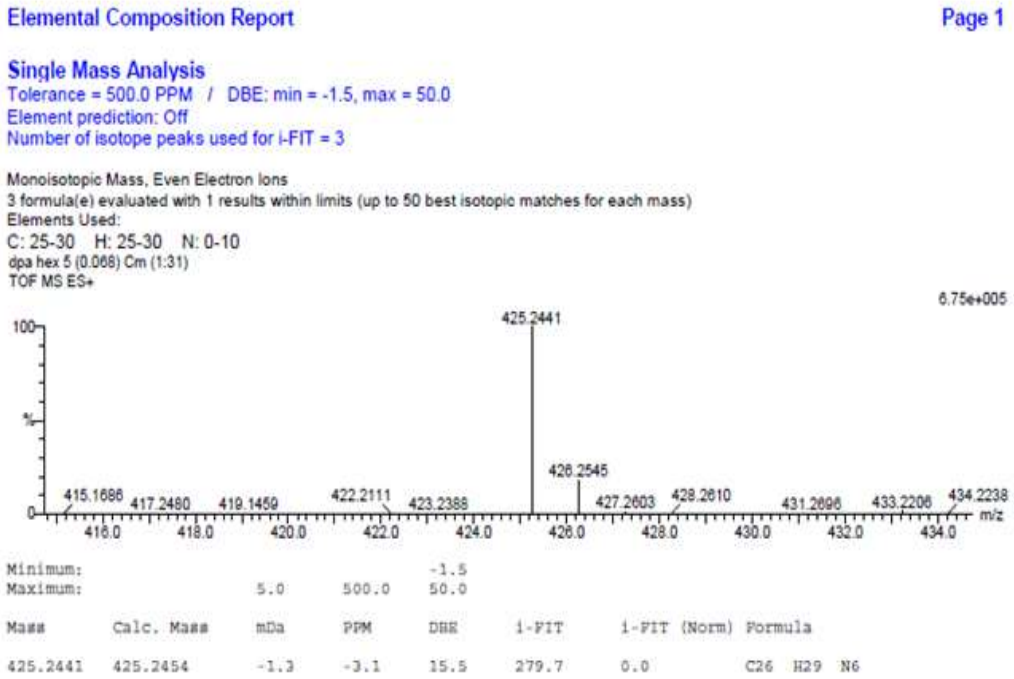

Figure S4.23: **TOF ESI mass spectrum of *N,N'*-1,6-bis(dipyridylamine)hexane (dpa_2Hex)**

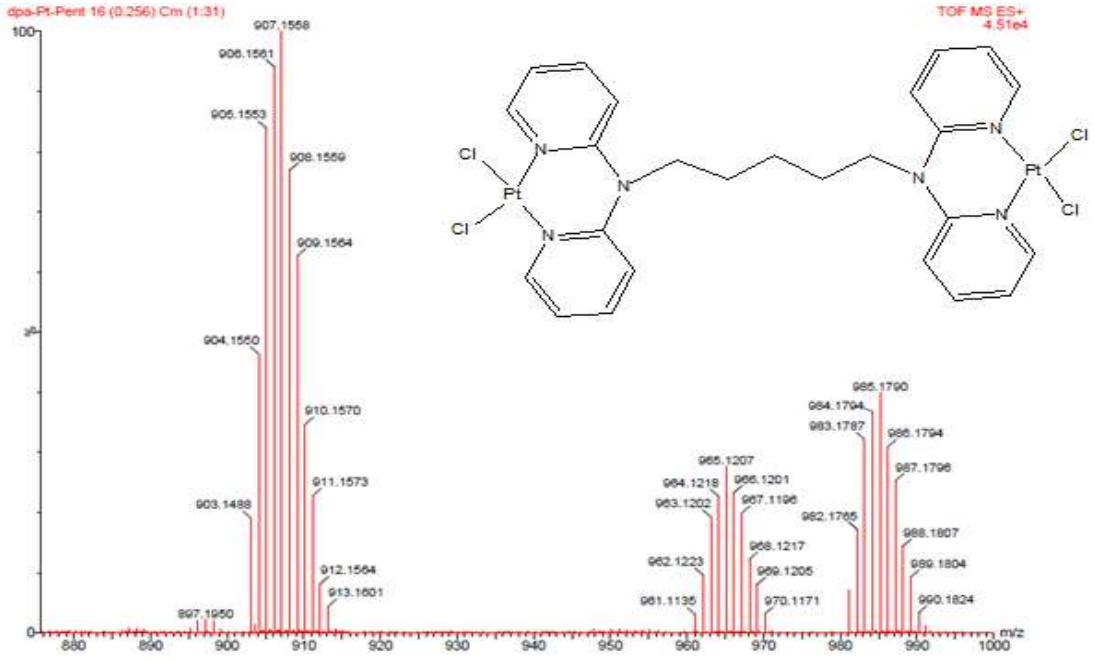

Figure S4.24: TOF ESI mass spectrum of PtL5

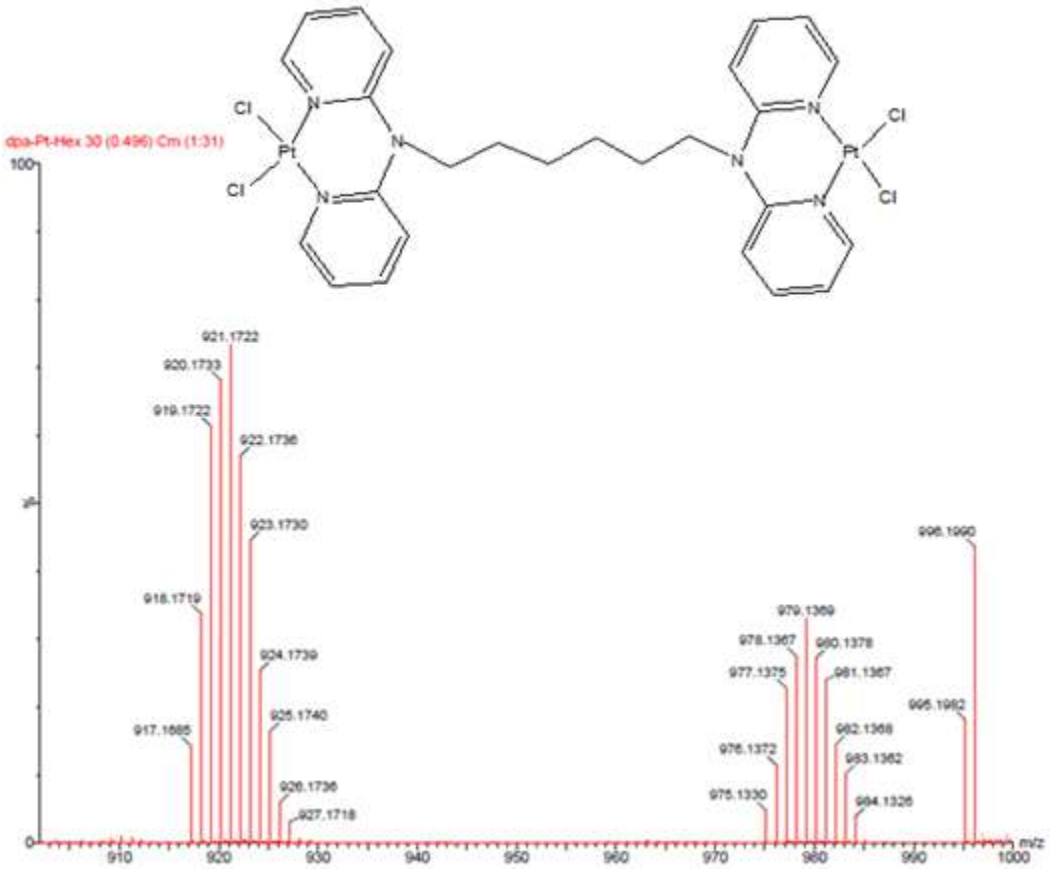

Figure S4.25: TOF ESI mass spectrum of PtL6

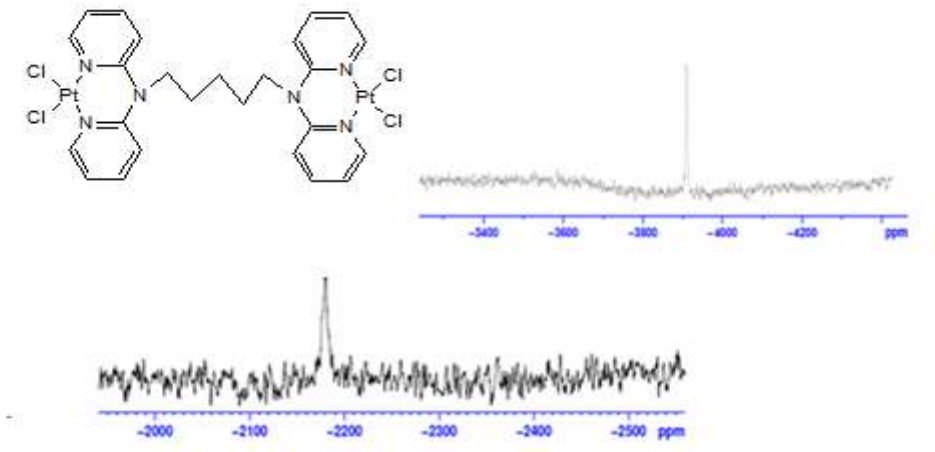

Figure S4.26: **^{195}Pt NMR spectrum of PtL5 in DMSO-d_6.**

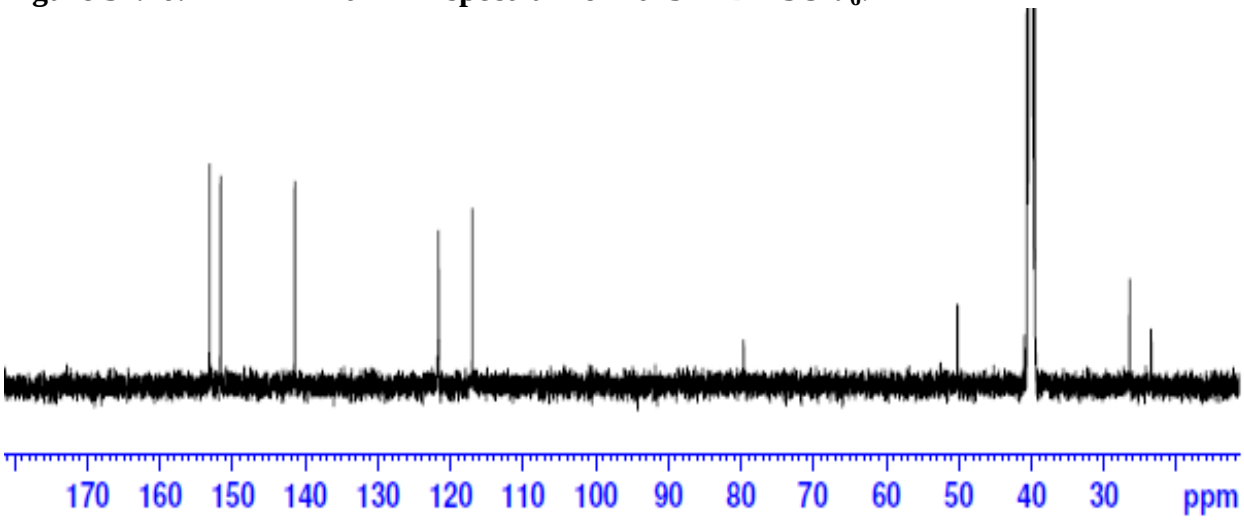

Figure S4.27: **^{13}C NMR spectrum for the complex PtL5 in DMSO-d_6.**

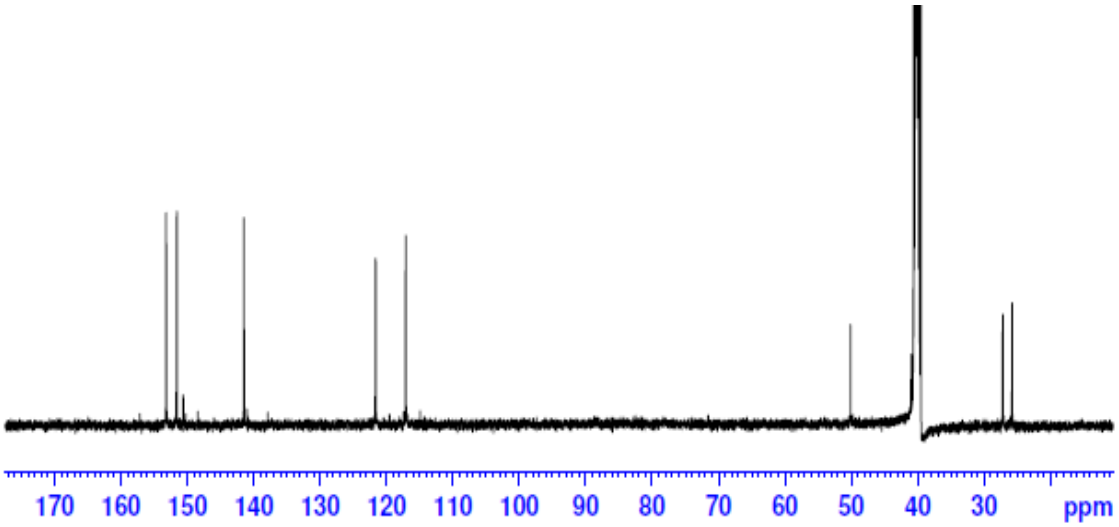

Figure S4.28: **^{13}C NMR spectrum for the complex PtL6 in DMSO-d_6.**

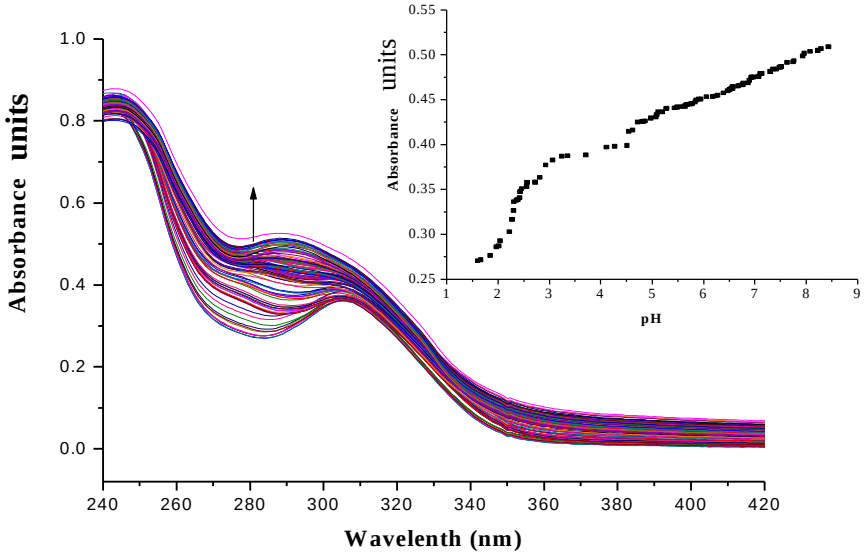

Figure S4.29: **UV-Vis spectral changes for the titration of 0.05 mM PtL4 within the pH range of 1-9; *Inset* shows the titration curve at λ = 290 nm**

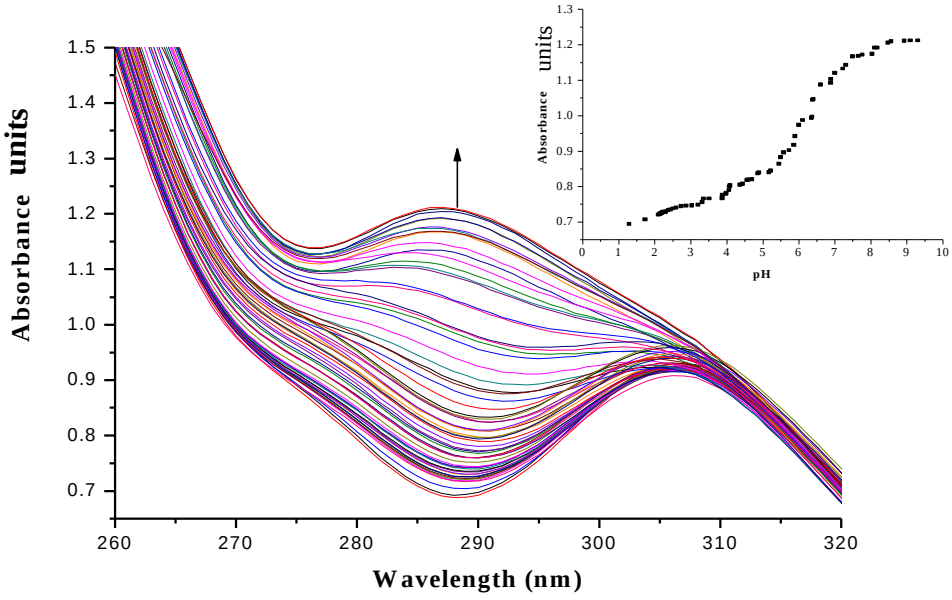

Figure S4.30: **UV-Vis spectral changes for the titration of 0.05 mM PtL5 within the pH range of 1-10; *Inset* shows the titration curve at λ = 288 nm.**

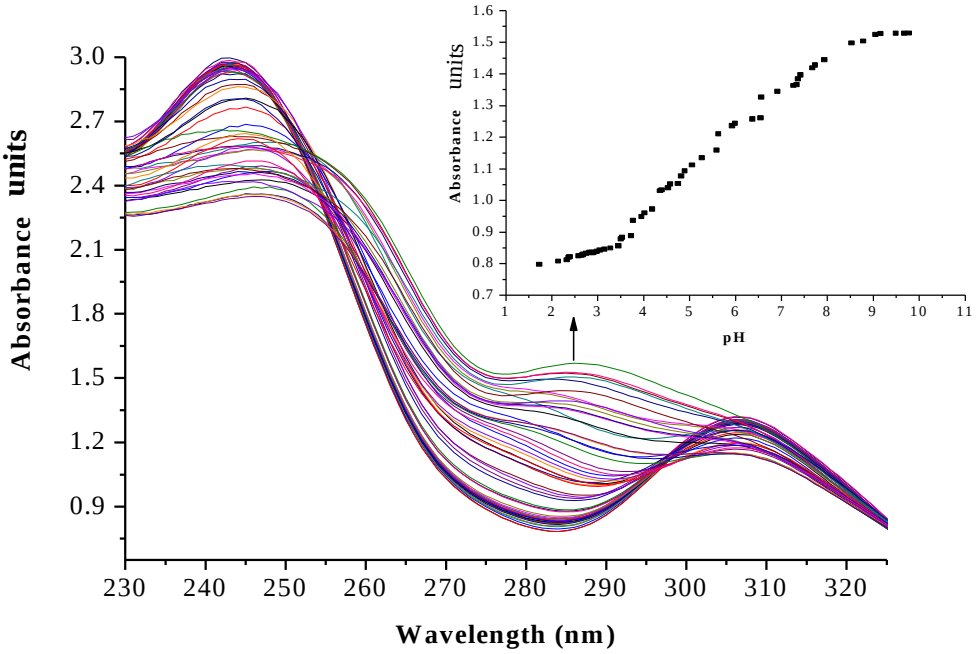

Figure S4.31: **UV-Vis spectral changes for the titration of 0.5 mM PtL6 within the pH range of 1-10; *Inset* shows the titration curve at λ = 284 nm.**

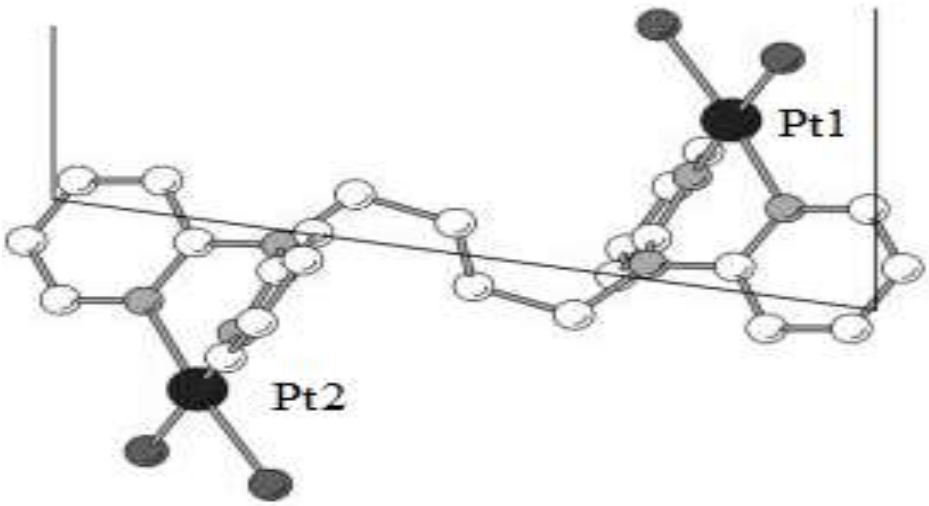

Figure S4.32: ***Anti*-conformational structure of alkyl complexes with even (-CH_2)n) group. Hydrogen atoms left out for clarity.**

Figure S4.33: ***Anti- and Syn*-conformational structure of alkyl complexes with even and odd (-CH_{2-})n group**.

With this variation in structural conformations, different substitution behaviour in the reactivity is expected as observed in this investigation

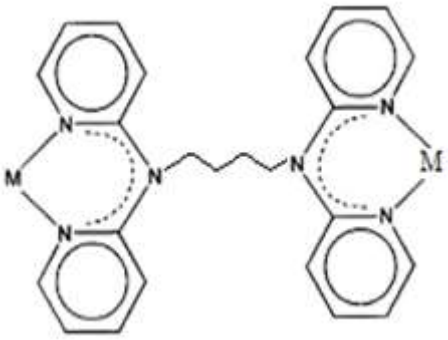

Figure S4.34: **Proposed conjugated system that stabilizes the metal centre (M)**

The metal atoms are in a conjugation six-membered ring, which makes the electron density to be delocalized into the rings causing deshielding of the alkyl protons. As such the metal alkyl protons are shifted downfield and the ligand protons shifted upfield as revealed in this study.

Figures S4.34 and S4.35 are full spectra of even numbered alkyl chain complexes showing similar substitution behaviour of two separate kinetic steps on the UV-Vis spectrophotometer. On the contrary Figures S4.36 and S4.37 are also full spectra of odd numbered alkyl chain complexes showing similar kinetic behaviour but different from even numbered alkyl chain complexes. Only one kinetic step was observed on the UV-Vis spectrophotometer for these moieties.

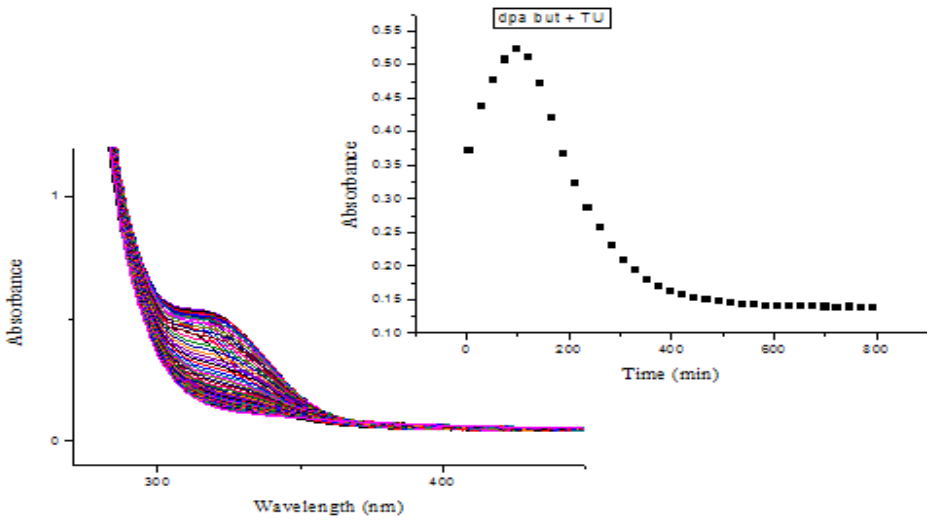

Figure S4.35: UV-Vis spectral changes observed during the reaction between 0.05 mM **PtL4** and **TU**; *inset* is a typical kinetic trace for time dependence of absorbance at 320 nm, T = 298 K, pH = 2.0 and I = 0.1 M $NaClO_4$.

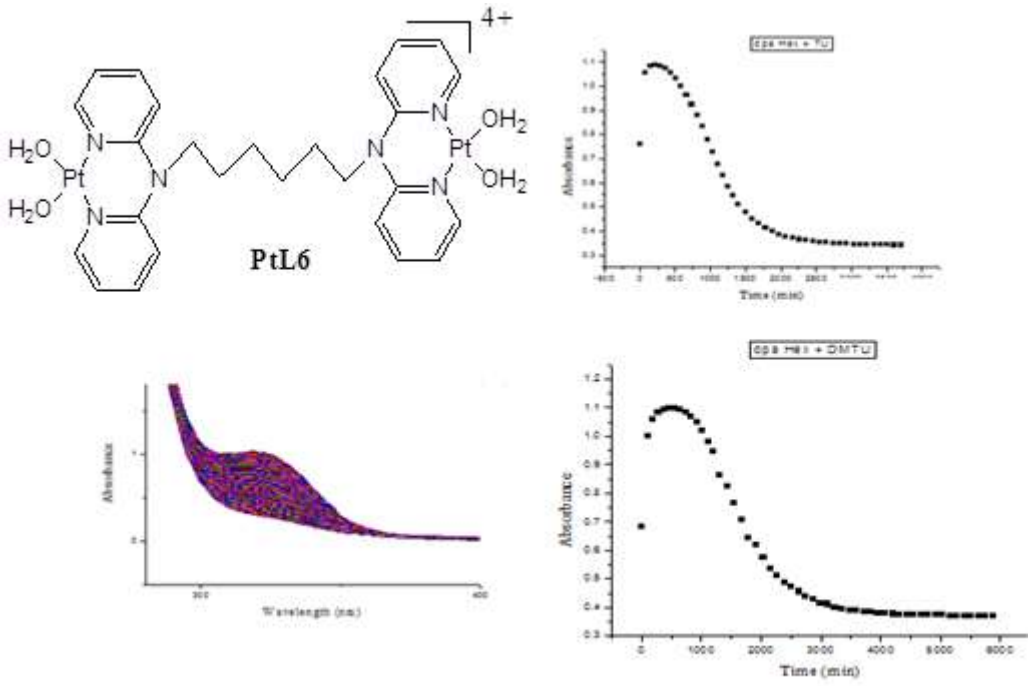

Figure S4.36: UV-Vis spectral changes observed during the reaction between **PtL6** and **TU** and **DMTU**; *inset* is a typical kinetic trace for time dependence of absorbance at 320 nm, T = 298 K, pH = 2.0 and I = 0.1 M $NaClO_4$.

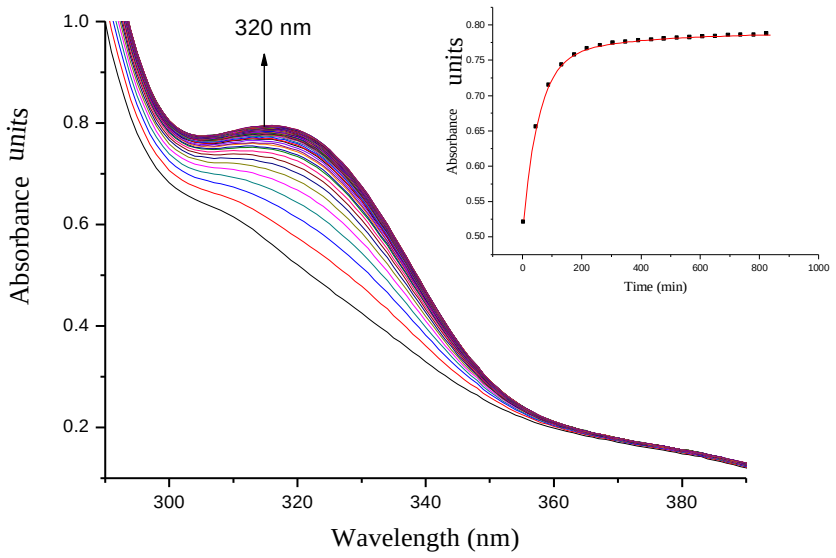

Figure S4.37: **UV-Vis spectral changes observed during the reaction between PtL3 and TU; *inset* is a typical kinetic trace for time dependence of absorbance at 320 nm, *T* = 298 *K*, pH = 2.0 and *I* = 0.1 M $NaClO_4$.**

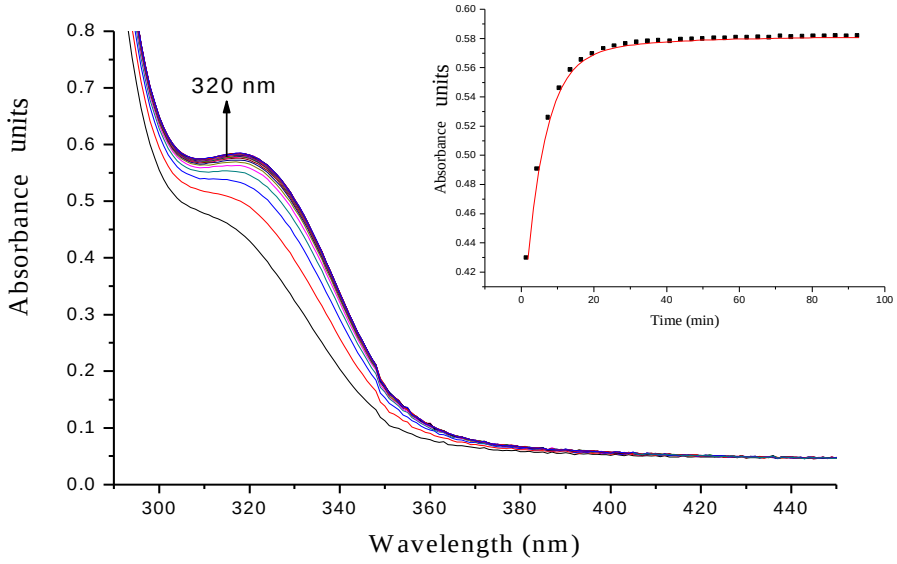

Figure S4.38: **UV-Vis spectral changes observed during the reaction between PtL5 and TU; *inset* is a typical kinetic trace for time dependence of absorbance at 320 nm, *T* = 298 *K*, pH = 2.0 and *I* = 0.1 M $NaClO_4$.**

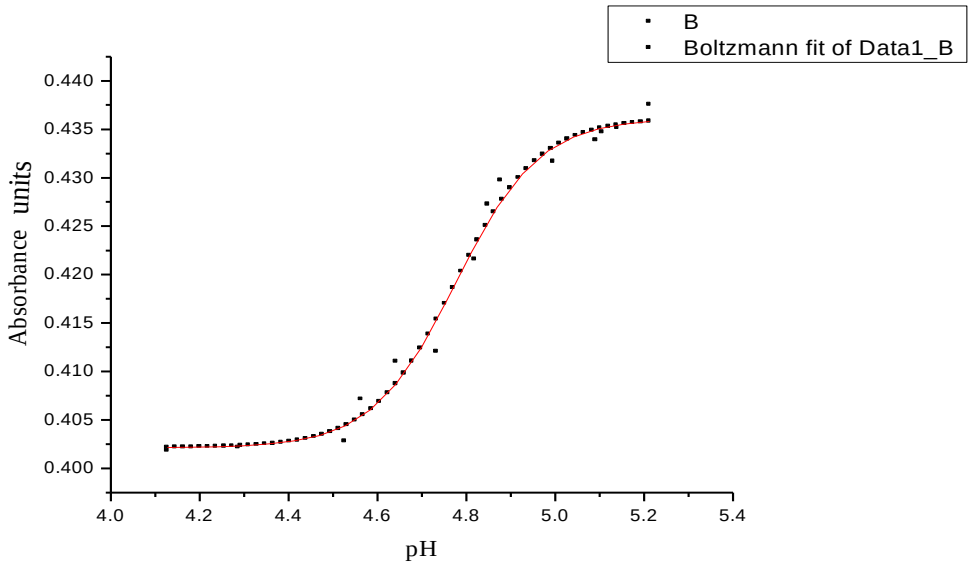

Figure S4.39: **Determination of third dissociation constant (pK_{a3}) for PtL5 using Boltzmann equation from the sigmoid curve at the inflection point**

Boltzmann Equation: $y = A_2+(A_1 - A_2)/(1 + \exp((x - x_0)/dx)$.

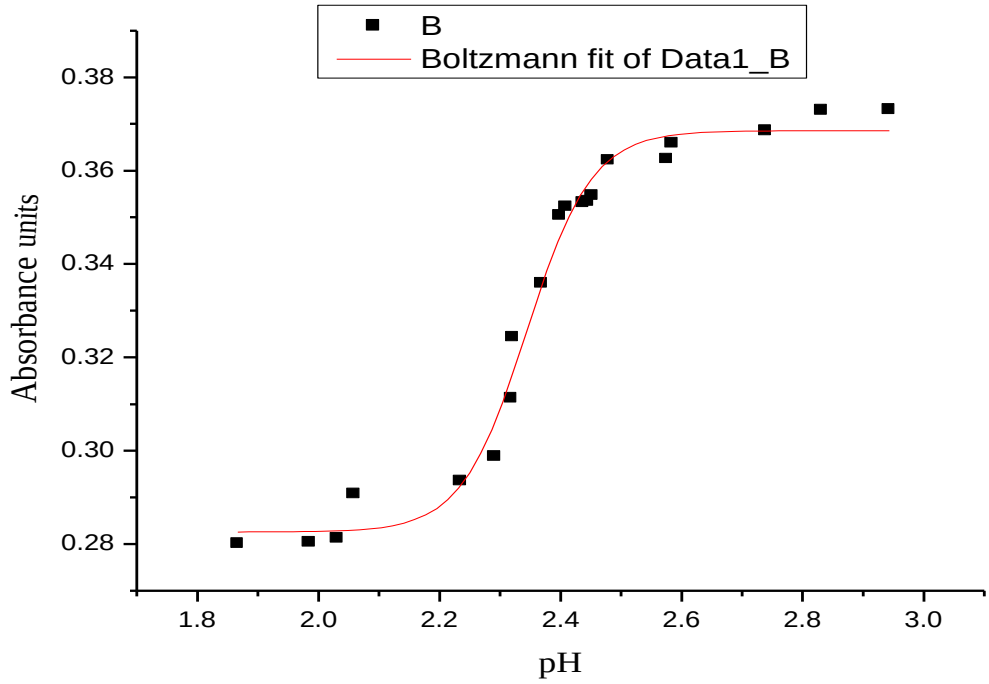

Figure S4.40: **Determination of first dissociation constant (pK_{a1}) for PtL4 using Boltzmann equation from the sigmoid curve at the inflection point**

APPENDIX 3 (CHAPTER 5)

A summary of wavelengths used for kinetic measurements for the investigated complexes, some of their kinetic traces, k_{obs} for reactions at different concentrations and temperatures and characterization of complexes using ^{1}H NMR, TOF ES^{+} mass spectra, ^{13}C NMR and ^{195}Pt' NMR are given in the following tables.

Table S5.1: Summary of the wavelengths used for monitoring kinetic reactions for Scheme 5.1

Complex	Nucleophile	Wavelength (λ) (nm)	
		Stopped-flow	UV-Visible
PtC1	**TU**	300	320
	DMTU	300	320
	TMTU	372	-
PtC2	**TU**	290	320
	DMTU	297	320
	TMTU	362	335
PtC3	**TU**	298	320
	DMTU	300	320
	TMTU	362	-
PtC4	**TU**	295	320
	DMTU	302	320
	TMTU	375	335
PtC5	**TU**	310	320
	DMTU	312	320
	TMTU	363	335

Table S5.2: Average observed rate constants, k_{obs}, s^{-1}, for the displacement of the aqua ligands in PtC1 with the nucleophiles, at pH = 2.0, T = 298 K, I = 0.1 M $NaClO_4$.

TU		**DMTU**		**TMTU**	
Conc., M	k_{obs} (s^{-1})	Conc., M	k_{obs} (s^{-1})	Conc., M	k_{obs} (s^{-1})
0.016125	0.83058	0.016125	0.76101	0.016125	0.59118
0.012900	0.67085	0.012900	0.57174	0.012900	0.47966
0.009675	0.50078	0.009675	0.44363	0.009675	0.36090
0.006450	0.34548	0.006450	0.27486	0.006450	0.24560
0.003225	0.15269	0.003225	0.13821	0.003225	0.12349

Table S5.3: Average observed rate constants, $k_{obs,}$ s^{-1}, for the displacement of the aqua ligands in PtC2 with the nucleophiles, at pH = 2.0, *T* = 298 *K*, *I* = 0.1 M $NaClO_4$.

TU		DMTU		TMTU	
Conc., M	k_{obs} (s^{-1})	Conc., M	k_{obs} (s^{-1})	Conc., M	k_{obs} (s^{-1})
0.016125	0.53421	0.016125	0.40385	0.016125	0.18325
0.012900	0.42926	0.012900	0.32699	0.012900	0.14884
0.009675	0.32268	0.009675	0.23933	0.009675	0.11175
0.006450	0.21844	0.006450	0.16504	0.006450	0.07404
0.003225	0.11941	0.003225	0.07383	0.003225	0.03665

Table S5.4: Average observed rate constants, $k_{obs,}$ s^{-1}, for the displacement of the aqua ligands in PtC3 with the nucleophiles, at pH = 2.0, *T* = 298 *K*, *I* = 0.1 M $NaClO_4$.

TU		DMTU		TMTU	
Conc., M	k_{obs} (s^{-1})	Conc., M	k_{obs} (s^{-1})	Conc., M	k_{obs} (s^{-1})
0.06767	2.73529	0.06767	2.59214	0.06756	1.05179
0.05414	2.20997	0.05414	1.98764	0.05405	0.86859
0.04060	1.65401	0.04060	1.45689	0.04053	0.63733
0.02707	1.14098	0.02707	0.98106	0.02702	0.40358
0.01353	0.54412	0.01353	0.45754	0.01351	0.17014

Table S5.5: Average observed rate constants, $k_{obs,}$ s^{-1}, for the displacement of the aqua ligands in PtC4 with the nucleophiles, at pH = 2.0, *T* = 298 *K*, *I* = 0.1 M $NaClO_4$.

TU		DMTU		TMTU	
Conc., M	k_{obs} (s^{-1})	Conc., M	k_{obs} (s^{-1})	Conc., M	k_{obs} (s^{-1})
0.06750	1.91429	0.06750	1.38655	0.06750	0.45313
0.05400	1.49708	0.05400	1.14257	0.05400	0.35876
0.04050	1.09269	0.04050	0.84842	0.04050	0.27975
0.02700	0.74312	0.02700	0.56997	0.02700	0.18237
0.01350	0.37140	0.01350	0.28478	0.01350	0.09568

Table S5.6: Average observed rate constants, $k_{obs,}$ s^{-1}, for the displacement of the aqua ligands in PtC5 with the nucleophiles, at pH = 2.0, *T* = 298 *K*, *I* = 0.1 M $NaClO_4$.

TU		DMTU		TMTU	
Conc., M	k_{obs} (s^{-1})	Conc., M	k_{obs} (s^{-1})	Conc., M	k_{obs} (s^{-1})
0.06766	3.53973	0.06766	2.75609	0.06766	1.11304
0.05413	2.85104	0.05413	2.11523	0.05413	0.88367
0.04059	2.12823	0.04059	1.59007	0.04059	0.66470
0.02706	1.41148	0.02706	1.13457	0.02706	0.45901
0.01353	0.69678	0.01353	0.64225	0.01353	0.21466

Table S5.7: Temperature dependence of $k_2/M^{-1}s^{-1}$, for the displacement of the aqua ligands in PtC1 by the nucleophiles at 60-fold at pH = 2.0, *I* = 0.1 M $NaClO_4$

TU		DMTU		TMTU	
1/T (K^{-1})	ln(k_{obs}/T)	1/T (K^{-1})	ln(k_{obs}/T)	1/T (K^{-1})	ln(k_{obs}/T)
0.00325	-5.89191	0.00325	-6.00960	0.00325	-6.19553
0.00330	-6.14219	0.00330	-6.22662	0.00330	-6.44841
0.00336	-6.38868	0.00336	-6.50986	0.00336	-6.71625
0.00341	-6.69014	0.00341	-6.76485	0.00341	-7.08424
0.00347	-7.00099	0.00347	-7.09416	0.00347	-7.39929

Table S5.8: Temperature dependence of $k_2/M^{-1}s^{-1}$, for the displacement of the aqua ligands in PtC2 by the nucleophiles at 60-fold at pH = 2.0, *I* = 0.1 M $NaClO_4$

TU		DMTU		TMTU	
1/T (K^{-1})	ln(k_{obs}/T)	1/T (K^{-1})	ln(k_{obs}/T)	1/T (K^{-1})	ln(k_{obs}/T)
0.00325	-6.35449	0.00325	-6.67358	0.00325	-7.37117
0.00330	-6.5635	0.00330	-6.9020	0.00330	-7.61058
0.00336	-6.82819	0.00336	-7.12701	0.00336	-7.88858
0.00341	-7.10562	0.00341	-7.39446	0.00341	-8.21252
0.00347	-7.43243	0.00347	-7.79678	0.00347	-8.45753

Table S5.9: Temperature dependence of k_2/$M^{-1}s^{-1}$, for the displacement of the aqua ligands in PtC3 by the nucleophiles at 180-fold at pH = 2.0, *I* = 0.1 M $NaClO_4$

TU		DMTU		TMTU	
1/T (K^{-1})	ln(k_{obs}/T)	1/T (K^{-1})	ln(k_{obs}/T)	1/T (K^{-1})	ln(k_{obs}/T)
0.00325	-4.70833	0.00325	-4.77858	0.00325	-4.98388
0.00330	-4.94389	0.00330	-5.01423	0.00330	-5.34314
0.00336	-5.19389	0.00336	-5.32079	0.00336	-5.65308
0.00341	-5.47569	0.00341	-5.56605	0.00341	-6.07657
0.00347	-5.78287	0.00347	-5.85662	5.56605	-6.42359

Table S5.10: Temperature dependence of k_2/$M^{-1}s^{-1}$, for the displacement of the aqua ligands in PtC4 by the nucleophiles at 180-fold at pH = 2.0, *I* = 0.1 M $NaClO_4$

TU		DMTU		TMTU	
1/T (K^{-1})	ln(k_{obs}/T)	1/T (K^{-1})	ln(k_{obs}/T)	1/T (K^{-1})	ln(k_{obs}/T)
0.00325	-5.24131	0.00325	-5.48643	0.00319	-6.35375
0.00330	-5.47217	0.00330	-5.65473	0.00325	-6.65710
0.00336	-5.72534	0.00336	-5.86147	0.00330	-6.90964
0.00341	-5.97951	0.00341	-6.07195	0.00336	-7.24638
0.00347	-6.29505	0.00347	-6.29417	0.00341	-7.57911

Table S5.11: Temperature dependence of k_2/$M^{-1}s^{-1}$, for the displacement of the aqua ligands in PtC5 by the nucleophiles at 180-fold at pH = 2.0, *I* = 0.1 M $NaClO_4$

TU		DMTU		TMTU	
1/T (K^{-1})	ln(k_{obs}/T)	1/T (K^{-1})	ln(k_{obs}/T)	1/T (K^{-1})	ln(k_{obs}/T)
0.00325	-4.43696	0.00325	-4.71093	0.00325	-5.44462
0.00330	-4.68599	0.00330	-4.93210	0.00330	-5.74217
0.00336	-4.94180	0.00336	-5.23332	0.00336	-6.10551
0.00341	-5.22304	0.00341	-5.56580	0.00341	-6.48275
0.00347	-5.49608	0.00347	-5.87408	0.00347	-6.82595

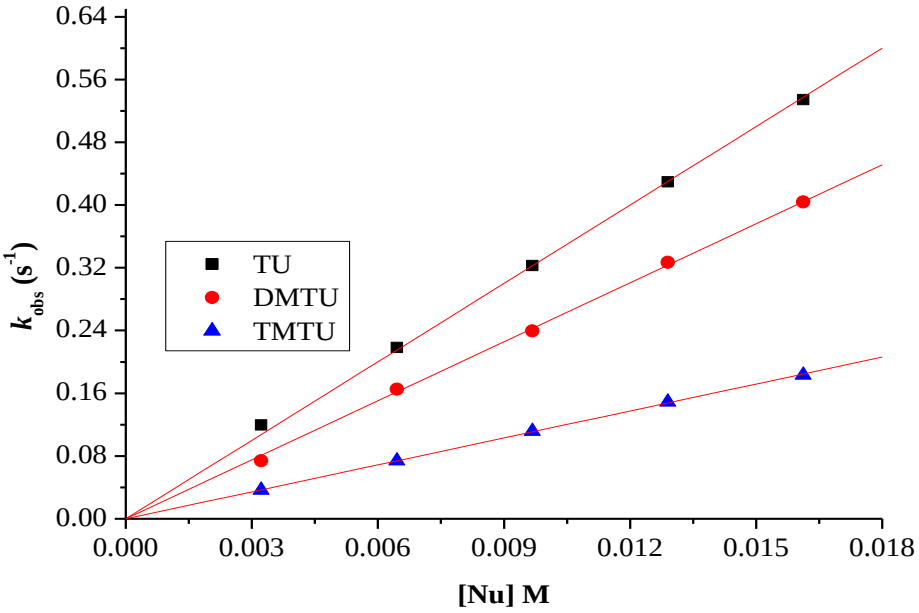

Figure S5.1: Dependence of the *pseudo* first-order rate constants (k_{obs}) on the concentrations of the nucleophiles for the aqua substitution for PtC2 in $NaClO_4$ (I = 0.1 M) at 298 K.

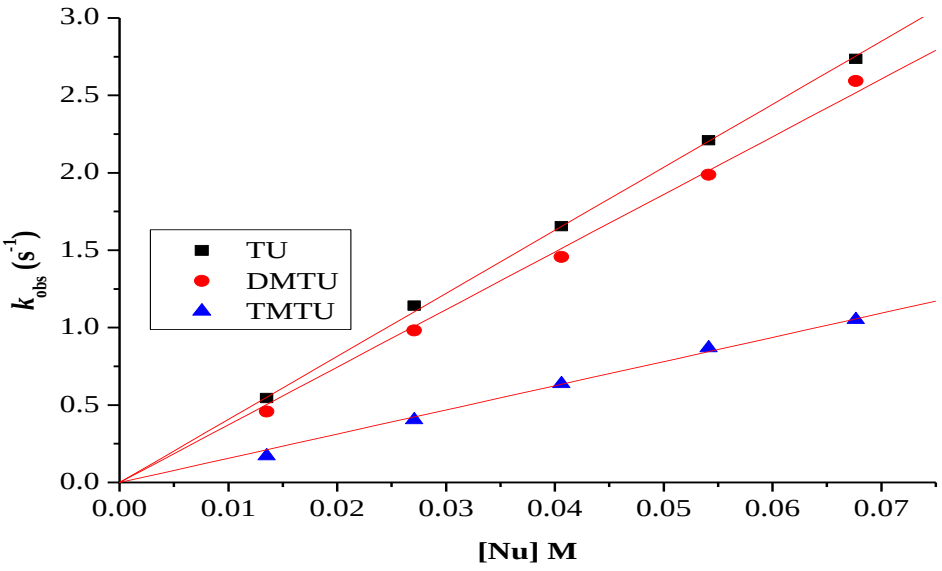

Figure S5.2: Dependence of the *pseudo* first-order rate constants (k_{obs}) on the concentrations of the nucleophiles for the aqua substitution for PtC3 in $NaClO_4$ (I = 0.1 M) at 298 K.

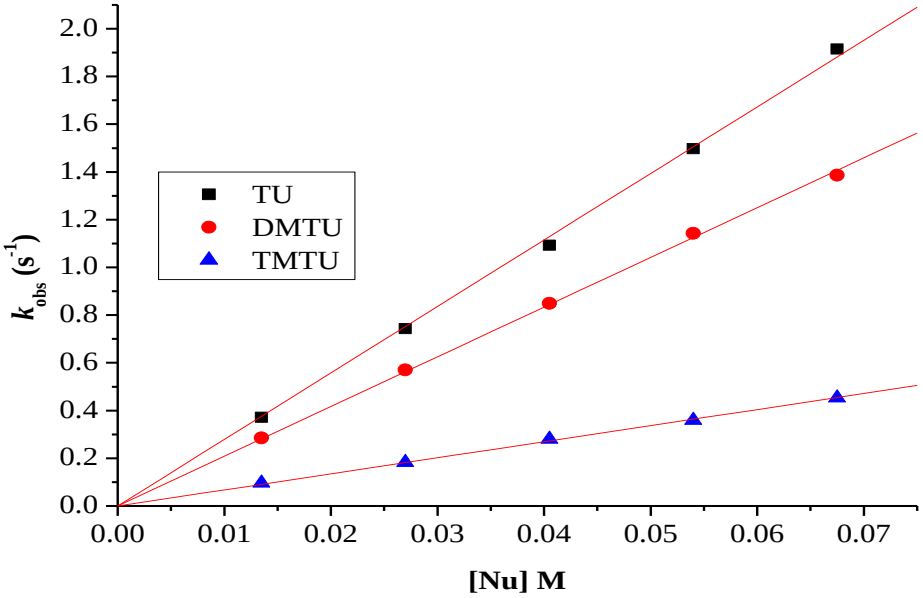

Figure S5.3: Dependence of the *pseudo* first-order rate constants (k_{obs}) on the concentrations of the nucleophiles for the aqua substitution for PtC4 in $NaClO_4$ (I = 0.1 M) at 298 K.

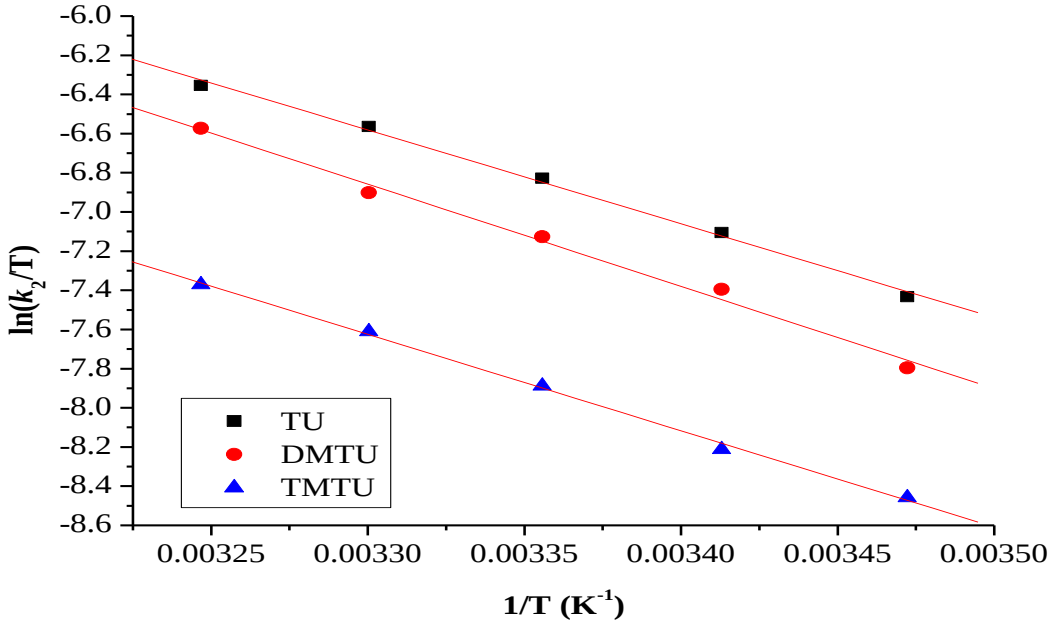

Figure S5.4: Eyring plots obtained for PtC2 with the nucleophiles for the substitution reactions over the temperature range 288 – 308 K in $NaClO_4$ (I = 0.1 M).

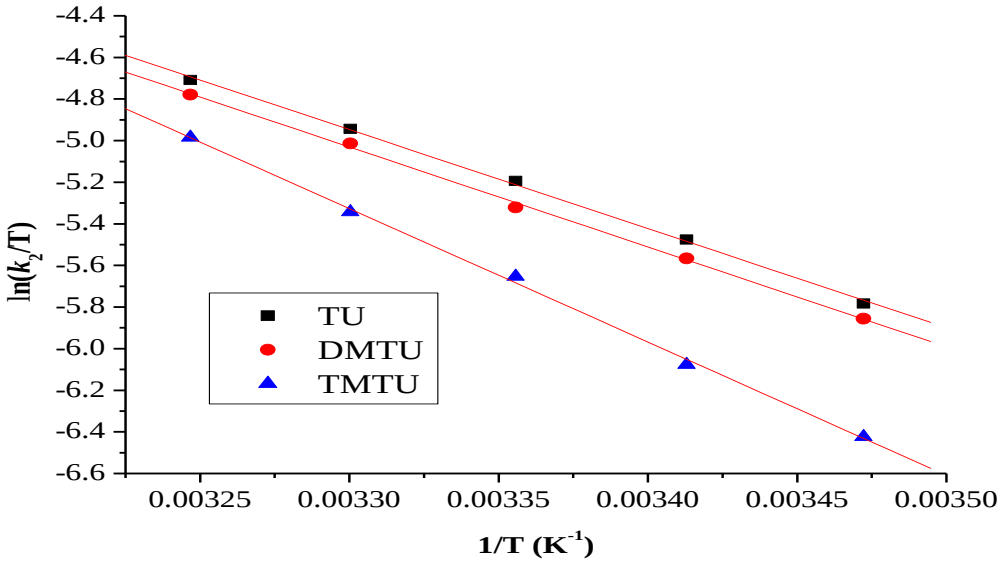

Figure S5.5: Eyring plots obtained for PtC3 with the nucleophiles for the substitution reactions over the temperature range 288 – 308 *K* in $NaClO_4$ (*I* = 0.1 M).

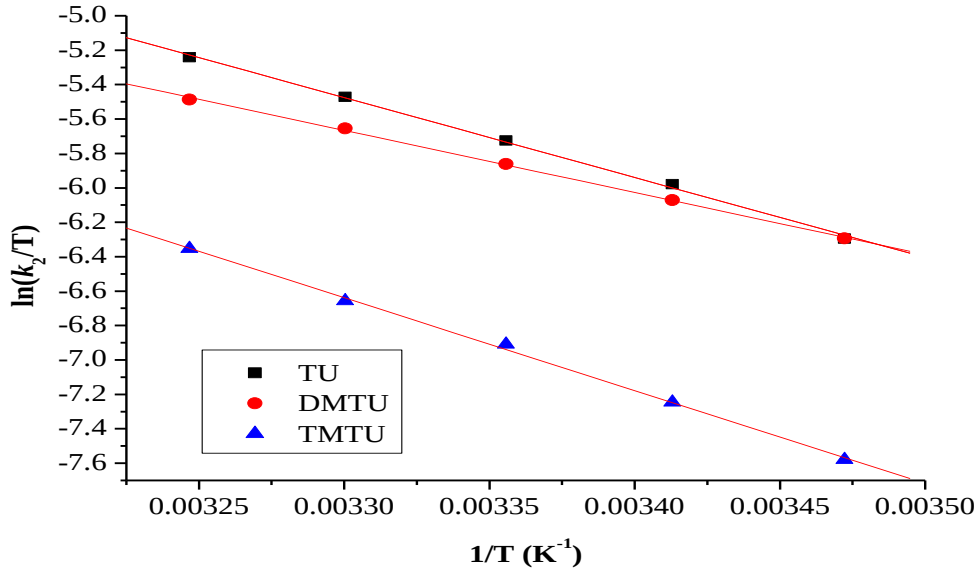

Figure S5.6: Eyring plots obtained for PtC4 with the nucleophiles for the substitution reactions over the temperature range 288 – 308 *K* in $NaClO_4$ (*I* = 0.1 M).

.

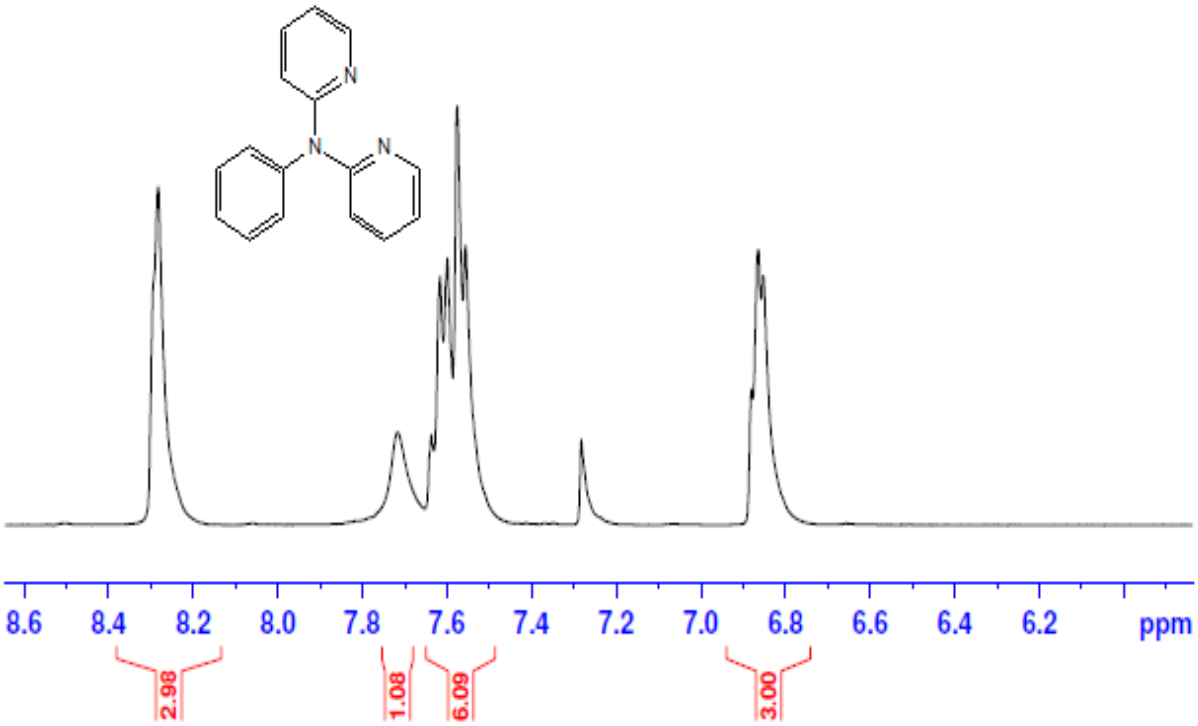

Figure S5.7 ^{1}**H NMR spectrum for Di-2-pyridylaminobenzene in** $CDCl_3$

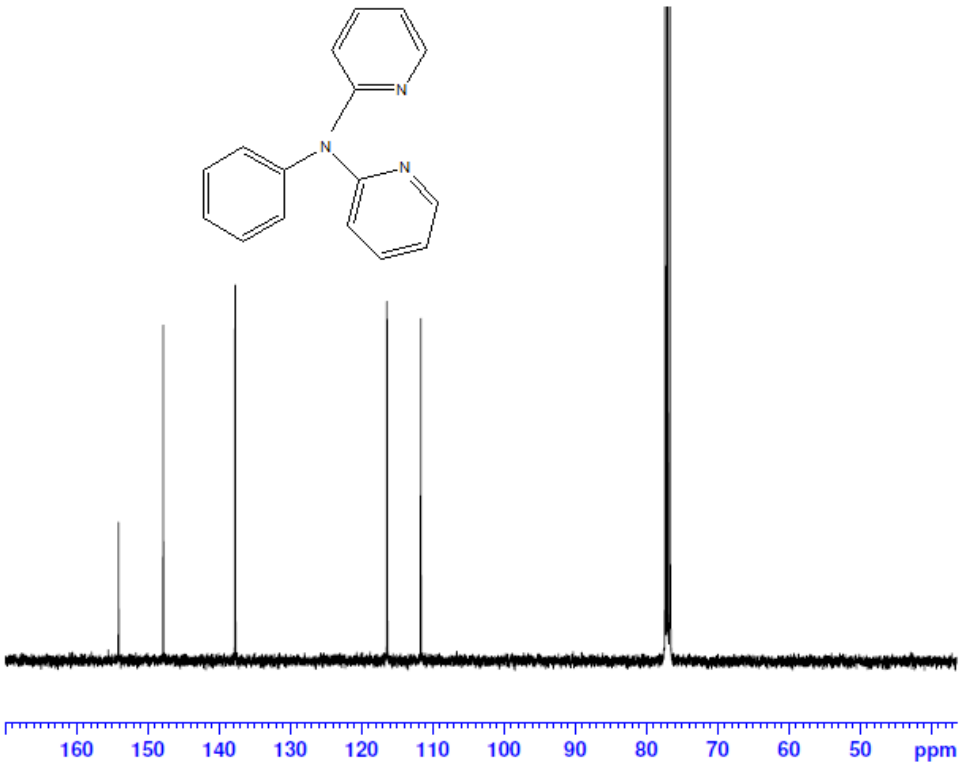

Figure S5.8 ^{13}**C NMR spectrum for Di-2-pyridylaminobenzene in** $CDCl_3$

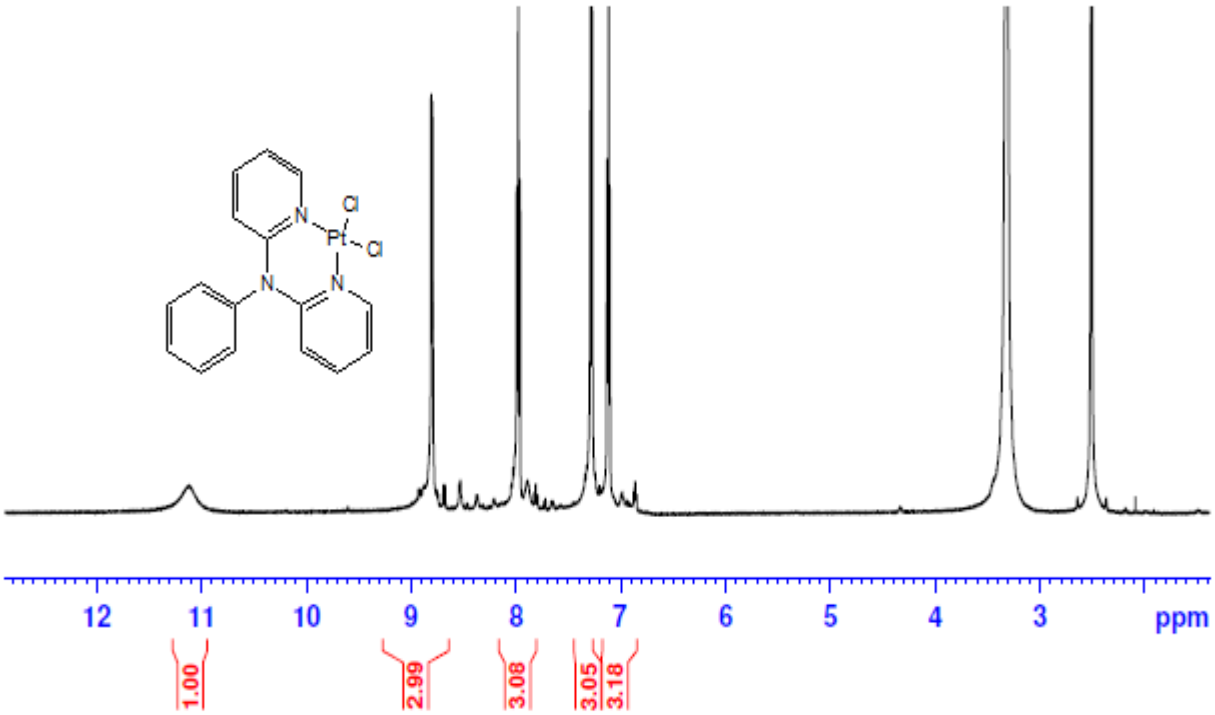

Figure S5.9: **^{1}H NMR spectrum for PtC1 in DMSO-d_6**

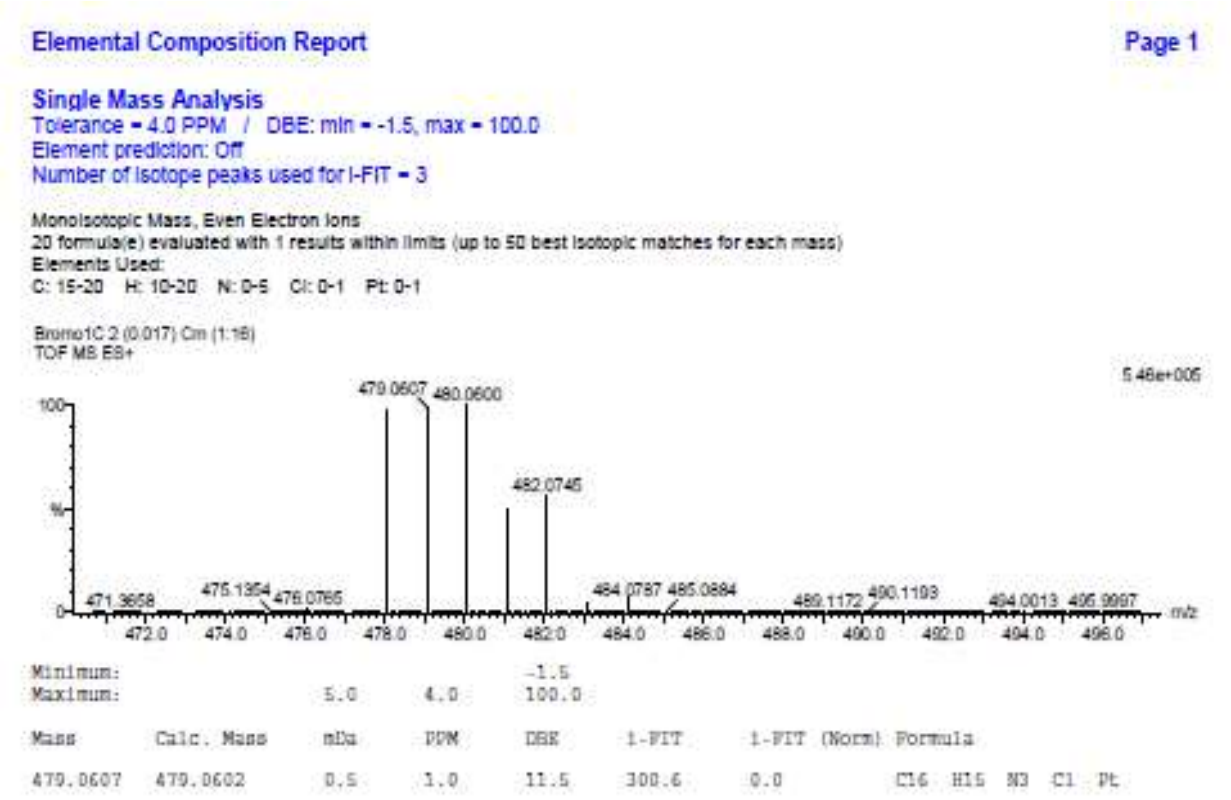

Figure S5.10: **TOF ESI mass spectrum of PtC1**

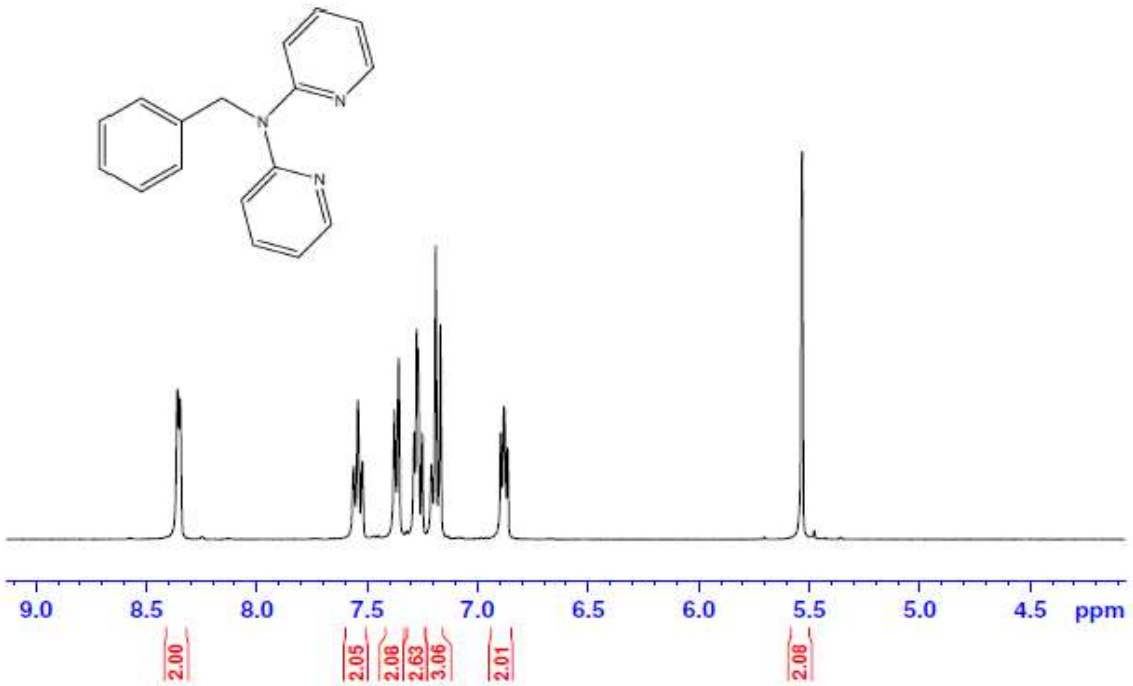

Figure S5.11 **^{1}H NMR spectrum for di-2-pyridylaminomethylbenzene in $CDCl_3$**

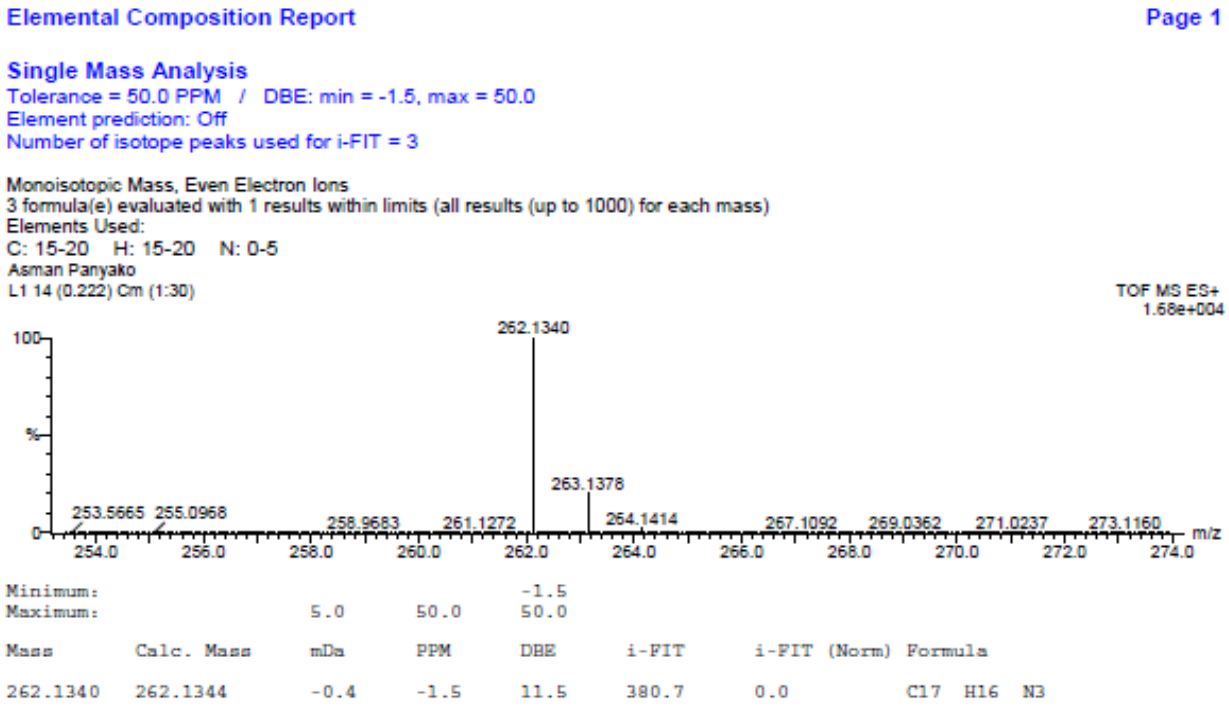

Figure S5.12: **TOF ESI mass spectrum of di-2-pyridylaminomethylbenzene**

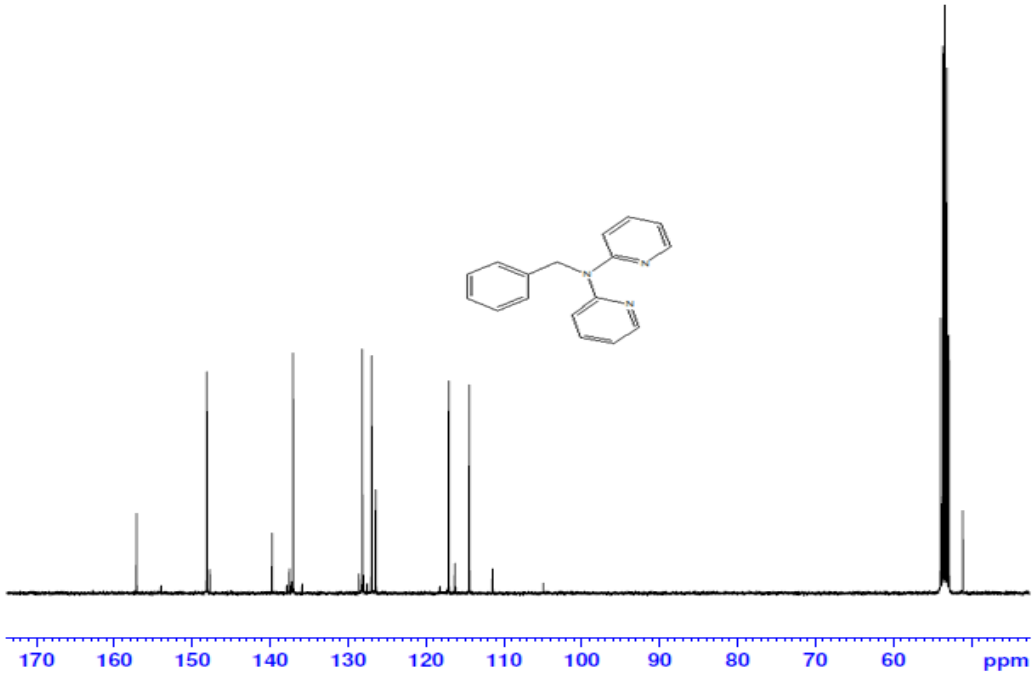

Figure S5.13: **^{13}C NMR spectrum of di-2-pyridylaminomethylbenzene in $CDCl_3$**

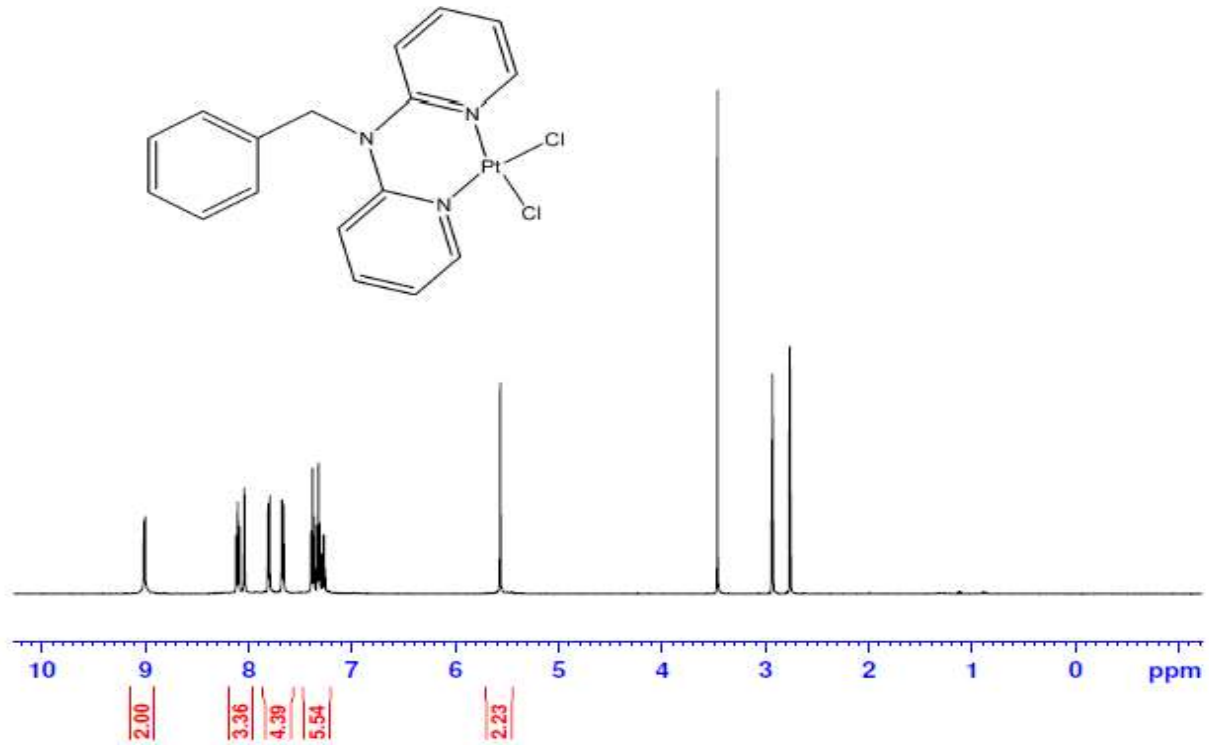

Figure S5.14: **^{1}H NMR spectrum of PtC2 in DMF-d_7.**

Elemental Composition Report **Page 1**

Single Mass Analysis
Tolerance = 5.0 PPM / DBE: min = -1.5, max = 50.0
Element prediction: Off
Number of isotope peaks used for i-FIT = 3

Monoisotopic Mass, Odd and Even Electron Ions
25 formula(e) evaluated with 1 results within limits (all results (up to 1000) for each mass)
Elements Used:
C: 15-20 H: 15-20 N: 0-5 Na: 1-1 Cl: 0-2 Pt: 0-1

Asman Panyako
CL1 26 (0.444) Cm (1:29)

TOF MS ES+
4.56e+003

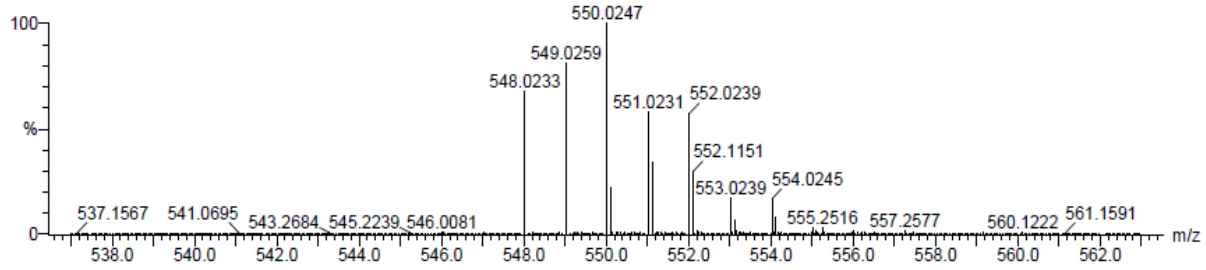

Minimum:				-1.5			
Maximum:		5.0	5.0	50.0			
Mass	Calc. Mass	mDa	PPM	DBE	i-FIT	i-FIT (Norm)	Formula
550.0247	550.0267	-2.0	-3.6	11.0	376.5	0.0	C17 H16 N3 Na Cl2 Pt

Figure S5.15: **TOF ESI mass spectrum of PtC2**

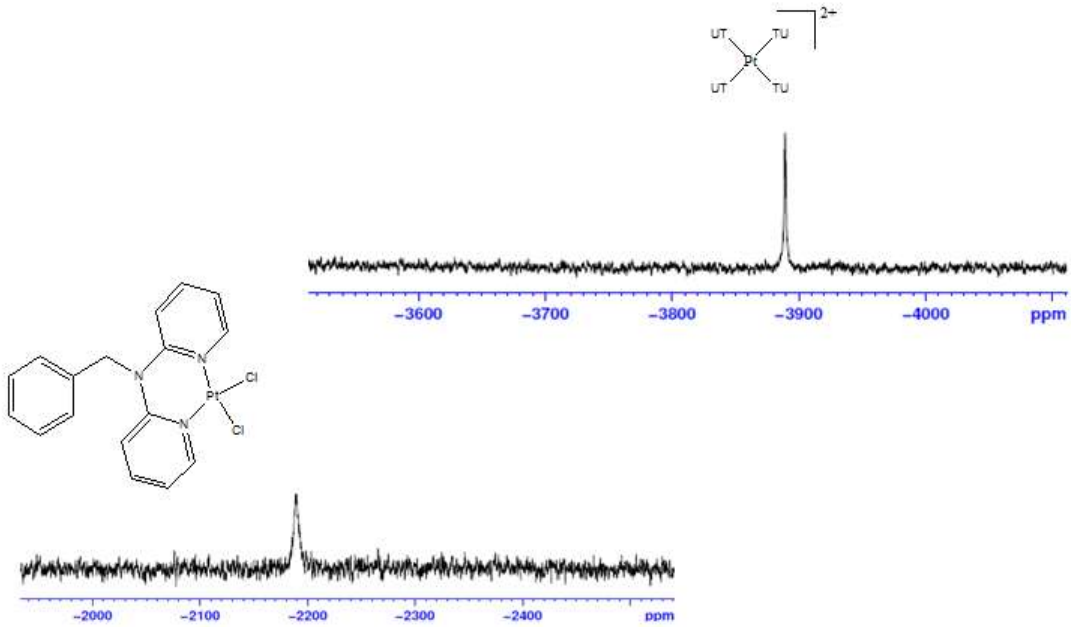

Figure S5.16: **^{195}Pt NMR spectrum of PtC2 in DMSO-d_6 showing the shifting of the peak from -2189.2 ppm to -3889.2 ppm**

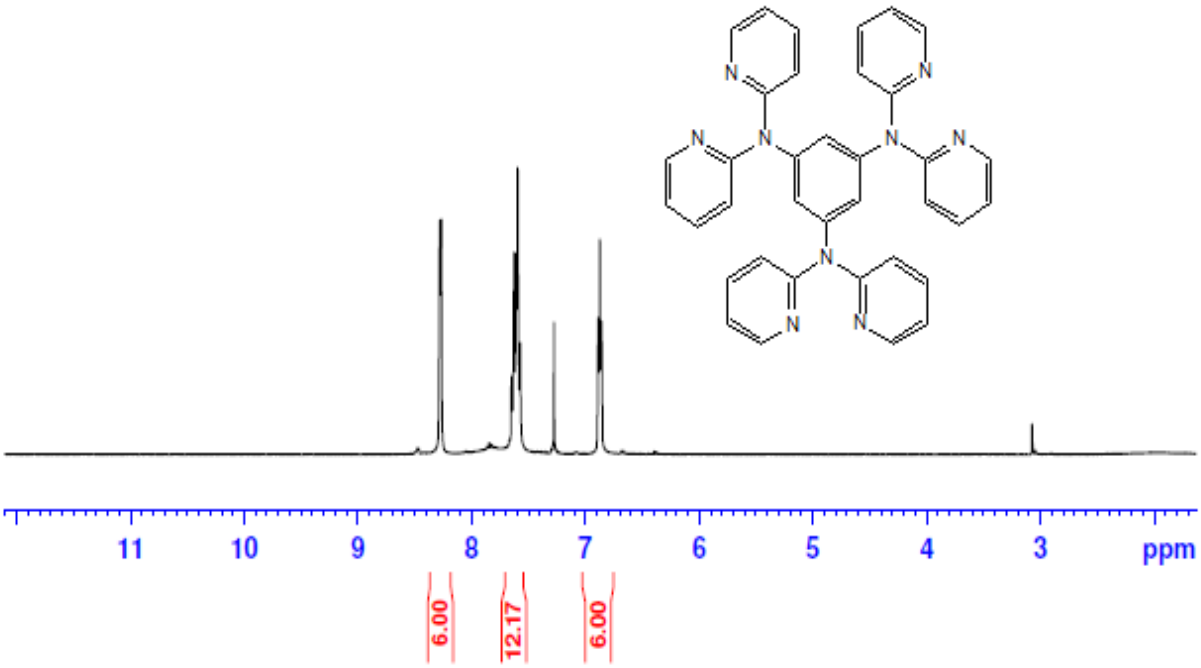

Figure S5.17: **^{1}H NMR spectrum of 1,3,5-tris(di-2-pyridylamino)benzene (tdab) in $CDCl_3$**

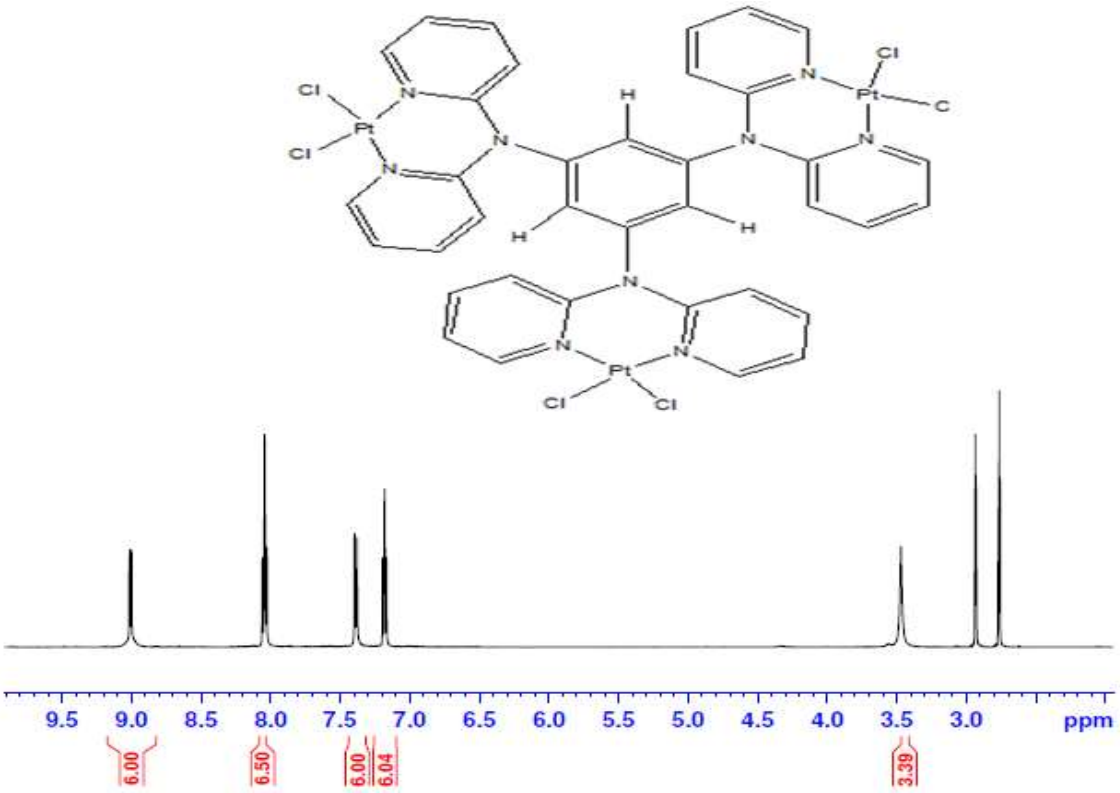

Figure S5.18: **^{1}H NMR spectrum for PtC3 in DMF-d_7**

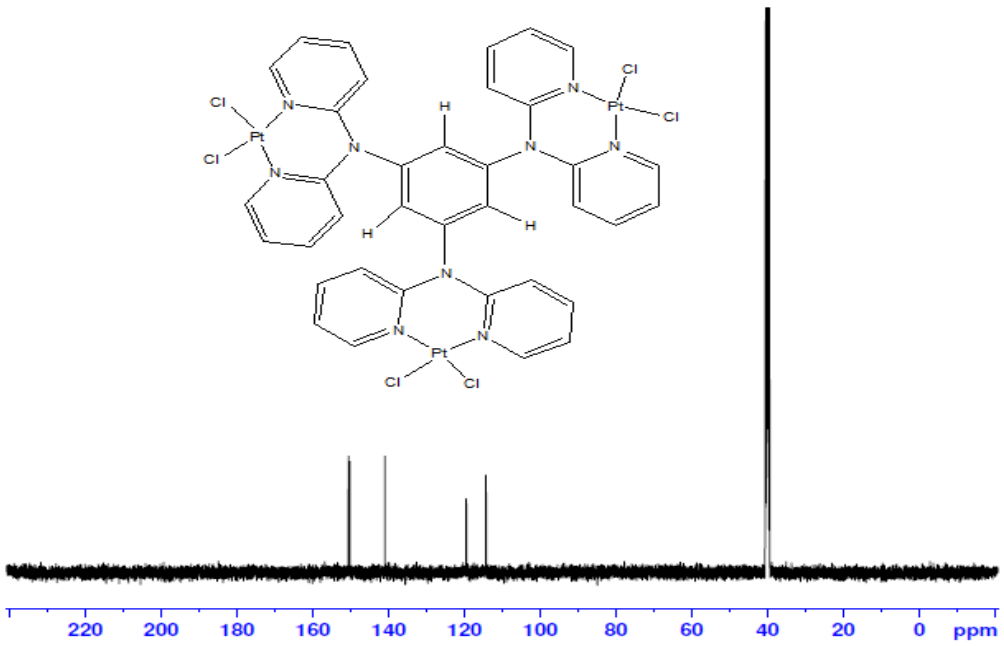

Figure S5.19: **^{13}C NMR spectrum of PtC3 in DMF-d_7**

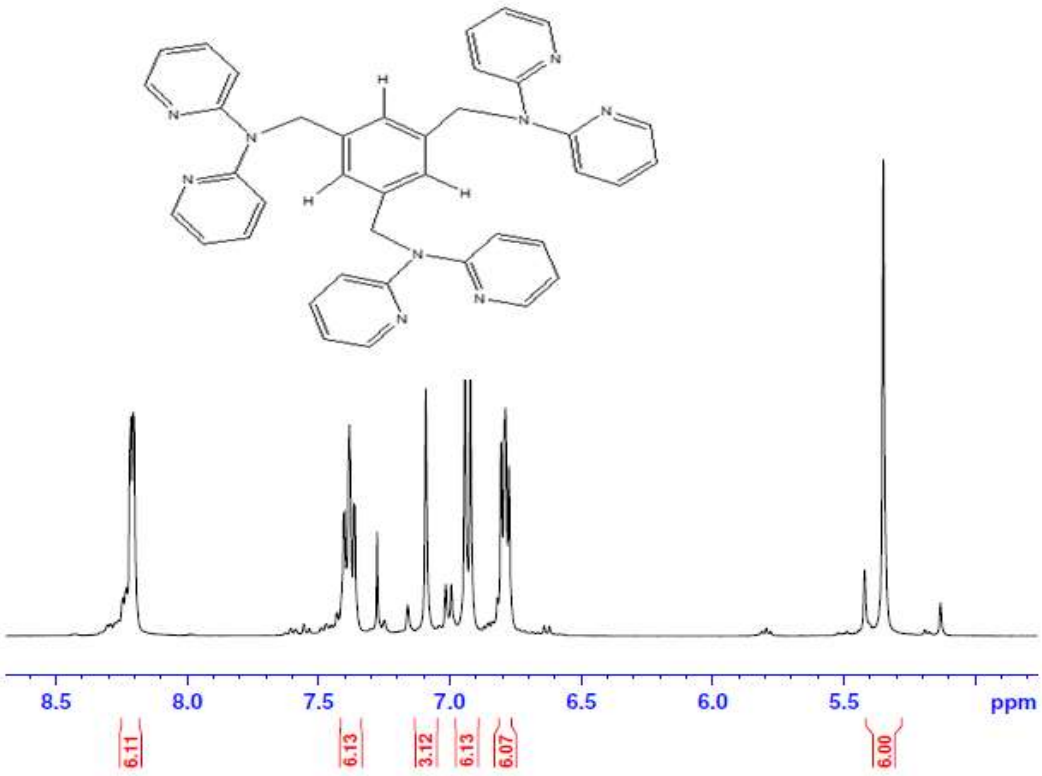

Figure S5.20: **^{1}H NMR spectrum of 1,3,5-tris(di-2-pyridylaminomethyl)benzene in $CDCl_3$**

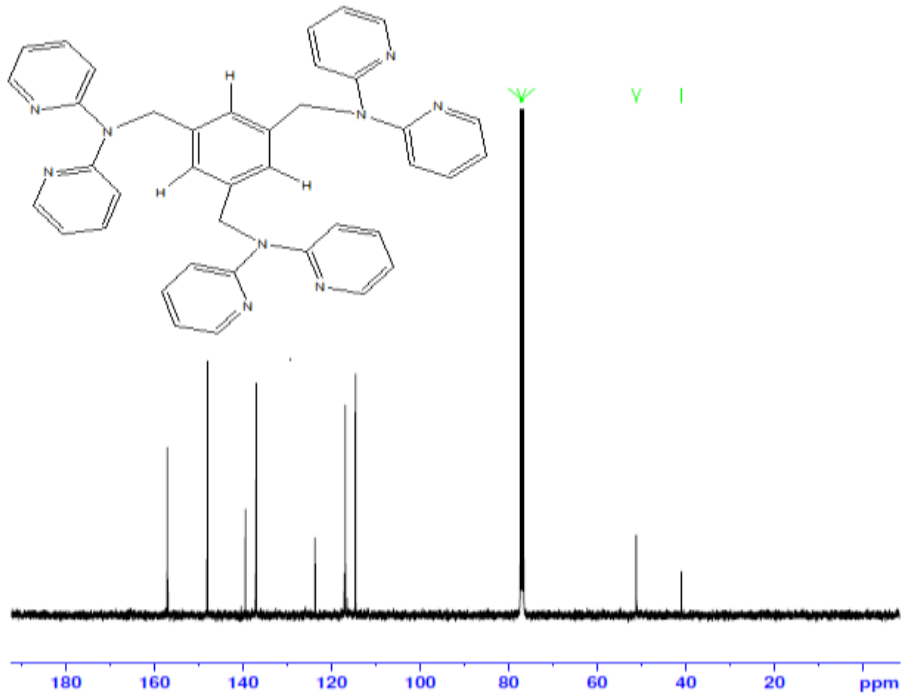

Figure S5.21: **^{13}C NMR spectrum of 1,3,5-tris(di-2-pyridylaminomethyl)benzene in $CDCl_3$**

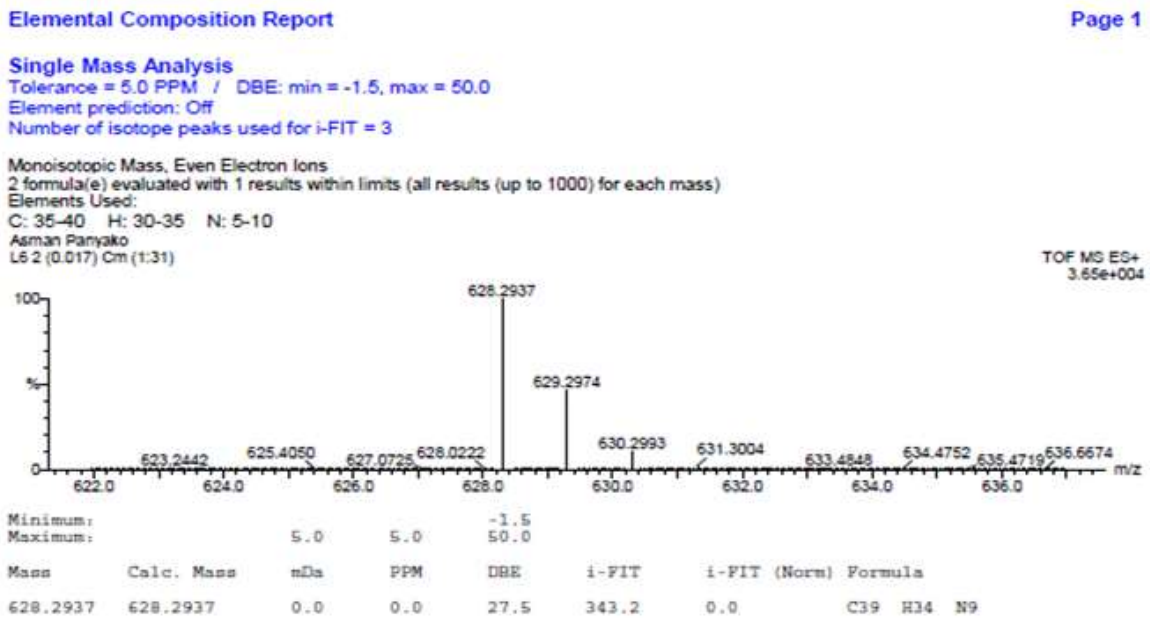

Figure S5.22: **TOF ESI mass spectrum of 1,3,5-tris(di-2-pyridylaminomethyl)benzene in $CDCl_3$**

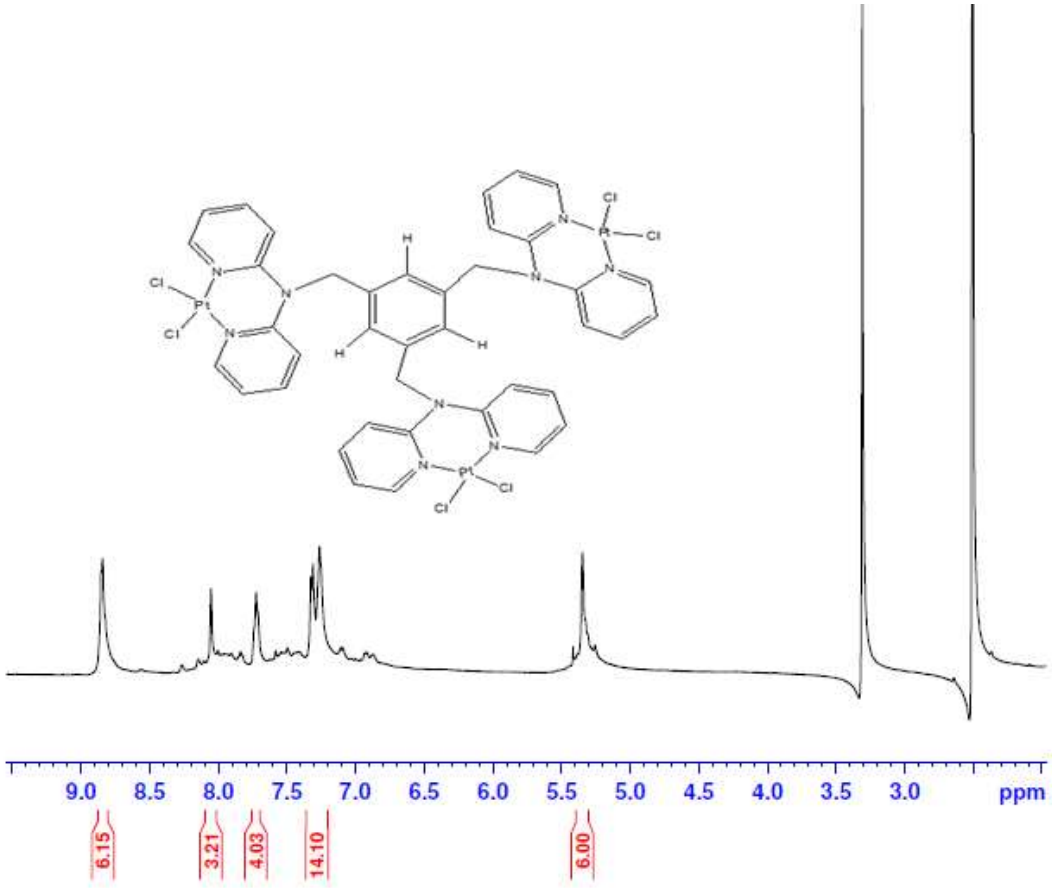

Figure S5.23: **^{1}H NMR spectrum of PtC4 in DMSO-d_6.**

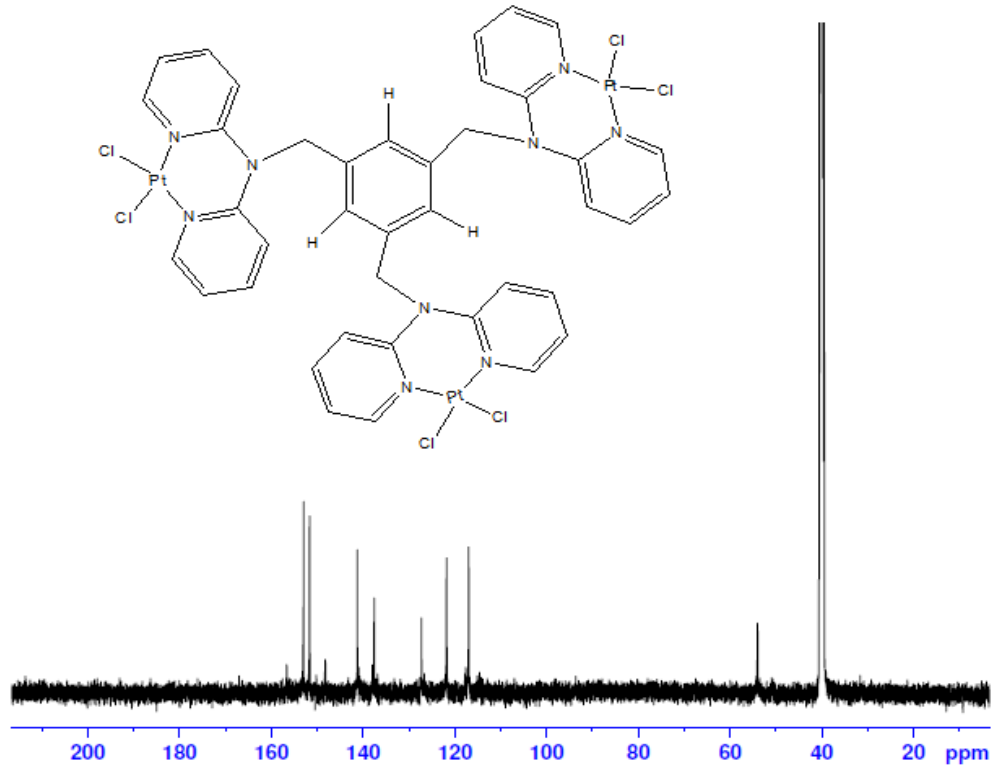

Figure S5.24: **^{13}C NMR of PtC4 in DMSO-d_6**

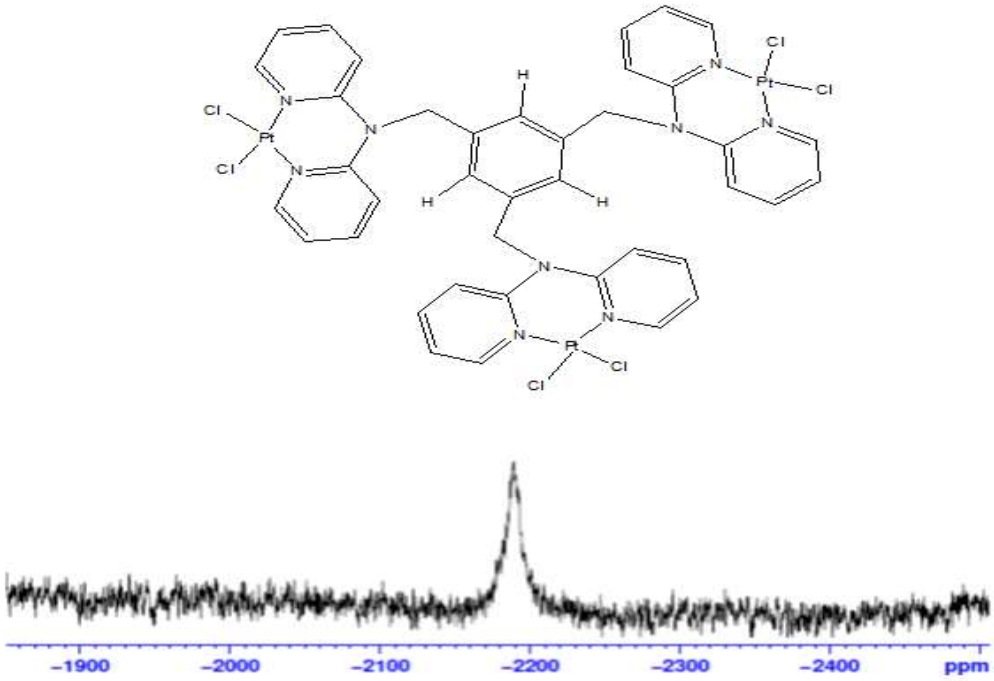

Figure S5.25: **^{195}Pt NMR spectrum of PtC4 (*inset*) in DMSO-d_6. The single peak confirms that all the three Pt(dpa)$_2$ are chemically equivalent**

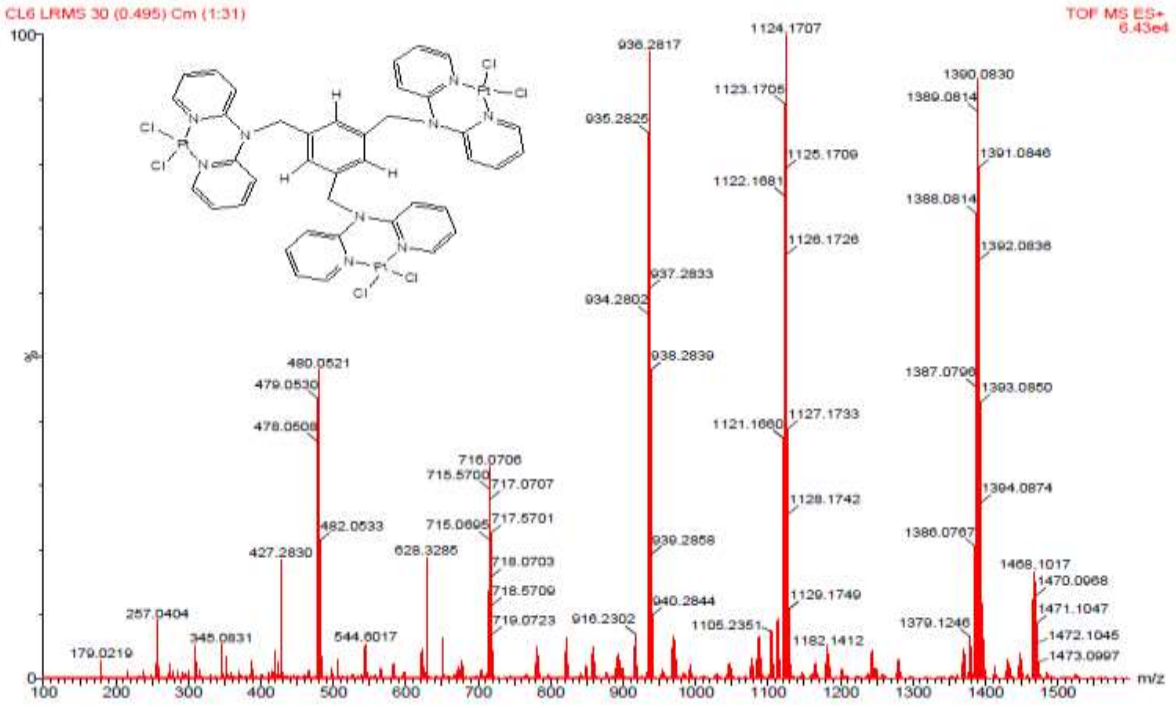

Figure S5.26: **TOF ESI mass spectrum of PtC4.**

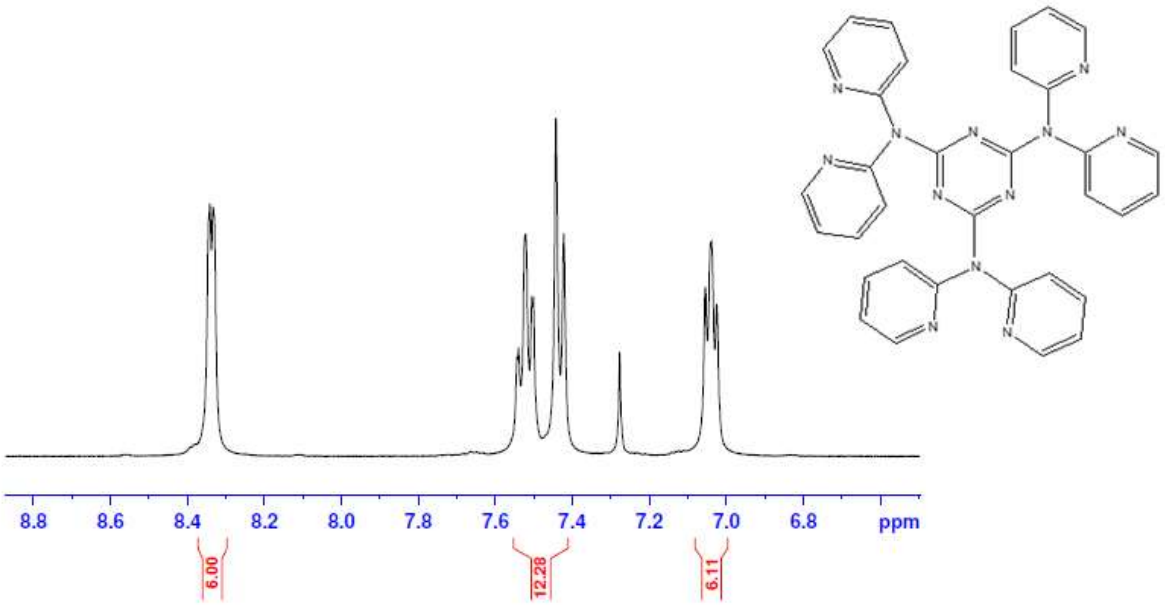

Figure S5.27: **^{1}H NMR spectrum of 2,4,6-tris(dipyridin-2-ylamino)–[1,3,5]-triazine (tdat),**

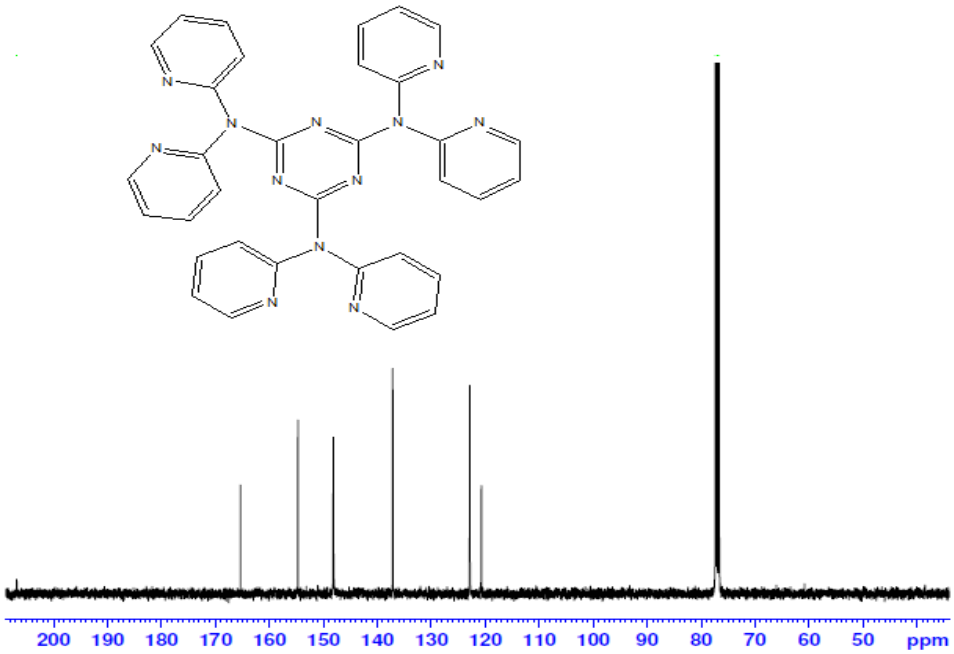

Figure S5.28: **^{13}C NMR spectrum of 2,4,6-tris(dipyridin-2-ylamino)–[1,3,5]-triazine (tdat),**

Elemental Composition Report Page 1

Single Mass Analysis
Tolerance = 4.0 PPM / DBE: min = -1.5, max = 50.0
Element prediction: Off
Number of isotope peaks used for i-FIT = 3

Monoisotopic Mass, Even Electron Ions
5 formula(e) evaluated with 1 results within limits (all results (up to 1000) for each mass)
Elements Used:
C: 30-35 H: 20-25 N: 10-15 Na: 0-1
Asman Panyako
L7 29 (0.478) Cm (1:30)

TOF MS ES+
8.94e+003

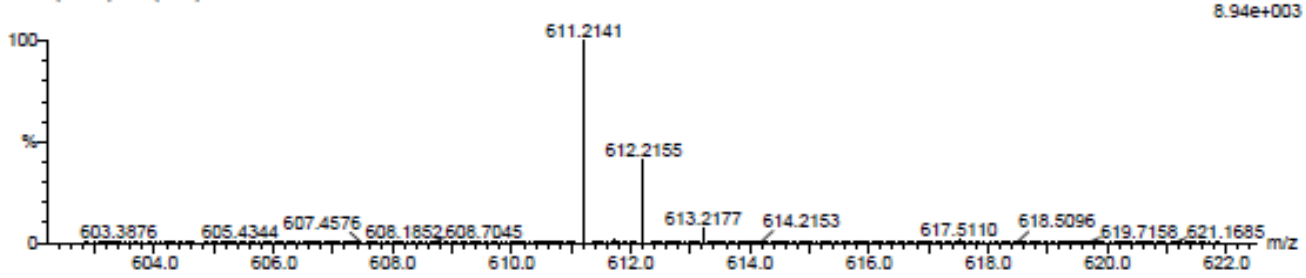

Minimum:				-1.5			
Maximum:		5.0	4.0	50.0			
Mass	Calc. Mass	mDa	PPM	DBE	i-FIT	i-FIT (Norm)	Formula
611.2141	611.2145	-0.4	-0.7	27.5	289.2	0.0	C33 H24 N12 Na

Figure S5.29: **TOF ESI mass spectrum of 2,4,6-tris(dipyridin-2-ylamino)–[1,3,5]-triazine (tdat),**

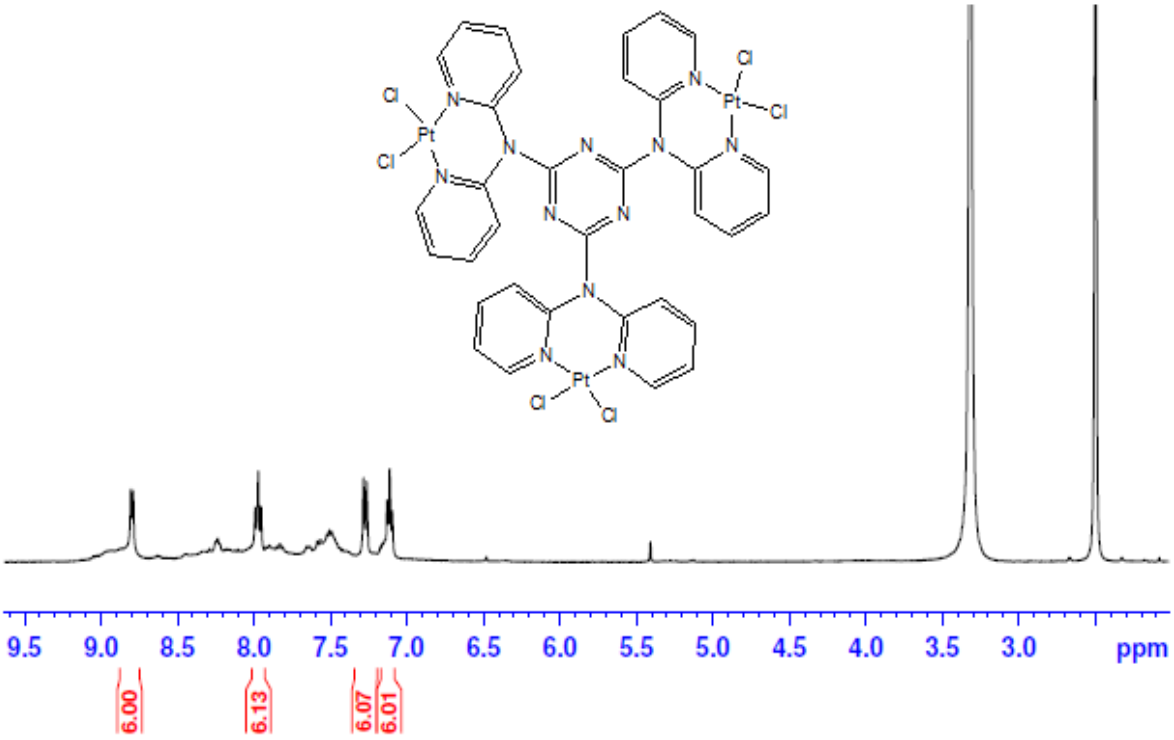

Figure S5.30: **^{1}H NMR spectrum for complex PtC5 in DMSO-d_6**

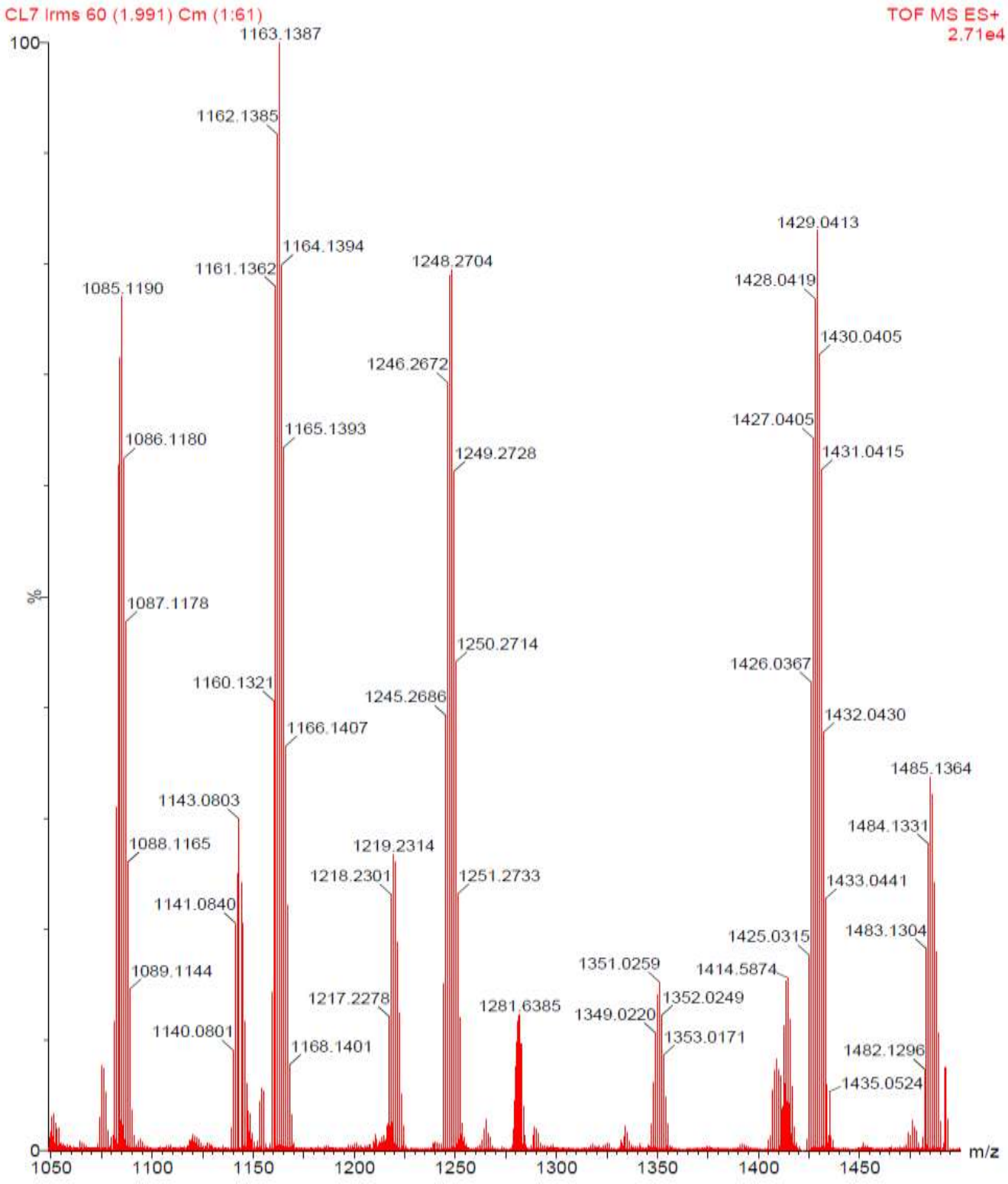

Figure S5.31: TOF ESI mass spectrum of PtC5

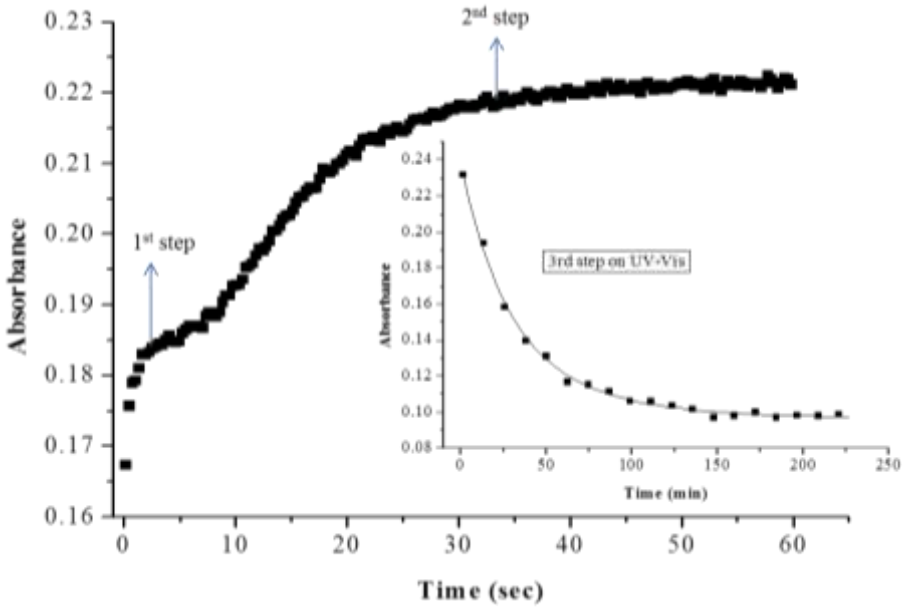

Figure S5.32: **A two-step typical kinetic trace for the reaction between PtC5 and DMTU at *T* = 298 *K*, pH = 2.0, *I* = 0.1 M ($NaClO_4$) on the stopped-flow at 304 nm, *inset* is the 3rd step obtained on UV-Vis spectrophotometer under similar conditions.**

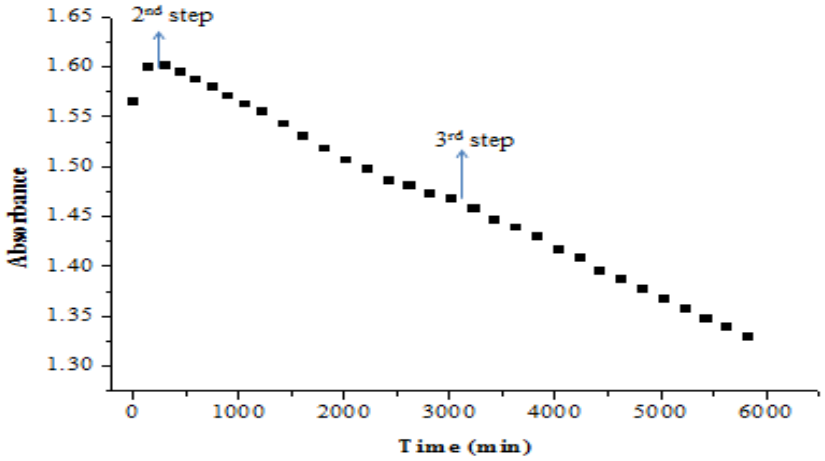

Figure S5.33: **A two-step typical kinetic trace for the reaction between PtC5 and TMTU at *T* = 298 *K*, pH = 2.0, *I* = 0.1 M ($NaClO_4$) on the UV-Vis at 335 nm.**

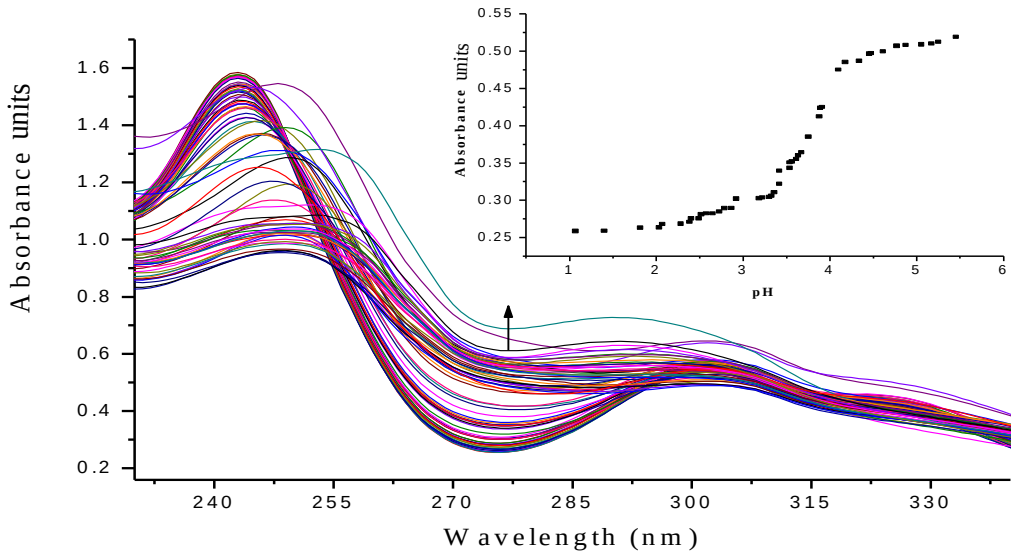

Figure S5.34: **UV-Vis spectral changes for the titration of PtC1 within the pH range of 1 to 9*; Inset* shows the titration curve at λ = 278 nm**

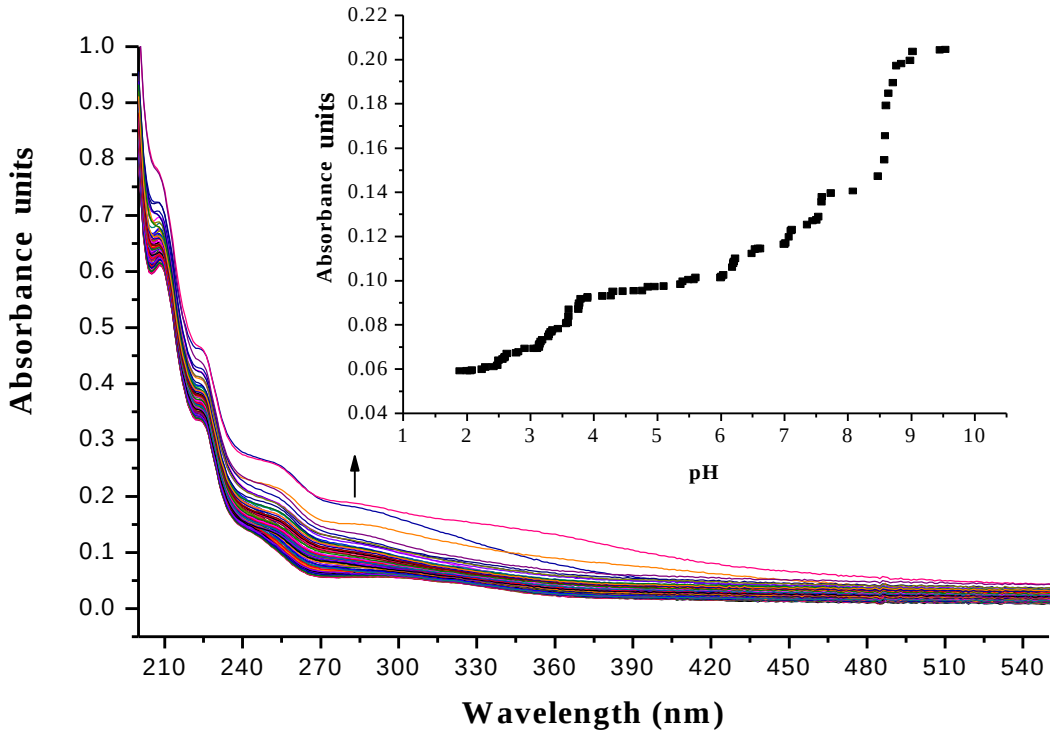

Figure S5.35: **UV-Vis spectral changes for the titration of PtC4 within the pH range of 1 to 10*; Inset* shows the titration curve at λ = 285 nm**

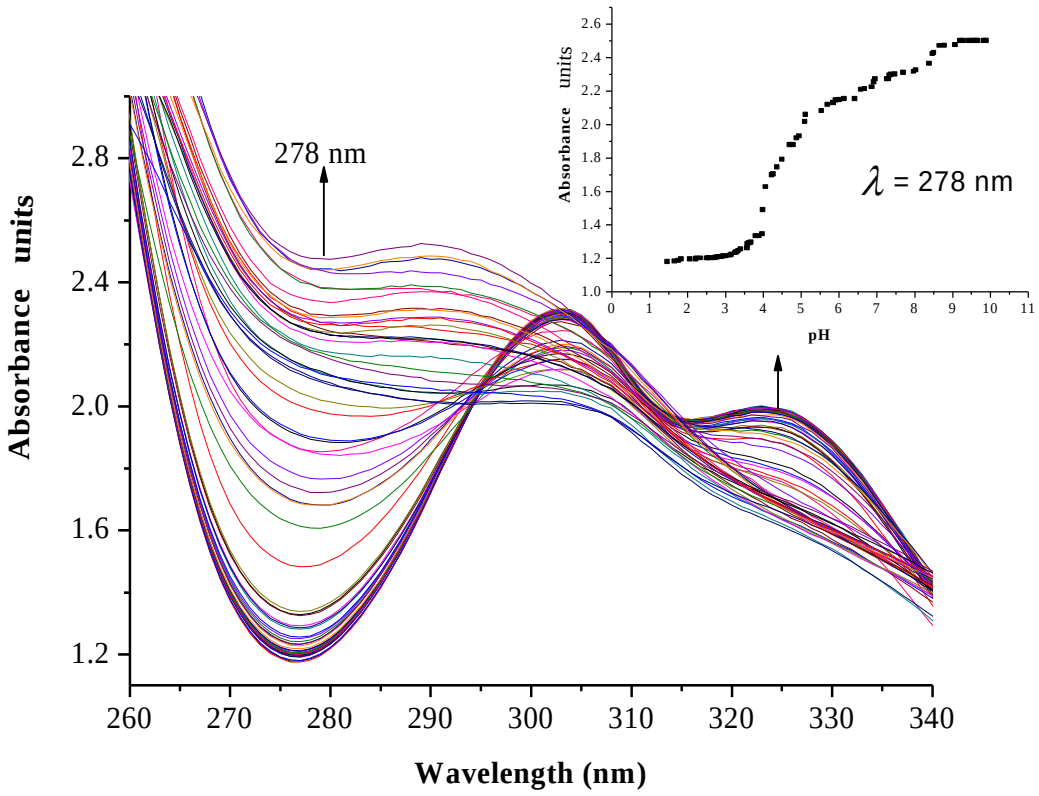

Figure S5.36: **UV-Vis spectral changes for the titration of PtC3 within the pH range of 1 to 10*; Inset* shows the titration curve at λ = 295 nm**

APPENDIX 4 (CHAPTER 6)

A summary of wavelengths used for kinetic measurements for the investigated complexes, some of their kinetic traces, k_{obs} for reactions at different concentrations and temperatures and characterization of complexes using ^{1}H NMR, TOF ES^{+} mass spectra, ^{13}C NMR and ^{195}Pt' NMR are given in the following tables.

Table S6.1: Summary of the wavelengths used for monitoring kinetic reactions for **scheme 1**

Complex	Nucleophile	Wavelength (λ) (nm)	
		Stopped-flow	UV-Visible
PtL1	**TU**	300	320
	DMTU	302	320
	TMTU	375	335
PtL2	**TU**	300	320
	DMTU	305	320
	TMTU	375	335
PtL3	**TU**	300	320
	DMTU	302	320
	TMTU	375	335
PtL4	**TU**	300	320
	DMTU	300	320
	TMTU	375	335
PtL5	**TU**	302	320
	DMTU	305	320
	TMTU	375	335

Table S6.2: Average observed rate constants, k_{obs}, s^{-1}, for the displacement of the aqua ligands in PtL1 with the nucleophiles, at pH = 2.0, T = 298 K, I = 0.1 M $NaClO_4$.

TU		**DMTU**		**TMTU**	
Conc., M	k_{obs} (s^{-1})	Conc., M	k_{obs} (s^{-1})	Conc., M	k_{obs} (s^{-1})
0.0675	2.67973	0.0675	2.48418	0.0675	0.48514
0.0540	2.16202	0.0540	1.98643	0.0540	0.38684
0.0405	1.54402	0.0405	1.48605	0.0405	0.29575
0.0270	1.06785	0.0270	0.96797	0.0270	0.19720
0.0135	0.49176	0.0135	0.48640	0.0135	0.09880

Table S6.3: Average observed rate constants, $k_{obs,}$ s^{-1}, for the displacement of the aqua ligands in PtL2 with the nucleophiles, at pH = 2.0, *T* = 298 *K*, *I* = 0.1 M $NaClO_4$.

TU		DMTU		TMTU	
Conc., M	k_{obs} (s^{-1})	Conc., M	k_{obs} (s^{-1})	Conc., M	k_{obs} (s^{-1})
0.0675	2.63923	0.0675	1.41019	0.0675	0.45750
0.0540	2.10068	0.0540	1.12935	0.0540	0.36404
0.0405	1.60625	0.0405	0.85079	0.0405	0.27305
0.0270	1.06166	0.0270	0.55912	0.0270	0.18495
0.0135	0.53292	0.0135	0.26372	0.0135	0.09105

Table S6.4: Average observed rate constants, $k_{obs,}$ s^{-1}, for the displacement of the aqua ligands in PtLL3 with the nucleophiles, at pH = 2.0, *T* = 298 *K*, *I* = 0.1 M $NaClO_4$.

TU		DMTU		TMTU	
Conc., M	k_{obs} (s^{-1})	Conc., M	k_{obs} (s^{-1})	Conc., M	k_{obs} (s^{-1})
0.0675	3.09714	0.0675	2.53003	0.0675	0.47574
0.0540	2.49119	0.0540	2.01663	0.0540	0.37827
0.0405	1.86182	0.0405	1.51655	0.0405	0.28714
0.0270	1.20742	0.0270	1.01172	0.0270	0.18097
0.0135	0.56601	0.0135	0.50499	0.0135	0.08777

Table S6.5: Average observed rate constants, $k_{obs,}$ s^{-1}, for the displacement of the aqua ligands in PtL4 with the nucleophiles, at pH = 2.0, *T* = 298 *K*, *I* = 0.1 M $NaClO_4$.

TU		DMTU		TMTU	
Conc., M	k_{obs} (s^{-1})	Conc., M	k_{obs} (s^{-1})	Conc., M	k_{obs} (s^{-1})
0.0675	3.39515	0.0675	2.43465	0.0675	0.49803
0.0540	2.60958	0.0540	1.94851	0.0540	0.40097
0.0405	2.00460	0.0405	1.43893	0.0405	0.29753
0.0270	1.26471	0.0270	0.95692	0.0270	0.19854
0.0135	0.48379	0.0135	0.45531	0.0135	0.09706

Table S6.6: Average observed rate constants, $k_{obs,}$ s^{-1}, for the displacement of the aqua ligands in PtL5 with the nucleophiles, at pH = 2.0, *T* = 298 *K*, *I* = 0.1 M $NaClO_4$.

TU		DMTU		TMTU	
Conc., M	k_{obs} (s^{-1})	Conc., M	k_{obs} (s^{-1})	Conc., M	k_{obs} (s^{-1})
0.0675	5.66781	0.0675	3.09459	0.0675	0.69696
0.0540	4.45017	0.0540	2.45073	0.0540	0.57570
0.0405	3.40003	0.0405	1.85136	0.0405	0.42805
0.0270	2.27112	0.0270	1.21153	0.0270	0.27314
0.0135	1.10509	0.0135	0.55964	0.0135	0.14751

Table S6.7: Temperature dependence of $k_2/M^{-1}s^{-1}$, for the displacement of the aqua ligands in PtL1 by the nucleophiles at 120-fold at pH = 2.0, *I* = 0.1 M $NaClO_4$

TU		DMTU		TMTU	
1/T (K^{-1})	ln(k_{obs}/T)	1/T (K^{-1})	ln(k_{obs}/T)	1/T (K^{-1})	ln(k_{obs}/T)
0.00325	-4.67291	0.00325	-4.58488	0.00325	-6.43877
0.00330	-4.91720	0.00330	-4.93993	0.00330	-6.65682
0.00336	-5.23083	0.00336	-5.30097	0.00336	-6.91533
0.00341	-5.51940	0.00341	-5.68669	0.00341	-7.12580
0.00347	-5.82144	0.00347	-6.09050	0.00347	-7.39401

Table S6.8: Temperature dependence of $k_2/M^{-1}s^{-1}$, for the displacement of the aqua ligands in PtL2 by the nucleophiles at 120-fold at pH = 2.0, *I* = 0.1 M $NaClO_4$

TU		DMTU		TMTU	
1/T (K^{-1})	ln(k_{obs}/T)	1/T (K^{-1})	ln(k_{obs}/T)	1/T (K^{-1})	ln(k_{obs}/T)
0.00325	-4.71467	0.00325	-5.08651	0.00325	-6.38768
0.00330	-4.97888	0.00330	-5.45175	0.00330	-6.64648
0.00336	-5.22319	0.00336	-5.85868	0.00336	-6.99519
0.00341	-5.49678	0.00341	-6.24438	0.00341	-7.29036
0.00347	-5.80912	0.00347	-6.64819	0.00347	-7.61813

Table S6.9: Temperature dependence of k_2/M^{-1}s^{-1}, for the displacement of the aqua ligands in PtL3 by the nucleophiles at 120-fold at pH = 2.0, *I* = 0.1 M NaClO$_4$

TU		DMTU		TMTU	
1/T (K^{-1})	ln(k_{obs}/T)	1/T (K^{-1})	ln(k_{obs}/T)	1/T (K^{-1})	ln(k_{obs}/T)
0.00325	-4.60811	0.00325	-4.48960	0.00325	-6.39080
0.00330	-4.82566	0.00330	-4.88036	0.00330	-6.66192
0.00336	-5.07554	0.00336	-5.28066	0.00336	-6.94488
0.00341	-5.31735	0.00341	-5.72450	0.00341	-7.26712
0.00347	-5.58562	0.00347	-6.14094	0.00347	-7.61503

Table S6.10: Temperature dependence of k_2/M^{-1}s^{-1}, for the displacement of the aqua ligands in PtL4 by the nucleophiles at 120-fold at pH = 2.0, *I* = 0.1 M NaClO$_4$

TU		DMTU		TMTU	
1/T (K^{-1})	ln(k_{obs}/T)	1/T (K^{-1})	ln(k_{obs}/T)	1/T (K^{-1})	ln(k_{obs}/T)
0.00325	-4.39478	0.00325	-4.62300	0.00325	-6.54239
0.00330	-4.68385	0.00330	-4.97514	0.00330	-6.85840
0.00336	-5.00165	0.00336	-5.33319	0.00336	-7.15510
0.00341	-5.32640	0.00341	-5.71814	0.00341	-7.49840
0.00347	-5.67204	0.00347	-6.10660	0.00347	-7.79920

Table S6.11: Temperature dependence of k_2/M^{-1}s^{-1}, for the displacement of the aqua ligands in PtL5 by the nucleophiles at 120-fold at pH = 2.0, *I* = 0.1 M NaClO$_4$

TU		DMTU		TMTU	
1/T (K^{-1})	ln(k_{obs}/T)	1/T (K^{-1})	ln(k_{obs}/T)	1/T (K^{-1})	ln(k_{obs}/T)
0.00325	-3.86670	0.00325	-4.37474	0.00325	-5.90663
0.00330	-4.14967	0.00330	-4.73060	0.00330	-6.20423
0.00336	-4.47331	0.00336	-5.08117	0.00336	-6.54561
0.00341	-4.78416	0.00341	-5.44686	0.00341	-6.89627
0.00347	-5.11337	0.00347	-5.81899	0.00347	-7.28161

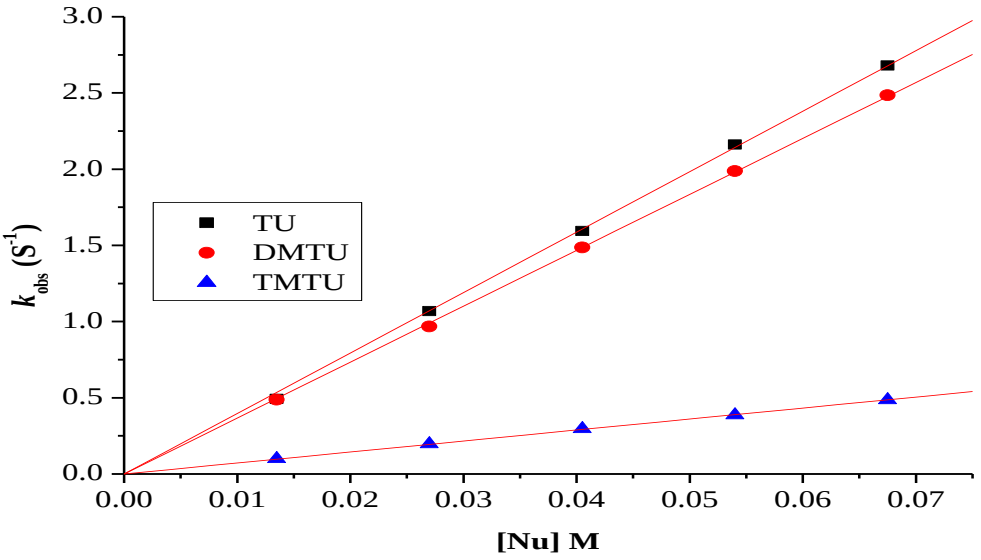

Figure S6.1: **Dependence of the *pseudo* first-order rate constants (k_{obs}) on the concentrations of the nucleophiles for the aqua substitution of PtL1 in $NaClO_4$ (I = 0.1 M) at 298 K.**

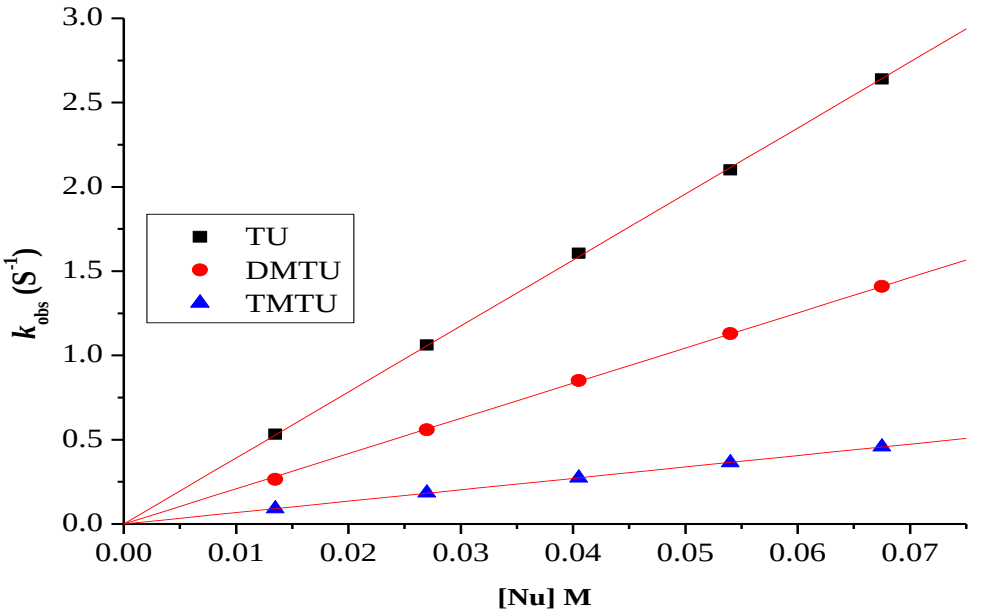

Figure S6.2: **Dependence of the *pseudo* first-order rate constants (k_{obs}) on the concentrations of the nucleophiles for the aqua substitution of PtL2 in $NaClO_4$ (I = 0.1 M) at 298 K.**

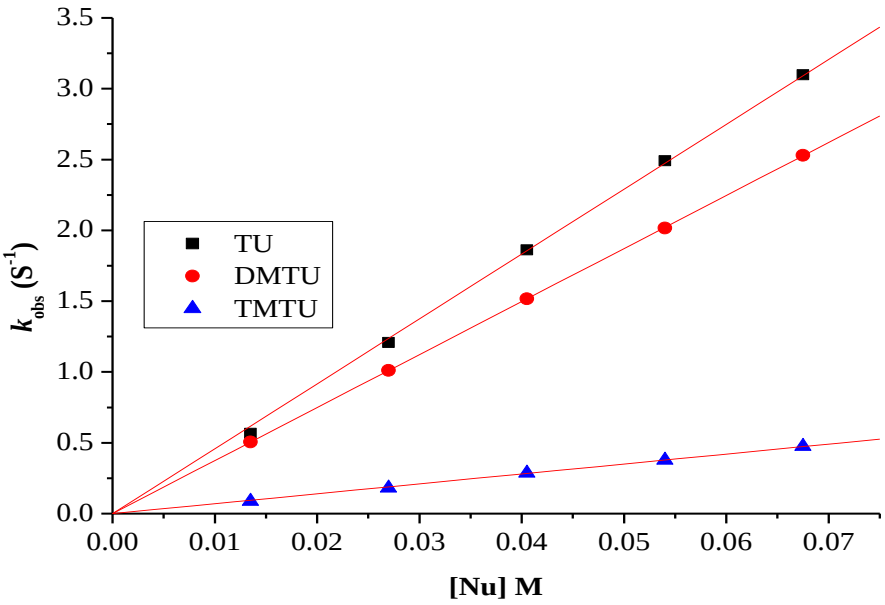

Figure S6.3: **Dependence of the *pseudo* first-order rate constants (k_{obs}) on the concentrations of the nucleophiles for the aqua substitution of PtL3 in $NaClO_4$ (I = 0.1 M) at 298 K.**

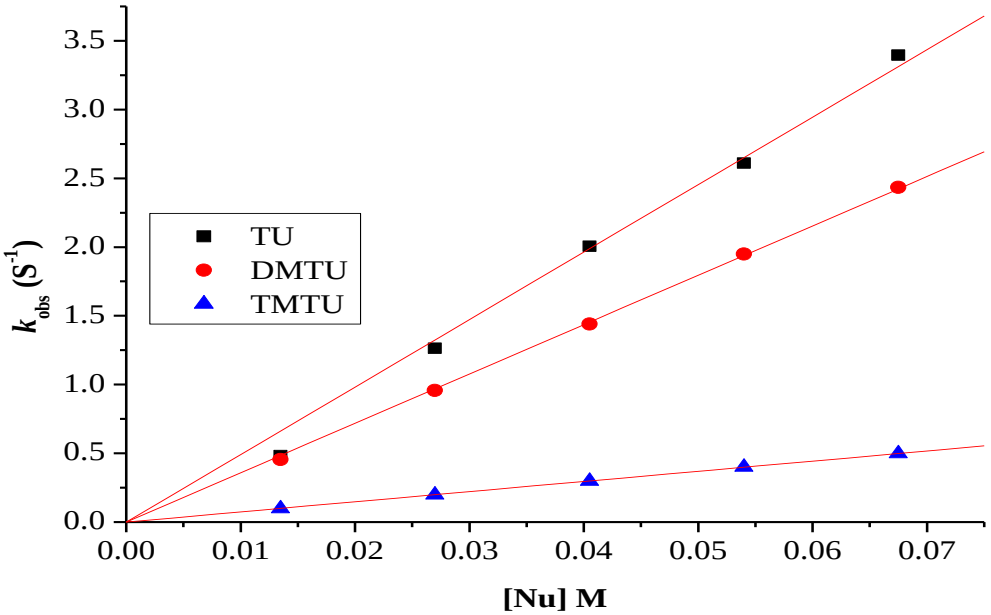

Figure S6.4: **Dependence of the *pseudo* first-order rate constants (k_{obs}) on the concentrations of the nucleophiles for the aqua substitution of PtL4 in $NaClO_4$ (I = 0.1 M) at 298 K.**

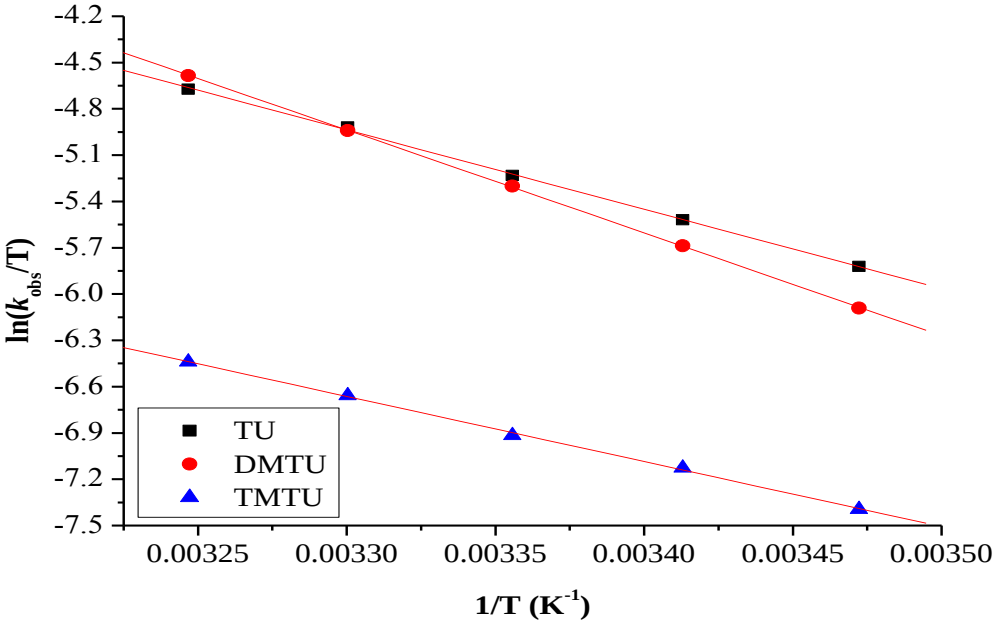

Figure S6.5: **Eyring plots obtained for PtL1 with the nucleophiles for the substitution reactions over the temperature range 288 – 308 *K* in $NaClO_4$ (*I* = 0.1 M).**

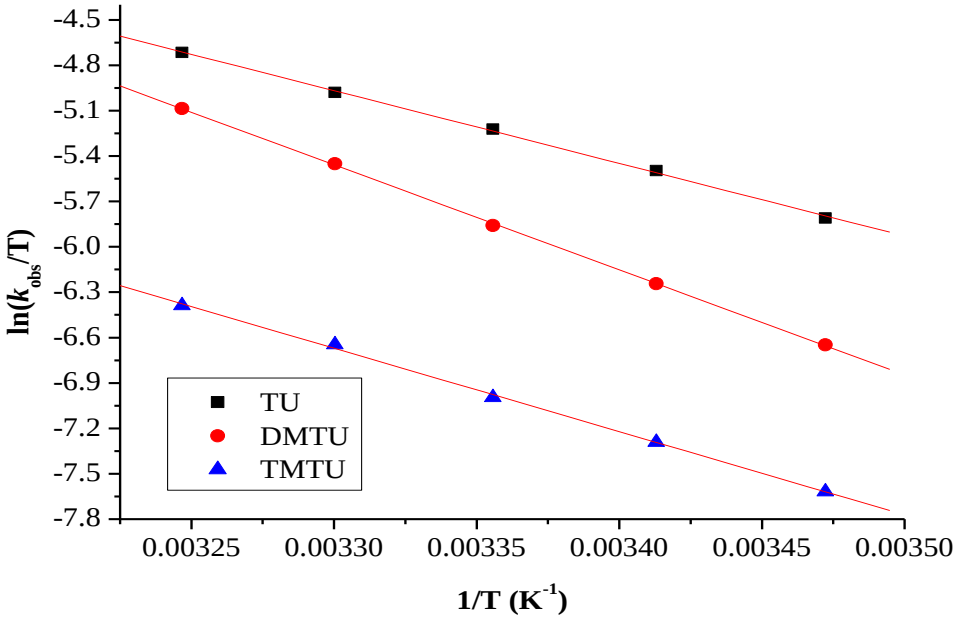

Figure S6.6: **Eyring plots obtained for PtL2 with the nucleophiles for the substitution reactions over the temperature range 288 – 308 *K* in $NaClO_4$ (*I* = 0.1 M).**

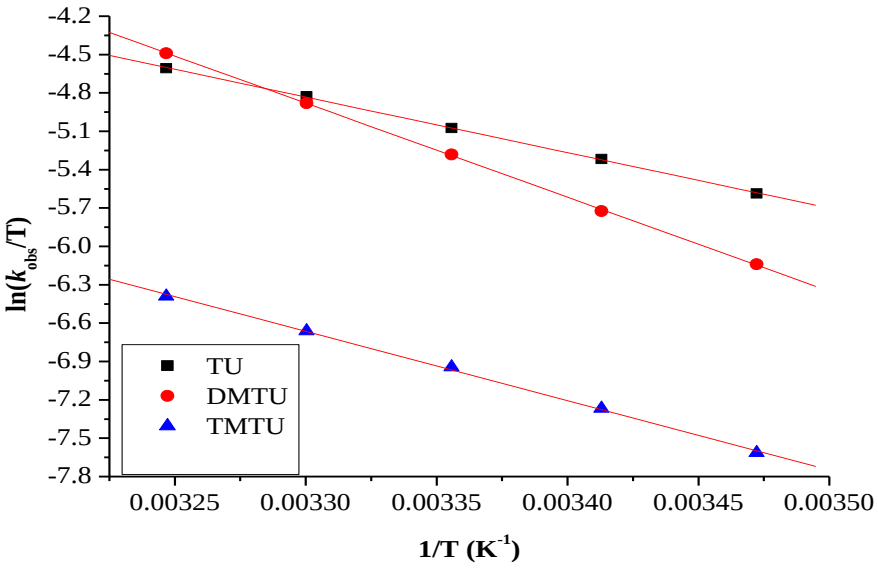

Figure S6.7: **Eyring plots obtained for PtL3 with the nucleophiles for the substitution reactions over the temperature range 288 – 308 *K* in $NaClO_4$ (*I* = 0.1 M).**

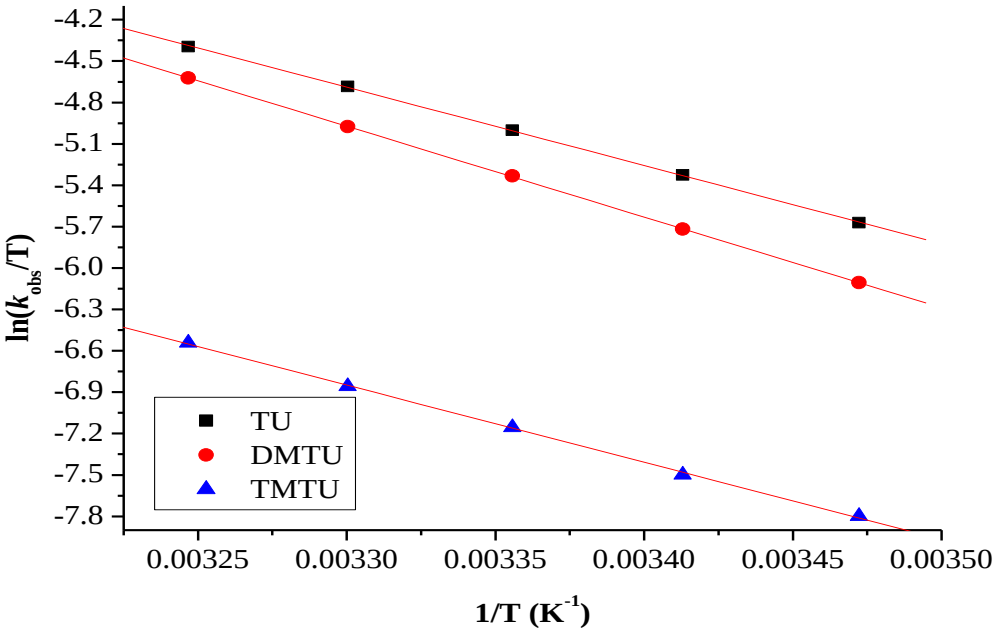

Figure S6.8: **Eyring plots obtained for PtL4 with the nucleophiles for the substitution reactions over the temperature range 288 – 308 *K* in $NaClO_4$ (*I* = 0.1 M).**

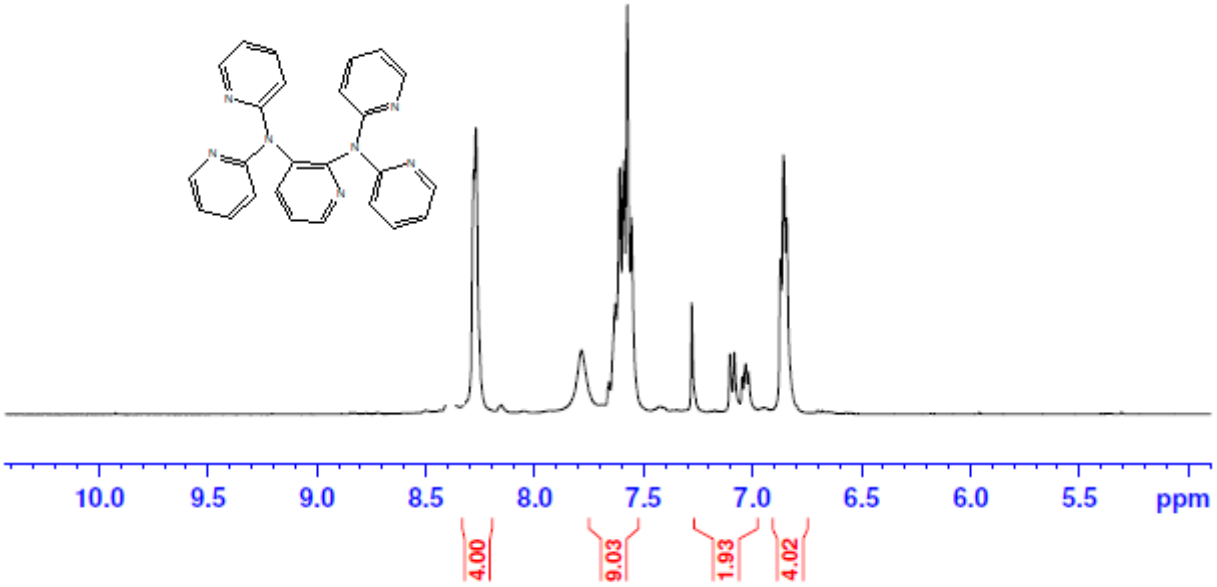

Figure S6.9: **^{1}H NMR spectrum of *N,N,N',N'*-tetrakis(2-pyridyl)-2,3-pyridinediamine (2,3-tppda)**

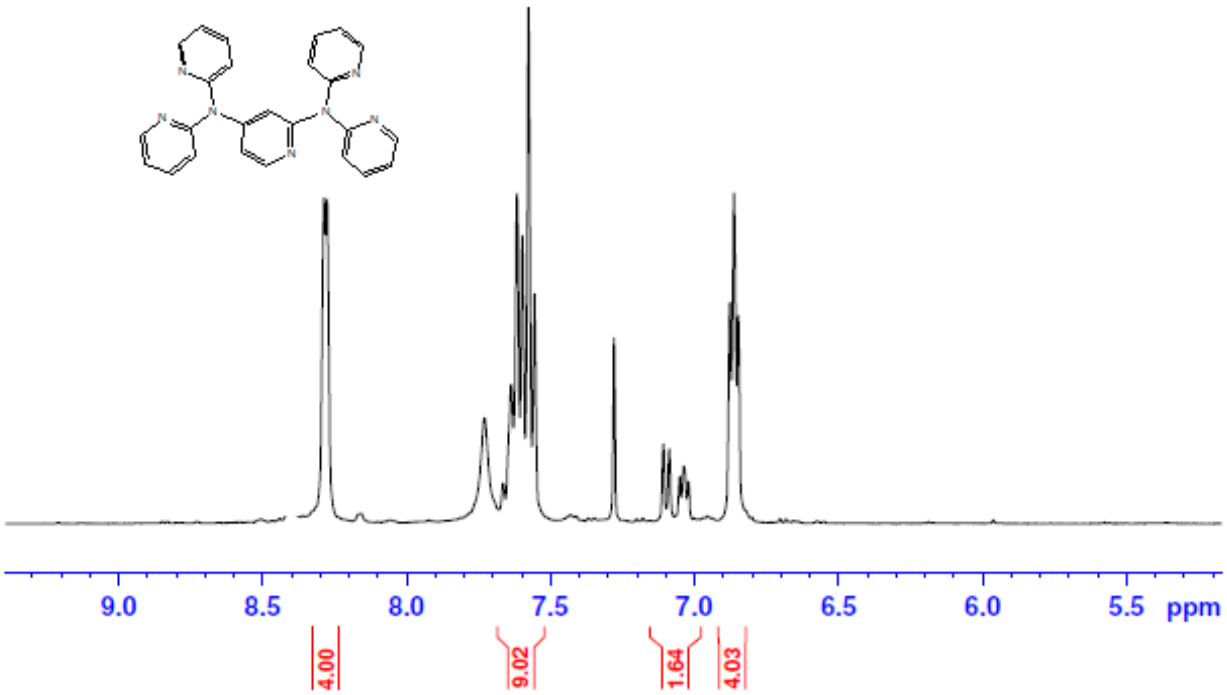

Figure S6.10: **^{1}H NMR spectrum of *N,N,N',N'*-tetrakis(2-pyridyl)-2,4-pyridinediamine (2,4-tppda)**

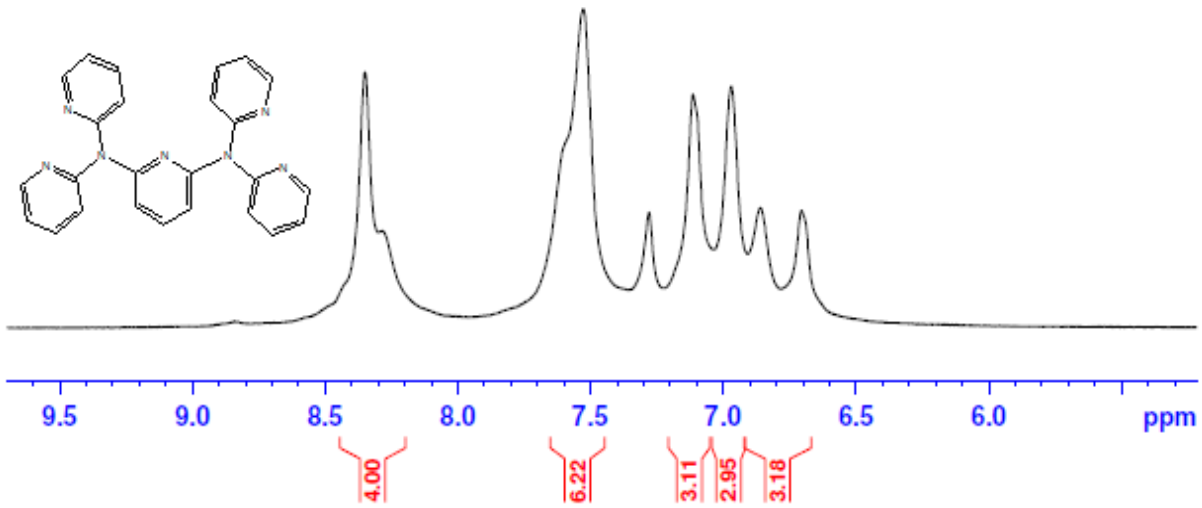

Figure S6.11: **^{1}H NMR spectrum of *N,N,N',N'*-tetrakis(2-pyridyl)-2,6-pyridinediamine (2,6-tppda).**

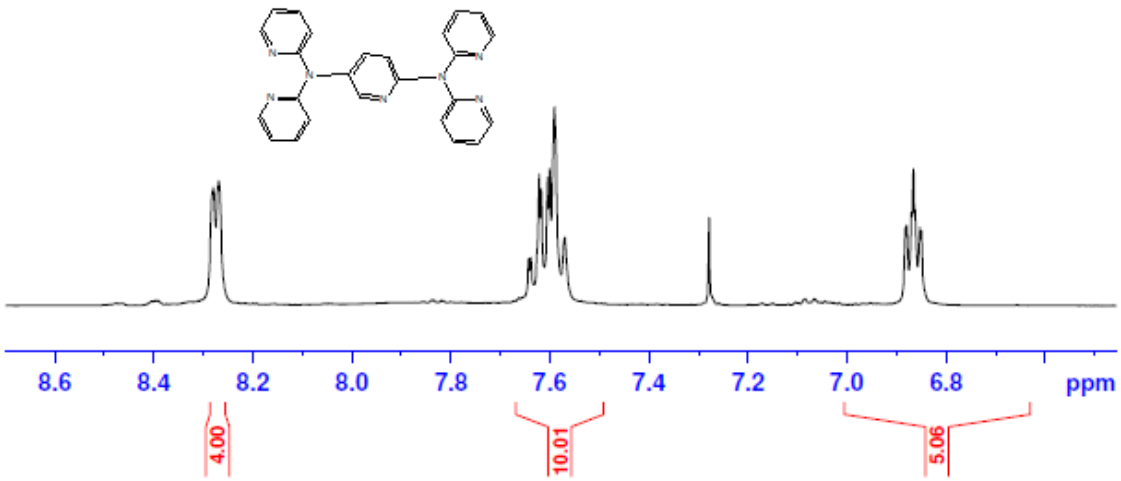

Figure S6.12: **^{1}H NMR spectrum of *N,N,N',N'*-tetrakis(2-pyridyl)-2,5-pyridinediamine (2,5-tppda)**

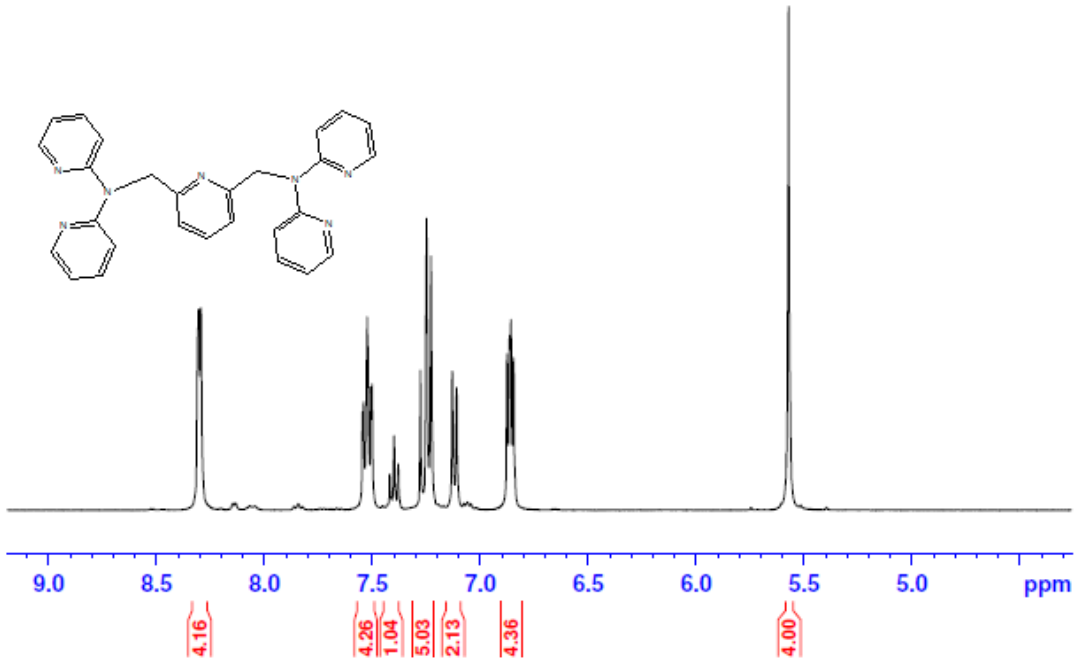

Figure S6.13: **^{1}H NMR spectrum of *N,N,N',N'*-tetrakis(2-pyridylaminomethyl)-2,6-pyridylamine (2,6-tpmpda)**

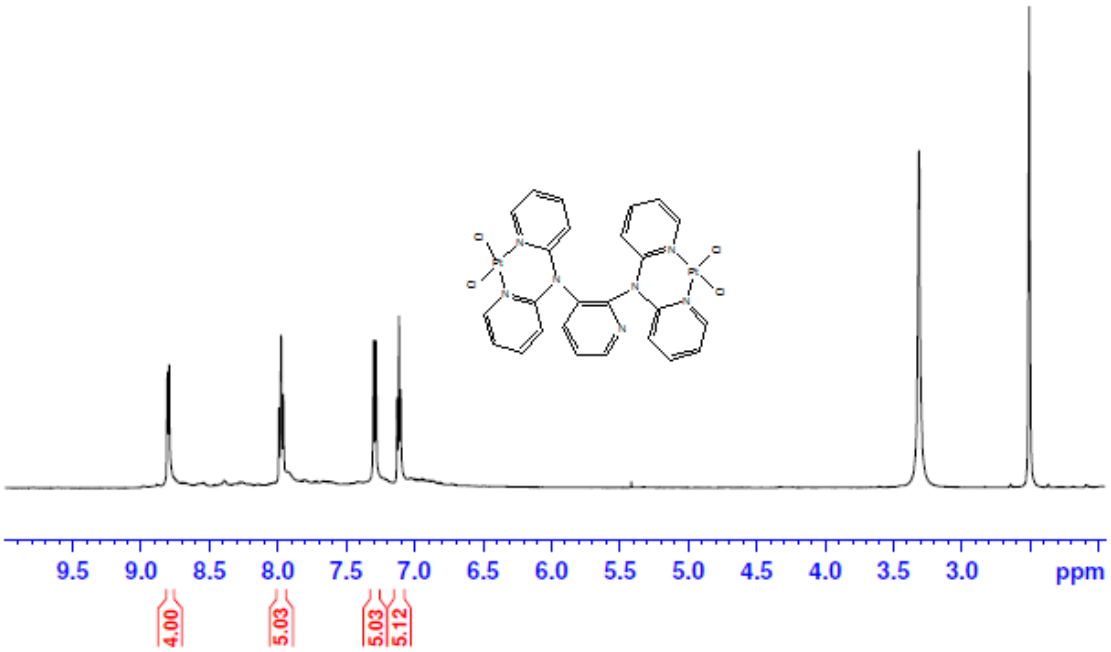

Figure S6.14: **^{1}H NMR spectrum of PtL1**

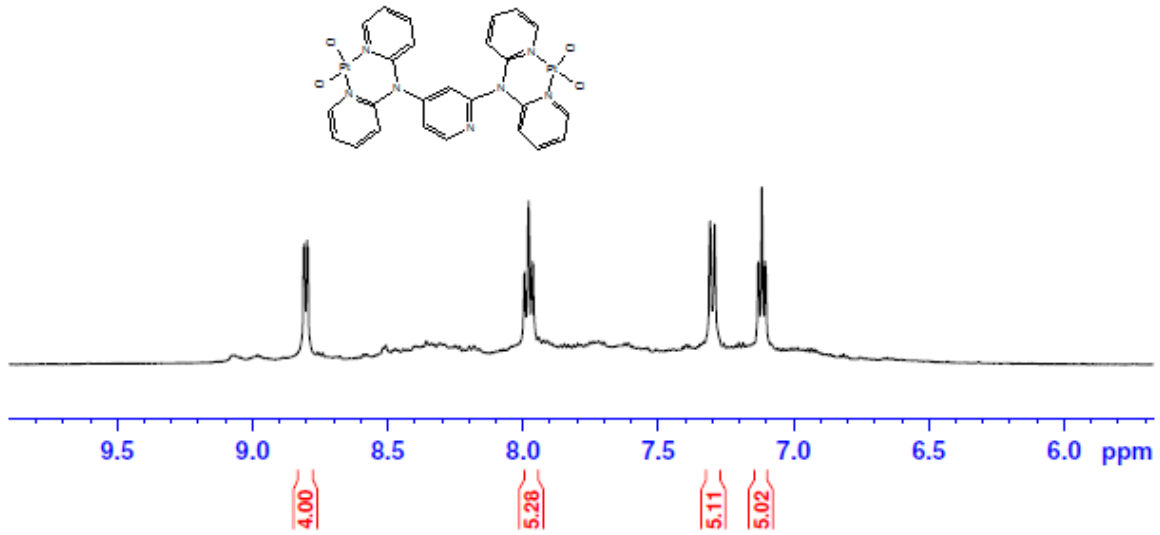

Figure S6.15: **^{1}H NMR spectrum of PtL2**

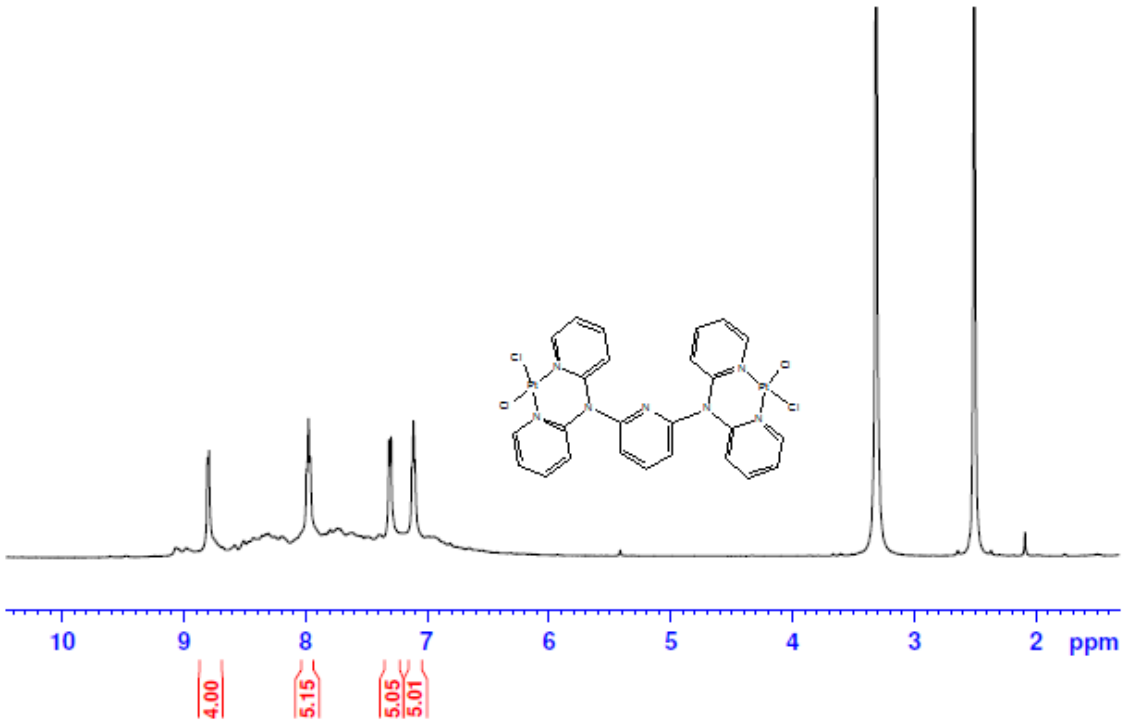

Figure S6.16: **^{1}H NMR spectrum of PtL3**

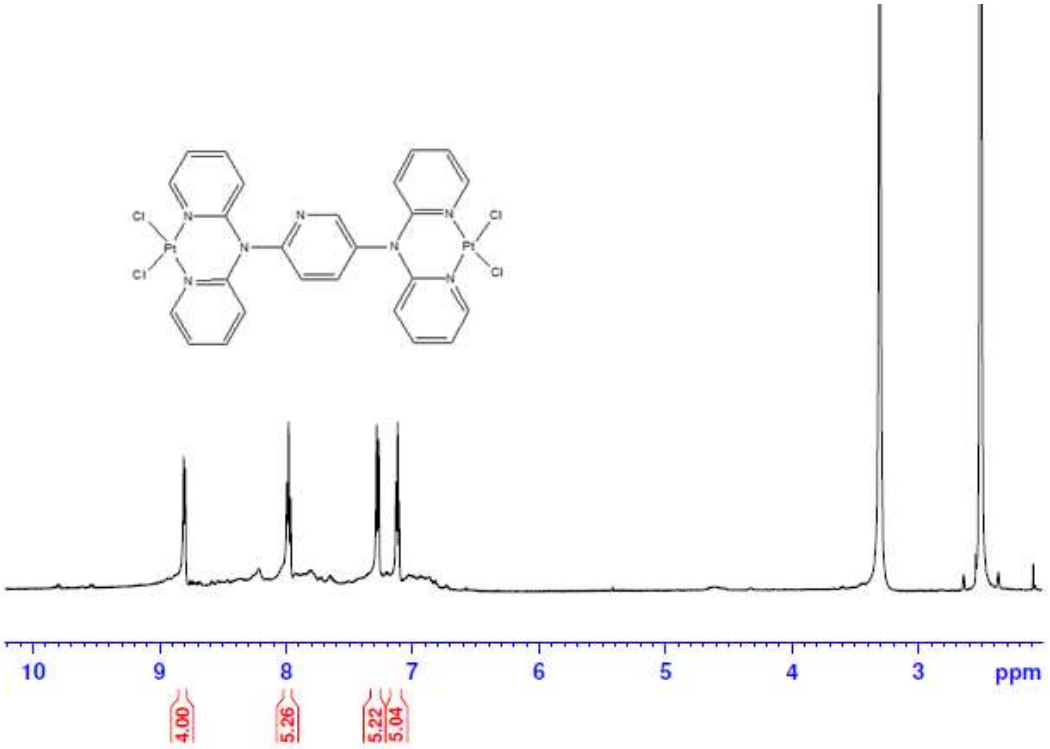

Figure S6.17: ^{1}**H NMR spectrum of PtL4**

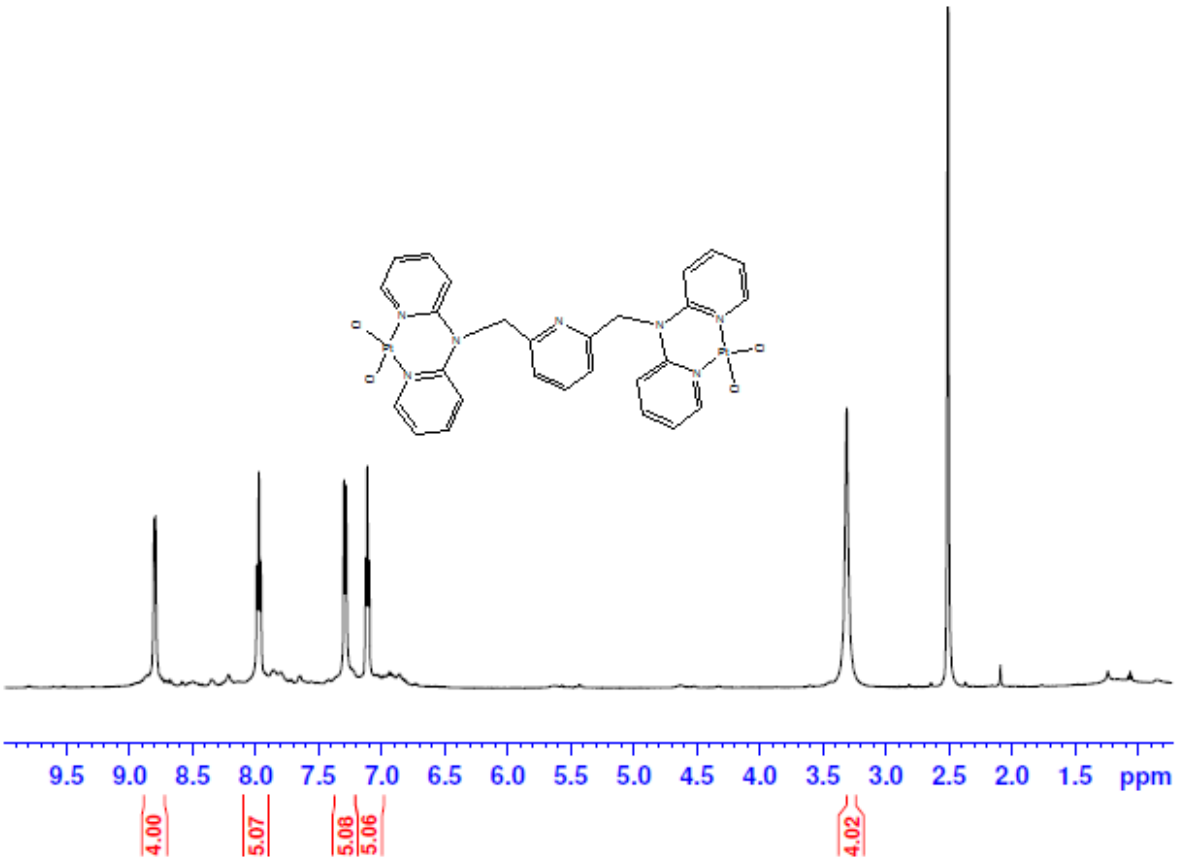

Figure S6.18: ^{1}**H NMR spectrum of PtL5**

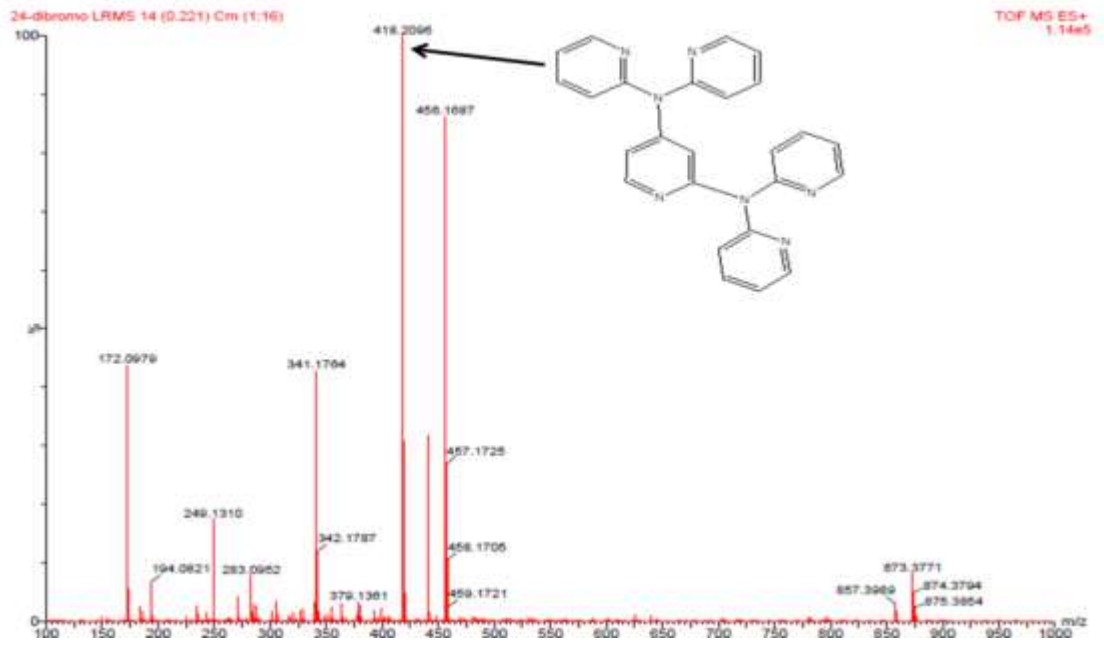

Figure S6.19: **TOF ESI mass spectrum of *N,N,N',N'*-tetrakis(2-pyridyl)-2,4-pyridinediamine (2,4-tppda)**

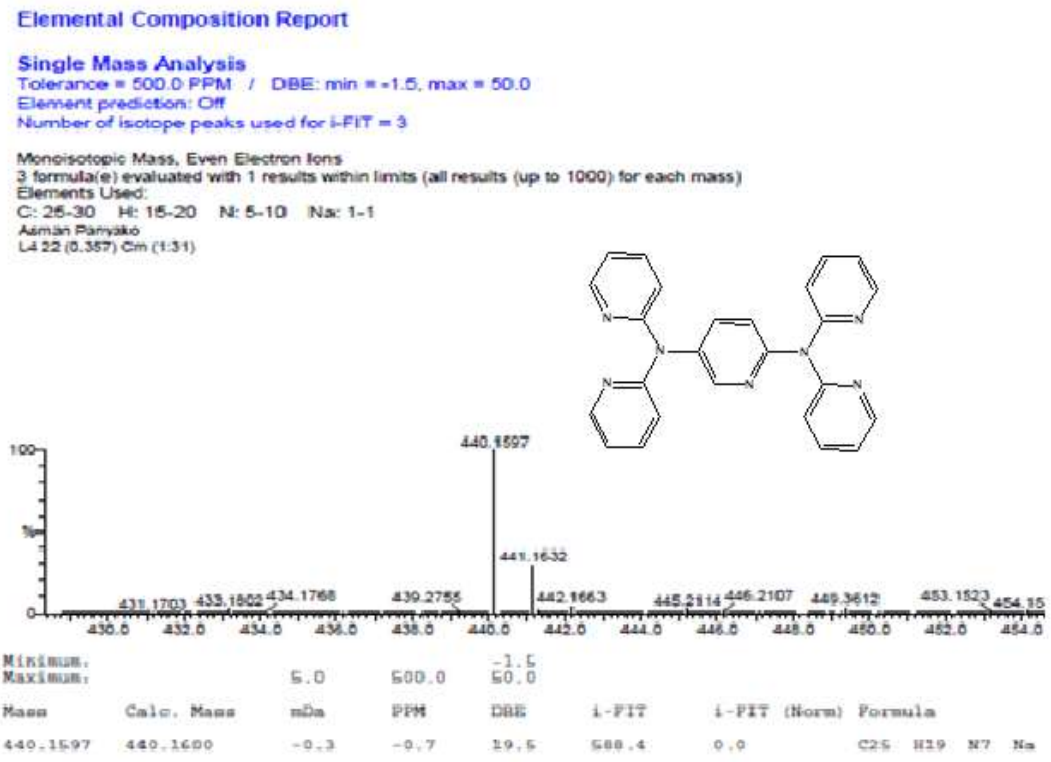

Figure S6.20: **TOF ESI mass spectrum of *N,N,N',N'*-tetrakis(2-pyridyl)-2,5-pyridinediamine (2,5-tppda)**

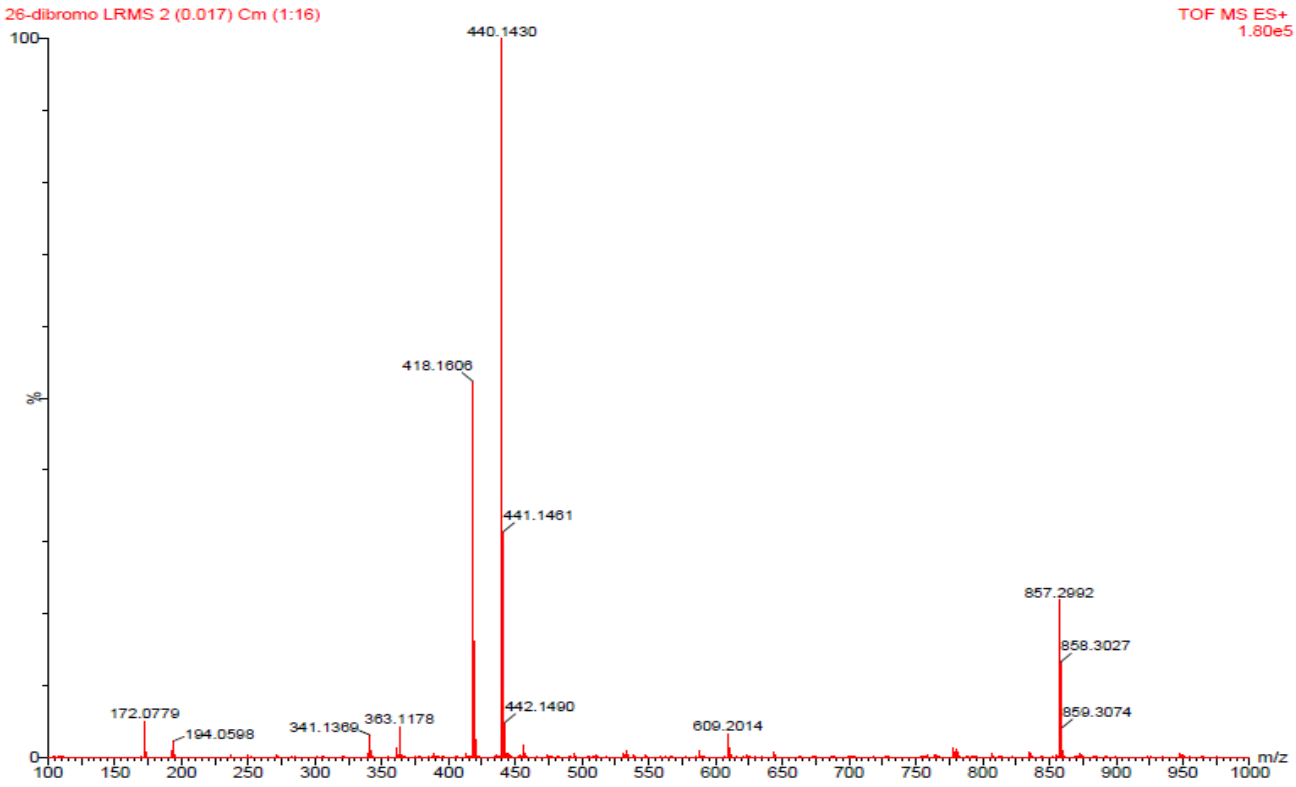

Figure S6.21: **TOF ESI mass spectrum of *N,N,N',N'*-tetrakis(2-pyridyl)-2,6-pyridinediamine (2,6-tppda)**

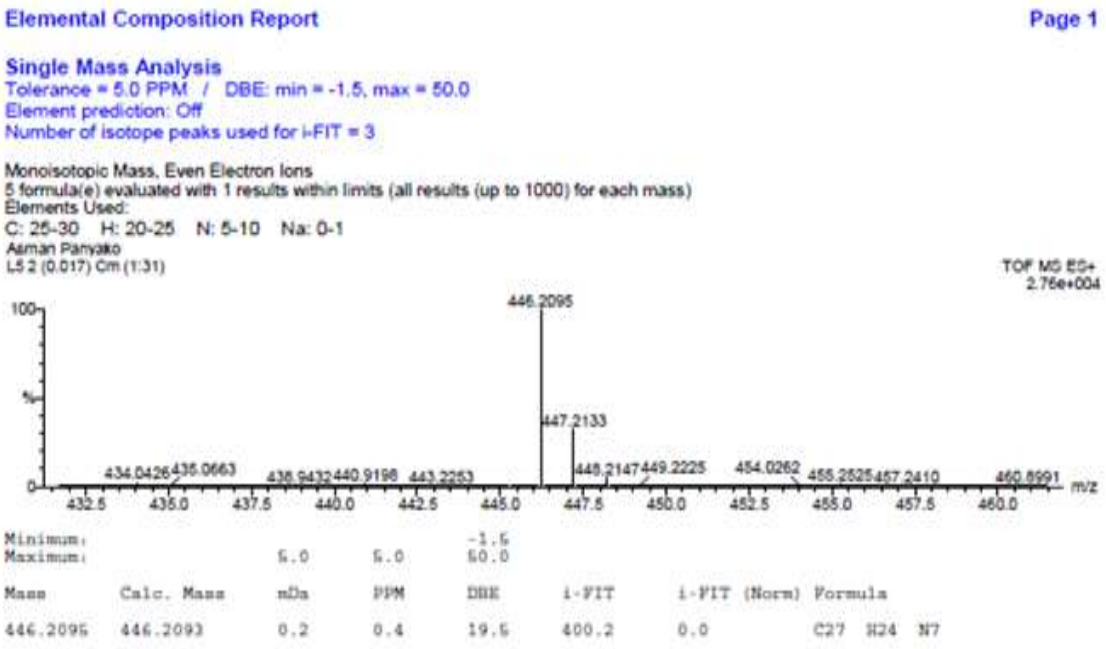

Figure S6.22: **TOF ESI mass spectrum of *N,N,N',N'*-tetrakis(2-pyridylaminomethyl)-2,6-pyridylamine (2,6-tpmpda)**

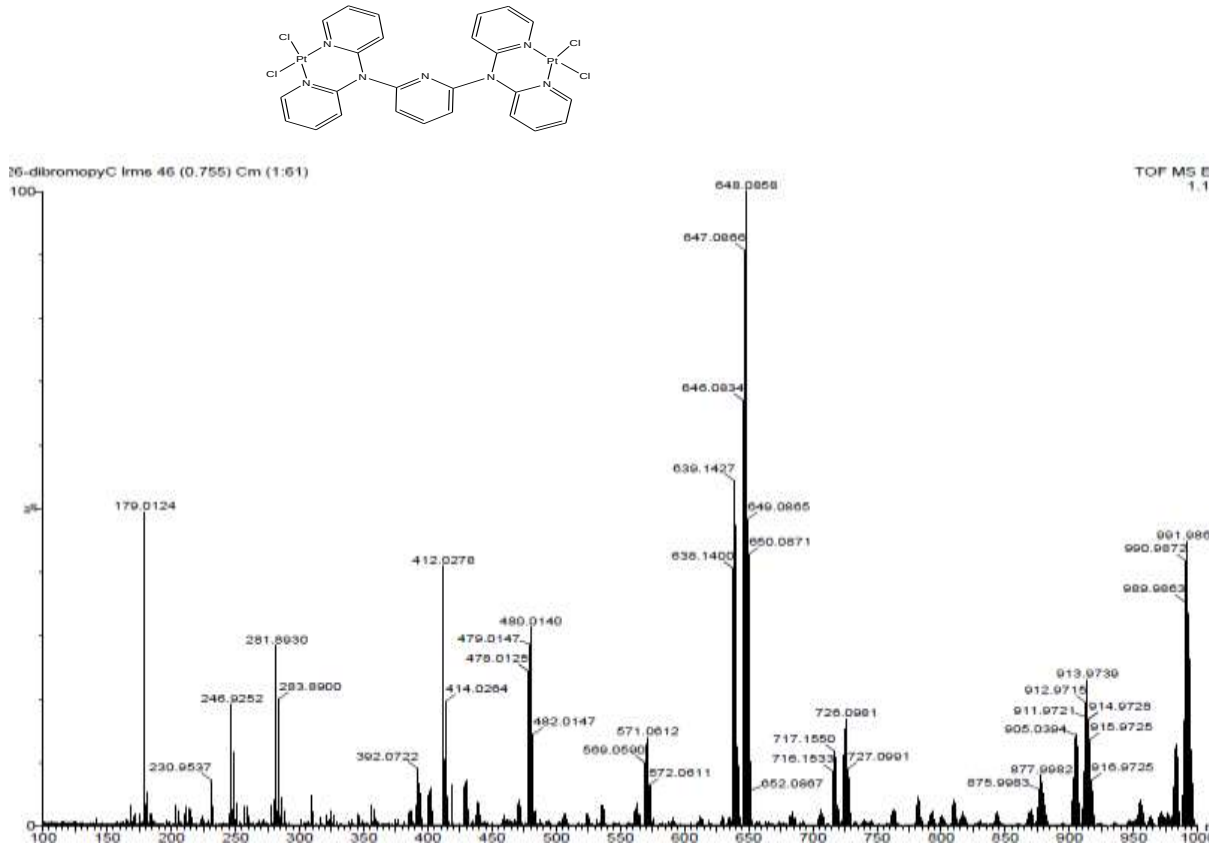

Figure S6.23: TOF ESI mass spectrum of PtL3

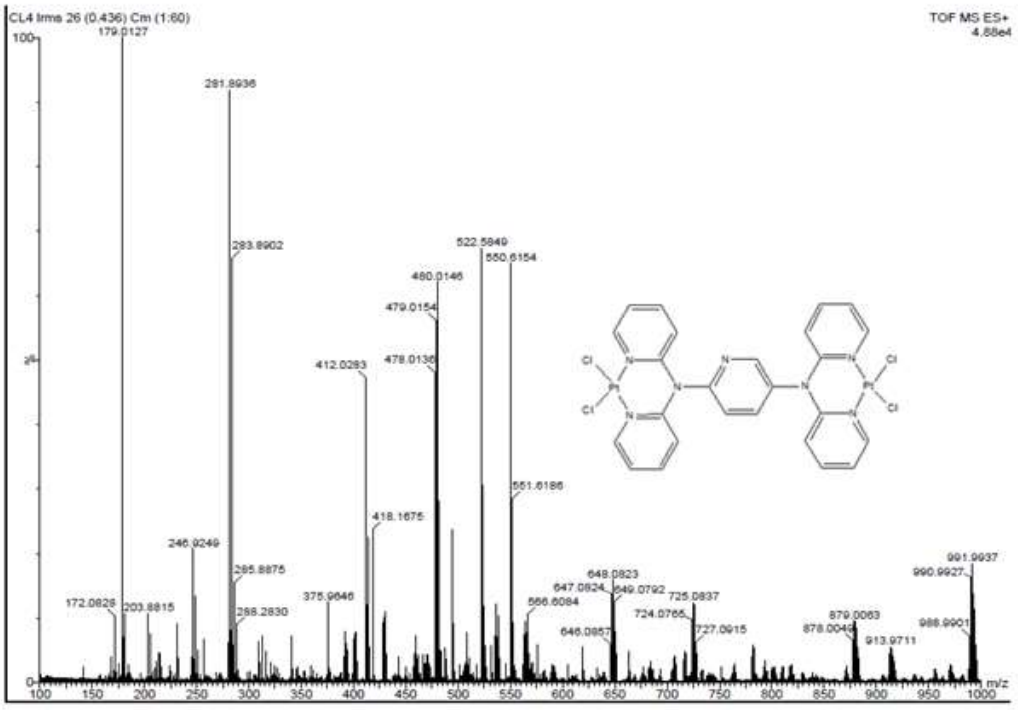

Figure S6.24: TOF ESI mass spectrum of PtL4

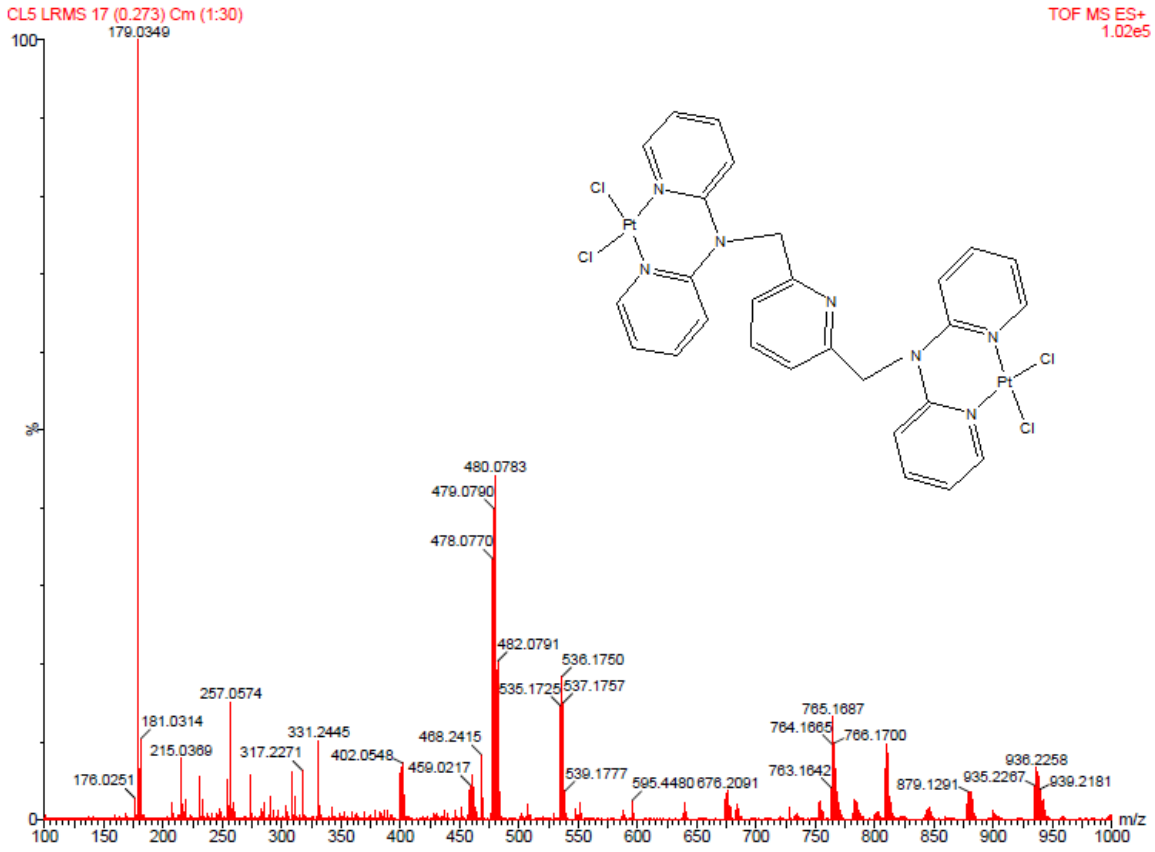

Figure S6.25: TOF ESI mass spectrum of PtL5

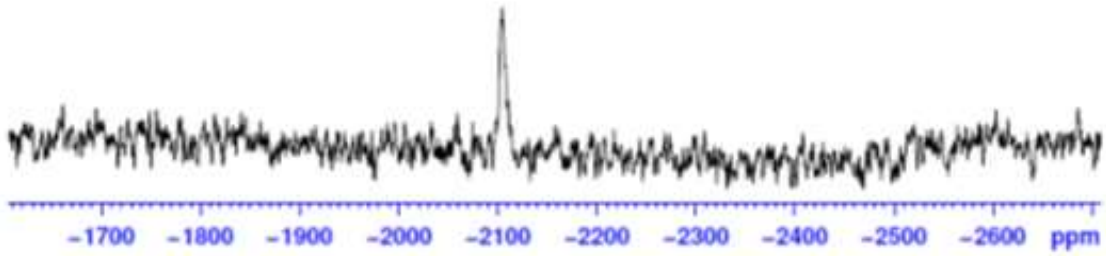

Figure S6.26: ^{195}Pt NMR spectrum of PtL1 in DMSO-d_6

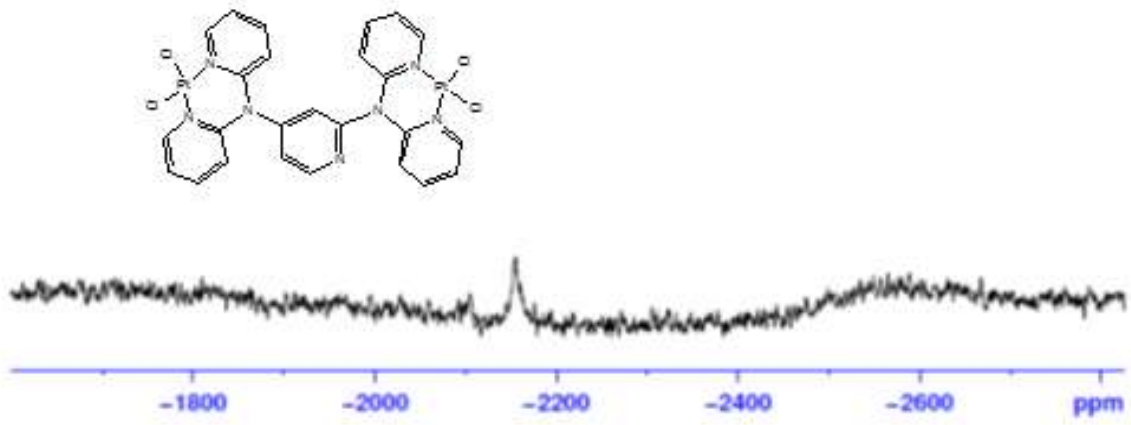

Figure S6.27: **^{195}Pt NMR spectrum of PtL4in DMSO-d_6**

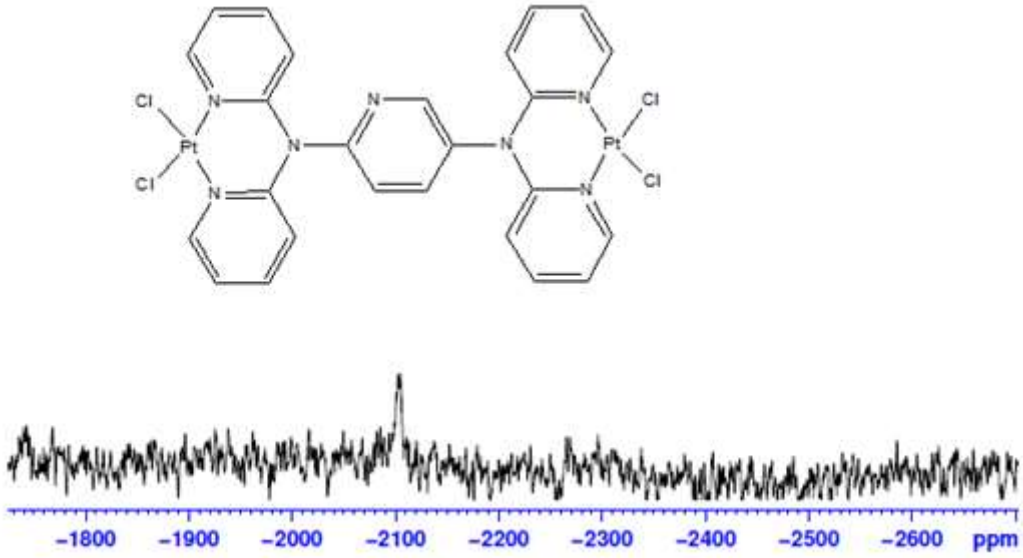

Figure S6.28: **^{195}Pt NMR spectrum of PtL4in DMSO-d_6**

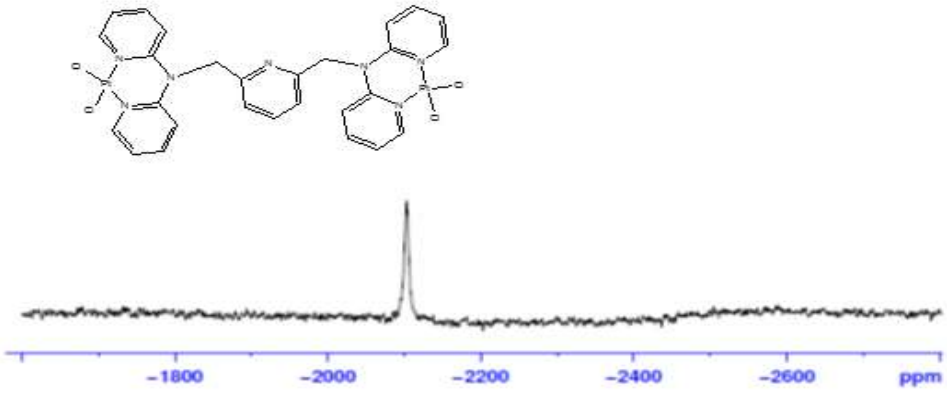

Figure S6.29: **^{195}Pt NMR spectrum of Pt2 in DMSO-d_6**

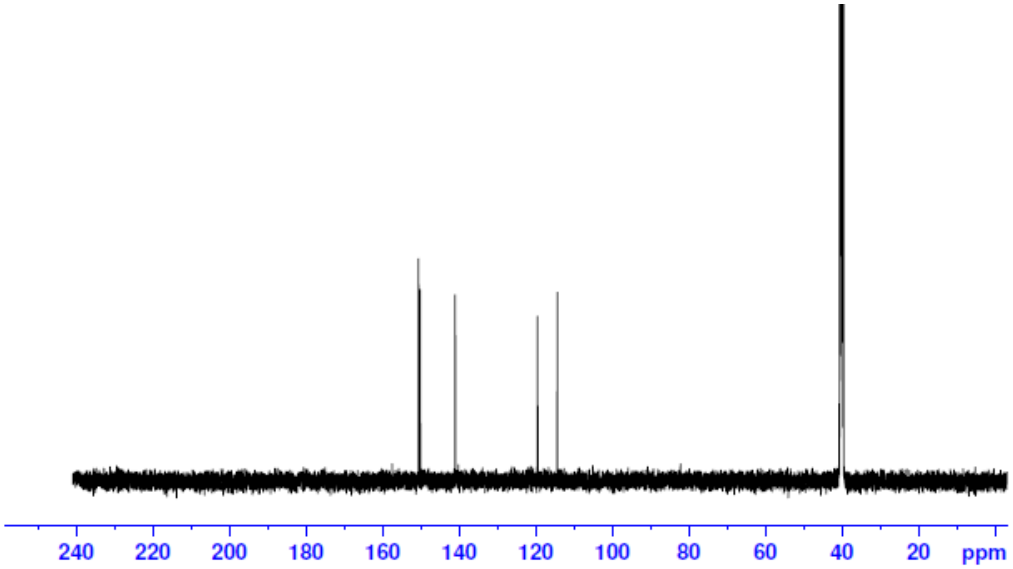

Figure S6.30: **^{13}C NMR spectrum of PtL1in DMSO-d_6**

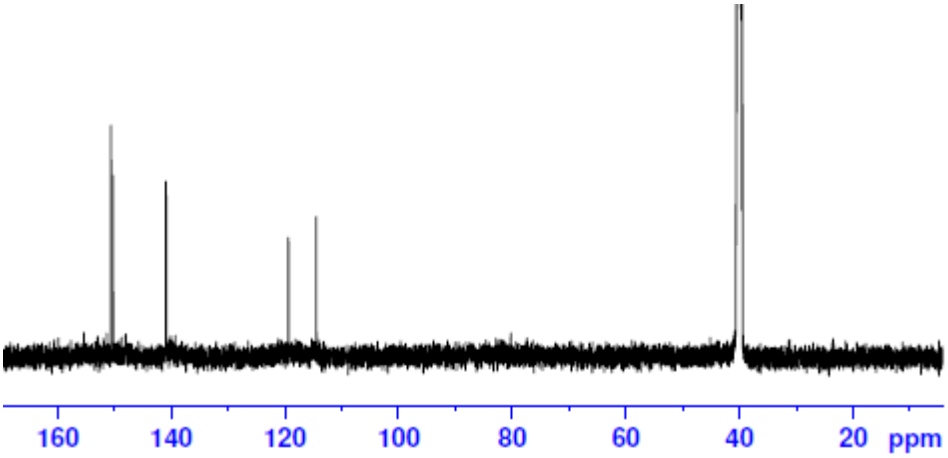

Figure S6.31: **^{13}C NMR spectrum of PtL4in DMSO-d_6**

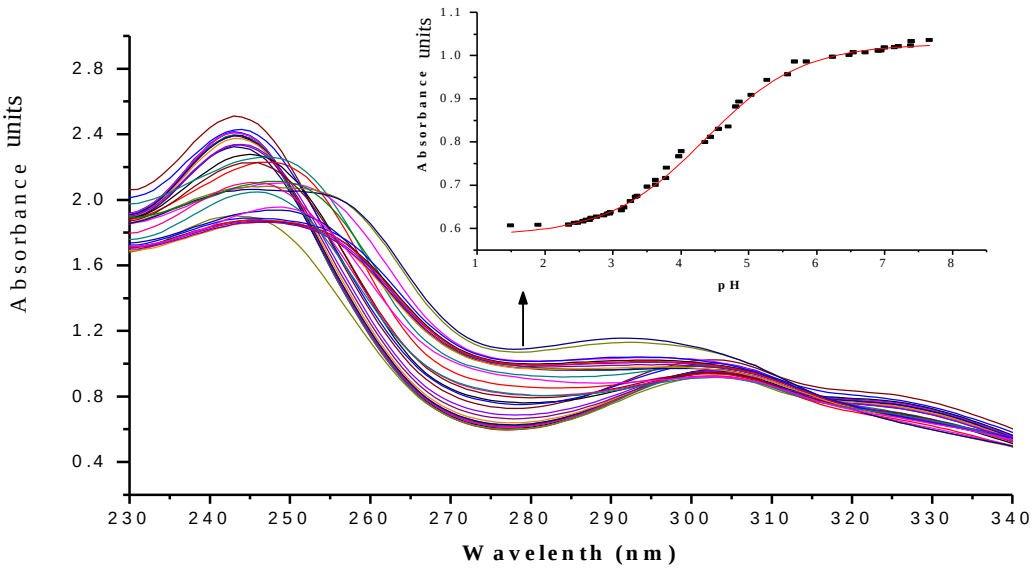

Figure S6.32: **UV-Vis spectrum of PtL1 complex recorded as a function of pH in the range of 2 to 10 at 25 ^{o}C, *Inset* Plot of absorbance versus pH at λ = 280 nm.**

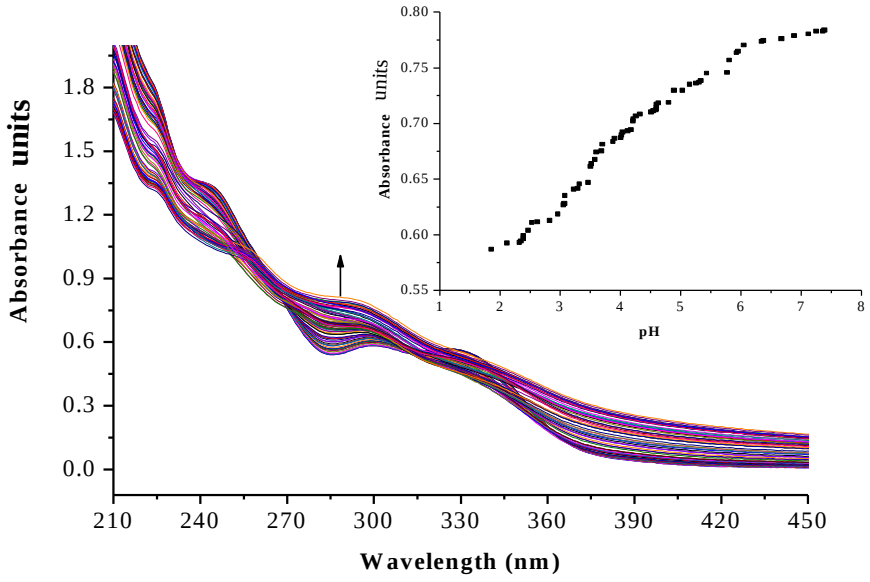

Figure S6.33: **UV-Vis spectrum of PtL3 complex recorded as a function of pH in the range of 2 to 10 at 25 ^{o}C, *Inset* Plot of absorbance versus pH at λ = 280 nm.**

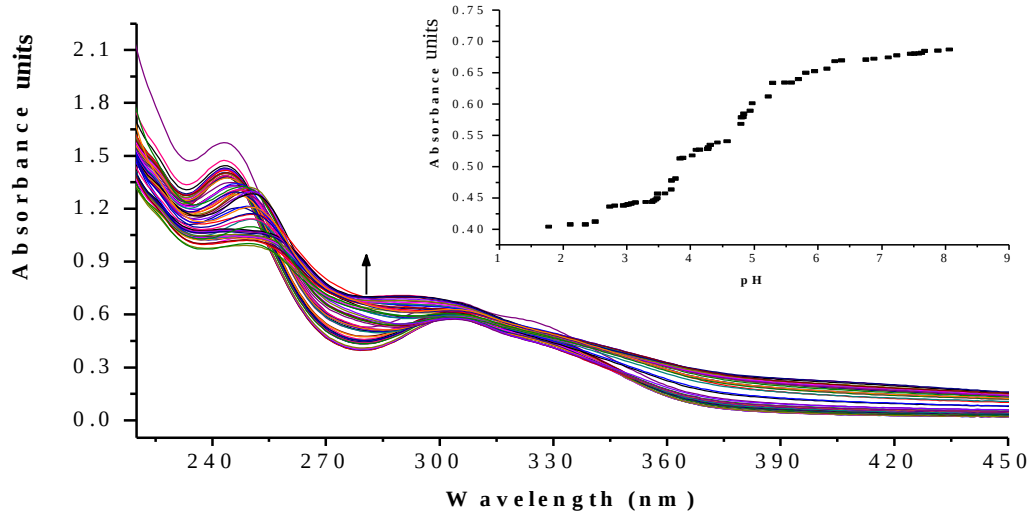

Figure S6.34: **UV-Vis spectrum of PtL4 complex recorded as a function of pH in the range of 2 to 10 at 25 ^{o}C, *Inset* Plot of absorbance versus pH at λ = 280 nm.**

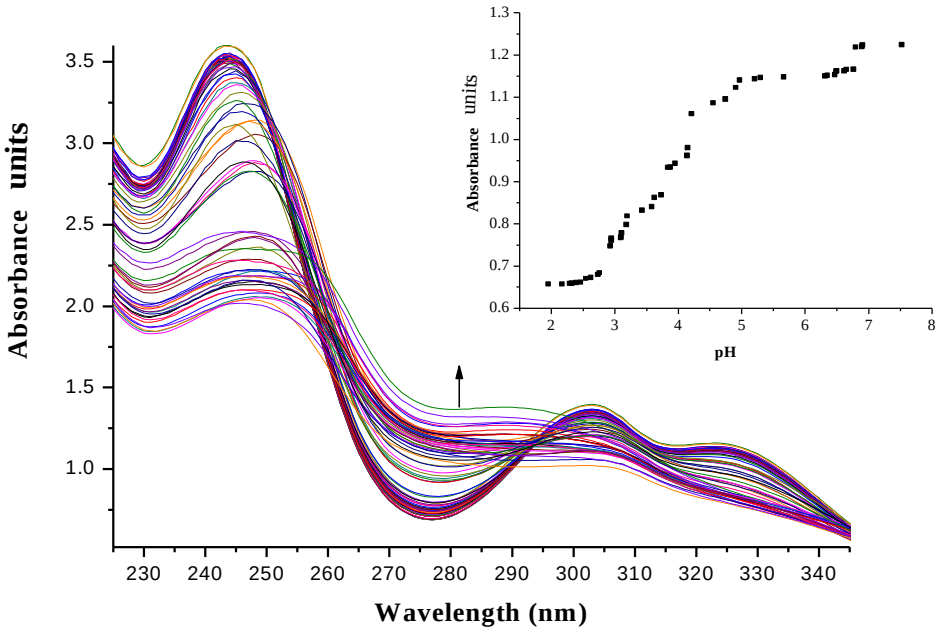

Figure S6.35: **UV-Vis spectrum of PtL5 complex recorded as a function of pH in the range of 2 to 10 at 25 ^{o}C, *Inset* Plot of absorbance versus pH at λ = 280 nm.**

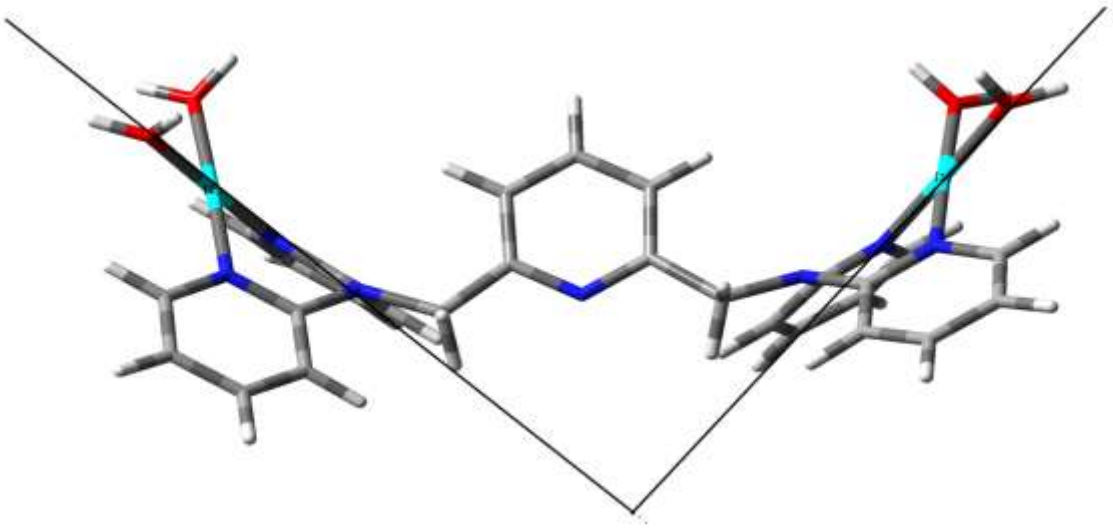

Figure S6.36: **Bowl shaped structure of complex PtL5; proposed for encapsulation of the nucleophiles causing acceleration in substitution kinetics of the complex**

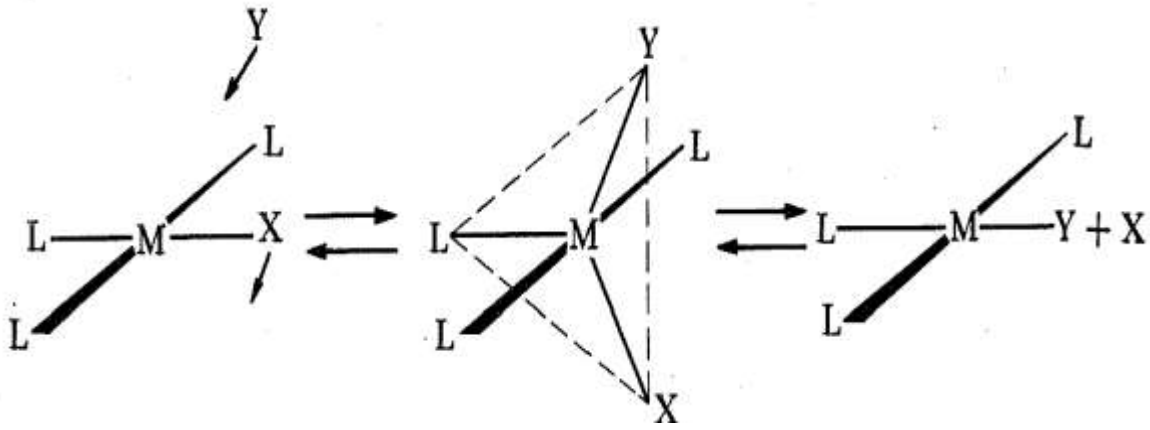

Figure S6.37: **Proposed penta-coordinated transition state of the complexes.**